LATE QUATERNARY PALAEOCEANOGRAPHY OF THE BENGUELA UPWELLING SYSTEM

MARK LITTLE

Thesis submitted for the degree of
Doctor of Philosophy

University of Edinburgh

1997

Declaration

I certify that the work presented in this thesis is my own, except where otherwise stated, and has not been submitted as a degree at this, or any other university.

Mark G. Little

Acknowledgements

Firstly to Dick Kroon for his insatiable and boundless enthusiasm. To Brian Price for giving me valuable advice and encouragement. To Ralph Schneider for replying to my endless e-mails and making me very welcome in Germany. Thank you.

This research was part of a joint collaboration with the Department of Geoscience, University of Bremen, Germany. I had a very enjoyable two months in Bremen, and an equally enjoyable (although I did not say this at the time), shipboard experience. Thanks especially to Peter Müller, Torsten Bickert, Gerold Wefer; Christian Baars, Ralph Kreutz, Ramses Hoek and Monika Segl.

To my colleagues, and in particular: Ian Alexander, Clare Bradshaw, Yvonne Cooper, Janet Cuthill, Sandy Tudhope, Kate Darling, Ian Snape, Al Matthewson, Bob Pringle, Ian Chisholm and Gordon Waugh. Thanks for all your help, advice and for bringing me back down to Earth when I needed it. Thanks for sharing my sense of humour. Thanks to my office mates Sally Brown, Paula McDade, Keerthi Perera, Alison Sowerbutts, Karen Mair and Pauline Thomson, for the obvious reasons.

Thanks to Martin Brasier for initiating my interest in Palaeoceanography.

And finally to my dearest Natalie.

TABLE OF CONTENTS

Abstract: Planktonic foraminifera recovered from nine cores in the Benguela Current system are used to ascertain the variability of upwelling intensity for the late Quaternary and its impact on atmosphere-ocean-cryosphere linkages. The analyses from high-resolution planktonic foraminiferal records for cores GeoB 1706, GeoB 1711 and PG/PC12, reveal striking variations in upwelling intensity during the last 160,000 years. Four species make up over 95% of the variation within the cores, and enable the record to be divided into episodes characterised by particular planktonic foraminiferal assemblages which have meaningful ecological significance when compared to those of the present-day and the relationship to their environment. The cold-water planktonic foraminifer, *Neogloboquadrina pachyderma* sinistral [*N. pachyderma* (s)], dominates the modern-day, coastal upwelling centres, and *Neogloboquadrina pachyderma* dextral and *Globigerina bulloides* characterise the fringes of the upwelling cells. *Globorotalia inflata* is representative of the offshore boundary between newly upwelled waters and the transitional, reduced nutrient levels of the sub-tropical waters. In the fossil record, episodes of high *N. pachyderma* (s) abundances are interpreted as evidence of increased upwelling intensity and the associated increase in nutrients. The *N. pachyderma* (s) record suggests rapid shifts in the intensity of upwelling, and corresponding trophic domains, that do not follow the typical glacial—interglacial pattern, but instead reflect the shifts of the Angola-Benguela Front situated to the north of the Walvis Ridge. Absence of high abundances of *N. pachyderma* (s) from the continental slope of the southern Cape Basin indicate that Southern Ocean surface water advection has not exerted a major influence on the Benguela Current system. The periods of high abundance in *N. pachyderma* (s) are referred to as 'PS events' and indicate increased intensity and zonality of the South Atlantic trade winds controlling the Benguela upwelling system.

During these intense upwelling phases, total organic carbon, abundance of *N. pachyderma* (s) and the benthic/planktonic foraminiferal ratio, provide the best indicators for palaeoproductivity away from coastal re-suspension. The offshore record of GeoB 1711 is used as the indicator for maximum offshore divergence and shelf-edge upwelling and is regarded as the best indicator for palaeoceanographic and palaeoproductivity variability. TOC content, measured in cores away from the conflicting signals of re-sedimentation and continental shedding, provides a quick method for analysing short-term climate and oceanic variability without the problems of temperature dominance associated with faunal populations studies. The good correlation between PS events, the North Atlantic Heinrich events, and the Dansgaard-Oeschger cycles from the Greenland ice core (GISP2) suggests large-scale oceanographic or

climatic teleconnections between the North and South Atlantic via the trade wind system. The radiocarbon constrained timing of PS events younger than 45 kyr indicates that the South Atlantic leads the North Atlantic's response to trade wind changes, particularly during isotope stages 4—2 when the Earth was dominated by large ice sheets. At times of increased trade wind strength, tropical and sub-tropical waters are forced across the equator on an 8 kyr periodicity, increasing the equatorial pool of warm water which can be transferred to the high latitudes of the North Atlantic. The increased supply of warm-water to the high latitudes of the northern hemisphere increases the ice-ocean moisture gradient and accelerates ice sheet growth, leading to eventual ice sheet collapse and iceberg calving (Heinrich event).

To the south of the Benguela Current system, the abundances of warm-water, tropical, planktonic foraminifera from GeoB 3602 correlate well to the meridional shifts of the sub-tropical convergence and the Antarctic polar front, indicating warm-water intrusion via the "Cape Valve". The co-occuring nature of deep-sea dissolution cycles in the Pacific, preservation cycles in the equatorial and North Atlantic, and the warm-water input via the Cape Valve, suggests that all three are closely linked with the production of North Atlantic Deep Water. The complete transect through the Benguela Current system, and correlation with the ice and sediment records, suggests that fluctuations in the input of saline-rich water from the Indian Ocean on glacial—interglacial timescales, and variability in the rate of heat/moisture flux to the high latitudes of the North Atlantic on sub-Milankovitch timescales, are extremely important for North Atlantic Deep Water production and global ocean-climate teleconnections.

Thesis Structure

This work is divided into five main sections —

(1) Introduction and background to palaeoceanography, and a review of recent research in the Benguela Current upwelling system and South Atlantic Ocean, with emphasis on their position in the global atmosphere-ocean system (CHAPTER 1).

(2) Chronostratigraphy and sediment history of the Benguela Current system and the records under study (CHAPTER 2).

(3) Results from sediment and micropalaeontological analysis in the northern Benguela Current system. This is further divided into three sections:

> (I) Local and regional oceanography and upwelling regime of the modern Benguela Current system and the late Quaternary history of palaeoceanographic change for the last 160,000 years (CHAPTER 3).
>
> (II) Palaeoproductivity variations in the Benguela Current system during the last glacial—interglacial cycle (CHAPTER 4).
>
> (III) Regional and global correlation of Benguela upwelling variability with South Atlantic—North Atlantic atmosphere-ocean teleconnections (CHAPTER 5).

(4) Record of change from the southern Benguela Current system for the last 500,000 years and its implications for warm-water advection, North Atlantic Deep Water production, and global climate instability (CHAPTER 6).

(5) Summary and conclusions. Long term records of warm-water advection versus short-term climate and upwelling variability (CHAPTER 7).

Introduction

Ch.1.

Chapter 1. Introduction

1.1. Previous research

Studies of sediments beneath modern and ancient oceanic settings have shown biological and geochemical proxies to be an important guide to past oceanography, productivity and climate changes on a decadal to millenial scale. The record of surface sediments distributed across the continental shelf and slope of southwestern Africa documents the palaeoceanographic history of possibly the most important continental margin, the Benguela upwelling system.

The continental margin of southwestern Africa is the site of intense upwelling and exceptionally high productivity recording amplified signals of climate change since the Benguela Current's evolution in the early Oligocene (~ 35 My. B.P.[1]). Recent work has focused on understanding the relationships of faunal variations to changes in upwelling intensity and location (*Lowry,* 1987, *Oberhänsli,* 1991, *Diester-Haass et al.,* 1992, *Giraudeau,* 1992, *Oberhänsli et al.,* 1992, *Schmidt,* 1992, *Dingle and Nelson,* 1993, *Giraudeau et al.,* 1993, *Giraudeau and Rogers,* 1994, *Dingle,* 1995, *Schmiedl,* 1995, *Summerhayes et al.,* 1995b, *van Leeuwen,* 1995, *Bleil and participants,* 1996, *Jansen et al.,* 1997, *Giraudeau et al.,* in prep., *Little et al.,* 1995; 1997a; 1997b), and to variations in geochemical and palaeoproductivity proxies (*Schneider,* 1991, *Schneider et al.,* 1992, *Giraudeau and Rogers,* 1994, *Schneider et al.,* 1995, *Summerhayes et al.,* 1995b, *Giraudeau et al.,* in prep.); have these relationships always existed or have they changed temporally or spatially? Does upwelling vary with climate changes forced by the orbital parameters, such as precession, which is thought to be dominant at the equator (*Imbrie et al.,* 1989, *McIntyre et al.,* 1989, *Ruddiman and Janecek,* 1989, *Molfino and McIntyre,* 1990, *Schneider et al.,* 1994, *Schneider et al.,* 1995)? Does upwelling vary at sub-Milankovitch frequencies similar to those recorded in many marine and terrestrial settings across the world (*Jouzel et al.,* 1987; *Heinrich,* 1988; *Yiou et al.,* 1991; *Bond et al.,* 1993; *Dansgaard et al.,* 1993; *Grootes et al.,* 1993; *Hagelberg et al.,* 1994; *Thouveny et al.,* 1994; *Kennett and Venz,* 1995; *Mix and Morey,* 1997; *van Kreveld et al.,* 1996)? Studies like this, of the glacial-interglacial change in a major component of the Earth's ocean-atmosphere system, are essential to establish the natural variability

[1] Million years before present.

of the global climate so that meaningful models of future climate change can be developed.

The sediments beneath the Benguela Current system (BCS) are primarily biogenic in origin, with planktonic foraminifera contributing the largest proportion (up to 96.6%) of skeletal calcium carbonate (*Bremner,* 1983). Planktonic foraminifera have been shown to vary with temperature, nutrients, productivity, and to a lesser extent salinity (*Bé and Tolderlund,* 1971, *Bé,* 1977, *Giraudeau,* 1992; 1993, *Ufkes and Zachariasse,* 1993) and have been extensively used for markers of palaeoceanographic change (*Berger et al.,* 1982; *Berger et al.,* 1987: *Kroon et al.* 1988; *Kroon and Ganssen,* 1989; *McIntyre et al.,* 1989; *Mix,* 1989a; 1989b; *Kroon et al.,* 1990; *Herguera,* 1992; *Oberhänsli et al.,* 1992, and others therein). In this study the modern-day spatial distribution of planktonic foraminifera is applied to interpret temporal changes of the last 160,000 years, and is assessed according to oceanographic frontal movements, trade wind zonality and upwelling intensity, and nutrient input into the Benguela Current system. The results are placed in a regional and finally global perspective of the atmosphere-ocean heat exchange.

Core	Position Latitude	Longitude	Water depth	Length	Sampling frequency
GeoB 1706-2	19°33.7 S	11°10.5 E	980 m	1120 cm	5 cm
GeoB 3608-2	22°21,5 S	12°12,0 E	1972 m	846 cm	20 cm
PG/PC 12	22°16.0 S	12°32.3 E	1017 m	702[2] cm	10 cm
GeoB 1711-4	23°18.9 S	12°22.6 E	1967 m	1066 cm	5 cm
GeoB 3606-1	25°28,0 S	13°05,0 E	1785 m	1074 cm	20 cm
GeoB 3605-2	31°26.7 S	15°17,8 E	1375 m	898 cm	20 cm
GeoB 3604-3	31°47,1 S	15°30,0 E	1514 m	942 cm	20 cm
GeoB 3603-2	35°07,5 S	17°32,6 E	2840 m	1130 cm	20 cm
GeoB 3602-1	34°47,9 S	17°45,3 E	1885 m	984 cm	5 cm

Table 1.1. Details of cores studied, listed according to latitude, north—south.

The material analysed for this research, was collected from the continental slope of southwest Africa, offshore Namibia and South Africa. Nine sediment cores were retrieved from the mid to upper continental slope along a north—south transect of the southwest African margin. Gravity cores, GeoB 1706 and GeoB 1711 were both collected on R/V METEOR cruise M20-2 (1991; *Schulz and cruise participants,* 1992); a piston core PC12 and its accompanying gravity core PG12 collected on R/V CHAIN

[2] Total combined length (PC12 + PG12)

cruise 115 (1973; *Summerhayes,* 1974); and cores GeoB 3602—3608 were collected on R/V METEOR cruise M34-1 (1996; *Bleil and cruise participants,* 1996). The complete transect of the Cape Basin allowed for a unique history of the palaeoceanographic fluctuations over the entire region to be ascertained, and for hypotheses in local oceanographic sources and causal mechanisms to be developed; core details are given in Table 1.1 and their geographical position is shown in Figure 1.1.

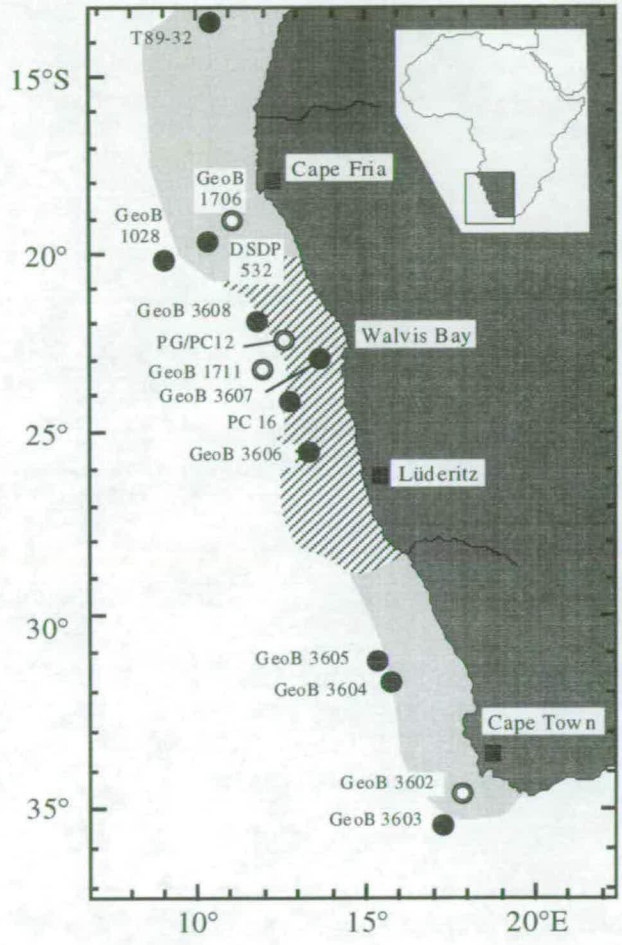

Figure 1.1. Geographical position of cores cited (black circles) and sampled (black rings) from the Cape Basin continental shelf and slope. Hashed area represents the zone of permanent upwelling in the northern Benguela region, dotted areas represent the zones of seasonal upwelling in the southern Benguela region, the southern Angola Basin and Walvis Ridge offshore Cape Fria. Core positions are given in Table 1.1.

1.2. Research objectives

The aim of this study is to assess the variation of planktonic foraminifera to determine changes in the palaeoceanography of the Benguela system in the expectation that this will enable us to asess the extent to which upwelling has changed temporally and spatially and to determine what controls those changes.

The high resolution foraminiferal record of cores GeoB 1706, GeoB 1711 and PG/PC12 are used to investigate the variability of palaeoceanography of the South African, Namibian and Angolan margins for the last 160 kyr. Previous analyses on planktonic foraminifera in this and other regions have linked foraminiferal variability to changes in temperature, nutrients, wind direction, monsoon strength, salinity, aridity, carbonate platform building and oceanographic frontal movements. Two hypotheses can be made: one relates to the timing of fluctuations and the other relates to the causes of fluctuations.

The first hypothesis, timing of fluctuations, is of importance in the BCS to relate proposed changes in upwelling intensity to previously described global or regional mechanisms. Do fluctuations in abundances of planktonic foraminifera co-vary with precession driven seasonality at the equator (*McIntyre et al.,* 1989); polar frontal shifts at high southern latitudes (*Howard and Prell,* 1992); heightened monsoon intensity (*Emeis et al.,* 1995); maximum deflection of the Benguela Current into the South Atlantic gyre (*Schneider et al.,* 1995); and/or Heinrich-type events recorded in terrestrial and marine events across the world (e.g. *Kotilainen and Shackleton,* 1995)? If so, do the abundances of planktonic foraminifera record changes on a Milankovitch or sub-Milankovitch time scale?

The second hypothesis, causes of fluctuations, is usually more local in origin. Do planktonic foraminifera in the BCS vary with flux in nutrient availability, with sea surface temperature, with trade wind zonality and upwelling intensity, or are they related to advection of cold waters from the south as has previously been stated as the main cause of change in abundance of planktonic foraminifera (*McIntyre et al.,* 1989, *Giraudeau,* 1993, *Summerhayes et al.,* 1995b; *Giraudeau et al.,* in prep.)?

The following is a list of objectives that we hope to resolve with this research in the Benguela Current system.

1. Can abundances of planktonic foraminifera be used as a proxy for past changes of upwelling intensity in the BCS?
2. To what degree is the BCS controlled by cold-water advection from the Southern Ocean as has previously been suggested (*McIntyre et al.,* 1989, *Giraudeau,* 1993, *Summerhayes et al.,* 1995; *Giraudeau et al.,* in prep.)?
3. Do planktonic foraminifera from the Cape Basin show changes in relation to the shifts in the position of the Angola-Benguela Front, corresponding to those of the Angola Basin?
4. Can we make any assumptions on past productivity using foraminiferal or organic carbon proxies, or is the sedimentological record not as applicable as it is in other areas?
5. Can we use total organic carbon as an easier and quicker method for recording short-term climatic and oceanic variability?
6. Do Milankovitch band frequencies appear in sediment records in the Cape Basin, like it does in the equatorial Atlantic?
7. Do we observe similar short-lived climatic events in the South Atlantic to those seen throughout the world, and can we gain further insight into their significance, relative timing, and possible driving mechanisms?
8. Finally, we attempt to place the BCS in a global perspective. Is the Benguela system as important climatically as the North Atlantic was first perceived to be? Are the South Atlantic—North Atlantic teleconnections important for short- or long-term climate variability, and is this an artefact of a Milankovitch-driven atmospheric system?

1.3. Scope of research

To assess the use of planktonic foraminifera as palaeoceanographic and palaeoproductivity proxies, I use a total of nine cores retrieved from the Benguela upwelling system from three separate collection expeditions to the South Atlantic. This research would not have been possible without the contributions from Ralph Schneider, Peter Müller, Torsten Bickert, Monika Segl and Gerold Wefer at Bremen University and Colin Summerhayes at Southampton University. I was fortunate enough to participate in the R/V METEOR cruise M34-1 (Cape Town - Walvis Bay; January 1996) and to be directly involved in collecting, sampling, preparing and both preliminary and secondary analyses of cores GeoB 3602—3608 both on-board ship

and later at Edinburgh University. Cores from R/V METEOR cruise M20-2 were kindly provided by Bremen University together with a complete oxygen and carbon isotope record (Ralph Schneider, Torsten Bickert, Monika Segl) and total organic carbon (TOC) measurements (Peter Müller). Combined core PG/PC12 was re-sampled for foraminiferal analysis by Colin Summerhayes at Woods Hole Oceanographic Institute and provided a higher resolution study for the last 60 kyr. This core was prepared and analysed at the University of Edinburgh.

The scope of this research was to analyse planktonic foraminiferal abundances from cores in the Benguela upwelling system using the oxygen isotope stratigraphy solely as a chronostratigraphic framework for the cores. Detailed assessment of the oxygen and carbon isotope variations with time was outside the scope of this project as this is, and will, be carried out by Bremen University. The stable isotope chronostratigraphic framework was developed as part of this research and later supported using Accelerated Mass Spectrometry (AMS) ^{14}C dating further provided by Bremen University (Ralph Schneider and Monika Segl), after analysis at the Leibniz-Labor AMS facility, Christian-Albrechts-University, Kiel, Germany. The chronostratigraphic framework for core PG/PC12 is constrained using AMS ^{14}C dating from published results in *Summerhayes et al.* (1995b).

1.4. Background to oceanography

1.4.1. Present-day surface circulation and upwelling

The general pattern of oceanic surface water circulation is shown in Figure 1.2, and records the present-day averaged global surface water current pattern. However, at any one time the local current flow may be very different to these averaged conditions; for example, small-scale eddies and rings at the Agulhas Retroflection (*Winter and Martin,* 1990, *Duncombe-Rae,* 1991). These small-scale variations of surface and intermediate waters may become increasingly important as climate dynamics are seen to vary on ever decreasing time scales. However, the discussion will concentrate on general ocean circulation and how these prevailing currents are driven.

The wind-driven currents of the sea surface are dominated by three mechanisms: wind stress, pressure gradients, and the Coriolis force. Each factor will be discussed briefly to provide an overview of the physical oceanography. The large-scale global wind

system blows in response to the differential heating on the ocean surface and to the rotation of the earth on its spin axis. The consequence of this is zonal wind flow, which produces the trade winds [3] of the sub-tropics, possibly the single most important factor in oceanographic and climate studies. Wind stress creates friction with the surface waters which instigates surface current flow [4]. We would assume therefore, that the ocean's surface mirrors the atmospheric circulation, but an additional factor, the Coriolis deflection, must be taken into consideration.

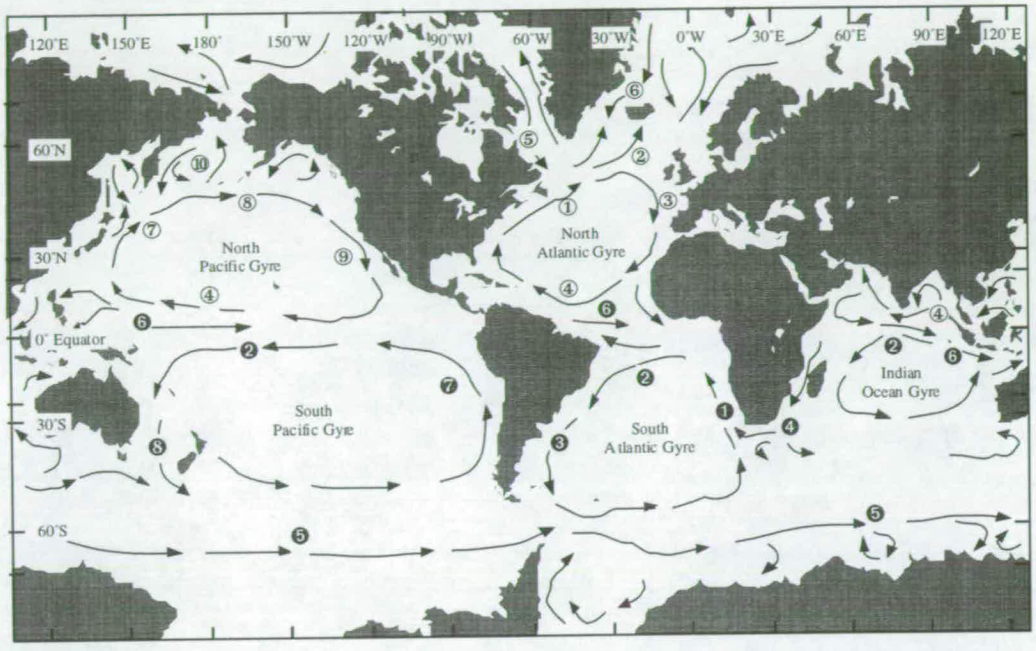

Northern Hemisphere Currents

① Gulf Stream
② N. Atlantic C.
③ Canary C.
④ N. Equatorial C.
⑤ Labrador C.
⑥ E. Greenland C.
⑦ Kuroshio C.
⑧ N. Pacific C.
⑨ California C.
⑩ Oyashio C.

Southern Hemisphere Currents

❶ Benguela C.
❷ S. Equatorial C.
❸ Brazil C.
❹ Agulhas C.
❺ Antarctic Circumpolar C.
❻ Equatorial Countercurrent
❼ Peru C.
❽ E. Australian C.

Figure 1.2. Global surface-water current pattern.

The rotational velocity of the Earth varies with latitude, so that the oceans, which are not rigidly fixed on the Earth, undergo an apparent deflection known as the Coriolis effect. The movement of water in the northern hemisphere is deflected to the right, and water in the southern hemisphere is deflected to the left. In conjunction with the uneven distribution of solar heat on the rotating earth, the Coriolis force causes the air

[3] Trade winds are zonally directed east—west, the antithesis of which are the westerlies in the mid-latitudes.
[4] Wind stress is proportional to the (wind speed)^2.

to deflect creating the trade winds and westerlies of both hemispheres. The result is paired cyclonic and anticyclonic gyres lying between the 60° lines of latitude in the ocean basins where water movement is not impeded by continental land mass. An interesting and important facet of the Coriolis force is Ekman transport (ET); the increasing deflection of currents with depth away from the direction of the generating wind. As the current deepens the water layer is further deflected, producing a spiralling current, the Ekman spiral, in which speed decreases with depth.

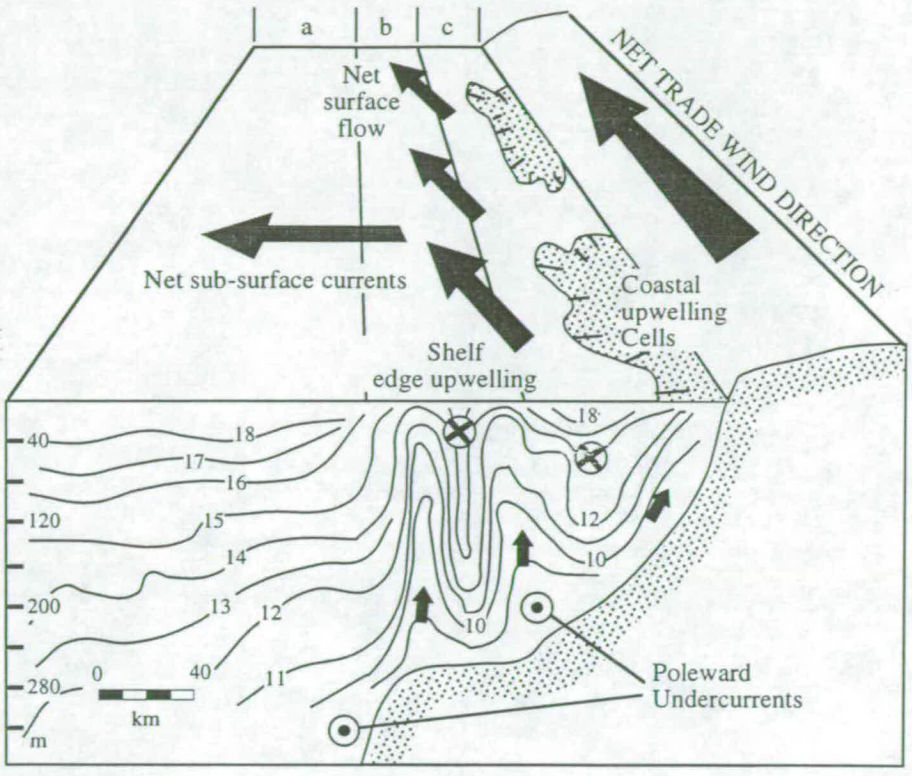

Figure 1.3. Conceptual three-dimensional model of the Benguela upwelling system off Namibia (adapted from *Bang,* 1971; *Barange and Pillar,* 1992; *Summerhayes et al.*, 1995b). Isotherms in °C, depths in meters; arrows in cross-section represent upwelling; dots in circles indicate poleward undercurrents; crosses in circles indicate equatorward motion. Region: a = trade wind drift; b = offshore divergence belt; c = Benguela Current (after *Summerhayes*, 1983).

Volume transport calculations have shown that surface currents move at up to 45° from the wind direction and net water transport is perpendicular to the generating wind (Figure 1.3). This becomes particularly important when we consider ET as a result of trade winds on the eastern boundaries of the world's oceans, for example southwestern Africa. Offshore South Africa, trade winds are directed south-east to

north-west, and thus equatorwards, for much of the year. The wind stress pattern and resultant ET creates an offshore drift of water away from the land. If this net volume displacement is not sufficiently replaced by horizontal flow then water must rise from below, creating vertical circulation, referred to as upwelling.

All the eastern boundary regions where the wind stress is nearly equatorward for part of the year are major upwelling regions [5]. The re-distribution of mass during coastal upwelling, with denser upwelled water accumulating along the coast as the winds transport the surface water offshore, results in an along-shore current that flows in the direction of the wind. This has been observed in many environments including Oregon, Peru and northwest Africa, where cross-shelf transport in the surface layer over the continental shelf is in good agreement with ET estimates.

1.4.2 Water mass structure of the Atlantic

Profiles through the ocean basins reveal that water temperature drops with increasing latitude and increasing depth, which becomes important when we consider heat, nutrient and biogenic fluxes in the oceans. Water that is warmer than 10° C is confined to a thin lens that straddles the equator. Solar radiation is at a maximum at the equator and heats this water to such an extent that it offsets the density effect of the high salinities, created by evaporation rates in the sub-tropics, and thus it floats above colder, denser water below. Poleward of 45°S, evaporation cools the sea-surface water and increases its density. As this dense water moves equatorward, it encounters warmer, less-dense surface water and sinks below it, thus producing a salinity and temperature dependent water stratification.

In the Atlantic Ocean the deep, bottom waters are dominated by the cold, dense Antarctic Bottom Water (AABW) produced primarily within the Weddell Sea (Figure 1.4). The overlying Antarctic Deep Water (AADW) forms in less extreme conditions, and tends to be less saline than the AABW. From the northern hemisphere, North Atlantic Deep Water (NADW), which is less cold and salty than either the AABW or AADW, is generated at such a high rate, by volume, that it is the most common of the bottom waters. It spreads across the North Atlantic floor before it is forced over the denser AABW and then the AADW, into intermediate depths where it mixes with the

[5] Except the west coast of Australia. Here, the along shore pressure gradient off western Australia is very large and dominates wind stress, suppressing upwelling and causing the poleward direction of the Leeuwin Current (*Smith et al.*, 1991).

Antarctic Circumpolar Current (AACC). At the top of the idealised water structure are the overlying less dense intermediate waters of the Antarctic and Arctic (AAIW and AIW respectively) and the central waters of the North Atlantic and South Atlantic (NACW and SACW respectively). An elongated tongue of highly saline Mediterranean Intermediate Water (MIW) spills over the Strait of Gibraltar and can be found at ~ 40°N.

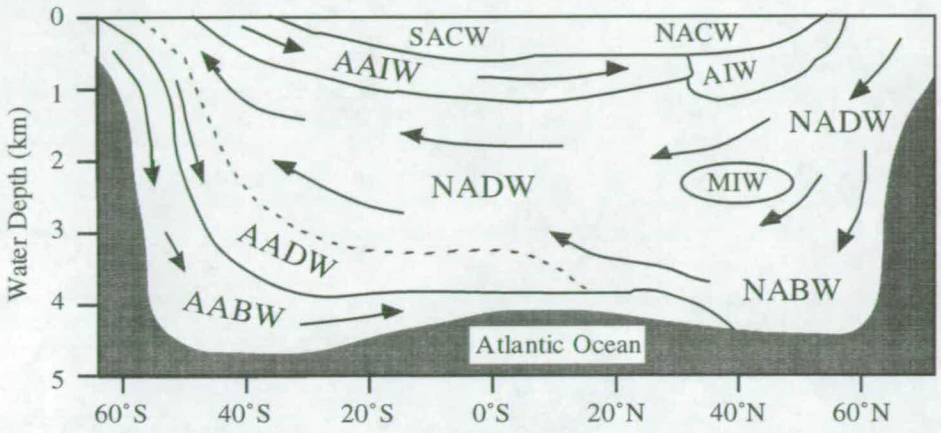

Figure 1.4. Longitudinal profile of idealised water mass structure for the Atlantic Ocean. SACW = South Atlantic Central Water; NACW = North Atlantic Central Water; AAIW = Antarctic Intermediate Water; AIW = Arctic Intermediate Water; NADW = North Atlantic Deep Water; MIW = Mediterranean Intermediate Water; AADW = Antarctic Deep Water; NABW = North Atlantic Bottom Water; AABW = Antarctic Bottom Water.

1.4.3. Global oceanography and heat flux

The global component of ocean-circulation is thought to be driven by temperature and salinity differences, thermohaline circulation, while basin-scale flow is considered to be wind-driven. Recently, authors have tried to bring these two components into a single coherent model of global ocean circulation (*Macdonald and Wunsch,* 1996). The main features of past inter-ocean thermohaline convection have involved the 'warm-route' and the 'cold-route', the possible paths needed to compensate for the rapid loss of heat in the high latitudes of the North Atlantic (*Stommel,* 1980). In the South Atlantic this has the effect of creating equatorward rather than poleward advective heat fluxes (*Baumgartner and Reichel,* 1975, Figure 1.5).

Circulation of oceanic water masses is the major driving force behind global heat and fresh water inter-oceanic transfer. Convective overturning of the world's major ocean basins links the entire ocean volume to the atmospheric and climate system at decadal to centennial time scales. Simplified schemes of inter-ocean thermohaline convection (Figure 1.6) driven by sinking of cold, saline-rich, waters in the North Atlantic the NADW.

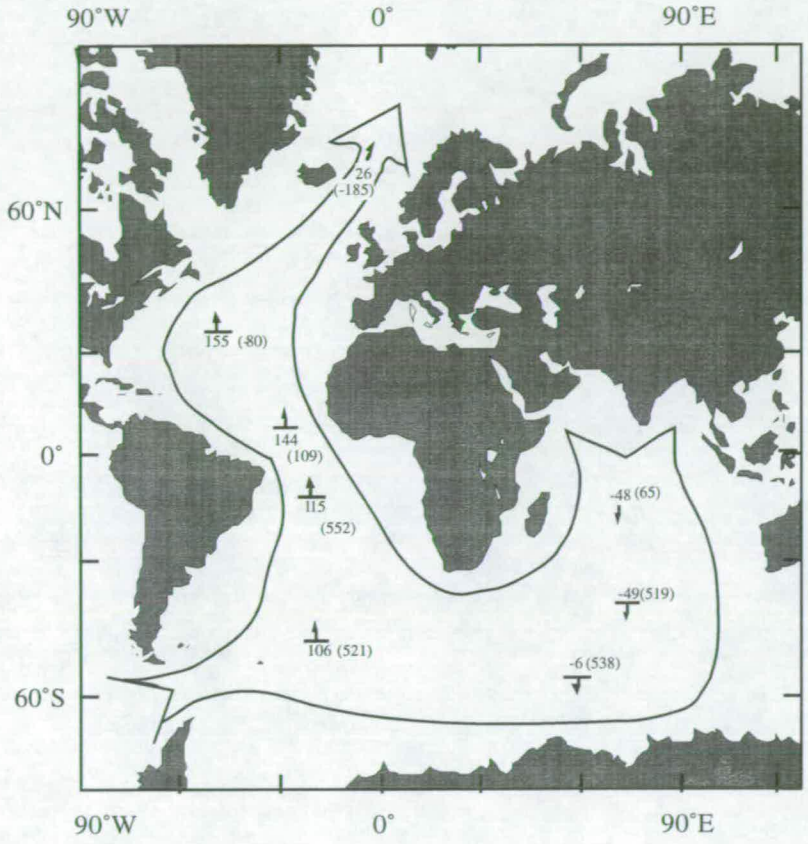

Figure 1.5. Meridional heat transport in the Indian and Atlantic Oceans. Heat flux (10^{13} W) and fresh-water flux (10^3 m^3 sec^{-1}) in brackets. Positive values indicate northward direction. Modified from *Stommel* (1980), and data from*Baumgartner & Reichel* (1975).

The NADW continues to the Southern Ocean along the sea floor, across the equator, until it is incorporated into the AACC along with similar cold, saline-rich, deep and bottom waters of the Weddell gyre region. Some of these waters upwell into the Agulhas region where they return westward into the Atlantic in the form of rings and eddies (*Winter and Martin,* 1990, *Duncombe-Rae,* 1991, *Gordon and Bosley,* 1991, *Gordon et al.,* 1992). The combined deep waters from the North Atlantic and Southern Ocean move into the Indian and Pacific basins within the AACC. Within the

Indian Ocean much of the water is returned through the Indian Ocean gyre system to the Agulhas Current. Here it's temperature and salinity are greatly increased before it re-enters the South Atlantic, the 'warm-route'.

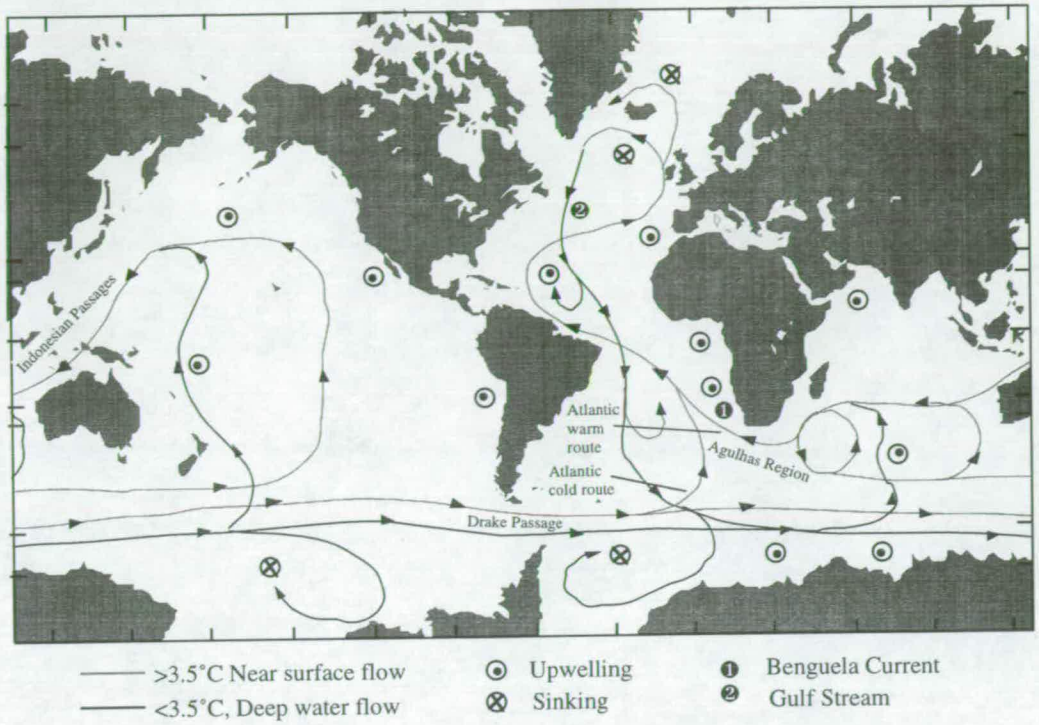

Figure 1.6. Inter-ocean thermohaline circulation (after *Gordon,* 1986, *Gordon et al.,* 1992).

Most of the controversy in global oceanic circulation relates to the origin of waters which eventually form deep water in the northern North Atlantic. Have these waters passed through the Pacific and back into the Indian Ocean, via the Indonesian Passages, before entering the South Atlantic around the southern tip of Africa (the warm-route), or have they remained cold within the AACC and circumnavigated the Southern Ocean passing back into the South Atlantic via the Drake Passage (the cold-route). *Macdonald and Wunsch* (1996) present a new model, following the work of *Stommel* (1980); *Gordon* (1986); *Rintoul* (1991); *Gordon et al.* (1992) and *Macdonald* (1993), which relates measured and modelled global oceanographic data to a complex two cell system rather than the single overall global pathway.

The first cell, acting independently, connects the sinking Atlantic waters to the Southern Ocean and AACC which carries deep waters to the Pacific and Indian oceans. From here it is mixed with intermediate waters before returning via the Drake

Passage (cold route, Figure 1.6). The second cell connects the Pacific and Indian basins via intermediate water exchange through the Indonesian Passages and waters re-enter the South Atlantic having been warmed up at the Agulhas Retroflection (warm route). Their results show that the 'warm-route' and the 'cold-route' act independently from the Pacific-Indian flow through the Indonesian Passages. The Pacific and Indian Oceans are linked to the Atlantic overturning cell via the 'warm-route' south of Africa, but the global-ocean model predicts that, within the steady-state constraints, this link is weak and intermittent. The modelled results for north of the Drake Passage signify a strong northward transfer of intermediate and surface waters originating from the Pacific Ocean. Thus, the Indonesian throughflow is not a significant part of a single global circulation model, effectively producing two cells which act almost independently of each other. Note, however, that this model deals with only two 'layers' of water column, that >3.5°C (~ upper 1000m) and that <3.5°C. Although it is important to understand the global oceanic pathways at all levels, it is particularly important to understand the fluctuations in surface water response which has the main interaction with the atmosphere and records rapid changes in climate and temperature. In this research, I am primarily investigating the fluctuations in surface waters to oceanic and global change, via the abundances of planktonic foraminifera which is discussed more fully in sections 1.5.2 and 1.5.3..

1.5. The Benguela upwelling system

1.5.1. Evolution of the Benguela Current

The Benguela Current constitutes the eastern limb of the South Atlantic anticyclonic gyre (SAAG), presently existing offshore South Africa, Namibia and Angola. The development of the Benguela Current, along with the major upwelling systems of the modern oceans, began to develop in the middle Miocene (late Tertiary, ~16 My B.P.). The following is a brief chronological description of the tectonic and hydrographic evolution of the South Atlantic Ocean.

The main steps leading towards the modern oceanographic circulation system was initiated with the rifting between Eurasia and North America in the early Cretaceous (~120 My B.P.; *Emery and Uchupi,* 1984) and the subsequent opening of the South Atlantic between 110—95 My B.P. (lower—middle Cretaceous). The rifting of the southern margins of the Atlantic is recorded by extensive black shales in the North and

South Atlantic, and evaporites in the shallow rift margin between South America and western continental Africa. By 75 My B.P. (late Cretaceous) there is evidence for the development of the Brazil, Guinea, Argentine and Cape deep-sea basins, and furthermore, the first deep cold-water inflow from the Southern Ocean. At the beginning of the Eocene global warming (55—42 My B.P.), the dominant sedimentation is pelagic, with nannoplankton (chalk) on the southwest African margin typical of marine shelf facies. With progressive rifting, passage to the North Atlantic is achieved and meridional [6] Atlantic surface and deep water flow is initiated, recorded by the first carbonate dissolution events (middle Eocene). In the early Oligocene (36—35 My. B.P.), Antarctica begins to separate from South America opening the Drake Passage, commencing thermal decoupling of high- and low-latitude surface oceans, and the onset of circumpolar circulation and thermal isolation of Antarctica. It is at this time, with the development of an east Antarctic ice sheet, that indicative high productivity sediments are recorded off southern Namibia, signifying the onset of the BCS circulation.

As stated previously, the major upwelling systems of the modern oceans began to develop in the middle Miocene (~15 My B.P.), as deep- and intermediate-water evolution led to the thermal stratification that we associate with the oceans today. This was brought about largely by the broad opening of the Drake Passage strengthening circumpolar deep water flow, further isolating the growing Antarctic ice mass. Sedimentary cores retrieved from DSDP sites 362 and 532 (*Siesser,* 1980, *Diester-Haass et al.,* 1988, *Oberhänsli,* 1991, *Diester-Haass et al.,* 1992) on the Walvis Ridge continental terrace, above the calcite compensation depth, provide a detailed history of upwelling-enhanced productivity and associated sediments since the middle Miocene (Neogene).

From the late Miocene (~ 6—3.5 My B.P.), maximum glaciation of the Antarctic continent, due to greatest isolation by circumpolar currents, produces a strong meridional temperature gradient between high southern latitudes and the tropics. Upwelling centres shifted north since the middle Miocene as the current is intensified, bringing upwelling centres to the Walvis Ridge during glacials. Prior to the late Miocene (~10 My B.P.) upwelling centres did not reach the Walvis Ridge and the associated high productivity sediments, diatoms and organic carbon, are not recorded.

---

[6] Meridional - approximately parallel to the lines of longitude running from the North to South pole. Zonal - direction perpendicular to polar meridian, parallel to equator.

In the Pliocene (~ 3.5—2 My B.P.), the Panama Strait is closed starting the modern day conveyor-like circulation. Glaciation in the northern hemisphere begins, and the continuing intensification of the Benguela Current produced an upwelling signal in both glacial- and interglacial-sediments.

The Quaternary (~1.7—0 My. B.P.) saw the onset of strong glacial to interglacial climate changes, which are of primary importance to this and other modern climate and oceanographic studies. The DSDP sites record a slight decrease in intensity of the Benguela Current during the late Quaternary as the BCS moves poleward, with intense upwelling in cold periods and less intense upwelling in warm periods. Although several authors have suggested upwelling variations to vary at Milankovitch orbital periodicities (*Diester-Haass et al.,* 1988, *Imbrie et al.,* 1989, *McIntyre et al.,* 1989, *Oberhänsli,* 1991, *Schneider et al.,* 1994), this and other recent studies suggest that upwelling is varying at much shorter time intervals (*Kennett and Venz,* 1995; *Mix and Morey,* 1997; *Little et al.,* 1997a; 1997b).

1.5.2. Regional surface oceanography

The oceanography off South Africa, Namibia and Angola is controlled by the coastal branch of the Benguela Current forming the northeastern limb of the anticyclonic gyre of the South Atlantic. In the South Atlantic Ocean the surface oceanography can be divided into two parts, the area south of the Angola-Benguela Front (ABF) and the area to the north. The hydrography of the BCS has been described in detail by a number of workers (*Shannon,* 1985, *Lutjeharms and Meeuwis,* 1987, *Lutjeharms and Stockton,* 1987, *Summerhayes et al.,* 1995b), and is summarised in Figure 1.7. The Benguela Oceanic Current (BOC) is the equatorward drift of cool surface waters flowing from 34°S (Cape Town) along southwestern Africa to 23°S (Walvis Bay) where it diverges from the coast. Inside the shelf break, along the entire coastline, a component of the BOC moves equatorwards forming the Benguela Coastal Current (BCC). The BCC continues northwards off Angola up to a maximum of 14°S (*Meeuwis and Lutjeharms,* 1990) where the line of upwelling centres terminate. The warm Angola Current (AC) forming the southeasterly limb of the South Equatorial Counter Current (SECC) flows polewards off Angola until it meets the cold BCC between 18—14°S at the ABF. This is the mixing site of warm relatively nutrient-poor waters, from the north, and colder relatively nutrient-rich waters, from the south. The front penetrates at its greatest extent 1000 km offshore, with a zone of maximum

frontal development within the first 250 km from the shore (*Meeuwis and Lutjeharms,* 1990). The front has a mean annual shift of 2—3° latitude, with a general frontal orientation NW—SE (*Meeuwis and Lutjeharms,* 1990).

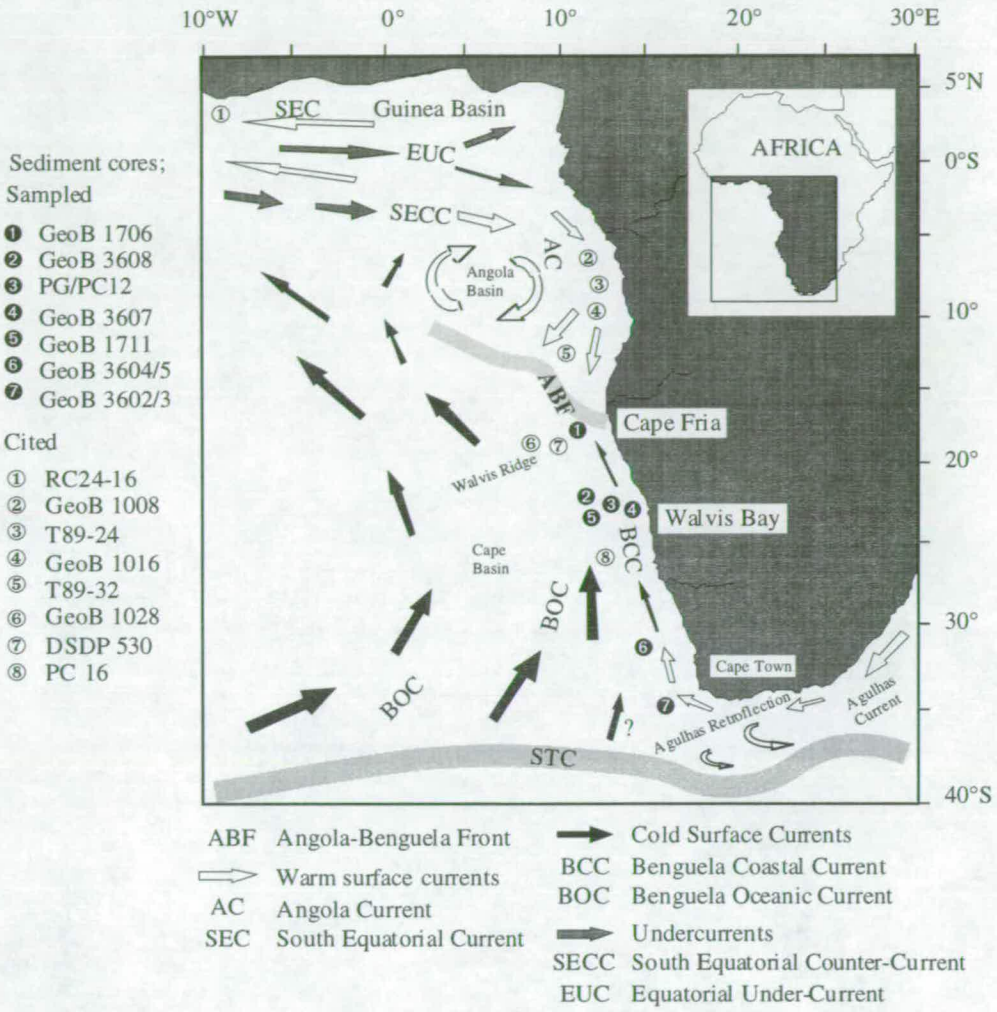

Figure 1.7. Regional surface-water circulation of western and southwestern Africa (after *Shannon,* 1985, *Lutjeharms and Meeuwis,* 1987, *Lutjeharms and Stockton,* 1987, *Meeuwis and Lutjeharms,* 1990).

In the south of the BCS a component of the warm-water Agulhas Current enters from the Indian Ocean (*Gordon,* 1986, *Gordon et al.,* 1992, *Macdonald and Wunsch,* 1996, *Schmitz,* 1996) and forms a thermal barrier, the Agulhas Retroflection. This has been observed from satellite imaging (*Duncombe-Rae,* 1991) as a series of dynamic eddies and rings from the east effectively limiting the equatorward flow of cool filaments of South Atlantic surface waters into the BOC (*Shannon et al.,* 1989).

Movement of the thermal barrier, which is controlled by the relative position and intensity of the sub-tropical convergence (STC) and the Agulhas Current, creates a variable supply of cold sub-Antarctic waters and warm Agulhas waters into the BCS. This has the effect of controlling the heat flux into the area from the south, and will be recorded in the planktonic foraminiferal record by changes in abundance of temperature-dominated species.

To the north of the ABF the BOC, SECC and AC, form the eastern South Atlantic cyclonic gyre (*Moroshkin et al.,* 1970, *Gordon and Bosley,* 1991). The BOC, which diverges from the coast at, or before, the Walvis Ridge, forms the western arm of the gyre and a component is deflected into the equatorial region (~0—5° N and S) by the south-westerly SECC, while the remaining cold-waters are transported across the equator into the southwestern North Atlantic. The eastern arm of the SAAG, transports warm, saline-poor, waters into the northerly reaches of the Cape Basin, before they too are deflected northwest from the coast. At the equator, the two major anticyclones dominating the Atlantic Ocean circulation force the surface currents from east to west (South Equatorial Current, SEC) creating major equatorial upwelling in the easterly Guinea Basin. The returning Equatorial Under-Current (EUC) balances the configuration with a component diverting into both the South and North Atlantic Oceans.

1.5.3. Local surface oceanography and modern-day upwelling

Coastal upwelling within the BCS varies with the seasonal extremes of summer and winter (*Shannon,* 1985), with water cooler than 16°C extending along the entire coast during austral [7] winter and spring. Upwelling intensity and the associated primary productivity is high all year round. However, the seasonal signal has the effect of dividing the system into a northern Benguela region (NBR) and a southern Benguela region (SBR; *Dingle,* 1995). This is seen in the modern day planktonic foraminiferal (*Giraudeau et al.,* 1993) and benthic ostracoda (*Dingle,* 1995) distributions and has been demonstrated using satellite imaging (*Lutjeharms and Meeuwis,* 1987). Seven major upwelling cells can be distinguished: at Luderitz (25°S), Namaqua (29°S), Columbine (32°S), Walvis (22°S), Namibia (19°S), Peninsula (34°S) and Kunene (17°S), in order of decreasing intensity (Figure 1.8). A strong correlation was found

[7] austral - southern hemisphere; boreal - northern hemisphere.

between strength of offshore winds and level of upwelling intensity (*Lutjeharms and Meeuwis,* 1987).

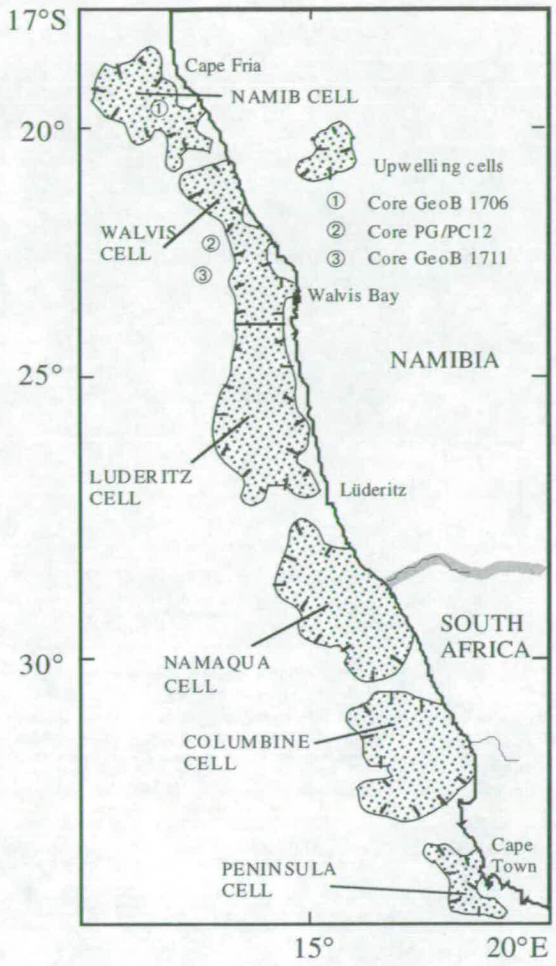

Figure 1.8. Upwelling cells of the Benguela system over the continental margin of southwestern Africa (after *Dingle*, 1995).

The boundary between the NBR and the SBR is the site of maximum upwelling intensity at 26—27°S (Luderitz), which has the coldest and the most persistent upwelling. The NBR is predominantly a winter phenomenon, but is typified by year round, permanent, high productivity and enhanced accumulation of phytoplankton (*Brown et al.,* 1991). Wind speeds are of medium intensity with a wide, oceanic, filamentous, mixing domain (*Lutjeharms and Stockton,* 1987). Surface sediments are rich in organic matter with a maximum in the nearshore diatom belt (*Bremner,* 1983, *Rogers and Bremner,* 1991). In the Recent setting the NBR has the lowest dissolved oxygen, related to a poor oxygen source in the Angola Basin, and highest marine

organic carbon levels and SSTs (*Dingle,* 1995). *Boyd et al.* (1987) found late summer intrusion of surface and sub-surface warm Angolan water down to Walvis Bay to be a common feature of late austral summer and early autumn.

In contrast, the SBR has a highly seasonal upwelling situation with its maximum in summer, and a restricted mixing domain (*Lutjeharms and Meeuwis,* 1987, *Giraudeau and Rogers,* 1994). Offshore there is a strong thermal front between the cold, dense, upwelled waters and the displaced, oligotrophic, tropical waters. Associated with the variable upwelling intensity there is a highly seasonal variability in nutrient supply, and average chlorophyll *a* is relatively low compared to the NBR (*Giraudeau,* 1993). In the recent sediments the SBR has the highest dissolved oxygen levels which supports a large benthic ostracod population (*Dingle,* 1995).

1.5.4. Late Quaternary upwelling record

The most extensive review of the Quaternary upwelling history and variability offshore Namibia was by *Summerhayes et al.* (1995b). Using geochemical and micropalaeontological analyses of a piston core (PG/PC12) from the slope off Walvis Bay, they discussed upwelling dynamics in the BCS during the last 70 kyr. The most productive time interval, derived from organic carbon data, was during glacial stages 4—2, peaking in isotope stage 3, and coinciding with the coldest sea surface temperatures (SSTs) from alkenone data. Upwelling and organic matter flux was found to increase in stage 4 and 3, but decline into stage 2, the last glacial maximum (LGM). This was attributed to a northward shift of the trade winds in stage 2, leading to a marked decrease in upwelling at site PG/PC12. The primary control on the system is believed to be the precessionally controlled position of the SAAG and corresponding variations in the upwelling favourable trade winds. Aside from this primary control on productivity, they also suggest variations in the supply of nutrients into the system via sub-surface waters which sink at the STC, and continued clockwise around the South Atlantic with the EUC and through the Angola Basin to Namibia.

Jansen et al. (1997) used planktonic foraminifera from three cores on the Angola-Zaire margin to reconstruct palaeopositions of the ABF for the last 180 kyr. Using a relatively low resolution record compared to this study, they suggest that the extreme shifts of the BCS can be described by the 100 kyr (eccentricity) period and the

meridional shifts by the 23 kyr (precession) component of the Earth's orbital parameters. *Jansen et al.* (1997) show strong northward shifts in stages 4 and 3.3—3.1, while the southernmost positions (similar to the present situation) were occupied in stages 6.3, 5.5 and stage 1. Similar to *Summerhayes et al.* (1995b), they associate the shifting of the ABF and accompanying upwelling cells to displacements and relative intensity of the SAAG and corresponding southeast trade winds.

Using alkenone-derived SSTs calculated from cores on the Angola Margin, the Walvis Ridge, the Congo Fan and the equatorial Atlantic, *Schneider et al.* (1995; 1997) found that the records closely matched each other indicating that the ABF has not shifted substantially in the last 200 kyr (*Schneider et al.,* 1995), and has remained between 12° and 20°S. The precedence of SST changes at the Walvis Ridge as well as in the equatorial Atlantic, with respect to the Angola and Cape Basins, suggests that south of the ABF variations in the zonality of trade winds are superimposed on changes in heat advection (from the Benguela). Thus, they suggest that the predominant precessional cycle observed, results from differential variations in trade wind forcing between both areas. During periods of increased trade wind zonality, it is likely that the BOC diverted more to the northwest before it crossed the Walvis Ridge (after *Jansen et al.,* 1984, *Jansen and van Iperen,* 1990), which would result in an increase in offshore transport of cold-water upwelling filaments south of the ABF and an increase in equatorial upwelling. The Angola Basin would then have received lesser amounts of cold, southern BOC as it is deflected offshore.

Schneider et al. (1995) conclude that the trade wind forced cycle observed in the ΔSST_{ABF} record [8], is a low-latitude phenomenon overprinting the trade wind signal as a result of monsoonal circulation changes over the east equatorial South Atlantic induced by boreal summer insolation over Africa. In contrast to the northern hemisphere, where trade wind forcing is controlled by the 41 and 100 kyr periodicities, eastern South Atlantic surface oceanography is additionally sensitive to low-latitude 23 kyr insolation changes in the northern hemisphere.

Schneider et al. (1997) compare organic carbon measurements with previously calculated SSTs, to understand the variation in palaeoproductivity. Total organic carbon (TOC) results, support the hypothesis of precessional sensitivity of sediments

[8] ΔSST_{ABF} = SST difference across the ABF calculated by subtracting the interpolated SST value of core GeoB 1028-5 (Walvis Ridge) from the corresponding values of core GeoB 1016-3 (Angola Basin).

in the equatorial South Atlantic as suggested previously by *Lyle* (1988), *McIntyre et al.* (1989) and *Molfino and McIntyre* (1990). Following *Imbrie et al.* (1989), *Schneider et al.* (1995) argue for trade wind forcing of coastal and equatorial upwelling, but also argue for an additional component of cold-water advected from the BCS.

1.6. Distribution of surface sediments

Sediments underlying upwelled water masses may reflect characteristic differences between those from the same latitudes that have no upwelling influence. However, these characteristics are only reflected in the sediments if the upwelling is prolonged for sufficient amounts of geological time. For example, in the southwest African upwelling region current sedimentation rates vary between 30 and 120 cm/1000 years in the inner diatom mud belt (*Calvert and Price,* 1983), but reduce to rates in the order of 5 cm/1000 years in the foraminiferal dominated slope facies [9], large enough for the history of upwelling to be recorded.

The modern sediments accumulating on the Namibian shelf are composed predominantly of biogenic material: organic matter, diatomaceous silica and calcium carbonate. The biogenics are split into three zones parallel to the coast, Figure 1.9, (*Bremner,* 1983, *Calvert and Price,* 1983). Nearest the shore is a diatomaceous, black mud belt, with waters at the surface sediment interface almost completely anoxic. Further away is the middle shelf dominated by faecal pellets and separated from the diatom belt by a zone of coarse sediment centred at about 150 m. On the slope at about 1000m is a carbonate-rich band, dominated by foraminifera, coccoliths and ostracodes (*Giraudeau,* 1992; 1993; *Giraudeau and Rogers,* 1994; *Dingle,* 1995). Terrigenous material is not abundant, although it can be blown in by easterly, offshore winds, or supplied by coastal rivers. It is thought that ever since the initiation of upwelling off southwest Africa since the early Miocene, these three belts have existed spatially similar to the modern situation.

Surface sediments do not reflect the contemporaneous hydrologic conditions like plankton, nor an annually averaged record like benthos, but instead reflect hydrologic

[9] Within the cores analysed, average sedimentation rates in the cores collected from a 2000 m water depth are 8—11 cm/1000 years consisting almost entirely of planktonic foraminifera without terrestrial influence. Values are not adjusted for compaction or dissolution. *Meyer* (1973) observed maximum sedimentation rates of 150 cm/1000 yrs in the small shelf basins.

changes on a decadal to centennial time scale. The major- and minor-element geochemistry of the surface sediments reflects the complex mixture of terrigenous, biogenic, and authigenic sedimentary components, and can be used to assess the extent of secondary diagenetic or geochemical enrichment. It can also be used to assess changes in local oceanography, and nutricline and/or thermocline structure, and their correlation to the dominant biogenic signatures.

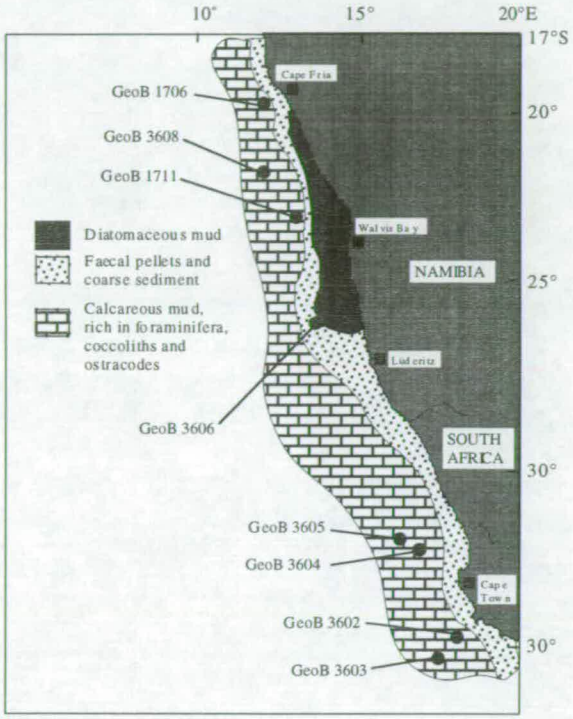

Figure 1.9. Generalised distribution of biogenic surface sediments (after *Bremner,* 1983, *Calvert and Price,* 1983, *Giraudeau,* 1992, 1993).

The use of minor element geochemistry has varied in its success in differing marine settings. Previous authors have used the fluctuation of major- and minor-elements to discuss changes in palaeoproductivity (*Müller and Suess,* 1979, *Müller et al.,* 1983, *Zahn et al.,* 1986, *Sarnthein et al.,* 1987, *Boyle,* 1988, *Berger et al.,* 1989), upwelling (*Siesser,* 1980, *Meyers,* 1992), anoxia (*Schlanger and Jenkyns,* 1976, *Emerson and Bender,* 1981), wind strength (*Boyle,* 1983, *Shimmield et al.,* 1990, *Weedon and Shimmield,* 1991), continental aridity (*Nair et al.,* 1989, *Sirocko and Sarnthein,* 1989, *Matthewson et al.,* 1995), weathering source (*Schneider et al.,* in press), diagenesis (*Bishop,* 1988, *von Breymann et al.,* 1992), and river discharge (*Schneider et al.,* 1994).

Diester-Haass (1978) provides a good review of indicative geochemistry and sedimentation within upwelling areas, and the BCS in particular. The main characteristics of the surface water masses of recent upwelling regions are: lowered temperatures, increased dissolved oxygen, high nutrient contents and thus increased productivity. Of which two of these characteristics, lowered temperatures and increased biological production, are important for geological observations as they may describe differences between sediments from cores at the same latitude with, and without, upwelling influence; for example, sediments beneath high productivity, and therefore generally anoxic [10] shelf and slope upwelling settings, have been found to be finely laminated and rich in organic carbon (*Yeats and Haq,* 1981, *Hay and Sibuet,* 1984, *Ruddiman and Sarnthein,* 1989, *Suess and von Huene,* 1990).

In the BCS five components are responsible for most of the variability in sediment composition (*Calvert and Price,* 1983): calcium carbonate, organic matter and biogenic opaline silica, terrigenous debris, phosphorite, and glauconite. Barium, considered by many to be important in the study of palaeoproductivity, is distributed with iodine independently of the these components.

The most widely used geochemical indicators of past productivity are total organic carbon [11] (TOC) and biogenic opaline silica (opal) as these are thought to be strongly related to the amount of excess organic carbon produced in productivity events, such as upwelling (*Müller and Suess,* 1979, *Dymond,* 1981, *Bishop,* 1988). Intense upwelling injects both cold-water and nutrients into the surface waters, and thus organic carbon burial is related to the subsequent changes in export productivity associated with nutrient input. These productivity/upwelling events should be accompanied by decreased SSTs at times of high organic carbon burial, characterising them apart from lateral cold-water advection (*Lyle et al.,* 1992).

Organic carbon is found at its maximum (15% TOC; *Calvert and Price,* 1983, *Rogers and Bremner,* 1991) in the narrow belt of anoxic diatom ooze (max 88% opal; *Bremner,* 1983), particularly predominant in the shallow waters of Walvis Bay. Organic carbon concentrations in the sediment reflect the TOC received on the sea

---

[10] If bottom waters lack oxygen or if H_2S is present from high amounts of organic matter, oxygen is removed through oxidation of organic matter leaving a thick sediment-water interface oxygen-poor or anoxic.

[11] Often referred to in other texts as C_{org}, with C_{Morg} as marine-derived organic carbon.

floor. Of special interest to palaeoproductivity estimates, TOC records the fluctuation of normal marine productivity and the episodes of enhanced productivity, but also records the added material from a terrigenous source diluting the signal. For any productivity assessment the terrigenous component must be quantified, often requiring correlation with other proxies (e.g. C/N ratio, *Müller et al.,* 1983; Barite, *Shimmield,* 1992; Uranium, *Shimmield and Pederson,* 1990; Zr/Al, *Matthewson et al.,* 1995). Surface water productivity records inferred from TOC must take into consideration other factors; dilution by terrigenous and carbonate material, sediment re-distribution, and type and extent of organic preservation and re-mineralization. However, recent work in the east-equatorial Atlantic has favoured changes in productivity over all other variables (*Lyle,* 1988, *Sarnthein et al.,* 1988, *Schneider,* 1991, *Struck et al.,* 1993, *Müller et al.,* 1994, *Schneider et al.,* 1997).

Of the TOC produced in the marine environment, including addition from a terrigenous source, only a very small proportion (~2%) reaches the geological record, so the signal is already subject to bias. Only very large shifts in the TOC production will be recorded, for example at times of intense productivity, or shedding from the innermost organic rich diatom mud belt where TOC is in excess of 10%, rather than 1—5% on the mid-upper slope facies. Plumes, filaments and eddies in the diffuse mixing zone of the NBR could transport material through the shelf break front onto the continental slope (*Lutjeharms and Stockton,* 1987, *Shillington,* 1992, *Waldron and Probyn,* 1992, *Waldron et al.,* 1992). *Shillington* (1992), however, suggests that these processes do not represent a large scale loss of productive coastal water to the open sea and are probably only a minor influence of TOC re-distribution and dilution. *Summerhayes et al.* (1995b) showed enrichment of organic matter at site PG/PC12 on the continental slope off Namibia to respond to changes in upwelling intensity and to a lesser extent mixing processes taking place in the shelf edge upwelling system. Both processes can be linked with seaward advection of coastal nutrient-rich upwelled water enhancing production at the shelf edge. Comparison with the SEEP experiment (*Biscaye et al.,* 1988), where only 20% of the organic flux reaching the slope is exported from the shelf, it is thought the rest represents in-situ production related to prolonged coastal upwelling.

1.7. Summary

The Benguela Current system is the site of exceptionally high productivity and intense upwelling, recording amplified signals of climate and ocean change since its evolution in the early Oligocene. The surface sediments covering the continental shelf and slope are characteristic of high productivity coastal upwelling margins dominated by diatoms and planktonic foraminifera in the overlying waters. High organic carbon contents record the fluctuation of palaeoproductivity with time, and allow the variation of productivity changes to be assessed. The hydrography of the Benguela Current system has been researched in detail, but the variation of the currents and water masses with time is still not fully understood. Movement of the Angola-Benguela Front, to the north of the Walvis Ridge, has been the subject of recent research, and is suggested to move with variations in the trade wind/monsoon system. Variations in upwelling dynamics are similarly suggested to vary with trade wind intensity, but also with the hypothesised advection of cool waters from the Southern Ocean. The main objective of this research, is to assess the variation of planktonic foraminifera to determine the nature and timing of changes in the palaeoceanography of the Benguela Current system. Four high resolution foraminiferal records are assessed to investigate the principal causes of faunal change in the BCS, and to quantify the relative influence from cold-water advection, upwelling and trade wind modulation.

Oxygen and carbon isotope chronostratigraphy

Ch.2.

Chapter 2. Oxygen and carbon isotope chronostratigraphy

2.1. Stable isotope theory and analysis

For any meaningful interpretation of palaeoceanography or palaeoclimatology, it is necessary to build a chronostratigraphic framework for the sediment cores under investigation. Stable oxygen isotope analysis is the most widely used method for chronostratigraphy, and is based on the ratio of oxygen's two isotopes ^{16}O and ^{18}O, expressed as $^{18}O/^{16}O$. This ratio is found to fluctuate through time in all of the world's oceans with a characteristic signature which is used for dating and core correlation (*Emiliani,* 1955, *Shackleton and Opdyke,* 1973, *Imbrie et al.,* 1984, *Prell et al.,* 1986, *Martinson et al.,* 1987), Figure 2.1.

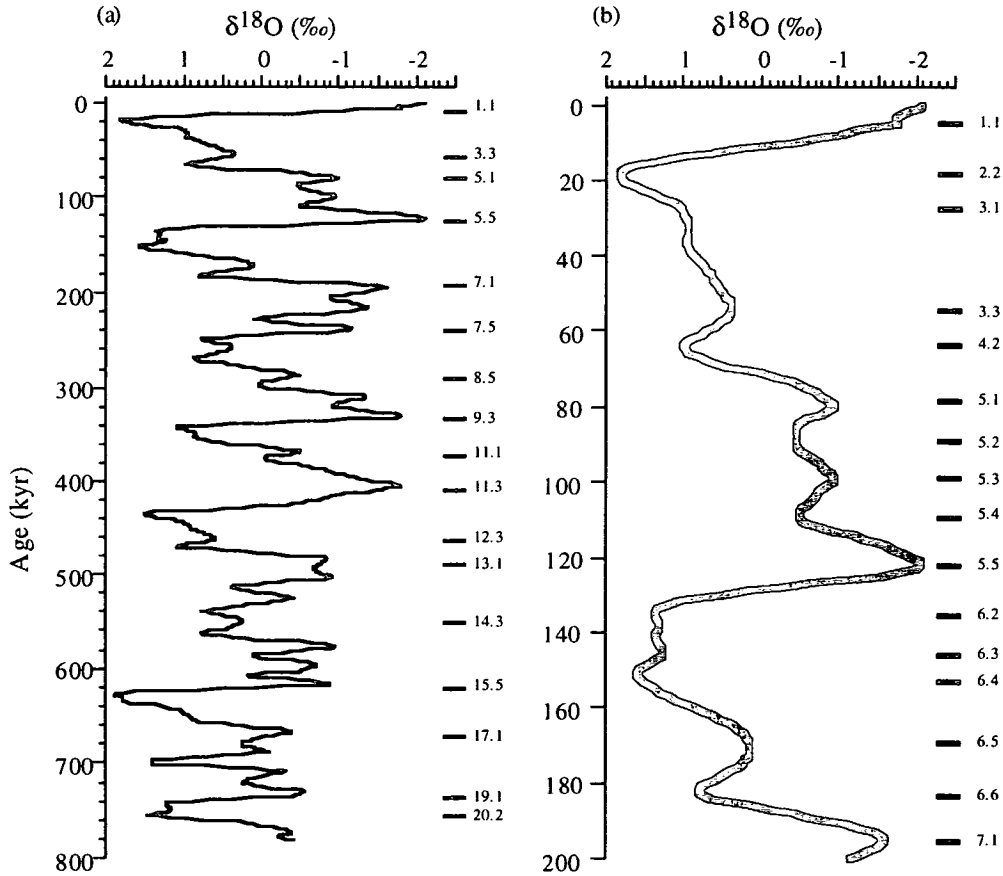

Figure 2.1. Standard SPECMAP stacked oxygen isotope curve, after (*Imbrie et al.,* 1984, *Prell et al.,* 1986); (a) Complete isotope record for the last 800 kyr, (b) Detailed analysis of the last 200 kyr.

Emiliani (1955) established the first oxygen isotope stratigraphy using isotopes extracted from the tests of foraminifera from a low latitude marine core. Foraminifera secrete a calcareous test in approximate equilibrium with the water mass they inhabit and thus preserve the oxygen and carbon isotopic record at the time of precipitation, although slight variations with changing species have been documented (see *Patience and Kroon,* 1991 for discussion). As the pelagic rain falls to the sea floor over time, a chronologic record of oxygen and carbon fluctuations is established and preserved. The usual interpretation of variation in the $^{18}O/^{16}O$ ratio is linked directly with changes in the global hydrological cycle. The following is a brief summary of this system.

The oxygen isotopic composition of the global oceans is dominantly controlled by low latitude evaporation and high latitude precipitation. In the process of evaporation, the lighter isotope, ^{16}O, is preferentially removed from the oceans and transported to the polar continents. Moving from low to high latitudes, atmospheric oxygen is enhanced in the lighter ^{16}O, and loses the heavy ^{18}O. Polar ice caps thus become relatively enriched in the light isotope, ^{16}O, whilst the oceans become enriched in ^{18}O. During a glacial period when polar ice caps expand, more ^{16}O is removed from the ocean system and thus foraminifera record a value with a relatively heavy $^{18}O/^{16}O$ ratio, and the trapped ice records a negative ratio. Inversely, foraminifera that have lived in an interglacial period, when polar ice caps have reduced in size and released ^{16}O back into the hydrological cycle, will record relatively light $^{18}O/^{16}O$ ratios, and ice caps will record relatively heavy ratios.

For calibration, the $^{18}O/^{16}O$ ratios are compared to a standard (PDB, Pee Dee Belemnite [1]), and then expressed as a deviation of ^{18}O in parts per thousand (‰) from this standard value (*Shackleton and Opdyke*, 1973), $\delta^{18}O$.

$$\delta^{18}O = \left[\frac{^{18}O/^{16}O_{sample}}{^{18}O/^{16}O_{reference}} - 1 \right] \times 1,000 \ (‰)$$

[1] PDB standard was obtained from carbonate from the belemnite *Belemnitella americana* from the upper Cretaceous Pee Dee Fm. from South Carolina (*Epstein and Urey,* 1951).

2.2 Radiocarbon dating

The influence of continuous high energy cosmic radiation and neutron collision in the upper atmosphere results in the production of carbon nuclei, of which the radiocarbon isotope, carbon-14 (^{14}C), forms only a small component of the total carbon produced (1 part in 10^{10} per cent of total carbon). As ^{14}C is radioactive there is a continual decay of ^{14}C to form the stable element ^{14}N via beta transformation (*Libby*, 1955). ^{14}C atoms are rapidly oxidised to carbon dioxide and, along with other molecules of $^{12}CO_2$, become mixed throughout the atmosphere and absorbed by the oceans and living organisms. It was initially assumed that (1) the production rate of ^{14}C was constant, and thus the atmospheric content of ^{14}C is also constant, and (2) that the ^{14}C:^{12}C ratio in the biosphere and hydrosphere is in equilibrium with the atmospheric ratio; although both of these assumptions has come under scrutiny in recent years. All living matter loses ^{14}C at the same rate at which they absorb it, broadly in equilibrium with atmospheric CO_2. Once the organism ceases to exist, exchange with the atmosphere cannot take place (closed system) and the amount of ^{14}C trapped in the organism will naturally decay. The rate of decay follows a negative exponential curve (half-life of radiocarbon used is 5568 years $\pm$ 30), and thus the date of death can be calculated from the measured residual ^{14}C activity. The point at which the amount of remaining ^{14}C falls below the limit of measurement provides the upper most limit of dating to be about 50,000 years, although at this extreme the measurement is subject to a large degree of error. Radiocarbon dating is used here to provide extra chronological control particularly during oxygen isotope stage 3 where correlation with other marine records is difficult with stable oxygen isotope stratigraphy alone.

2.2.1. Sources of error in ^{14}C dating

Discrepancies between calendar and radiocarbon ages determined from wood samples first suggested that the assumption of a constant ^{14}C production rate with time was inaccurate (*de Vries*, 1958), and has been subsequently confirmed using dendrochronology (*Suess*, 1970; *Stuiver et al.*, 1991; *Pearson et al.*, 1986), varved sediments (*Stuiver,* 1970), and U-Th (*Stuiver,* 1978; *Bard et al.,* 1990a; 1990b) dating of corals. The existence of ^{14}C plateaux's, that is a period of constant ^{14}C age, at around 12.7, 10 and 9.5 ka are thought to reflect changes in ^{14}C atmospheric reservoir previously not considered (see *Ammann and Lotter*, 1989).

On a longer time scale, direct comparison between AMS determination of ^{14}C and U-Th on fossil corals suggests that radiocarbon underestimates the true age by as much as 2.5 kyr at 16 ka BP, and 3.5 kyr at 20 ka BP (*Bard et al.,* 1990b; 1993). These results are explained mainly as the consequences of changes in the cosmogenic nuclide production linked to the gradual decrease of the Earth's magnetic field; and smaller effects from changes in the global carbon cycle linked to thermohaline convection and deep water production (see *Bard et al.,* 1990b; and 1993 for discussion). The divergence between ^{14}C age determinations and those obtained by other dating methods has been reconciled by the use of a conversion of ^{14}C years into a calendar age framework, and expressed as calendar years (*Bard et al.,* 1993), see section 2.3.2. and footnote [3].

A second important source of error occurs as a result of the slow mixing rate of surface and deep waters. Because ^{14}C is transferred from the atmosphere to the oceans only across the surface, and the mixing is slow, ^{14}C in deep ocean waters decays without replenishment and thus has an apparent age which differs from the surface waters. Hence a correction factor is therefore applied to marine-derived ^{14}C ages e.g. foraminifera, but this itself is subject to variation. In the surface waters of the North Atlantic this is around +400 years (*Bard et al.,* 1988), while in parts of the equatorial East Pacific the figure is +580 years (*Shackleton et al.,* 1988). Upwelling adds a further dimension to the problem as it brings 'older' water to the surface ocean and affects the apparent age of the surface waters. The results presented here use a constant reservoir correction factor of +400 years, as is used in the North Atlantic.

2.3. Materials and methods

2.3.1. Oxygen and carbon stable isotope analysis

For a high resolution analysis, samples were taken at 5cm intervals along the GeoB cores, and 10cm intervals along PG/PC12, allowing geochemical, micropalaeontological and stable isotopic analysis to be carried out at average sample intervals of about 650 years. For the GeoB cores, tests of *Globorotalia inflata* d'Orbigny and *Cibicidoides wuellerstorfi* Schwager (GeoB 1711 only) were hand-picked under a binocular microscope from the 250—500μm fraction to achieve an analytical weight between 0.05 and 0.10mg, composed of between 8—10 well-preserved and clean *Gr. inflata* specimens, and 2—4 *C. wuellerstorfi* specimens. For

core PG/PC12 oxygen and carbon stable isotope analysis was carried out using *N. pachyderma* specimens. Stable oxygen and carbon isotope analysis was conducted on a Finnigan MAT 251 mass spectrometer using a KIEL automated sampling device [2]. The tests of the foraminifera were reacted with concentrated orthophosphoric acid at 75°C. Calibration is through secondary standards calibrated via NBS 18, 19 and 20, data are normalised to the PDB scale with te defined value of NBS 20 of -4.14 and -1.06 ‰ for oxygen and carbon, respectively. Analytical precision for oxygen and carbon isotope analyses was ± 0.07‰ and ± 0.03‰ (1-sigma), respectively.

2.3.2. Radiocarbon dating

Detailed inter-core correlation was possible using measured radiocarbon ages from the upper parts of the southern Cape Basin cores. Radiocarbon ages were measured on foraminifera extracted from selected samples to provide information particularly in oxyegn isotope stage 3 where the isotope correlation was proving difficult. Radiocarbon dates for PG/PC12 were provided from *Summerhayes et al.* (1995) while new dates were measured for GeoB 1706 and GeoB 1711. Carbon dioxide generated from the samples by acid hydrolysis was reacted to graphite using Fe/H_2 catalytic reduction at the Fachbereich Geowissenschaften, Bremen, Germany. Graphite was pressed into targets which were analysed along with standards and process blanks on an accelerator mass spectrometer (AMS) at the Leibniz-Labor AMS facility, Christian-Albrechts-University, Kiel, Germany, following the procedures described in *Nadeau et al.* (1997). Analytical radiocarbon ages were calculated using 5568 years as the half-life of radiocarbon. The analytical ^{14}C ages obtained must be corrected for the age difference between atmosphere and the surface ocean. For the low-latitude range the reservoir age is generally 400 years and is not likely to have changed by more than 100—200 years during the late Pleistocene (*Bard,* 1988; *Bard et al.,* 1990b). We have corrected the analytical data ages for reservoir effect by + 400 years, and further calculated radiocarbon ages to calendar years according to *Bard et al.* (1990a, b) and *Bard et al.* (1993) [3].

---

[2] GeoB sampling and analysis was carried out at the Fachbereich Geowissenshaften, University of Bremen, Germany; PG/PC12 sampling and analysis was carried out on a VG Isotech PRISM isotope ratio mass spectrometer, at the Isotope Research Unit, East Kilbride, Scotland.

[3] < 18,000 ^{14}C years BP: "True age" = (1.24 x ^{14}C age) - 840 [yrs BP]
> 18,000 years BP: "True age" = [-5.85×10^{-6} x (^{14}C age)^2] + (1.39 x ^{14}C age) - 1807 [yrs BP]

2.4. Chronostratigraphy of the $\delta^{18}O$ records from the southeastern African continental slope

2.4.1. GeoB 1706 and GeoB 1711

The oxygen and carbon isotope stratigraphies for GeoB 1706 and GeoB 1711, are shown in Figures 2.2 and 2.3, and stable isotope age control points are given in Table 2.1. A benthic isotope record for GeoB 1711 (Figure 2.2) aided the chronostratigraphy of the planktonic foraminiferal-derived $\delta^{18}O$ records for GeoB 1706 and GeoB 1711. Five radiocarbon dates were measured for the upper 45 kyr in GeoB 1706, and together with a further five oxygen isotope control points allowed the core to be dated at regular intervals over the last 160 kyr.

GeoB 1706			GeoB 1711		
Depth (m)	Age (kyr)	Events	Depth (m)	Age (kyr)	Events
0.03	0	Core top	0	0	Core top
0.23	8.05	AMS	1.16	14.48	AMS
0.58	12.21	AMS	1.91	20.01	AMS
1.78	26.95	AMS	2.51	21.80	AMS
2.33	38.77	AMS	3.41	39.70	AMS
3.48	44.37	AMS	4.01	44.37	[a]AMS
6.93	71	5.0	4.61	53	3.3
8.38	87	5.2	5.56	65	4.2
8.43	87.6	Hiatus end	6.86	80	5.1
8.48	126.5	Hiatus start	7.46	87	5.2
8.73	128	6.0	8.21	99	5.3
9.93	135	6.2	9.01	111	5.4
10.68	151	6.4	9.81	123	5.5
			10.71	136	6.2

Table 2.1. Isotope control points for GeoB 1706 and GeoB 1711. Age picks for GeoB 1711 were allocated using the benthic foraminiferal record of *C. wuellerstorfi*. The hiatus in GeoB 1706 was best-fitted between the samples at 8.48m and 8.43m. Control points are from Imbrie *et al.* (1984). [a]AMS = ^{14}C age applied from GeoB 1706 after correlation of $\delta^{13}C$ records and later confirmation from planktonic foraminiferal abundance records.

The planktonic foraminiferal record for GeoB 1711 utilises four radiocarbon dates and a further age control point correlated from the oldest AMS ^{14}C age from GeoB 1706 (44 ka). This was deemed reasonable from direct correlation with the planktonic $\delta^{13}C$ records and later from planktonic foraminiferal abundance records. Older than early

stage 3, the benthic foraminiferal record for GeoB 1711 is correlated to the SPECMAP standard eight times to encompass the last 140 kyr. Correlation between the planktonic foraminiferal isotope records revealed a period of non-deposition at site GeoB 1706 during isotope sub-stages 5.5—5.2.

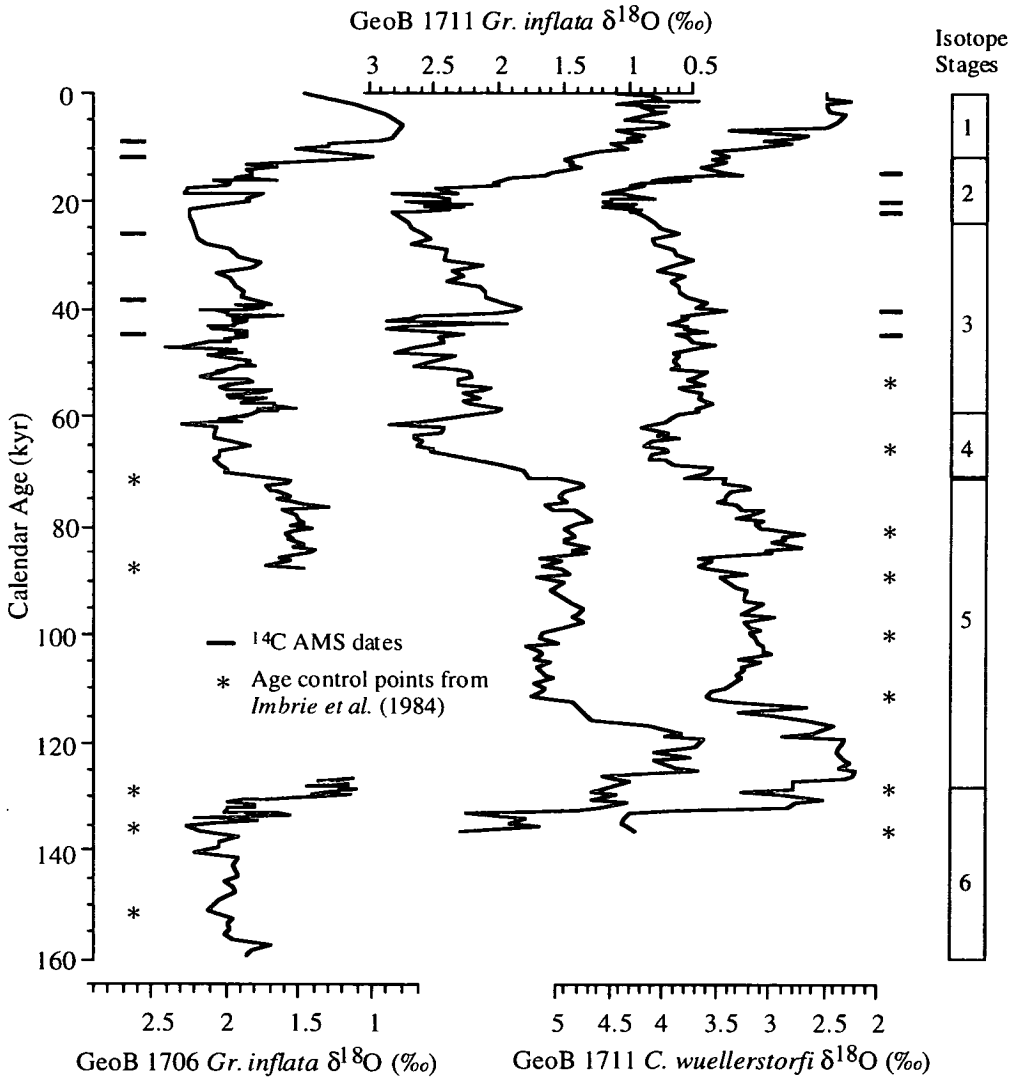

Figure 2.2. Oxygen isotope calendar age profiles for GeoB 1706 (planktonic record) and GeoB 1711 (planktonic and benthic records). The AMS dates and age control-points for each core are given, to the left for GeoB 1706 and to the right for GeoB 1711 (for GeoB 1711 these are derived from the benthic foraminiferal stratigraphy of *Cibicidoides wuellerstorfi*). The same stratigraphy is applied to the carbon isotope profiles (Figure 2.3).

The GeoB 1706 isotope records illustrate the missing heavy values of $\delta^{13}C$ in isotope sub-stage 5.3 (99 ka; Figure 2.3), and the missing light isotopic values of $\delta^{18}O$ in

isotopic sub-stage 5.5 (122 ka; Figure 2.2) . In all isotope records from the Angola and Cape Basins, and the continental slope off southwest Africa and equatorial west Africa (*Schneider,* 1991, *Schneider et al.,* 1997), isotope sub-stage 5.5 oxygen-isotope values reach Holocene $\delta^{18}O$ minima. The $\delta^{18}O$ values for GeoB 1706 in isotopic stage 5 are higher than the Holocene values.

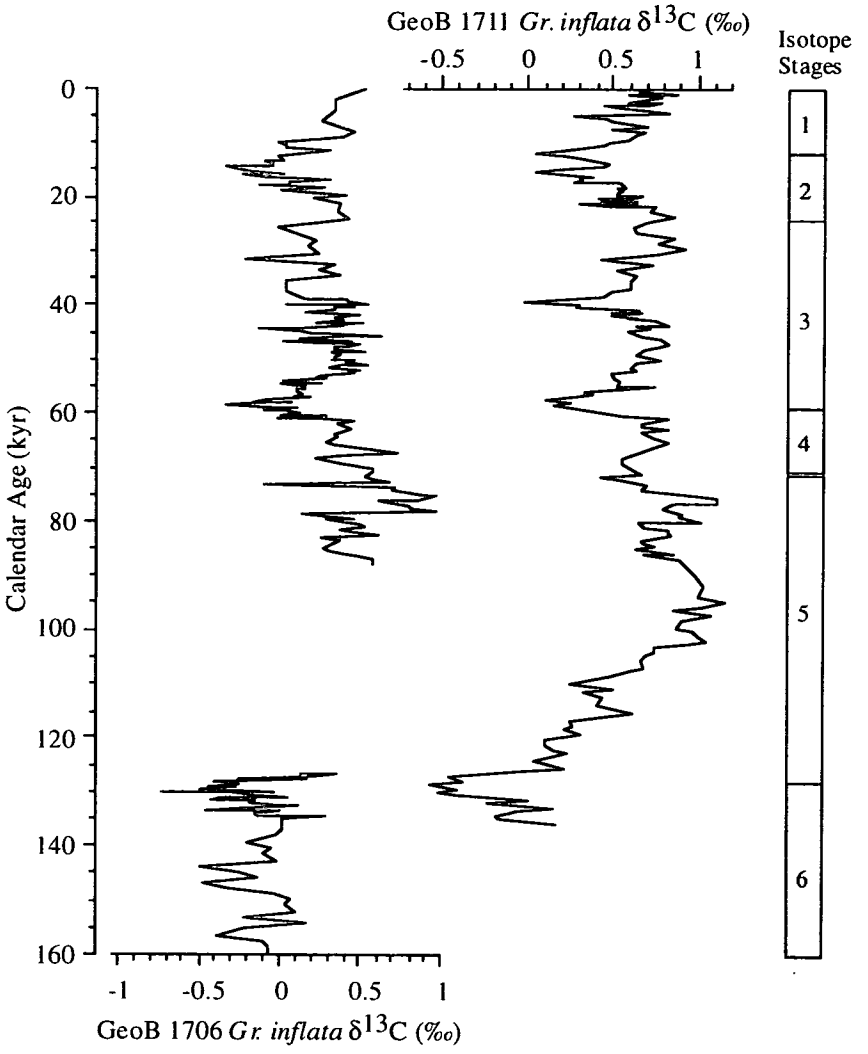

Figure 2.3. Carbon isotope stratigraphy for GeoB 1706 and GeoB 1711 with respect to calendar age. The excellent correlation of the two $\delta^{13}C$ records versus age clarifies the positioning of the hiatus boundaries in the interval of sub-stages 5.5—5.2. Together, the oxygen and carbon isotope records highlight the absence of sub-stages 5.5 (122ka)—5.3 (99ka), with the missing excursion to positive $\delta^{13}C$ values (sub-stage 5.3) in GeoB 1711 and the missing excursion to Holocene, or lower, $\delta^{18}O$ values (sub-stage 5.5) in GeoB 1706. Age control-points are given in Table 2.1 and AMS dates in Table 2.2).

Detailed examination of oxygen and carbon isotope signatures allowed the margins of the hiatus to be best-fitted for 848 cm and 843 cm in GeoB 1706, matching 126.5 kyr and 87.6 kyr, respectively, in GeoB 1711 (*Little et al.*, 1997a). Figure 2.3 shows the

Core	Depth (m)[a]	Analytical Age [b] (kyr)	Error +/- (yrs)	Calendar Age[c] (kyr)	Error +/- (yrs)
PG/PC12[d]	0.10	5.99	75	6.09	93
PG/PC12[d]	0.45	7.88	40	8.44	49
PG/PC12[d]	0.75	10.50	55	11.69	68
PG/PC12[d]	1.13	14.10	55	16.15	67
PG/PC12[e]	1.42	16.85	80	19.49	95
PG/PC12[e]	1.67	19.25	85	22.33	101
PG/PC12[e]	2.17	23.80	120	27.54	134
PG/PC12[e]	2.67	28.50	190	32.68	202
GeoB 1706[f]	0.23	7.49	50	7.95	62
GeoB 1706[f]	0.58	10.85	70	12.11	87
GeoB 1706[f]	1.78	23.23	250	26.9	284
GeoB 1706[f]	2.33	34.42	810	38.77	802
GeoB 1706[f]	3.48	40.28	1700	44.4	1369
GeoB 1711[f]	1.16	12.68	70	14.39	87
GeoB 1711[f]	1.91	17.14	120	19.84	144
GeoB 1711[f]	2.51	18.74	130	21.73	154
GeoB 1711[f]	3.41	35.37	980	39.71	959

[a] combined PC/PG12 depth, and combined GeoB 1711 gravity and box core depth.
[b] no reservoir corrections or calibration to calendar years.
[c] ages converted to calendar years following the methods of *Bard et al.*, 1990a; 1990b; 1993, after a + 400 years correction for marine reservoir effect.
[d] Age from *N. pachyderma* right coiling specimens.
[e] Age from *N. pachyderma* mainly left coiling specimens.
[f] Age from *Gr. inflata* specimens.

Table 2.2. Radiocarbon ^{14}C dates and calendar age calculation (after *Bard et al.* 1990) for PG/PC12, GeoB 1706 and GeoB 1711.

carbon-isotope records of GeoB 1711 and GeoB 1706 to directly compare the records adjusted for age. The maximum of $\delta^{13}C$ in sub-stage 5.3 is clearly missing, whilst the excellent correlation in early stage 5 marks the isotope sub-stage 5.5 start of the hiatus. The $\delta^{18}O$ stratigraphy of the complete benthic foraminiferal record (Figure 2.2) further clarifies the missing section of sediment, with the noticeable isotopic absences in mid-stage 5. Alkenone-derived SST data for both GeoB 1706 and GeoB 1711 reinforce the age model described (*Müller*, unpublished), and further suggests the presence of a hiatus between sub-stages 5.5 and 5.2 in GeoB 1706.

2.4.2. PG/PC12

Figure 2.4 shows the oxygen and carbon isotope stratigraphy for PG/PC12 (after *Summerhayes et al.*, 1995b). The planktonic foraminiferal isotope record was produced from the tests of *Neogloboquadrina pachyderma* Ehrenberg, and cannot, therefore, be directly correlated with GeoB 1706 or GeoB 1711. The oxygen isotope record was correlated with the stacked record of *Imbrie et al.* (1984) and, although with an overall similarity, precise correlation of isotope events could not be allocated.

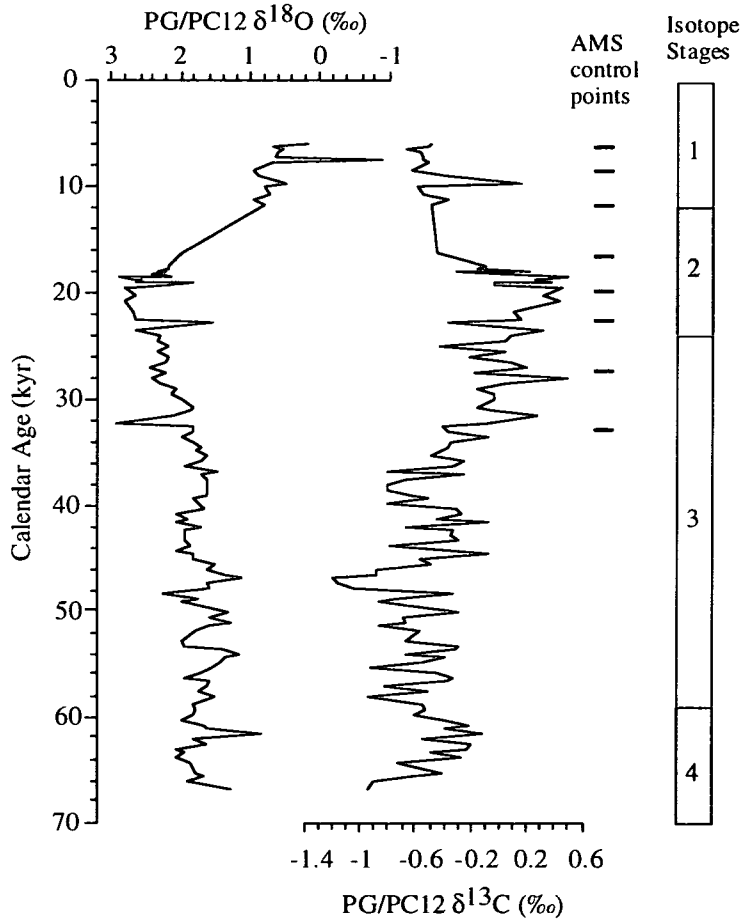

Figure 2.4. Oxygen and carbon isotope depth profiles for PG/PC12. AMS ^{14}C control points (calendar years) are shown to the right of the records, together with a graphical representation of glacial-interglacial isotope stages.

Summerhayes et al. (1995b) describe how an abrupt transition from light $\delta^{18}O$ values, averaging 0.7‰ in the pilot core PG12, to heavier $\delta^{18}O$ values of about 2‰ at the top

of the piston core PC12, indicated that there is a small amount of section missing between the pilot core and the piston core at the transition from the Holocene to the last

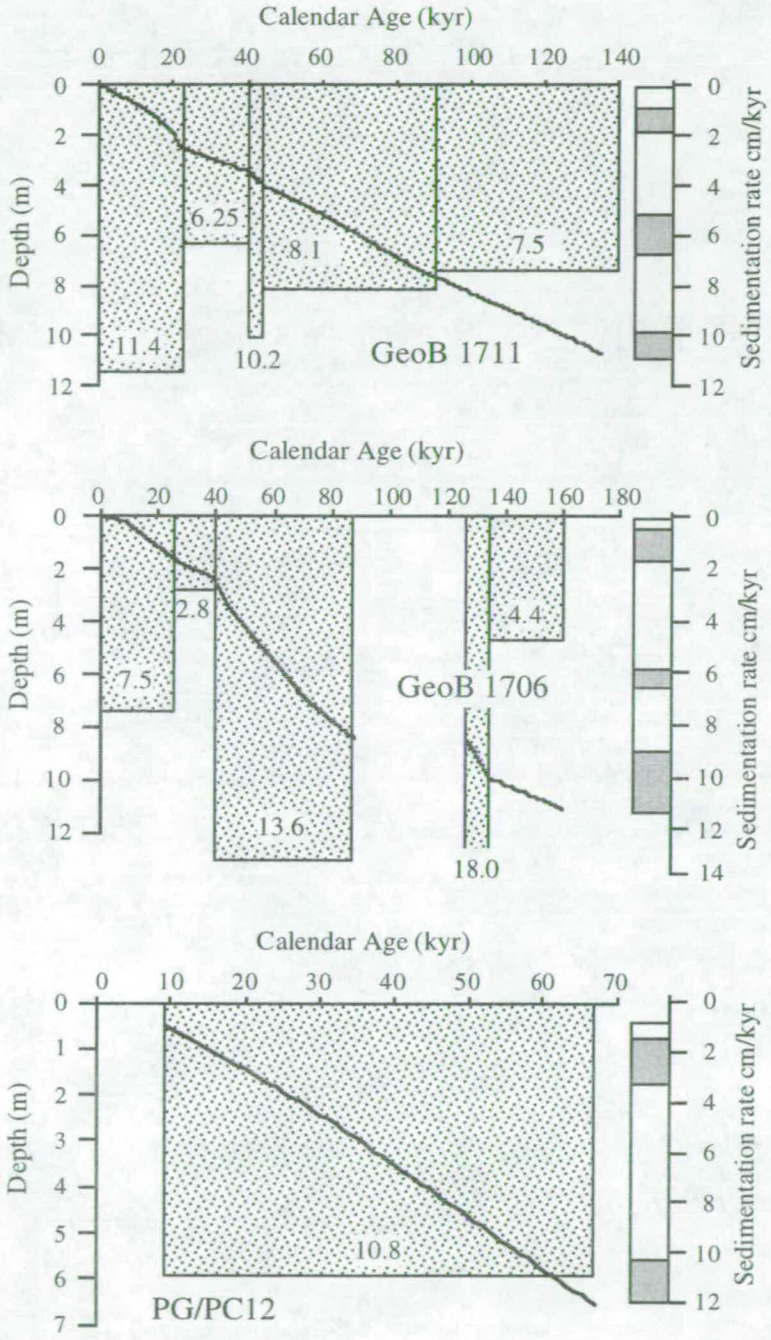

Figure 2.5. Sedimentation rates and age/depth profiles for GeoB 1711, GeoB 1706 and PG/PC12. Note the differences in age scale plotted on the horizontal axis. Stable isotope interglacial—glacial stages are given to the right of each record, glacial stages are shaded.

glacial maximum (LGM, isotope stage 2). The combined record, PG/PC12, has 30 cm missing, where the top of PC12 represents 112 cm (82 cm of pilot core PG12 + 30 cm of missing section). Combined (PG/PC12), the pilot and piston core represent at least 620 cm of sediment record, with a small hiatus between the two sediment cores, confirmed using carbonate content profiles from four other cores near the slope of PG/PC12 [PC16, 4778, 4804 and 4805] (*Summerhayes et al.,* 1995b).

No isotopic events could be identified with a good degree of certainty. Eight AMS ^{14}C dates for the top 270 cm of PG/PC12 are given graphically to the right of Figure 2.5 and listed in Table 2.3. Two of these dates, at 144 and 75 cm, correlate to isotope events 2.2 and 2.0, respectively. Linear interpolation from the control points gives a 64 kyr age (~ isotope sub-stage 4.2) for the core base (652 cm) [4]. However, comparison with the GeoB 1711 planktonic foraminiferal derived $\delta^{18}O$ record, would place the oxygen isotope stage 4.0 boundary (59 ka) at 563 cm, and therefore, the age of the core base at 67 kyr (mid isotope-stage 4).

2.5. Sedimentation rates

Figure 2.5 indicates that in the longer records from GeoB 1706 and GeoB 1711 sedimentation rates do vary with age. In all of the cores studied there is not a constant relationship between sedimentation rate and global temperature related to the glacial—interglacial cycles. In general, the average sedimentation rate for PG/PC12 is, as expected, higher than for the offshore core GeoB 1711 and the Walvis Ridge core GeoB 1706. PG/PC12 records an average 10.8 cm/1000 years for the last 70 kyr, while GeoB 1706 and GeoB 1711 record averages of 9.6 and 8.5 cm/1000 years respectively.

[4] Comparison of planktonic foraminiferal records (GeoB 1706, GeoB 1711 and PG/PC12) suggest that isotope sub-stage 4.2 is indeed recovered, but the Pleistocene did not penetrate isotope stage 5 (see Chapter 3 for discussion).

Rapid palaeoceanograpic changes in the Benguela upwelling system as indicated by abundances of planktonic foraminifera

Ch.3.

Chapter 3. Rapid palaeoceanograpic changes in the Benguela upwelling system as indicated by abundances of planktonic foraminifera

3.1. Introduction

Upwelling systems and the associated enhanced primary and secondary productivity, make a significant contribution to the total carbon reservoir in the ocean sediments (*Shaffer*, 1993). It is vital that a proper understanding of upwelling systems, their variability and driving mechanisms, is gained to quantify the carbon sinks in the oceans. The southwest African margin is an excellent area to study upwelling dynamics as it is the site of intense upwelling and exceptionally high productivity. Offshore displacement of more oligotrophic, transitional to sub-tropical waters by the southeast trade winds allows the intense upwelling of cold, nutrient-rich waters into the surface layer. This stimulates extreme phytoplankton growth (*Brown et al.* 1991) in a narrow shoreward zone of eutrophy resulting in most of the surface sediments being of biogenic origin (discussed in Chapter 1).

This chapter will outline the variation of planktonic foraminiferal abundances in both modern and fossil sediments to determine changes in the oceanography of the Benguela upwelling system, in the expectation that this will enable us to assess the extent to which upwelling has changed temporally and spatially, and to determine what controls these changes. Two main questions to be investigated are: (1) can abundance variations of planktonic foraminifera be used to determine past changes of upwelling intensity in the Benguela upwelling system?; (2) to what degree is the Benguela Current system (BCS) influenced by cold-water advection from the Southern Ocean as has previously been suggested (*McIntyre et al.*, 1989; *Giraudeau*, 1993; *Summerhayes et al.*, 1995b; *Giraudeau et al.*, in prep.)?

3.2. Modern-day water mass and nutrient distribution

The distribution of water masses is important in any discussion of foraminiferal variations. *Bé and Tolderlund* (1971) grouped planktonic foraminifera into five faunal zones, showing a bipolar and anti-tropical nature of preferred habitats with distinct faunas living in particular latitudinal zones, seemingly governed by the temperature regime. However, other studies brought the dominance of temperature into question,

with 'typically' cold-water species such as *Globigerina bulloides* d'Orbigny being found in tropical upwelling areas (*Thiede,* 1975, *Prell and Curry,* 1981, *Kroon,* 1991) reinforcing the idea that species distribution is governed by nutrient levels and not by temperature alone (*Reynolds and Thunnel,* 1985, *Kroon and Ganssen,* 1989, *Ten Haven and Kroon,* 1991).

Three water mass types adequately describe the BCS as observed by the modern distribution of planktonic foraminifera (*Giraudeau,* 1993) and satellite imaging (*Lutjeharms and Stockton,* 1987, *Meeuwis and Lutjeharms,* 1990). In the modern setting, *Giraudeau* (1993) mapped planktonic foraminifera into trophic and oceanographically distinct zones or belts, from Cape Town to Cape Fria. Figure 3.1 is a composite of the modern distribution of planktonic foraminifera (after *Giraudeau,* 1993) and shows the four main species components of the modern assemblage. In the southern Benguela region (SBR), the offshore waters are typical of oligotrophic, transitional to sub-tropical conditions with low nutrient levels and reduced primary productivity, suitable for *Globorotalia inflata* d'Orbigny. Inshore, the eutrophic, nutrient-rich, cooler upwelled waters form an area much more agreeable to primary and secondary producers, including *Neogloboquadrina pachyderma* sinistral (Ehrenberg) [*N. pachyderma* (s)]. The sharp break between the two zones of foraminifera dominance correlate precisely to the hydrography of the SBR (Figure 3.2).

Bang (1971) studied the water structure between 29°S and 32°S (SBR) and distinguished a coast-parallel coastal upwelling front over the continental shelf with a sharply defined thermal anomaly between an offshore divergence zone and the newly upwelled waters of the BCS. In the SBR, upwelled water is transported from a deeper origin than that in the northern Benguela region (NBR), and together with the seasonal run-off from the Orange River, the SBR (particularly the Namaqua upwelling cell) experiences some of the lowest sea-surface temperatures and salinities.

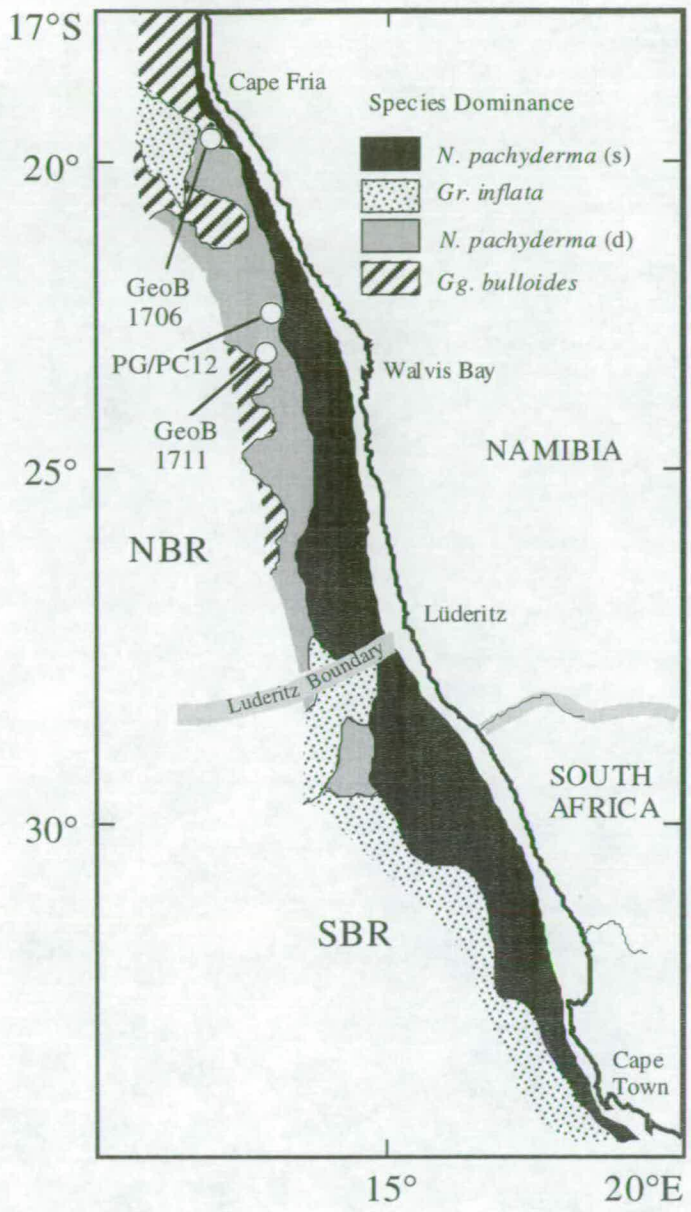

Figure 3.1. Recent distribution of planktonic foraminifera in the study area, after *Giraudeau* (1993). *N. pachyderma* (s) is found in eutrophic, cool upwelled waters; *Gr. inflata* is found in oligotrophic, transitional to sub-tropical conditions; and, *N. pachyderma* (d) and *Gg. bulloides* are found in the mixed, mesotrophic, sub-tropical and upwelled waters typical of the offshore northern Benguela region (NBR). The Lüderitz Boundary represents the boundary between the northern (NBR) and southern (SBR) Benguela regions .

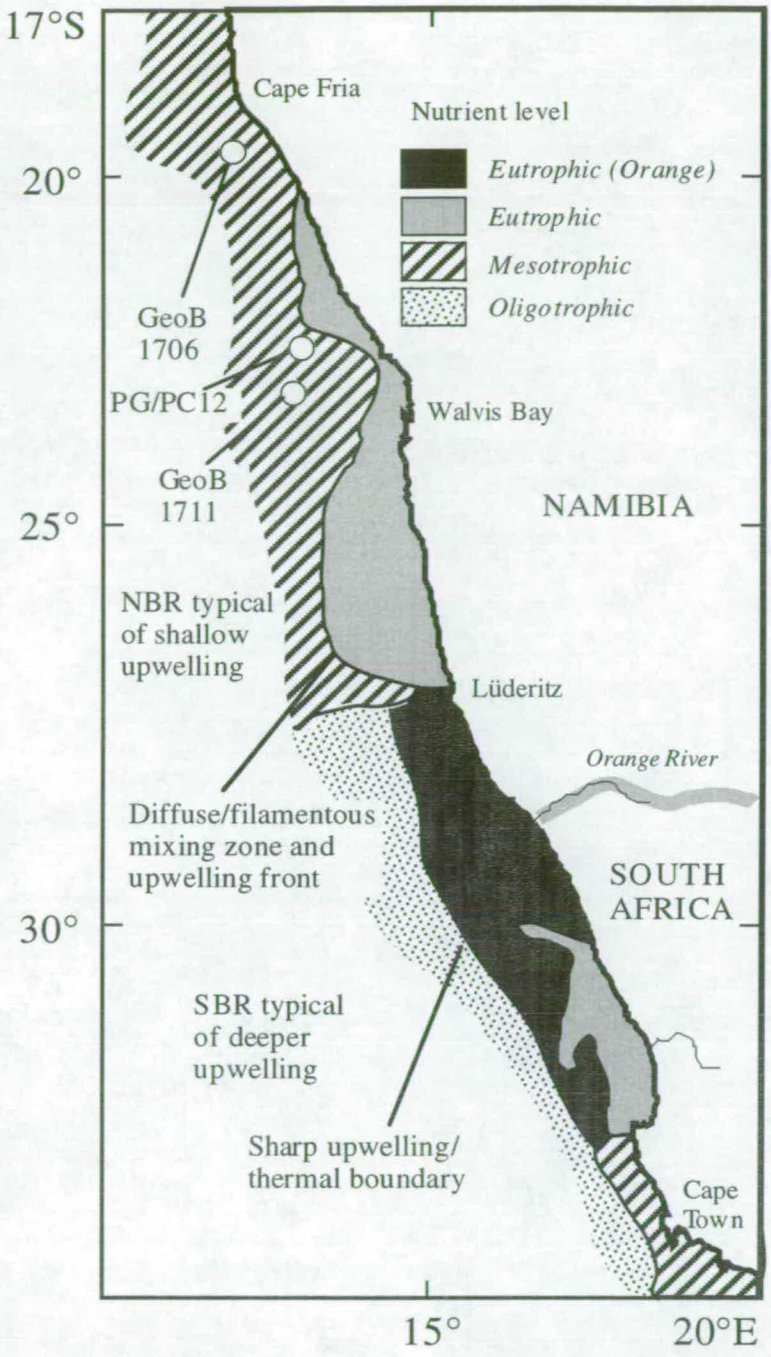

Figure 3.2. Composite map of the nutrient distribution in the Benguela upwelling system (after *Giraudeau et al.*, in prep.). Eutrophic (Orange) = High nutrient levels with added seasonal input from the Orange River; Eutrophic = High nutrient levels; Mesotrophic = Medium/High nutrient levels; Oligotrophic = Relatively reduced nutrient levels; NBR = northern Benguela region, and SBR = southern Benguela region.

Barange and Pillar (1992) extended the observations northwards to 17°S (NBR) and reported that the offshore divergence zone is a permanent feature independent of the wind stress. A 'tongue' of warm, oxygen- and nutrient-poor, Angola Basin water filters into the northern BCS intermittently throughout the year (*Boyd et al.,* 1987) further increasing the extent of the filamentous mixing domain in the NBR. As well as the offshore conditions in the SBR, *Gr. inflata* also inhabits the nutrient-poor, sub-tropical Angola Current filaments injected into the BCS in the NBR.

The offshore zone of the NBR is characterised by areas of mixed nutrient levels, suitable for *Neogloboquadrina pachyderma* dextral (Ehrenberg) [*N. pachyderma* (d)] and *Gg. bulloides*. *N. pachyderma* (d) prefers the mesotrophic, but higher nutrient levels of the upwelled filaments where the average SST is also lower, whilst *Gg. bulloides* prefers the relatively lower nutrient levels away from the upwelling filaments (*Giraudeau*, 1993). Nearshore waters, which upwell in this area, are of a shallower origin than in the SBR (*Shannon and Nelson,* 1997), and are less ideal for *N. pachyderma* (s) than the nearshore area to the south.

3.3. Late Quaternary planktonic foraminiferal variability

Oberhänsli (1991) and *Schmidt* (1992) used the abundances of planktonic foraminifera as indicators of past upwelling processes in the BCS. Both document cold periods during early stage 6 and within stages 4—2, from sites GeoB 1028 and DSDP 532 (see Figure 1.1), recorded by the greatest maxima of the 'cold water' species *N. pachyderma (s)*. However, although both showed distinct peaks in the planktonic assemblages, the records were of too low a resolution to ascertain a periodicity for the variations seen and to imply any forcing mechanisms for the system as a whole. Studies of U^{k}_{37} (*Schneider et al.,* 1995) and organic matter in PC12 (*Summerhayes et al.,* 1995b) revealed similar histories of cooling and production, suggesting that it may be related to an increased vigour of upwelling, not simply an introduction of cold water from the south.

3.4. Materials and methods

3.4.1 Cores collected from the R/V METEOR cruise M20-2 (1991) and R/V CHAIN cruise 115 (1973)

For a high-resolution analysis, samples were taken at 5 cm intervals along the GeoB cores, giving an average sampling spacing of 650 years. Micropalaeontological samples (10 cm^3) for foraminiferal counts were wet sieved, before foraminiferal analysis was made on the > 125 μm size fraction. Archived core material is kept at the Department of Geosciences, University of Bremen, Germany. PC12 and PG12 (combined as PG/PC12) were sampled on-board at 20 cm intervals for geochemical and isotopic analysis, and the remaining core material was stored in the core repository at the Woods Hole Oceanographic Institution. In October 1995, the cores were re-sampled at 10 cm intervals for planktonic foraminifera. Samples were wet sieved for fractions >125 μm. Archived core material is kept at the Woods Hole Oceanographic Institution, Woods Hole, Massachusetts, USA; and archived foraminiferal samples at the Department of Geology and Geophysics, Edinburgh University, Scotland.

3.4.2. Cores collected from the R/V METEOR cruise M34-1 (1996)

Cores from the recent cruise of the R/V METEOR (M34-1 Cape Town—Walvis Bay; *Bleil and cruise participants*, 1996) were sampled on-board for planktonic foraminiferal, geochemical and isotopic analysis. Micropalaeontological samples (10 cm^3) for foraminiferal counts were taken at 20 cm intervals and wet sieved, and dried in an oven at 40°C before on-board analysis was made on the > 125 μm size fraction. Archived core material is kept at the Department of Geosciences, University of Bremen, Germany.

3.4.3. Planktonic foraminifera classification

Planktonic foraminiferal species were identified using the taxonomic concepts of *Parker* (1962) and the Neogene planktonic foraminiferal classification of *Kennett and Srinivasan*, (1983); classification is given in Appendix 1.2. For the purpose of this work dextral neogloboquadrinids are grouped as *N. pachyderma* (d) excluding all

adult forms of *Neogloboquadrina dutertrei* d'Orbigny which are counted separately [1]. This method was used to account for the problem of the *N. pachyderma* intergrades of Kipp (1976), where a distinction between *N. pachyderma* and *N. dutertrei* is gradual, and the species definition between the two is already under question (*Dick Kroon* pers. comm.).

	GeoB 1706		GeoB 1711		PG/PC12	
	Ave	Max	Ave	Max	Ave	Max
G. hexagonus				1.1		
Ga. glutinata	2.6	17.2	1.6	6.2	0.9	4.8
Ga. siphonifera	0.3	2.9	0.2	2.3	0.4	1.1
Ga. uvula		1.3		0.3		0.3
Ge. calida	0.1	2.4		2.4		0.4
Gg. bulloides	25.3	50.2	21.5	48.7	24.1	55.9
Gg. conglobatus		0.8				
Gg. digitata		0.7		1.3		0.3
Gg. falconensis	0.2	2.8	0.2	1.5	0.1	1.4
Gg. humilis		0.8				
Gg. pyramidalis		0.5		0.3		
Gg. quinqueloba	1.6	6.7	3.5	14.2	3.0	11.3
Gg. ruber	0.2	2.7	0.2	4.1	0.1	2.5
Gg. rubescens	0.2	2.6				0.7
Gg. tenellus	0.4	3.3		1.3		
Gr. crassaformis	0.9	11.8	0.1	2.5	0.1	1.2
Gr. hirsuta	0.1	1.8				
Gr. inflata	11.8	57.6	5.6	36.8	4.5	15.0
Gr. menardii		0.8	0.1	0.4		0.5
Gr. scitula	0.6	10.1	0.4	2.4	0.2	1.4
Gr. theyeri		0.6				
Gr. truncatulinoides	0.3	3.8	0.3	2.9	0.4	2.1
Gr. tumida		0.4				
Gs. ruber	0.2	2.7	0.2	4.1	0.1	2.5
Gs. sacculifer	0.3	3.8	0.3	2.9	0.4	2.1
N. dutertrei			8.7	28.2	1.7	6.7
N. pachyderma (d)	27.8	58.2	31.4	82.1	30.3	63.4
N. pachyderma (s)	29.4	81.8	25.9	84.2	33.2	80.4
O. universa	0.9	9.3	0.4	4.6	0.8	5.4
P. obliquiloculata		1.1	0.1	0.7	0.1	6.7

Table 3.1. Planktonic foraminiferal abundances for GeoB 1706, GeoB 1711 and PG/PC12. Full species definitions and references are given in Appendix 1.

[1] This method is used for all core analyses with the exception of GeoB 1706. This was the first core analysed and it was considered at the time to merge all dextral coiling Neogloboquadrinids together including all adult forms of *N. dutertrei* which were later counted separately. Thus, GeoB 1706 does not have a separate record for *N. dutertrei*.

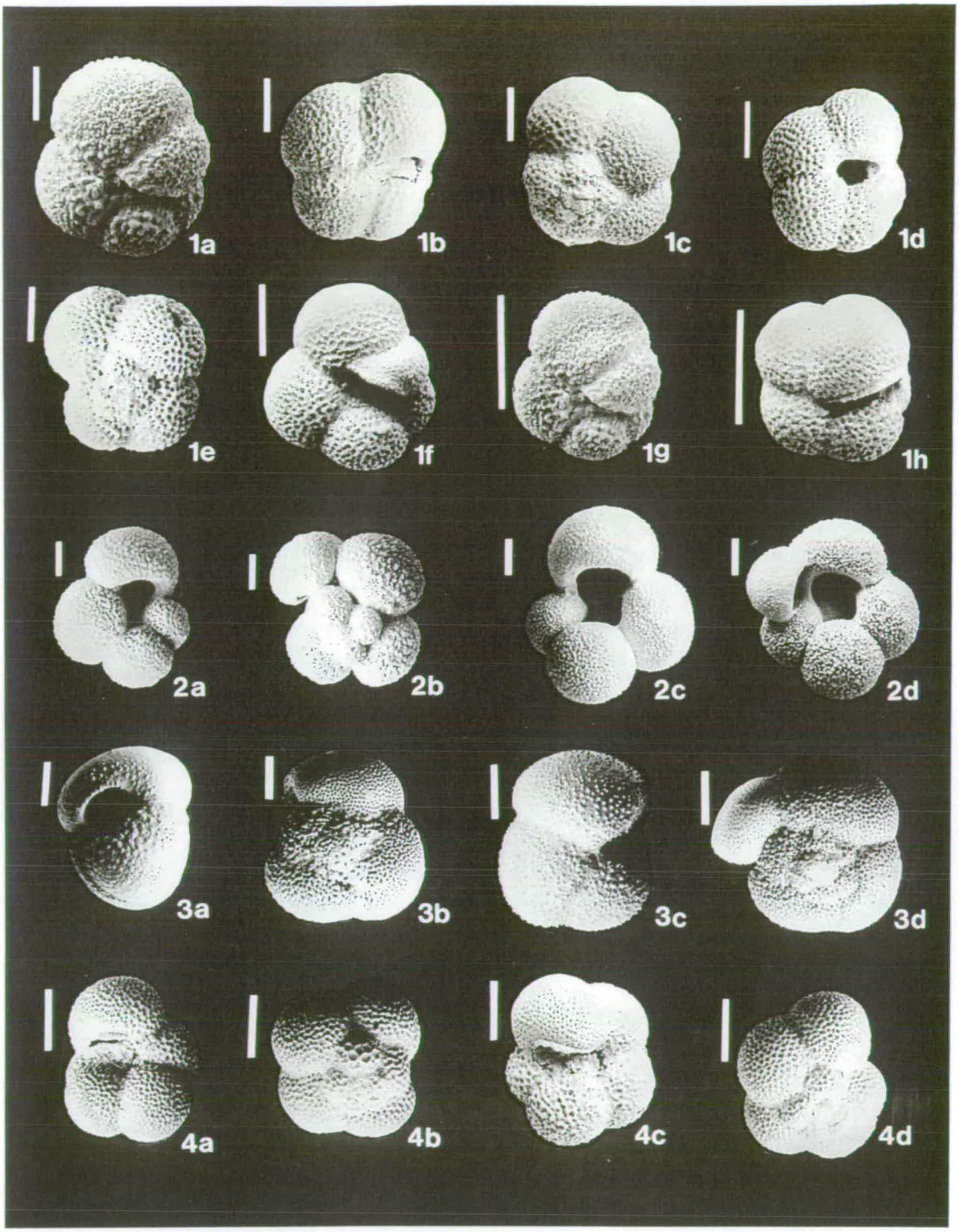

Plate 3.1. Photographs of the four main planktonic foraminifera from the Benguela upwelling system. Scale bar is 100 µm in length for all specimens.

1a—1h: *Neogloboquadrina pachyderma* (s) (Ehrenberg), 1861.
2a—2d: *Globigerina bulloides* d'Orbigny, 1826.
3a—3d: *Globorotalia inflata* d'Orbigny, 1839.
4a—4d: *Neogloboquadrina pachyderma* (d) (Ehrenberg), 1861.

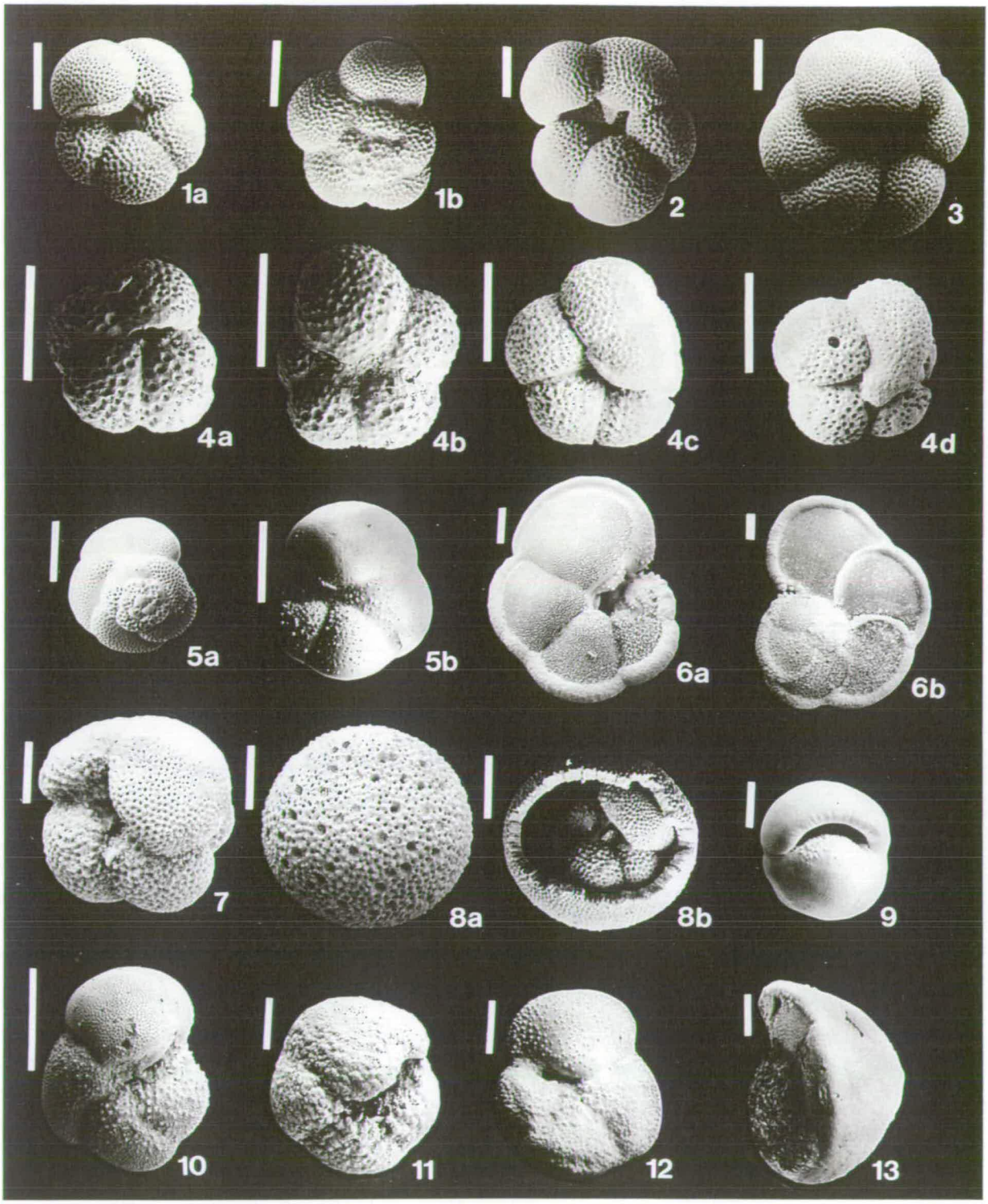

Plate 3.2. Photographs of planktonic foraminifera from the Benguela upwelling system. Scale bar is 100 μm in length for all specimens.

1a—1b: *Neogloboquadrina pachyderma* (d) (Ehrenberg), 1861.
2: *Neogloboquadrina pachyderma* (d) intergrade.
3: *Neogloboquadrina dutertrei* d'Orbigny, 1839.
4a—4d: *Globigerina quinqueloba* Natland, 1938.
5a—5b: *Globorotalia scitula* (Brady), 1882.
6a—6b: *Globorotalia menardii* (Parker, Jones and Brady), 1865.
7: *?Globoquadrina altispira* (Cushman and Jarvis), 1936: Miocene.
8a—8b: *Orbulina universa* (d'Orbigny), 1839.
9: *Pulleniatina obliquiloculata* (Parker and Jones), 1865.
10: *Globorotalia theyeri* Fleisher, 1970.
11: *Globorotalia crassaformis* (Galloway and Wissler), 1927.
12: *Globorotalia hirsuta* (d'Orbigny), 1839.
13: *Globorotalia truncatulinoides* (d'Orbigny), 1839.

Plate 3.1 shows the four dominant species in the Benguela upwelling system, and Plate 3.2 shows comparison between *N. pachyderma* (d) and an adult *N. dutertrei* for comparison. On average over two hundred specimens were counted for each sample, and where possible three hundred or more, to enable a good degree of certainty in the species abundance analyses. For a preliminary analysis while on-board the R/V METEOR (M34-1), a reduced sample size of between 50 and 100 specimens was counted. This was found, after testing, to be as reliable as using a larger sample size for a preliminary assessment. Core GeoB 3602 was re-sampled and re-counted at a higher frequency spacing and with an increased sample size in Edinburgh and was also found to be largely in agreement with the ship-board results of this same core.

3.5. Southwest African planktonic foraminiferal records

Twenty nine planktonic foraminifera species (Table 3.1) were identified in the sediments of the Benguela upwelling system. In GeoB 1711, seven species have an average abundance greater than 1%, six from GeoB 1706, and six also from PG/PC12. Of those, four species [*N. pachyderma* (s), *Gg. bulloides*, *N. pachyderma* (d) and *Gr. inflata*] make up, on average, over 90% of the total assemblage.

3.5.1 GeoB 1706 (Walvis Ridge)

As previously described, four species make up over 90% of the total planktonic foraminifera abundance recorded at the Walvis Ridge. *N. pachyderma* (s) constitutes the largest average fraction of the fossil record, with a very similar contribution from *N. pachyderma* (d) and *Gg. bulloides*, with approximately 12% of the total fossil abundance from *Gr. inflata*. The other species, with an average abundance over 1%, are *Globigerinita glutinata* (Egger) and *Globigerina quinqueloba* Natland. Figure 3.3 shows the variation of these main species with depth and also the sum total of all benthic foraminifera (as a percentage of the total foraminifera).

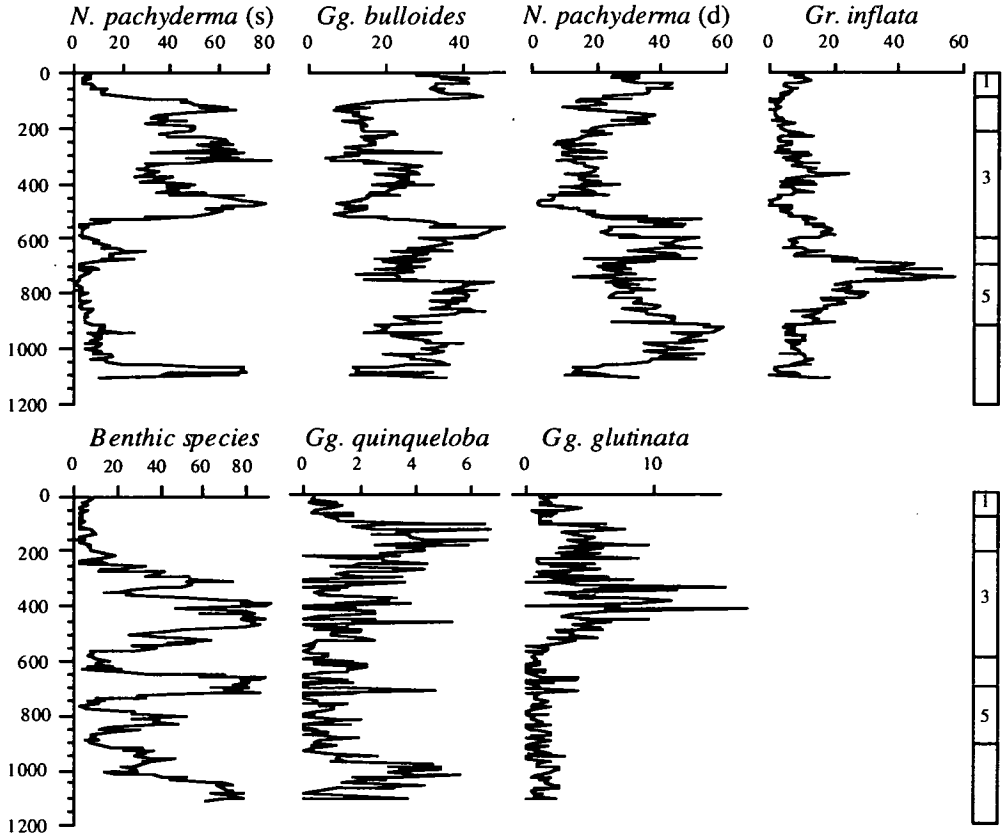

Figure 3.3. GeoB 1706. Abundances (% of total planktonic foraminifera) of the six main planktonic foraminifera and ratio of benthic to planktonic foraminifera, all against depth (cm). On the right hand side is a schematic representation of the interglacial—glacial stages 1—6; glacials are shaded.

3.5.2. GeoB 1711 (continental slope, Northern Cape Basin)

On the continental slope at a water depth of 1967 m, further offshore than GeoB 1706 and PG/PC12, GeoB 1711 would probably be expected to contain less planktonic foraminifera than the other sites, and in particular a decrease in the dominance of nearshore coastal foraminifera. However, *N. pachyderma* (s) still contributes a large fraction of the planktonic foraminifera to the fossil record, but with a slightly greater contribution from *N. pachyderma* (d), and a similar percentage from *Gg. bulloides*. Again *Gr. inflata* makes up the minority portion and, although further offshore, only has an average abundance of 5.6%. *Ga. glutinata* and *Gg. quinqueloba* are also present with 1.6% and 3.5% respectively, with *N. dutertrei* [1] recording an average of almost 9%. Figure 3.4 shows the variation of the four main species with depth and

also the sum total of all benthic foraminifera (as a percentage of the total foraminifera), *Gg. quinqueloba* and *N. dutertrei*.

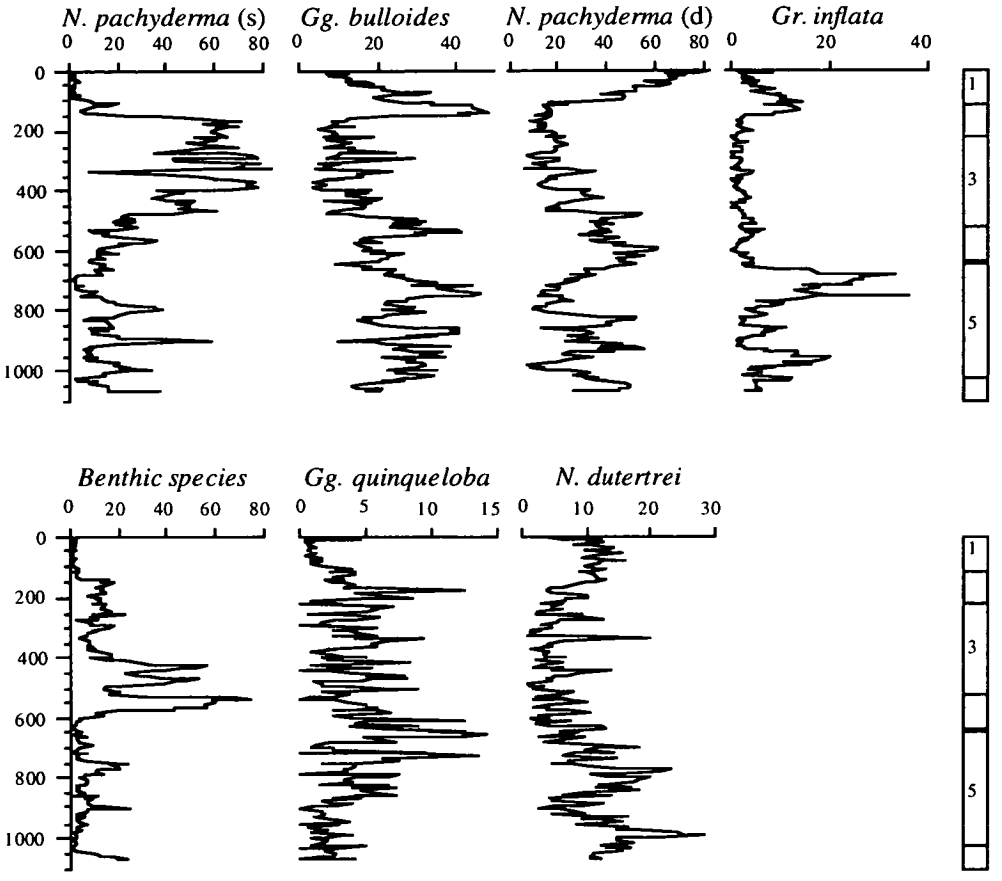

Figure 3.4. GeoB 1711. Abundances (% of total planktonic foraminifera) of the six main planktonic foraminifera and ratio of benthic to planktonic foraminifera species, all against depth (cm). On the right hand side is a schematic representation of the interglacial-glacial stages 1—6; glacials are shaded.

3.5.3. PG/PC12 (continental slope, Northern Cape Basin)

PG/PC12 is situated close by GeoB 1711 at a water depth of 1017m. Further inshore than GeoB 1711, *N. pachyderma* (s) again contributes the largest fraction of planktonic foraminifera at 33%. *N. pachyderma* (d), *Gg. bulloides* and *Gr. inflata* make up the other portion. *Gg. quinqueloba.* and *N. dutertrei* [1] have abundances of 3% and 2% respectively. Figure 3.5 shows the variation of the four main species with depth and also the sum total of all benthic foraminifera (as a percentage of the total foraminifera), *Gg. quinqueloba* and *N. dutertrei.*

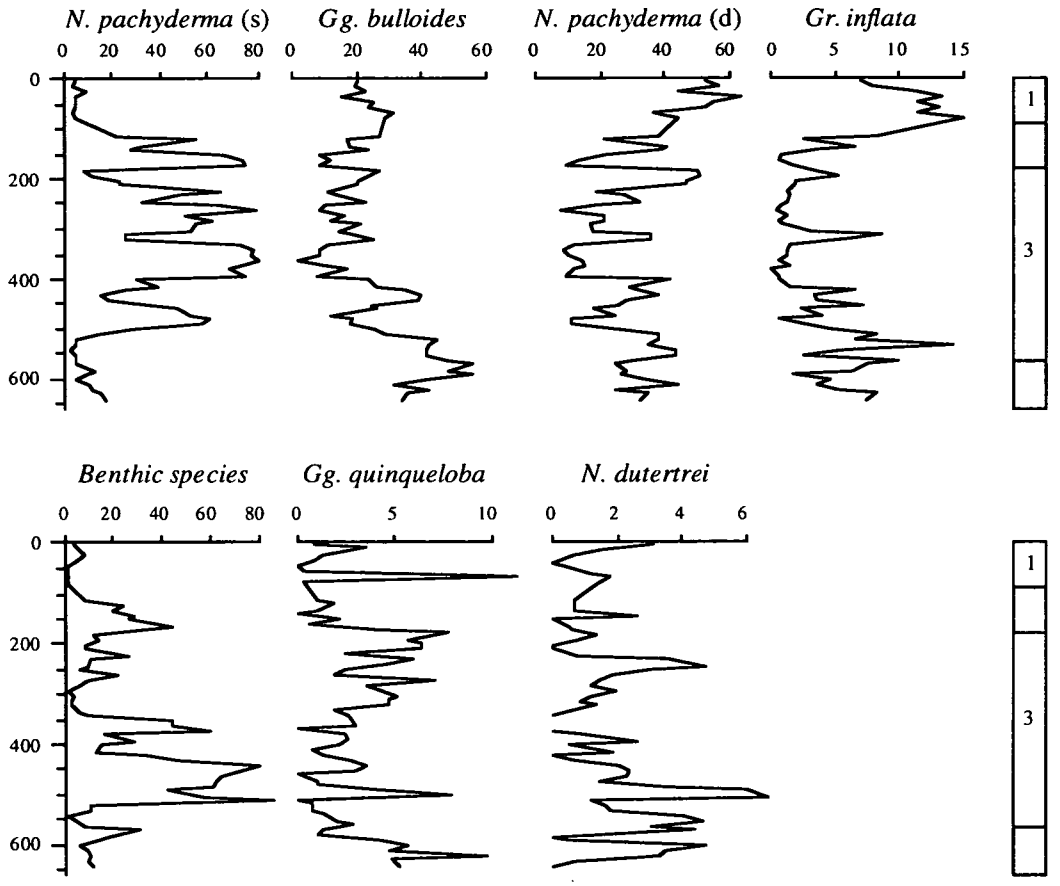

Figure 3.5. PG/PC12. Abundances (% of total planktonic foraminifera) of the six main planktonic foraminifera and ratio of benthic to planktonic foraminifera, all against depth (cm). On the right hand side is a schematic representation of the interglacial-glacial stages 1—4; glacials are shaded.

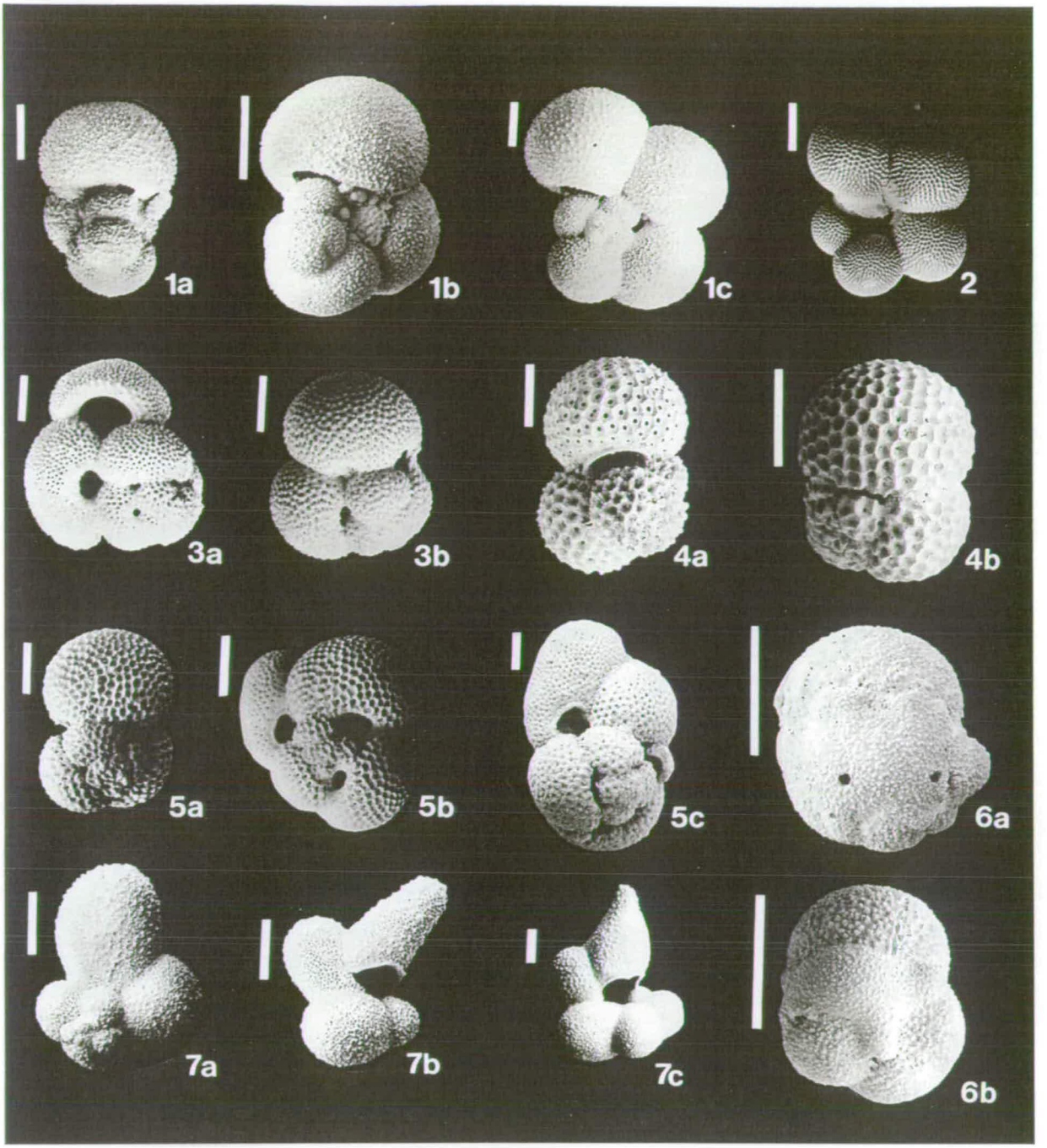

Plate 3.3. Photographs of tropical planktonic foraminifera from the Benguela upwelling system. Scale bar is 100 μm in length for all specimens.

1a—1c: *Globigerinella aequilateralis* (Brady), 1839 [*Globigerina siphonifera* d'Orbigny, 1839].
2: *Globorotalioides hexagona* (Natland), 1938.
3a—3b: *Globigerinoides ruber* (d'Orbigny), 1839.
4a—4b: *Globigerinoides sacculifer* (Brady), 1877 [*Globigerinoides trilobus* - form].
5a—5c: *Globigerinoides sacculifer* (Brady), 1877.
6a—6b: *Globigerinita glutinata* (Egger), 1897.
7a—7c: *Globigerina digitata* Brady, 1879.

3.5.4. Changes in abundance of sub-tropical species

Total sub-tropical species [2] make up to 30% of the total planktonic foraminifera recorded in the northern Benguela region. Of these, *N. dutertrei*, *Ga. glutinata*, *Globorotalia crassaformis* (Galloway and Wissler) and *Orbulina universa* (d'Orbigny) make up the majority percentage with maximum abundances of 28.2% [1] (GeoB 1711), 17.2% (GeoB 1706), 11.8% (GeoB 1706) and 9.3% (GeoB 1706) respectively.

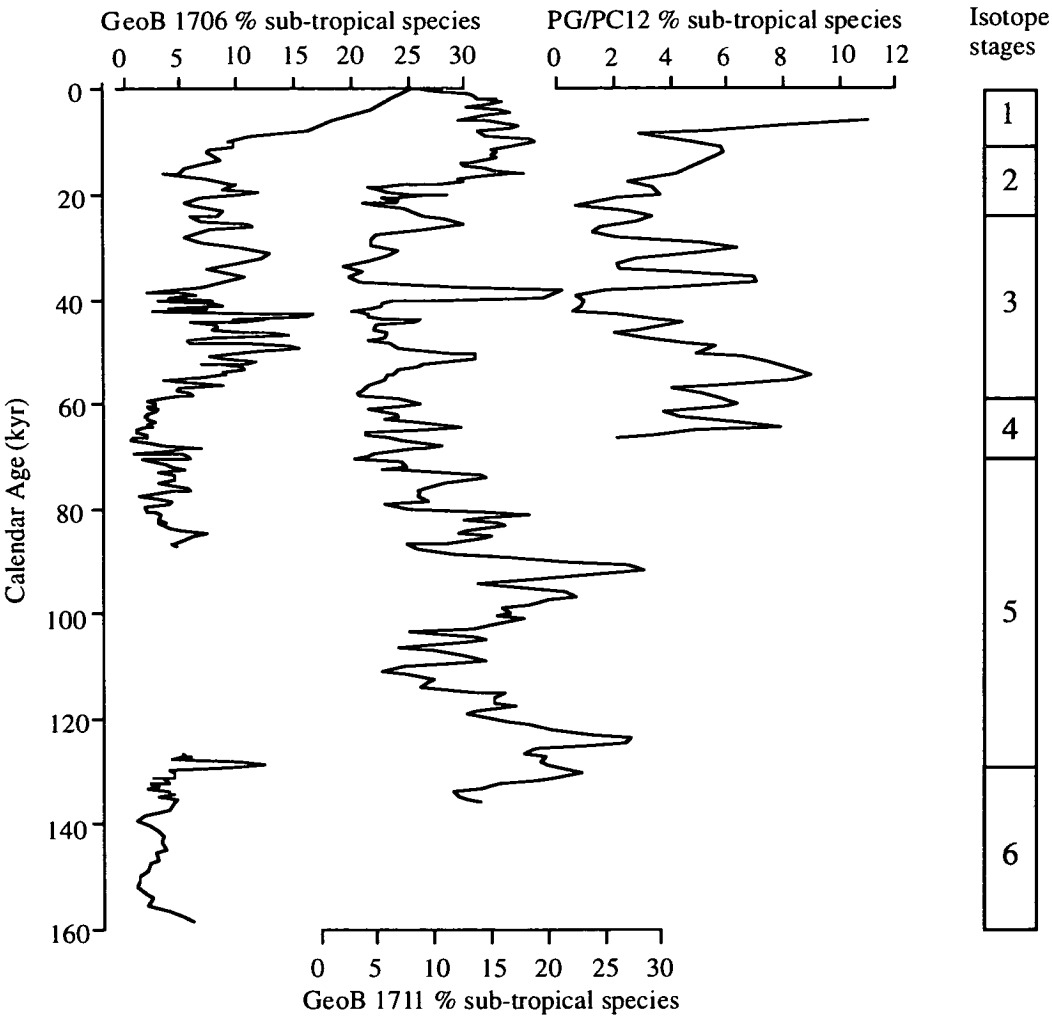

Figure 3.6. Abundances of the total sub-tropical planktonic foraminifera [2]. On the right hand side is a schematic representation of the interglacial-glacial stages.

[2] 'Sub-tropical' species = all tropical and sub-tropical species included in the sub-tropical and tropical zones (after *Bé and Tolderlund*, 1971) with the exception of *Gr. inflata*. Species included are: *Gg. falconensis*, *Ga. glutinata*, *Gr. truncatulinoides*, *N. dutertrei*, *Gr. crassaformis*, *O. universa*, *Ge. siphonifera*, *Gr. hirsuta*, *Gs. ruber*, *G.g conglobatus*, *Gg. rubescens*, *Gg. digitata*, *Gr. tumida*, *Gr. menardii*, *P. obliquiloculata*, and *Gs. sacculifer*.

The warm-water, tropical, spinose species, *Globigerinella aequilateralis* (Brady) [*Globigerina siphonifera* d'Orbigny], *Globigerinoides ruber* (d'Orbigny) and *Globigerinoides sacculifer* (Brady) (Plate 3.3), have an average abundance below 0.5% and do not significantly effect the total sub-tropical species numbers. As would be expected, the offshore record of GeoB 1711 records a higher average of total sub-tropical species than the more coastal PG/PC12, and the Walvis Ridge record of GeoB 1706 (Figure 3.6). The record for GeoB 1711 shows maxima in sub-tropical species abundance centered on 125 ka, 90 ka, 40 ka and the Holocene and, similar to the cold-water *N. pachyderma* (s), the numbers of sub-tropical species do not seem to be responding to the global glacial-interglacial changes as given by $\delta^{18}O$, instead they are oscillating with a higher frequency of change.

3.5.5. Time-series analysis of foraminiferal abundance variability

Time series background and methodology

Spectral, or time-series, analysis provides a way of partitioning a complicated problem into smaller units. Spectral analysis uses statistical methods adapted from Imbrie *et al.* (1989), to separate a complex waveform into its various components. In view of the planktonic foraminiferal and other datasets collected for this research, we are primarily dealing with a waveform which can to a first approximation be divided into one, or many, sinusoidal waves each with a period (one cycle), T. Consider an ideal geological situation of sinusoidal form, for example a 100,000 year cycle of sea level. The period of the waveform is 100 kyr, and the frequency is the reciprocal of the period, which is 0.01 (cycles per thousand years). However, in a 'natural' geological situation, for example a coastal marine setting, then the observed signal being measured, for example the variation in $\delta^{18}O$ from planktonic foraminifera tests, will be made up of many sinusoidal waveforms, each with a different timing (phasing), frequency and period. The aim of spectral analysis is to reduce the complexity of the initial dataset into the components that make up the signal, to be able to assess the possible forcing mechanisms at each measured frequency (or period). In the marine environment the most common forcing frequencies are well documented and are collectively called Milankovitch orbital mechanisms (further discussed in Chapter 5) which occur with frequencies at 100 kyr, 40 kyr and 23—19 kyr relating to the distance and shape of the Earth's orbit around the sun.

The following is a brief discussion of spectral analysis, estimates and plots before a discussion of the results. The analysis has been carried out using the SPECMAP Arand programs kindly given by Dr. Philip Howell, Brown University, Conneticut, USA.

A signal varying with time (age), will oscillate with a period, T, and frequency, f. As discussed above, most 'real' geological signals will be the sum of many components, which spectral analysis separates into the individual constituents. The results from spectral analysis may be plotted as variance [3] versus the frequency (and period). When a signal is made up of pure sine waves, or a combination of sine waves, the resultant spectrum is a series of vertical lines at the constituent frequencies. In geological signals this is rarely the case, and signals will be made up of data which does not occur regularly but is 'white noise', a random signal. Thus, when spectral plots of 'real' data are shown they are plotted as a curve with discrete peaks centered on the frequencies at which the dominant spectra occur. The log of spectral density (variance^2/frequency) is plotted versus frequency, as this provides a method for checking the confidence interval (the plus or minus error bar) over the entire frequency range, generally 80%. The method used to evaluate the true spectrum from a given time series, transforming the data from the time domain into the frequency domain, is Fourier transformation. In brief, the Fourier transformation approximates the signal by a sum of sine waves of different frequencies. The first Fourier component, or first harmonic, is a sine wave with a period equal to the data length, N Δt (where N = number of points in time, t; and Δt = the regular time interval between each data point). The second harmonic is a sine wave best fitting the residuals, it has a period N Δt / 2, and so on to higher order harmonics. Using the Blackman-Tukey method (*Jenkins and Watts,* 1968) which uses a Fourier analysis of the auto-corelation or auto-covariance function. This is defined by lagging the time series to a copy of itself and plotting the covariance or corelation factor calculated for each step of a defined lag interval against the number of lags. An increase in the number of lags increases the resolution of frequency information in the spectrum, but also increases the sampling error and therefore confidence interval; while a reduction in the number of lags has the reverse effect. When using this method it is therefore necessary to balance the output of uncertainty versus resolution. The results from a Blackman-Tukey time-series analysis of SPECMAP $\delta^{18}O$, are plotted in Figure 3.7.

---

[3] Variance is the average squared deviation from the mean. VAR = $\sigma_2 = \Sigma (x_1-x_2)^2/N$

For an honest appraisal of the dataset, it is necessary to compare the resultant high-frequency spectra, after time-series analysis, with a best estimate for 'background' periodicity. It is only those peaks that are elevated above the background record by the confidence interval (CI) that are statistically reliable. However, normally no such measure of 'background' periodicity is given, and instead it is left to the reader to consider which spectral peaks are statistically viable. Originally, SPECMAP suggested that a low-resolution record be measured, i.e. by using fewer lags (e.g. N/5—N/8) for background periodicity in which to compare with a higher resolution record. However, the choice of the low-resolution record is subject to 'red noise' bias (i.e. power at the low frequency end of the spectrum) and will accentuate some periods with respect to others, and the choice of a high resolution record is equally difficult. Deciding what the background periodicity should be is perhaps dangerous.

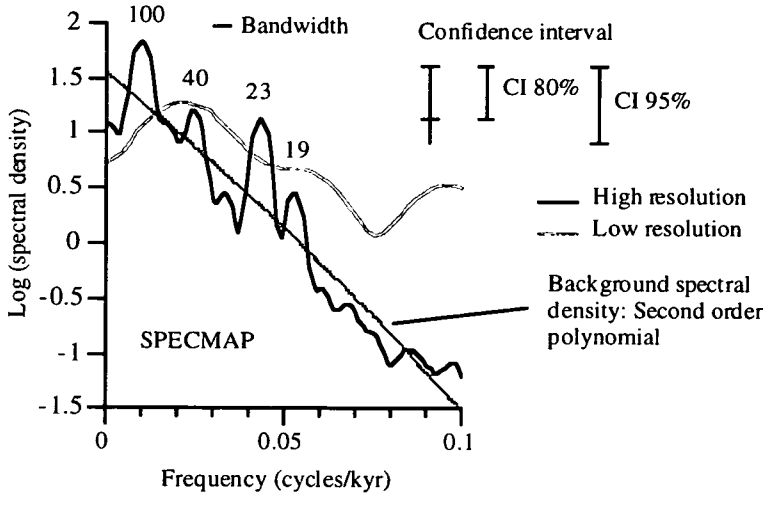

Figure 3.7. Spectral analysis results for SPECMAP. Spectral period analysed, 0—782 kyr; $\Delta t = 2$ kyr; N = 392; Number of lags = 100. The lower limit confidence interval, CI, is shown valid for the whole range of frequencies (period = 1/f). For comparison, a second order polynomial expression of the resultant log (spectral density) [i.e. that given as the output of Fourier transformation via the Blackman-Tukey method] is shown for the background spectral periodicity, together with the lower limit error bars of the 80 and 95% confidence intervals.

To try and give a more honest assessment of the datasets under study here, the spectral results from a high-resolution analysis are compared to a second order polynomial derived from the resultant spectral output after Blackman-Tukey analysis i.e. a quadratic curve-fit of the log of spectral density (*Graeme Weedon* pers. comm.; *Steens*

et al., 1991). The results from spectral analysis for SPECMAP $\delta^{18}O$, suggests that this method provides a better appraisal of the periods visually present in the dataset (Figure 3.7, see Figure 2.1). The lower limits for the 80% and 95% confidence intervals are given separately, but are combined in later figures. The spectral analysis shows discrete coherent peaks (valid at the 80% CI) at periods of 100 and 23 kyr, as would be expected if global sea level were to be controlled by the Milankovitch forcing criteria: eccentricity and precession. The measurement of the 'background' spectral density should be treated with caution, it only provides a reference point which is itself problematic. In instances where there is no spectral density observed at the low-frequency end of the spectrum, i.e. the long-term nature of the record is flat, or alternatively when the results record a high spectral density at the low-frequency end, then the polynomial is subject to bias at the low-end and the high-end of the spectrum respectively [4].

Spectral analysis results

Figure 3.8 shows the spectral results for the complete record of GeoB 1711 and Figure 3.9 gives the spectral results for the shorter records of PG/PC12 and GeoB 1706, although PG/PC12 is possibly too short for a meaningful analysis to be carried out. A time interval of 0.9 kyr was chosen for all of the records [5]. All bandwidths and lower confidence intervals are shown for the high-resolution analysis, and spectral peaks are labelled with the time period of oscillation (kyr). All of the main planktonic foraminiferal abundances were analysed for the continuous 136 kyr record of GeoB 1711 (Figure 3.8). All of the analyses indicate recurrent spectra at the 8 kyr period, within the 80% confidence interval constraint, and often within the 95% confidence limit, consistent with visual inspection of these records (Figures 3.4 and 3.6). Notably, *Gg. bulloides* has discrete, spectra at 11.5 and 23 kyr periods, of which the 11.5 kyr period is coherent at the 95% confidence interval. The spectral maxima at 12.5 and 12 kyr periods in the sub-tropical and *N. dutertrei* spectral results may be considered analogous to the 11.5 kyr period recorded in the *Gg. bulloides* time-series within the levels of observation. It may further suggest that these peaks are 'real' in the sub-tropical and *N. dutertrei* time-series analysis, although they are not found to be

[4] Note that removal of the polynomial from the figures leaves a usual graph of log(spectral density) vs frequency as is used in most journal publications.

[5] Although with an average sample of interval of 650 years, the cores studied had periods of higher sedimentation which, with a constant sample interval of 5 cm, increased the time interval to an average of 900 years in these periods.

confident with respect to the polynomial for background periodicity. Their prononced nature alone, and visual correlation in the temporal domain would suggest that these peaks are real.

Species abundances from cores PG/PC12 and GeoB 1706 also have coherent spectral peaks at sub-Milankovitch periodicities, centered on 6, 11—12 and 15 kyr (Figure 3.9). PG/PC12, with a greater sedimentation rate than GeoB 1706 and GeoB 1711 has only two discrete maxima, although this is largely due to the shortness of the record (67 kyr), at 6 kyr and 10—12 kyr. These periods of change are clearly obvious from visual inspection of the planktonic foraminiferal abundances (Figure 3.5). Although the analysed length of the record is short (87 kyr), visual inspection of the foraminiferal records for GeoB 1706 suggests a precessional effect in the period before 40 ka which is further supported by spectra at the ~40—23 kyr period from the sub-tropical foraminifera abundance, coherent at the 95% confidence level.

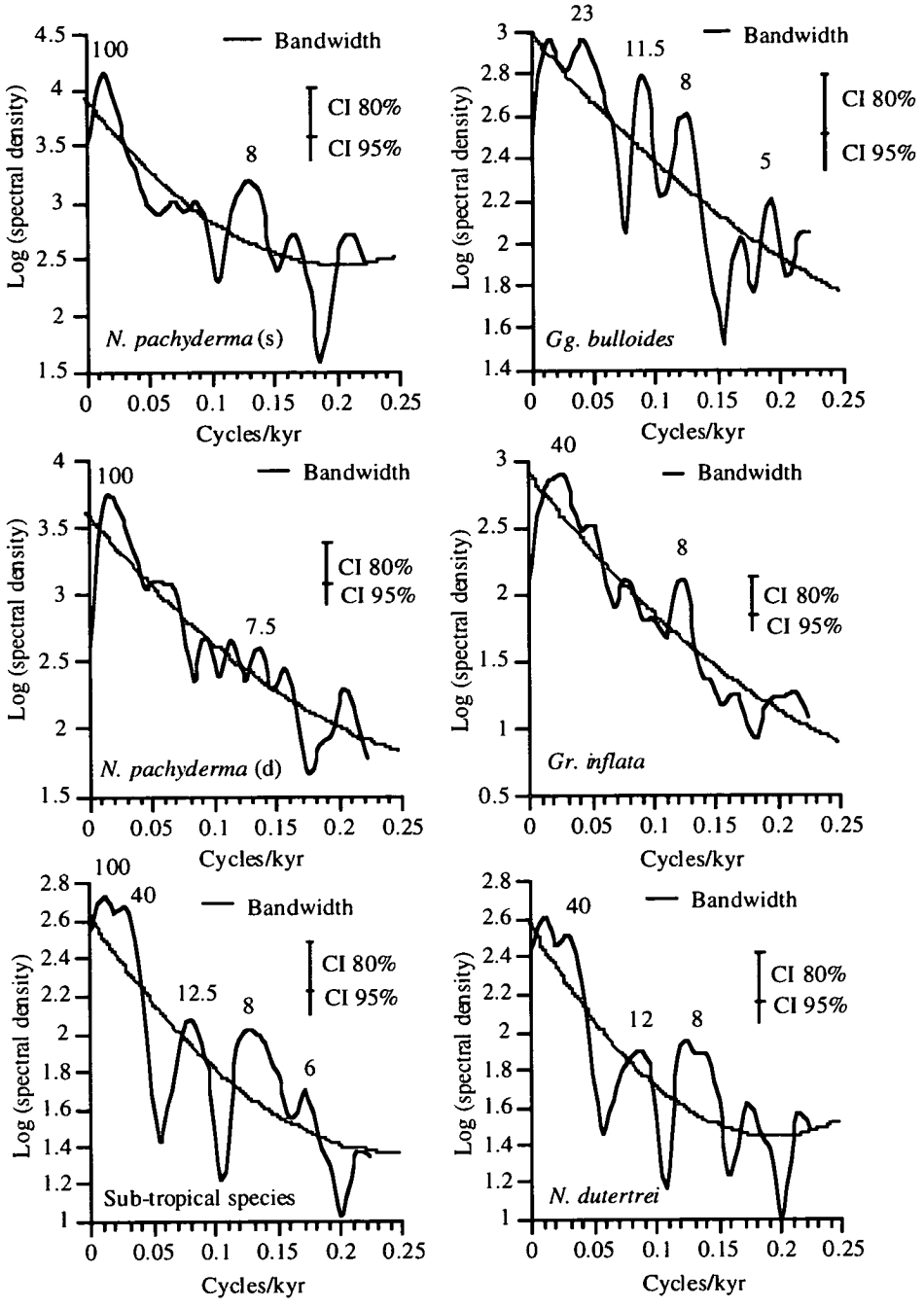

Figure 3.8. GeoB 1711 spectral analysis results. Statistical information: Spectral period analysed, 1—136 ka; $\Delta t = 0.9$ kyr; N = 151; CI is shown for 80 lags. For comparison, a second order polynomial expression of the spectral density is shown for the background spectral periodicity, together with the lower limit error bars of the 80 and 95% confidence intervals.

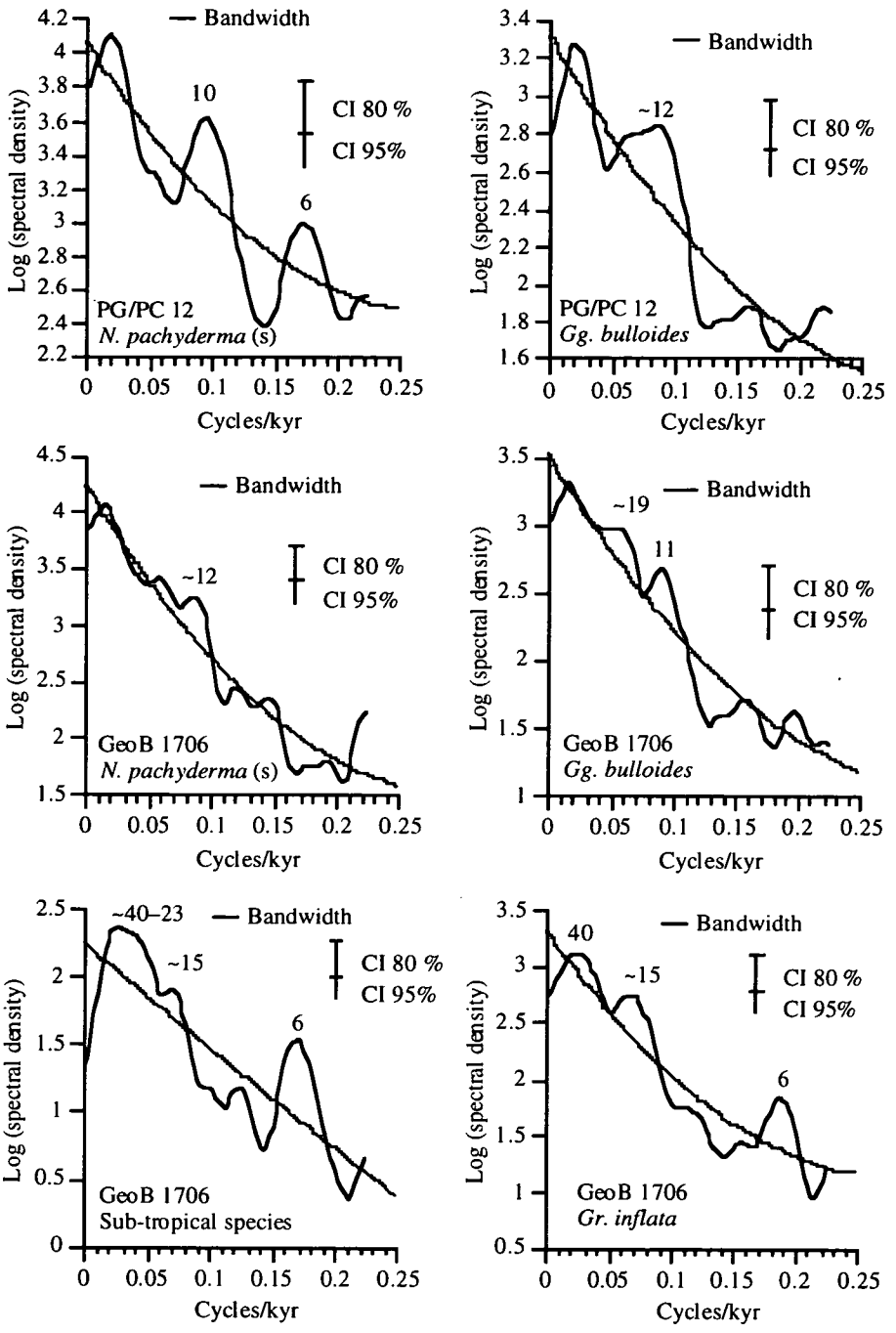

Figure 3.9. PG/PC12 and GeoB 1706 spectral analysis results. Statistical information: PG/PC12. Spectral period analysed, 1—67 ka; Δt = 0.9 kyr; N = 74; CI is shown for 50 lags. GeoB 1706. Spectral period analysed, 1—87 ka; Δt = 0.9 kyr; N = 96; CI is shown for 60 lags. For comparison, a second order polynomial expression of the spectral density is shown for the background spectral periodicity, together with the lower limit error bars of the 80 and 95% confidence intervals.

Sub-Milankovitch cyclicity is discussed in greater detail in Chapter 5, but the recurring coherent spectral density at the 8 kyr and 11—12 kyr periods strongly suggests the influence from mechanisms fluctuating on a sub-Milankovitch periodicity. *Hagelberg et al.* (1994) and more recently *McIntyre and Molfino* (1996) have shown sub-Milankovitch climate oscillation to be an important mechanism controlling eastern equatorial Atlantic oceanographic signals. The occurence of an 8 kyr and 11—12 kyr periodicity within faunal records from the South Atlantic, further suggests that sub-Milankovitch processes influence the marine environment. The relative absence of the direct influence from the precessional band on the faunal records is suprising, considering its documented relative dominance on equatorial and low latitude climate and oceanography (*Imbrie et al.*, 1989, *McIntyre et al.*, 1989, *Mix and Morey*, 1997, *Schneider et al.*, 1995; 1997; in press), which is assessed further in Chapter 5.

3.6. Temporal changes in nutrient supply as evidenced by variations in abundance of planktonic foraminifera

The relative abundances of planktonic foraminifera can be divided into a series of discrete episodes described with respect to the dominant species present in that time slice. There are four types of episode characterising the variation of assemblages seen offshore Namibia (Table 3.2).

<table>
<tr><th></th><th>N. pachyderma (s)</th><th>Gg. bulloides</th><th>N. pachyderma (d)</th><th>Gr. inflata</th></tr>
<tr><td>Episode A</td><td>> 40%</td><td></td><td></td><td rowspan="3"></td></tr>
<tr><td>Episode B</td><td colspan="3">> 20% each</td></tr>
<tr><td>Episode C</td><td rowspan="2"></td><td colspan="2">> 80% total</td></tr>
<tr><td>Episode D</td><td></td><td></td><td>> 20%</td></tr>
</table>

Table 3.2. Definition of episodes. Episode A, is dominated by *N. pachyderma* (s) when it is in abundances greater than 40% over all others. Episode B is not dominated by a single species, but consists of 20% each (or >) of *N. pachyderma* (s), *Gg. bulloides* and *N. pachyderma* (d). Episode C is dominated by two species, *Gg. bulloides* and *N. pachyderma* (d) both contributing to a total of ~80% (or >) of the total assemblage. Finally, *Gr. inflata* dominates Episode D when it is in abundance greater than 20%.

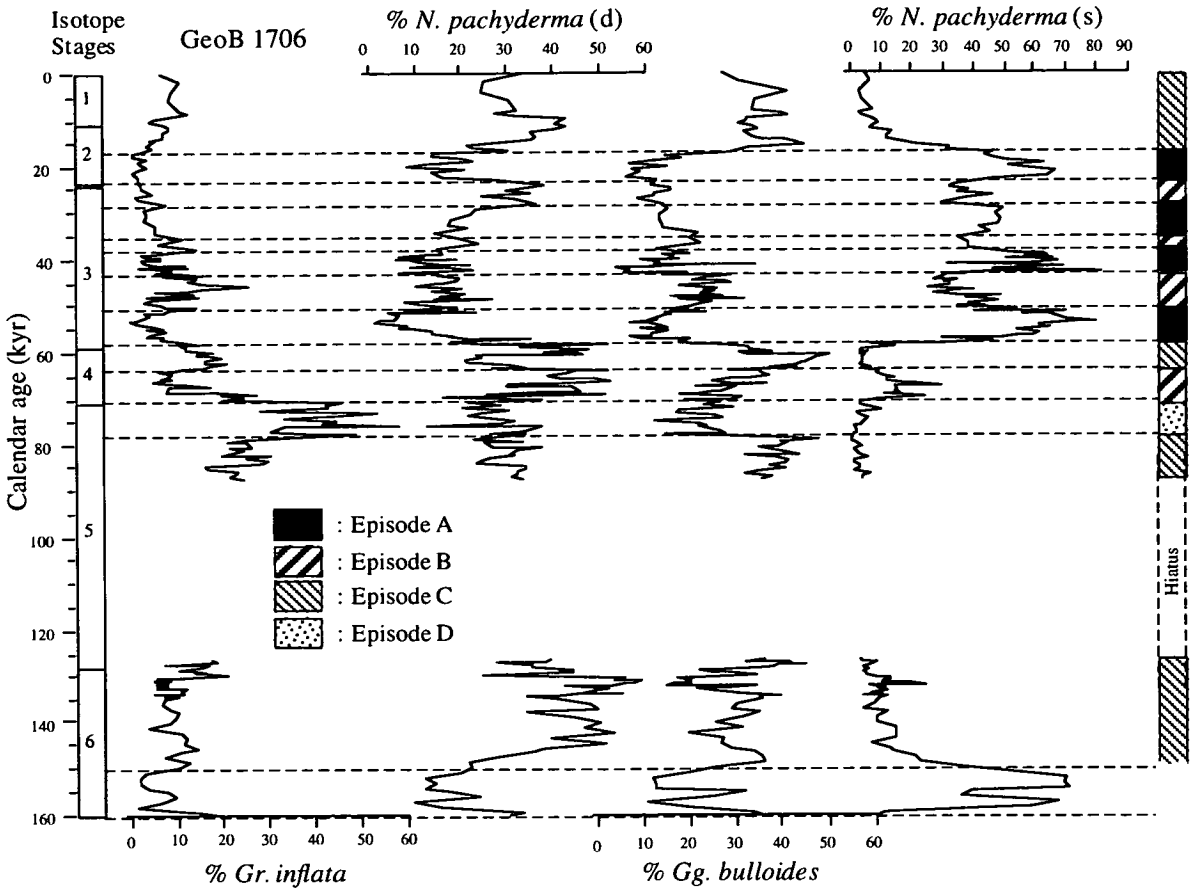

Figure 3.10. GeoB 1706. Fluctuations in the relative abundances of the four major species of planktonic foraminifera with age. Isotope stages are given on the left for reference, whilst a schematic reference for episode dominance is given on the right. Episode A: Dominance of *N. pachyderma* (s) > 40% over all others; Episode B: 20% each (or >) of *N. pachyderma* (s), *N. pachyderma* (d) and *Gg. bulloides* ; Episode C: Dominance of *N. pachyderma* (d) + *Gg. bulloides* both contributing to a total of ~80%; and, Episode D: *Gr. inflata* > 20%.

The graphic representation of the temporal variance in Episodes A–D (right hand side of Figures 3.10, 3.11 and 3.12) shows no obvious correlation with the glacial-interglacial pattern of the isotope stages (left hand side). *N. pachyderma* (s), which defines Episode A, has the greatest influence on the major fluctuations in the system, which could be demonstrated using principal component analysis. *N. pachyderma* (s) does not vary with the changes in the global hydrological cycle, described by $\delta^{18}O$ variations (*Imbrie et al.*, 1984), but instead shows a higher frequency of change with abundance maxima throughout isotope stages 6—2, including interglacial stage 5.

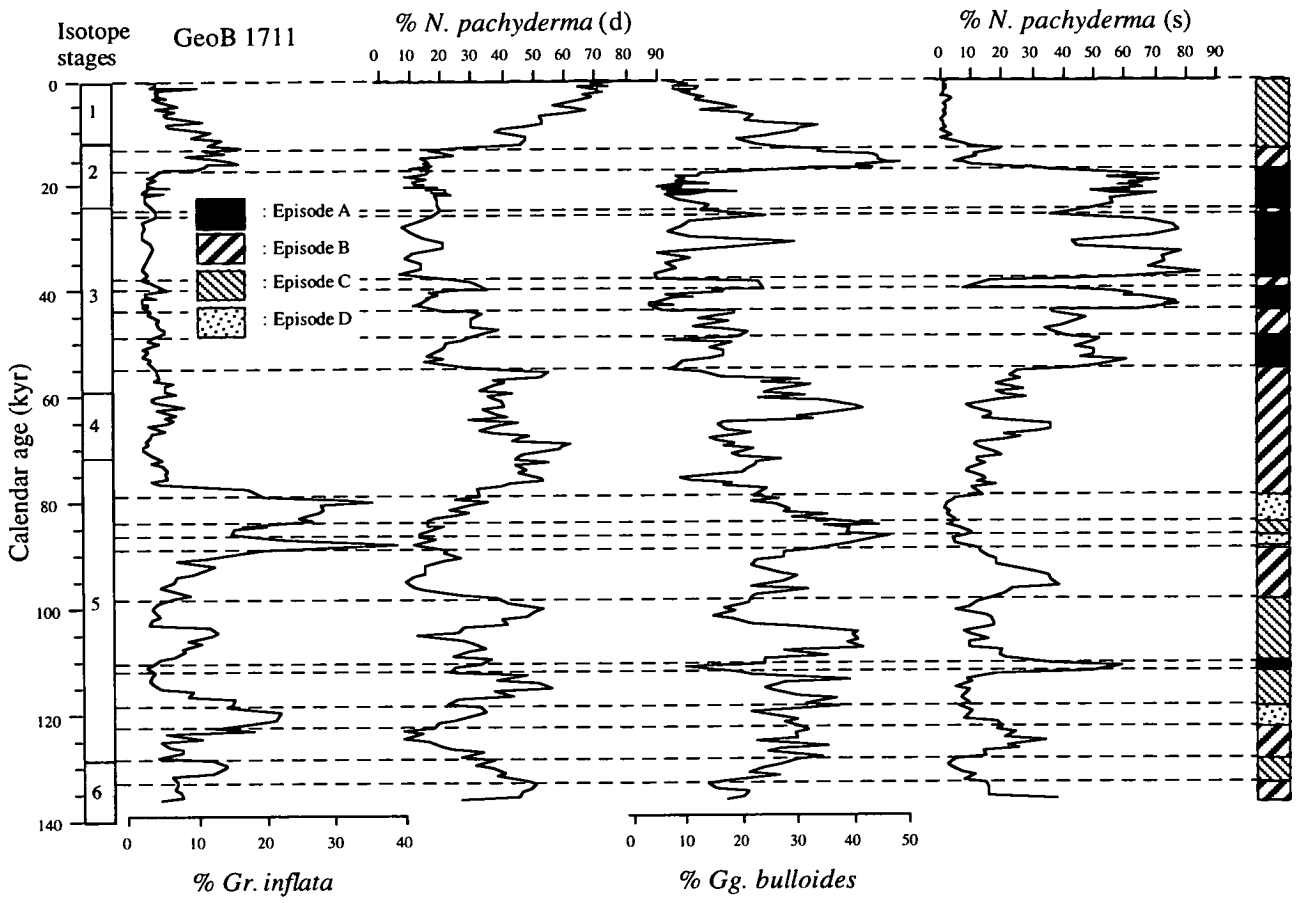

Figure 3.11. GeoB 1711. Fluctuations in the relative abundances of the four major species of planktonic foraminifera with age. Isotope stages are given on the left for reference, whilst a schematic reference for episode dominance is given on the right. Episode A: Dominance of *N. pachyderma* (s) > 40% over all others; Episode B: 20% each (or >) of *N. pachyderma* (s), *N. pachyderma* (d) and *Gg. bulloides* ; Episode C: Dominance of *N. pachyderma* (d) + *Gg. bulloides* both contributing to a total of ~80%; and, Episode D: *Gr. inflata* > 20%.

Previous investigations within the BCS have distinguished a good agreement with the distribution patterns of the planktonic foraminifera, nutrient levels and surface water hydrography (*Giraudeau,* 1993, *Ufkes and Zachariasse,* 1993, *Ufkes,* submitted). *Giraudeau et al.* (in prep.) found a similar pattern when they studied coccolith abundances in the same area. On the basis of factor analysis they correlated the abundances of coccolith species to the modern-day distribution of trophic areas.

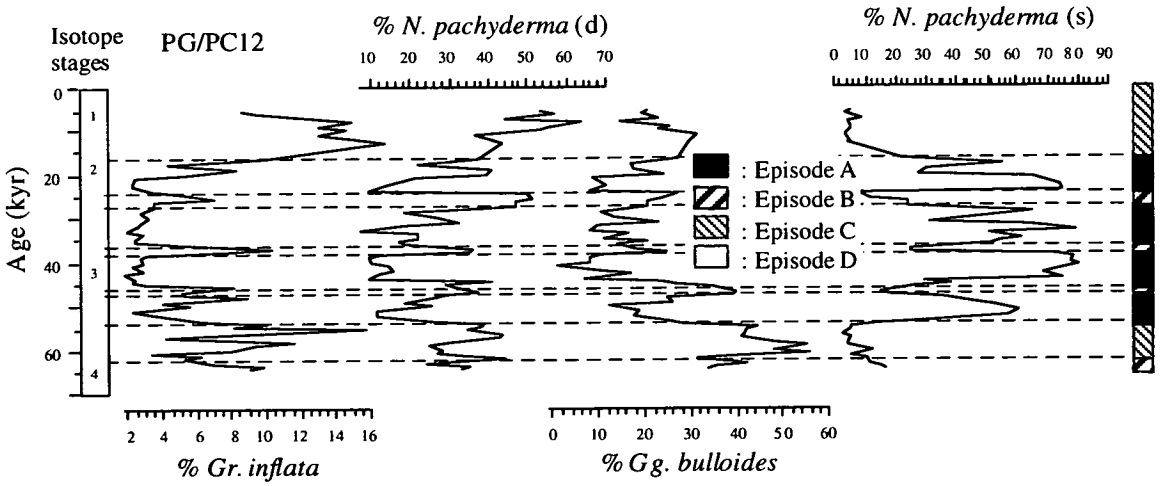

Figure 3.12. PG/PC12. Fluctuations in the relative abundances of the four major species of planktonic foraminifera with age. Isotope stages are given on the left for reference, whilst a schematic reference for episode dominance is given on the right. Episode A: Dominance of *N. pachyderma* (s) > 40% over all others; Episode B: 20% each (or >) of *N. pachyderma* (s), *N. pachyderma* (d) and *Gg. bulloides* ; Episode C: Dominance of *N. pachyderma* (d) + *Gg. bulloides* both contributing to a total of ~80%; and, Episode D: *Gr. inflata* > 20%.

A comparison of planktonic foraminifera (Figure 3.1) and coccolith distributions in Recent surface sediments (*Giraudeau,* 1993, *Giraudeau et al.,* 1993, *Giraudeau and Rogers,* 1994), reveals a striking similarity to the modern-day trophic-level distribution (Figure 3.2), indicating a relationship between foraminifera type/number and nutrient levels within the Benguela upwelling system, similar to other oceanic settings (*Reynolds and Thunnel*, 1985; *Kroon and Ganssen*, 1989; *Kroon*, 1991). The fossil assemblages are thus best interpreted with respect to a temporally varying nutrient availability or supply. Episodes type A and D infer eutrophic (high) and relatively oligotrophic (low) nutrient levels respectively, when the observed modern-day nutrient-foraminiferal relationship is applied. Eutrophic Episode A, would correlate with the trophic-situation presently occurring in the nearshore upwelling centres particularly intense off Lüderitz and further south in the SBR. The offshore, sub-tropical conditions of the SBR, would be representative of Episode D trophic levels. Episodes C and D would characterise intermediate, mesotrophic conditions, typical of the mixed zone offshore in the NBR and similar to the modern-day situation at the sites of GeoB 1706 and GeoB 1711. At the site of GeoB 1706, eutrophic conditions dominated the oceanographic setting during isotope sub-stage 6.4 and stages 3 and 2. At sites GeoB 1711 and PG/PC12, the planktonic foraminiferal record

similarly suggests upwelling conditions throughout stage 3 and into early stage 2. Both GeoB 1706 and GeoB1711 core sites record sub-tropical, relatively oligotrophic conditions dominating late stage 5.

3.7. Angola-Benguela Front migration, upwelling intensification or cold-water advection?

A fluctuation in nutrient supply could be explained by three different conditions within the BCS. Firstly, an increase in upwelling intensity, which would have the effect of widening the zone of *N. pachyderma* (s) displacing further offshore the boundary between eutrophic and mesotrophic water masses (Figure 3.2) and therefore the boundary between the dominance of *N. pachyderma* (s) and other species (Figure 3.1). Secondly, a physical shift of the ABF and corresponding trophic zones equatorwards, bringing increased nutrient levels to the north. Thirdly, a sporadic injection of cold, nutrient-rich water advecting from the Southern Ocean past Cape Town and along the eastern edge of the BCS. All of these conditions would be observed in the fossil record by a relative enhancement of the typical upwelling fauna, in particular *N. pachyderma* (s). An alternative hypothesis, an increase in the nutrient supply by poleward undercurrents from the Angola Basin, was postulated by *Summerhayes et al.* (1995a) and *Struck et al.* (1993) using the $\delta^{13}C$ record of the surface dweller *Gg. ruber*, although no firm evidence for nutrient enrichment from the north has been proven. Ideally, a record of deep currents would be obtained using a deeper dwelling organism, or a benthic species, as a surface water species will record productivity and temperatures from many different sources, however, unfortunately this what outside the scope and time of this research.

3.7.1. Temporal shifts of the Angola-Benguela Front

The distribution of planktonic foraminiferal zones is linked to the oceanographic regimes which are presently occurring off the southwest African coast. The coccoliths and planktonic foraminifera (*Giraudeau*, 1989) seem to be responding primarily to nutrient availability, and thus upwelling intensification and/or advection of Southern Ocean surface waters. *Jansen et al.* (1997) recorded high abundances of *N. pachyderma* (s), within the Angola Basin, with maximum abundances throughout the last 160 kyr, and a peak in abundance during early isotope stage 3. The variation in planktonic foraminiferal abundances, was correlated to physical shifts of the ABF,

using a foraminiferal transfer function, the Benguela index [BI=2/3 x left coiling + 1/3 x right coiling) *N. pachyderma*], to record latitudinal movements of the ABF. The ABF is recorded to vary in response to changes in the intensity and position of the South Atlantic anticyclonic gyre (SAAG) and the sub-tropical convergence (STC). An equatorwards deflection of the ABF would produce a shift of the more eutrophic areas [dominated by *N. pachyderma* (s)] to the north, whilst a poleward shift would decrease the relative nutrient supply at the Walvis Ridge by moving the upwelling centers south. In the extreme case, a large poleward displacement of the ABF as far as GeoB 1706 could be possible, extending the southerly intrusion of warm Angolan water onto the Walvis Ridge. If the whole Benguela upwelling system were to move with the ABF, we would predict maxima of *N. pachyderma* (s) in the NBR at times of equatorward shifts.

The Benguela index (BI; *Jansen et al.*, 1997) defines the timing of proposed shifts of the ABF from records in the Angola Basin. Records from the Cape Basin which include increased abundances of the cold-water species *N. pachyderma* (s) do not correlate well (Figure 9 in *Little et al.*, 1997a). The Benguela upwelling group [BUG = *N. pachyderma* (s) + *Gg. bulloides*] 'transfer function' (Figure 3.13) better describes the "true" shifts of the ABF either side of the front and takes into account the abundances of the upwelling species *Gg. bulloides*, which is found to dominate upwelling zones in warmer waters (e.g. Indian Ocean; *Brummer and Kroon,* 1988, *Kroon and Ganssen,* 1989, *Kroon et al.,* 1990). Indeed *Gg. bulloides* is always present in cores T89-32 (14°58.2'S 10°41.6'E; Figure 1.1), T89-24 (8°54.7' S 12°03.1' E) and GeoB 1008-3 which *Jansen et al.* (1997) used for their analysis, and it appears to fluctuate with *N. pachyderma* (s) at times of glacial cooling. However, both the BI and BUG transfer functions do not remove the glacial effect of increased upwelling intensity on the foraminiferal assemblages. The normalised BUG function (after removal of the 'best-fit' polynomial expression) gives a resultant upwelling intensity index which removes the long term glacial—interglacial trend superimposed on the upwelling variations, leaving perhaps a better guide to the actual ABF shifts (Figure 3.13).

A comparison between the temporal fluctuations of the ABF with the BI and BUG of GeoB 1711 is shown in Figure 3.14. Although all three *N. pachyderma* (s) records provide an excellent correlation with the timing of ABF shifts, the records for core GeoB 1711 show different amplitudes as a result of the high abundances of

N. pachyderma (s) in the Cape Basin. The fluctuations of the BI [6] for GeoB 1711 are directly comparable to similar peaks at 60—70 kyr in stage 4, and 45—50 kyr and 30—35 kyr in stage 3, as seen in T89-32 and T89-24 from the Angola Basin (*Jansen et al.*, 1997).

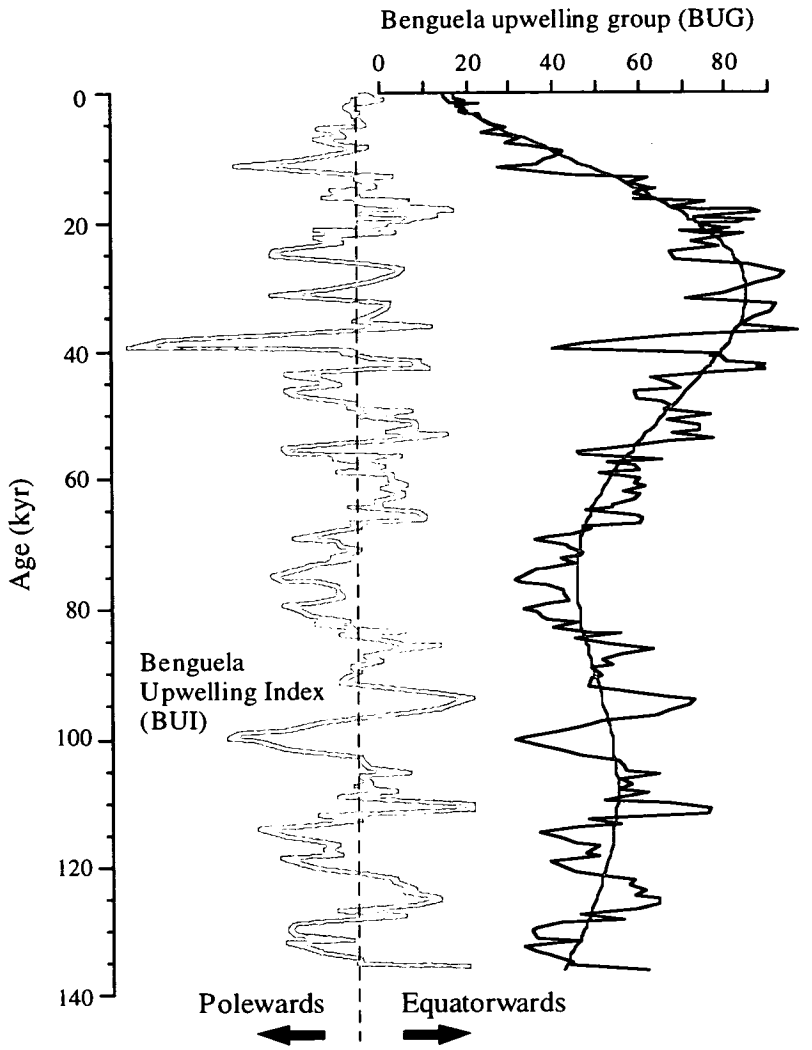

Figure 3.13. Benguela upwelling group (BUG) transfer function, polynomial expression and resultant Benguela upwelling index (BUI) for core GeoB 1711. BUI = BUG - 'best fit' sixth order polynomial expression for normalising the data and removing the long term glacial—interglacial trend.

[6] Benguela index (BI) is dominated by the abundance of *N. pachyderma* (s) and *N. pachyderma* (d) the two cold-water planktonic foraminifera in the Benguela system.
BI = (2/3 x left coiling + 1/3 x right coiling) *N. pachyderma* (*Jansen et al.*, 1997).

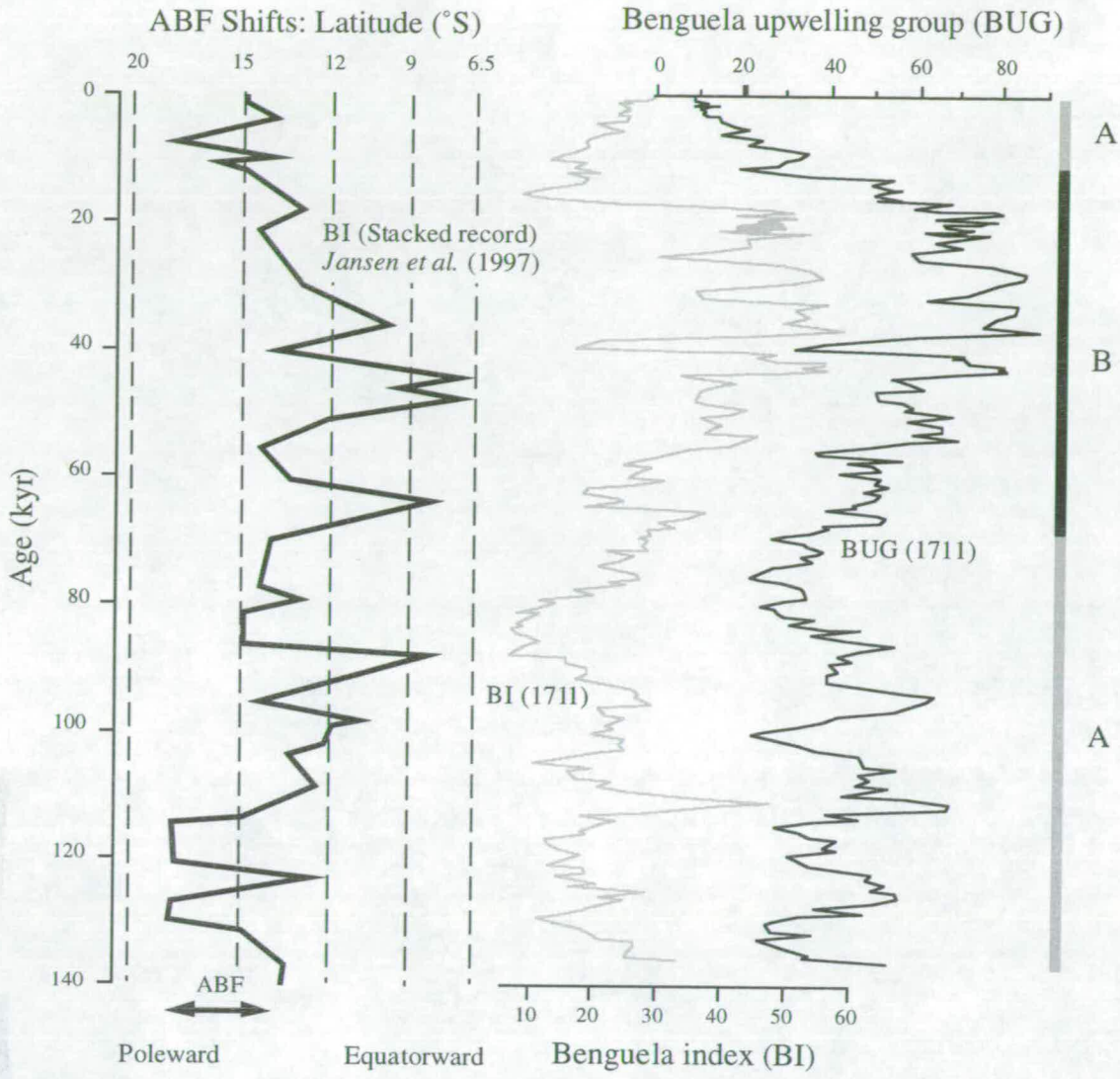

Figure 3.14. Comparison of the Benguela index (BI) 'transfer function' of *Jansen et al.* (1997) (left) with data from GeoB 1711 (right). The BI is used to assess relative N—S (equatorward—poleward) movements of the ABF, derived from *N. pachyderma* abundances in five cores from the Angola-Zaire margin. Periods of increased Cape Basin upwelling intensity (maxima in BUG) broadly coincide with the timing of equatorward shifts of the ABF. The time interval (A) is dominated by *Gg. bulloides* abundances when *N. pachyderma* (s) is relatively absent, and describes 'warmer' upwelling comparable to the northern side of the ABF, while interval (B) is dominated by *N. pachyderma* (s) and indicates 'cooler' upwelling comparable to the southern side of the ABF. The Benguela index is given as (2/3 x left coiling + 1/3 x right coiling) *N. pachyderma* (*Jansen et al.*, 1997). The BUG is given as (*N. pachyderma* (s) + *Gg. bulloides*).

Jansen et al. (1997) predict major equatorward shifts in isotope stage 4 and sub-stages 3.3—3.1, and maximum poleward shifts in isotope sub-stages 6.3, 5.5 and stage 1. In addition, the ABF record shows a similar position in late isotope stage 6—early stage 5 to that of the Holocene. These shifts are mirrored in the *N. pachyderma* (s) records of GeoB 1706 and GeoB 1711. The normalised BUG transfer function is thought to better represent the "true" shifts of the ABF without the influence from the glacial-interglacial trend. A good correlation exists between the suggested ABF shifts (*Jansen et al.*, 1997) and the upwelling index, and although there are differences, they are mainly related to discrepancies within the age models of the cores, particularly a small hiatus in core T89-32 during isotope sub-stage 5.2 which may 'correct' the anomaly at 100 kyr in GeoB 1711. GeoB 1706 records high abundances of *N. pachyderma* (s) in isotope sub-stage 6.4 correlating to an equatorward shift of the ABF not seen in the BI of the Angola Basin.

Alkenone-derived SST estimates (*Schneider et al.*, 1995; 1997, *Summerhayes et al.*, 1995b) indicate that the coolest period in the BCS and the Angola Basin is centred on the lower part of isotope stage 3, exactly when *N. pachyderma* (s) abundances are at their maximum (Figures 3.10, 3.11 and 3.12). *Jansen et al.* (1997) proposed the greatest equatorward shift of the ABF at this time based on a maximum of *N. pachyderma* (s) at site T89-32 (Figure 3.14). The implied temporal ABF movements are supported by a variety of data, primarily the general agreement of *N. pachyderma* (s) abundances, as seen in GeoB 1706, GeoB 1711 and PG/PC12, GeoB 1028 (*Schmidt,* 1992), DSDP 532 (*Oberhänsli,* 1991) and T89-32 (*Jansen et al.*, 1997), with alkenone-derived SSTs, which have been recorded by *Schneider et al.* (1995; 1997) and *Summerhayes et al.* (1995b). The seemingly anomalous, almost monospecific, assemblage at site GeoB 1706 in sub-stage 6.4, followed by a lack of *N. pachyderma* (s) in late stage 6, is corroborated by SST data from a core on the Angola Basin continental margin (GeoB 1016) with a corresponding cool sub-stage 6.4 and a warmer late stage 6 (*Schneider et al.*, 1995).

From cores on the Angola margin, the Walvis Ridge, the Congo fan and the equatorial Atlantic, *Schneider et al.* (1995; 1997), using alkenone-derived SSTs, indicated that the ABF has not shifted substantially in the last 200 kyr and has remained between 12°S and 20°S. *Jansen et al.* (1997), however, recorded high *N. pachyderma* (s) abundances in cores between 6.5°S and 20°S implying larger movements of the ABF. The difference between the two datasets may be related to the habitat of the

coccolithophores from which the alkenones and SSTs are derived. The alkenones, and therefore SSTs, are dependent upon the biogeographic limits of coccolithophorids (review by *Brassel,* 1993). The coccolithophores respond to averaged temperature changes within the watermass they inhabit, and often co-vary with the global glacial—interglacial regime (*Müller et al.*, in press, and others therein) and not directly with upwelling (*Ten Haven and Kroon,* 1991, *Emeis et al.,* 1995). *N. pachyderma* (s) in the BCS, however, is found in the cores of the upwelling cells (*Ufkes and Zachariasse,* 1993, *Ufkes,* submitted), and records the immediate, intensification of upwelling seemingly unaffected by the glacial—interglacial pattern. *N. pachyderma* (s) records the maximum fluctuations of the ABF, while the coccolith-derived SSTs are measuring the averaged effect of the upwelling cell fringes and global glacial—interglacial regime not the position of the upwelling cores themselves. Most likely it is the combined effect of the physical movement of the ABF and an increase in upwelling intensity which accounts for the planktonic foraminiferal variations seen in the Angola and Cape Basins.

3.7.2. Equatorward advection of sub-Antarctic surface water

Many of the previous studies in the BCS (*McIntyre et al.*, 1989; *Schneider et al.*, 1995; *Summerhayes et al.*, 1995b; *Jansen et al.*, 1997) have discussed advection of Southern Ocean surface or intermediate waters as a result of equatorward shifts of the sub-tropical convergence (STC). *Morley* (1989) and *Howard and Prell* (1992), studied the movements of the STC, situated to the south of Cape Town, marking the boundary between cold, polar-waters from the Southern Ocean and warmer waters of the South Atlantic. Using planktonic foraminiferal and radiolarian evidence from cores in the southern Indian Ocean, they recorded maximum poleward positions of the STC in isotope stages 11, 9, 5 and 1, while maximum equatorward positions in isotope stages 12, 10, 8, 6 and 4—2. The movements of the STC can be described by a two end-member system (Figure 3.15): a) maximum poleward position of the STC, permitting the largest pulses of Indian Ocean water entry into the Atlantic, which is accompanied by maximum equatorward heat advection into the BCS and the maximum poleward position of the ABF; and b) maximum equatorward position of the STC, limiting the amount of Agulhas Current advecting into the Atlantic by formation of a thermal barrier or gradient off Cape Town. This may, in extreme cases, allow an increase in cold-water advection from either the South Atlantic Surface Water (SASW)

or the Antarctic Intermediate Water (AAIW) below, without necessitating an unlikely shift of the polar front (*Shannon et al.*, 1989).

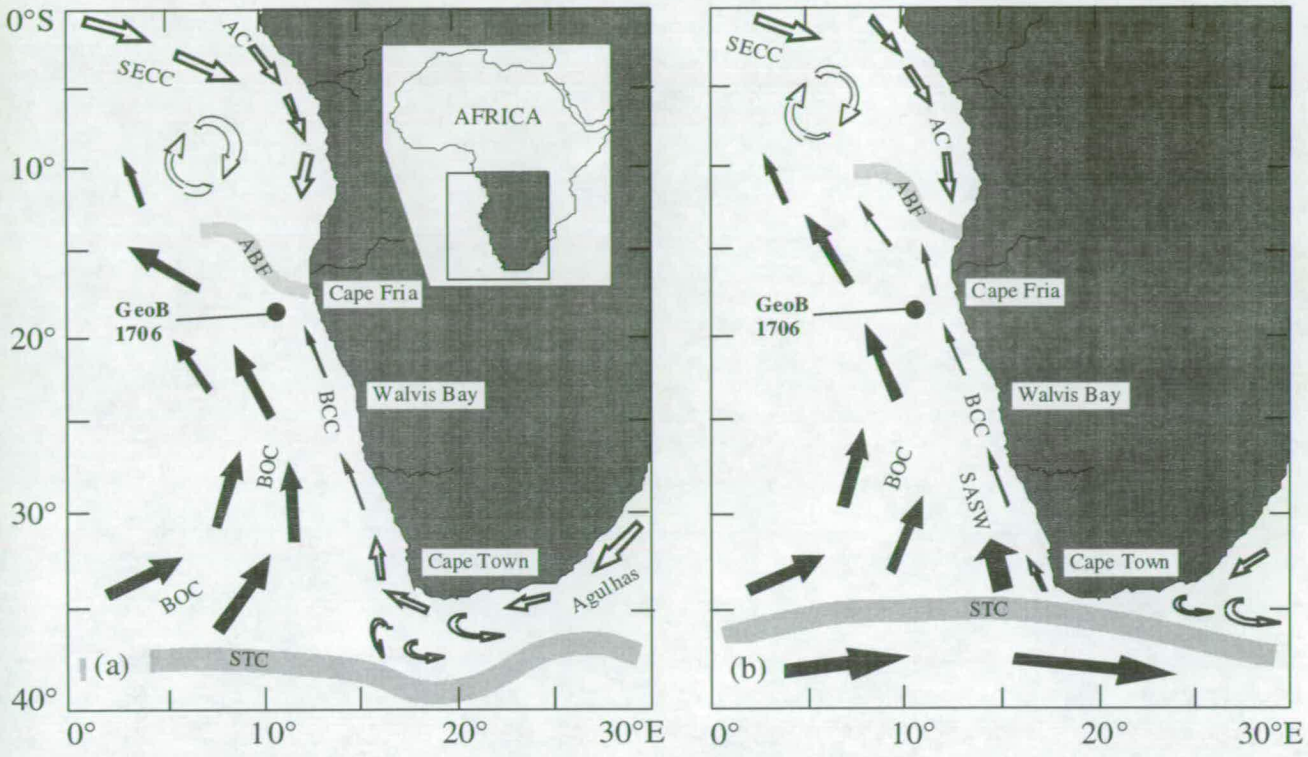

Figure 3.15. The movements of the STC can be described by a two end-member system: a) Interglacial, poleward position of the STC, permitting the largest pulses of Indian Ocean water entry into the Atlantic; and b) Glacial, equatorward position of the STC, limiting the amount of Agulhas Current advecting into the Atlantic by formation of a thermal barrier or gradient off Cape Town. Black arrows - cold currents, white arrows - warm currents. Size of arrows gives an indication of current strength.

However, although the timing of events links well with the shifting of the ABF, it still does not conclusively argue for or against advection from the Southern Ocean. For further evidence, planktonic foraminiferal or SST data from the SBR are needed to record equatorward heat flux around and past the Cape of Good Hope, via the Agulhas Retroflection.

3.7.3. Southern Benguela core material (Cruise M34-1: *Bleil and cruise participants*, 1996)

New core material and planktonic foraminiferal data were collected on the R/V METEOR cruise M34-1 (January 1996). On-board sampling and foraminiferal analysis yielded the first conclusive evidence against cold-water advection from the south. Seven cores were recovered from varying water depths along three transects covering the Cape Basin from Cape Point to the Walvis Ridge.

Core site (water depth, m) Listed north to south	Core position	Average abundance *N. pachyderma* (s)	Maximum abundance *N. pachyderma* (s)
GeoB 1706 (980)	19°33.7 11°10.5	29.38	81.76
GeoB 3608 (1972)	22°21,5 12°12,0	28.72	84.75
PG/PC12 (1017)	22°16,0 12°32,3	33.2	80.4
GeoB 1711 (1967)	23°18.9 12°22.6	25.90	84.2
GeoB 3606 (1785)	25°28,0 13°05,0	11.83	23.91 (38.60)
GeoB 3605 (1375)	31°26.7 15°17,8	6.04	21.28 (36.07)
GeoB 3604 (1514)	31°47,1 15°30,0	3.00	15.25
GeoB 3603 (2840)	35°07,5 17°32,6	0.85	4.00
GeoB 3602 (1885)	34°47,9 17°45,3	1.99	8.47 (21.54)

Table 3.3. Average and maximum relative abundances of *N. pachyderma* (s) for all cores analysed. Values for GeoB 3606, GeoB 3605 and GeoB 3602 are marked by single excursions (anomalies) to higher values; first number given is the second highest recorded abundance. Within the three most southerly (poleward) cores (GeoB 3602, GeoB 3603 and GeoB 3604), values of abundance only exceed 10% four times in 30 metres of core sampled. Note that average relative abundances are much lower in the southern reaches of the Cape Basin and that there is a positive trend to higher values equatorward into the northern Cape Basin.

The cold-water *N. pachyderma* (s) was found to be almost completely absent in continental-slope cores from 2000 and 3000 m off Cape Town for the last 200,000 years (Figure 3.16). No obvious sign of selective dissolution was observed, and the other planktonic forms typical of the SBR were in great abundance, with significant numbers of tropical spinose forms presumably intruding around the Cape from the Indian Ocean. Generally the southern Benguela cores recorded a very similar story to those of the northern Benguela. Marine sediments in the north are dominated by eutrophic and mesotrophic planktonic foraminifera largely due to the proximity of coastal upwelling cells and the overall character of a diffuse, filamentous mixing zone provides a wide area of nutrient availability.

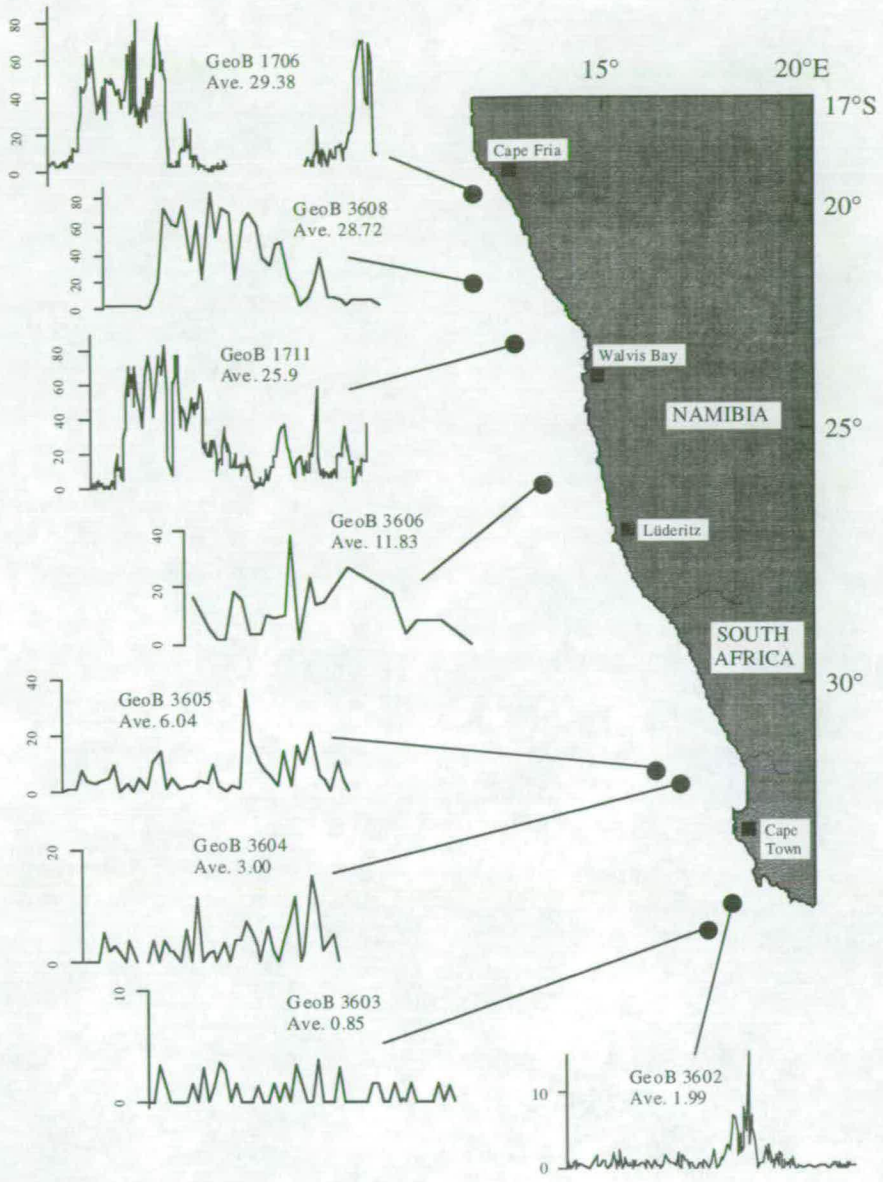

Figure 3.16. *N. pachyderma* (s) abundance records for GeoB 1706, GeoB 3608, GeoB 1711, GeoB 3606, GeoB 3605, GeoB 3604, GeoB 3603 and GeoB 3602 (given as % of total planktonic foraminifera). GeoB 1706, GeoB 1711 and GeoB 3602 are sampled at 5 cm intervals and have been dated and presented versus age (GeoB 1706, 0—160 kyr; GeoB 1711, 0—140 kyr; GeoB, 3602 0—520 kyr). The other cores have been sampled on-board, at a sample interval of 20 cm and have not been dated, and are thus presented versus depth. Core details are given in Table 1.1, average *N. pachyderma* (s) abundance is shown. Black circles indicate approximate core positions.

In the southern part of the Benguela system, sediment records record lower numbers of eutrophic species as the coastal upwelling is restricted to a narrow band with little

communication and mixing with the offshore sub-tropical waters. In this environment *Gr. inflata* dominates in both the modern-day setting and the fossil record, with additional numbers of sub-tropical and tropical planktonic foraminiferal species wrapping around with the Agulhas rings and eddies as the sub-tropical convergence (STC) is forced southwards by an expansion of the tropical Hadley cells.

Further information on the exact timing of abundance changes in the southern Cape Basin is not possible as stable oxygen-isotope age models have not yet been produced, and no ages assigned. However, GeoB 3608, located between the well dated cores GeoB 1706 and GeoB 1711, shows a very similar profile for *N. pachyderma* (s) abundances to those recorded in the cores either side, suggesting that this core passes into late stage 5 (core length 846 cm).

A trend to higher maxima and average values is clearly obvious in a traverse from the southern Cape Basin to the north (Table 3.3). If northward advection was to play a major role in the planktonic foraminiferal variations seen in the Benguela upwelling system, then we would almost certainly see the highest abundances of the cold-water *N. pachyderma* (s) in the south of the region, not the almost zero abundances actually recorded. We would therefore conclude that the ABF shifts described, are responding primarily to changes in upwelling intensity via fluctuations in the BCS.

3.7.4. Upwelling intensification via trade wind forcing

McIntyre et al. (1989) used planktonic foraminiferal estimates of SST to estimate seasonality in the equatorial Atlantic. Seasonality maxima, largest summer-winter temperature range, are recorded at similar times to greatest upwelling intensity in the BCS, and broadly coincide with the relative shifts of the ABF (*Jansen, et al.,* 1997). Trade wind zonality is strongly related to the seasonality at the equator (*Mix et al.*, 1986b; *Imbrie et al.*, 1989; *McIntyre et al.*, 1989; *Little et al.,* 1995; *Schneider et al.*, 1995; *Mix and Morey,* 1997), and also contributes to most of the SST, palaeoproductivity and palaeoceanography variations within the BCS (*Little et al.*, 1995; *Schneider et al.*, 1995; *Summerhayes et al.*, 1995b; *Jansen et al.*, 1997; *Mix and Morey,* 1997; *Schneider et al.*, 1997; in press). The records of GeoB 1706 and GeoB 1711 suggest intensification of upwelling in the northern Cape Basin coinciding with increased equatorial and Angola Basin upwelling, at times of increased trade wind intensity. There is no evidence in support of the advection of Southern Ocean water

across the STC, and equatorward heat advection, other than that from upwelling via the BCS, plays a minor if not insignificant role in equatorial and Angola Basin palaeoceanography. It is the injection of newly upwelled BCS waters, rather than advection of Southern Ocean water, which *McIntyre et al.* (1989) observed at the equator. The BCS is driven by atmospheric conditions controlling trade wind intensity and intensity over southwestern Africa (*McIntyre et al.*, 1989; *Schneider et al.*, 1995; 1997; *Mix and Morey*, 1997). Figure 3.17. shows a graphical representation of the hypothesised extremes of a meridional and zonal trade wind system.

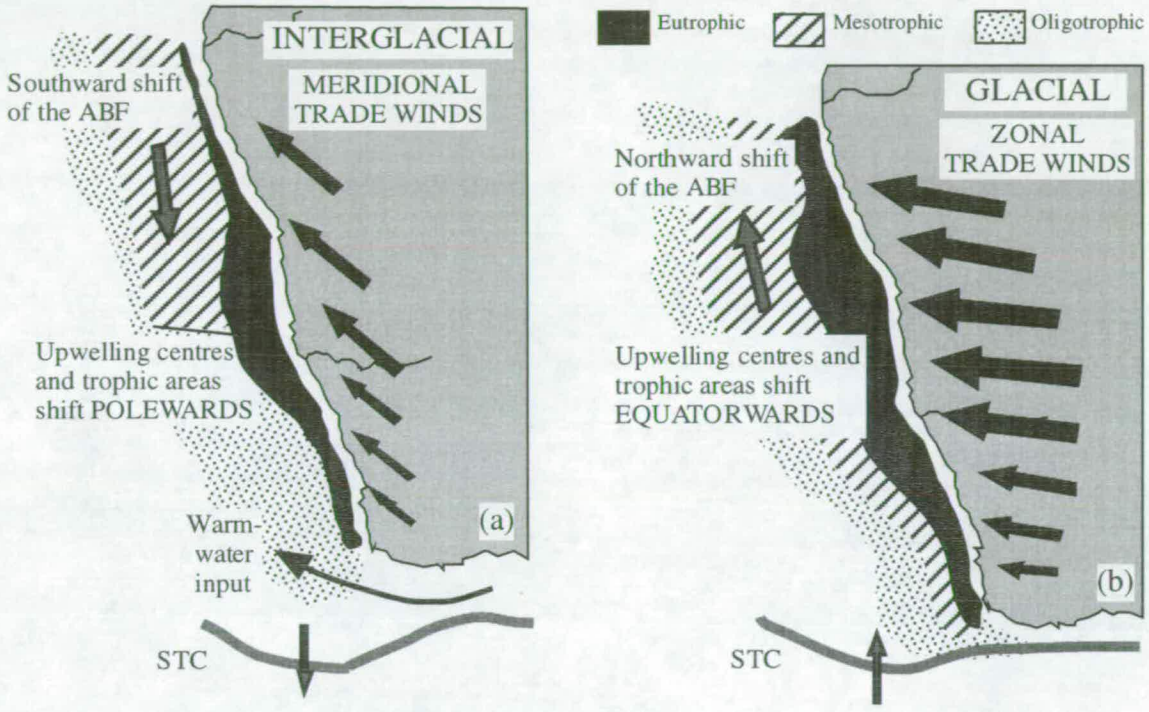

Figure 3.17. Sketch to show the hypothesised extremes of a dominant meridional (interglacial) and zonal (glacial) trade wind system on the hydrography and upwelling intensity of the Benguela upwelling system. Offshore hypothetical hydrographic situation resulting from trade wind intensity and direction modulation. Arrows indicate approximate net intensity and direction of trade winds. STC indicates approximate position of the sub-tropical convergence.

Times of maximum abundances of *N. pachyderma* (s), eutrophic-upwelling events, indicate maximum offshore divergence and associated upwelling intensity, at times of maximum trade wind intensity. This is recorded in the NBR sediment and planktonic foraminiferal record as a relative shift of the ABF equatorwards. During periods of trade wind intensity, the hydrography in the NBR will be similar to the modern-day situation offshore Lüderitz, upwelling will intensify, there will be more offshore

transport of cool, eutrophic waters and the area suitable for *N. pachyderma* (s) will expand. Inversely, periods of reduced trade wind intensity resulting from a net meridional wind direction will reduce the upwelling intensity in the NBR, although at these times the overall upwelling productivity will be reduced. In the sediment record this is recorded as a relative shift of the upwelling centres and the ABF polewards and the hydrography of the NBR will return to the present-day situation with a diffuse mixing zone suitable for mesotrophic faunas.

Summerhayes et al. (1995b) suggested that upwelling increased in stages 4 and 3, but declined into stage 2. This was attributed to an equatorward shift of the trade winds in stage 2, leading to a marked decrease in upwelling at site PG/PC12. However, the planktonic foraminiferal record of GeoB 1711, on the continental slope nearby to PG/PC12, indicates that upwelling off Walvis Bay was intense throughout isotope stage 3 into early stage 2, with a decrease of intensity, from 15 ka to the modern-day.

3.7.5. Timing of trade wind modulation

The exact timing and forcing by trade wind intensification will be discussed in greater detail and with respect to previous research and a global perspective in Chapter 5. However, the results of spectral analysis for GeoB 1711, GeoB 1706 and PG/PC12 (Figure 3.8 and 3.9), suggests discrete maxima occurring on sub-Milankovitch time scales (i.e. cyclicity on a higher frequency than 19—23 ka). In particular, the complete 140 kyr record for GeoB 1711, shows recurrent spectral power at the 8 kyr and 11—12 kyr periods, and the lack of significant spectral power in the precessional band which dominates low latitude climate and oceanographic change (*Imbrie et al.*, 1989, *McIntyre et al.*, 1989, *Mix and Morey*, 1997, *Schneider et al.*, 1995; 1997, in press).

N. pachyderma (s), the dominant species reflecting upwelling and hydrographic change in the Benguela system, shows coherent spectral density only at the 8 and 6 kyr periods and probably also at the ~12 kyr period, consistent with the other main species and the total sub-tropical species. In all cases the 8 kyr time period is within the 80% confidence interval. *Gg. bulloides*, also records coherent spectral power at the 8 kyr and ~12 kyr period, but also registers coherent spectra at the 23 kyr period. The additional spectra from the *Gg. bulloides* analysis, suggests that *Gg. bulloides* is responding to another factor influencing change in the Benguela system. The

discrepancy most likely relates to the species ecology, and in particular, each species distribution and relative temperature and nutrient requirements. From the sedimentary record (Figures 3.11, 3.12, 3.13), it is seen that *Gg. bulloides* is always in abundance greater than 10%, while *N. pachyderma* (s) is regularly at, or near, zero abundance. Periods of intense upwelling, which stimulate high nutrient levels and corresponding high abundance of *N. pachyderma* (s), occur predominantly in the SBR, and in particular offshore Lüderitz, in the modern setting (*Giraudeau et al.*, 1993; *Ufkes and Zachariasse*, 1993). The rapid fluctuations in *N. pachyderma* (s) abundance reflect the increased nutrient levels via advection of deeper upwelled waters, which occurs via trade wind intensification on an 8 kyr and 11—12 kyr periodicity, while *Gg. bulloides* fluctuates with background productivity levels, with trade wind changes superimposed.

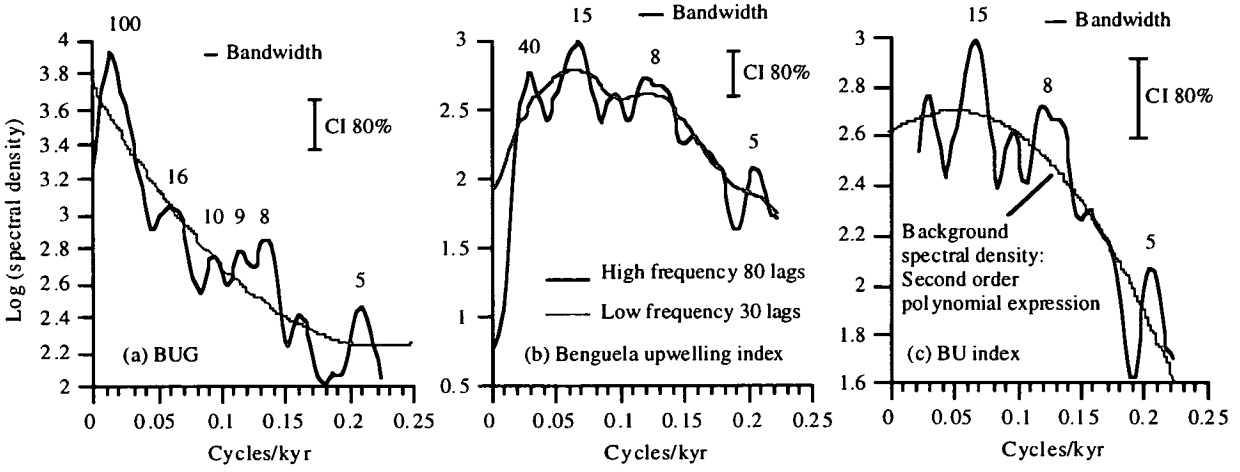

Figure 3.18. Spectral analysis of the Benguela upwelling index (BUI) and Benguela upwelling group (BUG) transfer functions. Spectral period analysed, 1—136 ka; Δt = 0.9 kyr; N = 151; CI is shown for 80 lags. In figure (a) and (c), a second order polynomial expression of the spectral density is shown for the background spectral periodicity, together with the lower limit error bar for the 80% confidence interval. In figure (b), a low resolution record is shown for comparison, as the polynomial would be biased against the high frequency spectra as a result of the missing 'red noise'. (c) Enlarged section from (b). Red noise part of the spectrum is removed, 100 kyr power is missing due to normalisation of the dataset.

From the record of GeoB 1711, the 23 kyr periodicity is clearly visible in interglacial stage 5 (Figure 3.11), at a time when *N. pachyderma* (s) is relatively absent from the sedimentary record, trade wind intensity is greatly reduced and the precessional

component of insolation is at its maximum amplitude (*McIntyre et al.,* 1989). At this time, warm-waters from the Angola Basin may accentuate the precessional signal in the Benguela system. Indeed, from core GeoB 1706 on the Walvis Ridge, coherent spectral power occurs in the precessional band from both the sub-tropical foraminifera and *Gg. bulloides*, consistent with visual inspection, of which both faunal records indicate a relatively warm-water signal compared to *N. pachyderma* (s).

Gg. bulloides, which dominates upwelling zones in environments with warmer sea-surface temperatures (for example the Indian Ocean and Arabian Sea: *Brummer and Kroon,* 1988, *Kroon and Ganssen,* 1989, *Kroon et al.,* 1990), is thought to record background productivity and upwelling changes in the absence of the intensity recorded in glacial periods by large *N. pachyderma* (s) abundances. The BUG transfer function and resultant upwelling index, incorporates the relatively warm-water and cold-water upwelling signals, *Gg. bulloides* and *N. pachyderma* (s) respectively, in an attempt to gain a better record of the shifts of the ABF and upwelling changes in the Benguela system. Spectral analysis of the BUG (unsmoothed) dataset shows coherent spectral density at the 100, 8 and 5 kyr periods, coherent with visual analysis of the record (Figure 3.14). Results for the BUI (smoothed with a 7 point weighted average), document spectral power at the 15, 8 and 5 kyr periods. In this instance, with the long term glacial—interglacial effect removed, the ~16 kyr frequency observed in the BUG spectral analysis is now coherent as is expected from visual inspection of the record (Figure 3.14 and 3.15). The results suggest that the relative ABF shifts and corresponding trade wind and upwelling intensity vary on an approximately 8 and 15 kyr periodicity.

Core GeoB 1711 provides a complete high resolution record for the last 140 kyr covering the entire last glacial period, at a time when the global climate was dominated by large ice sheets. At this time the external forcing from Milankovitch parameters was reduced as precession and eccentricity amplitudes decreased rapidly to a nadir within the last glacial. The results from GeoB 1711, GeoB 1706 and PG/PC12 suggest that sub-Milankovitch cyclicity dominates trade wind modulation during the relative absence of precessional forcing, which is at a maxima in interglacial stage 5 (*Berger*, 1978; *McIntyre and Molfino,* 1996). In Chapter 5, the timing of upwelling and trade wind intensification is compared to other records of rapid marine and climate variability to investigate the forcing mechanisms behind these short-lived, high frequency climate changes.

3.8. Summary

The planktonic foraminiferal records for GeoB 1706, GeoB 1711 and PG/PC12 illustrate that the abundance of the cold-water planktonic foraminifer, *N. pachyderma* (s), does not vary with the global glacial—interglacial pattern. Four species make up over 95% of the variation within the core, and enable the record to be divided into episodes characterised by specific planktonic foraminiferal assemblages, with meaningful ecological significance when compared to those of the modern-day. *N. pachyderma* (s), dominates the modern-day, coastal upwelling centres; *Gr. inflata* characterises the oligotrophic, offshore zone of the SBR; and together, *Gg. bulloides* and *N. pachyderma* (d) inhabit the mesotrophic areas of the mixed zone in the NBR. In the fossil record, the planktonic foraminifera are thought to be varying largely with changing nutrient supply, and the subsequent levels of primary productivity, according to local water hydrography and oceanography currently existing offshore Namibia and the west coast of South Africa. In cores GeoB 1706 and GeoB 1711, episodes of high *N. pachyderma* (s) abundances are interpreted as evidence of increased upwelling intensity, and the associated increase in nutrients. Periods of high *N. pachyderma* (s) abundance describe rapid, discrete events dominating isotope stages 3 and 2, the timing of which correlate to the temporal shifts of the Angola-Benguela Front, situated to the north of the Walvis Ridge. The physical movement of the ABF cannot be disassociated from the increase in upwelling intensity recorded in the fossil record. The absence of high abundances of *N. pachyderma* (s) from the continental slope of the southern Cape Basin, conclusively rules out Southern Ocean surface water advection.

Spectral analysis of the faunal records and Benguela upwelling index (BUI), demonstrates recurrent variability at the 8 kyr period, and relative intensification of upwelling, and the relative shifts of the ABF, on a 15 kyr period. Precessional climate forcing does not appear to influence the planktonic foraminifera inhabiting the Benguela Current system, or the relative shifts of the ABF. Upwelling intensification along the entire coast of western and southwestern Africa is generated by changes in the strength of the trade wind system, responding to similar shifts and intensity of the atmospheric and oceanic gyres controlling the position of the ABF.

Palaeoproductivity proxies in the Benguela upwelling system - *N. pachyderma* (s), benthic foraminifera and total organic carbon (TOC)

Ch.4.

Chapter 4. Palaeoproductivity proxies in the Benguela upwelling system - *N. pachyderma* (s), benthic foraminifera and total organic carbon (TOC)

4.1. Introduction

The biological productivity of the oceans is sensitive to changes in climate which can effect essential factors such as nutrient and light availability. In turn, ocean productivity may influence climate by regulating the partitioning of CO_2 between the atmosphere and ocean. Productivity fluctuations therefore, are important in providing feedbacks to the climate system. It is vital that we gain an understanding of the 'biological pump' which pulls carbon out of the surface waters and buries it at depth, essentially removing it from the carbon cycle. The efficiency of the pump depends largely on the biological removal and associated downward transport and burial of organic matter. Favourable sites for organic carbon removal and burial are on the upper continental slope, for several reasons: (1) the coastal setting results in high, pulsating productivity; (2) the shelf can supply additional carbon; and (3) settling and decomposition in the water column are of short duration and as a result a higher percentage of the carbon is buried. Several proxies have been used with a certain degree of success in identifying the dynamics of palaeoproductivity. Total organic carbon (TOC) content and variation of $\delta^{13}C$ of carbonate with time have proved the most useful techniques, but more recently transfer equations for reconstructing palaeoproductivity based on the deep-sea sediment record of planktonic foraminifera (overview by *Sarnthein et al.,* 1992) have been used to supplement and support organic carbon measurements. Following the studies of *Müller and Suess* (1979) and *Suess* (1980), workers have based productivity estimates on the rates of organic carbon accumulation (*Sarnthein et al.*, 1987; *Sarnthein et al.*, 1988; *Lyle et al.*, 1988; *Lyle,* 1988), the accumulation rates of siliceous fossils (*Abrantes*, 1991; *Lyle et al.,* 1988), the faunal composition of planktonic foraminifers and comparison with carbon-based evidence (*Mix,* 1989b; *Giraudeau*, in prep.), and from the benthic/planktonic foraminifera ratio (*Berger and Diester-Haass,* 1988).

Upwelling areas are regions of high primary productivity with a high input of planktonic skeletal material and organic matter to the underlying sea floor. These regions play a crucial role in controlling the oceanic carbon budget and atmospheric CO_2 level (*Sarnthein et al.,* 1988). The Benguela upwelling system is no exception to

this rule. Upwelled water is relatively enriched in nutrients and cooler than the displaced surface water (*Dingle*, 1995), and the sediments accumulating beneath the upwelling cells are dominated by an organic- and diatom-rich mud, containing up to 22% organic carbon (*Calvert and Price*, 1971). The bottom sediments may also be organic-rich largely as a result of oxygen-poor bottom waters adversely affecting the benthos and preserving the organic carbon. However, below the oxygen-minimum zone the life conditions for benthos are greatly improved, as a consequence of high plankton production, and as a result large numbers of benthic foraminifera thrive. Both planktonic and benthic foraminifers favour upwelling-influenced regions. However, when the ratio of planktonic to benthic foraminifers is taken, one can see that benthic foraminifers increase more than planktonic foraminifers in fertile regions (for example N.W. Africa; *Diester-Haass*, 1978). The association with benthic foraminifers and high levels of primary productivity could be a useful tool for measuring past palaeoproductivity in coastal upwelling areas.

The carbon cycle is a very complex system, but one of the major interactions is the utilisation of CO_2 in the photic zone by marine phytoplankton. Photosynthesis, and the export of organic carbon from the surface waters of the ocean as either particulate or dissolved organic carbon, acts as a 'biological pump' which lowers the partial pressure of CO_2 in the photic zone (*Berger et al.*, 1989). Removal of carbon from the ocean-atmosphere system buried in marine sediments, although only accounting for a small fraction of the carbon in the global cycle, may reflect natural variations in the concentration of atmospheric CO_2. Upwelling areas cover only a small portion of the ocean's surface, however they account for at least 10% of the total oceanic productivity (*Berger et al.*, 1989) which is reflected in the TOC records of sediments at upwelling margins.

Organic carbon contents are commonly used as a proxy for palaeoproductivity in upwelling areas (*Müller and Suess*, 1979; *Sarnthein et al.*, 1987; 1988; 1992; *Berger et al*, 1989; *Summerhayes et al.*, 1995b). Recent studies have concentrated on mapping the variation with respect to changing upwelling intensity and primary productivity levels (*Schneider et al.*, 1994; 1995; *Summerhayes et al.*, 1995b; *Rutsch et al.*, 1995; *Schmiedl*, 1995). Organic carbon variability within the water column, is largely controlled by nutrient availability and primary productivity levels, which in turn is related to the remineralisation of organic matter in surface sediments. The debate as to whether past TOC records are a true representation of palaeoproductivity,

or are an artefact of preservation, diagenesis, erosion and re-suspension from bottom currents, and/or dilution from terrigenous debris from the neighbouring continent, will not easily be resolved.

The two main aims of this chapter are: (1) to assess the relative use of planktonic foraminifera, total organic carbon (TOC) content, and the benthic/planktonic foraminifera (B/P) ratio, as proxies for palaeoproductivity in the Bengela upwelling system; and (2) to examine the TOC signatures for evidence of sub-Milankovitch variability as is observed in the planktonic foraminiferal records, in the hope that this will provide a quick method for high-resolution analysis in other high productivity areas effected by rapid climate and oceanic instability.

4.2. Materials and methods

For the determination of TOC content, 100 mg aliquots of freeze-dried sediment samples were weighed in ceramic crucibles, wetted with a few drops of ethanol to suppress foaming during acidification, decalcified by addition of 6 M HCL, and dried on a hot plate at about 80°C. TOC was then determined by combustion in a LECO C/S-244 Elemental Analyser. The relative precision of the measurements, based on replicates and control analyses of lab-internal reference sediments, was better than 3%. TOC measurements have kindly been provided by Peter Müller, Fachbereich Geowissenshaften, Bremen University, Germany.

4.3. Changes in the benthic/planktonic foraminiferal ratio

Benthic foraminifera and the $\delta^{13}C$ signal of their tests, have long been used to reconstruct water depth, salinity, nutrient supply, and deep ocean circulation, but are now used more and more as palaeoproductivity indicators (*Altenbach*, 1985; *Lutze et al.*, 1986; *Berger and Diester-Haass*, 1988; *Berger and Wefer,* 1988; *Altenbach*, 1989; *Herguera and Berger,* 1991; *Berger and Herguera*, 1992; *Berger et al.,* 1994), including the relative abundance of benthic to planktonic foraminifera (*Diester-Haass*, 1978; *Lutze*, 1980; *Berger and Diester-Haass*, 1988). Many examples from modern and ancient settings demonstrate that high accumulation rates of organic matter on the seafloor underlie regions of high primary productivity, and are demarcated by high abundances of benthic foraminifera (*Lutze and Coulbourn*, 1984; *van Leeuwen*, 1989). The rapid change in the fallout of organic carbon as a result of productivity

changes, both spatially and temporally, appears to be the primary cause for fluctuations of benthic foraminiferal numbers off northwest Africa (*Altenbach and Sarnthein*, 1989). The abundances of benthic foraminifera, record spatial and temporal changes of the fertility in the surface waters, governed largely by the expansion of the region of upwelling productivity and carbon flux (*Lutze et al.*, 1986).

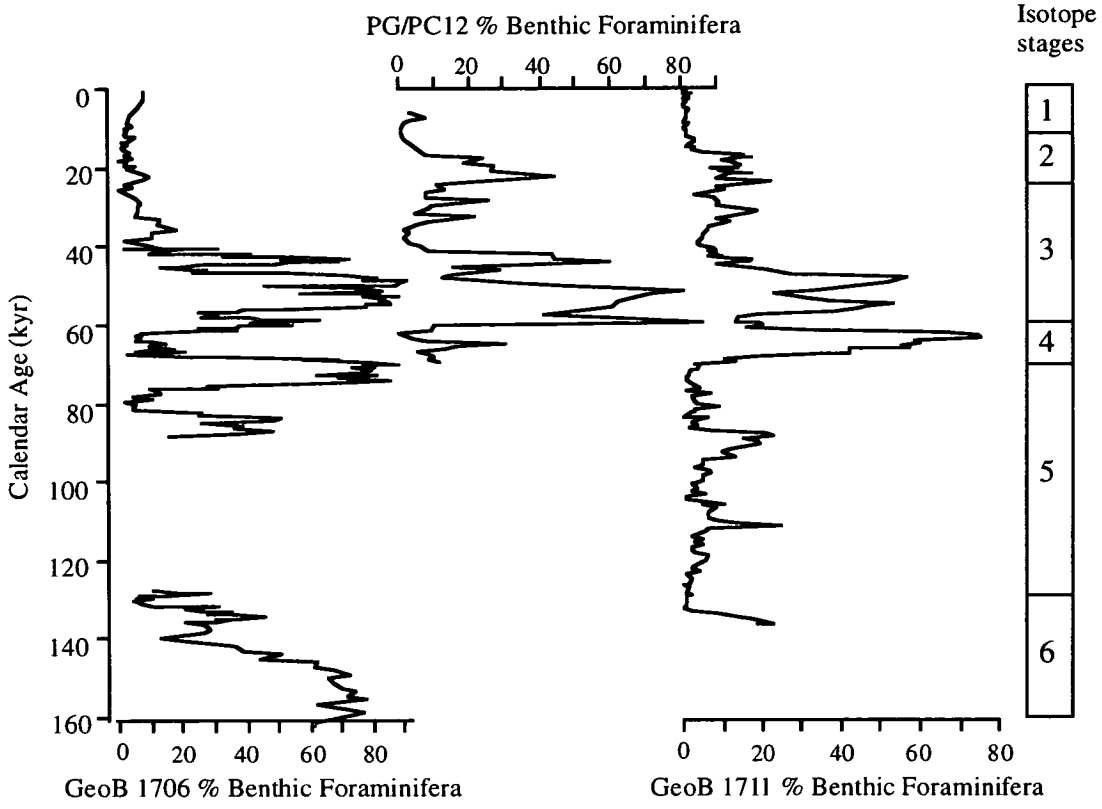

Figure 4.1. Benthic/planktonic foraminiferal ratios for GeoB 1706, PG/PC12 and GeoB 1711. % Benthic foraminifera indicates, the percentage of benthic foraminifera of the total foraminifera (planktonics + benthics).

Berger and Diester-Haass (1980) found that the abundance of benthic foraminifera, relative to planktonic foraminifera (B/P ratio), is governed by the supply of food to the sea floor, which is a function of depth and proximity to the shelf. On the continental margin off northwest Africa the B/P ratio is a useful guide to palaeoproductivity, and a useful tool to qualitatively, if not quantitatively, measure the amount of organic matter delivered to the seafloor. The three records of benthic foraminiferal relative abundance from the northern Cape Basin (Figure 4.1), although showing differences, all have maxima (up to 90% benthic foraminifera) in the period late isotope stage 5—early

isotope stage 3. All three records show very rapid changes in the benthic/planktonic ratio of over 80% in less than 1—2 ka, presumed to be reflecting total palaeoproductivity.

The geographical position of the three cores may account for the variations in exact timing of change in the B/P ratio. GeoB 1706, situated on the Walvis Ridge in the north of the Benguela system, records sustained maxima during isotope stage 6, late stage 5, early stage 4, and a prolonged although variable maximum throughout early to mid stage 3. GeoB 1706 does not record a relative change in the B/P ratio after 40 ka. GeoB 1711 and PG/PC12, with core sites located on the continental slope off Namibia, record corresponding maxima in stage 4, early—mid stage 3, and also late stage 3 to mid stage 2. GeoB 1711, with the only complete record of oxygen isotope stage 5, records maxima during isotope sub-stages 5.4 and 5.2, although somewhat reduced relative to the maxima recorded later in stages 4 and 3.

4.4. Total organic carbon (TOC) variability

Upwelling, high productivity, and the low oxygen content in bottom waters, control the distribution and quantity of organic matter in the sediments of the Benguela system. Also, as off California, faecal pellets play a major role in the sedimentation of organic matter (*Summerhayes*, 1983), which is clear from the high numbers of faecal pellets preserved in the sediments. As described previously in section 1.6, the highest TOC abundance in Recent sediments is recorded in the diatom ooze on the inner shelf between Lüderitz and the Kunene River (*Calvert and Price,* 1971).

Figure 4.2 shows the modern-day distribution of TOC on the continental shelf and slope of southwest Africa, with the highest TOC measurements in the diatom mud belt (*Summerhayes et al.,* 1983). Slope sediments from beneath the offshore divergence belt are enriched in TOC at water depths of 500—1500 m, almost certainly as a result of shelf edge upwelling. Abundances of TOC are much greater in the northern Benguela region (NBR) than the southern (SBR), as a direct result of prolonged, year-round, intense upwelling rather than the seasonal, although more intense, upwelling in the south. The region inshore of the orange river is also effected by dilution from terrigenous supplies further enhancing the differences between the NBR and the SBR. Piston cores from the continental slope, show that the NBR is consistently rich in

organic matter in water depths down to 2000 m (*Bremner,* 1983, *Summerhayes,* 1983, *Diester-Haass,* 1985, *Summerhayes et al.,* 1995b).

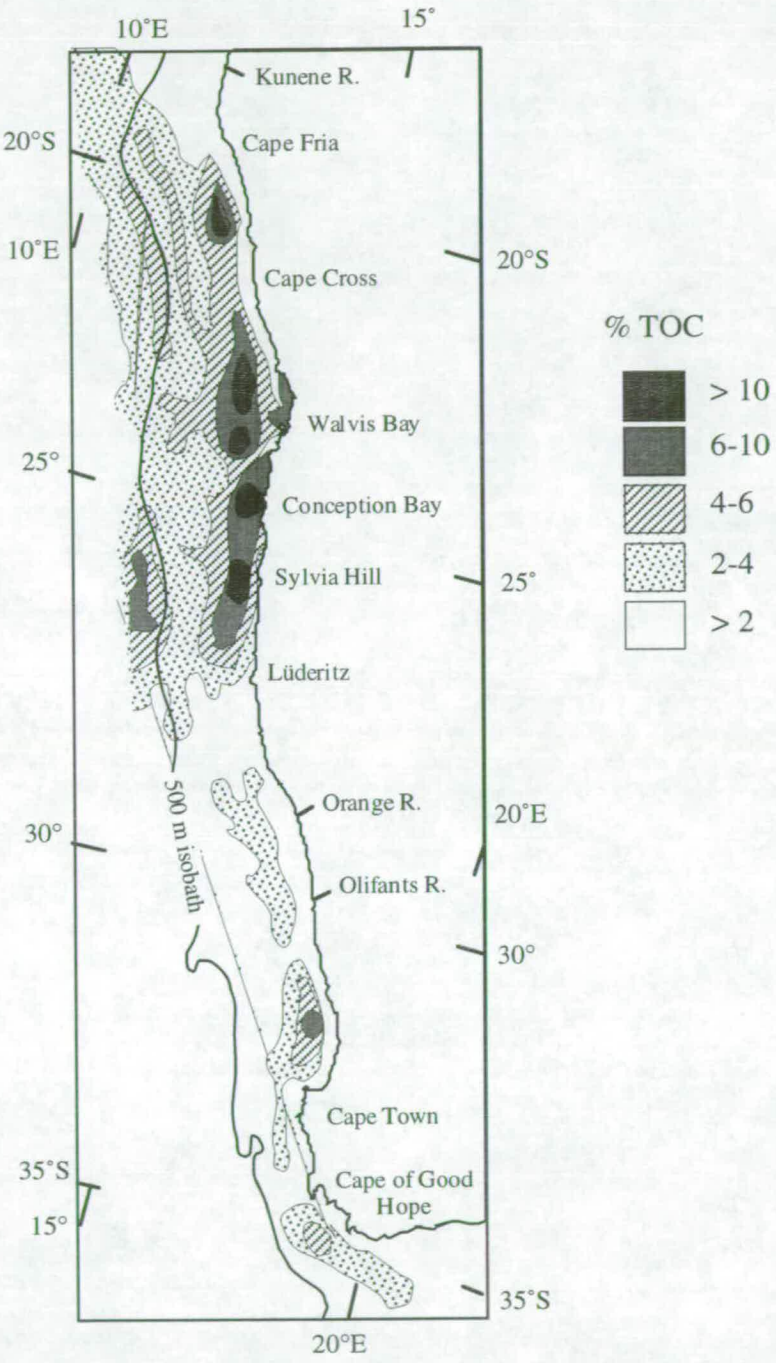

Figure 4.2. Distribution of TOC on the continental shelf and slope of southwest Africa. Adapted from *Summerhayes* (1983). Shelf edge is approximately at the 500 m isobath (dark line).

Almost all of the organic matter in samples from the continental slope and shelf off southwest Africa is amorphous, bacterially degraded, marine material, typical of high phytoplankton production (*Bremner,* 1983). The three cores treated in this study were recovered from two geographically distinct areas. GeoB 1706 was collected from a water depth of 1000 m on the Walvis Ridge, whilst PG/PC12 and GeoB 1711 were collected from the Namibian continental slope from water depths of 1000 and 2000 m respectively. Although still beneath the active upwelling system, the Walvis Ridge acts as a natural barrier for mixing between the Angola and Cape Basins. GeoB 1711, the deepest and farthest offshore, records the extreme limits of the Benguela upwelling (Chapter 3) and may be the key to separating local and regional productivity effects.

4.4.1. Productivity record from GeoB 1706

The following is an assessment of the productivity records from GeoB 1706, PG/PC12, and GeoB 1711, comparing the organic carbon record with the upwelling indicator, *N. pachyderma* (s), and the B/P ratio. The history of upwelling intensity given by the planktonic foraminifer *N. pachyderma* (s) largely correlates with the TOC content within the sediments, especially within the last 80 ka (Figure 4.3.). The abundance of benthic foraminifera has a relatively good correlation with TOC content before 60 ka, as would be expected if both were recording palaeoproductivity as previous workers have suggested, but after 60 ka the direct positive correlation breaks down.

The TOC/*N. pachyderma* (s) correlation suggests additional input of TOC not directly related to upwelling intensity, if *N. pachyderma* (s) is recording the total upwelling input, at four intervals in the last 160 kyr (not including the hiatus, 125—90 ka): 150—140 ka; 140—130 ka; 90—80 ka and 50—38 ka. At these times TOC content is greater than would be expected given the *N. pachyderma* (s) abundances alone. Interestingly, in the intervals before 60 ka, the B/P ratio is high, probably as a result of the increased TOC delivered to the sea floor, but suggesting that overall productivity is higher than expected. Although *N. pachyderma* (s) is not a useful indicator of productivity for all of the last 140 kyr due to its relative absence in the warm interglacials, it is perhaps the best productivity indicator overall. At times when *N. pachyderma* (s) is low in abundance, different species of planktonic foraminifera e.g. *Gg. bulloides*, or indeed other primary and secondary producers, may account for the change in TOC content within the sediments. The discrepancies could also be

accounted for by changes lower in the food chain for example; and abundance of diatoms instead of coccoliths as the primary producers varying the habitat for grazers.

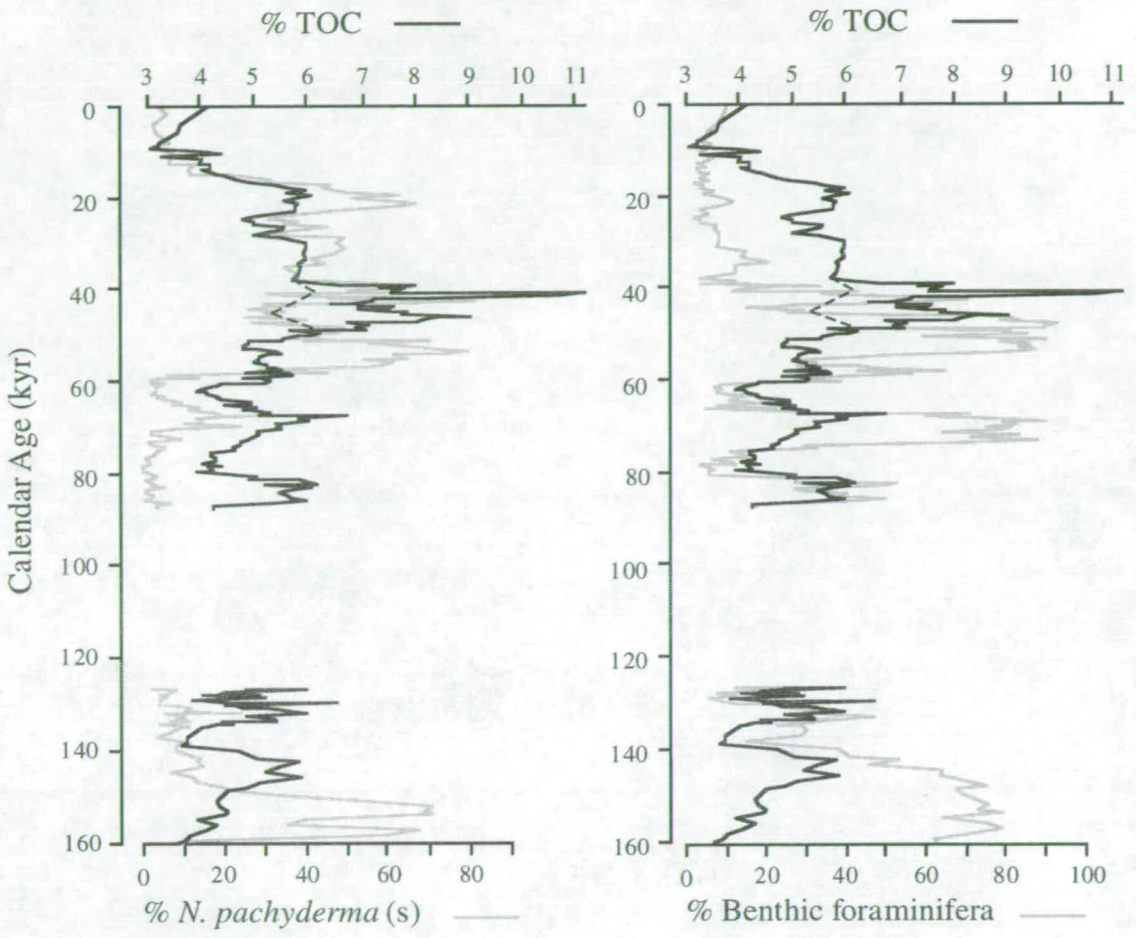

Figure 4.3. GeoB 1706: Total organic carbon (TOC) as a percentage of the total sediment (wt %) (black line) with % *N. pachyderma* (s), as a percentage of the total planktonic foraminifera, and % benthic foraminifera, as a percentage of the total foraminifera (benthics + planktonics). For the interval 50—40 ka a dashed line links the TOC curve either side of the 'anomalous' TOC content (see discussion in text).

The 50—38 ka peak of TOC is 'anomalous' however, and is not accounted for by increased abundances of benthic foraminifera or with any other planktonic foraminiferal proxy (Figure 3.3). This will be discussed later in connection with the TOC record from PG/PC12. Disregarding the 'anomalous' peak of TOC and assuming that it did not pass its ceiling value of 6%, which is maintained throughout the previous 110 ka, then an excellent correlation exists between TOC content and *N. pachyderma* (s) abundances for the last glacial—interglacial cycle, where

N. pachyderma (s) dominates the surface waters in abundances up to 80% of the total planktonic foraminifera. Before the last glacial there is a good positive correlation between TOC and benthic foraminifera, particularly in the intervals 140—130 ka and 90—80 ka. The relationship between all three productivity proxies at the base of the core is not understood. Maxima in both B/P ratio and *N. pachyderma* (s) abundance at this time, suggests an interval of intense upwelling and productivity and therefore an increased deposition of organic carbon should be expected. However, although organic carbon levels reach a maximum at 145 ka, they do not record a maximum at the peak of upwelling intensity at 160—150 ka.

The *N. pachyderma* (s) abundances suggest that during the last glacial period when the Walvis Ridge was a site of intense upwelling, the greatest contributor to the TOC record was upwelling induced productivity. At times when the upwelling intensity was reduced, i.e. before 80 ka, the TOC record is primarily correlated to the B/P ratio, suggesting a site of reduced upwelling intensity with more oxygen available at the sediment-water interface suitable for benthic activity and increased numbers of benthic foraminifera. This 'switch' does not seem to have been an immediate process. Benthic foraminiferal abundances are high within the period of intense upwelling, 40—60 ka, although there is not a good positive correlation with either TOC or *N. pachyderma* (s) abundances. Possibly oxygen-rich bottom waters still provided a suitable environment for benthos. At present the benthic foraminiferal record for the Walvis Ridge is poorly understood, the *N. pachyderma* (s) abundances seem to correlate to the TOC content of the sediments when *N. pachyderma* (s), and therefore upwelling intensity, are greatest, but other than recording the relationship of the B/P ratio, no firm conclusion can be made. A full assessment of individual benthic foraminiferal components, as undertaken by *van Leeuwen* (1989; Angola Basin), could probably extrapolate the relationships further.

4.4.2. Productivity record from PG/PC12

PG/PC12, from a water depth of 1000 m inshore of core GeoB 1711 on the continental slope offshore Namibia, records a higher average TOC content than GeoB 1706. TOC is abundant in PG/PC12, ranging from 4% near the core-top to 10% in the interval 50—40 ka in isotope stage 3. The core-top values reflect those of the modern slope sediments (Figure 4.2.), while the maximum down-core, approach those values found in muds from the inner shelf upwelling area (*Bremner*, 1981;

Summerhayes et al., 1995b; Figure 4.2.). As at core site GeoB 1706, during the last 70 ka the TOC variation is largely governed by production relating to fluctuations in upwelling intensity, indicated by the abundance of *N. pachyderma* (s). However, there are seeming anomalies, although some of these may just relate to increased abundance of other upwelling species e.g. *Gg. bulloides*, at the expense of *N. pachyderma* (s). The increased TOC content in the period 50—38 ka seen in GeoB 1706, is also present in the TOC record for PG/PC12, and in the TOC record, although less pronounced, for GeoB 1711 (Figure 4.5).

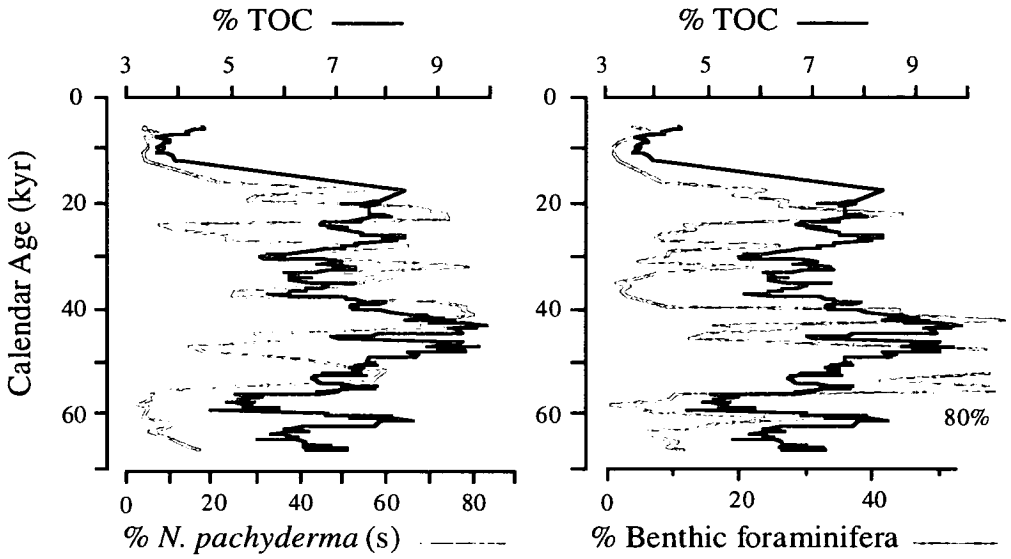

Figure 4.4. PG/PC12: Total organic carbon (TOC) as a percentage of the total sediment (wt %) (black line) with % *N. pachyderma* (s), as a percentage of the total planktonic foraminifera, and % benthic foraminifera, as a percentage of the total foraminifera (benthics + planktonics)..

The main sources of organic matter on the slope would have been deposition from: (1) the shelf edge upwelling system; (2) intensification and enlargement of the inner shelf upwelling cells, bringing primary and secondary production seawards; (3) periodic input from filaments and offshore currents; and (4) an increased rate of supply from the addition of re-suspended organic-rich muds from the inner shelf, by tidal or bottom currents. A net increase in production and/or re-suspension of organic material would enhance the accumulation of TOC further offshore. *N. pachyderma* (s) abundances from GeoB 1706, PG/PC12 and GeoB 1711 indicate that upwelling intensity had already increased to its maximum levels, and did not increase further during the glacial period. With the present data available, this would suggest that the increased accumulation of organic carbon during mid-isotope stage 3 (~ 50 ka) is

primarily a result of re-suspension and offshore deposition of organic material removed from the inner shelf high productivity belt. The use of *N. pachyderma* (s) as the upwelling productivity signal, is an attempt to remove the upwelling derived TOC signature, from the re-suspended TOC signal.

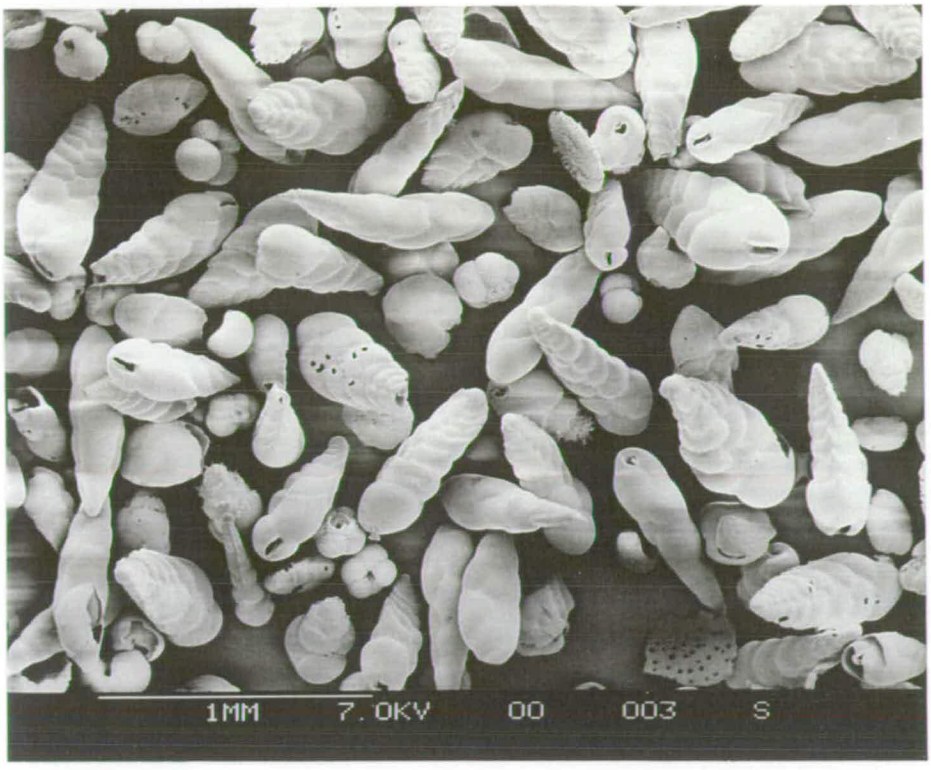

Plate 4.1. Scanning electron micrograph from a 'benthic productivity event" (high B/P ratio). Bolivinids largely dominate the assemblage. Note the presence of left coiling *N. pachyderma*. Sample taken from isotope stage 3, GeoB 1711.

The record for benthic foraminifera (B/P ratio), does to a large extent follow the productivity from upwelling intensity, as indicated by *N. pachyderma* (s). The benthos are responding to increased food supply when upwelling at the surface provides cool, nutrient-rich waters suitable for primary productivity. Interestingly, the B/P ratio records two pronounced maxima in benthic foraminifera during 60—40 ka, certainly related to the timing of intense upwelling, but with abundances twice what they are in later intense upwelling episodes in late stage 3 and stage 2. As before, a similar 'anomaly' is observed in GeoB 1706 and also in GeoB 1711. What is certain is that there was a benthic productivity event at approximately this time recorded throughout the northern Cape Basin from 1000 m water depth on the Walvis Ridge to 2000 m water depth offshore Namibia. GeoB 1706 records two other related benthic

productivity events, seemingly not related to the surface water hydrography, during 160—140 ka and 80—65 ka. At present there is not an unequivocable answer to these benthic events, possibly they relate to changes in the supply of oxygen-rich sub-surface waters not just to upwelling intensity alone. Nutrient-rich water from a poleward undercurrent is an option, possibly with an origin in the Angola Basin, as previous authors have suggested (*Hart and Currie*, 1960; *Shannon*, 1985; *Chapman and Shannon*, 1985; *Dingle and Nelson*, 1993). This is likely to be oxygen-poor and may not sustain a large benthos. It is also possible that a nutrient- and oxygen-rich Antarctic water mass could influence the Benguela shelf and slope at this time, providing a more suitable environment for a rich benthos. It is reasonable to suggest that the species-type may be of importance to each of these benthic 'blooms'. Largely bolivinids dominate the assemblages (Plate 4.1), which previous workers (*Phleger and Soutar*, 1973; *Douglas and Woodruff*, 1981; *Bernhard*, 1986; *van Leeuwen*, 1989; *Murray*, 1991) have suggested represent high organic carbon contents and productivity levels, as are recorded here. However, the high abundances of benthic foraminifera still largely remain an enigma, and cannot be used as a quantitative guide to palaeoproductivity until they are better understood.

4.4.3. Productivity record from GeoB 1711

GeoB 1711 is the deepest, and farthest offshore, core studied here. The abundances of *N. pachyderma* (s) document the greatest intensity of upwelling and therefore trade winds, increasing the width of the upwelling dominated *N. pachyderma* (s) fields and increasing the offshore divergence of sub-tropical waters (*Little et al.*, 1997a). This core site was chosen to record sedimentation away from the influence of continental shedding, dust input, re-suspension of organic matter, and bottom current erosion.

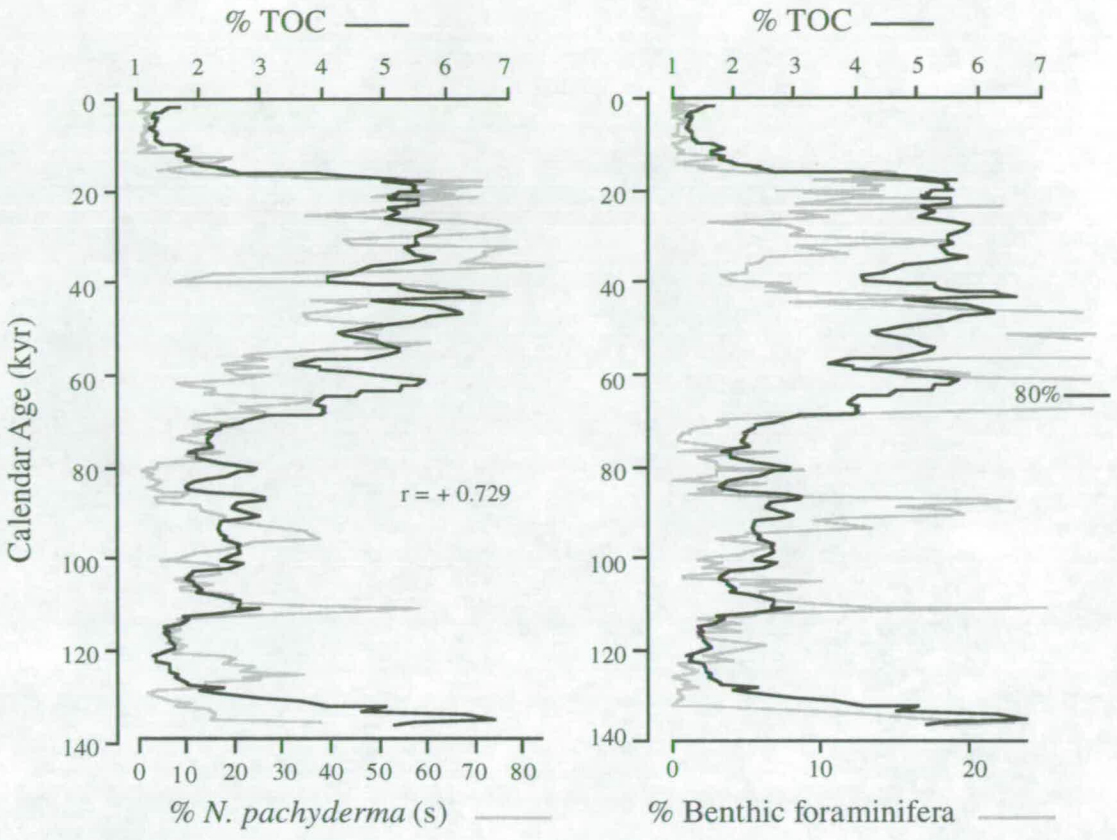

Figure 4.5. GeoB 1711: Total organic carbon (TOC) as a percentage of the total sediment (wt %) (black line) with % *N. pachyderma* (s), as a percentage of the total planktonic foraminifera, and % benthic foraminifera, as a percentage of the total foraminifera (benthics + planktonics). Correlation coefficient between TOC and *N. pachyderma* (s), r, = + 0.729.

The graphic correlation emphasises the overall trend between TOC and *N. pachyderma* (s) abundances, and although there are a few anomalies these occur when *N. pachyderma* (s) is not dominating the assemblage, and therefore at a time when the upwelling intensity has dropped below maximum levels (interglacial stage 5). At this time, TOC content is only between 1—2 % of the total sediment, reflecting much reduced productivity. This level of organic content may be reflecting the background primary productivity rather than the extra input from increased upwelling intensity in the last glacial period.

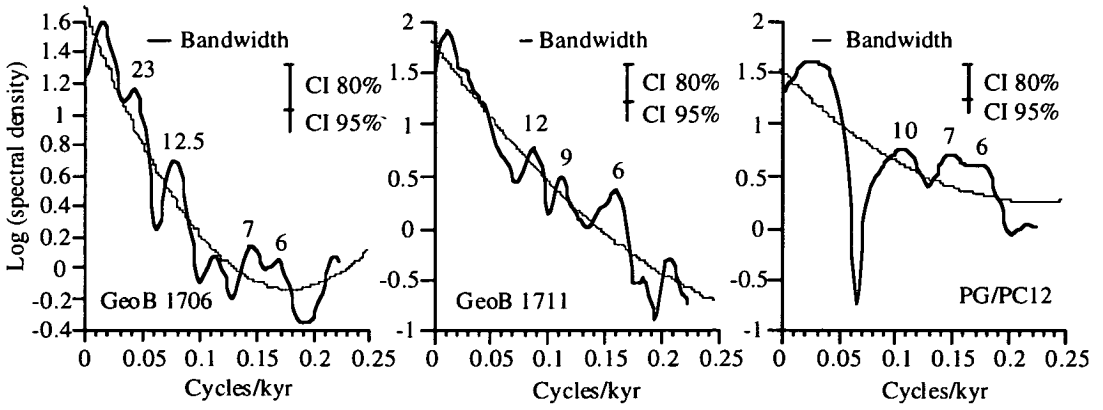

Figure 4.6. Spectral analysis for TOC in GeoB 1706, GeoB 1711 and PG/PC12. Statistical information: GeoB 1706. Spectral period analysed, 1-87 ka; Δt = 0.9 kyr; N = 96; CI shown for 60 lags. GeoB 1711. Spectral period analysed, 1-136 ka; Δt = 0.9 kyr; N = 151; CI is shown for 80 lags. PG/PC12. Spectral period analysed, 1-67 ka; Δt = 0.9 kyr; N = 74; CI is shown for 50 lags. For comparison, a second order polynomial expression of the spectral density is shown for the background spectral periodicity, together with the lower limit error bars of the 80 and 95% confidence intervals.

The number of benthic foraminifera in this core, is far below the levels recorded at the Walvis Ridge from GeoB 1706, or from the shallower record of PG/PC12. Total relative benthic foraminiferal abundance has a maximum, i.e. large B/P ratio, of 80% at 65 ka, and 55% at 50 ka (Figure 4.5), but at all other times has relative abundances of less than 20%, low B/P ratio. Removing the influence of the large maxima between 70—40 ka, the relative abundance of benthic foraminifera have an excellent correlation with TOC and abundance of *N. pachyderma* (s), with all of the maxima and minima in phase with those of TOC. It would seem that if the enhanced numbers of benthic foraminifera during 70—40 ka was 'anomalous' then benthic foraminifera, TOC and *N. pachyderma* (s) percentages could be used as proxies for productivity away from the immediate coastal upwelling situation. All proxies suggest that periods of increased upwelling stimulated increased productivity and an increased supply of organic carbon to the sea floor stimulating a thriving benthic community.

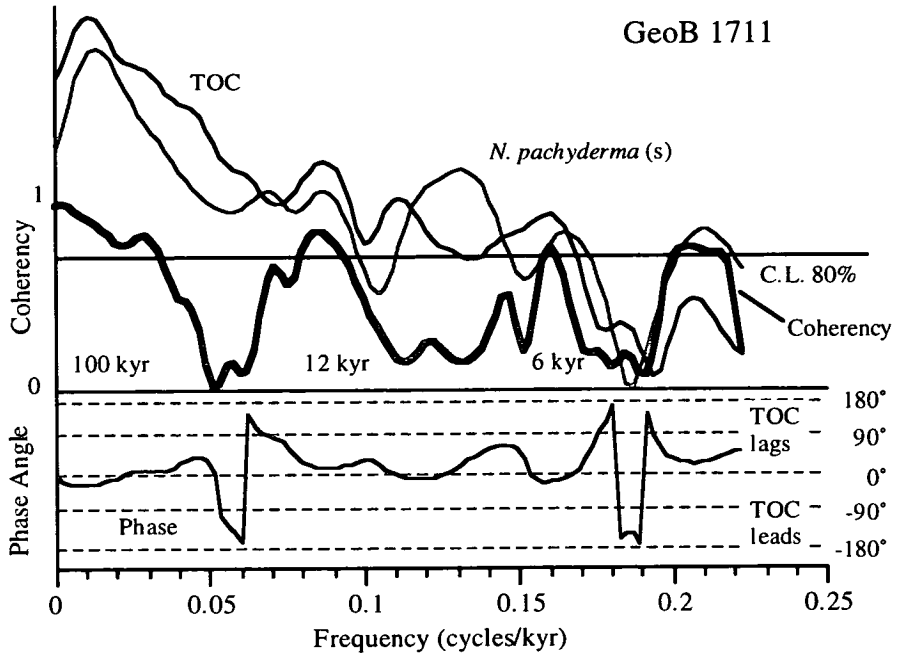

Figure 4.7. Cross-spectral analysis results between GeoB 1711 *N. pachyderma* (s) and GeoB 1711 TOC (1—136 ka). Cross-spectral statistics: Sample time interval, Δt, = 0.9 kyr; Number of samples, N, = 151; Confidence level for the 80% non-zero coherency is indicated; Bandwidth for all analyses = 0.16 cycles/kyr. Spectral maxima are highlighted with the period of oscillation (kyr). Phase angle is given graphically below the cross-spectral results. Note TOC and *N. pachyderma* (s) are in phase (0° within error margin) at the coherent periods of oscillation 12 and 6 kyr.

Time-series analysis for TOC measurements, document pronounced spectral maxima at the sub-Milankovitch periods of 12, 9 and 6 kyr (Figure 4.6), while *N. pachyderma* (s), and other planktonic foraminiferal abundances in the NBR, record recurrent coherent spectral maxima at 8 and 12 kyr (Figure 3.8). The cross-spectral analysis between *N. pachyderma* (s) and TOC for GeoB 1711, records coherency at the 12 kyr, and possibly 6 kyr, periods (Figure 4.7). Given the error margins on such a time-series analysis, the presence of an 8 kyr and 9 kyr periodicity within *N. pachyderma* (s) and TOC datasets respectively suggests that sub-Milankovitch forcing 'controls' both datasets. TOC measurements do not record significant spectra in the precessional band (19—23 kyr), which are documented from organic matter records at the equator, in the Angola Basin and from the Congo Fan (*Schneider et al.*, 1995; 1997). Similarly, results presented by *Schneider et al.* (1996), do not record coherent spectra in the precessional band from the Walvis Ridge (core GeoB 1028-5; 20°06.2'S 09°11.1'E, water depth 2209 m) from a 400 kyr

record, in agreement with the faunal and TOC records from within the Benguela Current (GeoB 1711 and PG/PC12), and from the Walvis Ridge (GeoB 1706), Figures: 3.8, 3.9, and 4.6. The TOC results, provide good supporting evidence that sub-Milankovitch periodicity is a true feature of the upwelling and productivity in the Benguela system and that precession appears to play a secondary if not minor role. TOC measurements may provide a quicker method for analysing climate and oceanic variability, away from the conflicting effects of re-suspension and continental shedding, than faunal population studies, although *N. pachyderma* (s) abundances are probably a more reliable method for cross-correlation between local core sites with possibly fewer influencing factors superimposed.

4.5. Late Quaternary palaeoproductivity in the northern Benguela upwelling system

Comparing the productivity records from GeoB 1706, PG/PC12 and GeoB 1711 we find basic similarities between all three core sites. Overall there is a general positive correlation between increased TOC and increased *N. pachyderma* (s) abundances and an increased B/P ratio. TOC records from the Peruvian (e.g. *Schrader,* 1992), Californian (e.g. *Summerhayes,* 1983), and northwest African margins (e.g. *Müller et al.,* 1983, *Thiede and Junger,* 1992) also suggest this overall correlation between productivity and offshore wind intensity with organic carbon content. In the Benguela system, as in most other upwelling systems, there is no linear correlation between measured TOC and the other palaeoproductivity proxies. The correlations suggest that *N. pachyderma* (s) abundances seem to be the most useful indicator for upwelling palaeoproductivity. However, at times of reduced upwelling intensity the correlation is not so clear (e.g. GeoB 1711 > 80 ka). Marine primary productivity contributes the largest percentage (90—95%; *Summerhayes,* 1983) to the TOC measured in the sediments, but proxies for primary or secondary productivity, such as *N. pachyderma* (s), do not necessarily reflect the total variation of TOC within the sediment record. As is the problem with the TOC sediment record, it results from the interplay of supply, sedimentation, re-suspension, terrestrial input, diagenesis and benthic activity, of which these components can never fully be quantified individually. Together with *N. pachyderma* (s), the TOC record for GeoB 1711 is the most useful indicator of upwelling and its influence on the palaeoproductivity record in the Benguela system. The variation in abundance of *N. pachyderma* (s), records maximum upwelling intensity away from the effects of re-suspension and the excellent correlation with

TOC, particularly in the glacial isotope stages 4—2, reflects an increase in organic carbon deposition over background productivity.

The B/P ratio, although largely suggesting a direct relationship with *N. pachyderma* (s) abundance and TOC, does present problems, indicating that until more is known about the relative benthic foraminiferal contributions it is not suitable, as yet, as a palaeoproductivity indicator in the Benguela system. The positive trend between TOC and *N. pachderma* (s) abundances with the B/P ratio has two main problems: (1) relative absence of benthic foraminifera after 40 ka on the Walvis Ridge; and (2) a benthic productivity event during ~ 60—40 ka. The relative lack of benthic foraminifera on the Walvis Ridge could reflect two things, firstly an increase in planktonic foraminifera relative to benthic foraminifera via a changing food or water supply, thus diluting the ratio, or secondly, a true lack of benthic foraminifera, reflecting a change in the benthic environment. The dilution of the B/P ratio would necessitate a huge increase in planktonic foraminifera abundance, which cannot easily be envisaged given that upwelling intensity is already at or near its maximum. While the reduction of benthic foraminiferal numbers, could be relatively easy to facilitate. A disruption to the benthic environment, for example decreasing the dissolved oxygen content, removing nutrient input to the benthic environment, or relatively deepening the depth of the oxygen-minimum zone via relative sea-level change, would have severe adverse effects to the benthic community, which is reflected in a very low B/P ratio (Figure 4.1). *Dingle* (1995) showed that in the present setting, the Walvis Ridge is the site of minimum oxygen content and the least hospitable for a thriving benthic community. The benthic oxygenation on the Walvis Ridge is largely controlled by the intensity of surface upwelling via primary productivity and the contribution of warm, saline, oxygen-poor water which impinges as a poleward undercurrent from the Angola Basin. Given the geographical location of GeoB 1706, an intermittent input from the Angola Basin provides the most logical explanation for the lack of benthic foraminifera from 40 ka to the present.

The benthic productivity events recognised in the NBR between 70 and 40 ka, primarily at site GeoB 1711 but also present at sites GeoB 1706 and PG/PC12, suggest a favourable change in the benthic environment. The most likely cause of the environmental modification at the sediment-water interface, would again be a variation in oxygen levels. The greatest effects of the benthic change are observed offshore in the record for GeoB 1711, where normal benthic/planktonic ratios are below 15%,

whilst in the period 70—40 ka the ratio increases to almost 80% and there is an extra benthic productivity maximum associated with this centered on 65 ka not recorded inshore at site PG/PC12, although it is recorded at site GeoB 1706 at 70 ka. The absence of the Angola Basin poleward undercurrent could produce this relative change, however, a more likely relative oxygen increase could come from an oxygen-rich intermediate/deep water incursion from the south onto the Namibian continental slope and lower shelf.

The organic carbon measurements from the offshore record of GeoB 1711, highlight the dominance of sub-Milankovitch periodicity in the Benguela system, and do not record significant, coherent spectra in the precessional band (19—23 kyr). Records from the Walvis Ridge (GeoB 1706, this paper; GeoB 1028, *Schneider et al.,* 1997) show precession to be a minor control on faunal and productivity records, in contrast to the Angola Basin which is strongly influenced by the precession controlled trade wind/monsoon intensification (*Mix et al.,* 1986a; 1986b, *McIntyre et al.,* 1989, *Schneider et al.,* 1995; 1997). Although the high resolution records are not long enough to measure the timing of variability conclusively, the absence of the precession component within the last 140 kyr is very apparent. Direct Milankovitch orbital forcing, in particular the precessional band, is not represented in the faunal and organic carbon records from the Benguela system and instead sub-Milankovitch forcing, primarily at the harmonic of precession (~12 kyr), dominates the organic carbon records.

N. pachyderma (s) varies dramatically in isotope stages 3—2, with swings in abundance from 0—80% in all three NBR core records, particularly PG/PC12 and GeoB 1711, which are away from the Walvis Ridge. During periods of upwelling intensification, lateral expansion of the upwelling fringes over the core sites generates immediate and dramatic responses from the planktonic foraminifera, recorded as rapid, large changes in *N. pachyderma* (s) abundance oscillating on an 8—9 kyr periodicity via trade wind changes. TOC however, records a smoother profile with less dramatic swings in organic carbon content in the sedimentary record, as excess organic carbon is either utilised or lost in the process of sedimentation. Both the planktonic foraminifera and TOC records from GeoB 1711, however, document recurrent periodicity at the 6 and 8—9 kyr periods. Although TOC may provide a quicker method for analysing sub-Milankovitch oceanographic change, *N. pachyderma* (s)

abundances record the immediate response to climate forcing and allow for a more accurate assessment of the forcing mechanisms [1].

4.6. Summary

The relative abundance of *N. pachyderma* (s), total organic carbon (TOC) content and the benthic/planktonic foraminifera ratio, indicate an overall positive correlation and contemporaneous variability. In the glacial isotope stages 4—2, there is an excellent correlation between *N. pachyderma* (s) abundances and TOC. During these intense upwelling phases almost all of the TOC in the sediments is derived from upwelling-driven primary production. The offshore record of site GeoB 1711 is used as the indicator for maximum offshore divergence and shelf-edge upwelling, away from the interference and dilution from re-suspension of inner shelf organic matter. At this locality the correlation is particularly good with a correlation coefficient of + 0.729, and the benthic/planktonic (B/P) ratio also corresponds to the surface productivity.

Anomalies between the B/P ratio and TOC are thought to represent a changing oxygen supply. The relative absence of benthic foraminifera from 40 ka to the present, in GeoB 1706 on the Walvis Ridge, is thought to indicate the presence of a warm, saline, oxygen-poor, poleward undercurrent impinging on the Walvis Ridge, making the benthic environment inhospitable for most organisms. In the Cape Basin at the site of GeoB 1711 and PG/PC12, benthic favourable conditions are present between ~ 70 and 40 ka. This is thought to represent enriched oxygenation of the sediment-water interface, with a possible incursion of oxygen-rich intermediate/deep waters, such as the AAIW and/or AABW. $\delta^{13}C$ measurements from cores in the Cape Basin further suggest that Southern Ocean water masses impinged on the Cape Basin during this time (*Bickert and Wefer*, 1997).

The faunal and TOC records for GeoB 1711, record spectral maxima at sub-Milankovitch periodicities, in particular at 12, 8—9 and 6 kyr. The faunal records are dominated by the rapid changes in *N. pachyderma* (s) abundance which records swings in abundance from 0—80% in all three NBR core records. During periods of upwelling intensification, lateral expansion of the upwelling fringes generates immediate and dramatic responses in *N. pachyderma* (s) abundance oscillating on an 8 kyr periodicity via trade wind changes. TOC however, records a smoother profile

[1] Sub-Milankovitch forcing mechanisms are discussed in Chapter 5.

with less dramatic swings in organic carbon content in the sedimentary record. *N. pachyderma* (s) appears to exist in a state of equilibrium and a slight change in environmental conditions, probably via nutrient availability, stimulates an immediate and dramatic response. For future analysis, TOC contents may provide a quicker method for analysing climate and oceanic variability without the super-position of temperature dominance which effects faunal population studies. TOC variability reflects the change in upwelling intensification best expressed away from the coastal upwelling situation and from dilution and re-sedimentation, but the B/P ratio is not yet a suitable method for quantifying palaeoproductivity. *N. pachyderma* (s) abundance is probably the best proxy for palaeoceanographic and palaeoproductivity changes and may better record the timing and periodicity of climate instability in the Benguela Current system.

South Atlantic upwelling events and sub-Milankovitch climate variability as observed by changes in the abundance of *N. pachyderma* (s) - links to trade wind forcing and North Atlantic Heinrich events

Ch.5

Chapter 5. South Atlantic upwelling events and sub-Milankovitch climate variability as observed by changes in the abundance of left coiling *Neogloboquadrina pachyderma* - links to trade wind forcing and North Atlantic Heinrich events

5.1. Introduction

The abundance of the left coiling planktonic foraminifer, *N. pachyderma* (s), shows a higher frequency of change than would be expected if the Benguela upwelling system was dominated solely by the global glacial—interglacial cycles. These rapid events are investigated to ascertain the extent, cause and timing of South Atlantic—North Atlantic teleconnections in global oceanic and atmospheric linkages. The abundance of *N. pachyderma* (s) is used as the indicator of maximum trade wind intensity and corresponding offshore expansion of the coastal upwelling front (*Little et al., 1997a*). The planktonic foraminiferal record of GeoB 1711 is used in preference to the records from GeoB 1706 and PG/PC12 which, as well as being either incomplete or too short in length, lie inshore of GeoB 1711 and do not give an indication of the maximum divergence of the upwelling front from its present position. The aim of this chapter is to assess the correlation of rapid oceanic events documented in the South Atlantic sediment records with the global records of similar short-lived climate variability recorded in previous marine, terrestrial and ice-core studies.

Many authors have studied the well-defined rapid pulses of ice-rafted debris (IRD) in marine sediments during the last glacial cycle (*Pastouret et al.,* 1975, *Ruddiman,* 1977, *Aksu and Piper,* 1979, *Fillon and Duplessy,* 1980, *Ruddiman et al.,* 1980, *Molnia,* 1983, *Broecker,* 1988; 1990, *Jansen and Veum,* 1990, *Broecker et al.,* 1992, *Bond et al.,* 1992, *Duplessy et al.,* 1992, *Bond et al.,* 1993, *Grousset et al.,* 1993, *Keigwin and Lehman,* 1994, *Maslin et al.,* 1995, *Porter and Zhisheng,* 1995, *van Kreveld et al.,* 1996). These short lived 'Heinrich-events' (*Bond et al.,* 1992) occur on sub-Milankovitch time scales at intervals of between 8—11 kyr, and are commonly associated with peak abundances of the Arctic/sub-Arctic fauna, as represented by *N. pachyderma* (s) (*Bond et al.,* 1992, *Broecker and Maier-Reimer,* 1992, *Bond et al.,* 1993, *Grousset et al.,* 1993, *van Kreveld et al.,* 1996; *Elliot et al.,* 1997). Periods of cooling terminated by an abrupt warming, represent similar rapid climate changes in the Greenland ice cores (*Broecker et al.,* 1990, *Johnsen,* 1992, *Bond et al.,* 1993, *Dansgaard et al.,* 1993, *Grootes et al.,* 1993, *Alley et al.,* 1993, *Bender et al.,* 1994).

The ice-records suggest climate fluctuations at a higher frequency than Milankovitch orbital forcing, with more oscillations in the last 60 ka than are recorded in the *N. pachyderma* (s) and IRD records from the North Atlantic sediments (e.g. *Bond et al.,* 1992; 1993). *Dansgaard et al.* (1993), showed that the $\delta^{18}O$ record from the GRIP ice core contains 23 interstadials within the last 120kyr, with 17 interstadials recognised between the LGM (last glacial maximum) and oxygen isotope-stage 4, compared with only 5 Heinrich events recognised in marine sediments within this period (*Heinrich,* 1988, *Bond et al.,* 1992; 1993, *Grousset et al.,* 1993).

The Heinrich events are thought to be the result of fluctuations in the thermohaline convective conveyor which draws warm, tropical, saline-rich waters from the equatorial regions into the high latitudes of the North Atlantic via the Gulf Stream and North Atlantic Drift (*Broecker and Denton,* 1989, *Berger,* 1990, *Broecker et al.,* 1990, *Bond et al.,* 1993, *Paillard and Labeyrie,* 1994). Previously, meltwater input from the large Laurentide ice sheets was thought to be the principal cause of disturbance to the thermohaline convection (*Boyle et al.,* 1982; 1987, *Broecker et al.,* 1985, *Watts,* 1985, *Broecker,* 1988, *Broecker and Denton,* 1989, *Berger,* 1990, *Broecker et al.,* 1990, *Teller,* 1990, *Andrews et al.,* 1993, *Bond et al.,* 1993, *Paillard and Labeyrie,* 1994), decreasing the salinity of the Gulf Stream, and therefore density, and lowering its potential to sink in the polar regions of the North Atlantic, thus reducing the rate of convective overturn and deep water mixing. The subsequent decrease in warm-water advection from the tropics is suggested to stimulate a rapid cooling and sudden ice sheet build up, with ice sheets expanding to their maximum seaward position before final collapse and release of icebergs into the North Atlantic, further cooling the surface polar waters (*Johnson and Andrews,* 1979, *Paillard and Labeyrie,* 1994). If this model is coupled with the Gulf Stream and the cross-equatorial transfer of heat and moisture from the South Atlantic to the North Atlantic via the SEC, as previous models of oceanic convection suggest (*Stommel,* 1980, *Gordon,* 1986, *Berger,* 1990, *Gordon et al.,* 1992, *Berger and Kroon,* 1995, *Macdonald and Wunsch,* 1996), then the impact of thermohaline changes on the conveyor could also be affected by changes in the rate of moisture input from the tropics at times of increased trade wind intensity (*Ruddiman and McIntyre,* 1981; *Imbrie et al.,* 1989; *Little et al.,* 1995; 1997a). An increase in moisture supply to the North Atlantic ice sheets, contemporaneous with a northern hemisphere cooling, would enhance rapid ice build-up and subsequent ice-sheet calving (*MacAyeal,* 1993a; 1993b; *Boulton and Payne,* 1994), and would account for the anomalous warm-water

SSTs which prevail into the phase of maximum ice building in the northwestern sub-tropical gyre and sub-polar ocean (*Ruddiman and McIntyre,* 1981).

Occurrences of other Heinrich-type events outside the North Atlantic region (*Broecker,* 1994, *Thouveny et al.,* 1994, *Porter and Zhisheng,* 1995; *Schmelzer et al.,* 1997) bring into question whether the discrete Heinrich events are wholly a North Atlantic phenomena or whether they should be considered with seasonality and insolation changes which dominate low latitude climate. If, as *Berger and Kroon* (1995) suggest, "seasonality is at the heart of Milankovitch forcing", can this be related to changes on the sub-Milankovitch scale, such as the Dansgaard-Oeschger cycles (*Dansgaard et al.,* 1993, *Grootes et al.,* 1993) seen in the Greenland ice cores? Should we be looking for a system which influences all three: seasonality, Heinrich events and sub-Milankovitch forcing. *Mix et al.* (1986a; 1986b), *McIntyre et al.* (1989) and *Little et al.* (1997a) have suggested that the trade wind system exerts a dominant control in the eastern equatorial and south eastern Atlantic and that this system forms an important link in Atlantic and global heat transfer. Here we examine the relative abundances of planktonic foraminifera in cores from the northern Cape Basin for evidence of short-lived climate events related to the trade wind system and their link to equatorial seasonality and Heinrich events.

5.2. Background

5.2.1. Global distribution of Heinrich Layers

Rapid episodes of massive iceberg release (Heinrich events) into the North Atlantic Ocean during the last glaciation, have been associated with cold air temperatures over Greenland recorded from GRIP and GISP2 ice cores (Dansgaard-Oeschger cycles; *Dansgaard et al.*, 1993; *Grootes et al.*, 1993). Recent research has reported the occurrence of Henrich-type events, with a periodicity at Dansgaard-Oeschger cyclicity, outside of the North Atlantic IRD belt (*Yiou et al.,* 1991, *Broecker,* 1994, *Thouveny et al.,* 1994, *Kennett and Ingram,* 1995a; 1995b, *Kotilainen and Shackleton,* 1995, *Behl and Kennett,* 1996, *Charles et al.,* 1996, *McIntyre and Molfino,* 1996, *Little et al.,* 1997a; *Cayre et al.*, 1997; *Schmelzer et al.*, 1997; Figure 5.1). Four of the youngest of these cold events (H1—H4) have been recorded from several sites outside of the North Atlantic, but the full suite of Heinrich events (H1—H6) have been

recorded in only a few locations (*Thouveny et al.,* 1994, *Porter and Zhisheng,* 1995, *Little et al.,* 1997a).

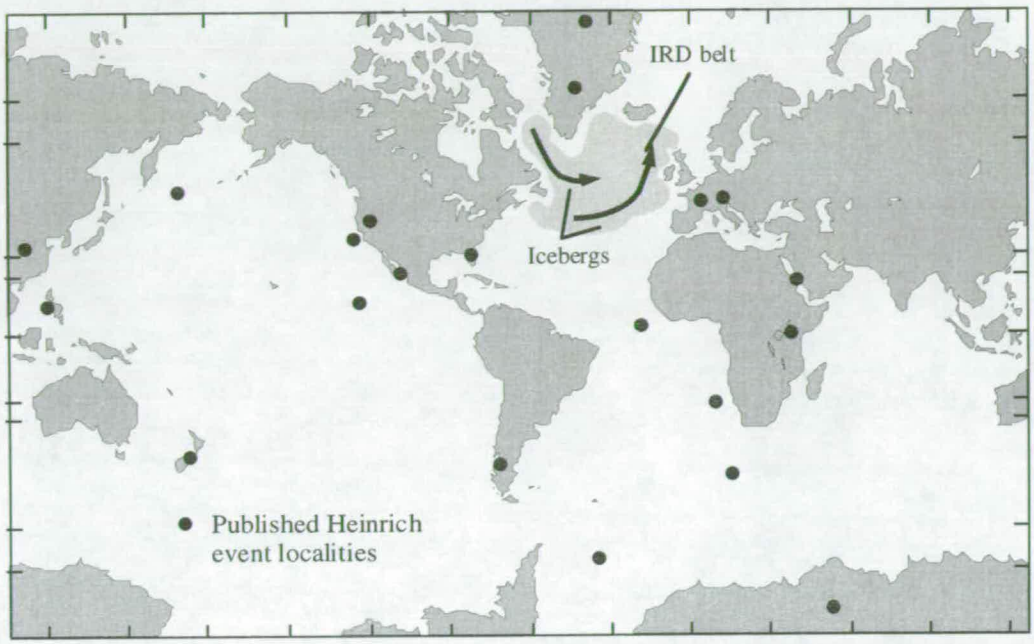

Figure 5.1. Global distribution of published Heinrich events, the IRD belt and the iceberg track (after Broecker, 1994). [Data from: *Broecker and Denton,* 1990, *Linsley and Thunell,* 1990, *Yiou et al.,* 1991, *Bond et al.,* 1992, *Dansgaard et al.,* 1993, *GRIP,* 1993, *Grootes et al.,* 1993, *Grousset et al.,* 1993, *Roberts,* 1993, *Broecker,* 1994, *Hagelberg et al.,* 1994, *Thouveny et al.,* 1994, *Bond and Lotti,* 1995, *McIntyre and Molfino,* 1996, *van Kreveld et al.,* 1996; *Cayre et al.,* 1997; *Schmelzer et al.,* 1997.]

Porter and Zhisheng (1995) compared magnetic susceptibility and grain-size variations in the Luochuan loess/palaeosol succession with North Atlantic Heinrich events, *N. pachyderma* (s) abundances and Greenland ice core $\delta^{18}O$ variations. The grain-size analysis in particular, showed an excellent correlation with Heinrich events in the North Atlantic, but also highlighted correlations with other events in the GRIP ice core and the *N. pachyderma* (s) abundances from core V28-31 (*Bond et al.,* 1993). *Dansgaard et al.*(1993) and *Grootes et al.* (1993) present similar findings, with more 'Heinrich-type' events than are present in the North Atlantic sediment records but are well documented in the Greenland summit ice cores. The Chinese loess grain-size fluctuations are a direct result of dust influx variability controlled by changes in the direction and intensity of the East Asian summer monsoon (*Porter and Zhisheng*, 1995). *Behl and Kennett* (1996) reported on rapid climate instability from ODP site

893 in the Santa Barbara Basin. Using a bioturbation index, they record 19 of the 20 Dansgaard-Oeschger events, in the form of laminated sediments deposited under anoxic conditions. The authors use this as evidence to suggest that short-term events were not restricted to the North Atlantic region; similar events in the Gulf of California (*Kennett and Ingram,* 1995b) and preliminary oxygen isotope results from the Red Sea (*Schmelzer et al.*, 1997), which record all of the interstadials in the last glacial cycle suggest that these events are a global phenomena.

5.2.2. Forcing mechanisms

Milankovitch orbital forcing

The most important changes occuring on the time scale of 10^4—10^6 years are those related to the Earth's orbital parameters (*Milankovitch,* 1930, *Hays et al.,* 1976, *Imbrie and Imbrie,* 1980, *Imbrie et al.,* 1984; 1992; 1993a; 1993b).

In the abscence of any other celestial bodies, the earth would describe an elliptic orbit with the sun as one of the foci. The shape and position of the ellipse would be fixed. Furthermore, if the earth were a perfectly spheroidal, homogeneous body its axis of rotation would have a fixed direction in space, and make a constant angle with the normal to the plane of the ecliptic [1]. The gravitational attraction of the other planets in the solar system disrupts the Earth's elliptic motion around the sun, but as the masses of the planets are small compared to the sun, the ellipse is only slightly disturbed. It is practical, therefore, to describe the motion of the Earth as an ellipse with orbital elements that vary slowly in time.

The ellipse, and its temporal variation, is described using three orbital parameters: eccentricity, tilt (obliquity), and precession. The Earth's orbit through time is defined by the precession of the equinoxes (the time when the earth is nearest the Sun [perihelion] changes from January to July on a period of approximately 21kyr), the tilt, or obliquity, of the Earth's rotation axis (currently 23.4° but varying between 22—24° on a time scale of 41kyr) and changes in the eccentricity of the orbit of the Earth around the Sun (period of nearly 100kyr). The other orbital elements necessary to describe the position and velocity of the Earth in space and that of its axis of rotation, vary on even slower time scales than eccentricity, tilt and precession.

---

[1] Ellipse described by the Earth's passage around the sun.

It is necessary to understand how variation in the Earth's parameters can effect the Earth's climatic system. Of most importance is the amount of solar radiation received by the Earth and its variation with time. The direct effect from orbital changes affecting the climate system is actually very small. Eccentricity modifies the globally and annually averaged insolation recieved at the top of the atmosphere, of which the total change in insolation over the Quaternary is calculated to be about one part in a thousand over the same period (*Held,* 1982).

Obliquity and precession have no net global and annual effect on insolation at all, they only change the contrast between the seasons. Importantly, for obliquity this change of contrast is the same in both hemispheres, for precession the contrast is largest in one hemisphere when it is smallest in the other. The precessional effect is the same at all latitudes within one hemisphere, while the obliquity effect increases with latitude. As a result, insolation changes due to obliquity might dominate at higher, polar-latitudes, while precessional changes might dominate at lower, equatorial-latitudes.

Sub-Milankovitch frequencies

High-resolution climate records suggest that variability in the atmosphere and ocean occurs at higher frequencies than those of orbital forcing, i.e. cycling on a period less than 19—23 kyr. These higher frequencies are grouped as millenial or sub-Milankovitch frequencies. Sub-Milankovitch frequencies are not known to have direct linear forcing mechanisms, unlike Milankovitch frequencies which are forced by changes in the Earth's orbit. Evidence from high-resolution sediment records documents sub-Milankovitch frequencies in many localities over the world: the eastern equatorial Pacific (ODP site 846; *Hagelberg et al.,* 1994); eastern equatorial Atlantic (ODP site 663; *Hagelberg et al.,* 1994); the northeastern Atlantic (DSDP site 609; *Hagelberg et al.,* 1994); the Red Sea (*Schmelzer et al.,* 1997); and the South Atlantic (DSDP site 516F; *Park et al.,* 1993); and in ice cores (Vostok, *Yiou et al.,* 1991; and Greenland, *Mayewski et al.,* 1994). Several studies have predicted that sub-Milankovitch cyclicities should occur as a non-linear response to Milankovitch forcing (*Wigley,* 1976, *Ghil and Le Treut,* 1981, *Le Treut and Ghil,* 1983, *Ghil,* 1984, *Le Treut et al.,* 1988, *Short et al.,* 1991, *Crowley et al.,* 1992). Using a non-linear climatic oscillator model to which orbital forcing is applied, *Ghil and Le Treut* (1981) and *Le Treut and Ghil* (1983) demonstrated that harmonic responses to precessional

forcing arise at 11.5, 10.4 and 9.5 kyr, where 75% of the variance in the 10—12 kyr band is non-linearly transferred from precession band variations (*Hagelberg et al.,* 1994).

Le Treut and Ghil (1983) demonstrate that the peak at 10.4 kyr corresponds to the 'combination tones' of $f_1 + f_2$ (where $f_1 = 1/19$, $f_2 = 1/23$, $f_3 = 1/41$ and $f_4 = 1/100$ cycles/kyr; *Ghil and Childress,* 1987) while the smaller peaks at 11.5 and 9.5 kyr correspond to $2f_2$ and $2f_1$ respectively. *Yiou et al.* (1991) present an extra peak at 14.1 kyr corresponding to the slightly different combination tone of $f_2 + f_3$ and *Pisias and Rea* (1988) describe combination tones of $f_2 + f_4$ and $f_3 + f_4$ for strong spectral density at the 28—31 kyr period. More recently, *McIntyre and Molfino* (1996) have proposed that the dominant sub-Milankovitch frequency in equatorial Atlantic sediment records is centered on 8.4 kyr, correlating to a combination tone harmonic from eccentricity and precession i.e. $2(f_2 + f_4)$. These harmonics (e.g. $2f_1$ or $2f_2$), as well as combination tones (e.g. $f_1 + f_2$), are only possible in the presence of system non-linearities (*Le Treut and Ghil,* 1983).

Short et al. (1991) used an energy balance climate model to show the presence of oscillation at frequencies equal to precession harmonics. Their model predicts a surface temperature response to insolation forcing in equatorial regions where the twice-yearly passage of the Sun over the equator creates a precession harmonic of 10—12 kyr, and also increases the 100 kyr and 400 kyr power spectrum (*Crowley et al.,* 1992). Using the modelled present-day geography at low latitudes, the response of the monsoon system to the modelled forcing was an amplification of the non-linear components (*Short et al.,* 1991, *Crowley et al.,* 1992). In addition to these modelling studies, the non-linear climate response to Milankovitch forcing at 9.5—12 kyr has been suggested from a number of datasets (*Molfino et al.,* 1984, *Pokras and Mix,* 1987; *Hagelberg et al.,* 1994; *Park et al.,* 1993; *Yiou et al.,* 1991; *Mayewski et al.,* 1994).

Crowley et al. (1992) and later *Hagelberg et al.* (1994) discussed potential problems with interpreting time-series analyses on the basis of non-linearities in the recording system. *Hagelberg et al.* (1994) demonstrated that a clipped precessional system with a mean value of zero (thus only the positive values remain) produced extra power spectral peaks at 10—11 kyr and 50 kyr, the harmonics of the precessional and eccentricity indexes. These harmonics are an artefact of the clipping and represent

non-linearities in the recording system not non-linearities in the climate system (*Crowley et al.*, 1992). The only way to be assured that high-frequencies exist within the time-series, is to detect them in the time domain as well as the frequency domain, i.e. before and after spectral analysis.

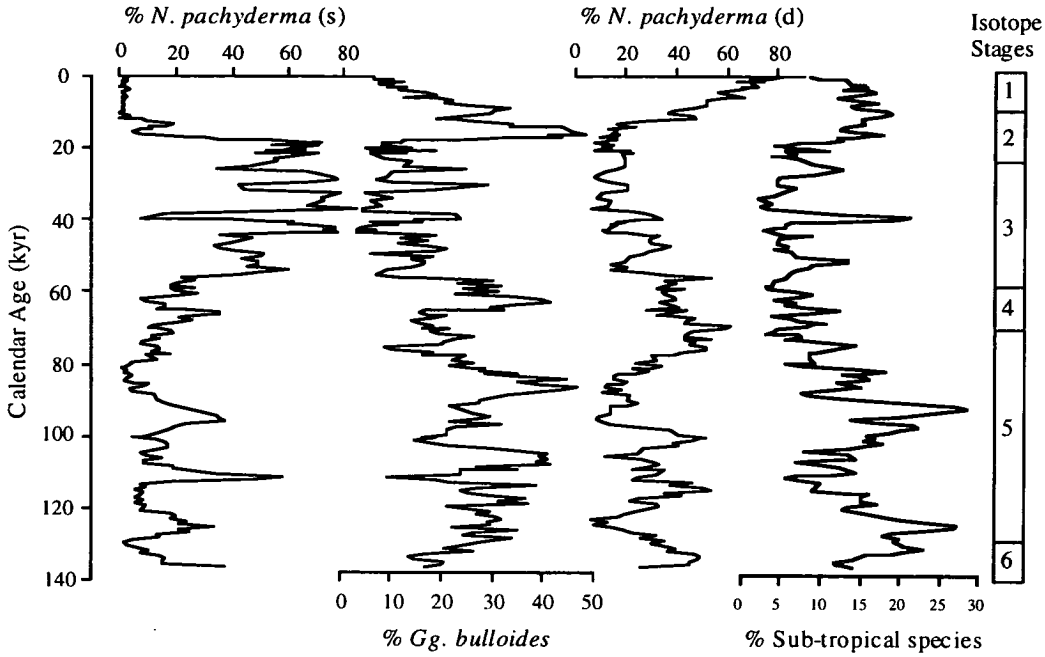

Figure 5.2. GeoB 1711. Abundances (% of total planktonic foraminifera) of the main planktonic foraminifera components, all against depth (cm). On the right hand side is a schematic representation of the interglacial—glacial oxygen isotope stages.

5.3. Correlation of South Atlantic PS-events with equatorial seasonality and the Greenland $\delta^{18}O$ ice-core record

The changing down-core abundance of the cold-water planktonic foraminifer, *N. pachyderma* (s), records rapid oscillations in relative abundances between 0 and 80% of the total planktonic foraminiferal assemblage (Figure 5.2). The *N. pachyderma* (s) records do not follow the glacial—interglacial regime described by the oxygen isotope profile, but instead show a higher frequency of change on a sub-Milankovitch cyclicity with *N. pachyderma* (s) maxima describing discrete PS events (pachyderma sinistral) approximately every 8—10 kyr (PS events; Table 5.1), although the spacing is not entirely regular.

The *N. pachyderma* (s) records off southwest Africa have been shown to vary primarily according to the local oceanographic and upwelling regime, which is driven by the intensity and direction of the southeast trade winds (*Little et al.*, 1997a). The extent of the coastal upwelling cells at any one time will dictate the hydrography and therefore planktonic foraminiferal record. Owing to its geographical position, GeoB 1711, at a water depth of 1967 m, is thought to reflect the maximum extent of the upwelling offshore and therefore the most intense upwelling and corresponding strong trade winds, while cores inshore of GeoB 1711 generally have broader maxima of *N. pachyderma* (s) reflecting a more sustained position below upwelling cells not reflecting the maximum intensity of trade winds (*Little et al.*, 1997a).

Pachyderma Sinistral		Heinrich			
Event	Calendar Age, kyr	Event	Age,[a] kyr	Error (+/-)	Calendar Age,[b] kyr
PS1	19.2-21.7	H1	13.65-14.99	90-230	15.59-17.25
PS2	26.1-29.0	H2	20.37-21.77	330-220	23.64-25.25
PS3	32.7-36.7	H3	26.57-29.57	310-660	30.60-33.80
PS4	42.4	H4[c]			38-42
PS5	53	H5[c]			50-52
PS6	65-71	H6[c]			67[d]
PS7	95				
PS8	111				
PS9	125				

[a]Analytical age from *Bond et al.* [1992].
[b]Ages converted to calendar years following the methods of *Bard et al.* (1990a; 1990b; 1993) after a + 400-years correction for marine reservoir effect.
[c]From *Grousset et al.* (1993).
[d]H6 covers the whole of stage 4 (*Bond et al.*, 1992) but peaks at 67 kyr.

Table 5.1. Pachyderma Sinistral Events and Heinrich Events correlation. PS event calendar age ranges are taken as an average from cores GeoB 1711, PG/PC12 and GeoB 1706.

Upwelling events PS1—PS9 punctuate the record for the last 140 kyr with an average spacing in the order of 10 kyr in the glacial stages 4—2 and with a longer ~20 kyr spacing during interglacial stage 5 (Figure 5.3). The calendar ages for PS events PS1—PS9 and Heinrich events H1—H6 are given in Table 5.1 with PS1—PS6 correlating well with the timing of H1—H6 in the North Atlantic with a consistent 3-kyr phase lead of the southern hemisphere to the Heinrich events of the northern

hemisphere. Considering this lead, PS-events PS1—PS6 in GeoB 1711 and PG/PC12, correlate well to the six Heinrich events in the North Atlantic, within analytical and calendar age correction error margins.

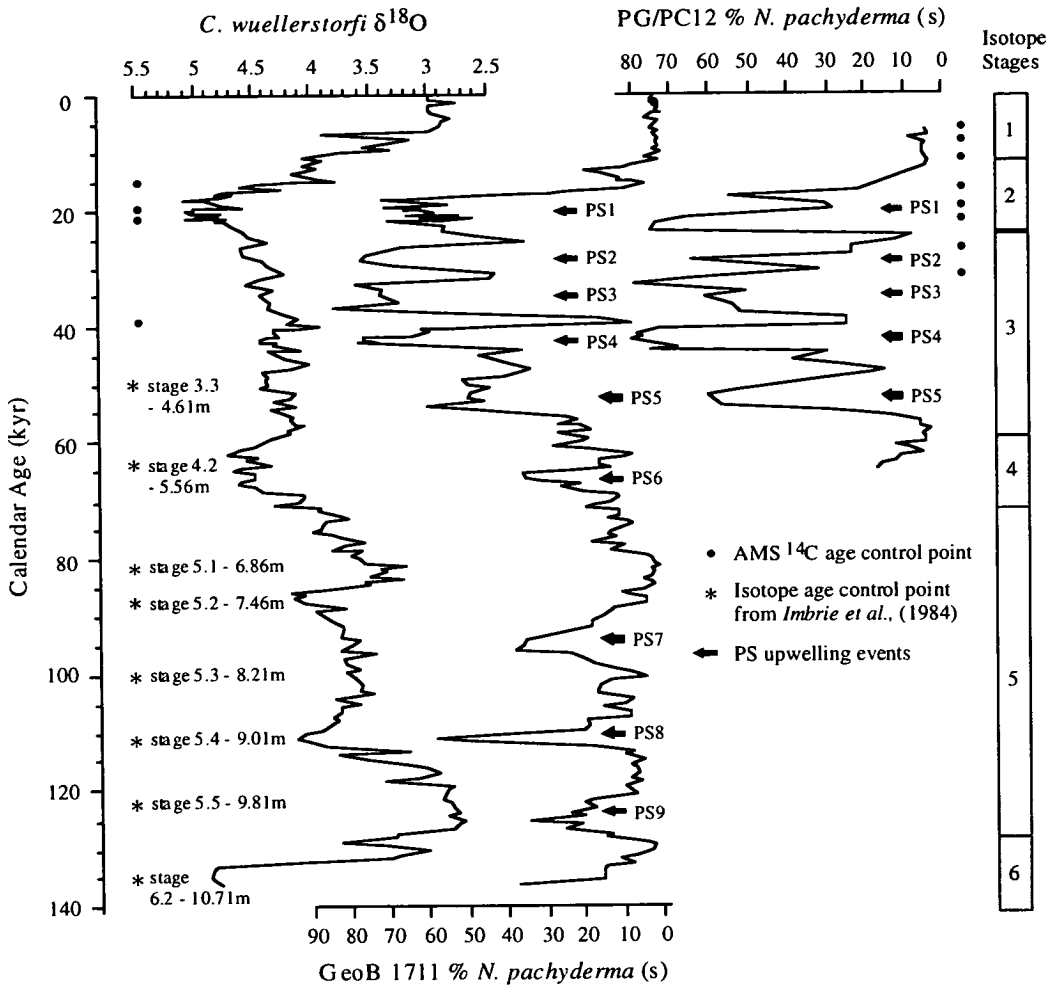

Figure 5.3. Planktonic foraminifera derived oxygen isotope stratigraphy for GeoB 1711 versus calendar age (kiloyears before present). The $\delta^{18}O$ age control points (asterisks) and ^{14}C AMS age control points (solid circles) for GeoB 1711 are shown to the left of the $\delta^{18}O$ *C. wuellerstorfi* record, and to the right of the *% N. pachyderma* (s) data for PG/PC12. PS (pachyderma sinistral) upwelling events are highlighted on the GeoB 1711 and PG/PC12 *N. pachyderma* (s) abundance data. Graphic representation of the isotope stages is given to the right of the figure.

With regard to PS and Heinrich events preceeding H6 (PS6), there is no general agreement as to how many events exist and to their exact timing. *Heinrich* (1988) observed an 'extra' 5 events during interglacial stage 5 and more recently *McManus et al.* (1994) reported the occurrence of IRD deposits together with increased abundances

of *N. pachyderma* (s) during interglacial stage 5. Heinrich events H1—H6 from sediment records in the North Atlantic are associated with peak abundances of *N. pachyderma* (s) and large fluxes of IRD principally at times of large ice sheets during global cooling, specifically during glacial isotope stages 4—2. During warmer interglacial periods, when ice sheets are near their minimum size and insolation is near a maximum, it is unlikely that fluctuations in ice sheet growth will be recorded in IRD and *N. pachyderma* (s) abundances, as ice sheets will never grow to a sufficient size to enable ice sheet calving or to produce "true" Heinrich events. The presence of PS events during interglacial stage 5 further supports the studies of *Heinrich* (1988) and *McManus et al.* (1994) for climate instability during non-glacial periods when high-latitude climate amplification is not as pronounced.

Using a similar graphic correlation to that used in previous Heinrich studies (*Bond et al.*, 1993, *Dansgaard et al.*, 1993, *Grousset et al.*, 1993, *Bender et al.*, 1994), tie-lines have been drawn between the *N. pachyderma* (s) record of GeoB 1711 and their temporal equivalents in the GISP2 ice core. Additionally, the equatorial seasonality record derived from planktonic foraminiferal abundances at core RC24-16 (5°2.3'S 10°11.5'W; *McIntyre et al.*, 1989) is also correlated with the GeoB 1711 *N. pachyderma* (s) record. *Bender et al.* (1994), using the stratigraphy of *Dansgaard et al.* (1993), correlated the 23 interstadials found in the GRIP ice core record to those in the nearby Greenland ice core, GISP2. The graphic correlation in Figure 5.4 suggests that almost all of the 23 interstadials, particularly in the glacial stages 4—2 (IS1—IS20; *Bender et al.*, 1994), can be found in the GeoB 1711 *N. pachyderma* (s) record as higher frequency maxima in *N. pachyderma* (s) abundances (NP events), and therefore cold events at site GeoB 1711, superimposed on the more dramatic changes in *N. pachyderma* (s) abundance (PS events). All of the NP events can also be found in the RC24-16 seasonality record with cooler upwelling maxima occuring simultaneous with maximum eastern equatorial seasonality and therefore maximum seasonal SST variability between summer and winter extremes. Notably, it is the maxima in the *% N. pachyderma* (s) record, and hence cool intervals of increased upwelling intensity, that match $\delta^{18}O$ maxima in the GISP2 ice core, and therefore warm atmospheric temperatures over Greenland (Figure 5.3). The *N. pachyderma* (s) abundances suggest that the pronounced PS events PS6, PS7 and PS8 record cold stages in a predominantly warm interglacial period, whilst PS1—PS5 record the base values in a cold glacial period punctuated by anomalously low *% N. pachyderma* (s) values.

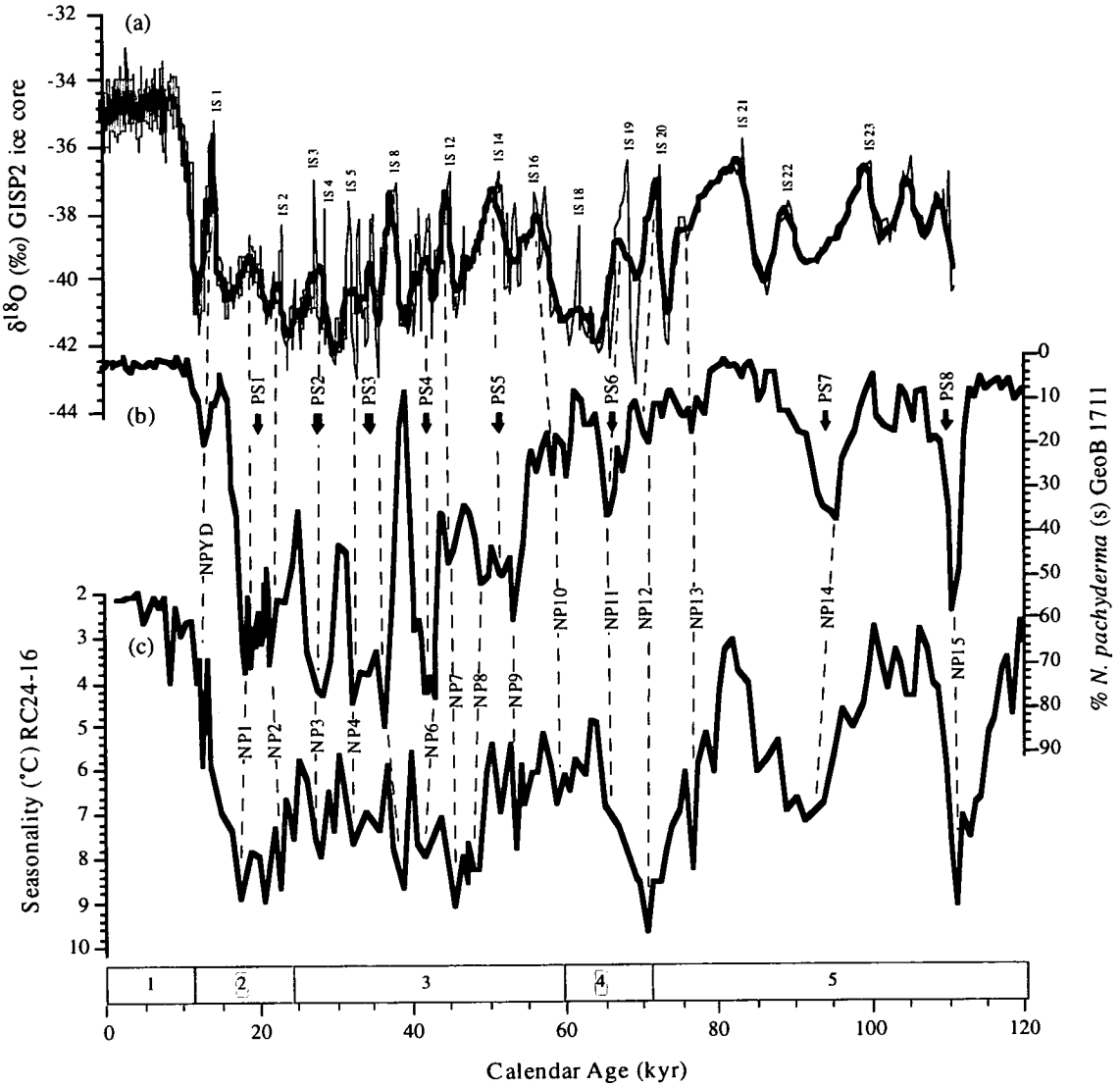

Figure 5.4. Correlation between: (a) Greenland, GISP2 ice core ($\delta^{18}O$); (b) *N. pachyderma* (s) from GeoB 1711 (% of total planktonic foraminifera); (c) Equatorial seasonality (°C), *McIntyre et al.* (1989). The GISP2 $\delta^{18}O$ data (*Grootes et al.*, 1993) has been smoothed for graphic correlation [thick line; 21pt smooth < 70 kyr, 9 pt smooth > 70 kyr], with the original data (thin line) superimposed. *N. pachyderma* (s) maxima (PS-events) are labelled PS1—PS8. The high frequency NP events in GeoB 1711 (dashed lines) are superimposed on the PS event stratigraphy, and are correlated to temporal equivalents in the GISP2 $\delta^{18}O$ ice core record and equatorial seasonality (dashed lines). NP events are listed later in Table 5.2.

The correlation suggests that the cold NP events within the GeoB 1711 and RC24-16 records, consistently lead the corresponding cold periods within the GISP2

atmospheric record, in the ^{14}C constrained 0—45 kyr period, consistent with the findings of *Bender et al.* (1994) and *Charles et al.* (1996). Alternatively, cooling in the southern hemisphere is in phase with warming in the Greenland ice core record and vice versa. Statistical correlation between GeoB 1711 *N. pachyderma* (s) abundances and RC24-16 (seasonality) and GISP2 ($\delta^{18}O$ ice) gives coefficients 0.532 and -0.522 respectively without taking any correlation into consideration. After accounting for a 'typical' graphic correlation, which aligns cold events with cold events (i.e. a relative shift of the GISP2 data ~3 kyr), the correlation coefficients improve to 0.651 and -0.714 respectively without a phase difference between any of the datasets.

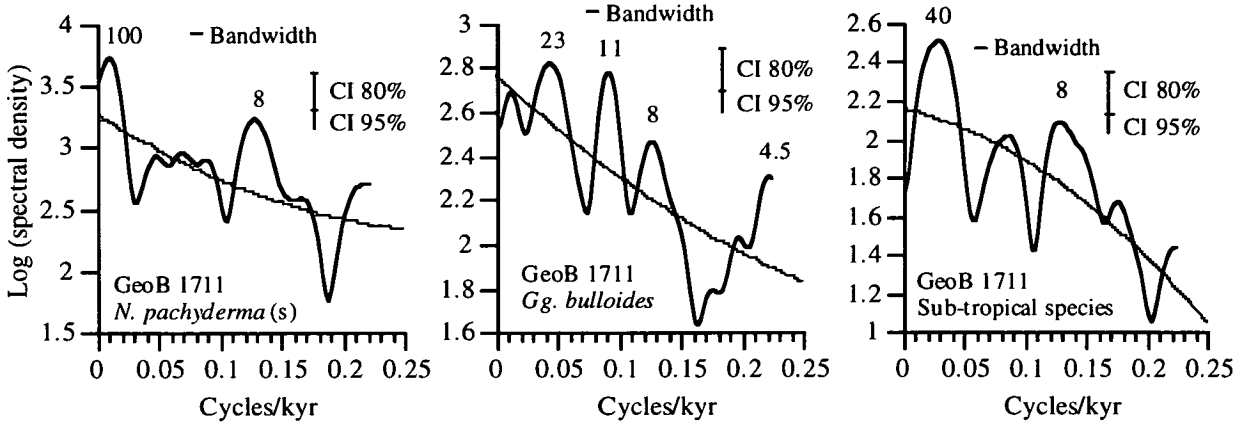

Figure 5.5. GeoB 1711 spectral analysis results. Statistical information: Spectral period analysed, 16—136 ka; Δt = 0.9 kyr; N = 134; CI is shown for 80 lags. For comparison, a second order polynomial expression of the spectral density is shown for the background spectral periodicity. Coherent spectral maxima are highlighted with the period of oscillation (kyr).

The South and equatorial Atlantic lead the North Atlantic response documented by Heinrich layers and are opposing at the higher frequency scale of atmospheric response indicated by the interstadials IS1—IS23. Supporting planktonic foraminiferal abundances from cores GeoB 1706 on the Walvis Ridge, and PG/PC12 on the continental slope demonstrate that with further AMS ^{14}C control on the younger part of these records, the apparent lead visible in Figure 5.4 and calculated in Table 5.1 is a true feature of the South Atlantic records. Indeed, *Imbrie et al.* (1989) showed that South Atlantic SST records consistently lead the North Atlantic SST response by 3-kyr in the precessional cycle. The inter-hemisperic correlation, suggests that the cross-equatorial geostrophic/thermohaline flux plays an important role in northern hemisphere climate change.

Spectral analysis of the entire record for GeoB 1711, of all the main planktonic foraminiferal abundances for the last 140 kyr (Figure 3.8), indicates recurrent spectral power at the 8 and 11—12 kyr periods, generally within the 80% confidence interval constraints and consistent with visual inspection of the records (Figures 5.2). Figure 5.5 presents the results of an iterative spectral analysis, with the Holocene removed from the records, as the large transition from high *N. pachyderma* (s) abundance to almost zero abundance at ~15 ka was thought to disrupt the overall spectral assessment. The spectral analysis for the period 16—136 ka further amplifies the spectra at the 8 kyr period in all of the 'main' components of the Benguela system: *N. pachyderma* (s), *Gg. bulloides* and sub-tropical foraminifera. *Gg. bulloides* also records power at the 23 and 11 kyr periods as discussed in Chapter 3, but with the removal of the last 15 ka gives spectral maxima above the 95% confidence level. The continued recurrence of coherent spectral power above the 80% confidence level at the 8 kyr period, indicates that sub-Milankovitch periodicity is a true feature of the records, and is the dominant forcing in the Benguela upwelling system. This was tested further, by varying the time interval (Δt) and the resolution of the spectral analysis (results not shown). In all cases the records showed spectral power centered on an 8 kyr period, and suggested that the spectral analysis and statistical results are robust.

For comparison, the spectral signatures for the GISP2 $\delta^{18}O$ ice-core and the RC24-16 record of equatorial seasonality are shown in Figure 5.6. The record of planktonic foraminifera derived equatorial seasonality for core RC24-16 has pronounced spectral power at the 23 kyr period, but no spectral power above the 80% confidence level for sub-Milankovitch periodicities, although they can be readily identified by visual inspection of the seasonality record (Figure 5.4). The GISP2 ice core record, with 23 interstadials identified in the last 100 kyr (*Dansgaard et al.*, 1993; *Bender et al.*, 1994), records spectral power at the ~5 kyr period at which the Dansgaard-Oeschger cycles are thought to occur, but not at any other sub-Milankovitch frequency.

The relative mismatch between a consistent 8 kyr periodicity identified in faunal records from the South Atlantic, and the absence of the 8 kyr period in equatorial seasonality, are thought to result from the amplitude differences between the two sets of signals. *N. pachyderma* (s) appears to respond 'immediately' to oceanographic change in the Benguela system, and shows rapid swings in relative abundance. However, its relative disappearence from the record in warm, interglacial periods is

opposing to relative change in equatorial seasonality. Seasonality documents large differences between seasonal SSTs in the glacial stages without the large swings identified in the Benguela system, while it records greater amplitudinal changes in the warm interglacials.

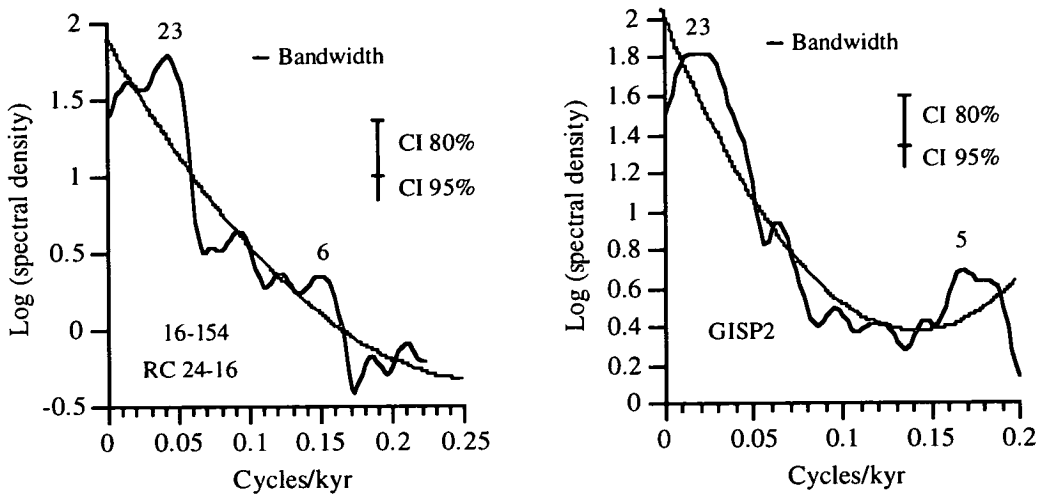

Figure 5.6. Spectral density plots for RC24-16 equatorial seasonality and GISP2 $\delta^{18}O$. Statistical information: (a) RC24-16 (1—183 ka); Δt = 0.9 kyr; N = 203; (b) GISP2 (1—110 ka); Δt = 0.9 kyr; N = 121; A second order polynomial expression of the spectral density is given for the background spectral periodicity, together with the lower limit error bars of the 80 and 95% confidence intervals (CI). RC24-16: CI for 90 lags and GISP2: CI for 60 lags.

The results presented in Figure 3.8 and Figure 5.5 should not be regarded as conclusive proof of high-frequency cyclicity, but are intended to show the increased spectral density in the planktonic foraminiferal variability. The proof for high-frequency cyclicity is the visual inspection of the records themselves, which are highlighted further with a graphic correlation of the filtered records for *N. pachyderma* (s) versus the original dataset (Figure 5.7).

The filtered signals from the *N. pachyderma* (s) record from GeoB 1711 (Figure 5.7) are used to further highlight the dominance of sub-Milankovitch cyclicity. The 8 kyr period was chosen for the sub-Milankovitch filter as it is expressed in all of the spectral analyses as the predominant period of forcing. The filters of the GeoB 1711 *N. pachyderma* (s) record, show that the PS events are concordant with the 8 kyr maxima throughout the dataset but particularly in glacial stages 4—2, when the precessional effect is reduced.

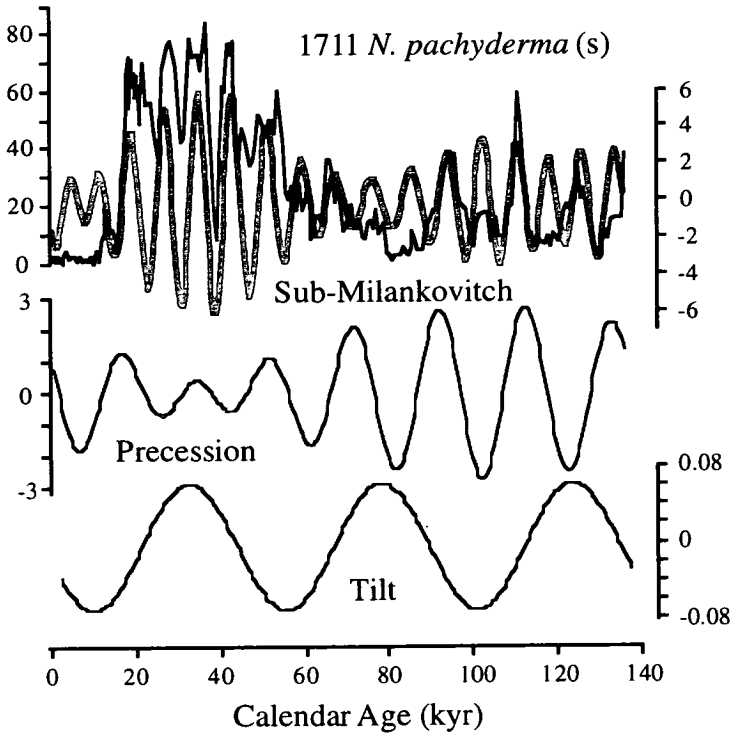

Figure 5.7. Filtered signals of the *N. pachyderma* (s) record of GeoB 1711 (using the Analyseries package of Paillard, CFR/LMCE). The filters are centered on 8, 23 and 41 kyr, with a bandwidth of ~ ± 2 kyr, the sub-Milankovitch filter therefore utilises the frequency range 6—10 kyr. This figure demonstrates that the contributions from the sub-Milankovitch and precessional frequencies dominate late and early sections of the signal, respectively. The sub-Milankovitch filter shows a good correlation with maxima in *N. pachyderma* (s) particularly in the glacial stages 4—2 where the contribution from these frequencies noticeably increases.

The precessional band filter (19—23 kyr) shows an inverse relationship to the sub-Milankovitch filter, with the greatest component transferred from the interval before its nadir at 40—30 ka. The PS events before the glacial period align well with the precessional maxima with the only exception at 125 ka. The 41 kyr filtered record was largely stable throughout the last 120 kyr, i.e. amplitudes of the filtered record do not change, suggesting that there was not a strong influence from tilt on the faunal populations. PS events, at least for the glacial period 60—16 ka, are cycling on a sub-Milankovitch frequency when precession is less dominant than during interglacial stage 5 (*Berger,* 1978b, *McIntyre and Molfino,* 1996).

Moreover, all sediment and ice records, in particular equatorial seasonality, show an interesting feature whereby the data show a clear change of the dominance of frequency at about 60—65 ka. Visual inspection of the seasonality record in particular, shows greatest amplitudinal variations in the earlier part of the record with an enhanced 23 kyr frequency, while the period between 65 and 15 ka has a much higher frequency of change (Figure 5.4 and 5.7). The variable frequency of change suggests that precession seems to be more dominant before 65 ka in the warmer global interglacial regime, but younger than this, the northern Cape Basin is affected by a higher frequency of change, at a time when the normal precessional variation, and insolation, is at its weakest (*Berger et al.,* 1984) and the average global temperature is reduced. The change at 65 ka is also reflected in the GISP2 ice core, with an overall trend from longer term cycles before isotope stage 4 to shorter, higher-frequency change in the glacial stages 4—2 (Figure 5.4).

The concentration of sub-Milankovitch oscillation at the 8 kyr period, is in the maximum glacial interval 16—62 ka. Spectral analysis for *Gg. bulloides,* indicates 'extra' spectral power at the 23 kyr period not significant at the 80% confidence level in the *N. pachyderma* (s) record. This largely results from the on-off nature of the *N. pachyderma* (s) signal, relating to its ecology. *N. pachyderma* (s) records the maximum intensity of upwelling, associated with the highest levels of nutrients and the coolest SSTs, and fluctuates between 0 and 80%, and vice versa, in an interval of less than 5 kyr. This suggests that *N. pachyderma* (s) responds when the equilibrium situation ideal for its habitat is changed, primarily via nutrient availability and the relative shift of the upwelling front across the site of GeoB 1711. As discussed in Chapter 3, *Gg. bulloides* does not respond in the same way, but records the intermittent change in upwelling intensification superimposed on longer term cycles identified as spectral power at the 23 kyr period. Precession is found to dominate climate change at the equator and within the Angola and Guinea Basins (*McIntyre et al,* 1989*; Schneider et al.* 1995; 1997), and the intermittent intrusion of Angola Basin currents over the Walvis Ridge may provide the 23 kyr signal in the *Gg. bulloides* response to change. Unfortunately, the Walvis Ridge record (GeoB 1706) has a missing section during the period of maximum precessional control, and the hypothesis cannot be confirmed conclusively. However, sub-tropical foraminifera which will record the warmest SSTs on the Walvis Ridge, do contain spectral power at the 23 kyr period significant at the 95% confidence level, in agreement with visual inspection of the record for the last 80 kyr (Figure 3.6). This suggests that the

precessional influence at lower latitudes, may play a role in the faunal abundances via communication between the Angolá and Cape Basins at the Walvis Ridge.

Recent studies have used, and often rely, on cross-spectral analysis to prove the correlation and concordancy between two or more seemingly co-varying datasets in an attempt to draw conclusions about forcing mechanisms for the system under consideration. It was thought that the graphic correlation (Figure 5.4) would be ideal for cross-spectral analysis, and that mathematical analysis could resolve the complex integration between ice-core, seasonality and faunal population data. However, after numerous attempts using the full range of statistically viable input parameters (Δt, N, Bw, No. of lags, time interval to be examined) it was realised that a range of results and phasing could be gained. Changing the time interval alone enabled varying levels of coherency between equatorial seasonality (RC24-16) and planktonic foraminifera abundances at different periods (e.g. GeoB 1711 *N. pachyderma* (s) record from 1-136 ka and without the Holocene, 16-136 ka). This also yielded a full range of phasing between the records at different periods of oscillation, (e.g. at the 23 kyr period the 1711 record could lead or lag by up to 4 kyrs, or be in phase with RC24-16 seasonality). Similarly, the filtered signals from either record, centered at different periods with varying ranges of bandwidth and with varying time intervals assessed, resulted in a full spectrum of phasing, but consistently with the GISP2 $\delta^{18}O$ ice record lagging the faunal abundances from GeoB 1711, GeoB 1706 and PG/PC12, correlating with the visual inspection of the records. There are several reasons why cross-spectral analysis is not of use in this situation. *Ralph Schneider* (pers. comm.) suggests that the terminations of the *N. pachyderma* (s) maxima at 55 ka and 15 ka (GeoB 1711) will disrupt the primary signals that Fourier tranformation requires to assess co-correlation between the two datasets, introducing non-linearities in the recording system. *Andrew McIntyre* (pers. comm.) believes the geographical positioning and nature of the dataset acquisition used in the correlation, also provides many possibilities for a poor cross-spectral analysis. Cross-spectral analysis is not considered to be a useful method for quantifying correlation given the spectrum of results which can be achieved by varying the input paramaters. Visual inspection of the records (supported, but not proved by spectral analysis), and graphic correlation, as previously used as the main supporting argument for most Heinrich studies (*Bond et al.*, 1993, *Dansgaard et al.*, 1993, *Grousset et al.*, 1993, *Bender et al.*, 1994), although being subject to interpretation, is considered the most subjective and reasonable method of assessment between the different records when stratigraphic

control is provided using unrelated proxies. In this instance the upper part of all of the records are governed by AMS ^{14}C dates and the lower core-sections using the $\delta^{18}O$ isotope stratigraphy (foraminiferal abundances are not tuned for any periodicity).

5.4. Correlation of palaeoceanographic proxies in the South Atlantic

The *N. pachyderma* (s) abundances from the South Atlantic Ocean show a history of rapid events punctuating the last 140 kyr, temporally consistent with equatorial seasonality and with most of the events recognisable in Greenland ice records. As both northern and southern hemispheres are linked via the oceanic conveyor system, the correlation suggests that the cross-equatorial geostrophic/thermohaline flux plays an important role in northern and southern hemisphere climate change. Before discussing the implications for the North Atlantic, it is necessary to understand the forcing mechanisms behind the observed rapid changes in the Cape Basin and at the equator.

Using planktonic foraminifera derived SSTs from sediment cores in the eastern equatorial Atlantic Ocean, *McIntyre et al.* (1989) concluded that the variations seen in the seasonality records were controlled by two separate factors. First is equatorial trade wind and monsoon-controlled divergence, which controls trade wind meridionality/zonality and, in turn, upwelling intensity. Second is the increased abundance of transitional and sub-polar fauna in the equatorial Atlantic, which led them to believe that heat advection from high southern latitudes also plays a significant role. *Mix et al.* (1986b) suggested that glacial cooling and an enhanced seasonal cycle in the eastern equatorial Atlantic was due to stronger trade winds and equatorial upwelling linked to reduced monsoonal advection. These mechanisms were linked into a two end-member system (section 3.7.2., Figure 3.10): (1) furthest southerly position of the sub-tropical convergence (STC), permitting the greatest pulses of Indian Ocean water to enter into the Atlantic, accompanied by maximum northward heat advection into the Benguela Current; and (2) farthest northerly position of the STC preventing Indian Ocean water entry into the Atlantic by formation of a thermal barrier south of Cape Town and accompanied by equatorward advection of cold water from south of the STC. Equatorward advection of cold waters from the STC should be reflected in very high abundances of cold-water planktonic foraminifera as are used to describe cool SSTs at the equator. Cores taken from the southern Cape Basin, (Section 3.7.3.) show that the cold-water *N. pachyderma* (s) was almost completely

absent offshore Cape Town for at least the last 200,000 years, and in abundances less than 50% in the north of the SBR, even though it is in abundances of up to 90% in the NBR (*Oberhänsli,* 1991, *Schneider,* 1991, *Schmidt,* 1992, *Jansen et al.,* 1997, *Little et al.,* 1997a). If northward advection of cool Southern Ocean surface and intermediate waters was to be playing a major role in the planktonic foraminiferal variations seen in the Benguela upwelling system, then we would almost certainly see the highest abundances of the cold-water *N. pachyderma* (s) in the south of the region. Their absence strongly suggests against cold-water advection of sub-Antarctic surface and intermediate waters from the STC.

A third possibility we must consider is the extension of the Benguela Current into the more northerly Angola Basin and equatorial Guinea Basin by the intensification of the along shore component of the Benguela Current in glacial periods (*Gardner and Hays,* 1976, *Morley and Hays,* 1979, *Diester-Haass,* 1985, *Pokras,* 1987, *Diester-Haass et al.,* 1988, *Mix and Morey,* 1997). This necessitates a westward deflection of the Benguela Coastal Current in the region of 0—5°S, and a shift from the present cyclonic gyre where the Benguela Current is deflected at 23°S. Recent studies do not indicate an intensification of the along shore component of the Benguela Current into the Angola or Guinea Basins (*Jansen and Van Iperen,* 1991, *Schneider et al.,* 1995, *Jansen et al.,* 1997, *Mix and Morey,* 1997). *Schneider et al.* (1996), by using SST records from the Angola Basin and on the Walvis Ridge, show that the Angola-Benguela Front has remained between 12 and 20°S during the last 200 kyr and that the current cyclonic gyre centred on the Angola Basin has existed during this time. The relationship with *N. pachyderma* (s) abundances and the modern day upwelling situation strongly argue that upwelling in the Benguela System is dominated by the trade winds and that its fluctuation corresponds to the movements of the Angola-Benguela Front (*Little et al.,* 1997a).

Direct along shore intensification of the Benguela Current into the Angola Basin is not significant, and instead, an intensification of equatorial upwelling coinciding with intensification of upwelling farther south in the northern Cape Basin should be considered. The result correlating to cold SSTs in the equatorial region and an increased annual SST range promoting increased equatorial seasonality (*Mix et al.,* 1986a; 1986b; *Imbrie et al.,* 1989; *McIntyre et al.,* 1989; *Mix and Morey,* 1997).

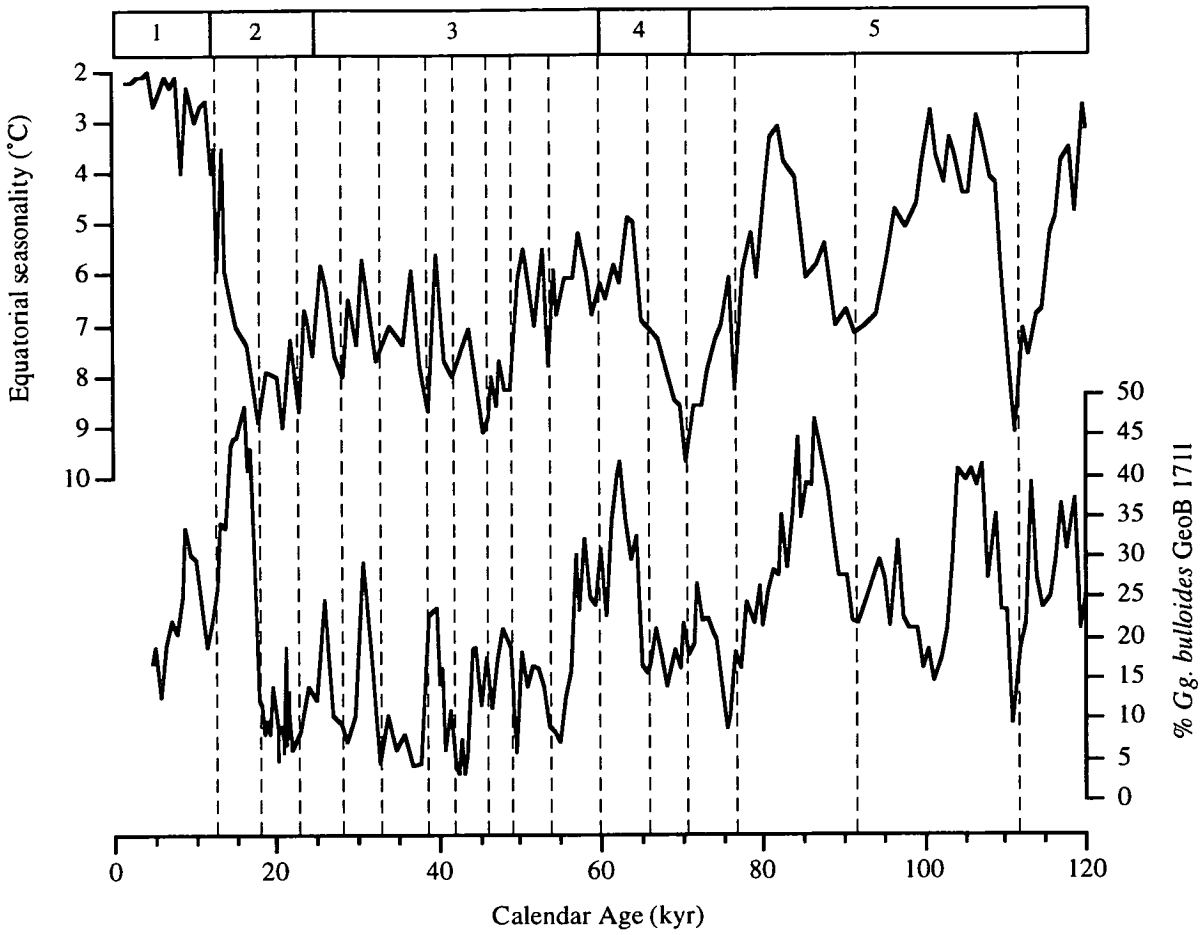

Figure 5.8. Correlation of short-term events in equatorial seasonality (*McIntyre et al.* 1989) and *Gg. bulloides* (GeoB 1711). A graphic representation of oxygen isotope stages is given at the top.

As expressed by the spectral analysis results (Figure 3.8 and 5.5), spectral power at the 23 kyr period in *Gg. bulloides* variability suggests an influence from the equatorial regions particularly at a time when *N. pachyderma* (s) fluctuations do not dominate the relative faunal abundances. When *Gg. bulloides* abundance is compared to the record for equatorial seasonality it is clear that there is an excellent visual correlation (Figure 5.8), except for the Holocene. The short-term variability identified in the *N. pachyderma* (s) fluctuations and correlated to intertadials in the GISP2 ice core, are identified in the record for equatorial seasonality and applied to the *Gg. bulloides* record. The only major discrepancy occurs in the Holocene, when *Gg. bulloides* abundances are less than expected, probably relating to ecology and food type/source. Notably, it is the seasonality maxima (upwelling maxima) that correlate to minimum

abundances of *Gg. bulloides*, as the upwelling in the Benguela is dominated by *N. pachyderma* (s).

There was clearly an intensification of upwelling in the northern Cape Basin at regular intervals over the past 140 kyr (*Little et al.,* 1997a), which was most intense during isotope stages 2 and 3, but was still active, although at a reduced intensity, during stages 4 and 5; similar planktonic foraminiferal analysis, agrees in most part with this assessment (*Oberhänsli,* 1991; *Diester-Haass et al.,* 1992; *Schmidt,* 1992; *Giraudeau et al.,* in prep.; *Jansen et al.,* 1997). Upwelling intensity in the Benguela system correlates to maximum equatorial seasonality, and therefore greatest summer—winter temperature variations, as expressed by *N. pachyderma* (s). There is no evidence in support of the advection of sub-Antarctic waters from the STC, but instead there is ample evidence of extensive cooling associated with trade wind driven upwelling. It is the input of this latter type of cold upwelled water, simultaneous with Benguela coastal upwelling, which *McIntyre et al.* (1989) observed at the equator rather than advection of Southern Ocean surface waters.

Trade wind zonality is strongly related to the seasonality at the equator, as *McIntyre et al.* (1989), *Imbrie et al.* (1989), *Schneider et al.* (1995), *Little et al.* (1995; 1997a) and *Mix and Morey*, (1997) have suggested; but equatorward surface cold-water advection from the Southern Ocean, other than that from upwelling, plays a minor if not insignificant role. At times of maximum trade wind zonality, the eastern boundary of the South Atlantic Ocean and equatorial seasonality records, respond to increased upwelling intensity and relatively cooler SSTs. Equatorial seasonality could be further enhanced if offshore divergence of the Benguela Current intensified the direct input into the equatorial regions via the South Equatorial Countercurrent. Increased trade wind intensity along the entire eastern margin of the South Atlantic, should increase the divergence of warm surface waters away from the coastal upwelling cells and force tropical and sub-tropical waters across the equator via the South Equatorial Current. This will increase the equatorial pool of heat which can be transported to the high northern latitudes by the Gulf Stream and North Atlantic Drift. The BUI transfer function utilises the 'glacial' *N. pachyderma* (s) and the 'interglacial' *Gg. bulloides* as indicators of maximum upwelling intensity, and is thought to give the best qualitative guide to relative intensity and variability of upwelling in the Benguela system.

5.5. Teleconnections in the Atlantic Ocean and atmospheric circulation system

Using the relative abundance of the coccolith species *Florisphaera profunda*, *McIntyre and Molfino* (1996) present a correlation between the millenial-scale pulses of IRD in the North Atlantic to those of *F. profunda* at three equatorial sites situated on the east side of the mid-Atlantic ridge: RC24-02 (0°34.0'N 13°39.0'W, at a depth of 3837 m); RC24-08 (1°20.0'S 11°54.0'W, at a depth of 3885 m); and RC24-17(5°3.0'S 10°11.0'W, at a depth of 3530 m). *F. profunda* is restricted to the lower euphotic zone, and in the equatorial Atlantic its abundance is controlled by the thermocline-nutricline gradient (*Okada and Honjo,* 1973, *Okada and McIntyre,* 1977, *Molfino and McIntyre,* 1990) which is a direct function of trade wind-forced current velocity. Temporal variations in the maximum abundance of *F. profunda* describe a sub-Milankovitch cyclicity centered on the 8.4 kyr period, concordant with calendar ages for Heinrich events H1, H2 and H3, and within reasonable error margins for H4 and H5.

South Atlantic			Mid-equatorial Atlantic	
NP-Event	PS-Event	Calendar Age [a] (kyr)	*F. profunda* Minima	Calendar Age (kyr)
NPYD		13.23	1a	13
NP1	PS1	19.27	2a	19-21
NP2		21.81		
NP3	PS2	28.76	3a	27-29
NP4	PS3	32.74		
NP5		36.71	4a	37
NP6	PS4	42.42	5a	43
NP7		45	6a	45-50
NP8		49		
NP9	PS5	53	7a	55
NP10		61	8a	60-65
NP11	PS6	65		
NP12		71	9a	68-73
NP13		77	10a	75
NP14		95		
NP15		111		

[a] PS-Event centered about this calendar age.

Table 5.2. Comparison of the contemporaneity of NP [*Neogloboquadrina pachyderma* (s)] events from the Benguela system with *F. profunda* maxima from the mid-equatorial Atlantic. NP events record the smaller scale oscillations superimposed on the PS event stratigraphy given in Table 5.1, and graphically correlated to equatorial seasonality and the GISP2 interstadials in Figure 5.4 (dashed lines). NPYD = younger dryas recorded in *N. pachyderma* (s) abundances in GeoB 1711.

Maxima in *F. profunda* are interpreted as intervals of reduced trade winds (*Molfino and McIntyre,* 1990), largely coincident but with a slight phase lead (~500 years), with North Atlantic IRD maxima (*Bond and Lotti,* 1995). *F. profunda* maxima (trade wind meridionality) occur at approximately 8, 16, 25, 33 and 41 ka (calendar years from AMS ^{14}C dating), with corresponding minima (trade wind intensity) at 13, 19—21, 27—29, 37 and 43 ka from the record of RC24-08 and additional minima at approximately 45—50, 55, 60—65, 68—73, and 75 ka (calendar years from oxygen isotope stratigraphy) from the longer record of RC24-02.

These rapid intervals of trade wind intensification are contemporaneous with the NP events recorded in core GeoB 1711, with the exception of NP 4 (32.74 ka); Table 5.2. NP events highlight the higher frequency variations in trade wind intensity, superimposed of the PS event stratigraphy, which are correlated with interstadials in the GISP2 ice core and similar events in the record of equatorial seasonality (Figure 5.4). The mid-equatorial Atlantic records from RC24-08 and RC24-02 further suggest that increased trade wind zonality is the dominant forcing mechanism affecting equatorial and eastern South Atlantic faunal populations. The following is a discussion of the hypothesised forcing mechanisms required to produce the contemporaneity of phasing of the southern, equatorial and northern Atlantic climate signatures.

From the correlation of *F. profunda* variability with North Atlantic IRD deposits, *McIntyre and Molfino* (1996) hypothesised a long-term El Niño-type mechanism to account for the cross-equatorial transfer of heat to higher northern latitudes. Strong zonal trade winds increase the net displacement of warm tropical and sub-tropical waters from the eastern equatorial belt to the Caribbean and Gulf of Mexico increasing the dynamic height in the Caribbean to ~1 m above the Atlantic at the same latitude, and ~2 m above the sub-polar North Atlantic. The increase in intensity is recorded by minima in *F. profunda* abundances, and corresponding maxima in *N. pachyderma* (s) abundances and equatorial seasonality (*McIntyre et al*, 1989). The following decrease in trade wind intensity from GeoB 1711, decreases cross-equatorial displacement and 'releases' the warm waters 'stored' in the Gulf of Mexico and Caribbean. As there is no direct oceanographic connection to the equatorial corridor, these warm saline-rich waters flow into the western boundary current and intensify the heat and moisture flux into the Gulf Stream and to the high latitudes of the North Atlantic. Although the *F. profunda* abundances most certainly reveal variations in trade wind intensity, it is

unlikely that warm-water will be 'stored' in the Gulf of Mexico without overflowing and enhancing the warm-water transport in the Gulf Stream at times of trade wind intensification.

The *N. pachyderma* (s) records from GeoB 1711, GeoB 1706 and PG/PC12 suggest another relationship between the ice-calving and subsequent IRD deposits which correlate to times of diminished trade winds (*F. profunda* maxima). During the period of increased trade wind and upwelling intensity in glacial stages 4—2, the *N. pachyderma* (s) record is punctuated by anomalous abundance minima. These periods of low percentage relative abundance of *N. pachyderma* (s) represent rapid short-lived warmer intervals at a time of glacial cooling, reflecting decreased trade wind strength as monsoonal winds increased over eastern and central Africa. Contrary to this, the cool NP events, which are thought to be typical for the eastern South Atlantic continental margin, correlate to warmer climate intervals in the Greenland ice records and sub-Arctic ocean SSTs (*Ruddiman and McIntyre,* 1981). The Benguela Current system could be regarded as the major component influencing cross-equatorial teleconnections between the South Atlantic and North Atlantic via the South Equatorial and the North Brasil Currents into the Gulf Stream, driven by variations in atmospheric conditions controlling trade wind intensity. Cold water resulting directly from intense trade wind-driven upwelling, will produce cold SSTs and lowered salinities along the entire eastern South Atlantic margin. Direct cross-equatorial transfer of this cooler water into the Gulf Stream, similar to that from hypothesised meltwater models, would have had an almost instantaneous cooling effect on North Atlantic records rather than a lead of 3-kyr as is implied from correlation with the timing of Heinrich events. With respect to northern hemisphere climate change indicated in the GISP2 record, it appears that southern hemisphere trade winds have been reduced at times of maximum cooling and vice versa, thus another hypothesis is required.

The ^{14}C constrained upper part of the four southern hemisphere records (Figure 5.3; Table 5.1), suggests a 3 kyr lead of the southern hemisphere to the northern hemisphere. The variation of SST at 16 sites in the Atlantic Ocean (*Imbrie et al.,* 1989) produced the same result, and without exception, all coherent temperature responses south of the equator lead changes in ice volume in the precessional band (also recorded by *McIntyre et al.,* 1989), and all coherent North Atlantic responses lag ice volume change. The greatest leads occur in the equatorial and South Atlantic, and

describe a 3 kyr phase lead to the changes in ice volume over the precessional band. The lagging warmth in the high latitudes of the North Atlantic were discussed by *Ruddiman and McIntyre* (1981; 1984) and can be explained using a model of feedback mechanisms to increase moisture flux to the high latitudes of the North Atlantic to accelerate iceberg growth.

Ruddiman and McIntyre (1981) discuss the relationships between summer insolation, ice sheet build-up and moisture flux, and describe how moisture made available to the ice sheets in the North Atlantic Ocean forms a mechanism for the rapid growth and decay of Northern Hemisphere ice. The northwestern sub-tropical gyre and the sub-Arctic ocean remain near their maximum SST into the phase of maximum ice building, creating optimal conditions for rapid ice growth by providing moisture due to the large temperature gradient between the atmosphere and ocean. The GeoB 1711 data set reinforces this relationship but suggests that enhanced cross-equatorial transfer of warm waters into the Gulf Stream at times of trade wind intensity, increases warm-water advection to the higher latitudes of the North Atlantic and maintains the elevated SSTs into the phase of maximum ice building. Without very high resolution records the precise timing of events in the northern and southern hemisphere cannot be quantified conclusively, but the phase difference suggested by this and previous work (*Imbrie et al.*, 1989; *Charles et al.*, 1996; *Abelmann et al.*, 1997) suggests a real lead of the South Atlantic Ocean.

Boulton and Payne (1994) modelled mid-latitude northern hemisphere ice sheet growth and have suggested that Heinrich scale instabilities and ice calving could result from internal thermal instabilities as a result of changes in the basal boundary conditions of the ice sheets. A reduction in basal friction, leading to relatively rapid reduction in ice sheet thickness and eventual calving of icebergs, could result from an increase in the accumulation rate of snow, melting at the base of the ice sheet, and/or from an expansion of the ice sheet over a deformable surface. Modelled results suggest that ice sheet calving could occur approximately every 4 kyr, following a 2—3 kyr increase in the accumulation of snow, as is predicted by the 3-kyr lead of the southern Atlantic Ocean. Furthermore, *Boulton and Payne* (1994) believe that the basal geology beneath the margins of the Laurentide and European ice sheets will be susceptible to sliding and aid calving very similar to the modelled results. A relative increase in moisture supply to the atmosphere in the higher latitudes of the North Atlantic would be enough to create basal instability leading to a rapid ice-calving event and IRD deposit.

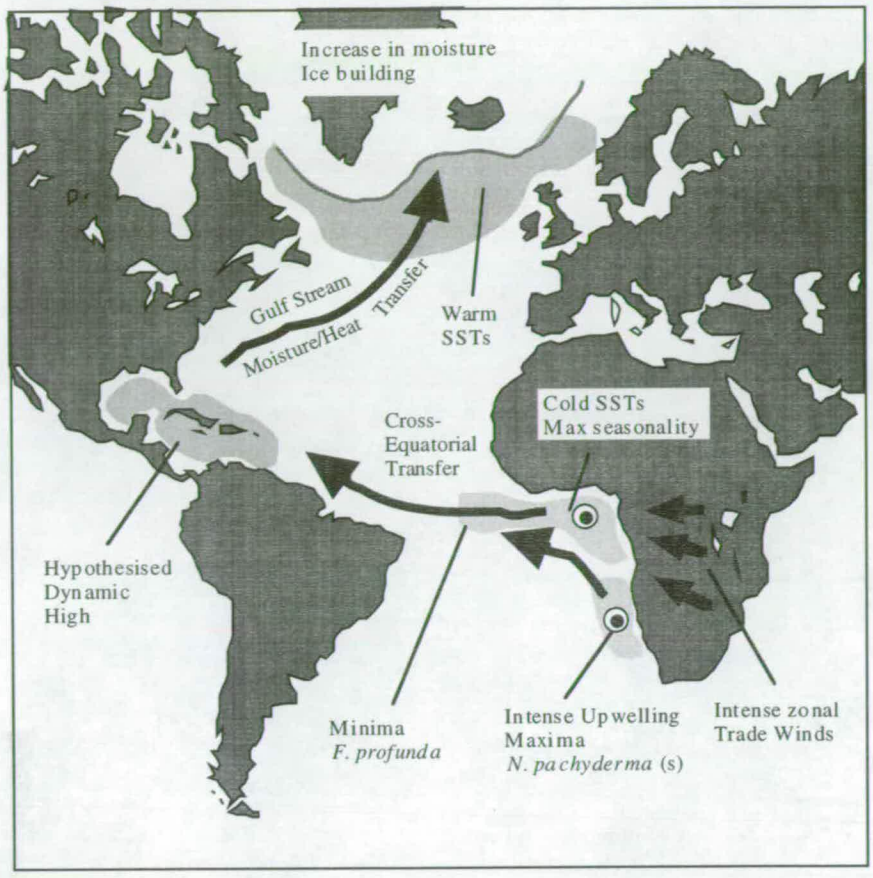

Figure 5.9. Schematic diagram illustrating the inferred seqence of events in a PS event. Intense zonal trade winds: As polar glaciation begins, increased thermal gradients drive stronger zonal trade winds, strong equatorial and NBR upwelling, and maximum cross-equatorial divergence of warm water. Associated with high abundances of *N. pachyderma* (s) and other upwelling species, and low abundances of *F. profunda* at the mid-Atlantic ridge. Strong winds are hypothesised to create a dynamic high in the Gulf of Mexico and Caribbean whilst 'excess' warm water intensifies the net flux of moisture and heat to the high latitudes of the North Atlantic via the Gulf Stream. Elevated SSTs in the sub-Arctic ocean increase moisture supply and precipitation on the neighbouring ice sheets enhancing ice sheet growth and lateral expansion. Ice sheets expand latitudinally and approach basal friction equilibrium which inevitably leads to ice sheet instability and iceberg discharge. The increased supply of saline-poor, cold water from the ice sheets, together with the reduced cross-equatorial flow of warm, sub-tropical water, slows the rate of the thermohaline conveyor further accentuating North Atlantic cooling.

Bond and Lotti (1995) used a high resolution record for the interval 10,000 to 38,000 radiocarbon years ago covering Heinrich events H4—H1 in the North Atlantic and

reported 13 ice-rafting cycles with an average duration of between 2000 and 3000 years, correlating to the Dansgaard-Oeschger temperature cycles recorded in the Greenland Summit ice cores. The rapid intervals of IRD reflect an increase in the amount of glacial ice discharged into the North Atlantic Ocean every 2000—3000 years in the cold glacial period. The findings from this research point to a dominant mechanism operating within the atmosphere that caused rapid oscillations in air temperatures above Greenland and a recurring internal process, such as basal sliding (*Boulton and Payne,* 1994), to produce icebergs calved from more than one ice sheet to alter the North Atlantic's heat conveyor. The resulting ocean surface coolings triggered further iceberg discharges and amplified the temperature shifts. The compositional data, derived from an analysis of the lithic fragments constituting the IRD deposits, do not rule out iceberg discharges from the Greenland, Barents or Scandinavian ice sheets, but suggest the greatest component came via the Gulf of St Lawrence (*Bond and Lotti,* 1995).

The observations from the southern, northern and equatorial Atlantic can be collectively described using a model of oceanic response to trade wind forcing. During intervals of trade wind intensification (Figure 5.9) equatorial divergence is at a maximum, recorded by minimum abundances of *F. profunda* and maximum equatorial seasonality. Trade wind intensification increases upwelling intensity in the northern Benguela region shifting the system and ABF equatorwards, this is recorded as maximum abundances of the upwelling fauna along the entire coastal belt of the eastern South and equatorial Atlantic. There is a net increase in the cross-equatorial transfer of heat to the Gulf of Mexico and higher northern latitudes via the Gulf Stream, delivering warm saline water to the northwestern sub-tropical gyre and sub-polar ocean. At these high latitudes of the North Atlantic the large temperature gradient between the atmosphere and ocean, caused by the raised SST at a time of glacial cooling, provides increased moisture and precipitation onto the increasing ice masses. When the trade winds diminish, identified by maxima of *F. profunda* and equatorial seasonality, and minima of *N. pachyderma* (s), ice sheets have grown to their maximum latitudinal extent and become internally unstable (basal friction). As the hypothesised dynamic high in the Gulf of Mexico and Caribbean (*McIntyre and Molfino,* 1996) is directly released into the Gulf Stream and not delayed, then the thermal gradient in the sub-polar North Atlantic is intensified, amplifying the ice sheet instability and accelerating iceberg calving into the North Atlantic. Iceberg release

further amplifies the temperature shifts recorded in the North Atlantic sediment records and the Greenland atmospheric records.

Our observations, and the new record correlating marine sediment core and ice core records from the Southern Ocean (*Charles et al.,* 1996), suggests millenial scale 'conveyor-belt' changes occur in all of the Earth's major ocean basins in both northern and southern hemispheres. The entire dataset is strongly suggestive of a globally linked atmosphere-ocean system varying via changes in trade wind intensity, linked to sub-Milankovitch climate variability derived from the insolation-linked precessional band.

5.6. Summary

Relative abundances of the cold-water planktonic foraminifera, *N. pachyderma* (s), record rapid upwelling events (PS events) punctuating the last 140 kyr, on a sub-Milankovitch cyclicity between 8—10 kyr. Records in the equatorial Guinea Basin and the more southerly Angola and Cape Basins have also shown upwelling intensification to be the primary control on faunal and SST patterns. Correlation between *N. pachyderma* (s) abundances from the northern Cape Basin and eastern equatorial seasonality record (*McIntyre et al.,* 1989), and *F. profunda* abundances on the equatorial Mid-Atlantic Ridge, suggests that the western margin of southern and equatorial Africa is dominated by fluctuations in trade wind intensity. Radiocarbon dating for the last 45 kyr permits a further correlation between PS events in the northern Cape Basin with Heinrich events of the North Atlantic, and suggests teleconnections in South Atlantic—North Atlantic and global heat transfer.

Intense upwelling events on a sub-Milankovitch cyclicity occurred throughout the last 140 kyr, in particular during the last glacial cycle (isotope stages 4—2), controlled by changes in intensity of the trade winds at times of maximum ice build-up and minimum solar insolation, and indicate a 3-kyr phase lead of the South Atlantic to corresponding changes in northern hemisphere sediment records. The increase in trade wind controlled offshore displacement of tropical and sub-tropical waters may have implications for the strength of equatorial transfer into the North Atlantic, via the South and North Equatorial Currents and the Gulf Stream, and for the global thermohaline conveyor and Atlantic convection. The tropical warm-water which is forced across the equator, is transported to the high latitudes of the North Atlantic into the phase of

maximum ice building. This intensifies the moisture gradient between the sub-Arctic ocean and the northern hemisphere ice sheets, increasing the rate of snow accumulation until eventual ice sheet collapse and iceberg calving.

Furthermore, the sub-Milankovitch frequencies at which these rapid upwelling events occur have also been described for sediment cores within the Pacific (*Kennett and Ingram,* 1995, *Behl and Kennett,* 1996), northern (*Hagelberg et al.,* 1994), and southern Atlantic Oceans (*Park et al.,* 1993; *Charles et al.,* 1996) and within the Greenland (*Bender et al.,* 1994, *Mayewski et al.,* 1994) and Vostok (*Yiou et al.,* 1991) ice cores. The palaeoceanographic records analysed in this study demonstrate further, that high frequency sub-Milankovitch cyclicity is a global phenomenon and that cross-equatorial heat transfer via trade wind intensification may have serious repercussions for global climate.

Surface circulation of the southern Benguela system and its relationship to variable warm-water input from the Indian Ocean and movement of the sub-tropical convergence

Ch.6

Chapter 6. Surface circulation of the southern Benguela system and its relationship to variable warm water input from the Indian Ocean and movement of the sub-tropical convergence

6.1. Introduction

Previous research in the Southern Atlantic Ocean and Southern Indian Ocean has put much emphasis on the temporal patterns and timing of shifts in the Antarctic Polar Front (APF) and the sub-tropical convergence (STC) with the timing of relative flux of the North Atlantic Deep Water (NADW) [*Hays et al.,* 1976, *Corliss,* 1982, *Imbrie et al.,* 1984, *Oppo and Fairbanks,* 1987, *McIntyre et al.,* 1989, *Morley,* 1989a; 1989b, *Howard and Prell,* 1992, *Charles et al.,* 1996]. The STC marks the boundary between the South Atlantic and the Southern Ocean and also represents the boundary between the Antarctic Circumpolar Current (ACC) and the South Atlantic anticyclonic gyre (SAAG) near to 40°S. Surface circulation and mixed-layer dynamics in this region are linked to southern high-latitude wind and sea ice fields, influencing cross-equatorial surface heat flux and inter-hemispheric atmospheric mechanisms. The abundance of planktonic foraminifera are used to assess their suitability as palaeoceanographic and palaeoproductivity indicators with the anticipation that this will allow further insight into warm-water Indian Ocean input via the Agulhas Retroflection and its effect on Atlantic and global climate change.

The objectives of this chapter were to assess the influence of sub-Milankovitch periodicity on warm-water input from the Indian Ocean, and its correlation with PS events in the NBR. However, the sedimentation rate offshore Cape Town was found to be much less than that for the NBR, and a suitable high resolution record could not be gained. Direct comparison between the timing of advection from the Agulhas Retroflection with respect to upwelling in the northern Cape Basin is thus not possible. Instead, this chapter analyses the longer term changes affecting South Atlantic and Indian Ocean communication. Is Milankovitch orbital forcing the dominant mechanism driving instability in faunal records, as seen in the equatorial Atlantic (*McIntyre et al.,* 1989, *Schneider et al.,* 1995; 1997)? Can we recognise relative shifts of the STC, or warm-water input from the Indian Ocean, in the variabilty of the planktonic foraminiferal abundances? The relative shifts of the STC, or warm-water advection, may have serious implications for the long-term nature of the thermohaline circulation. The addition of warm, saline-rich water to the conveyor,

which transports this heat to the high latitudes of the North Atlantic across the equator, will increase the ocean's potential to sink and accelerate deep water production. Inversely, a reduction in the amount of water added to the system, will relatively decelerate deep water production and oceanic convection. The implications of this mechanism are far reaching as NADW production is considered probably the most important key to oceanographic change, including amplification of glacial—interglacial cycles, and therefore global warming and cooling, and initiation of carbonate dissolution or preservation (*Luz and Shackleton,* 1975, *Crowley,* 1985, *Peterson and Prell,* 1985, *Farrell and Prell,* 1989, *Haddad and Droxler,* 1996). This new core from the continental shelf offshore Cape Town, is in an ideal position to monitor warm- and cold-water input into the Benguela and oceanic system, and to test global teleconnections with NADW production and timing of dissolution and preservation cycles in the Atlantic and Pacific Oceans.

6.2. Regional surface oceanography

The STC marks the southern edges of the sub-tropical gyres with a surface expression of increased sea surface temperature (SST) and salinity located at about latitude 40°S (Figure 6.1). The STC is usually characterised as a zone of rapid SST change between the 10°C and 14°C winter isotherms, and between the 14°C and 18°C summer isotherms (*Garner,* 1959, *Peterson and Whitworth,* 1989, *Howard and Prell,* 1992). In the South Atlantic at 30°S the boundary of the STC is defined by surface temperatures near 16°C. The warmer, more saline water to the north appears to have its source in the Brazil Current, the colder, fresher water to the south coming from the Falkland Current branch of the Antarctic Circumpolar Current (*Webb,* 1997).

The Agulhas Current is the western boundary current of the southern Indian Ocean and is most intense between Durban and Port Elizabeth along the eastern coastline of southern Africa. It extends deeper than 2000 m and has surface speeds that often exceed 2 m/s and a mean transport of about 100 million m^3/s. South of Africa, it turns abruptly eastwards in a tight retroflection loop, the southern part of which is known as the South Indian Ocean Current. The STC is very pronounced to the south of Africa where Agulhas Current water is forced into the system (Figure 6.1).

There are a number of water masses present off the coast of southwestern Africa, including tropical and sub-tropical surface waters, thermocline water (comprising

South Atlantic Central Water, South Indian Central Water, and tropical Atlantic Central Water), AAIW, NADW, and AABW. The thermocline waters overlie the AAIW, the core of which lies at an average depth of 700—800 m in the southeast Atlantic (*Shannon and Nelson,* 1997) and somewhat deeper in the Agulhas Retroflection area. *Valentine et al.,* (1993) have estimated that, on a volumetric basis, AAIW accounts for 52% of the water masses above the 1500 m bathymetric contour off southern Africa. An input of relatively fresh and oxygen-rich AAIW enters into the Benguela Current from the southwest diluting the input of AAIW from the Indian Ocean, which has been estimated to be about 50% of the AAIW in the Benguela area (*Gordon et al.,* 1992).

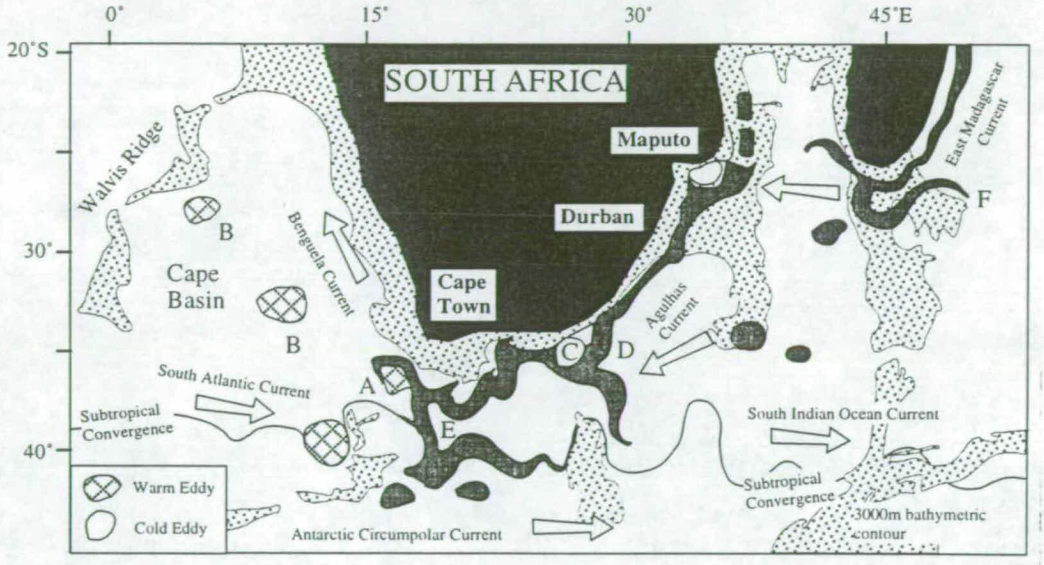

Figure 6.1. Oceanography and bathymetry of the main mesoscale and larger features of circulation in the upper ocean layers of the southern Benguela upwelling system (modified from *Lutjeharms,* 1997). **A** is an Agulhas ring, recently shed from the Agulhas retroflection (**E**), being encircled by an Agulhas filament. **B**s are Agulhas rings drifting off into the South Atlantic. **C** is a cyclonic cold eddy forming part of the Agulhas Current causing an upstream retroflection (**D**) at the Agulhas Plateau. **F** is the retroflection of the East Madagascar Current.

6.3. Southern Atlantic GeoB 3602 Chronostratigraphy

GeoB 3602 is situated at a water depth of 1885 m on the continental slope offshore Cape Town (34°47'9 S 17°45'3 E; Figure 1.1). Stratigraphic age control comes from the oxygen isotopes of the tests of the planktonic foraminifer, *Gr. inflata,* measured at the Fachbereich Geowissenschaften, Universitat Bremen, Germany. The oxygen

isotope record is correlated using the oxygen isotopic event classification for the Pleistocene provided by *Prell et al.* (1986), and age assignments after *Imbrie et al.* (1984). The oxygen isotope record for GeoB 3602 is placed on the SPECMAP time scale for graphic correlation in Figure 6.2 and the isotope control points are given in Table 6.1. In addition to oxygen isotope stratigraphy, a preliminary nannofossil study detailed the absence of *Emiliana huxleyi* [1] but the presence of *G. lacunosa* and large abundances of *G. oceanica* at the bottom of the core (*Martin Cépek* and *Ralph Schneider*, pers. comm.) making the core base at least 461 ka [*G. lacunosa* last appearence = 461 ka (oxygen isotope sub-stage 12.33); *Thierstein et al.*, 1977]. The ages have been assigned by linear interpolation to depths that lie between listed isotope control points.

Depth (m)	Age (kyr)	Events	Depth (m)	Age (kyr)	Events
CT 0.03	0	Present	5.43	287	8.5
1.03	19	2.2	5.53	299	8.6
1.18	53	3.3	5.73	310	9.1
1.63	80	5.1	6.13	331	9.3
3.03	122	5.5	6.43	341	10.2
3.38	151	6.4	6.68	362	11.0
3.63	171	6.5	8.33	423	12.0
3.78	183	6.6	8.63	478	13.0
4.08	205	7.2	8.88	491	13.12
4.53	228	7.4	9.18	502	13.13
4.88	249	8.2	9.68	513	13.2
5.08	269	8.4	CB 9.88	524	14.0

Table 6.1. Oxygen isotope control points for GeoB 3602. Age picks for GeoB 3602 were allocated using the oxygen isotope stratigraphy for GeoB 3602. Control points are from *Imbrie et al.* (1984); CT = core top; CB = core base.

6.4. Planktonic foraminiferal records from the southern Benguela region, Cape Town

The relative abundance of planktonic foraminifera in the South Atlantic core GeoB 3602 are presented in Table 6.2. Of the twenty four planktonic foraminifera species identified in GeoB 3602, 78% of the overall downcore average abundance is accounted for by three species *Gr. inflata, N. pachyderma (d),* and *Gg. bulloides.* The remaining, largely sub-tropical fauna, make up on average 19% of the total

[1] First appearence of *Emiliana huxleyi* is 265 ka (*Thierstein et al.*, 1977).

assemblage of which almost 7% is attributable to the spinose warm-water tropical species of *Gg. ruber, Gs. sacculifer* and *Ge. siphonifera* (*Ge. aequilateralis*).

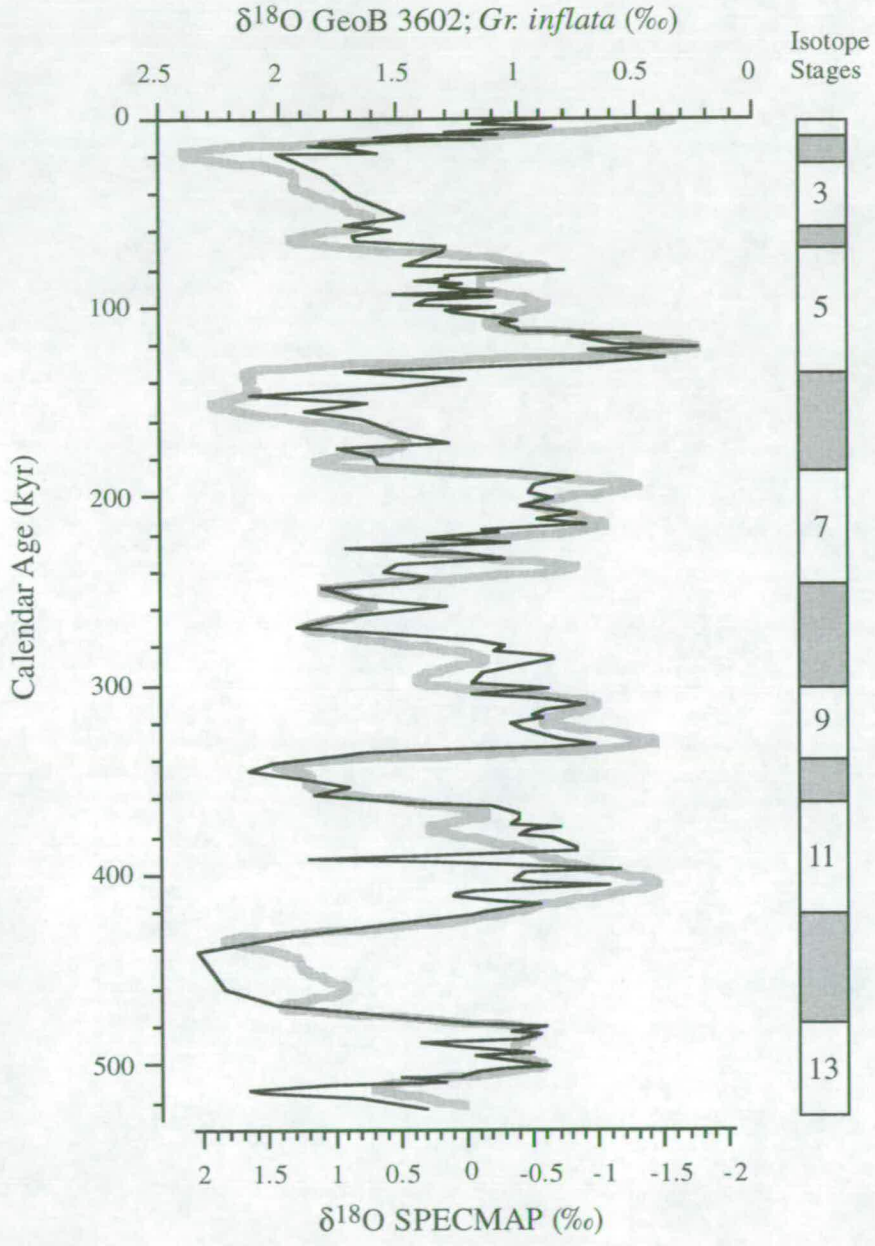

Figure 6.2. Oxygen isotope control points for GeoB 3602, and correlation with SPECMAP. Age control points are derived from *Imbrie et al.* (1984).

Three species make up almost 80% of the total planktonic foraminifera abundance recorded offshore Cape Town. *Gr. inflata* constitutes the largest average fraction of the fossil record, with a slightly smaller contribution from *N. pachyderma* (d) and

Gg. bulloides, with approximately 20% of the total fossil abundance from sub-tropical and tropical species. Overall the species diversity of planktonic foraminifera, with an average abundance greater than 1%, is larger offshore Cape Town than it is nearer the equator in the NBR. The abundances of the main species, together with the sum total of sub-tropical species [2], tropical spinose species [3] and total benthic foraminifera (as a percentage of the total foraminifera), are plotted against depth and given in Figure 6.3.

Species	Average (%)	Maximum (%)
Gr. inflata	30.8	53.5
N. pachyderma (d)	26.1	65.0
Gg. bulloides	21.5	42.1
N. dutertrei	5.8	13.8
Gs. ruber	5.0	11.9
Gr. truncatulinoides	3.4	12.6
Ga. glutinata	1.8	6.6
N. pachyderma (s)	1.1	15.5
Gs. sacculifer	1.0	5.9
Gr. scitula	0.6	2.9
Ge. siphonifera	0.6	2.7
O. universa	0.5	3.9
Gg. quinqueloba	0.5	3.7
Gr. crassaformis	0.3	4.2
P. obliquiloculata	0.2	1.9
Gr. hirsuta	0.2	1.5
Gr. menardii	0.2	1.4
Gg. tenellus	0.1	2.9
Gg. falconensis	0.1	1.4
Gg. digitata	0.1	1.4
Ge. calida	0.1	1.1
Gg. conglobatus		2.0
Ga. uvula		0.5
Gg. rubescens		0.4
Tropical spinose foraminifera	6.6	16.0
Sub-tropical foraminifera	19.1	34.5
Benthic foraminifera	3.8	31.4

Table 6.2. Summary of downcore planktonic foraminiferal species abundances for GeoB 3602.

[2] Sub-tropical species = *N. dutertrei, Gs. ruber, Gr. truncatulinoides, Ga. glutinata, Gs. sacculifer, Ge. siphonifera, O. universa, P. obliquiloculata, Gr. hirsuta, Gr. menardii, Gg. digitata, Ge. calida, Gg. conglobatus, Ga. uvula* and *Gg. rubescens*

[3] Spinose species = *Gs. ruber, Gs. sacculifer* and *Ge. siphonifera*

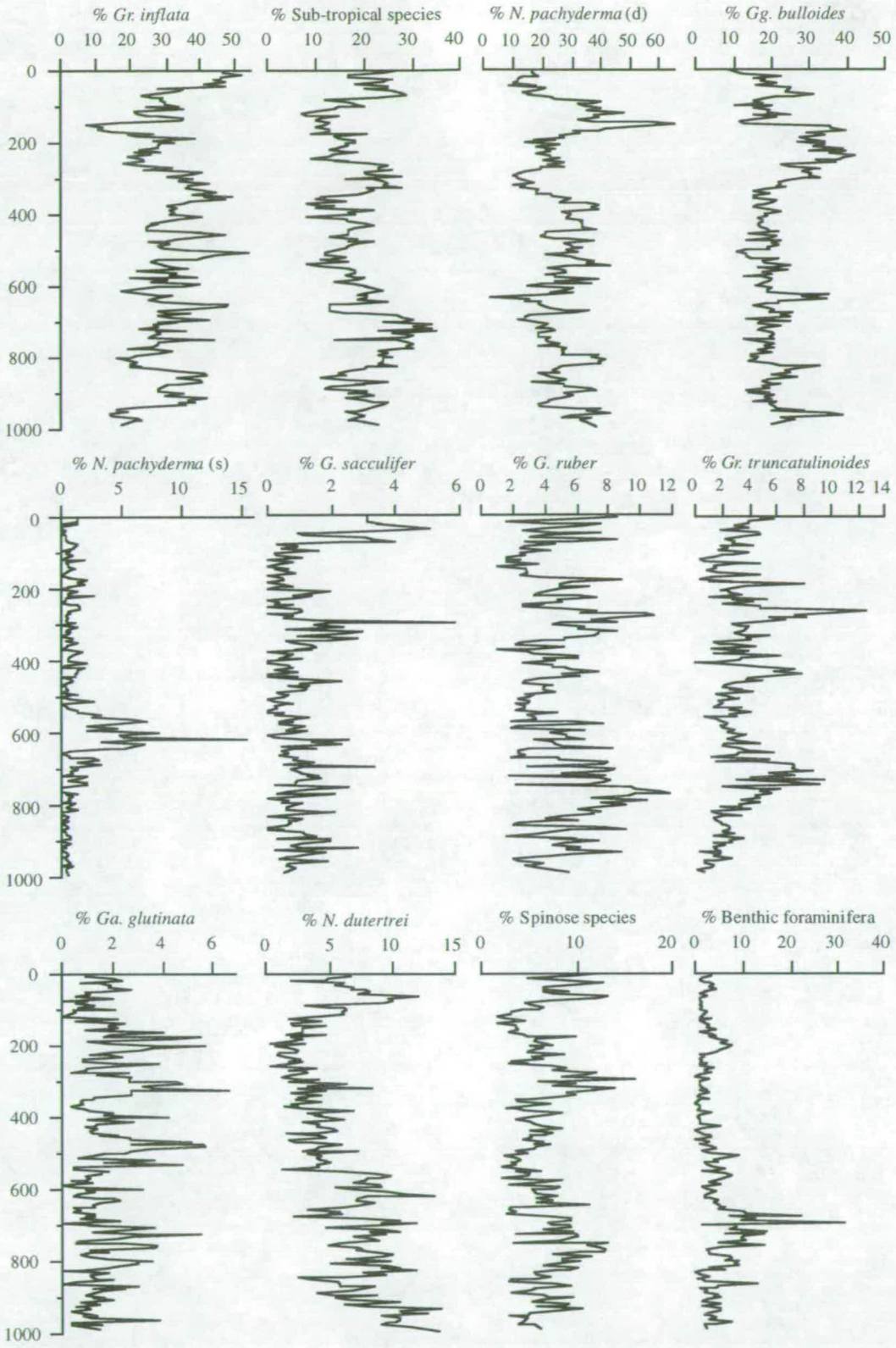

Figure 6.3. GeoB 3602. Abundances of the main planktonic foraminifera (as a percentage of the total foraminifera), sub-tropical species, tropical spinose species, and the ratio of benthic-planktonic foraminifera, all against depth (cm).

In the southern Indian Ocean, *Gr. inflata* is thought to be an indicator of the southern margin of the sub-tropical Gyre, most abundant during the interglacial oxygen isotope stages (*Howard and Prell*, 1992). Exceptions to this pattern occur in some intervals where carbonate dissolution has increased the abundance of the solution-resistant *Gr. inflata*.

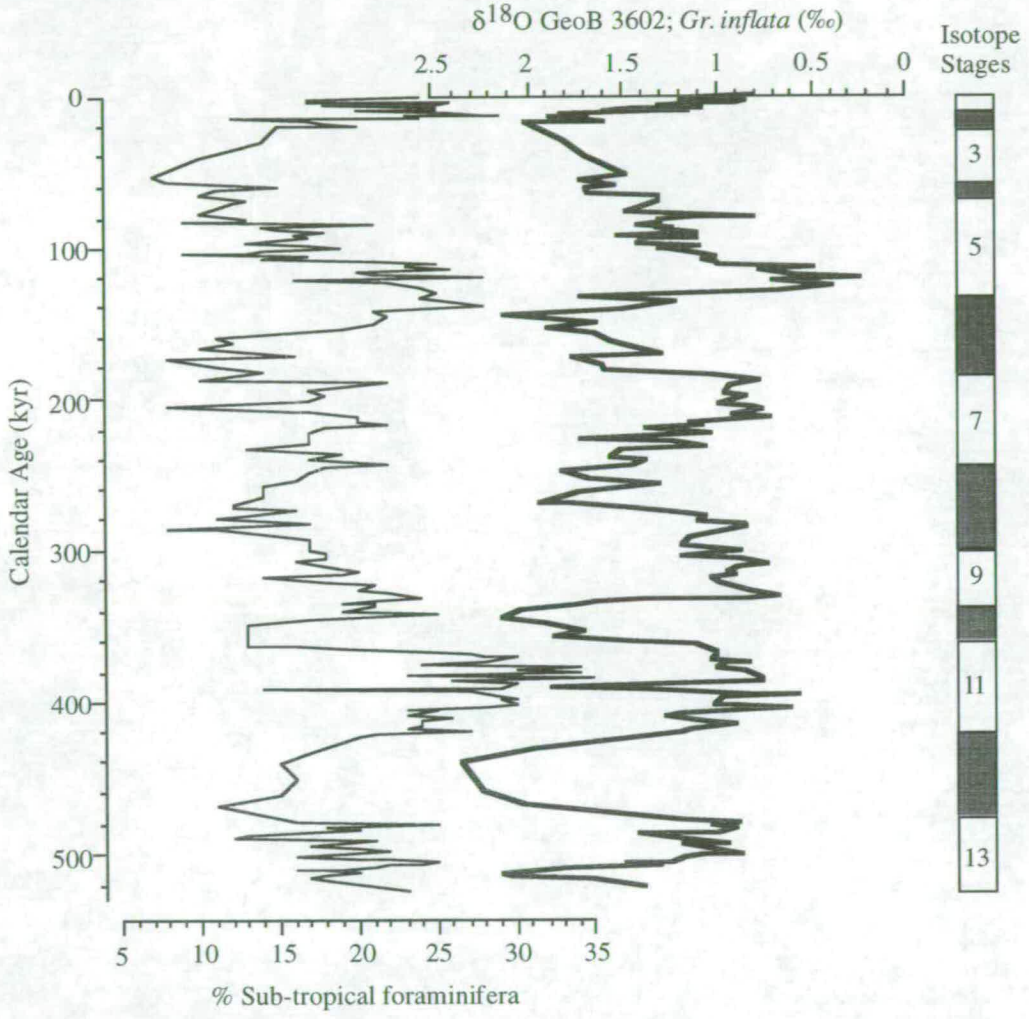

Figure 6.4. Correlation of sub-tropical planktonic foraminiferal abundance (as a % of the total) with $\delta^{18}O$ *Gr. inflata*. Graphic representation of oxygen isotope stages is given to the right hand-side (interglacials - white; glacials - shaded).

However, in core GeoB 3602 the thin-walled spinose foraminifera *Gs. sacculifer*, *Gs. ruber* and *Ge. siphonifera* show highest abundances generally coinciding with intervals of maximum abundance of *Gr. inflata* (Figure 6.3). This suggests that

dissolution does not play an important role in the relative abundance of the planktonic foraminifera. The total abundance of sub-tropical planktonic foraminifera, largely follows the glacial—interglacial changes described by oscillations in the $\delta^{18}O$ record (Figure 6.4). Differences between the records are roughly within the noise level of such fluctuations.

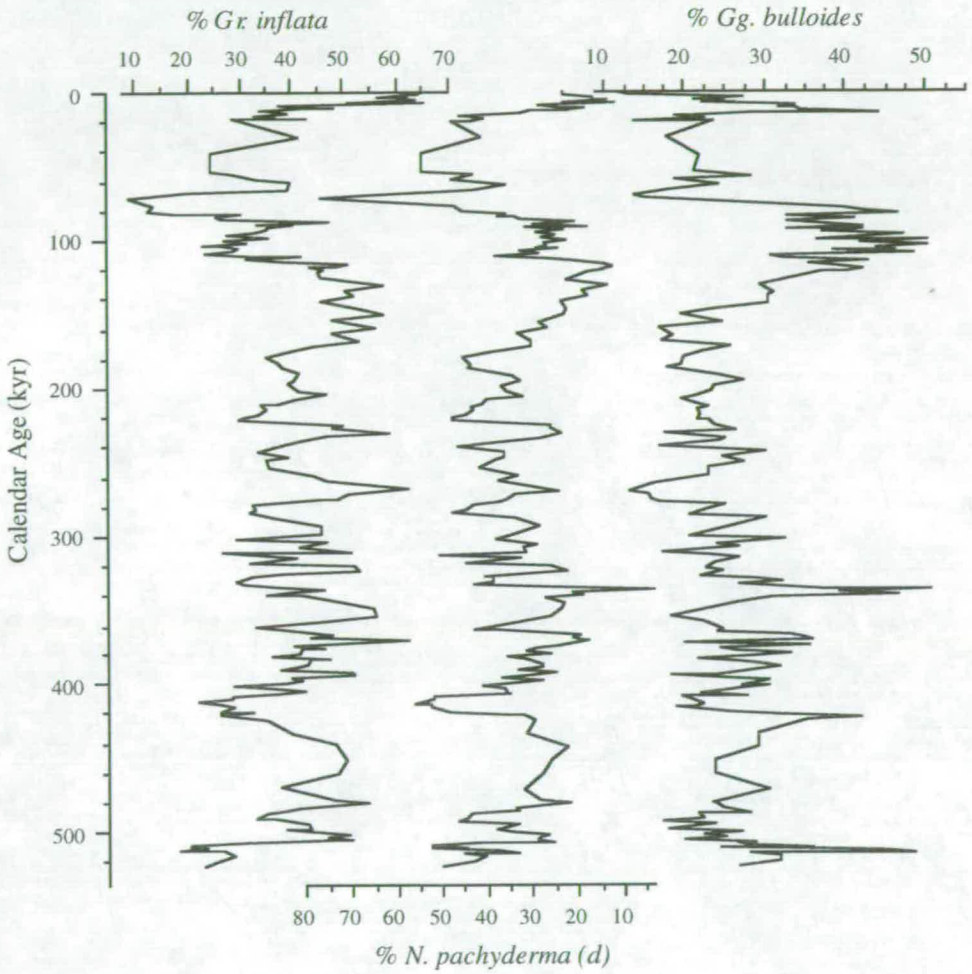

Figure 6.5. Variation in abundance of the transitional assemblage (as a % of the total) from GeoB 3602. Note the excellent, but inverse, correlation of *Gr. inflata* with *N. pachyderma* (d).

Sub-tropical planktonic foraminifera have highest abundances in the interglacial periods, up to a maximum of 34.5% during isotope stage 11, and to a low of ~7% during the glacial interval of isotope stages 4—2. The abundance of sub-tropical foraminifera significantly influences the variability in the foraminiferal assemblage and alternates with the typical transitional fauna of *Gr. inflata*, *Gg. bulloides* and *N. pachyderma* (d) which form the greatest percentage of the planktonic foraminifera.

If the foraminifera were significantly affected by selective dissolution, then *Gr. inflata* should record an increase in abundance, supressing the sub-tropical fauna (*Howard and Prell*, 1992). If this was the case, the values for sub-tropical foraminiferal abundance would therefore be regarded as a low estimate. However, the recorded abundance of the transitional fauna in GeoB 3602, is typical for the modern-day planktonic foraminiferal distribution offshore Cape Town, and the higher abundances of sub-tropical and spinose planktonic foraminifera are considered representative for the modern-day Indian Ocean (*Bé and Hutson,* 1977). The coincidence of high numbers of *Gr. inflata* and sub-tropical plankonic foraminifera during interglacial periods, further indicates that dissolution does not significantly effect the sedimentary record of GeoB 3602. The relative abundances of the transitional and sub-tropical fauna in GeoB 3602, correlate to the modern-day distribution levels of planktonic foraminifera in the SBR and northern Indian Ocean respectively. The mixture of sub-tropical and transitional faunas suggests that during interglacials there is an increased delivery of warm Indian Ocean water from the Agulhas Retroflection into the Benguela Current.

The variation in abundance documented by *Gr. inflata* is followed with an inverse relationship with *N. pachyderma* (d), while *Gg. bulloides* documents far less dramatic swings with an average 22% abundance, with the exception of interglacial stage 5 to the present day (Figure 6.5). It is likely that if selective dissolution did affect the relative abundances of planktonic foraminifera that *Gg. bulloides* would be affected first, due to its thin test and wall structure.

Given the modern distribution of the faunal components dominated by *Gr. inflata, Gg. bulloides*, *N. pachyderma* (d), and the sub-tropical foraminifera within distinct water masses in the modern southern South Atlantic and Indian Ocean (*Bé and Tolderlund,* 1971, *Bé and Hutson,* 1977, *Hutson,* 1977, *Kroon and Ganssen,* 1989, *Giraudeau,* 1993: *Little et al.,* 1997a), the down core changes in the abundance of these species groups document both the intrusion of warm-waters around Cape Town from the Agulhas Current, but also the local hydrographic conditions governing the southernmost reaches of the Benguela upwelling system. The maxima of sub-tropical foraminifera are interpreted as evidence of major warm-water input into the Benguela system largely at times of least global ice volume. Maximum warm water input is thus thought to have occurred during interglacial stages 11, 5 (including the isotope stage 6/5 transition), and stage 1, where the abundance of sub-tropical foraminifera is

greatest. During interglacial stages 13, 9, and 7 the percentage of sub-tropical foraminifera is lower, suggesting slightly reduced amounts of warm-water wrapping around the southern tip of Africa.

The variation in abundance within the typical transitional fauna off Cape Town, reflects localised hydrographic changes as seen in the NBR (*Little et al.*, 1997a). *Gr. inflata* in the SBR is thought to reflect the strong thermal and hydrographic boundary between newly upwelled, cool, nutrient-rich waters and the displaced, warmer, nutrient-poor waters typical offshore Cape Town. Variations in the intensity of upwelling further north in the NBR will have a direct influence on the hydrography of the SBR (*Little et al.*, 1997a). Small changes in the nature and extent of the nutrient supply and structure of the thermocline, are reflected in the relative abundances of *Gr. inflata, N. pachyderma* (d) and *Gg. bulloides*.

In the modern setting, intense upwelling is only present seasonally in a narrow, coastal belt in the SBR (*Giraudeau,* 1993 [surface sediment]; *Kate Darling* pers. comm. [plankton nets]). The thermocline at these times is almost non-existent, as cool waters are advected from deep in the water column. Offshore in the SBR, there is a strong hydrographic/thermal boundary separating upwelled waters from sub-tropical to transitional waters. In the Recent transitional environment of the southern STC, there is a well developed, deep thermocline with abundant *Gr. inflata*, as the relative position of the STC southwards permits an increased input of warm Indian Ocean water entry into the Benguela system (Figure 3.17). During glacial periods, when trade winds have intensified as a result of the expansion of the atmospheric polar cells, the APF and STC are relatively northwards preventing Indian Ocean water entry into the Benguela system. Although upwelling is not as intense in the SBR as it is in the NBR, the thermal boundary between the upwelled waters and the offshore transitional waters is more diffuse. A shallow thermocline is developed, with fingers of upwelled water filtering offshore as in the modern-setting of the NBR. Upwelling intensity in the SBR is thought to be best interpreted using *Gg. bulloides* as is suggested for the Angola Basin and has been used in the Arabian Sea (*Prell and Curry,* 1981; *Kroon and Ganssen,* 1989; *Kroon,* 1991; *Curry et al.*, 1992; *Steens et al.,* 1992).

6.5. Discussion

6.5.1. Comparison with previous studies

Meridional shifts of the STC and APF have been discussed previously as the major factor affecting faunal and floral populations within Southern Ocean and southern Indian Ocean waters (*Hays et al.*, 1976, *Williams,* 1976, *Prell et al.*, 1979; 1980, *Morley,* 1989b, *Howard and Prell,* 1992). *Howard and Prell* (1992) presented six deep sea cores spanning the last 500 kyr from the southern Indian Ocean along a transect through the APF to the southernmost point of the STC (between 48°—42° S). The results from *Howard and Prell* (1992), demonstrate that the palaeoceanographic history of the southern Indian Ocean, as recorded by the relative abundances of planktonic foraminifera, can be explained by the movement of the STC and APF, distributing water masses which vary the SST of the surface waters. In the southern Indian Ocean (*Howard and Prell*, 1992), a transitional assemblage made up almost entirely of *Gr. inflata* and *Gg. bulloides* varies inversely with the cold, polar assemblage *N. pachyderma* (s) which is prevalent in the Southern Ocean and increases in abundance in cores from successively higher latitudes.

Howard and Prell (1992) found that polar species of planktonic foraminifera dominated the sediments when the core site was equatorward of the modern APF (46°N) during six glacial intervals of the past 500 kyr, isotope stages 12, 10, 8, 6, and 2. Species typical of the sub-tropical gyre edges and STC have only been abundant poleward of 42°S at the early parts of interglacial stages, 11, 9, 5 and 1, which was interpreted as reflecting the meridional shifts of the boundaries of the STC and sub-polar gyres (Figure 6.6). The most equatorward of these records, core E49-21 (SST - winter), shows that maximum poleward positions of the STC which correlate well with the maximum abundances of tropical spinose foraminifera from GeoB 3602 indicating warm-water input from the Indian Ocean. The Cape Town record also suggests an additional poleward shift of the STC during interglacial stage 13. Similarly, all of the other cores studied by *Howard and Prell* (1992) and *Morley* (1989) provide further excellent supporting evidence that planktonic foraminiferal abundances from GeoB 3602 accurately record shifts of the STC.

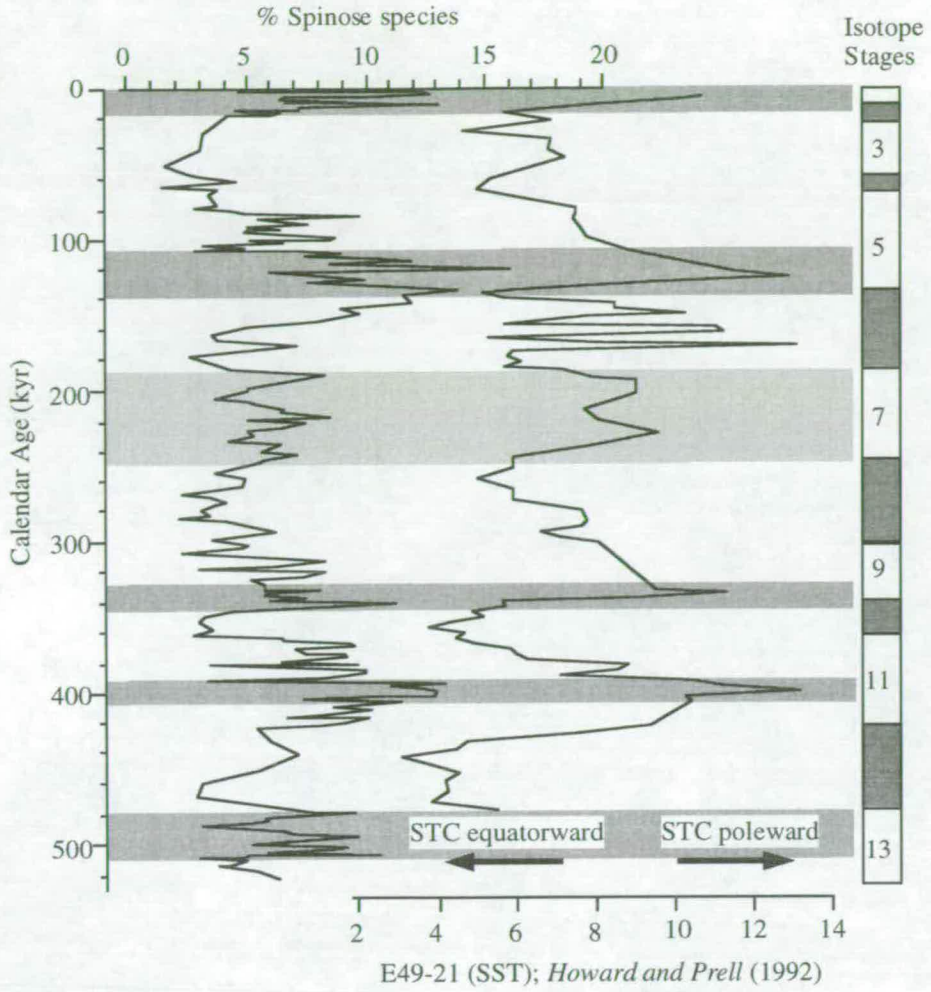

Figure 6.6. Comparison of the planktonic foraminiferal-derived SST transfer function from E49-21 (southern Indian Ocean; *Howard and Prell,* 1992) with abundance of tropical, spinose planktonic foraminifera (*Gs. ruber, Gs. sacculifer* and *Ge. siphonifera*). Graphic representation of oxygen isotope stages is given to the right hand-side (interglacials - white; glacials - shaded). The anomalous SST maxima at approximately 160—130 ka in E49-21 are not seen in any of the other cores sampled in the transect through the STC and APF (*Howard and Prell,* 1992). The higher sampling frequency in GeoB 3602 obviously describes more short-term SST oscillations than are suggested by the low-resolution southern Indian Ocean core.

Globorotalia menardii (Parker, Jones and Brady), a tropical, warm-water, planktonic foraminifer has been suggested to be of particular importance for understanding the intrusion of warm-waters from the Agulhas Retroflection around the Cape of Good Hope (*Schott,* 1935, *Berger,* 1970). *Schott* (1935) found *Gr. menardii* to 'disappear' during glacial intervals in the Atlantic and re-appear in interglacials, primarily as a

result of SST change. However, the CLIMAP (1976) sea-level and temperature reconstruction suggests that temperatures are well within the range of the modern habitat of *Gr. menardii*. Why then, does *Gr. menardii* seemingly disappear in the southern Atlantic glacial ocean? Previously, it has been suggested that the delivery of warm-water around the Cape re-seeds the *Gr. menardii* population within interglacials, during expansion of the central South Atlantic gyre (*Berger et al.,* 1985, *Berger and Wefer,* 1997). *Gr. menardii* occurs in greatest abundance during interglacial isotope stages 13, 11, 9 and 5, with an anomalous peak in *Gr. menardii* abundances at 440 ka occuring as a result of the weak chronology in the low-sedimentation glacial interval stage 12 (Figure 6.7). *Gr. menardii* is largely absent in stages 12, 10, 8, 4, and 3 but is certainly present during isotope stage 6 where there is a more reliable glacial isotope chronostratigraphy. Certainly the highest abundances of *Gr. menardii* correlate to maximum warm-water intrusion around the Cape as is recorded by sub-tropical and spinose foraminiferal numbers (Figure 6.6) and warmer SSTs (*Howard and Prell,* 1992), but the dataset does not conclusively argue for a re-seeding during interglacials. The presence of *Gr. menardii* in glacial isotope stage 6, which does not record a major change in sedimentation rate similar to the other glacial periods, suggests that *Gr. menardii* is 're-seeded' from the Indian Ocean more regularly than during interglacials alone, but flourishes during times of maximum warm-water advection. When *Gr. menardii* is absent from the sediment record (e.g. *Imbrie and al.,* 1973), it is suggested that the "Cape Valve" (*Berger et al.,* 1985) is closed, denying warm-water flow to the South Atlantic. Does the STC converge on the Cape of Good Hope to 'shut off' the Cape Valve at times of maximum northerly expansion of the APF, and if so, "is this why less heat is transported from the South Atlantic to the North Atlantic during glacials *(Berger and Wefer, 1997)*".

Core GeoB 3602 is in an excellent position to assess the extent of closure of the Cape Valve during glacials. The planktonic foraminiferal record for GeoB 3602 indicates that the Cape Valve is never fully closed but instead reduces the warm-water advection from the Indian Ocean. Sub-tropical foraminifera only fall below 10% in abundance during six brief intervals, including interglacial stages 7 and 5, for the last 520 kyr. The tropical, spinose foraminifera also remain abundant, and never fall below 2% of the total planktonic foraminifera; *Gr. menardii* also, is not solely restricted to the interglacial intervals and is abundant intermittently throughout the core. It is most likely that *Gr. menardii* does not respond well to the reduced warm-water advection during glacial periods, probably related to its ecology. *Gr. menardii* may have

problems with its reproductive cycle, or the change in thermocline stratification. In a 'Cape Valve open'—'Cape Valve closed' system the Cape Valve will never fully shut off the flow of Indian Ocean waters into the Atlantic. Eddies, rings and filaments will filter as off shoots from the main retroflection intermittently 'feeding' the Benguela system and providing suitable environments for sub-tropical and tropical species. During these intervals of an equatorward STC, *Gr. menardii, Gs. sacculifer* and *Gs. ruber* will be in lesser abundance, occupying small environmental niches until the conditions are wamer once again.

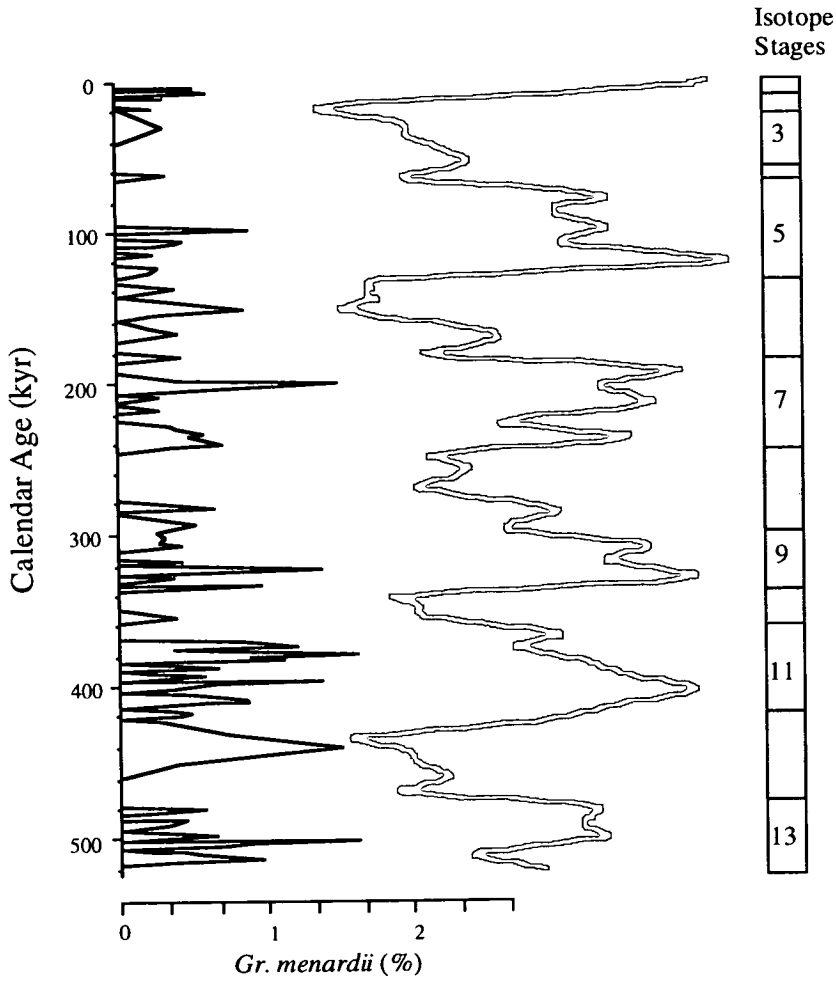

Figure 6.7. Variation in abundance of *Gr. menardii* for the last 520 kyr. SPECMAP $\delta^{18}O$ stacked record is shown with the graphic representation of oxygen isotope stages given to the right hand-side (interglacials - white; glacials - shaded) for comparison.

6.5.2 Ice age cycles and inter-hemispheric climate-ocean linkages

The similarity between the $\delta^{18}O$ profile from the South Atlantic GeoB 3602 record and the stacked SPECMAP reconstruction (Figure 6.1) is not suprising if the South Atlantic is responding primarily to the dominance of global ice volume changes. The cross-spectral analysis of SPECMAP with GeoB 3602 $\delta^{18}O$ further enforces the correlation, with coherency at the 95% level in all of the Milankovitch orbital periods (100, 40 and 23 kyr), with the exception of the 19 kyr band which is absent in the GeoB record largely as a result of the low-sedimentation rates within the glacial intervals (Figure 6.8a). Although not coherent with SPECMAP, the $\delta^{18}O$ record for GeoB 3602 shows coherent spectral power at the 10—11 kyr period, similar to that seen higher up in the NBR. Time series analysis of the relative abundance of sub-tropical planktonic foraminifera shows dominant Milankovitch frequencies of the eccentricity and precessional cycles (centered on 21 kyr), but additional strong power at the 28 kyr period and at the harmonic frequencies of 15 and 10—8 kyr periods, of which the 15 kyr spectral power may be an artefact of the precessional variability (Figure 6.8b). The further presence of sub-Milankovitch frequencies, higher than the 23 kyr period, cannot be assessed fully due to the relatively low resolution of the records. Interestingly however, the 31—28 kyr period which is above the 80% confidence interval, has been reported from late Quaternary South and Equatorial Atlantic sediment and TOC records (*Verardo and McIntyre,* 1994, *Berger and Wefer,* 1997, *Bickert and Wefer,* 1997, *Wefer et al.,* 1997), and in central equatorial Pacific divergence and wind intensity (*Pisias and Rea,* 1988). The mechanisms controlling the generation of the 31—28 kyr periodicity are not fully understood, but may be a result of non-linear responses to the climatic system (*Pisias and Rea,* 1988). The 28 kyr period observed in the foraminiferal record from GeoB 3602 could be an artefact of the time scale developed for this core reflecting errors in correlation of GeoB 3602 $\delta^{18}O$ to the SPECMAP stacked record. However, good agreement between the isotope records, especially in the interval between isotope stages 11—5 (Figure 6.2), argue against this possibility and the fact that this spectral component is found in several other oceanic sediment records suggests that this frequency component is real. As seen equatorwards in the Benguela system and equatorial Atlantic (*Hagelberg et al.*, 1994; *Little et al.,* 1997a; 1997b), non-linear interactions may produce strong powers in higher frequencies transferred from the Milankovitch orbital periodicities. An interaction between the 100 kyr eccentricity cycle and the 41 kyr tilt cycle, or the 23 kyr precession cycle, could produce periods of 29 kyr and 30 kyr respectively

(*Pisias and Rea,* 1988). Given the latitude of core GeoB 3602 seemingly affected by the more 100 and 40 kyr dominated movements of the STC and APF, and with warm-water input from the Indian Ocean, which at equatorial latitudes is strongly dominated by the precessional 23 kyr component (*Kroon et al.,* 1990, *Clemens et al.,* 1991, *Weedon and Shimmield,* 1991), it is not suprising that the sub-tropical foraminiferal input into the Benguela Current will record an interaction of these two signals. Due to the reduced sedimentation rates within the glacial periods it is not possible to accurately distinguish which of the two documented periodicities (29 or 30 kyr) that the system is responding to, but it does further suggest that the Benguela system responds to non-linear interactions transferred from Milankovitch orbital forcing.

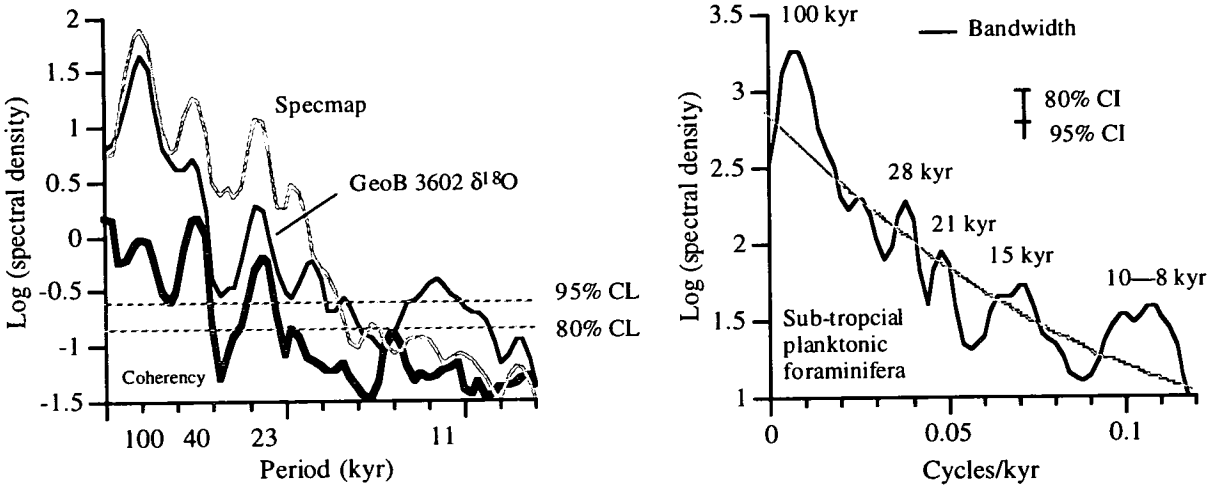

Figure 6.8. GeoB 3602 cross-spectral and spectral analysis. (a) Cross-spectral analysis results for GeoB 3602 $\delta^{18}O$ versus SPECMAP stacked $\delta^{18}O$ isotope record (1—520 ka). Statistics: t = 1 kyr; N = 521; bandwidth and confidence interval, CI, are shown for 180 lags; coherency levels are shown for 80% and 90%. Coherent spectral maxima are highlighted with the period of oscillation (kyr). (b) Spectral analysis results for GeoB 3602 sub-tropical planktonic foraminiferal abundance (1-520 kyr). Statistics: t = 1 kyr; N = 521; bandwidth and confidence interval, CI, are shown for 180 lags. Coherent spectral maxima are highlighted with the period of oscillation.

6.5.3. South—North Atlantic heat transport via the Cape Valve: Implications for Atlantic and Pacific deep-sea dissolution during the Bruhnes Chron

The relative shifts of the STC, or warm-water advection, as indicated by the correlation with SSTs from the southern Indian Ocean (*Howard and Prell,* 1992) and

from the variation in abundance of *Gr. menardii*, may have implications for global thermohaline circulation. The addition of warm, saline-rich water to the conveyor, which transports this heat to the high latitudes of the North Atlantic across the equator, will increase the ocean's potential to sink and accelerate deep water production (*Little et al.,* 1997b). Inversely, a reduction in the quantity of water added to the system, will relatively decelerate deep water production and oceanic convection. NADW production is considered probably the most important key to oceanographic change, including amplification of glacial—interglacial cycles, as discussed in Chapter 5, and the degree of carbonate dissolution or preservation (*Luz and Shackleton,* 1975, *Crowley,* 1985, *Peterson and Prell,* 1985, *Farrell and Prell,* 1989, *Haddad and Droxler,* 1996).

The distribution, preservation, and accumulation of $CaCO_3$ on the seafloor is largely determined by the balance between the biogenic production of $CaCO_3$ in the supersaturated surface waters and its dissolution in the generally undersaturated deep waters. Although productivity determines the input of $CaCO_3$ to the deep-sea, dissolution is the dominant control on $CaCO_3$ preservation which is largely affected by the position of the lysocline, the depth at which carbonate dissolution rapidly accelerates (*Berger,* 1968, *Berger,* 1975). The degree of saturation of the abyssal waters acts as a first order boundary condition for carbonate preservation or dissolution, upon which is superimposed the effects of organic matter degradation within the sediments. The CO_2 released by oxidation of organic carbon causes a decrease in the $CaCO_3$ saturation of the pore waters, and thus an increase in $CaCO_3$ dissolution. Pumping CO_2 out of the ocean, e.g. by increasing terrestrial biomass (*Shackleton,* 1977), would give rise to good preservation of $CaCO_3$. Below the lysocline (approximately 3800m in the Indian Ocean), the progressive intensification of dissolution and the physical loss of carbonate from the sediments reflects the increasing degree of carbonate undersaturation of the bottom waters (*Peterson and Prell,* 1985).

Fluctuations in $CaCO_3$ dissolution are largely controlled by changes in the global mass balance of $CaCO_3$ and ocean circulation, which in turn are mediated by global climate conditions. Core records demonstrate that the depths of the lysocline, the carbonate critical depth (CCrD) and the carbonate compensation depth (CCD) have changed significantly over geological time scales (*Berger,* 1968, *Berger,* 1973, *Gardner,* 1975, *Luz and Shackleton,* 1975, *Crowley,* 1985, *Peterson and Prell,* 1985, *Farrell and*

Prell, 1989). These changes, observed as fluctuations in $CaCO_3$ preservation, are recorded in many deep-sea cores in the Pacific, equatorial and North Atlantic documenting changes in deep water circulation (Figure 6.9; fro example *Farrell and Prell*, 1989).

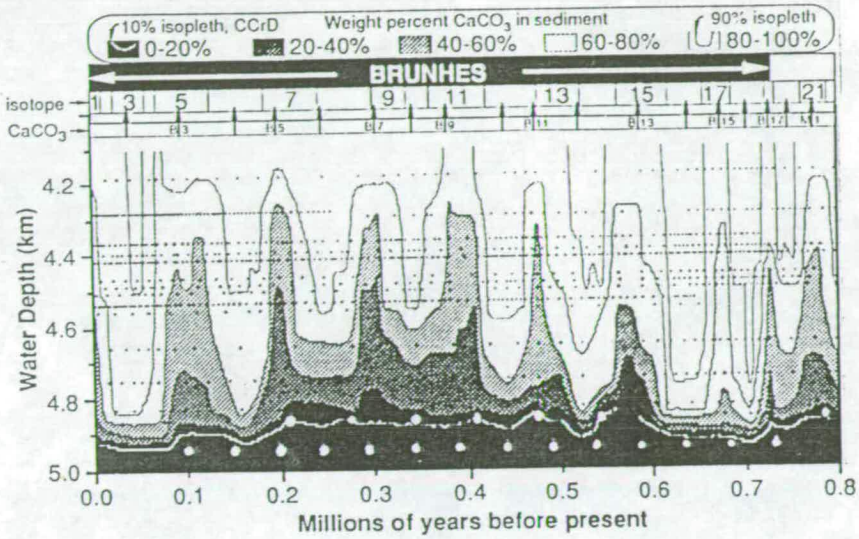

Figure 6.9. Bathymetric variations in $CaCO_3$ preservation through time, as expressed by $CaCO_3$, from 16 cores in the East Equatorial Pacific Ocean. The values were contoured with six isopleths at the 90, 80, 60, 40, 20 and 10% $CaCO_3$ levels. If the % $CaCO_3$ records are primarily the results of dissolution, and assuming the $CaCO_3$ to non-$CaCO_3$ sediment ratio was constant at 9:1, then these isopleth levels respectively represent apparent $CaCO_3$ losses of 0, 56, 83, 93, 97, and 99%. The SPECMAP oxygen isotope stages are given above the plot (from *Imbrie et al.*, 1984) with the odd numbers referring to interglacial intervlas, and the $CaCO_3$ event scale with the midpoints of the preservation maxima and minima marked by arrows. Preservation minima arrows are labelled by event name (from *Farrell and Prell,* 1989).

Although not entirely conclusive, *Crowley* (1985) presents records from the North Atlantic which show dissolution to be relatively low during interglacials while conversely, the Pacific Ocean has dissolution maxima in the interglacials and preservation maxima in the glacials. More recently, from records in the Caribbean and western North Atlantic (*Haddad and Droxler,* 1996), show that shallow water (655m—1933m water depth) Bahama records resemble deep Atlantic carbonate records with dissolution during glacial isotope stages and preservation during interglacial isotope stages, for the past 200 kyr. Basin-basin fractionation of carbonate was proposed (*Luz and Shackleton,* 1975, *Crowley,* 1985) to explain the out-of-phase dissolution patterns between the Atlantic and Pacific (*Crowley,* 1983). This

fractionation was mediated by the production rate of the NADW which, in the present day accumulates CO_2 oxidised from falling organic debris on its long journey to the Pacific via the Antarctic Circumpolar Current (AACC). As a result the Pacific Deep Water (PDW) is more corrosive to carbonate than the NADW (*Broecker and Peng,* 1982).

During interglacial periods, when there is an increased supply of warm, saline-rich water into the South Atlantic via the Cape Valve, cross-equatorial transfer delivers warm water to the Gulf Stream with an increased Indian Ocean component, which increases NADW production. Increased production of NADW intensifies bottom water transfer and dramatically reduces the residence time for bottom waters in the Atlantic Ocean. The AABW and AAIW are mixed with an intensified NADW creating an enhanced intermediate and bottom water circulation, and strong heterogeneity in the North and South Atlantic Oceans. Young NADW, concentrated with organic carbon, crosses the Atlantic Ocean bottom rapidly reducing its potential for carbonate dissolution and remaining largely un-corrosive. The Atlantic at this time has an enhanced preservation potential and maintains well preserved carbonate records. In the Pacific however, the NADW forms a greater component of the PDW, after its long journey within the AACC. When it mixes with the PDW it is of a different character than at the start of its journey, with greatly increased CO_2 content increasing its corrosive potential and removing $CaCO_3$ from deep water sediments. Pacific sediments thus record dissolution cycles during interglacials, inverse to the Atlantic.

During glacials (Figure 6.10b), NADW production was slowed as less heat is transferred to the high latitudes of the North Atlantic, and less CO_2 was pushed into the deep Pacific by the NADW (*Boyle and Keigwin,* 1985). The Atlantic becomes sluggish, even though surface currents are intense, but these deliver cooler, less saline, water to the high latitudes of the North Atlantic reducing their sinking potential. The residence time for NADW is increased in the Atlantic, as oceanic botton circulation is sluggish, increasing the disolution potential for the Atlantic, but decreasing the corrosive input into the PDW, increasing the Pacific's preservation potential. Thus in a simple context, the inverse nature of the Pacific and Atlantic basins (*Gardner,* 1975, *Crowley,* 1983, *Crowley,* 1985, *Curry and Lohman,* 1985, *Haddad and Droxler,* 1996) can be explained by basin-basin fractionation (*Le and Shackleton,* 1992) with basin-shelf fractionation only enhancing this relationship.

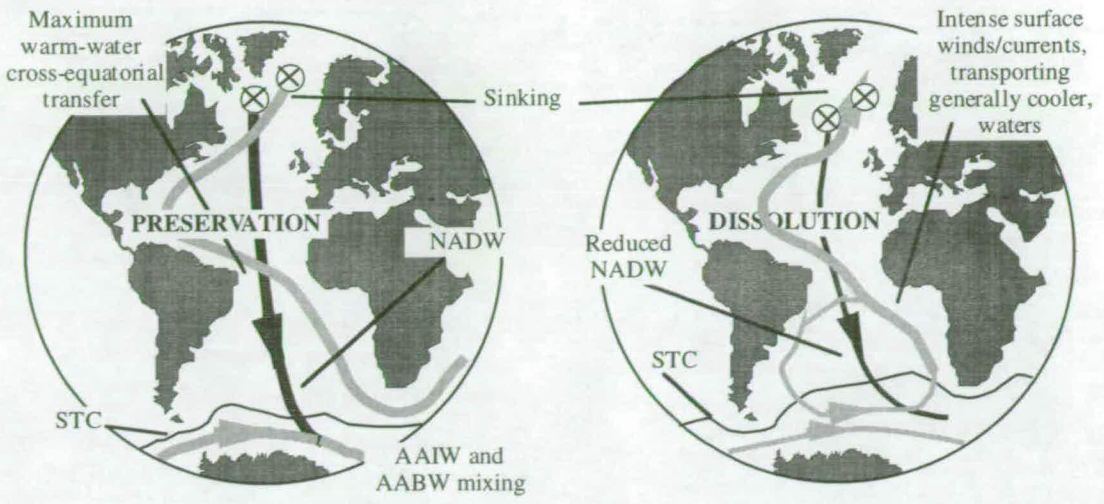

Figure 6.10. Schematic diagrams representing hypothesised Atlantic circulation during interglacial and glacial intervals. (a) Cape valve open: Changes in circulation reflect maximum warm-water advection from the Indian Ocean during an interval when expansion of the SAAG produces a retreat of the APF and STC. (b) Cape valve closed: Reduced warm-water advection from the Indian Ocean prodcues less favourable conditions for NADW production resulting in reduced surface and bottom ocean circulation and convecton. Adapted from *Haddad and Droxler* (1996).

The relationship between the deep sea dissolution cyles in the Pacific, preservation cycles in the equatorial and North Atlantic, and the warm-water input via the Agulhas Retroflection is more than just a coincidence. Basin-basin fractionation together with shelf-basin fractionation can account for the inverse relationship between the Pacific 'dissolution cycles' and the Atlantic 'dilution cycles' [4], but also suggest that these changes are a result of a varying NADW production. Together, the SST and faunal records from the Southern Ocean and southern Indian Ocean suggest that the Cape Valve has contracted and expanded largely with global ice-volume and sea level changes allowing warm-water intrusion into the Atlantic from the Indian Ocean. The

[4] Atlantic dilution cycles co-occur, although conversely, with Pacific dissolution cycles and are thought to reflect the increased supply of terrigenous materials from the continents during glacial, sea level low stands.

faunal record for GeoB 3602 documents the warm-water intrusion of Indian Ocean waters wrapping around the Cape of Good Hope into the Benguela Current at times when NADW production is intensified. Recent studies suggest that the South Atlantic leads the North Atlantic's response to climate change and NADW production (*Charles et al.,* 1996, *Abelmann et al.,* 1997, *Little et al.,* 1997a; 1997b), and *Imbrie et al.,* (1989) report that the precessional component of SST in the South Atlantic similarly leads the response of the North Atlantic. Although the faunal record for GeoB 3602 is not of high enough resolution to determine a lead-lag relationship with NADW production, in conjunction with the NBR data (*Little et al.,* 1997a) the correlation suggests that input via the Agulhas Retroflection may play a major role in North Atlantic climate change, NADW production and global hydrographic control of the lysocline.

6.6. Summary

The planktonic foraminiferal record for GeoB 3602 illustrates that the changes in abundance of the total warm-water, 'sub-tropical' planktonic foraminifer are synchronous with the global glacial—interglacial regime. Three species make up over 78% of the overall downcore average abundance, with sub-tropical planktonic foraminifera accounting for an average 19% of the assemblage of which almost 7% is attributable to the spinose warm-water tropical species (*Gs. ruber, Gs. sacculifer,* and *Ge. siphonifera*). These abundances are considered normal with respect to the modern-day transitional envionment offshore Cape Town and the tropical environment in the Arabian Sea, respectively (*Bé and Hutson,* 1977). As recorded equatorwards in the northern Benguela region, and in the Angola and equatorial Guinea Basins, the variation in the abundances of planktonic foraminifera largely vary according to the local hydrography and upwelling intensity.

The abundances of tropical, spinose planktonic foraminifera correlate well to the meridional shifts of the STC and APF within the southern Indian Ocean and Southern Ocean, indicating warm-water intrusion around the Cape of Good Hope largely during interglacials when the STC is in its most poleward position and the Cape Valve is open. However, the presence of *Gr. menardii* within glacial isotope stage 6 does not conclusively argue for re-seeding only during interglacials but suggests that *Gr. menardii* may be present most of the time, flourishing during times of maximum warm-water advection from the Indian Ocean. The Cape Valve closed situation does

not fully shut off the warm-water advection from the Indian Ocean, but eddies, rings and filaments filter off intermittently providing an environment suitable for *Gr. menardii, Gs. ruber*, and *G. sacculifer*.

The strong power at the 28 kyr period is superimposed on the longer 100 kyr period of warm-water Indian Ocean advection into the South Atlantic. This spectral power has been suggested to be a further result of non-linear responses to the climatic system (*Pisias and Rea*, 1988), and is the result of interaction between the 100 kyr dominated STC and APF meridional shifts and the 23 kyr precession dominated monsoonal/trade wind fluctuations which affects the Benguela system and Indian Ocean upwelling.

The co-occurring nature of deep-sea dissolution cycles in the Pacific, preservation cycles in the equatorial and North Atlantic, and the warm-water input via the Agulhas Retroflection suggests that all three are closely related to the production of NADW. NADW production is controlled primarily by the transport of warm, saline-rich water to the high latitudes of the North Atlantic which is affected by the warm-water, Indian Ocean component from the Cape Valve. The subsequent production rate of NADW is thought to be the main cause for disturbance to the thermohaline-conveyor and the residence time for bottom waters in the Atlantic and Pacific basins, affecting the hydrology of the lysocline. Fluctuations in the input of saline-rich water from the Indian Ocean, on the glacial-interglacial timescale, and in particular on the sub-Milankovitch timescales suggested by *Little et al.* (1997b) in the Benguela system, are extremely important for NADW production and global ocean-climate linkages.

Summary and conclusions

Ch.7.

Chapter 7. Summary and conclusions

7.1. Introduction

The Benguela upwelling system, situated on the southeastern continental slope of Africa, is the site of intense, variable, upwelling and high productivity, recording amplified signals of climate change. The cores analysed in this study provide information from one of the key positions within the global geostrophic/thermohaline circulation controlling the atmosphere-ocean teleconnections via heat transfer to the high latitudes of the North Atlantic Ocean. Studies like this, of the glacial—interglacial change in a major component of the Earth's ocean-atmosphere-cryosphere system, are essential to establish the natural variability of global climate so that meaningful models of future climate change can be developed.

7.2. Upwelling variability via trade wind modulation

In the modern setting of the BCS, the water mass types adequately describe the distribution of planktonic foraminifera, and allow the fossil assemblages to be interpreted with a meaningful ecological and hydrological significance. In the SBR, the offshore waters are typical of oligotrophic, transitional to sub-tropical conditions with much reduced nutrient and primary productivity levels of the inshore upwelling centres. Surface sediment studies (*Giraudeau,* 1993) show the offshore waters to be dominated by *Gr. inflata* while the inshore upwelling centres are dominated by *N. pachyderma* (s), and *Gg. quinqueloba* in the smaller size fraction (< 125μm). A distinct break between the two zones of foraminifera dominance correlate precisely to the hydrography of the region with a sharp thermal anomaly separating the offshore divergence zone and the newly upwelled waters of the coastal upwelling belt (*Bang,* 1971). Results from plankton samples taken across a transect from Cape Town to the outer shelf and slope, revealed that the modern-day assemblage agrees with this assessment and further identified a concentration of sub-tropical planktonic foraminifer species at the thermal boundary (*Kate Darling*, pers. comm.), with *Gr. inflata* slightly further offshore and *N. pachyderma* (s) and *Gg. quinqueloba* in the inshore upwelling centre.

To the north of the Benguela Current system, the hydrography, and resultant planktonic foraminiferal distribution, is more complex. The upwelled water in the

NBR is advected from a shallower depth than that from the SBR and does not produce a sharp thermal boundary zone (*Barange and Pillar,* 1992). The offshore zone of the NBR is characterised by a wide filamentous mixing domain with the inclusion of cold, nutrient-rich, filaments and eddies from the inshore upwelling centres. The mixing domain is dominated by *Gg. bulloides* and *N. pachyderma* (d) which both prefer relatively lower nutrient levels away from the upwelling filaments (*Giraudeau,* 1993). Inshore, the upwelled waters are dominated by *N. pachyderma* (s).

The temporal fluctuations of the planktonic foraminifera enable the record to be divided into episodes characterised by particular planktonic foraminiferal assemblages which indicate the prevailing hydrological and upwelling conditions. The fluctuation of the foraminiferal abundances, in particular the *N. pachyderma* (s) record, suggests temporal shifts in the intensity of upwelling, and corresponding trophic domains, that do not follow the typical glacial—interglacial pattern, and instead describe the shifts of the Angola-Benguela Front (ABF), marking the boundary between the warm Angola Current and the cool Benguela Current, to the north of the Walvis Ridge (*Jansen et al.*, 1997). The normalised Benguela upwelling group (BUG) 'transfer function' better describes the shifts of the ABF either side of the front, than the Benguela Index used in the Angola Basin. The Benguela upwelling index (BUI) incorporates the cool-water upwelling species, *N. pachyderma* (s), and the warmer water upwelling species, *Gg. bulloides*, which is common in upwelling centres in more tropical climates (e.g. Indian Ocean; *Kroon*, 1991; *Kroon and Ganssen,* 1989). The BUI removes the effects of the long term glacial—interglacial trend which is superimposed on the upwelling variations, and is thought to better represent the 'true' shifts of the ABF and temporal changes in upwelling intensity.

The shifts of the ABF and variability of upwelling in the Benguela system, were thought to be primarily controlled by advection of cold surface and/or intermediate waters from the Southern Ocean (*Summerheys et al.,* 1995; *Jansen et al.,* 1997). However, if northward advection was to play a major role in the planktonic foraminiferal variations seen in the Benguela Current, then we would almost certainly see the highest abundances of the cold-water, *N. pachyderma* (s) in the south of the region, not the almost zero abundances actually recorded (Table 3.3). *McIntyre et al.* (1989) used planktonic foraminiferal estimates of SST to estimate seasonality in the equatorial Atlantic. Seasonality maxima, largest summer-winter temperature range, are recorded at similar times to greatest upwelling intensity in the BCS. Trade wind

zonality is strongly related to the seasonality at the equator (*Mix et al.*, 1986; *Imbrie et al.*, 1989; *McIntyre et al.*, 1989; *Little et al.*, 1995; *Schneider et al.*, 1995; *Mix and Morey*, 1997), and also contributes to most of the SST, palaeoproductivity and palaeoceanography variations within the BCS (*Litte et al.*, 1995; *Summerhayes et al.*, 1995b; *Jansen et al.*, 1997; *Mix and Morey*, 1997; *Schneider et al.*, 1995; 1997; in press). The records of GeoB 1706 and GeoB 1711 suggest intensification of upwelling in the northern Cape Basin coinciding with increased equatorial and Angola Basin upwelling, at times of increased trade wind zonality. There is no evidence in support of the advection of Southern Ocean water across the STC, and equatorward heat advection, other than that from upwelling via the BCS, plays a minor if not insignificant role in equatorial and Angola Basin palaeoceanography. It is the injection of newly upwelled waters, rather than advection of Southern Ocean water, which *McIntyre et al.* (1989) observed at the equator. Upwelling intensification along the entire coast of western and southwestern Africa is generated by changes in the strength and zonality of the trade wind system, responding to similar shifts and intensity of the atmospheric and oceanic gyres.

7.3. Palaeoproductivity

Upwelling areas are regions of high primary productivity with a high input of planktonic skeletal material and organic matter to the underlying sea floor. The Benguela upwelling system is no exception to this rule. Upwelled water is relatively enriched in nutrients and cooler than the displaced surface water (*Dingle*, 1995), and the sediments accumulating beneath the upwelling cells are dominated by an organic and diatom-rich mud, containing up to 22% organic carbon (*Calvert and Price*, 1971). The bottom sediments are so organic-rich largely as a result of oxygen-poor bottom waters adversely affecting the benthos and preserving the organic carbon. However, below the oxygen-minimum zone the life conditions for benthos are greatly improved, as a consequence of high plankton production, and large numbers of benthic foraminifera are able to thrive.

The high-resolution palaeoproductivity records from the NBR indicate a general positive correlation between increased TOC contents and increased *N. pachyderma* (s) abundances, with an increased benthic/planktonic foraminifera (B/P) ratio. TOC records from the Peruvian (e.g. *Schrader*, 1992), Californian (e.g. *Summerhayes*, 1983), and northwest African margins (e.g. *Müller et al.*, 1983; *Thiede and Junger*,

1992) also suggest this overall correlation between productivity and offshore wind intensity with organic carbon content. However, in the Benguela system, as in most other upwelling systems, there is no direct linear correlation between measured TOC and the palaeoproductivity proxies. In the glacial isotope stages 4—2, there is an excellent correlation between *N. pachyderma* (s) abundances and TOC. During these intense upwelling phases almost all of the TOC in the sediments is derived from upwelling driven primary production. The offshore record of site GeoB 1711 is used as the indicator for maximum offshore divergence and shelf-edge upwelling, away from the interference and dilution from re-suspension of inner shelf organic matter. TOC variability reflects the change in upwelling intensification, best expressed away from the coastal upwelling situation away from dilution effects, but the B/P ratio is not yet a suitable method for quantifying palaeoproductivity. *N. pachyderma* (s) abundance is probably the best proxy for palaeoproductivity and palaeoceanographic changes, and may better record the timing and periodicity of climate instability in the Benguela system.

Time series analysis of the organic carbon record for GeoB 1711, positioned offshore and away from the main effects of continental dust input and re-sedimentation, documents pronounced, coherent, spectral maxima at the sub-Milankovitch periods of 12, 9—8 and 6 kyr. The faunal records are dominated by *N. pachyderma* (s), which records large changes in abundance between 0 and 80% of the total abundance, responding to lateral expansion of the coastal upwelling cells. Organic carbon does not record these dramatic swings, and instead records a smoother profile. The analyses provide further supporting evidence that sub-Milankovitch forcing is a significant control on upwelling and productivity fluctuations in the Benguela system. Organic carbon measurements may provide a quicker method for analysing climate and oceanic variability without the superposition of temperature dominance which effects faunal population studies, but only when away from the conflicting effects of re-suspension and continental shedding.

7.4. Global climate instability via trade wind forcing

The 'cold-water' planktonic foraminifer, *N. pachyderma* (s), shows rapid fluctuations in relative abundance, indicating changes in upwelling and trade wind intensity. The changing down-core abundance of *N. pachyderma* (s), records rapid oscillations in relative abundances between 0 and 80% of the total planktonic foraminiferal

assemblage. The *N. pachyderma* (s) records do not follow the glacial—interglacial regime, described by the oxygen isotope profile, but instead show a higher frequency of change on a sub-Milankovitch cyclicity with *N. pachyderma* (s) maxima describing discrete PS events (pachyderma sinistral) approximately every 8—10 kyr (Table 5.1). Upwelling events PS1—PS9 punctuate the record for the last 140 kyr, of which PS1—PS6 have a good correlation with the timing of Heinrich events H1—H6 in the North Atlantic with a consistent 3-kyr phase lead of the southern hemisphere to the Heinrich events of the northern hemisphere.

The graphic correlation between PS events and the GISP2 ice core suggests that almost all of the 23 interstadials, particularly in the glacial stages 4—2 (IS1—IS20; *Bender et al.*, 1994), can be found in the GeoB 1711 *N. pachyderma* (s) record as maxima in *N. pachyderma* (s) abundances, and therefore cold events at site GeoB 1711 (Figure 5.3). All of the short-term features of upwelling events PS1—PS8 can also be found in the RC24-16 equatorial seasonality record with cooler upwelling maxima occuring simultaneous with maximum eastern equatorial seasonality and therefore maximum seasonal SST variability between summer and winter extremes. Notably, it is the minima in the % *N. pachyderma* (s) record, and hence warm intervals of reduced upwelling intensity, that match $\delta^{18}O$ minima in the GISP2 ice core and minima in the equatorial seasonaltiy record. The *N. pachyderma* (s) abundances suggest that the pronounced PS events PS6, PS7 and PS8 record cold stages in a predominantly warm interglacial period, whilst PS1—PS5 record the base values in a cold glacial period punctuated by anonamously low percentage *N. pachyderma* (s) values.

The South and equatorial Atlantic lead the North Atlantic response documented by Heinrich layers and are opposing at the higher frequency scale of atmospheric response indicated by the interstadials IS1—IS23. Supporting planktonic foraminiferal abundances from cores GeoB 1706 on the Walvis Ridge, and PG/PC12 on the continental slope demonstrate that with further AMS ^{14}C control on the younger part of these records, the apparent lead of the South Atlantic is a true feature of the South Atlantic records, similar to previous published results (*Imbrie et al.*, 1989; *Charles et al.*, 1996; *Abelmann et al.*, 1997). Further correlation with trade wind variability measured at the mid-equatorial Atlantic ridge (*McIntyre and Molfino*, 1996), shows the short-term instability in the Benguela system (NP events; ~4—5 kyr), superimposed on the longer-term (10 kyr) PS events, to be represented by variations

in *F. profunda* abundances as well as interstadials IS1—IS23 in the GISP2 and GRIP Greenland ice cores. The mid-equatorial Atlantic records from RC24-08 and RC24-02 further suggest that increased trade wind zonality is the dominant forcing mechanism affecting equatorial and eastern South Atlantic faunal populations.

Correlation between *N. pachyderma* (s) abundances from the northern Cape Basin and eastern equatorial seasonality record (*McIntyre et al.*, 1989), and *F. profunda* abundances on the equatorial Mid-Atlantic Ridge, suggests that the entire eastern margin of the northern, southern and equatorial Africa is dominated by fluctuations in trade wind zonality and intensity. Radiocarbon dating for the last 45 kyr permits a further correlation between PS events in the northern Cape Basin, with Heinrich events of the North Atlantic and suggests teleconnections in South Atlantic—North Atlantic and global heat transfer. Maximum abundances of *N. pachyderma* (s) coincide with interstadials in the GISP2 ice core and further suggest that warm-water advection to the North Atlantic stimulates rapid ice sheet growth via moisture feedback mechanisms.

Intense upwelling events on a sub-Milankovitch cyclicity occurred throughout the last 140 kyr, in particular during the last glacial cycle (isotope stages 4—2), controlled by changes in intensity of the trade winds at times of maximum ice build-up and minimum solar insolation, and indicate a 3-kyr phase lead of the South Atlantic to corresponding changes in northern hemisphere sediment records. The increase in trade wind controlled offshore displacement of tropical and sub-tropical waters may have implications for the strength of equatorial transfer into the North Atlantic, via the South and North Equatorial Currents and the Gulf Stream, and for the global thermohaline conveyor and Atlantic convection. The tropical warm-water which is forced across the equator, is transported to the high latitudes of the North Atlantic into the phase of maximum ice building. This intensifies the moisture gradient between the sub-Arctic ocean and the northern hemisphere ice sheets, increasing the rate of snow accumulation until eventual ice sheet collapse and iceberg calving (Heinrich event).

7.5. Warm-water advection via the Cape Valve: Implications for inter-hemispheric climate-ocean linkages

The high abundances of sub-tropical and tropical planktonic foraminifera in the south of the Benguela Current system describe a different history of planktonic foraminifera diversity than at the Walvis Ridge or in the northern Cape Basin where trade wind driven upwelling dominates. Meridional shifts of the STC and APF have been discussed previously as the major factor affecting faunal and floral populations within Southern Ocean and southern Indian Ocean waters (*Hays et al.,* 1976; *Prell et al.,* 1980; *Morley,* 1989a; *Morley,* 1989b; *Howard and Prell,* 1992). Previous studies of planktonic foraminiferal faunal abundances indicate that the meridional shifts of the STC and APF can be adequately described by the species typical of the sub-tropical gyre edges and the polar front. The correlation between SSTs, derived from the southern Indian Ocean records (*Howard and Prell,* 1992), and the abundance of tropical, spinose species from GeoB 3602, suggests that the Cape Town core records the mid-latitude affects of the STC and APF meridional shifts. Similarly, all of the other cores studied by *Howard and Prell* (1992) and *Morley* (1989) provide further excellent supporting evidence that planktonic foraminiferal abundances from GeoB 3602 accurately record shifts of the STC. Sub-tropical planktonic foraminifera account for an average 19% of the assemblage of which almost 7% is attributable to the spinose, warm-water, tropical species (*Gs. ruber, Gs. sacculifer,* and *Ge. siphonifera*). These abundances are considered typical for the modern-day transitional envionment offshore Cape Town and the tropical environment in the Arabian Sea, respectively (*Bé and Hutson,* 1977), and further suggest that the faunal fluctuations offshore Cape Town result from the largely interglacial advection of warm-waters via the Agulhas Retroflection. As recorded equatorwards in the northern Benguela region, and in the Angola and equatorial Guinea Basins, the variation in the abundances of the transitional planktonic foraminifera [*Gr. inflata, Gg. bulloides* and *N. pachyderma* (d)] vary according to the local hydrography and upwelling intensity.

The relative shifts of the STC, or warm-water advection, as indicated by the correlation with SSTs from the southern Indian Ocean (*Howard and Prell*, 1992) and from the variation in abundance of *Gr. menardii*, may have serious implications for global thermohaline circulation. The addition of warm, saline-rich water to the conveyor, which transports this heat to the high latitudes of the North Atlantic across the equator, will increase the ocean's potential to sink and accelerate deep water

production (*Little et al.*, 1997b). Inversely, a reduction in the quantity of water added to the system, will relatively decelerate deep water production and oceanic convection. NADW production is considered probably the most important key to oceanographic change, including amplification of glacial—interglacial cycles, and the degree of carbonate dissolution or preservation (*Luz and Shackleton,* 1975, *Crowley,* 1985, *Peterson and Prell,* 1985, *Farrell and Prell,* 1989, *Haddad and Droxler,* 1996).

The co-occurring nature of deep-sea dissolution cyles in the Pacific, preservation cycles in the equatorial and North Atlantic, and the warm-water input via the Agulhas Retroflection is more than just a coincidence. Basin-basin fractionation together with shelf-basin fractionation can account for the inverse relationship between the Pacific 'dissolution cycles' and the Atlantic 'dilution cycles' (*Luz and Shackleton*, 1975; *Crowley,* 1985; *Farrell and Prell*, 1989; *Haddad and Droxler*, 1996), but also suggest that these changes are a result of a varying NADW production. Together, the SST and faunal records from the Southern Ocean and southern Indian Ocean have suggested that the Cape Valve has contracted and expanded largely with global ice-volume and sea level changes allowing warm-water intrusion into the Atlantic from the Indian Ocean. The faunal record for GeoB 3602 documents the warm-water intrusion of Indian Ocean waters wrapping around the Cape of Good Hope into the Benguela Current at times when NADW production is intensified. Although the faunal record for GeoB 3602 is not of high enough resolution to determine a lead-lag relationship with NADW production, in conjunction with the NBR data (*Little et al.,* 1997b) the correlation suggests that input via the Agulhas Retroflection may have serious implications for North Atlantic climate change, NADW production and global hydrological control of the lysocline.

7.6. Short-term climate instability versus long term warm-water advection

The high-resolution studies from the Benguela Current system, document sub-Milankovitch climate instability during cool, glacial intervals when warm, saline-rich, surface water advection to the high latitudes is reduced, although surface currents and wind speeds are increased. Seemingly inverse to this, NADW production in glacial periods is reduced and bottom water oceanic convection is sluggish. The reduced delivery of warm-waters to the North Atlantic results from removing the supply of Indian Ocean waters in a closed Cape Valve situation. Although this may seem to

conflict with the rapid climate instability during glacial periods, it does not. The rapid climate instability described by the PS and NP events in the Benguela system correlate to similar events in the equatorial and mid-equatorial Atlantic, and the interstadials and Heinrich events of the Greenland ice cores and North Atlantic, document short-lived changes in the atmosphere-ocean system via trade wind modulation. The upwelling events in the Benguela, record the surface and intermediate water response to trade wind changes, while the interstadials in the Greenland ice cores record the atmosphere—ocean temperature contrast from the increased rate of delivery of warm-water to the high latitudes of the North Atlantic. The Heinrich events, however, describe the resultant collapse of the ice sheets after a period of climate change and further amplify the North Atlantic cooling by slowing the rate of oceanic thermohaline convection, and thus are a result and amplifier of climate change not a cause. The short-term climate instability occurs at a time of overall sluggish bottom water circulation which may account for the 'super-conveyor' events recorded by the PS and resultant Heinrich events. If the system had an efficient and rapid bottom to surface communication, then possibly the rapid climate instability would not occur but would be equilibrated with longer-term changes. This may explain the enhancement of sub-Milankovitch cyclicity within glacials and the dominance of more precession and obliquity forcing during periods of good bottom water circulation.

During interglacials, when there is an increased supply of warm, saline-rich water into the South Atlantic via the Cape Valve, cross-equatorial transfer delivers warm-water to the Gulf Stream with an increased Indian Ocean component, which increases NADW production. Increased production of NADW intensifies bottom water transfer and dramatically reduces the residence time for bottom waters in the Atlantic Ocean. Although deep water convection is increased and there is good inter-basin exchange of waters, the increased insolation in the equatorial belt causes expansion of the Hadley cells and drives the inter-tropical convergence zone to higher latitudes, compressing the polar cells and thus reducing trade wind intensity. Surface water currents and offshore wind speeds are reduced, and the rate of cross-equatorial transfer and flux of warm-waters to the high latitudes of the North Atlantic is also reduced, although the potential to sink is increased due to the greater inclusion of Indian Ocean waters via the Cape Valve.

With regard to short-term climate variability within interglacial periods, there is no general agreement as to what happened. *Heinrich* (1988) observed an 'extra' five IRD

events during interglacial stage 5 and more recently *McManus et al.*(1994) report the occurrence of IRD deposits together with increased abundance of *N. pachyderma* (s). Heinrich events H1—H6 from sediment records in the North Atlantic are associated with peak abundances of *N. pachyderma* (s) and large fluxes of IRD principally at times of large ice sheets during global cooling, specifically glacial isotope stages 4—2. During warmer interglacial periods, when ice sheets are near their minimum size and insolation is near a maximum, it is unlikely that fluctuations in ice sheet growth will be recorded in IRD and *N. pachyderma* (s) abundances, as ice sheets will never grow to a sufficient size to enable ice sheet calving or to produce 'true' Heinrich events. The presence of PS events during interglacial stage 5 further supports the studies of *Heinrich* (1988) and *McManus et al.,* (1994) for climate instability during non-glacial periods when high-latitude climate amplification is not as pronounced, although the increased spacing of these events (~ 20 kyr) suggests that precession may play a more important role than it does during glacials when it is at a minimum. Indeed, the strong power at the 28 kyr period is superimposed on the longer 100 kyr period of warm-water Indian Ocean advection into the South Atlantic. This spectral power has been suggested to be a further result of non-linear responses to the climatic system (*Pisias and Rea*, 1988), and is the result of interaction between the 100 kyr dominated STC and APF meridional shifts and the 23 kyr precession dominated monsoonal/trade wind fluctuations which affects the Benguela System and Indian Ocean upwelling.

The significant high frequency, sub-Milankovitch, variation seen in all records from the Benguela Current system suggests that in the mid-latitudes in particular, the balance of the relative components from polar and equatorial regions determines the resultant forcing on the system. Sub-Milankovitch frequencies have also been recorded for sediment cores in the eastern equatorial Pacific (ODP site 846; *Hagelberg et al.,* 1994), North Pacific (ODP site 893, *Kennett and Ingram,* 1995a; California margin, *Thunell and Mortyn,* 1995; ODP sites 882 and 883, *Kotilainen and Shackleton,* 1995), eastern equatorial Atlantic (ODP site 663; *Hagelberg et al.,* 1994), the northeastern Atlantic (DSDP site 609; *Hagelberg et al.,* 1994), the South Atlantic (DSDP site 516F; *Park et al.,* 1993), the Southern Ocean, *Charles et al.,* 1996); terrestrial sediment cores (Massif Central, France, *Thouveny et al.,* 1994); and in ice cores (Vostok, *Yiou et al.,* 1991; *Bender et al.,* 1994, and *Charles et al.,* 1996; and Greenland, *Bender et al.,* 1994; *Mayewski et al.,* 1994), and are an important element to understand further for future climate models.

The Benguela Current system could be regarded as the major component influencing cross-equatorial teleconnections between the South Atlantic and North Atlantic. The palaeoceanographic records analysed in this study demonstrate further that high-frequency sub-Milankovitch cyclicity is a global phenomenon and that cross-equatorial heat transfer via trade wind intensification may have serious repercussions for global climate change.

Bibliography

Bibliography

Abelmann, A., U. Brathauer, R. Gersonde, R. Sieger and U. Zielinski, Late Quaternary sea-surface temperature reconstructions in the Southern Ocean and their coupling to global atmosphere and ocean circulation changes, *Terra Nova, 9*, 609, 1997.

Abrantes, F., Variability in upwelling of NW Africa during the latest Quaternary: diatom evidence, *Paleoceanography, 6*, 431-460, 1991.

Adelseck, C.G., Jr., Recent and late Pleistocene sediments from the eastern equatorial Pacific Ocean: Sedimentation and dissolution. *Ph.D. Thesis, Univ. of California at San Diego, La Jolla*, 1977.

Adelseck, C.G., Jr., and T.F. Anderson, The late Pleisotcene record of productivity fluctuations in the eastern equatorial Pacific Ocean, *Geology, 6*, 388-391, 1978.

Aksu, A.E. and D.J.W. Piper, Baffin Bay in the past 100,000 yr, *Geology, 7*, 245-248, 1979.

Alley, R.B., D.A. Meese, C.A. Shuman, A.J. Gow, K.C. Taylor, P.M. Grootes, J.W.C. White, M. Ram, E.D. Waddington, P.A. Mayeweski and G.A. Zielinski, Abrupt increase in Greenland snow accumulation at the end of the Younger Dryas event, *Nature, 362*, 527-529, 1993.

Altenbach, A.V. and M. Sarnthein, Productivity record in benthic foraminifera. In: Berger, W. H., Smetacek, V. S. and Wefer, G. (eds), *Productivity of the Oceans: Present and Past.* John Wiley and Sons, 255-269, 1989.

Ammann, B. and A.F. Lotter, Late-glacial radiocarbon and palynostratigraphy on the Swiss Plateau, *Boreas, 18*, 109-126, 1989.

Andrews, J.T., A.S. Dyke, K. Tedesco and J.W. White, Meltwater along the Arctic margin of the Laurentide ice sheet (8-12 ka): Stable isotopic evidence and implications for past salinity anomalies, *Geology, 21*, 881-884, 1993.

Bang, N.D., The southern Benguela Current region in February 1966. Part 2. Bathymetry and air/sea interactions, *Deep Sea Res., 18*, 209-265, 1971.

Bang, N.D. and W.R.H. Andrews, Direct current measurements of a shelf-edge frontal jet in the southern Benguela system, *J. Mar. Res., 32(3)*, 405-417, 1974.

Barange and Pillar, Cross-shelf circulation, zonation and maintenance mechanisms of *Nyctiphanes capensis* and *Euphasia hanseni* (Euphausiacea) in the northern Benguela upwelling system, *Cont. Shelf Res., 12*, 1027-1042, 1992.

Bard, E., Correction of Accelerator Mass Spectrometer ^{14}C ages measured in planktonic foraminifera, *Paleoceanography, 3*, 635-645, 1988.

Bard, E., M. Arnold, R.G. Fairbanks and B. Hamelin, ^{230}U, ^{234}U and ^{14}C ages obtained by mass spectrometry on corals, *Radiocarbon, 35*, 191-199, 1993.

Bard, E., B. Hamelin and R.G. Fairbanks, U-Th ages obtained by mass spectrometry in corals from Barbados: sea level during the past 130,000 years, *Nature, 346*, 456-458, 1990a.

Bard, E., B. Hamelin, R.G. Fairbanks and A. Zindler, Calibration of the ^{14}C timescale over the past 30,000 years using mass spectrometric U-Th ages from Barbados corals, *Nature, 345*, 405-410, 1990b.

Barnola, J.M., D. Raynaud, Y.S. Korotkevich and C. Lorious, Vostok ice cores provide 160,000 year record of atmospheric CO_2, *Nature, 329*, 1987.

Baumgartner, A. and E. Reichel, *The world water balance*, Elsevier/North-Holland, 1975.

Bé, A.W.H. An ecological, zoogeographic and taxonomic review of recent planktonic foraminifera. In: Ramsay, A. T. S. (ed), *Oceanic Micropal.*, Academic Press 1-100, 1977.

Bé, A.W.H. and W.H. Hutson, Ecology of planktonic foraminifera and biogeographic patterns of life and fossil assemblages in the Indian Ocean, *Micropal., 23*, 369-414, 1977.

Bé, A.W.H. and D.S. Tolderlund, Distribution and ecology of living planktonic foraminifera in surface waters of the Atlantic and Indian Oceans. In: Funnel, B. M., and Riedel, W.R. (eds), *The Micropalaeontology of the Oceans*, Cambridge University Press 105-149, 1971.

Behl, R.J., Sedimentary facies and sedimentology of the late Quaternary Santa Barbara Basin, site 893, *Proc. Ocean Drill. Prog. Sci. Res., 146*, 295-308, 1995.

Behl, R.J. and J.P. Kennett, Brief interstadial events in the Santa Barbara Basin, NE Pacific, during the past 60 kyr, *Nature, 379*, 243-246, 1996.

Bender, M., T. Sowers, M.-L. Dickson, J. Orchado, P. Grootes, P.A. Mayeweski and D.A. Meese, Climate correlations between Greenland and Antarctica during the past 100,000 years, *Nature, 372*, 663-666, 1994.

Berger, A., Longterm variations of caloric insolation resulting from the Earth's orbital elements, *Quat. Res., 9*, 139-167, 1978b.

Berger, A., Accuracy and frequency stability of the Earth's orbital elements during the Quaternary. In: Berger, A., Imbrie, J., Hays, J., Kukla, G. and Saltzman, B. (eds), *Milankovitch and Climate, Part I*, Reidel 3-40, 1984.

Berger, A., J. Imbrie, J. Hays, G. Kukla and B. Saltzman, *Milankovitch and Climate*, Reidel 510pp., 1984.

Berger, W.H., Planktonic foraminifera: Selective solution and paleoclimatic interpretation, *Deep Sea Res., 15*, 31-43, 1968.

Berger, W.H., Biogenous deep-sea sediments: fractionation by deep-sea circulation, *Bull. Geol. Soc. Am., 81*, 1385-1402, 1970.

Berger, W.H., Deep-sea carbonates: Pleistocene dissolution cycles, *J. Foram. Res., 3*, 187-195, 1973.

Berger, W.H., Deep-sea carbonates: Dissolution profiles from foraminiferal preservation, *Spec. Pub. Cush. Found. Foram. Res., 13*. 82-86, 1975.

Berger, W.H., Global maps of ocean productivity. In: Berger, W. H., Smetacek, V. S., and Wefer, G. (eds), *Productivity in the oceans: Present and Past*, Wiley & Sons, 429-455, 1989.

Berger, W.H., The Younger Dryas cold spell - a quest for causes., *Palaeogeog., Palaeoclim., Palaeoecol., 89*, 219-237, 1990.

Berger, W.H., M.C. Bonneau and F.L. Parker, Foraminifera on the deep-sea floor: lysocline and dissolution rate, *Oceanol. Acta, 5*, 249-258, 1982.

Berger, W.H. and L. Diester-Haass, Paleoproductivity: the benthic/planctonic ratio in foraminifera as a productivity index, *Mar. Geol., 81*, 15-25, 1988.

Berger, W.H., K. Fischer, C. Lai and G. Wu, Ocean productivity and organic carbon flux. (Part I: Overview and maps of primary productivity and export production), *Repts. San Diego: University of California, SIO Reference, 67*, 87-30, 1987.

Berger, W.H., J.S. Killingley, C.V. Metzler and E. Vincent, Two-step deglaciation: ^{14}C-dated high-resolution $\partial^{18}O$ records from the tropical Atlantic Ocean, *Quat. Res., 23*, 258-271, 1985.

Berger, W.H. and D. Kroon, Possible causes for the Younger Dryas: a brief survey. In: Troelstra, S. R., van Hinte, J. E. and Ganssen, G. M. (eds), *The Younger Dryas*. North-Holland, 221-224, 1995.

Berger, W.H., V.S. Smetacek and G. Wefer, Ocean productivity and palaeoproductivity - an overview. In: Berger, W. H., Smetacek, V.S. & Wefer, G. (eds), *Productivity of the oceans: Present and Past*, Wiley 1-34, 1989.

Berger, W.H. and G. Wefer, Benthic deep-sea foraminifera: possible consequences of infaunal habitat for paleoceanographic interpretation, *J. Foram. Res., 18*, 147-150, 1988.

Bernhard, J.M., Characteristic assemblages and morphologies of benthic foraminifera from anoxia, organic-rich deposits; Jurassic through to Holocene, *J. Foram. Res., 16*, 207-215, 1986.

Bickert, T. and G. Wefer, Late Quaternary deep water circulation in the South Atlantic: Reconstruction from carbonate dissolution and benthic stable isotopes. In: Wefer, G., Berger, W. H., Siedler, G. and Webb, D. (eds), *The South Atlantic: Present and Past Circulation,* Springer 599-620, 1997.

Biscaye, P.E., R.F. Anderson and B.L. Deck, Fluxes of particles and constituents to the eastern United States continental slope and rise: SEEP 1, *Cont. Shelf Res., 8*, 855-904, 1988.

Bishop, J.K.B., The barite-opal-organic carbon association in oceanic particulate matter, *Nature, 332*, 341-363, 1988.

Bleil, U. and cruise participants, Bericht und erst Ergenbnisse über die METEOR-Fahrt M32/1, Cape Town-Walvis Bay, 2.1.1996 - 28.1.1996, *Ber. Fachber. Geowiss. Uni. Bremen,* 1996.

Blow, W.H., Age correlation biostratigraphy of the upper Tocuyo (San Lorenzo) and Pozón Formations, Eastern Falcón, Venezuela, *Bull. Amer. Paleontol., 39*, 59-251, 1959.

Bond, G., W. Broecker, S. Johnsen, J. McManus, L. Labeyrie, J. Jouzel and G. Bonani, Correlations between climate records from North Atlantic sediments and Greenland ice, *Nature, 365*, 143-147, 1993.

Bond, G., H. Heinrich, W. Broecker, L. Labeyrie, J. McManus, J. Andrews, S. Huon, R. Jantschik, S. Clasen, C. Simet, K. Tedesco, M. Klas, G. Bonani and S. Ivy, Evidence for massive discharges of icebergs into the North Atlantic ocean during the last glacial period, *Nature, 360*, 245-249, 1992.

Bond, G.C. and R. Lotti, Iceberg discharges into the North Atlantic on millenial time scales during the last glaciation, *Science, 267*, 1005-1009, 1995.

Boulton, G.S. and T. Payne Mid-Latitude ice sheets through the last glacial cycle: Glaciological and geological reconstructions. In: Duplessy, J.-C. and Spyriadakis, M.-T. (eds), *NATO ASI Series, Vol. I22 Long Term Climatic Variations*. Springer-Verlag 177-212, 1994.

Boyd, A.J., J. Salat and M. Maso, The seasonal intrusion of relatively saline water on the shelf off northern and central Namibia, *S. Afr. J. Mar. Sci., 5*, 107-120, 1987.

Boyle, E.A., Chemical accumulation variations under the Peru Current during the past 130,000 years, *J. Geophys. Res., 88*, 7667-7680, 1983.

Boyle, E.A., The role of vertical chemical fractionation in controlling late Quartenary atmospheric carbon dioxide, *J. Geophys. Res., 93*, 15701-15714, 1988.

Boyle, E.A. and L. Keigwin, North Atlantic thermohaline circulation during the past 20,000 years linked to high-latitude surface temperature, *Nature, 330*, 35-40, 1987.

Boyle, E.A. and L.D. Keigwin, Deep circulation of the North Atlantic over the last 200,000 years: Geochemical evidence, *Science, 218*, 784-787, 1982.

Boyle, E.A. and L.D. Keigwin, Comparison of Atlantic and Pacific paleochemical records for the last 215,000 years: changes in deep ocean circulation and chemical inventories, *Earth Planet. Sci. Lett., 76*, 135-150, 1985.

Brady, H., B, Supplementary note on the foraminifera of the Chalk of the new Britain Group, *Geol. Mag. Lon., 4*, 54-546, 1877.

Brady, H.B., Notes on some of the reticularian Rhizopoda of the Challenger expedition II: Additions to the knowledge of porcellaneous and hyaline types, *Quat. J. Micropal. Sci., 19*, 20-63, 1879.

Brady, H.B., Report of the foraminifera, *Roy. Soc. Edin., 11*, 708-717, 1882.

Brady, H.B., Report on the foraminifera dredged by H.M.S. Challenger during the years 1873-1876, *Challenger Expedition 1873-1876, Rept. Lon. Zool., 22*, 1-814, 1884.

Brassel, S.C., Applications of biomarkers for delineating marine palaeoclimatic fluctations during the Pleistocene. In: Engel, M. H. and Macko, S. A. (eds), *Organic Geochemistry: Principles and Applications*. Plenum Press 699-738, 1993.

Bremner, J.M., Biogenic sediments on the South West African (Namibian) continental margin. In: Thiede, J. and Suess, E. (eds), *Coastal Upwelling: Its Sediment Record. Part B: Sedimentary Records of Ancient Coastal Upwelling*. Plenum 73-104, 1983.

Breymann, M.T., von, K.-C. Emeis and E. Suess, Water depth and diagenetic constraints on the use of barium as a palaeoproductivity indicator. In: Summerhayes, C. P., Prell, W. L. and Emeis, K. C. (eds), *Upwelling Systems: Evolution Since the Early Miocene*. Geol. Soc. Spec. Pub., *64* 273-284, 1992.

Broeck, E., van den, Etude sur les foraminiféres de la Barbade (Antliles), *Soc. Belge Micr., 1*, 55-152, 1876.

Broecker, W., G. Bond Klas, M., E. Clark and J. McManus, Origin of the northern Atlantic's Heinrich events., *Clim. Dyn., 6*, 265-273, 1992.

Broecker, W.G., The chronology of the last glaciation: Implications to the causes of the Younger Dryas event, *Paleoceanography, 3 (1)*, 1-19, 1988.

Broecker, W.G., Massive iceberg discharges as triggers for global climate change, *Nature, 372*, 421-424, 1994.

Broecker, W.S., Salinity history of the northern Atlantic during the last deglaciation, *Paleoceanography, 5*, 459-467, 1990.

Broecker, W.S., G. Bond, M. Klas, G. Bonani and W. Wolfli, A salt oscillator in the glacial Atlantic?, 1, The concept, *Palaeoceanography, 5*, 469-477, 1990.

Broecker, W.S. and G.H. Denton, The role of ocean-atmosphere reorganizations in glacial cycles, *Geochim. Cosmo. Acta, 53*, 2465-2501, 1989.

Broecker, W.S. and E. Maier-Reimer, The influence of air and sea exchange on the carbon isotope distribution in the sea, *Global Biogeochem. Cycles, 6*, 315-320, 1992.

Broecker, W.S., D.M. Peteet and D. Rind, Does the ocean-atmosphere system have more than one stable mode of operation?, *Nature, 315*, 21-26, 1985.

Brummer, G.-J.A. and D. Kroon, *Planktic Foraminifers as Tracers of Ocean-Climate History*, Free University Press, 1988.

Calvert, S.E. and N.B. Price, Geochemistry of Namibian shelf sediments. In: Suess, E. and Thiede, J. (eds), *Coastal Upwelling, its Sediment Record: Part A: Responses of the Sediment Regime to Present and Coastal Upwelling*. Plenum 337-375, 1983.

Cayre, O., E. Vincent, N.J. Shackelton and Y. Lancelot, Planktonic foraminifera record off the Iberian margin during the last glacial cycle: Palaeotemperatures, palaeosalinities and Heinrich events, *Terra Nova, 9*, 618, 1997.

Chapman, P. and L.V. Shannon, The Benguela Ecosystem. Part II. Chemistry and related processes., *Oceanog. Mar. Bio. Ann. Rev., 23*, 183-251, 1985.

Charles, C.D. and R.G. Fairbanks, Evidence from Southern Ocean sediments for the effect of North Atlantic deep-water flux on climate, *Nature, 355*, 416-419, 1992.

Charles, C.D., J. Lynch-Stieglitz, U.S. Ninnemann and R.G. Fairbanks, Climate connections between the hemisphere revealed by deep sea sediment core/ice core correlations, *Earth Planet. Sci. Lett., 142*, 19-27, 1996.

CLIMAP project members, Seasonal reconstructions of the Earth's surface at the last glacial maximum, *GSA Map and Chart Ser. MC-36*, 1981.

Crowley, T.C., North Atlantic Deep Water cools the southern hemisphere, *Paleoceanography, 7*, 489-497, 1992.

Crowley, T.J. Late Quaternary carbonate dissolution changes in the North Atlantic and Atlantic/Pacific comparisons. In: Sundquist, E. and Broecker, W. (eds), *The Carbon Cycle and Atmospheric CO_2: Natural Variations Archean to Present. Geophys. Monogr. Ser., 32.* AGU, 271-285, 1985.

Crowley, T.J., K.-Y. Kim, J.G. Mengel and D.A. Short, Modelling 100,000 year climate fluctuations in pre-Pleistocene time series, *Science, 255*, 705-707, 1992.

Curry, W.B. and G.P. Lohman, Carbon deposition rates and deep water residence time in the equatorial Atlantic Ocean throughout the last 160,000 years. In: Sundquist, E. T. and Broecker, W. S. (eds), *The Carbon Cycle and Atmospheric CO_2 Natural Variations Archaean to Present, Geophys. Monogr. Ser., 32.* AGU 285-301, 1985.

Curry, W.B., D.R. Ostermann, M.V.S. Guptha and V. Ittekot, Foraminiferal production and monsoonal upwelling in the Arabian Sea: evidence from sediment traps. In: Summerhayes, C. P., Prell, W. L. and Emeis, K. C. (eds), *Upwelling Systems: Evolution Since the Early Miocene.* Geol. Soc. Spec. Pub., *64*, 93-106, 1992.

Cushman, J.A. and Jarvis, P.W., Three new foraminifera of the upper, middle and lower part of the Lower Miocene of Florida, *Bull. Florida State Geol. Surv., 9*, 7-147.

d'Orbigny, A.D., Tableau méthodique de la classe des Céphalopodes, *Ann. Sci. Nat. Paris, France, ser 1, vol. 7*, 1-277, 1826.

d'Orbigny, A.D. Foraminiferés. In: de la Sagra, R. (eds), *Histoire physique, politique et naturelle de l'Ile de Cuba,* Betrand, 1-224, 1839.

Dansgaard, W., S.J. Johsen, H.B. Clausen, D. Dahl-Jensen, N.S. Gundestrup, C.U. Hammer, C.S. Hvidberg, J.P. Steffensen, A.E. Sveinbjörnsdottir, J. Jouzel and G. Bond, Evidence for general instability of past climate from a 250-kyr ice-core-record, *Nature, 364*, 218-220, 1993.

Diester-Haass, L., Sediments as indicators of upwelling. In: Boje, R. and Tomczak, M. (eds), *Upwelling Ecosystems.* Springer-Verlag 261-281, 1978.

Diester-Haass, L., Late Quaternary sedimentation on the eastern Walvis Ridge, SE Atlantic (HPC 532, Leg 75, and four piston cores), *Mar. Geol., 65*, 145-189, 1985.

Diester-Haass, L., K. Heine, P. Rothe and H. Schrader, Quaternary history of continental climate and the Benguela Current off southwest Africa, *Paleogeog., Paleoclim., Paleoecol., 65*, 81-91, 1988.

Diester-Haass, L., P.A. Meyers and P. Rothe, The Benguela Current and associated upwelling on the southwest African Margin: A synthesis of the Neogene-Quaternary sedimentary record at DSDP sites 362 and 532. In: Summerhayes, C. P., Prell, W. L. and Emeis, K. C. (eds), *Upwelling Systems: Evolution Since the Early Miocene.* Geol. Soc. Spec. Pub., *64*, 331-342, 1992.

Dingle, R.V., Continental shelf upwelling and benthic ostracoda in the Benguela System (southeastern Atlantic Ocean), *Mar. Geol., 122*, 207-225, 1995.

Dingle, R.V. and G. Nelson, Sea bottom temperature, salinity and dissolved oxygen on the continental margin off south-western Africa, *S. Afr. J. Mar. Sci., 13*, 33-49, 1993.

Douglas, R.G. and F. Woodruff, Deep-sea benthic foraminifera. In: Emiliani, C. (ed), *The Sea, Vol. 7: The Oceanic Lithosphere.* J.Wiley and Sons, 1233-1327, 1981.

Duncombe-Rae, C.M., Agulhas retroflection rings in the South Atlantic Ocean: an overview, *S. Afr. J. Mar. Sci., 11*, 327-344, 1991.

Duplessy, J.C., L. Labeyrie, M. Arnold, M. Paterne, J. Duprat and T.C.E. van Weering, Changes in surface salinity of the North Atlantic Ocean during the last deglaciation, *Nature, 358*, 485-487, 1992.

Dymond, J., Geochemistry of Nazca plate surface sediments: An evaluation of hydrothermal, biogenic, detrital, and hydrogenous sources, *Geol. Soc. Am. Mem., 154*, 133-173, 1981.

Egger, J.G., Foraminiferen aus Meeresgrundproben, gelothet von 1874 bis 1876 von S.M. Sch. Gazelle, *Akad. Wiss. Berlin, Ber.*, 357-381, 1893.

Ehrenberg, C.G., Elemente des tiefen Meeresgrundes in Mexikanische Golfstrome bei Florida; Über die tiefgrund-Verhältnisse des oceans am eingange der Davisstrasse und bei island. In: Preuss, K. (eds), *Science Academy*. 222-240 and 275-317, 1861.

Elliot, M., L. Labeyrei, B. Lheman, C. Kissel, M. Arnold and T. Rasmussen, Rapid variations of deep water circulation in the North Atlantic during isotope stage 3 as evidenced by oxygen and carbon isotopes and magnetic susceptibility records, *Terra Nova, 9*, 610, 1997.

Emeis, K.-C., D.M. Anderson, H. Doose, D. Kroon and D. Schultz-Bull, Sea surface temperatures and the history of monsoon upwelling in the NW Arabian Sea during the last 500 kyr., *Quat. Res., 43*, 355-361, 1995.

Emerson, S. and M. Bender, Carbon fluxes at the sediment-water interface of the deep-sea: calcium carbonate preservation, *J. Mar. Res., 39*, 139-162, 1981.

Emerson, S. and J.I. Hedges, Processes controlling the organic carbon content of open ocean sediments, *Paleoceanography, 3*, 621-634, 1988.

Emery, K.O. and E. Uchupi, *The Geology of the Atlantic Ocean*, Springer, 1050 pp, 1984.

Emiliani, C., Pleistocene temperatures, *J. Geol., 63*, 538-578, 1955.

Epstein, S., R. Buchsbaum, H.A. Lowenstam and H.C. Urey, Revised carbonate-water isotopic temperature scale, *Bull. Geol. Soc. Am., 64*, 1315-1325, 1953.

Epstein, S. and H.C. Urey, Carbonate water isotopic temperature scale, *Geol. Soc. Am. Bull., 62*, 417-425, 1951.

Farrell, J.W. and W.L. Prell, Climatic change and $CaCO_3$ preservation: An 800,000 year bathymetric reconstruction from the central equatorial Pacific Ocean, *Paleoceanography, 4*, 447-466, 1989.

Fillon, R.H. and J.C. Duplessy, Labrador Sea bio-, tephro-, oxygen isotopic stratigraphy and late Quaternary palaeoceanographic trends, *Can. J. Earth Sci., 17*, 831-854, 1980.

Galloway, J.J. and S.G. Wissler, Pleistocene foraminifera from the Lomita Quarry, Palos Verdes Hills, California, *J. Palaeo., 1*, 35-87, 1927.

Gardner, J.V., Late Pleistocene carbonate dissolution cycles in the eastern equatorial Atlantic, *Spec. Pub. Cush. Found. Foram. Res., 13*, 129-141, 1975.

Gardner, J.V. and J.D. Hays, Responses of sea-surface temperature and circulation to global climate changes during the past 200,000 years in the eastern equatorial Atlantic Ocean, *Mem. Geol. Soc. Am., 145*, 221-246, 1976.

Garner, D.M., The Sub-Tropical Convergence in New Zealand surface waters, *N.Z. J. Geol. Geophys., 2*, 315-337, 1959.

Genthon, C., J.M. Barnola, D. Raynaud, C. Lorius, J. Jouzel, N.I. Barkov, Y.S. Korotkevich and V.M. Kotlyakov, Vostok ice core: climatic response to CO_2 and orbital forcing changes over the last climatic cycle, *Nature, 329*, 414-418, 1987.

Georgi, D.T., Circulation of bottom waters in the southwestern South Atlantic, *Deep Sea Res., 28*, 959-979, 1981.

Ghil, M., Climate sensitivity, energy balance models, and oscillatory climate models, *J. Geophys. Res., 89*, 1280-1284, 1984.

Ghil, M. and S. Childress, *Topics in geophysical fluid dynamics: Atmospheric dynamics, dynamo theory and climate dynamics*, Springer-Verlag, 1987.

Ghil, M. and H. Le Treut, A climate model with cryodynamics and geodynamics, *J. Geophys. Res., 86*, 5262-5270, 1981.

Giraudeau, J., Distribution of recent nannofossils beneath the Benguela system: southwest African continental margin, *Mar. Geol., 108*, 219-237, 1992.

Giraudeau, J., Planktonic foraminiferal assemblages in surface sediments from the southwest African continental margin., *Mar. Geol., 110*, 1-16, 1993.

Giraudeau, J., P.M.S. Monteiro and K. Nikodemus, Distribution and malformation of living coccolithophores in the northern Benguela upwelling system off Namibia, *Mar. Micropal., 22*, 93-110, 1993.

Giraudeau, J. and J. Rogers, Phytoplankton biomass and sea-surface temperature estimates from sea-bed distribution of nannofossils and planktonic foraminifera in the Benguela upwelling system, *Micropal., 40(3)*, 275-285, 1994.

Giraudeau, J., C.P. Summerhayes and D. Kroon, Upwelling variability off Namibia from phytoplankton biomass estimates over the last 70,000 years, in prep.

Gooday, A.J., A response by benthic foraminifera to the deposition of photodetritus in the deep sea, *Nature, 322*, 70-73, 1988.

Gordon, A.L., Interocean exchange of thermocline water, *J. Geophys. Res., 91*, 5037-5046, 1986.

Gordon, A.L. and K.T. Bosley, Cyclonic gyre in the tropical South Atlantic, *Deep Sea Res., 38*, S323-S343, 1991.

Gordon, A.L., R.F. Weiss, W.M. Smethie and M.J. Warner, Thermocline and intermediate water communication between South Atlantic and Indian Oceans, *J. Geophys. Res., C97*, 7223-7240, 1992.

GRIP, P.M., Climate instability during the last interglacial period recorded in the GRIP ice core, *Nature, 364*, 203-207, 1993.

Grootes, P.M., M. Stuiver, J.W.C. White, S. Johnsen and J. Jouzel, Comparison of oxygen isotope records from the GISP2 and GRIP Greenland ice cores, *Nature, 366*, 552-554, 1993.

Grousset, F.E., L. Labeyrie, J.A. Sinko, M. Cremer, G. Bond, J. Duprat, E. Cortijo and S. Huon, Patterns of ice rafted detritus in the glacial North Atlantic (40-55°N), *Paleoceanography, 8*, 175-192, 1993.

Haddad, G.A. and A.W. Droxler, Metastable $CaCO_3$ dissolution at intermediate water depths of the Caribbean and western North Atlantic: Implications for intermediate water circulation during the past 200,000 years, *Paleoceanography, 11*, 701-716, 1996.

Hagelberg, T.K., G. Bond and P. deMenocal, Milankovitch band forcing of sub-Milankovitch climate variability during the Pleistocene, *Paleoceanography, 9*, 545-558, 1994.

Hart, W.W. and R.I. Currie, The Benguela Current, *Discovery Reports, 31*, 123-298, 1960.

Hay, W.W. and J.C. Sibuet (eds) *Init. Repts. Deep Sea Drill. Proj., 75*, 1984.

Hays, J.D., J. Imbrie and N.J. Shackleton, Variations in the Earth's orbit: Pacemaker of the ice ages, *Science, 194*, 1121- 1132, 1976.

Heinrich, H., Origin and consequences of cyclic ice rafting in the northeast Atlantic Ocean during the past 130,000 years, *Quat. Res., 29*, 142-152, 1988.

Held, I.M., Climate models and the astronomical theory of the ice ages, *Icarus, 50*, 449-461, 1982.

Herguera, J.C., Deep-sea benthic foraminifera and biogenic opal: glacial to postglacial productivity changes in the western equatorial Pacific, *Mar. Micropal., 19*, 79-98, 1992.

Hofker, J., Foraminifera Dentata, foraminifera of Santa Cruz and Thatch Island, Virgin Archipelago, West Indies, *Spolia Zool. Mus. Kbenhavn, 15*, 1-237, 1956.

Howard, W.R. and W.L. Prell, Late Quaternary surface circulation of the southern Indian Ocean and its relationships to orbital variations., *Paleoceanography, 7*, 79-117, 1992.

Hutson, W.H., Variations in planktic foraminiferal assemblages along north-south transects in the Indian Ocean, *Mar. Micropal., 2*, 47-66, 1977.

Imbrie, J., A. Berger and N.J. Shackleton Role of orbital forcing: A two-million year perspective. In: Eddy, J. A. and Oeschger, H. (eds), *Global changes in the perspective of the past.* John Wiley and Sons 1993a.

Imbrie, J., E.A. Boyle, S.C. Clemens, A. Duffy, W.R. Howard, G. Kukla, J. Kutzbach, D.G. Martinson, A. McIntyre, A.C. Mix, B. Molfino, J.J. Morley, L.C. Peterson, N.G. Pisias, W.L. Prell, M.E. Raymo, N.J. Shackleton and J.R. Toggweiler, On the structure and origin of major glaciation cycles, 1, Linear responses to Milankovitch forcing, *Paleoceanography, 7*, 701-738, 1992.

Imbrie, J., E.A. Boyle, S.C. Clemens, A. Duffy, W.R. Howard, G. Kukla, J. Kutzbach, D.G. Martinson, A. McIntyre, A.C. Mix, B. Molfino, J.J. Morley, L.C. Peterson, N.G. Pisias, W.L. Prell, M.E. Raymo, N.J. Shackleton and J.R. Toggweiler, On the structure and origin of major glaciation cycles. 2. The 100,000-year cycle, *Paleoceanography, 8*, 699-735, 1993b.

Imbrie, J., J.D. Hays, D.G. Martinson, A. McIntyre, A.C. Mix, J.J. Morley, N.G. Pisias, W.L. Prell and N.J. Shackleton, The orbital theory of pleistocene climate: support from a revised chronology of the marine $\delta^{18}O$ record. In: Berger, A., Imbrie, J., Hays, J., Kukla, G. and Saltzman, B. (eds), *Milankovitch and Climate, Part I.* D. Reidel 269-305, 1984.

Imbrie, J. and J.Z. Imbrie, Modelling the climatic response to orbital variations, *Science, 207*, 943-953, 1980.

Imbrie, J., A. McIntyre and A. Mix, Oceanic response to orbital forcing in the Late Quaternary: Observational and experimental strategies. In: Berger, A. (ed), *Climate and Geo- Sciences.* Kluwer Academic Publishers 121-164, 1989.

Janacek, T.R. and D.K. Rea, Pleistocene fluctuations in northern hemisphere trade winds and westerlies. In: Berger, A., Imbrie, J., Hays, J., Kukla, G. and Saltzman, B. (eds), *Milankovitch and climate, Part I.* D. Reidel 269-305, 1984.

Jansen, E. and T. Veum, Evidence for two-step deglaciation and its impact on North Atlantic deep-water circulation, *Nature, 343*, 612-616, 1990.

Jansen, F., Ufkes and R. Schneider, Late Quaternary movements of the Angola-Benguela Front, SE Atlantic, and implications for advection in the equatorial Ocean. In: Wefer, G., Berger, W. H., Siedler, G. and Webb, D. (eds), *The South Atlantic: Present and Past Circulation.* Springer-Verlag 553-575, 1997.

Jansen, J.H.F. and J.M. Van Iperen, A 220,000 year climate record for the east equatorial Atlantic Ocean and equatorial Africa: evidence from diatoms and opal phytoliths in the Zaire (Congo) deep-sea fan, *Paleoceanography, 6 (5)*, 573-591, 1990.

Jansen, J.H.F., T.C.E. Van Weering, R. Gieles and J. Van Iperen, Late Quaternary oceanography and climatology of the Zaire-Congo fan and the adjacent eastern Angola Basin, *Neth. J. Sea Res., 17*, 201-249, 1984.

Jenkins, G.M. and D.G. Watts, *Spectral analysis and its application*, Holden Day 525 pp., 1968.

Johnsen, S.J., Irregular glacial interstadials recorded in a new Greenland ice core, *Nature, 359*, 311-312, 1992.

Johnson, R.G. and J.T. Andrews, Rapid ice sheet growth and initiation of the last glaciation, *Quat. Res., 12*, 119-134, 1979.

Jouzel, J., Ice cores north and south, *Nature, 372*, 612-613, 1994.

Jouzel, J., C. Lorius, J.R. Petit, C. Genthon, N.I. Barkov, V.M. Kotlyakov and V.M. Petrov, Vostok ice core: a continuous isotope temperature record over the last climatic cycle (160,000 years), *Nature, 329*, 403-408, 1987.

Keigwin, L.D. and S.J. Lehman, Deep circulation linked to Heinrich event 1 and Younger Dryas in a mid-depth North Atlantic core, *Paleoceanography, 9*, 185-194, 1994.

Kennett, J.P. and B.L. Ingram, A 20,000 year record of ocean circulation and climate change from the Santa Barbara Basin, *Nature, 377*, 510-513, 1995a.

Kennett, J.P. and B.L. Ingram, Palaeoclimatic evolution of Santa Barbara Basin during the last 20 kyr: Marine evidence from Hole 893A, *Proc. Ocean Drill. Prog. Sci. Res., 146*, 309-325, 1995b.

Kennett, J.P. and M.S. Srinivasan, *Neogene Planktonic Foraminifera: A Phylogenetic Atlas*, Hutchison Ross Publishing Co., 265 pp., 1983.

Kennett, J.P. and K. Venz, Late Quaternary climatically related planktonic foraminiferal assemblage changes: Hole 893A, Santa Barbara Basin, California., *Proc. Ocean Drill. Prog. Sci. Res., 146*, 281-293, 1995.

Kipp, N.G., New transfer function for estimating past sea-surface conditions from sea-bed distribution of planktonic foraminiferal assemblages in the North Atlantic. In: Cline, R. M. and Hays, J. D. (eds), *Investigation of Southern Ocean Palaeoceanography and Palaeoclimatology*. Geol. Soc. Am. Mem. 145. 1976.

Koc Karpuz, N. and E. Jansen, A high resolution diatom record of the last deglaciation from the SE Norwegian Sea: documentation of rapid climatic changes, *Paleoceanography, 7*, 499-520, 1992.

Kotilainen, A.T. and N.J. Shackleton, Rapid climate variability in the North Pacific Ocean during the last 95,000 years, *Nature, 377*, 323-326, 1995.

Kreveld, S.A., van, M. Knappertsbusch, J. Ottens, G.M. Ganseen and J.E. van Hinte, Biogenic carbonate and IRD (Heinrich Layer) accumulation in deep sea sediments from a northeast Atlantic piston core, *Mar. Geol., 131*, 21-46, 1996.

Kroon, D., Distribution of extant planktic foraminiferal assemblages in Red Sea and nothern Indian Ocean surface waters, *Rev. Esp. Micropal., 23 (1)*, 37-74, 1991.

Kroon, D., K. Beets, S. Mowbray, G. Shimmield and T. Steens, Changes in northern Indian Ocean monsoonal wind activity during the last 500 kyr., *Mem. Soc. Geol. It., 44*, 189-207, 1990.

Kroon, D. and G. Ganssen, Northern Indian Ocean upwelling cells and the stable isotope composition of living planktonic foraminifera, *Deep Sea Res., 36*, 1219-1236, 1989.

Le, J. and N.J. Shackleton, Carbonate dissolution fluctuations in the western equatorial Pacific during the late Quaternary, *Paleoceanography, 7*, 21-42, 1992.

Leeuwen, R.J.W., van, Sea floor distribution and late Quaternary faunal patterns of planktic and benthic foraminifera in the Angola Basin. *Ph.D. Thesis, Utrecht, The Netherlands*, 1995.

Le Treut, H. and M. Ghil, Orbital forcing, climatic interactions, and glaciation cycles, *J. Geophys. Res., 88*, 5167-5190, 1983.

Le Treut, H., J. Portes, J. Jouzel and M. Ghil, Isotopic modelling of climatic oscillations: Implications for a comparative study of marine and ice records, *J. Geophys. Res., 93*, 9365-9383, 1988.

Libby, W.F., *Radiocarbon Dating*, 2nd edition. University of Chicago Press, Chicago, 1955.

Linsley, B.K. and R.C. Thunell, The record of deglaciation in the Sulu Sea: Evidence for the Younger Dryas event in the tropical western Pacific, *Paleoceanography, 5*, 1025-1039, 1990.

Little, M.G., D. Kroon, R.R. Schneider, B. Price, P. Müller and G. Wefer, Late Quaternary palaeoceanography and palaeoproductivity of the Benguela upwelling system for the last 180,000 years. *ICP IV Conference*, Halifax, Nova Scotia, 1995.

Little, M.G., R.R. Schneider, D. Kroon, N.B. Price, T. Bickert and G. Wefer, Rapid palaeoceanographic changes in the Benguela upwelling system for the last 160,000 years, as indicated by abundances of planktonic foraminifera, *Palaeogeog., Palaeoclim., Palaeoecol.*, 130, 135-161, 1997a.

Little, M.G., D. Kroon, R.R. Schneider, N.B. Price and C.P. Summerhayes, Trade wind forcing of upwelling, seasonality, and Heinrich events as a response to sub-Milankovitch climate variability, *Paleoceanography*, 12 (4), 568-576, 1997b.

Lorius, C., J. Jouzel, D. Raynaud, J. Hansen and H. LeTreut, The ice-core record: climate sensitivity and future greenhouse warming, *Nature, 347*, 139-145, 1990.

Lowry, F.M.D., Foraminiferal thanataconeses from the continental shelf of Southern Africa. *Ph.D. Thesis, Uni. College London*, 1987.

Lutjeharms, J.R.E., The exchange of water between the South Indian and South Atlantic Oceans. In: Wefer, G., Berger, W. H., Siedler, G. and Webb, D. (eds), *The South Atlantic: Present and Past Circulation.* Springer 125-162, 1997.

Lutjeharms, J.R.E. and J.M. Meeuwis, The extent and variability of SE Atlantic upwelling, *S. Afr. J. Mar. Sci., 5*, 51-62, 1987.

Lutjeharms, J.R.E. and P.L. Stockton, Kinematics of the upwelling front off southern Africa, *S. Afr. J. Mar. Sci., 5*, 35-49, 1987.

Lutze, G.-F. and W.T. Coulbourn, Recent benthic foraminifera from the continental margin of Northwest Africa: community structure and distribution., *Mar. Micropal., 8*, 361-401, 1984.

Lutze, G.-F., U. Pflaumann and P. Weinholz, Jungquartäre Fluktuationen der benthischen Foraminiferenfaunen in Tiefsee-Sedimenten vor NW-Africa: eine Raktion auf Produktivitätsanderungen im Oberflächenwasser, *METEOR Forsch. Ergeb., C 40*, 163-180, 1986.

Lutze, G.F., Benthic foraminifers at site 397; Faunal fluctuations and ranges in the Quaternary (leg 47), *Deep Sea Drill. Proj. Init. Res., 47*, 419-431, 1980.

Luz, B. and N.J. Shackleton, $CaCO_3$ solution in the tropical east Pacific during the last 130,000 years, *Spec. Pub. Cush. Foram. Res. 13.* 142-150, 1975.

Lyle, M.W., F.G. Prahl and M.A. Sparrow, Upwelling and productivity changes inferred from a temperature record in the central equatorial Pacific, *Nature, 355*, 812-815, 1992.

MacAyeal, D.R., Binge/Purge oscillations of the Laurentide ice sheet as a cause of the North Atlantic's Heinrich events, *Paleoceanography, 8*, 775-784, 1993a.

MacAyeal, D.R., A low-order model of the Heinrich events cycle, *Paleoceanography, 8*, 767-773, 1993b.

Macdonald, A.M. and C. Wunsch, An estimate of global circulation and heat fluxes, *Nature, 382*, 436-439, 1996.

Macdonald, A.M.J., Property fluxes at 30°S and their implications for the Pacific-Indian throughflow and the global heat budget, *J. Geophys. Res., C98*, 6851-6868, 1993.

MacDonald, G.J., Spectral analysis of time series generated by nonlinear processes, *Rev. Geophys., 27*, 449-469, 1989.

Manabe, S. and R.J. Stouffer, Century scale effects of increased atmospheric CO_2 on the ocean-atmosphere system, *Nature, 364*, 215-218, 1993.

Martinson, D.G., N.G. Pisias, J.D. Hays, J. Imbrie, T.C. Moore and N.J. Shackleton, Age dating and the orbital theory of the ice ages: development of a high-resolution 0 to 300,000-year chronostratigraphy, *Quat. Res., 27*, 1-29, 1987.

Maslin, M.A., N.J. Shackleton and U. Pflaumann, Surface water temperature, salinity, and density changes in the northeast Atlantic during the last 45,000 years: Heinrich events, deep water formation, and climatic rebounds, *Paleoceanography, 10*, 527-544, 1995.

Matthewson, A.P., G.B. Shimmield, D. Kroon and A.E. Fallick, A 300 kyr high-resolution aridity record of the North African continent, *Paleoceanography, 10*, 677-692, 1995.

Mayewski, P.A., L.D. Meeker, S. Whitlow, M.S. Twickler, M.C. Morrison, P. Bloomfield, G.C. Bond, R.B. Alley, A.J. Gow, P.M. Grootes, D.A. Meese, A. Ram, K.C. Taylor and W. Wumkes, Changes in atmospheric circulation and ocean ice cover over the North Atlantic during the last 41,000 years, *Science, 263*, 1747-1751, 1994.

McIntyre, A. and B. Molfino, Forcing of Atlantic Equatorial and subpolar millenial cycles by precession, *Science, 274*, 1867-1870, 1996.

McIntyre, A., W.F. Ruddiman, K. Karlin and A.C. Mix, Surface water response of the equatorial Atlantic Ocean to orbital forcing, *Paleoceanography, 4*, 19-55, 1989.

McManus, J.F., G.C. Bond, W.S. Broecker, S. Johnsen, L. Labeyrie and S. Higgins, High-resolution climate records from the North Atlantic during the last interglacial, *Nature, 371*, 326-329, 1994.

Meeuwis, J.M. and J.R.E. Lutjeharms, Surface thermal characteristics of the Angola-Benguela front, *S. Afr. J. Mar. Sci., 9*, 261-279, 1990.

Meyer, K., Uran-Prospektion vor Südwestafrika, *Erzmetall, 26*, 1973.

Meyers, P.A., Organic matter variations in sediments from DSDP sites 362 and 532: evidence of upwelling changes in the Benguela Current upwelling system. In: Summerhayes, C. P., Prell, W. L. and Emeis, K. C. (eds), *Upwelling Systems: Evolution Since the Early Miocene.* Geol. Soc. Spec. Pub., *64*, 323-330, 1992.

Milankovitch, M., *Mathematische Klimalehre und Astronomische Theorie der Klimaschwankungen, Gebruder Borntraeger,* 176 pp., 1930.

Mix, A.C., Influence of productivity variations on long-term atmospheric CO_2, *Nature, 337*, 541-544, 1989a.

Mix, A.C., Pleistocene paleoproductivity: evidence from organic carbon and foraminiferal species. In: Berger, W. H., Smetacek, V. S. and Wefer, G. (eds), *Productivity of the Ocean: Present and Past.* J. Wiley & Sons 313-340, 1989b.

Mix, A.C. and A.E. Morey, Climate feedback and Pleistocene variations in the Atlantic South Equatorial Current. In: Wefer, G., Berger, W. H., Siedler, G. and Webb, D. J. (eds), *The South Atlantic: Present and Past circulation.* Springer 503-525, 1997.

Mix, A.C., W.F. Ruddiman and A. McIntyre, Late Quaternary palaeoceanography of the tropical Atlantic, 1: Spatial variability of annual mean sea-surface temperatures, 0—20,000 years B.P., *Paleoceanography, 1*, 43-66, 1986a.

Mix, A.C., W.F. Ruddiman and A. McIntyre, Late Quaternary paleoceanography of the tropical Atlantic, 2: The seasonal cycle of sea surface temperatures, 0-20,000 years B.P., *Paleoceanography, 1*, 339-353, 1986b.

Molfino, B., L.H. Heusser and G.M. Woillard, Frequency components of a Grande Pile pollen record: evidence of precessional orbital forcing. In: Berger, A., Imbrie, J., Hays, J., Kukla, G. and Saltzman, B. (eds), *Milankovitch and Climate.*, Riedel, 269-305, 1984.

Molfino, B., N.G. Kipp and J.J. Morley, Comparison of foraminiferal coccolithophoroid, and radiolarian palaeotemperature equations: Assemblage coherency and estimate concordancy, *Quat. Res., 17*, 279-313, 1982.

Molfino, B. and A. McIntyre, Precessional forcing of nutricline dynamics in the Equatorial Atlantic, *Science, 29*, 766- 769, 1990.

Molnia, B.F. Distal glacial-marine sedimentation: Abundance, composition and distribution of North Atlantic ocean Pleistocene ice-rafted sediment. In: Molnia, B. F. (eds), *Glacial-marine sedimentation*. Plenum Press 593-629, 1983.

Morley, J.J., Radiolarian-based transfer functions for estimating conditions in the South Indian Ocean, *Mar. Micropal., 13*, 293-307, 1989a.

Morley, J.J., Variations in high-latitude oceanographic fronts in the southern Indian Ocean: An estimation based on faunal changes, *Paleoceanography, 4*, 547-554, 1989b.

Morley, J.J. and J.D. Hays, Comparison of glacial and interglacial oceanographic conditions in the South Atlantic from variations in calcium carbonate and radiolarian distribution, *Quat. Res., 12*, 396-408, 1979.

Moroshkin, K.V., V.A. Bubnov and R.P. Bulatov, Water circulation in the eastern South Atlantic, *Oceanology,* English Translation, *10*, 27-34, 1970.

Müller, P.J., M. Cepek, G. Ruhland and R.R. Schneider, Alkenone and coccolithophorid species changes in late Quaternary sediments from the Walvis Ridge: Implications for the alkenone palaeotemperature method, *Palaeogeog., Palaeoclim., Palaeoecol.*, in press.

Müller, P.J., H. Erelenkeuser and R. Von Grafenstein, Glacial-interglacial cycles in oceanic productivity inferred from organic carbon contents in eastern North Atlantic sediment cores. In: Thiede, J. and Suess, E. (eds), *Coastal Upwelling: Part B*. Plenum 365-398, 1983.

Müller, P.J., R. Schneider and G. Ruhland, Late Quaternary pCO_2 variations in the Angola Current: Evidence from organic carbon $\delta^{13}C$ and alkenone temperatures. In: Zahn, R., Pedersen, T. F., Kaminski, M. A. and Labeyrie, L. (eds), *Carbon Cycling in the Glacial Ocean: Constraints on the Ocean's Role in Global Change.*, NATO ASI Series, vol. 117, Springer, 343-366, 1994.

Müller, P.J. and E. Suess, Productivity, sedimentation rate, and sedimentary organic matter in the oceans. I. Organic carbon preservation, *Deep Sea Res., 26*, 1347-1362, 1979.

Murray, J.W., *Ecology and Palaeoecology of Benthic Foraminifera*, Longman, 1991.

Nadeau, M.-J., M. Schleicher, P.M. Grootes, H. Erlenkeuser, A. Gottdang, D.J.W. Mous, J.M. Sarnthein and H. Willkomm, Nuclear Instruments and Methods, B. Leibniz-Labor AMS facility at the Christian-Albrechts-University, Kiel, Germany, 1997.

Nair, R.R., V. Ittekot, S.J. Manganini, V. Ramsaswamy, B. Haake, E.T. Degens, B.N. Desai and S. Honjo, Increased particle flux to the deep ocean related to monsoons, *Nature, 338*, 749-750, 1989.

Natland, M.L., New species of foraminifera from off the west coast of North America and from the later Tertiary of the Los Angeles Basin, *Ibid, 4*, 137-164, 1938.

Oberhänsli, H., Upwelling signals at the northeastern Walvis Ridge during the past 500,000 years, *Paleoceanography, 6*, 53-71, 1991.

Oberhänsli, H., C. Bénier, G. Meinecke, H. Schmidt, R. Schneider and G. Wefer, Planktonic foraminifers as tracers of ocean currents in the eastern South Atlantic, *Paleoceanography, 7*, 607-632, 1992.

Okada, H. and S. Honjo, The distribution of oceanic coccolithophorids in the Pacific, *Deep Sea Res., 20*, 355-374, 1973.

Oppo, D.W. and R.G. Fairbanks, Variability in the deep and intermediate water circulation of the Atlantic Ocean during the past 25,00 years: Northern hemisphere modulation of the Southern Ocean, *Earth Planet. Sci. Lett., 86*, 1-15, 1987.

Oppo, D.W. and R.G. Fairbanks, Atlantic Ocean thermohaline circulation of the last 150,000 years: relationship to climate and atmospheric CO_2, *Paleoceanography, 5*, 277-288, 1990.

Paillard, D. and L. Labeyrie, Role of the thermohaline circulation in the abrupt warming of the Heinrich events, *Nature, 372*, 162-164, 1994.

Park, J., L.D. D'Hondt, J.W. King and C. Gibson, Late Cretaceous precessional cycles in double time: A warm-Earth Milankovitch response, *Science, 261*, 1431-1434, 1993.

Parker, F. and W.H. Berger, Faunal and solution patterns of planktonic foraminifera in surface sediments of the South Pacific, *Deep Sea Res., 18*, 73-107, 1971.

Parker, F.L., Eastern Mediterranean foraminifera, *Repts. Swedish Deep-sea Exped., 8*, 219-254, 1958.

Parker, F.L., Planktonic foraminiferal species in Pacific sediments, *Micropal., 8*, 219-254, 1962.

Parker, W.K. and T.R. Jones, On some foraminifera from the North Atlantic and Arctic Oceans, including Davis Straits and Baffin Bay, *Roy. Soc. Lon. Phil. Trans., 155*, 325-441, 1865.

Parker, W.K., T.R. Jones and H.B. Brady, On the nomenclature of the foraminifera; Part XII. The species enumerated by d'Orbigny in the "Annales des Sciences Naturales, vol. 7, 1826", *Ann. Mag. Nat. Hist. Lon. Series 3, 12*, 429-441, 1865.

Patience, A.J., and D. Kroon, Oxygen isotope chronostratigraphy, In: P.L. Smart and P.D. Frances, *Quaternary Dating Methods - A User's Guide*, 199-228, 1991.

Pastouret, L., G.A. Auffret, M. Hoffert, H.D. Needham and C. Latouche, Sedimentation sur la ride de Terre-Neuve, *Can. J. Earth Sci., 12*, 1019-1035, 1975.

Pearson, G.W., Pilcher, J.R., Bilie, M.G.L., Corbett, D.M., and Qua, F. High precision ^{14}C measurement of Irish oaks to show the natural ^{14}C variations from AD 1840 to 5210 BC, *Radiocarbon,* 35, 25-34, 1986.

Peterson, L.C. and W.L. Prell, Carbonate dissolution in recent sediments of the eastern equatorial Indian Ocean: Preservation patterns and carbonate loss above the lysocline, *Mar. Geol., 64*, 259-290, 1985.

Peterson, R.G. and T. Whitworth, The subantarctic and polar fronts in relation to deep water masses through the Southwestern Atlantic, *J. Geophys. Res., 8*, 817-838, 1989.

Phleger, A.J. and A. Soutar, Production of benthic foraminifera in three east Pacific oxygen minima, *Micropal., 19*, 110-115, 1973.

Pisias, N.G. and D.K. Rea, Late Pleistocene paleoclimatology of the central equatorial Pacific: Sea surface response to the southeast trade winds, *Paleoceanography, 3*, 21-37, 1988.

Pokras, E.M., Diatom record of Late Quaternary climatic change in the eastern equatorial Atlantic and tropical Africa, *Paleoceanography, 2*, 273-286, 1987.

Pokras, E.M. and A.C. Mix, Earth's precession cycle and Quaternary climatic change in tropical Africa, *Nature, 326*, 486-487, 1987.

Porter, S.C. and A. Zhisheng, Correlation between climate events in the North Atlantic and China during the last glaciation, *Nature, 375*, 305-308, 1995.

Prell, W.L., The stability of low-latitude sea surface temperatures: An evaluation of the CLIMAP reconstruction with emphasis on the positive SST anomalies. *Technical Report. TRO25*, 60pp. Department of Energy, Washington D.C., 1985.

Prell, W.L. and W.B. Curry, Faunal and isotopic indices of monsoonal upwelling: Western Arabian Sea, *Oceanol. Acta., 4*, 1981.

Prell, W.L., W.H. Hutson and D.F. Williams, The subtropical convergence and late Quaternary circulation in the southern Indian Ocean, *Mar. Micropal., 4*, 225-234, 1979.

Prell, W.L., W.H. Hutson, D.F. Williams, A.W.H. Bé, K. Geitzenauer and B. Molfino, Surface circulation of the Indian Ocean during the Last Glacial Maximum, approximately 18,000 yr BP, *Quat. Res., 14*, 1980.

Prell, W.L., J. Imbrie, D.G. Martinson, J.J. Morley, G. Pisias, N.J. Shackleton and H.F. Streeter, Graphic correlation of oxygen isotope stratigraphy application to the late Quaternary, *Paleoceanography, 1*, 137-162, 1986.

Prell, W.L. and J.E. Kutzbach, Monsoon variability over the past 150,000 years, *J. Geophys. Res., 92*, 8411- 8425, 1987.

Reynolds, L.A. and R.C. Thunnel, Seasonal succession of planktonic foraminifera in the subpolar North Pacific, *J. Foram. Res., 15*, 282-301, 1985.

Rintoul, S.R., South Atlantic interbasin exchange, *J. Geophys. Res., C96*, 2675-2692, 1991.

Roberts, N., M. Taieb, P. Barker, B. Dumnati, M. Icole and D. Williamson, Timing of the Younger Dryas event in east Africa from lake level changes, *Nature, 366*, 146-148, 1993.

Rogers, J. and J.M. Bremner, The Benguela Ecosystem. Part VII. Marine geological aspects., *Oceano. Mar. Bio. Ann. Rev., 29*, 1-85, 1991.

Ruddiman, W.F., Late Quaternary deposition of ice rafted sand in the subpolar North Atlantic (lat 40-65N), *Geol. Soc. Am. Bull., 88*, 1813-1827, 1977.

Ruddiman, W.F. and A. McIntyre, Oceanic mechanisms for amplification of the 23,000-year ice-volume cycle, *Science, 212*, 617-627, 1981.

Ruddiman, W.F., A. McIntyre, V. Niebler-Hunt and J.T. Durazzi, Oceanic evidence for the mechanism of rapid northern hemisphere glaciation, *Quat. Res., 13*, 33-64, 1980.

Ruddiman, W.F., M.E. Raymo, D.G. Martinson, B.M. Clement and J. Backman, Pleistocene evolution: Northern hemisphere ice sheets and North Atlantic Ocean, *Paleoceanography, 4*, 353-412, 1989.

Ruddiman, W.F. and M. Sarnthein (eds), *Proc. Ocean Drill. Prog. Sci. Res., 108*, 1989.

Rutsch, H.-J., A. Mangini, G. Bonani, B. Dittrich-Hannen, P.W. Kubik, M. Suter and M. Segl, ^{10}Be and Ba concentrations in West African sediments trace productivity in the past, *Earth Planet. Sci. Lett., 133*, 129-143, 1995.

Sancetta, C. and S. Silvestri, Pliocene-Pleistocene evolution of the North Pacific ocean-atmosphere system, interpreted from fossil diatoms, *Paleoceanography, 1*, 163-180, 1986.

Sarnthein, M., U. Pflaumann, R. Ross, R. Tiedemann and K. Winn, Transfer functions to reconstruct ocean productivity: a comparison. In: Summerhayes, C. P., Prell, W. L. and Emeis, K. C. (eds), *Upwelling Systems: Evolution Since the Early Miocene*. Geol. Soc. Spec. Pub., *64*, 411-427, 1992.

Sarnthein, M., K. Winn, J.C. Duplessy and M.R. Fontugne, Global variations of surface ocean productivity in low and mid latitudes: Influence on CO^2 reservoirs of the deep ocean and atmosphere during the last 21,000 years, *Paleoceanography, 3*, 361-399, 1988.

Sarnthein, M., K. Winn and U. Zahn, Palaeoproductivity of oceanic upwelling and the effect on atmospheric CO^2 and climatic change during deglaciation times. In: Berger, W. H. and Labeyrie, L. D. (eds), *Abrupt Climate Change*. 311-337, 1987.

Schlanger, S.O. and H.C. Jenkyns, Cretaceous oceanic anoxic events causes and consequences, *Geol. Mjinbouw, 55 (3-4)*. 179-184, 1976.

Schmelzer, I., C. Hemleben and M. Segl, Dansgaard-Oescher events in the Red Sea, *Terra Nova, 9*, 621, 1997.

Schmidt, H., Der Benguela Strom im Bereich des Walfisch Rückens im Spätquartär. *Ph.D. Thesis, Univerisität Bremen,* 1992.

Schmiedl, G., Late Quaternary benthic foraminiferal assemblages from the eastern South Atlantic Ocean: Reconstruction of deep water circulation and productivity changes, *Repts. Polar Res., 160*, 1995.

Schmitz, W.J., On the eddy field in the Agulhas Retroflection, with some global considerations, *J. Geophys. Res., 101*, 16259-16271, 1996.

Schneider, R.R., Spätquartäre Produktivitätsänderungen im östlichen Angola-Becken: Reaktion auf Variationen im Passat-Monsun-Windsystem und in der Advektion des Benguela-Küstenstroms. *Ph.D. Thesis, Uni. Bremen,* 1991.

Schneider, R.R., P.J. Müller, D. Kroon, B. Price and I. Alexander, Monsoon related Zaire (Congo) discharge fluctuations and influence of fluvial silicate supply on marine productivity in the east equatorial Atlantic over the last 200,000 years, *Paleoceanography,* in press.

Schneider, R.R., P.J. Müller and G. Ruhland, Late Quaternary surface circuation in the east-equatorial south Atlantic: Evidence from Alkenone sea-surface temperatures, *Paleoceanography, 10*, 197-219, 1995.

Schneider, R.R., P.J. Müller, G. Ruhland, G. Meinecke, H. Schmidt and G. Wefer, Late Quaternary surface temperatures and productivity in the east-equatorial South Atlantic: Response to changes in trade/monsoon wind forcing and surface water advection. In: Wefer, G., Berger, W. H., Siedler, G. and Webb, D. (eds), *The South Atlantic: Present and Past Circulation.* Springer 527-551, 1997.

Schneider, R.R., P.J. Müller and G. Wefer, Late Quaternary palaeoproductivity changes off the Congo deduced from stable carbon isotopes of planktonic foraminifera, *Palaeogeog., Palaeoclim., Palaeoecol., 110*, 255-274, 1994.

Schott, W., Die foraminiferen in dem äquatorialen teil des Atlantischen Ozeans, *Deutl. Atl. Exped. Meteor 1925-1927, 3*, 43-134, 1935.

Schrader, H., Peruvian coastal primary palaeo-productivity during the last 200,000 years. In: Summerhayes, C. P., Prell, W. L. and Emeis, K. C. (eds), *Upwelling systems: Evolution Since the Early Miocene.* Geol. Soc. Spec. Pub., *64*, 391-409, 1992.

Schulz, H.D. and crusie participants, Bericht und erst Ergenbnisse über die METEOR-Fahrt M20/2, Abidjan-Dakar, 27.12.1991 - 3.2.1992, *Ber. Fachber. Geowiss. Uni. Bremen, 25*, 1992.

Schwager, C., Fossile foraminiferen von Kar Nikobar, NOVARA Expedition, Geologische Thiel vol. 2(2), 258, 1866.

Shackleton, N.J. Carbon-13 in Uvigerina: Tropical rainforest history and the equatorial Pacific carbonate dissolution cycles. In: Anderson, N. R. and Malahoff, A. (eds), *The Fate of Fossil Fuel CO_2 in the Oceans.* Plenum 145-165, 1977.

Shackleton, N.J. and N.D. Opdyke, Oxygen isotope and palaeomagnetic stratigraphy of equatorial Pacific core V 28-238: Oxygen isotope temperatures and ice volumes on a 10^5 year scale, *Quat. Res., 3*, 39-55, 1973.

Shackleton, N.J., J., -C., Duplessy, M. Arnold, P. Maurice, M.A. Hall, J. Cartlidge, Radiocarbon age of last glacial Pacific deep water, *Nature*, 335, 708-711, 1988.

Shannon, L.V., The Benguela Ecosystem Part 1: Evolution of the Benguela, physical features and processes., *Oceano. Mar. Bio. Ann. Rev., 23*, 105-182, 1985.

Shannon, L.V., J.J. Agenbag and M.E.L. Buys, Large and mesoscale features of the Angola-Benguela Front, *S. Afr. J. Mar. Sci.*, 5 11-34, 1987.

Shannon, L.V., J.R.E. Lutjeharms and J.J. Agenbag, Episodic input of Subantarctic water into the Benguela region, *S. Afr. J. Mar. Sci., 85*, 1989.

Shannon, L.V. and G. Nelson, The Benguela: Large scale features and processes and system variability. In: Wefer, G., Berger, W. H., Siedler, G. and Webb, D. (eds), *The South Atlantic: Present and Past Circulation.* Springer 163-210, 1997.

Shannon, L.V. and S.C. Pillar, The Benguela Ecosystem. Part III. Plankton, *Oceano. Mar. Bio. Ann. Rev., 24*, 65-170, 1986.

Shillington, F.A., L. Hutchings, T.A. Probyn, H.N. Waldron and W.T. Peterson, Filaments and the Benguela frontal zone; offshore advection or recirculating loops?, *S. Afr. Mar. Sci., 12*, 207-218, 1992.

Shimmield, G.B., Can sediment geochemistry record changes in coastal upwelling palaeoproductivity? Evidence from northwest Africa and the Arabian Sea. In: Summerhayes, C. P., Prell, W. L. and Emeis, K. C. (eds), *Upwelling systems: Evolution since the early Miocene.* Geol. Soc. Spec. Pub., *64*, 9-20, 1992.

Shimmield, G.B. and T.F. Pederson, The geochemistry of reactive trace metals and halogens in hemipelagic continental margin sediments, *Critical Revs. Aquatic Sci., 3*, 255-279, 1990.

Shimmield, G.B., N.B. Price and T.F. Pederson, The influence of hydrography, bathymetry and productivity on sediment type and composition of the Oman Margin and in the northwest Arabian Sea. In: Robertson, A. H. F., Searle, M. P. and Ries, A. C. (eds), *The Geology and Tectonics of the Oman Region.* Geol. Soc. Lon. Spec. Pub., *49*, 761-771, 1990.

Short, D.A., J.G. Mengel, T.J. Crowley, W.T. Hyde and G.R. North, Filtering of Milankovitch cycles by Earth's geography, *Quat. Res., 35*, 157-173, 1991.

Siesser, W.G., Late Miocene origin of the Benguela upwelling system off northern Namibia, *Science, 208*, 283-285, 1980.

Sirocko, F. and M. Sarnthein, Wind-bourne deposits in the northwestern Indian Ocean: record of Holocene sediments versus modern satellite data. In: Leinen, M. and Sarnthein, M. (eds), *Paleoclimatology and paleometry: Modern and Past Patterns of Global Atmospheric Transport.* Kluwer, Dordrecht 401-433, 1989.

Smith, R.L., A. Huyer, J.S. Godfrey and J.A. Church, The Leeuwin Current off Western Australia, 1986—1987, *J. Phys. Oceano., 21*, 323-345, 1991.

Steens, T.N.F., G. Ganssen and D. Kroon, Oxygen and carbon isotopes in planktonic foraminifers as indicators of upwelling intensity and upwelling-induced high productivity in sediments from the northwestern Arabian Sea. In: Summerhayes, C. P., Prell, W. L. and Emeis, K. C. (eds), *Upwelling Systems: Evolution Since the Early Miocene.* Geol. Soc. Spec. Pub., *64*, 107-120, 1992.

Stommel, H., Asymmetry of interoceanic fresh-water and heat fluxes, *Procs. Nat. Acad. Sci., 77*, 2377-2381, 1980.

Stuiver, M., In: Turekian K.K. (ed), *Late Glacial Cenozoic Ages.* Yale University Press, New Haven, 57-70, 1970.

Stuiver, M., T.F. Brazunias, B. Becker, B. Kromer, Climatic, solar, oceanic and geomagnetic influences on late-glacial and Holocene atmospheric $^{14}C/^{12}C$ change, *Quaternary Research,* 35, 1-24, 1991.

Stuiver, M., *Nature,* 273, 1978.

Stramma, L. and R.G. Peterson, Geostrophic transport in the Benguela Current Region, *J. Phys. Oceano., 19*, 1440-1448, 1989.

Struck, U., M. Sarnthein, L. Westerhausen, J.M. Barnola and D. Raynauld, Ocean-atmosphere carbon exchange: impact of the 'biological pump' in the Atlantic equatorial upwelling belt over the last 330,000 years, *Palaeogeog., Palaeoclim., Palaeoecol., 103*, 41-56, 1993.

Suess, H.E., Bristle-cone pine calibration of the radiocarbon time-scale 5,000 BC to the present. In: Olsson, I.U., *Radiocarbon Variations and Absolute Chronology*, John Wiley, 303-311, 1990.

Suess, E.R. and R. Von Huene (eds), *Proc. Ocean Drill. Prog. Sci. Res., 112*, 1990.

Summerhayes, C.P., Sedimentary processes in the northern Cape Basin, South Atlantic. Cruise report, CHAIN cruise 115 "Southlant" Leg 2: Dakar, Senegal to Cape Town, South Africa, December 14, 1973 - January 10, 1974. Woods Hole Oceanographic Institution, 12pp., 1974.

Summerhayes, C.P., Sedimentation of organic matter in upwelling regimes. In: Thiede, J. and Suess, E. (eds), *Coastal Upwelling: Its Sediment Record; Part B: Sedimentary Records of Ancient Coastal Upwelling*. Plenum Press, 29-72, 1983.

Summerhayes, C.P., K.C. Emeis, M.V. Angel, R.L. Smith and B. Zeitzschel, Upwelling in the ocean: Modern processes and ancient records. In: Summerhayes, C. P., Emeis, K. C., Angel, M. V., Smith, R. L. and Zeitzschel, B. (eds), *Upwelling in the Ocean. Dahlem Workshop Report*. John Wiley, 1-38, 1995a.

Summerhayes, C.P., D. Kroon, A. Rosel-Melé, R.W. Jordan, H.J. Schrader, R. Hearn, J. Villanueva, J.O. Grimalt and G. Eglinton, Variability in the Benguela Current System over the last 70,000 years., *Prog. Oceanog., 35*, 207-251, 1995b.

Teller, J.T., Meltwater and precipitation runoff to the North Altantic, Arctic and Gulf of Mexico from the Laurentide ice sheet and adjacent regions during the Younger Dryas, *Paleoceanography, 5*, 897-905, 1990.

Ten Haven, H.L. and D. Kroon, Late Pleistocene sea surface temperature variations off Oman as revealed by the distribution of long-chain alkenones, *Proc. Ocean Drill. Prog. Sci. Res., 117*, 445-452, 1991.

Thiede, J., Distribution of foraminifera in surface waters of a coastal upwelling area, *Nature, 253*, 712-714, 1975.

Thiede, J. and B. Junger, Faunal and floral indicators of coastal upwelling (NW African and Peruvian Continental Margins). In: Summerhayes, C. P., Prell, W. L. and Emeis, K. C. (eds), *Upwelling systems: Evolution Since the Early Miocene*. Geol. Soc. Spec. Pub., *64*, 47-76, 1992.

Thierstein, H.R., K.R. Geitzenauer, B. Molfino and N.J. Shackleton, Global synchroneity of Quaternary coccolith datum levels: Validation by oxygen isotopes, *Geology, 5*, 400-404, 1977.

Thouveny, N., J.L. de Beaulieu, E. Bonifray, K.M. Creer, J. Guiot, M. Icole, S. Johnsen, J. Jouzel, M. Reille, T. Williams and D. Williamson, Climate variations in Europe over the past 140 kyr deduced from rock magmnetism, *Nature, 371*, 503-506, 1994.

Thunell, R.C. and P.G. Mortyn, Glacial climate instability in the northeast Pacific Ocean, *Nature, 376*, 504-506, 1995.

Ufkes, E., Planktonic foraminifera in the surface waters of the eastern South Atlantic during springtime, *Oceanol. Acta.*, submitted.

Ufkes, E. and W.-J. Zachariasse, Origin of coiling differences in living negloboquadrinids in the Walvis Bay region, off Namibia, southwest Africa, *Micropal., 39*, 283-287, 1993.

Valentine, H.R., J.R.E. Lutjeharms and G.B. Brundrit, A fine scale volumetric census of the water masses of the Agulhas Retroflection area, *Rep. S. Afr. Coun. Sci. Ind. Res., EMA-R 691*, 105pp, 1993.

Verardo, D.J. and A. McIntyre, Production and destruction: Control of biogenous sedimentation in the tropical Atlantic 0-300,000 years B.P., *Paleoceanography, 9*, 63-86, 1994.

De Vries, H., Variation in concentration of radiocarbon with time and location on Earth, Koninkijk Nederlandse Akademie von Wetenschappen, Amsterdam, Proc., B61, 94-102, 1958.

Waldron, H.N. and T.A. Probyn, Nitrate supply and potential new production in the Benguela upwelling system, *S. Afr. J. Mar. Sci., 12*, 29-39, 1992.

Waldron, H.N., T.A. Probyn, J.R.E. Lutjeharms and F.A. Shillington, Carbon export associated with the Benguela upwelling system, *S. Afr. J. Mar. Sci., 12*, 369-374, 1992.

Webb, D.J., The southern boundary of the South Atlantic. In: Wefer, G., Berger, W. H., Siedler, G. and Webb, D. (eds), *The South Atlantic: Present and Past Circulation.* Springer, 211-217, 1997.

Weedon, G.P. and G.B. Shimmield, Late Pleistocene upwelling and productivity variations in the northwest Indian Ocean deduced from spectral analyses of geochemical data from ODP sites 722 and 724, *Proc. Ocean Drill. Prog. Sci. Res., 117*, 431-443, 1991.

Wefer, G., W.H. Berger, T. Bickert, B. Donner, G. Fischer, S. Kemle von Mücke, G. Meinecke, P.J. Müller, S. Mulitza, H.-S. Niebler, J. Pätzold, H. Schmidt, R.R. Schneider and M. Segl, Late Quaternary surface circulation in the South Atlantic: The stable isotope record and implications for heat transport and productivity. In: Wefer, G., Berger, W. H., Siedler, G. and Webb, D. (eds), *The South Atlantic: Present and Past Circulation.* Springer 461-502, 1997.

Wigley, T.M.L., Spectral analysis and the astronomical theory of climatic change, *Nature, 264*, 629-631, 1976.

Williams, D.F., Southern Ocean fluctuations of the polar front and subtropical convergence in the southeast Indian Ocean, *Mar. Micropal., 1*, 363-375, 1976.

Winter, A. and K. Martin, Late Quaternary history of the Agulhas Current, *Paleoceanography, 5*, 479-486, 1990.

Yeats, R.S. and B.U. Haq (eds) *Init. Repts. Deep Sea. Drill. Proj., 63*, 1981.

Yiou, P., C. Genthon, M. Ghil, J. Jouzel, H. Le Treut, J.M. Barnola, C. Lorius and Y.N. Korotkevitch, High-frequency palaeovariability in climate and CO_2 levels from Vostok ice core records, *J. Geophys. Res., 96*, 20,365-20,378, 1991.

Zahn, R., K. Winn and M. Sarnthein, Benthic foraminiferal $\delta^{13}C$ and accumulation rates of organic carbon: *Uvigerina perigrina* group and *Cibicidoides wuellerstorfi*, *Paleoceanography, 1*, 27-42, 1986.

Zhao, M., N.A.S. Beveridge, N.J. Shackleton, M. Sarnthein and G. Eglinton, Molecular stratigraphy of cores off northwest Africa: Sea surface temperature history over the last 80 ka, *Paleoceanography, 10*, 661-675, 1995.

Abbreviations and figure listings

A.1.

Appendix 1.1. List of abbreviations used

AABW	Antarctic Bottom Water
AACW	Antarctic Central Water
AADW	Antarctic Deep Water
AAIW	Antarctic Intermediate Water
AIW	Arctic Intermediate Water
ABF	Angola-Benguela Front
AC	Angola Current
AMS	Accelerated mass spectrometry
BCC	Benguela Coastal Current
BCS	Benguela Current system
BI	Benguela index
BOC	Benguela Oceanic Current
CCD	Carbonate compensation depth
CCrD	Carbonate critical depth
CI	Confidence interval
cm	Centimeters
DSDP	Deep sea drilling project
EUC	Equatorial Under-Current
ET	Ekman transport
F.	*Florisphaera*
Ga.	*Globigerinita*
Ge.	*Globigerinella*
GeoB	Geowissenschaften Bremen
Gg.	*Globigerina*
GISP2	Greenland ice-sheet project
Gr.	*Globorotalia*
GRIP	Greenland ice-core project
Gs.	*Globigerinoides*
H1-H6	Heinrich layers 1—6
IRD	Ice rafted debris
ka	Thousand years ago (date)
kyr	Kiloyear (interval)
LB	Lüderitz boundary
LGM	Last glacial maximum
m	Meters
MIW	Mediterranean Intermediate Water
My B.P.	Million years before present
N.	*Neogloboquadrina*
NACW	North Atlantic Central Water
NADW	North Atlantic Deep Water
NBR	Northern Benguela region
O.	*Orbulina*
P.	*Pulleniatina*
PDB	Pee Dee belemnite
PDW	Pacific Deep Water
PG/PC12	Combined gravity and piston core
PS-event	*N. pachyderma* (s) event
SAAG	South Atlantic Anticyclonic Gyre
SACW	South Atlantic Central Water
SASW	South Antarctic Surface Water
SBR	Southern Benguela region
SEC	South Equatorial Current
SECC	South Equatorial Counter Current
SST	Sea surface temperature
STC	Sub-tropical convergence
TOC	Total organic carbon
VOSTOK	East Antarctica ice-core
yrs	Years

Appendix 1.2. Planktonic foraminifera classification

Globigerina bulloides d'Orbigny, 1826
Globigerina falconensis Blow, 1959
Globigerina quinqueloba Natland, 1938
Globigerina rubescens Hofker, 1956
Globigerina tenellus Parker, 1958
Globigerinella calida (Parker), 1962
Globigerinita digitata Brady, 1884
Globigerinita glutinata (Egger), 1893
Globigerinita humilis (Brady), 1884
Globigerinita siphonifera d'Orbigny, 1839 [*Globigerinella aequilateralis* (Brady), 1839]
Globigerinita uvula (Ehrenberg), 1861
Globigerinoides conglobatus (Brady), 1879
Globigerinoides pyramidalis (van den Broeck), 1876
Globigerinoides ruber (d'Orbigny), 1839
Globigerinoides sacculifer (Brady), 1877
Globoquadrina altispira (Cushman and Jarvis),1936
Globorotalia inflata (d'Orbigny), 1839
Globorotalia crassaformis (Galloway and Wissler), 1927
Globorotalia hirsuta (d'Orbigny), 1839
Globorotalia menardii (Parker, Jones and Brady), 1865
Globorotalia scitula (Brady), 1882
Globorotalia theyeri Fleisher, 1974
Globorotalia truncatulinoides (d'Orbigny), 1839
Globorotalia tumida (Brady), 1877
Globorotalioides hexagona (Natland), 1938
Neogloboquadrina dutertrei (d'Orbigny), 1839
Neogloboquadrina pachyderma (Ehrenberg), 1861
Orbulina universa (d'Orbigny), 1839
Pulleniatina obliquiloculata (Parker and Jones), 1865

Appendix 1.3. List of figures, tables and plates

Chapter 1.

Chapter 2.

Chapter 3.

Stable oxygen and carbon isotope measurements

A.2.

Appendix 2. Oxygen and carbon isotope measurements

Appendix 2.1. Oxygen and carbon isotope data from GeoB 1706, using the planktonic foraminifer, *Globorotalia inflata.*

Depth (cm)	δ13C (‰)	δ18O (‰)	Depth (cm)	δ13C (‰)	δ18O (‰)	Depth (cm)	δ13C (‰)	δ18O (‰)
3	1.46	0.52	258	1.89	0.44	508	2.00	0.19
8	1.12	0.33	263	2.18	0.45	513	1.98	-0.01
13	0.91	0.34	268	2.06	0.34	518	1.70	0.15
18	0.81	0.25	273	1.99	0.32	523	1.76	0.15
23	0.88	0.46	278	2.00	0.33	528	1.99	0.10
28	0.97	0.39	283	1.85	0.15	533	1.97	0.10
33	1.31	0.19	288	1.62	0.16	538	1.72	0.12
38	1.31	-0.02	293	1.94	0.49	543	1.87	0.08
43	1.53	0.03	298	1.96	0.36	548	1.89	0.18
48	1.18	0.03	303	1.87	0.44	553	1.67	-0.08
53	1.01	0.30	308	1.93	0.34	558	1.67	-0.16
58	1.21	0.01	313	1.93	0.38	563	1.52	0.06
63	1.53	-0.01	318	1.94	0.22	568	1.80	-0.06
68	1.87	0.01	323	2.12	0.51	573	1.74	-0.34
73	1.65	-0.10	328	1.98	0.47	578	1.66	-0.04
78	1.68	-0.05	333	2.04	0.31	583	1.78	-0.13
83	1.87	-0.06	338	2.10	0.39	588	1.81	0.10
88	1.83	-0.35	343	1.86	0.12	593	1.89	-0.09
93	1.82	-0.19	348	1.93	-0.14	598	1.87	0.02
98	1.93	0.02	353	1.85	0.12	603	1.91	0.12
103	1.65	-0.23	358	1.86	0.20	608	2.02	0.00
108	2.07	-0.10	363	2.01	0.29	613	2.05	0.10
113	1.98	0.30	368	1.97	0.63	618	1.90	0.28
118	1.99	0.04	373	2.13	0.39	623	1.95	-0.03
123	2.27	0.05	378	2.12	0.12	628	2.05	0.23
128	2.27	-0.13	383	2.20	0.44	633	2.31	0.45
133	2.28	0.27	388	2.30	0.03	638	2.06	0.36
138	1.75	-0.00	393	2.41	0.48	643	2.07	0.44
148	1.85	0.42	398	1.93	0.42	648	2.08	0.34
153	1.84	0.20	403	2.05	0.33	653	1.99	0.36
158	2.26	0.37	408	1.89	0.33	658	1.84	0.29
163	2.25	0.36	413	2.11	0.52	663	2.03	0.33
168	2.24	0.42	418	2.00	0.31	668	2.05	0.73
173	2.20	-0.01	423	1.84	0.36	673	2.08	0.39
178	2.19		428	1.85	0.35	678	2.04	0.23
183	2.14	0.23	433	1.87	0.33	683	2.00	0.37
188	1.97	0.17	438	1.82	0.31	688	2.01	0.56
193	1.92	0.23	443	1.80	0.44	693	1.71	0.57
198	1.76	-0.22	448	1.90	0.40	698	1.56	0.52
203	1.83	0.34	453	1.96	0.54	703	1.58	0.58
208	2.06	0.23	458	2.07	0.38	708	1.73	0.67
213	1.97	0.37	463	2.02	0.30	713	1.70	-0.10
218	1.94	0.04	468	2.09	0.48	718	1.65	0.71
223	1.88	0.04	473	2.17	0.43	723	1.55	0.70
228	1.89	0.03	478	2.07	0.44	728	1.64	0.89
233	1.70	0.15	483	1.85	0.25	733	1.54	0.97
238	1.81	0.42	488	1.83	0.22	738	1.47	0.85
243	1.94	0.43	493	2.00	0.29	743	1.29	0.60
248	1.80	0.55	498	1.94	0.02	748	1.62	0.79
253	1.75	0.03	503	2.04	0.24	753	1.52	0.80

Depth (cm)	δ13C (‰)	δ18O (‰)	Depth (cm)	δ13C (‰)	δ18O (‰)	Depth (cm)	δ13C (‰)	δ18O (‰)
758	1.53	0.97	878	1.22	-0.41	998	2.18	0.02
763	1.50	0.13	883	1.11	-0.26	1003	1.91	0.01
768	1.47	0.44	888	1.28	-0.44	1008	2.05	-0.02
773	1.55	0.30	893	1.42	-0.27	1013	2.05	-0.21
778	1.42	0.49	898	1.15	-0.49	1018	2.22	-0.05
783	1.55	0.53	903	1.40	-0.04	1023	1.91	-0.11
788	1.59	0.38	908	1.42	-0.72	1028	1.96	-0.02
793	1.54	0.45	913	1.74	-0.28	1033	1.93	-0.49
798	1.58	0.60	918	1.88	-0.20	1038	1.90	-0.27
803	1.46	0.24	923	1.99	0.05	1043	2.01	-0.15
808	1.54	0.37	928	1.80	-0.35	1048	1.96	-0.48
813	1.40	0.31	933	1.80	-0.43	1053	1.93	-0.32
818	1.44	0.26	938	1.81	-0.16	1058	2.03	-0.04
823	1.55	0.30	943	1.99	-0.19	1063	2.09	0.07
828	1.64	0.39	948	2.00	-0.02	1068	2.13	0.04
833	1.56	0.48	953	2.01	0.11	1073	1.95	0.11
838	1.74	0.56	958	1.66	-0.21	1078	1.99	-0.21
843	1.48	0.56	963	1.56	-0.45	1083	1.97	0.17
848	1.12	0.12	968	2.21	-0.03	1088	2.01	-0.22
853	1.37	0.36	973	2.00	0.00	1093	1.96	-0.39
858	1.28	0.20	978	2.04	-0.15	1098	1.69	-0.10
863	1.17	-0.26	983	1.79	-0.13	1103	1.83	-0.07
868	1.45	-0.05	988	2.07	0.29	1108	1.85	-0.07
873	1.18	0.16	993	2.28	0.02			

Appendix 2.2. Oxygen and carbon isotope data from GeoB 1711, using the planktonic foraminifer, *Globorotalia inflata.*

Depth (cm)	δ13C (‰)	δ18O (‰)	Depth (cm)	δ13C (‰)	δ18O (‰)	Depth (cm)	δ13C (‰)	δ18O (‰)
1	0.67	1.08	81	0.47	1.01	201	0.60	2.44
4	0.72	0.82	86	0.43	1.25	206	0.41	2.22
7	0.65	0.76	91	0.20	1.43	211	0.58	2.41
10	0.88	0.88	96	0.04	1.49	216	0.62	2.45
11	0.63	0.46	101	0.22	1.42	221	0.46	2.27
13	0.58	0.91	106	0.31	1.45	226	0.43	2.57
16	0.78	1.10	111	0.47	1.37	231	0.63	2.52
19	0.59	0.71	116	0.44	1.61	236	0.64	2.47
21	0.60	0.90	121	0.20	1.65	241	0.30	2.38
22	0.77	0.86	131	0.03	1.92	246	0.50	2.66
25	0.70	0.81	141	0.37	1.97	251	0.74	2.83
26	0.45	0.72	146	0.29	2.05	256	0.71	
31	0.55	0.85	151	0.32	2.00	261	0.86	2.70
36	0.84	1.03	156	0.27	2.05	266	0.70	2.67
41	0.28	0.76	161	0.53	2.49	271	0.62	2.59
46	0.46	0.70	166	0.58	2.32	276	0.63	2.52
51	0.50	0.81	171	0.53	2.84	281	0.87	2.69
56	0.69	1.08	176	0.57	2.51	286	0.77	2.40
61	0.49	0.87	181	0.53		291	0.92	
66	0.68	1.01	186	0.52	2.39	296	0.76	2.42
71	0.63	0.91	191	0.66	2.37	301	0.42	2.14
76	0.58	1.15	196	0.67	2.74	306	0.73	2.36

Depth (cm)	δ13C (‰)	δ18O (‰)	Depth (cm)	δ13C (‰)	δ18O (‰)	Depth (cm)	δ13C (‰)	δ18O (‰)
311	0.52	2.29	551	0.73	2.60	841	1.04	1.78
316	0.64	2.40	556	0.79	2.65	846	0.93	1.68
321	0.60	2.16	561	0.83	2.50	851	0.76	1.67
326	0.60	2.10	566	0.79	2.52	856	0.75	1.73
331	0.48	2.10	586	0.55	1.98	861	0.70	1.61
336	0.44	1.97	596	0.56	1.81	866	0.66	1.71
341	-0.02	1.83	606	0.63	1.77	876	0.69	1.63
346	0.29	1.88	611	0.66	1.54	881	0.60	1.59
351	0.28	2.03	616	0.43	1.37	886	0.48	1.73
356	0.65	2.56	621	0.54	1.36	891	0.34	1.64
361	0.49	2.63	631	0.70	1.48	896	0.24	1.67
366	0.67	2.68	636	0.66	1.54	901	0.51	1.76
371	0.50	2.88	646	0.99	1.48	906	0.32	1.60
376	0.64	1.95	651	1.11	1.64	911	0.44	1.44
381	0.59	2.16	656	1.12	1.59	921	0.41	1.34
386	0.74	2.72	661	0.86	1.42	931	0.62	1.29
391	0.82	2.86	666	0.79		941	0.25	0.83
396	0.63	2.50	676	0.91	1.28	946	0.27	0.58
401	0.71	2.27	681	0.89	1.40	951	0.21	0.72
406	0.59	2.47	686	1.02	1.49	956	0.32	0.42
411	0.66	2.42	691	0.65		966	0.11	0.48
416	0.79	2.51	696	0.68	1.44	971	0.11	0.80
421	0.84	2.65	701	0.84	1.41	976	0.14	0.53
426	0.77	2.80	706	0.83	1.49	981	0.24	0.79
431	0.68	2.35	711	0.84	1.50	991	0.04	0.63
436	0.64	2.50	716	0.67	1.30	996	0.10	0.46
441	0.78	2.66	721	0.69	1.42	1001	0.21	1.20
446	0.62	2.36	726	0.75	1.32	1006	-0.05	1.12
451	0.60	2.22	731	0.63	1.48	1011	-0.45	0.98
456	0.64	2.22	736	0.87	1.68	1016	-0.38	1.21
461	0.48	2.32	741	0.69	1.51	1021	-0.57	1.28
466	0.51	2.31	746	0.89	1.66	1026	-0.40	1.11
471	0.54	2.07	751	0.92	1.52	1031	-0.52	1.29
476	0.52	2.14	756	0.93	1.46	1036	-0.42	1.01
481	0.74	2.27	761	0.98	1.70	1041	0.01	1.22
486	0.34	2.15	766	0.99	1.48	1046	-0.23	1.38
491	0.38	2.27	776	1.03	1.60	1051	0.15	2.26
496	0.10	2.24	791	1.01	1.44	1056	-0.05	1.80
501	0.24	2.00	796	1.16	1.36	1061	-0.20	1.92
506	0.15	2.04	801	1.03	1.39	1066	-0.17	1.68
521	0.56	2.63	806	0.85	1.43	1071	0.17	2.30
526	0.83	2.85	811	1.08	1.33			
531	0.68	2.44	816	0.91	1.49			
536	0.67	2.45	826	0.87	1.66			
541	0.84	2.65	831	0.97	1.67			
546	0.67	2.65	836	1.00	1.54			

Appendix 2.3. Oxygen isotope data from GeoB 1711, using the benthic foraminifer, *Cibicidoides wuellerstorfi.*

Depth (cm)	$\delta^{18}O$ (‰)	Depth (cm)	$\delta^{18}O$ (‰)	Depth (cm)	$\delta^{18}O$ (‰)	Depth (cm)	$\delta^{18}O$ (‰)
1	2.49	251	4.25	501	3.70	751	3.57
6	2.50	256	4.16	506	3.66	756	3.22
11	2.24	261	4.08	511	3.84	761	3.47
16	2.48	266	4.02	516	3.89	766	3.40
21	2.48	271	3.86	521	3.98	771	3.33
26	2.46	276	4.11	526	4.11	776	3.23
31	2.30	281	4.08	531	4.21	781	3.24
36	2.35	286	3.91	536	3.95	786	3.25
41	2.39	291	3.87	541	4.06	791	3.07
46	2.44	296	3.72	546	3.83	796	3.17
51	2.48	301	3.91	551	4.11	801	3.26
56	3.40	306	4.05	556	4.18	806	2.95
61	2.64	311	3.80	561	3.99	811	3.23
66	2.77	316	3.93	566	3.97	816	3.20
71	3.05	321	3.84	571	4.11	821	3.10
76	2.80	326	3.86	576	4.13	826	3.21
81	3.26	331	3.76	581	3.98	831	3.13
86	3.56	336	3.60	586	3.91	836	3.11
91	3.39	341	3.70	591	3.56	841	3.07
96	3.54	346	3.41	596	3.58	846	3.09
101	3.43	351	3.63	601	3.60	851	2.98
106	3.53	356	3.80	606	3.80	856	3.30
111	3.65	361	3.82	611	3.41	861	3.10
116	3.45	366	3.76	616	3.46	866	3.27
121	3.27	371	3.86	621	3.24	871	3.25
126	3.55	376	3.93	626	3.18	876	3.33
131	3.96	381	3.94	631	3.37	881	3.28
136	4.10	386	3.78	636	3.41	886	3.35
141	3.76	391	3.81	641	3.42	891	3.41
146	4.22	396	3.59	646	3.49	896	3.55
151	4.31	401	3.88	651	3.32	901	3.61
156	4.18	406	3.77	656	3.27	906	3.54
161	4.30	411	3.71	661	3.05	911	3.36
166	4.57	416	3.52	666	3.20	916	2.67
171	4.39	421	3.67	671	3.32	921	3.29
176	4.27	426	3.91	676	3.06	926	3.02
181	4.08	431	3.85	681	3.16	931	2.66
186	4.49	436	3.90	686	3.09	936	2.53
191	4.50	441	3.87	691	3.04	941	2.40
196	4.56	446	3.93	696	2.69	946	2.59
201	4.51	451	3.62	701	2.89	951	2.88
206	4.26	456	3.69	706	2.86	956	2.31
211	4.41	461	3.80	711	2.99	961	2.33
216	4.48	466	3.62	716	2.70	966	2.36
221	4.45	471	3.83	721	3.04	971	2.38
226	4.28	476	3.77	726	2.99	976	2.33
231	4.55	481	3.64	731	3.39	981	2.30
236	4.27	486	3.67	736	3.66	986	2.26
241	4.21	491	3.62	741	3.55	991	2.34
246	4.31	496	3.56	746	3.66	996	2.20

Depth (cm)	$\delta^{18}O$ (‰)	Depth (cm)	$\delta^{18}O$ (‰)	Depth (cm)	$\delta^{18}O$ (‰)	Depth (cm)	$\delta^{18}O$ (‰)
1001	2.23	1021	3.27	1041	2.85	1061	4.37
1006	2.30	1026	2.91	1046	3.86	1066	4.34
1011	2.79	1031	2.51	1051	4.32	1071	4.27
1016	2.79	1036	2.76	1056	4.35		

Appendix 2.4. Oxygen and carbon isotope data from PG/PC12, using the planktonic foraminifer, *Globorotalia inflata.*

Depth (cm)	$\delta^{18}O$ (‰)	$\delta^{13}C$ (‰)	Depth (cm)	$\delta^{18}O$ (‰)	$\delta^{13}C$ (‰)	Depth (cm)	$\delta^{18}O$ (‰)	$\delta^{13}C$ (‰)
5	0.17	-0.48	182	2.31	0.09	367	2.08	-0.09
10	0.69	-0.51	187	2.34	0.04	372	1.69	-0.67
15	0.52	-0.66	192	2.17	-0.44	377	1.95	-0.34
20	0.61	-0.57	197	2.32	0.04	382	1.93	-0.35
25	0.66	-0.54	202	2.19	-0.23	387	1.95	-0.29
30	-0.88	-0.56	207	2.24	0.08	392	1.87	-0.78
35	0.67	-0.50	212	2.47	0.19	397	2.05	-0.31
45	0.95	-0.63	217	2.24	-0.18	402	1.84	-0.08
50	0.89	-0.39	222	2.40	0.49	407	1.81	-0.58
55	0.49	0.17	227	2.30	0.03	412	1.53	-0.50
60	0.82	-0.59	232	2.07	-0.15	417	1.64	-0.89
65	0.72	-0.54	237	2.14	-0.04	422	1.36	-0.89
70	0.96	-0.37	242	2.00	-0.04	427	1.10	-1.20
75	0.81	-0.49	247	1.84	-0.15	432	1.65	-1.17
113	2.01	-0.45	252	1.87	-0.07	437	1.60	-1.06
124	2.17	-0.10	257	2.12	0.29	442	2.25	-0.33
126	2.19	-0.16	262	2.95	-0.11	447	1.77	-0.76
127	2.32	0.21	267	1.83	-0.41	452	1.99	-0.87
129	2.23	-0.31	272	1.83	-0.37	462	1.32	-0.30
130	2.43	0.08	277	1.97	-0.09	467	1.60	-0.70
131	2.29	0.09	282	1.83	-0.35	472	1.30	-0.67
132	2.13	0.49	287	1.71	-0.38	477	1.60	-0.87
133	2.87	0.49	292	1.79	-0.41	482	1.78	-0.57
134	2.72	0.26	297	1.63	-0.49	492	1.98	-0.66
135	2.57	0.27	302	1.70	-0.25	497	1.92	-0.30
136	2.66	0.38	307	1.92	-0.34	502	1.38	-0.31
137	1.82	-0.04	312	1.44	-0.81	507	1.15	-0.67
139	2.20	-0.04	317	1.69	-0.26	512	1.37	-0.40
140	2.67	0.40	322	1.65	-0.67	517	1.43	-0.56
141	2.68	0.37	327	1.62	-0.82	522	1.56	-0.93
142	2.80	0.45	332	1.62	-0.82	527	1.72	-0.46
147	2.63	0.32	337	1.63	-0.64	532	1.94	-0.33
152	2.81	0.42	342	1.84	-0.51	537	1.59	-0.38
162	2.71	0.11	347	1.75	-0.81	542	1.61	-0.83
167	2.64	0.17	352	1.68	-0.31	547	1.76	-0.51
172	1.56	-0.37	357	2.04	-0.29	552	1.54	-0.95
177	2.63	0.31	362	1.91	-0.46	562	1.81	-0.55

Depth (cm)	$\delta^{18}O$ (‰)	$\delta^{13}C$ (‰)	Depth (cm)	$\delta^{18}O$ (‰)	$\delta^{13}C$ (‰)	Depth (cm)	$\delta^{18}O$ (‰)	$\delta^{13}C$ (‰)
567	1.78	-0.53	597	1.83	-0.55	627	1.84	-0.58
572	1.82	-0.60	602	1.61	-0.19	632	1.78	-0.42
577	1.97	-0.40	607	2.04	-0.23	637	1.67	-0.62
582	1.67	-0.22	612	1.92	-0.49	642	1.91	-0.91
587	1.61	-0.40	617	2.04	-0.28	652	1.27	-0.95
592	0.83	-0.11	622	1.85	-0.73			

Appendix 2.5. Oxygen and carbon isotope data from GeoB 3602, using the planktonic foraminifer, *Globorotalia inflata.*

Depth	$\delta^{18}O$	$\delta^{13}C$	Depth	$\delta^{18}O$	$\delta^{13}C$	Depth	$\delta^{18}O$	$\delta^{13}C$
0.03	0.95	0.97	2.18	1.37	0.89	4.38	1.08	0.53
0.08	0.8	0.93	2.23	1.42	0.93	4.43	1.38	0.17
0.13	1.13	1.21	2.28	1.09	0.7	4.48	1.03	0.08
0.18	1.12	1.22	2.33	1.29	0.7	4.53	1.72	0.59
0.23	1.18	1.17	2.38	1.26	0.59	4.58	1.22	0.55
0.28	0.85	1	2.48	1.08	0.6	4.63	1.05	0.25
0.33	0.89	1.04	2.53	1	0.67	4.68	1.5	0.09
0.38	1.04	0.99	2.58	1.06	0.69	4.73	1.56	0.27
0.43	1.3	0.94	2.68	1	0.3	4.78	1.37	0.21
0.48	1.07	0.92	2.73	0.98	0.21	4.83	1.45	0.43
0.53	1.43	0.78	2.78	0.48	0.49	4.88	1.82	0.34
0.58	1.59	0.62	2.83	0.77	0.75	4.93	1.67	0.19
0.63	1.14	0.68	2.93	0.58	0.58	4.98	1.3	0.26
0.68	1.31	0.7	2.98	0.23	0.29	5.03	1.73	0.34
0.73	1.82	0.64	3.03	0.69	0.66	5.08	1.93	0.17
0.78	1.67	0.49	3.08	0.37	0.44	5.13	1.78	0.63
0.83	1.87	0.49	3.13	0.67	0.41	5.18	1.44	0.93
0.88	1.71	0.31	3.18	1.72	-0.02	5.23	1.17	0.76
0.98	1.58	0.31	3.23	1.21	-0.04	5.28	1.05	0.71
1.03	2.01	0.56	3.28	1.5	0.08	5.33	1.1	0.57
1.08	1.8	0.44	3.33	2.12	0.34	5.38	0.86	0.6
1.13	1.69	0.35	3.38	1.63	0.24	5.43	0.85	0.54
1.18	1.47	0.36	3.43	1.89	0.18	5.48	1.14	0.6
1.23	1.72	0.73	3.48	1.65	0.17	5.53	1.19	0.86
1.28	1.53	0.46	3.53	1.56	-0.23	5.58	0.87	0.62
1.33	1.69	0.42	3.58	1.46	-0.25	5.63	1.19	0.9
1.38	1.68	0.59	3.63	1.28	0.09	5.68	0.87	0.81
1.43	1.29	0.79	3.68	1.75	0.45	5.73	0.72	0.76
1.48	1.31	0.94	3.73	1.6	0.56	5.78	0.88	0.53
1.58	1.47	0.61	3.78	1.58	0.48	5.83	0.94	0.8
1.63	0.8	0.76	3.83	1.01	0.38	5.88	0.89	0.82
1.68	1.11	0.46	3.88	0.77	0.43	5.93	1.03	0.99
1.73	1.29	0.67	3.93	0.93	0.75	5.98	0.98	0.76
1.78	1.28	0.85	3.98	0.95	0.89	6.08	0.82	0.75
1.83	1.42	0.89	4.03	0.85	0.63	6.13	0.67	0.7
1.88	1.23	0.82	4.08	0.98	0.69	6.18	0.84	0.46
1.93	1.32	1.02	4.13	0.81	0.55	6.23	1.39	0.5
1.98	1.23	0.76	4.18	0.75	0.53	6.28	1.65	0.52
2.03	1.1	0.39	4.23	0.91	0.56	6.33	1.73	0.38
2.08	1.51	1.15	4.28	0.71	0.46	6.43	2.03	0.63
2.13	1.1	0.83	4.33	1.14	0.36	6.48	2.13	0.42

Depth	$\delta^{18}O$	$\delta^{13}C$	Depth	$\delta^{18}O$	$\delta^{13}C$	Depth	$\delta^{18}O$	$\delta^{13}C$
6.53	1.9	0.32	7.78	1.02	0.65	8.93	1.2	1.13
6.58	1.71	0	7.83	0.91	0.74	8.98	0.94	0.84
6.63	1.86	0.62	7.88	0.62	0.69	9.03	1.18	1.22
6.68	1.44	0.4	7.93	1.18	0.95	9.13	0.87	1.19
6.73	1.11	0.67	7.98	1.26	0.97	9.18	1.07	1.01
6.83	1	1.25	8.03	1.27	0.82	9.23	1.17	0.97
6.93	0.99	0.87	8.08	1.07	0.89	9.33	1.25	0.93
6.98	1.03	1.22	8.13	0.9	0.48	9.38	1.49	1.04
7.03	0.82	1.01	8.23	1.14	0.67	9.43	1.36	0.88
7.08	0.95	1.12	8.28	1.19	0.29	9.48	1.33	0.98
7.13	0.99	1.27	8.38	1.96	0.17	9.53	1.31	0.78
7.18	0.86	1.04	8.43	2.36	0.71	9.58	1.8	1.07
7.28	0.78	1.15	8.53	2.24	0.6	9.68	2.13	0.87
7.33	0.75	0.95	8.58	2.02	0.65	9.73	2.08	0.87
7.38	0.75	1.02	8.63	1.19	1.22	9.78	1.66	0.4
7.48	1.88	0.57	8.68	0.88	1.19	9.88	1.39	0.97
7.53	1.36	0.81	8.73	1.03	1.26			
7.58	0.82	1.02	8.78	0.9	1.11			
7.63	0.57	0.83	8.83	1	1.02			
7.68	0.97	1.01	8.88	1.41	0.8			

Core records of planktonic foraminifera

A.3.

Appendix 3. High resolution planktonic foraminifera records

Appendix 3.1. Numbers of planktonic foraminifera from GeoB 1706. Abbreviations are as follows: Fraction (1/) = fraction of sample counted to gain between 200 and 300 specimens (where possible); Depth (cm) = Depth of core sample; pachy (s) = *N. pachyderma* (s); bull. = *Gg. bulloides*; pachy (d) = *N. pachyderma* (d); inf. = *Gr. inflata*; quin. = *Gg. quinqueloba;* glut. = *Ga. glutinata;* crass. = *Gr. crassaformis*; univ. = *O. universa;* scit. = *Gr. scitula;* Other = All species unidentified and with an average below 0.5% (see Table 3.1); Total = Total planktonic foraminifera specimens counted; Benthics = Total number of benthic foraminifera counted.

Fraction (1/)	Depth (cm)	pachy. (s)	bull.	pachy. (d)	inf.	quin.	glut.	crass.	univ.	scit.	Other	Total	Benthics
32	3	11	69	83	15	1	6	28	19	2	17	251	24
32	8	16	78	64	26	1	3	30	19	1	14	254	23
64	13	9	127	74	28	1	5	24	24	1	14	307	23
64	18	9	92	81	22	3	4	23	16		16	267	12
64	23	31	152	146	46	3	5	34	7	1	21	449	16
128	28	13	178	122	56	1	8	27	12	4	24	445	26
128	33	14	175	137	37	3	4	20	11	2	19	423	9
128	38	27	144	190	23	6	7	10	4		26	442	17
512	43	26	109	139	14	3	14	6	2		15	335	9
256	48	23	80	105	19	1	7	10		2	8	259	9
512	53	15	73	92	18	1	1	4	2	1	9	216	13
1024	58	21	113	130	27	1	3	4	4	3	17	323	10
1024	63	30	71	79	15	4	5	3	4	1	9	223	4
512	68	33	97	106	21	1	6	5	2	1	13	291	12
512	73	39	124	119	14	6	7	8			19	341	6
256	78	33	111	95	15	2	3	4			8	271	7
512	83	53	113	55	9	3	3	4	2	1	9	252	11
256	88	125	132	89	17	5	4	3	6	2	13	399	11
512	93	103	101	101	9	5	6	1	3		2	331	16
256	98	144	88	45	2	14	3	5	2		7	312	4
512	103	121	41	37	1	18	17	2		1	27	275	9
512	108	131	51	57	10	9	6		4		8	281	8
512	113	89	21	40	3	3	9	1	2	1	6	178	11
256	118	177	20	35	6	7	20	1	1		12	280	9
512	123	123	37	21	9	16	18	3	3		5	239	16
512	128	106	14	38	3	6	5		1		4	181	18
512	133	158	23	33	1	8	9	1	2		1	236	27
512	138	130	13	33	3	5	8	2	1		6	203	20
512	148	172	48	105	6	14	14	2	2		6	372	8
512	153	96	34	109	6	11	15		2		10	287	14
512	158	95	47	103	7	13	13	2	1		14	302	3
512	163	145	61	113	12	25	12	2			5	378	8
512	168	76	27	76	10	10	9	1	2		2	217	6
512	173	106	29	57	2	6	19	2	4		4	232	16
512	178	78	18	64	3	12	19		1		5	202	13
512	183	64	31	81	17	11	10		3		4	223	18
512	188	120	37	56	6	8	6		5	2	1	242	18
256	193	144	41	67	11	13	18		1		4	305	22
256	198	80	22	29	5	7	7		8		1	162	11
128	203	102	30	37	11	6	5		20		4	215	36
128	208	153	52	79	20	10	21	4	16		9	366	53
128	213	119	58	38	14	9	10		9	1	6	264	64
128	218	150	88	85	47	15	14	7	10	2	8	429	55
256	223	154	90	97	24		11		8	4	12	403	53
256	228	93	32	36	34	4	21	3	2	2	12	242	7
128	233	206	77	63	16	11	3	6			4	386	50
128	238	222	50	50	8	10	3	2	1		5	356	37

Fraction (1/)	Depth (cm)	pachy. (s)	bull.	pachy. (d)	inf.	quin.	glut.	crass.	univ.	scit.	Other	Total	Benthics
128	243	217	57	24	13	15	3	1	6		4	341	58
256	248	118	33	21	13	4	11		2	1	4	208	6
64	253	202	54	42	18	6	7	2	2	1	5	341	164
256	258	197	47	19	18	5	8	3	2		1	301	81
256	263	114	39	43	14	2	6		4		2	225	34
512	268	162	26	25	6	12	16	3	1	3	18	276	33
256	273	274	56	47	11	13	3		2		2	409	53
128	278	104	23	30	10	3	6	2			2	181	131
64	283	53	59	38	9	2	2	4	1	1	2	171	103
32	288	68	40	28	22	4	12	4	2		4	186	92
32	293	119	16	16	3	6	1	6			4	171	188
32	298	117	26	19	26	7	4	2	4		2	207	229
16	303	81	5	21	5		3	1			2	119	331
32	308	61	9	30	12	1	11	3			3	133	141
16	313	130	10	11	8							159	361
32	318	94	26	19	11	6	4				4	164	200
32	323	93	39	27	20	4	8	6	4			201	243
8	328	62	29	33	32		32	7	6		2	207	201
64	333	72	42	29	19	3	16	4	2	2	3	192	128
128	338	65	61	32	15	1	14	4	3	7	3	210	75
64	343	142	111	98	70	6	22	13	1	8	12	486	122
128	348	65	52	48	32	2	29		1	7	11	250	41
128	353	91	71	51	32	1	4	4	3	4	1	263	85
128	358	90	87	49	46	3	11	5	1	4	6	302	118
64	363	101	82	48	46	2	17	1	2	5	7	316	101
32	368	76	42	24	60	8	8	2	4		10	238	251
32	373	66	68	53	39	8	17				10	261	654
64	378	46	26	16	13	3	9				1	114	457
64	383	35	25	14	5	3	11		1		5	99	455
64	388	46	38	35	23	2	15	2		3	4	170	578
32	393	28	21	12	3	3	7			1	3	78	884
32	398	37	12	15	11							75	632
32	403	26	22	10	3	1	5				2	69	517
32	408	85	37	57	9	4	13		1		5	213	187
32	413	48	25	8	3	1	8		2	2	3	100	407
16	418	60	35	18	10		27				5	157	560
32	423	34	16	13	6	2	5				2	78	417
32	428	67	38	37	27	5	7	2	1	2	8	194	271
32	433	76	22	11	11	3	5	11	2			141	662
32	438	83	49	49	15	1	6		1		5	209	730
32	443	79	17	5	3		6		1		2	113	931
32	448	70	20	8	5		12	1			8	126	429
64	453	78	18	8	5	3	5		4			121	676
32	458	159	26	12	3	4	13		2		7	226	1051
64	463	53	10	2		4	5				2	76	428
128	468	66	6	1	1		3	1	1		4	83	514
64	473	111	17	4	1	1	8		6		3	152	553
64	478	118	26	17	9	3	11	1	3	1	2	193	689
64	483	182	44	19	20	1	11		6		4	289	302
256	488	199	29	28	11	2	18	7	3		7	306	203
256	493	160	45	41	22	6	7	1	3	2	6	294	181
256	498	222	43	50	17	7	9	1	5	1	3	364	124
128	503	159	32	50	10	3	10			1	1	268	125
128	508	113	14	35	14	2	7	4	3	2	9	206	77
256	513	96	20	43	14	4	11	1	3	1	3	196	143
128	518	71	50	87	15	5	4		4	3	4	247	210
128	523	70	27	28	17	4	6		1			153	270
128	528	38	27	33	19	1	4	2		3	4	131	96
64	533	13	54	112	23	1	8	1	1	1	2	216	269

Fraction (l/)	Depth (cm)	pachy. (s)	bull.	pachy. (d)	inf.	quin.	glut.	crass.	univ.	scit.	Other	Total	Benthics
256	538	40	92	93	34	1	7	1	5	1	6	284	177
32	543	15	140	201	49		5		4	3	4	423	257
128	548	6	97	98	45	1				2	4	257	90
32	553	19	113	165	54	1	6		2	1	2	367	225
256	558	9	116	165	51		5		1	3	5	356	132
256	563	13	142	66	47		1	1	1	10	1	283	22
256	568	8	116	60	48					3	9	246	23
256	573	14	182	81	62	1	5	1	2	31	10	393	24
128	578	13	165	80	59	3	2			32	9	366	32
256	583	10	135	71	62	2	2		2	15	3	305	23
256	588	6	98	70	39	2	1	1		3	2	227	16
256	593	15	94	87	39		2	1		14	1	255	28
512	598	6	73	46	20	3	1		1	17	2	169	31
256	603	14	77	142	25	3	2		1	8	3	275	38
256	608	27	99	128	17	1	3		2	3	5	285	31
512	613	17	79	95	19	5				5	2	222	48
512	618	24	93	97	20	1	3		1	6	4	249	39
128	623	37	85	109	17	6				6	1	261	17
128	628	21	53	89	16	3					1	183	50
512	633	23	49	102	9	3	3		2	3	1	195	8
64	638	45	75	103	26	4	4			2		259	79
32	643	35	65	54	21	1			1	1		178	96
64	648	30	22	31	18	1					2	104	241
128	653	20	44	64	12		1		1	3		145	204
128	658	12	21	36	6		1				3	79	285
64	663	7	12	19	9		2					49	416
32	668	20	27	33	35	2	5	6			1	129	771
64	673	16	27	78	30	2						153	534
64	678	22	29	15	22		2		1		1	92	409
64	683	14	52	67	35	3	1		1		4	178	511
64	688	10	22	44	28	1		10			1	117	477
64	693	3	31	25	53		1				3	116	402
64	698	4	43	53	78		2	2	2		2	186	317
64	703	4	19	13	27	1						64	288
64	708	14	26	45	41	7	6	2			6	147	344
64	713	1	10	14	31				1		1	58	379
32	718	3	32	27	56	1	1	3		2	1	126	244
32	723	12	57	55	69	4	2	1	1	1	5	210	85
32	728	8	23	58	81		1	7	2		4	184	86
64	733	10	56	73	105		2		3		2	254	28
128	738	4	34	18	83		1	3			1	144	21
64	743	3	53	90	79	1	4	2	2		3	238	39
64	748	5	80	99	90	1	5	7	8		4	300	17
64	753	5	71	67	101	1	3	2			3	255	29
64	758	2	24	55	79		2				1	163	20
128	763	1	154	73	81	5	2	2		3	1	323	8
64	768		154	128	79	2	2	4	3	1	14	387	23
128	773	2	183	111	111	4	8	1	1	7	12	443	23
64	778	15	176	120	116	5	3			1	12	449	22
128	783	4	56	61	34	1					5	161	48
32	788	2	88	74	55	1		4	2	1	3	230	84
32	793	6	91	63	40				3		4	208	73
16	798	4	60	59	57		3			2	3	188	198
16	803	15	107	72	67	1		2	1		9	274	262
32	808	2	73	43	52		1	2	2		2	177	64
32	813	3	104	60	73	3	1		2	1	5	255	96
32	818	4	55	50	24	3	1	1			10	148	97
32	823	3	59	49	24	1	2		3		4	145	84

Fraction (1/)	Depth (cm)	pachy. (s)	bull.	pachy. (d)	inf.	quin.	glut.	crass.	univ.	scit.	Other	Total	Benthics
32	828	2	61	57	40		1	4	3		7	175	168
32	833	12	58	59	41	3	2	3	1		4	183	112
64	838	9	101	82	57	1		3	5		6	265	54
64	843	11	124	115	84		7	1	1		4	347	66
64	848	4	68	74	32			2	3	1	3	187	23
32	853	8	74	89	43	1	1	1	4		13	234	54
32	858	19	99	66	43		2	2	1		6	240	102
128	863	16	105	85	21	2	5		2	1	7	249	47
256	868	13	100	78	16		4	2	2		6	222	16
128	873	12	76	68	32	1	1		1		4	195	22
128	878	16	146	137	57	2	6			3	20	387	26
64	883	13	67	110	25	3	3	1	1	4	18	249	30
256	888	9	45	85	25	4		4	6		23	206	10
128	893	21	128	226	81	3	10	7	1	3	28	515	32
256	898	13	82	127	40	1	2			2	24	293	25
64	908	11	88	62	52	3			7		28	255	33
128	913	24	64	171	29	1	4	1		3	14	311	65
256	918	23	32	98	10	2	3	1			14	169	86
923	923	34	57	146	22	1	1	3	1	3	9	268	77
256	928	27	47	146	12	1			4		9	237	96
128	933	27	55	159	21		3	2	1		8	268	158
64	938	66	57	193	19	3	7	1			2	346	142
256	943	71	43	152	15	2	1	1		1	5	286	136
256	948	14	90	112	20	7	8	2	1	2	6	256	105
128	953	30	80	149	16	4	1	2		4	6	286	158
256	958	19	51	125	28	3		1	1	4	9	232	206
256	963	20	45	86	19	2					5	172	102
64	968	18	83	123	30	4	5			1	5	264	123
256	973	17	61	111	10	2	3					204	111
128	978	37	117	174	27	18	3	2	2	2	4	382	172
128	983	16	155	157	27	17	3		3	2	9	380	155
256	988	38	113	111	31	10	6	5		1	10	315	87
128	993	26	100	113	19	14	7		1		1	280	108
256	998	23	96	151	21	11	8		3	3	4	316	132
128	1003	12	88	149	24	15	7	1	1	1	1	298	116
128	1008	38	113	111	31	10	6	5		1	10	315	54
256	1013	26	104	146	31	13	4			2	5	326	84
256	1018	20	64	124	20	14	2		2	1	2	247	145
256	1023	30	68	100	7	7	1			2	1	215	144
128	1028	23	32	88	17	3	3					166	179
256	1033	34	63	92	27	4	4			1	6	225	187
256	1038	11	45	86	19	5	2		1			169	287
256	1043	22	52	67	25	4	3		2		3	175	298
256	1048	39	96	102	30	4	4		1	3	6	279	628
256	1053	28	49	39	10	6	3			2	1	137	390
256	1058	35	58	35	20	6	4			3		161	316
256	1063	85	61	53	24	6	6			4	2	239	517
256	1068	98	36	37	5	6	1				1	183	456
256	1073	120	20	20	3	2	3		1		1	169	501
256	1078	141	26	30	4	1	1				1	203	533
256	1083	115	20	20	6		1					162	592
128	1088	87	71	39	17		3	2			3	219	386
256	1093	60	42	40	16	3	1		1	2	3	165	466
256	1098	90	14	13	8	5	3					133	467
256	1103	82	27	22	1	3			2		1	137	326
128	1108	19	62	61	27		1	2	10		3	182	293
256	1113	13	50	43	26	1			5	1	1	139	227

Appendix 3.2. Numbers of planktonic foraminifera from GeoB 1711. Abbreviations are as follows: Fraction (1/) = fraction of sample counted to gain between 200 and 300 specimens (where possible); Depth (cm) = Depth of core sample; pachy (s) = *N. pachyderma* (s); pachy (d) = *N. pachyderma* (d); bull. = *Gg. bulloides*; dut. = *N. dutertrei;* inf. = *Gr. inflata*; glut. = *Ga. glutinata;* quin. = *Gg. quinqueloba;* Other = All species unidentified and with an average below 0.5% (see Table 3.1); Total = Total planktonic foraminifera specimens counted; Benthics = Total number of benthic foraminifera counted.

Depth (cm)	Fraction (1)	pachy. (s)	pachy. (d)	bull.	dut.	inf.	glut.	quin.	Other	Total	Benthics
*1	512	6	229	19	10	2		2	11	268	
*4	412	6	201	17	16	6	5	3	7	254	2
*7	512	3	151	22	14	5	1	10	13	206	2
*10	512	3	229	24	37	4		3	9	300	
11	512	10	275	52	45	34	3	1	6	420	7
*13	512	3	247	41	34	8	4	3	15	340	1
16	512	8	291	32	52	9	3	2	15	397	6
*19	512	3	241	36	41	7	2	3	10	333	1
21	512	4	220	28	31	8	2	1	10	294	4
*22	512	4	231	38	44	7	3	2	20	329	
*25	512		161	31	19	9	1	2	12	223	2
26	1024	6	189	34	29	5		1	10	264	3
31	512	13	220	39	45	8	1	4	8	330	
36	512	4	209	63	52	20	6	3	14	357	1
41	1024	5	150	46	32	5	1	1	1	240	3
46	1024	7	204	39	29	15		2	8	296	2
51	1024	3	225	71	51	12	1	3	3	366	2
56	512	11	277	118	83	21	5	6	14	521	3
61	1024	1	150	59	32	25	5	1	13	273	1
66	1024	6	216	104	37	15	3	7	25	388	1
71	1024	2	135	97	29	12	2	2	9	279	4
76	1024	6	112	86	41	21	1	3	13	270	2
81	512	0	143	114	61	38	6	3	18	365	1
86	1024	11	128	66	33	20		4	11	262	1
91	1024	1	167	67	41	40	7	3	25	326	3
96	1024	24	146	71	31	31	4	6	7	313	1
101	512	25	67	68	29	37	7	10	13	243	8
106	512	53	44	92	34	25	4	7	9	259	8
111	1024	32	42	68	21	24	3	6	6	196	3
116	1024	31	71	127	25	19	3	6	8	282	2
121	512	38	45	149	32	35	2	14	18	315	10
126	1024	16	32	95	23	27	2	9	9	204	4
131	512	9	35	96	23	29	3	5	8	200	5
136	256	17	34	115	28	23	5	8	6	230	11
141	256	11	19	45	14	10	2	2	7	103	19
146	256	76	32	139	34	25	2	8	3	316	57
151	512	143	78	163	54	19		16	11	473	66
156	512	54	25	36	14	4	1	5	12	139	32
161	256	197	55	46	28	8	4	15	17	353	61
166	256	290	44	52	27	6	4	14	3	437	47
171	256	266	30	30	17	3	1	18	6	365	57
176	256	117	32	21	8	4		27	5	209	31
181	256	204	33	23	12	2	1	12	1	287	47
186	128	157	30	36	17	2	1	11	1	254	39
191	128	183	40	24	14	2	1	11	2	275	45
196	256	226	48	18	37	7	4	23	4	363	29
201	128	203	28	31	35	14	3	30	4	344	48
206	128	223	64	32	26	9	1	18	7	373	42
211	128	180	55	27	19	2	3	2	3	288	42
216	128	282	66	32	11	4	8	13	15	416	50

Depth (cm)	Fraction (1)	pachy. (s)	pachy. (d)	bull.	dut.	inf.	glut.	quin.	Other	Total	Benthics
221	128	241	82	22	13	2	5	11	6	376	37
226	256	71	30	26	8		1		1	136	23
231	128	198	56	22	14	1	3	23	5	317	
236	128	130	48	30	11	3	3	13	4	238	33
241	128	124	53	34	16	8	3	15	3	253	38
246	128	125	51	23	5	1		11	6	216	46
251	128	140	36	12	4	1		1	5	194	26
256	128	175	61	27	29	2	5	10	6	309	29
261	64	146	51	37	11	4	2	8	2	259	74
266	128	200	85	53	38	9	5	26	11	416	37
271	128	104	50	73	37	6	6	13	6	289	35
276	128	322	60	50	27		2	13	7	474	13
281	128	317	30	39	22	2	1	6	1	417	34
286	128	287	36	26	11		2	5	4	367	35
291	128	163	33	25	7		2	5	2	235	20
296	64	73	35	50	7	2	1		3	168	38
301	32	107	49	43	11	4	2	14	10	230	45
306	128	168	23	10	2	3		5	3	211	20
311	128	215	26	31	8	3	3	11	2	297	40
316	128	245	48	21	3	2	2	15	2	336	22
321	128	171	35	21	5	1	5	14	3	252	16
326	128	261	20	13	2	3	2	7	2	308	17
331	256	148	62	12	14		7	15	8	258	14
336	256	41	75	58	51	4	7	10	8	246	9
341	512	22	99	68	45	11	4	27	8	276	12
346	256	101	68	38	17	9	4	17	9	254	22
351	128	101	30	30	7	1	3	10	2	182	16
356	128	237	74	24	14	2	3	22	5	376	26
361	128	149	37	28	8	5	4	13	5	244	23
366	128	197	50	24	14		1	18	1	304	24
371	128	231	43	13	4	1	1	6	3	299	32
376	256	145	26	6	3	2	1	5	2	188	13
381	256	178	27	18	10	2	2	2	5	239	33
386	128	187	31	8	8	1		5	1	240	49
391	128	164	52	15	9	3		8	5	251	51
396	128	81	64	42	15	3	2	11	8	218	40
401	128	89	81	46	9	2	5	4	9	236	21
406	128	119	76	30	8	6	2	7	5	248	42
411	64	68	45	27	3	3	2	3	3	151	41
416	128	65	50	19	10	4	2	14	2	164	63
421	32	110	125	56	8	10	6	4	4	319	159
426	32	52	51	31	5	5		1	1	145	192
431	128	52	37	24	2	2	1	5	4	123	134
436	64	96	50	11	12	2	2	10	3	183	156
441	64	77	34	28	7	4			4	150	98
446	64	90	42	29	28		3	4	9	196	101
451	128	104	40	35	18	2		8	3	207	61
456	64	107	32	35	15		1	17	8	207	82
461	64	109	50	34	12	3	1	12	19	221	110
466	64	172	41	26	12	3	3	23	5	280	170
471	64	84	45	14	6	3		9	5	161	189
476	64	85	75	14	9	4	3	9	1	199	171
481	64	49	108	25	9	4		2	1	197	150
486	64	53	126	39	1	6	5	4	9	234	147
491	64	96	132	110	4	6	2	5	7	355	83
496	64	71	135	78	11	15	3	11	10	324	56
501	256	57	115	102	6	11	1	20	4	312	50
506	256	48	57	45	3	6	3	16	0	178	27

Depth (cm)	Fraction (1)	pachy. (s)	pachy. (d)	bull.	dut.	inf.	glut.	quin.	Other	Total	Benthics
511	128	42	99	55	13	11		6	2	226	51
516	128	54	90	81	20	6		4	5	255	65
521	64	91	119	75	21	4		12	5	322	61
526	64	32	66	59	3	3	2	4	1	169	77
531	16	15	73	73	9	11		1	0	182	372
536	16	13	43	54	9	3	4		3	126	382
541	32	19	45	41	2	6	1	3	1	117	360
546	32	30	77	56	12	6	1	5	1	187	264
551	32	19	40	46	14	6	6	5	5	136	209
556	32	51	100	37	9	8	2	11	5	218	274
561	32	67	72	29	3	2		9	4	182	249
566	32	79	73	38	9	7	1	13	2	220	161
571	32	68	82	47	8	3	1	9	3	218	160
576	32	66	151	57	18	4	1	8	10	305	179
581	32	125	212	67	34	5	1	28	4	472	108
586	32	116	245	89	60	3	8	39	7	560	63
591	64	26	133	40	5	2		5	5	211	32
596	128	24	130	36	9		6	9	5	214	7
601	128	26	117	44	2		1	9	2	199	8
606	64	57	149	57	8	4	1	40	4	316	12
611	256	70	158	69	16	7	6	26	4	352	7
616	128	63	245	150	42	17	4	28	13	549	8
621	256	33	159	65	6	4	4	12	8	283	4
626	256	48	148	76	16	10	3	30	7	331	3
631	512	19	102	44	26	8	5	8	2	212	1
636	256	19	106	47	30	8	7	15	3	232	1
646	256	22	83	14	9	6	1	20	5	155	5
651	256	46	172	34	29	5	5	32	4	323	15
656	256	27	96	41	17	6	3	32	4	222	1
661	512	31	67	28	4	15	4	21	2	170	13
666	256	25	78	62	24	38	3	12	10	242	4
676	256	47	113	76	11	61	5	25	7	338	11
681	256	7	41	44	6	47	6	12	3	163	5
686	256	6	66	41	7	63		4	2	187	7
691	128	9	127	110	45	110	13	5	5	419	40
696	256	2	66	84	54	78	5	2	4	291	9
701	256	7	72	69	29	63	3	6	0	249	8
706	512	5	58	84	23	57	1	6	4	234	4
711	256	9	57	93	46	73	2	31	12	311	
716	256	13	41	92	29	64	4		17	243	18
721	512	7	37	108	19	35	4	18	13	228	8
726	512	4	42	71	13	36	6	28	3	200	4
731	256	14	49	105	33	35	3	18	10	257	9
736	512	15	19	56	21	18	2	9	4	140	2
741	256	19	28	106	16	37	1	17	2	224	17
746	256	6	27	65	12	30	1	6	2	147	39
751	128	5	13	45	5	43	1	2	3	114	35
756	128	24	40	62	14	32	6	8	2	186	33
761	32	34	54	72	26	37	16	11	10	250	60
766	64	25	42	45	25	15	4	6	1	162	40
771	64	51	58	63	65	14	7	9	16	267	38
776	64	36	29	43	42	20	9	7	11	186	21
786	64	77	35	65	35	18	5		9	235	37
791	64	88	27	75	26	13	2	19	2	250	13
796	128	120	28	92	45	15	7	22	7	329	18
801	256	93	28	53	48	6	4	10	4	242	8
806	128	69	42	93	53	12	5	9	7	283	18
811	128	52	66	58	44	18	6	10	3	254	19

Depth (cm)	Fraction (l)	pachy. (s)	pachy. (d)	bull.	dut.	inf.	glut.	quin.	Other	Total	Benthics
816	128	40	85	48	29	10	6	3	4	221	12
821	128	47	159	82	58	9	8	18	7	381	19
826	256	21	127	40	29	3	3	16	4	239	6
831	256	20	212	79	71	7	4	16	13	409	8
836	256	36	122	38	30	7	3	19	5	255	9
841	256	53	129	58	59	5	5	15	3	324	7
846	512	30	73	38	16	2		10	9	169	10
851	512	46	72	79	17	25		19	7	258	3
856	512	15	51	83	12	22	4	8	8	195	2
861	512	15	19	63	22	16	3	8	13	146	18
866	256	31	53	81	8	13		5	7	191	10
871	128	21	73	94	14	21		11	8	234	22
876	128	17	67	82	9	11	3	3	6	192	12
881	128	47	70	66	25	15	6	6	6	235	15
886	256	29	36	54	19	7		6	2	151	10
891	256	49	87	57	22	6	4	6	10	231	22
896	128	79	72	53	11	3		2	4	220	35
901	128	99	42	16	4	1	2		5	164	56
906	128	161	75	63	19	6	1		5	325	20
911	128	64	164	76	27	4	4	6	4	345	21
916	256	29	134	137	33	3	2	6	7	344	7
921	256	31	163	88	15	5	1	6	10	309	16
926	256	11	120	52	23	6		3	4	215	6
931	256	17	72	50	32	14	4	2	7	191	10
936	256	16	98	68	21	15	1	5	5	224	4
941	256	14	61	88	29	32	1	6	9	231	4
946	256	23	59	84	42	35		10	17	253	8
951	256	12	70	81	19	26	3		7	211	15
956	128	18	60	38	15	35		5	7	171	10
966	512	17	58	72	40	46		1	7	234	6
971	1024	42	45	64	35	38	2	4	4	230	5
976	512	71	61	110	63	37		7	7	349	15
981	1024	31	12	56	42	28		1	5	170	1
986	512	50	28	61	52	7		8	2	206	3
991	1024	49	18	70	66	20		7	4	230	4
996	1024	74	34	48	45	6	1	4	4	212	3
1001	512	73	67	120	51	13		4	13	328	
1006	512	83	77	87	49	18	1	2	13	317	5
1011	1024	27	66	49	29	11	3	4	11	189	2
1016	512	46	82	108	54	6	3	5	12	304	6
1021	1024	8	68	56	23	19		1	13	175	1
1026	512	6	89	77	45	35	4	14	22	270	1
1031	512	8	95	63	45	31	5	7	10	254	2
1036	512	15	88	46	29	22	5		15	205	1
1041	512	21	72	51	28	8	2	5	6	187	
1046	512	13	80	29	26	8	1	3	9	160	4
1051	256	27	91	25	20	9	1	5	5	178	19
1056	256	31	95	29	21	9	2	5	4	192	28
1061	256	36	104	48	24	12	1	4	1	229	47
1066	128	40	119	53	32	15	1		4	260	79
1070	128	75	52	34	21	5	1	8	5	196	45

Appendix 3.3. Numbers of planktonic foraminifera from PG/PC12. Abbreviations are as follows: Fraction (1/) = fraction of sample counted to gain between 200 and 300 specimens (where possible); Depth (cm) = Composite depth of core sample (PC12 and PG12 combined); pachy (s) = *N. pachyderma* (s); bull. = *Gg. bulloides*; pachy (d) = *N. pachyderma* (d); inf. = *Gr. inflata*; quin. = *Gg. quinqueloba*; glut. = *Ga. glutinata*; univ. = *O. universa;* dut. = *N. dutertrei;* Other = All species unidentified and with an average below 0.5% (see Table 3.1); Total = Total planktonic foraminifera specimens counted; Benthics = Total number of benthic foraminifera counted.

Depth (cm)	Fraction (1/)	Level	pachy. (s)	bull.	pachy (d)	inf.	quin.	glut.	univ.	dut.	Other	Total	Benthics
3	128	0-5.5	10	44	116	15	2	4	10	7	11	219	8
13	128	11.5-14.5	7	38	110	15	7		7	3	7	194	11
24	128	22.5-25.5	14	37	71	18	2	6	6	1	6	161	14
35	256	33.5-36.5	10	33	144	30	2	1	6		0	226	8
46	256	44.5-48	13	67	146	30		4	2	1	2	265	4
57	512	55.5-59	17	77	175	43	1	1	1	4	12	331	3
68	256	66.5-70	15	134	159	49	49	8	2	8	10	434	4
79	256	77.5-81	17	105	158	54	1	2	4	5	14	360	6
113	32	0-3	88	109	152	33	4	12	2	3	2	405	36
123	32	10.5-12.5	86	26	34	4	3	2		1	0	156	49
133	8	20-22	97	56	130	21	3	2	4	2	4	319	73
143	16	30-32	63	54	89	8		4		6	2	226	86
153	16	40-42	182	24	59	2	6	2			3	278	98
163	8	50-52	297	46	53	2	2	1		2	0	403	324
173	32	60-62	270	28	34	6	14	3	1	2	2	360	178
183	64	70-72	35	125	231	15	36	2	1	6	10	461	60
193	32	80-82	28	58	125	13	14		2	2	5	247	38
203	32	90-92	65	57	130	5	18	2	2		0	279	23
213	16	100-102	65	57	130	5	18	2	2		0	279	23
223	32	110-112	246	40	71	4	9	1		3	5	379	133
233	32	120-122	202	57	113	6	25	4		15	0	422	43
243	128	130-132	119	87	124	4	17	7	3	18	3	382	36
253	128	140-142	230	36	67	3	9	2		11	1	359	18
263	64	150-152	294	30	28	1	7			7	4	371	103
273	64	160-162	136	44	58	3	19	2	1	4	2	269	25
283	128	170-172	203	37	72	2	12			4	3	333	18
293	128	180-182	223	85	70	3	16	1	3	8	4	413	6
303	32	190-192	258	70	91	15	25	1	27	6	4	497	15
313	128	200-202	87	64	125	30	16	4	17	3	5	351	7
323	128	210-212	69	69	99	15	13	1	3	4	6	279	8
333	64	220-222	228	33	38	4	6	2		1	2	314	20
343	128	230-232	150	15	17	2	5				2	191	18
353	64	240-242	145	15	19	2	5				1	187	148
363	32	250-252	193	2	34	1	7	2			1	240	191
373	64	260-262	117	17	25	2		1			0	162	243
383	64	270-272	231	56	40		8			3	0	338	65
393	32	280-282	115	11	14	1	4	1	2	4	1	153	61
403	64	290-292	57	45	79	1	4	1	1	1	4	193	34
413	64	300-302	61	42	46	2	1		2	3	1	158	22
423	16	310-312	60	82	73	15	3		4		0	237	118
433	16	320-322	22	59	56	5	4		1	1	1	149	130
443	4	330-332	26	56	41	5	5	4		3	3	143	597
453	16	340-342	60	41	43	12	5	2		4	1	168	429
463	16	349-352	61	34	24	3			1	3	5	131	247
473	16	360-362	108	25	52	8	2	5	1	3	3	207	340
483	32	369-372	121	37	23	1	2	3	2	7	5	201	314
493	64	389-392	141	44	28	6	10	1	1	15	3	249	175
503	64	400-402	69	60	60	11	19	1		16	3	239	328
513	32	409-412	11	24	32	7		4	2	1	3	84	531
523	128	420-422	20	168	143	24	3	3	2	6	9	378	43

Depth (cm)	Fraction (l/)	Level	pachy. (s)	bull.	pachy (d)	inf.	quin.	glut.	univ.	dut.	Other	Total	Benthics
533	128	430-432	15	116	95	39	2		1	5	5	278	29
543	256	440-442	7	122	128	17	4	1		12	3	294	1
553	128	450-452	20	168	176	10	8	2	1	19	5	409	17
563	32	460-462	11	122	75	25	7	2		8	5	255	21
573	64	470-472	6	87	39	12	2	1		7	3	157	68
583	16	480-482	25	100	59	13	2	3			6	208	41
593	32	490-492	16	105	50	3	8	2		1	3	188	28
603	32	500-502	14	111	91	12	15	4	2	13	7	269	16
613	16	510-512	37	107	151	12	16	2	2	12	5	344	33
623	8	520-522	39	139	80	17	32	4	6	11	2	330	39
633	16	530-532	41	96	95	22	13		2	2	1	272	27
643	32	540-542	32	64	62	14	10	2			6	190	25

Appendix 3.4. Numbers of planktonic foraminifera from GeoB 3602. Abbreviations are as follows: Fraction (1/) = fraction of sample counted to gain between 200 and 300 specimens (where possible); Depth (cm) = Composite depth of core sample (PC12 and PG12 combined); inf. = *Gr. inflata*; pachy (d) = *N. pachyderma* (d); bull. = *Gg. bulloides*; dut. = *N. dutertrei*; sacc. = Gs. sacculifer; ruber = *Gg. ruber*; trunc. = *Gr. truncatulinoides*; men. = *Gr. menardii*; univ. = *O. universa*; pachy (s) = *N. pachyderma* (s); siph. = *Ge. siphonifera*; glut. = *Ga. glutinata*; quin. = *Gg. quinqueloba*; scit. = *Gr. scitula*; Other = All species unidentified and with an average below 0.5% (see Table 3.1); Ben. = Total number of benthic foraminifera counted. Spin. = tropical, spinose foraminifera; Trops = Sub-tropical foraminifera; Total = Total planktonic foraminifera specimens counted.

Fraction (1/)	Depth (cm)	Inf.	pachy (d)	bull.	dut.	sacc.	ruber	trunc.	men.	univ.	pachy (s)	siph	glut.	quin.	scit.	Other	Ben.	Spin	Trops	Total
8	3	198	70	36	28	13	36	20	2	2	5	3	4		2	1	11	52	113	425
8	8	213	76	45	22	14	26	26	2	7	6	2	4	1	2	1	15	42	109	453
16	13	131	48	30	12	8	4	10	3	1			5		3		4	12	43	255
16	18	117	33	56	5	9	11	10			3	2	6		2		2	22	44	255
16	23	200	52	68	27	15	33	13	2	2		6	3		4	1	8	54	115	440
16	28	181	46	75	22	17	26	16		3		9	6	1	2		13	52	104	409
16	33	197	42	70	28	21	17	15		3	1	3	8	2	2		15	41	101	415
32	38	111	50	58	18	10	7	5	1			1	5		6		7	18	48	273
16	43	176	32	60	29	6	17	17	2	3		1	10	2	4	4	16	24	95	373
32	48	121	91	108	36	4	33	21		3	1	3	6		4	6	8	40	110	441
64	53	121	64	86	25	4	14	11		1	1	5	3		4	3	8	23	68	347
64	58	124	47	87	43	11	11	12			1	6	4	1	3	6	4	28	94	363
32	63	113	63	93	38	13	33	9	1	2	2	5	2	1	7	3	9	51	108	391
32	68	71	46	93	29	12	17	9		5	2	7	6		2		3	36	88	302
64	73	111	94	106	42	10	11	12		5	5	9		3		4	3	30	95	418
64	78	115	96	83	36	1	18	17		2	4	9	4		1		4	28	92	391
64	83	154	213	96	16	5	14	10		2	5	5	3		1		8	24	63	533
128	88	145	178	75	25	2	12	12		7		11	6		1	1	4	25	85	488
128	93	152	165	92	32	8	22	9	1	7	4	3	3		3	5	7	33	92	514
256	98	133	135	42	25	5	15	15		3	1	3	8				3	23	79	390
256	103	110	180	89	27	1	11	12			4	7	2			2	4	19	66	452
256	108	133	133	57	23	1	10	8	1	6	1	1	2		1	2	8	12	54	381
256	113	99	222	90	19	5	7	7		2		2	1	2	1	1	9	14	46	466
512	118	58	127	50	10		4	1		2	5			2	2	3	4	4	19	266
256	123	72	108	71	5		7	2			1		5	4	2	3	3	7	24	287
256	128	75	106	42	12	2	4	13			1	2	6		3	2	9	8	42	274
128	133	126	114	77	7	1	13	11	1		2	2	2		1		3	16	39	359
256	138	97	106	45	6		3	4		1	3	1	7		1	1	5	4	28	282
32	143	54	184	38	15	2	8	5		2	3	2	6	1		1	8	12	42	324
32	148	31	271	53	12	1	11	4		1	2	2	9	2	6	1	9	14	51	417
64	158	28	100	85	7	2	7	4		1			2	1	1		10	9	25	240
64	163	26	97	89	4		6	12			2	1	10	1	2		2	7	33	250
64	168	38	79	102	12	1	10	3		2	1		5	2			9	11	34	256
64	173	65	81	71	5	1	10	1		1	5	1	4		2		10	12	23	247
64	178	81	108	129	12	2	37	12			6	2	23	2	1	2	11	41	90	420
32	183	61	75	94	5		16	3		1	5		12	3	1		12	16	38	280
16	188	153	67	107	1	2	19	31			2		4	1	2		26	21	59	392
16	193	71	63	79	8	2	13	10		2	2	2	5		4		14	17	47	266
16	198	129	56	135	3	1	27	11		3		2	15		5	2	31	30	72	400
32	203	125	112	115	9		21	8		1	5	1	25		5	1	34	22	72	437
16	208	140	92	169	13	10	21	12		2	2	1	18	4	6	1	35	32	83	502
16	213	106	94	119	9	5	14	10		2	2	1	12		1	1	21	20	59	387
16	218	88	80	151	4	3	13	13		1	10	3	7	2	3	4	17	19	50	393
32	223	109	86	112	3	5	23	4	3	1	1	5	4	1	2		8	33	66	380
64	228	68	56	125	5	3	23	17			1	1	6	6	3	1	3	27	60	320
64	233	77	67	103	8		14	8		1		1	7	3	2		5	15	42	294
64	238	53	63	117	5	1	14	12			2	3	2	1	3	1	3	18	37	278
64	243	130	142	213	16	1	14	12		1	7	2	4	5	5		9	17	51	553

Fraction (1/)	Depth (cm)	Inf.	pachy (d)	bull.	dut.	sacc.	ruber	trunc.	men.	univ.	pachy (s)	siph	glut.	quin.	scit.	Other	Ben.	Spin	Trops	Total
64	248	64	53	100	5	2	10	13	1	2	4	1	6		1		3	13	44	266
32	253	75	85	99	1		8	15	1		5	1	12		4	1	7	9	44	314
32	258	92	111	191	20	5	27	30	1		2	5	11	2	6		5	37	109	514
32	263	68	81	66	5	3	21	37		1	2	2	3		1	1	11	26	74	293
16	268	77	47	59	7	2	15	25		2	1	1	2			1	4	18	55	241
32	273	82	67	112	11		35	25			1	1	1	1	2		8	36	77	342
32	278	135	69	152	10	4	54	40	1	3	3	1	13		4		17	59	128	493
32	283	151	42	105	5	2	32	20		2	1	7	5				3	41	75	374
64	288	172	45	140	13	7	32	31		1	2		13		5	1		39	99	464
64	293	93	32	91	13	18	26	15			3	5	8		1		9	49	86	306
128	298	100	30	87	5	5	13	7		1		4	7		2		3	22	43	264
64	303	145	57	120	27	6	19	14	1	3	5		19	1		1	3	25	93	423
64	308	185	91	132	17	13	35	21	1	5	2	6	26		1	1	5	54	129	544
128	313	147	34	75	29	2	21	13		3	1	3	11	1	1		4	26	86	346
128	318	141	53	87	10	11	33	14			3	9	14	3	1	1	5	53	93	383
64	323	221	74	129	29	18	44	18	2	6	4	8	40	1	3	1	13	70	169	604
256	328	107	56	71	6	7	22	11		2		7	8		1		2	36	64	301
256	333	132	56	59	14	3	23	18	1	1	3	3	9	2		1	8	29	72	325
256	338	179	72	61	10	11	21	15	3	2	3	7	11	1	1		3	39	82	400
256	343	182	109	94	16	9	25	20	1	9	1	4	6	1	5	1	2	38	90	483
256	348	166	79	50	8	2	13	5		3	4	2	4	1			9	17	38	339
256	353	226	160	88	24	4	13	10	1	2	2	2	4	1	3	2	3	19	64	548
512	358	138	79	45	6	4	6	8	1	1	1	1	2				1	11	29	293
512	363	99	68	57	7	4	14	12		2		1	2		1			19	43	268
256	368	125	124	72	5	3	12	4			2	2	1	3			2	17	28	354
128	373	129	168	74	13	6	4	17		1	7	1	3	3			5	11	47	429
256	378	86	102	45	19		8	6	1	2	3	2	2	1			2	10	40	277
64	383	93	108	43	9	2	9	4		1	2	1	3		1		1	12	29	277
32	388	110	93	65	15	2	21	22			2	6	7		3	1	12	29	76	350
32	393	103	84	70	12	1	19	11			2	2	5		3	2	3	22	53	317
32	398	89	83	53	14	3	11	9	1	1	1		12	1	1	2	1	14	52	282
32	403	100	87	56	19		14	4	4		6	1	7	1	2		1	15	51	303
32	408	126	88	58	9		8		1		1	3	3	3	9	1	3	11	25	312
32	413	107	105	52	13	2	14	9		1			9		3		2	16	49	316
32	418	128	141	74	18	3	19	20	1	3	8	1	6	2	4		5	23	71	430
32	423	129	166	87	20	4	26	36		2	7	2	6		6		24	32	99	494
32	428	136	167	83	26	1	28	30		1	6	3	4	2	4		26	32	97	497
32	433	114	151	74	25	4	33	26	1		5	1	6	2	6		7	38	97	449
32	438	69	105	48	11		14	22			3		3	3	2			14	51	281
32	443	104	165	80	7	4	27	25		4		1	5	3	3		4	32	74	429
128	448	114	60	54	12		17	11		2	2	1	6		3		5	18	49	283
128	453	132	73	73	16	3	12	13	1	3	3	2	5	1			9	17	57	340
256	458	144	58	43	5	7	8	15	1	5	1	1	8		3	3	10	16	51	304
256	463	160	99	85	9	4	10	12	2	1		3	11	3	1			17	54	403
128	468	158	135	93	17	6	21	11	2	3	1	4	25	3		1	12	31	91	483
256	473	96	121	44	19	2	13	7	2		1	3	9	3	2		6	18	55	323
256	478	86	94	77	14	4	13	12	1	5	2	7	19	3	2		3	24	75	339
64	483	137	129	86	18	5	17	11				3	25	3	4		15	25	80	439
256	488	97	106	76	10	1	16	15		4	4	2	12	3	1		14	19	60	347
256	493	128	150	82	32	2	12	7		3	3	2	12	4	2		6	16	70	439
256	498	123	92	64	11	2	11	8		2		3	8		3		10	16	46	329
256	503	174	140	60	19	2	13	13			4	6	7	1	1		13	21	62	442
1024	508	186	72	39	14		8	11		4	9		4				32	8	42	348
128	513	208	139	64	20	1	14	8		2		1	3	1	2		31	16	54	468
256	518	153	111	50	17	3	11	8		1		1	14	1			14	15	59	375
256	523	133	108	49	17	2	7	6		4	1	3	6		2		16	12	45	338
64	528	141	188	108	20	1	13	7	1		2	1	8	1	2		10	15	53	497
128	533	92	126	64	15	1	10	12	2		5	1	17	4	2		8	12	62	356

Fraction (l/)	Depth (cm)	Inf.	pachy (d)	bull.	dut.	sacc.	ruber	trunc.	men.	univ.	pachy (s)	siph	glut.	quin.	scit.	Other	Ben.	Spin	Trops	Total
256	538	69	103	44	4		5	6			3		1		1		8	5	19	239
64	543	75	70	62	3		10	10		2	4		1	1	5		15	10	28	245
32	548	155	98	88	26	2	21	11	2		14	4	8	7	5		15	27	75	443
32	553	167	124	75	39	1	13	14	1		11	2	7	3			7	16	77	457
32	558	86	112	95	39	5	13	3	1	1	24	2	6	4	2		24	20	71	396
32	563	147	93	76	39	3	15	7	1	2	31	3	4	9	3	1	33	21	77	440
32	568	87	68	56	22	1	5	5	1	6	18		3		3		17	6	43	276
32	573	96	59	32	19	2	14	6			11		2	3			11	16	44	245
32	578	63	122	55	22	1	24	7		5	6	1	1	3	3		15	26	63	315
32	583	79	64	52	23	3	6	5		1	12	7	3		4		7	16	50	261
32	588	72	101	53	25	2	5	6	1		6	1		1	5		15	8	40	278
32	593	148	74	65	20	2	24	11		3	10	4	2	2	2		5	30	68	369
32	598	86	37	40	17	3	14	6	3	1	20	1	8	8	3		6	18	53	247
32	603	105	112	60	35	3	16	13		3	18		3	3	1		8	19	74	373
32	608	72	87	64	34		17	12	1		16	1	4	8	2		13	18	70	319
32	613	89	119	98	70	1	28	16		3	82	1	3	12	2		13	30	126	528
32	618	91	125	78	33	5	27	10		2	28	1	2	6			8	33	85	413
32	623	131	94	131	34	12	15	15	4	1	15		6	6	1		8	27	91	470
32	628	146	11	160	32	6	20	22	2	1	32		9	7			12	26	96	456
64	633	108	60	108	33	9	18	9		2	23	2	9	1	1	3	17	29	83	388
128	638	70	38	94	20	1	14	6		2	14	1	4	4	1		10	16	51	273
64	643	99	65	73	25	5	28	11		2	13	5	4		1		16	38	85	340
128	648	164	75	86	25	3	12	15		1	3	2	5		2		21	17	68	399
256	653	123	52	48	8	1	6	15				1	1				16	8	34	257
512	658	146	69	47	18	2	7	10	1		2		2		3		15	9	41	308
256	663	111	80	54	14	1	8	9		3	2	1	1	1	1	1	29	10	38	288
128	668	92	121	69	20	3	6	4		1	8		4		2		35	9	44	336
64	673	72	72	45	5	2	11	13			7	2	2		1		52	15	37	234
8	678	91	38	63	19	2	12	4			3	2	3	1	1		18	16	47	246
8	683	79	39	63	29	4	22	13			9		2	2	3		34	26	76	279
8	688	71	30	56	20	1	17	16			3	3	5				21	21	62	222
8	693	117	33	37	32	9	8	20	2	2	2	2		1	1		86	19	82	274
16	698	80	48	70	25	3	16	20	3		4	2	4				4	21	78	282
8	703	101	65	53	14	2	25	23	1	1	2		3	6			25	27	72	300
8	708	86	65	54	30	3	26	28	1	5	3	1	12	6			28	30	112	326
8	713	79	49	63	29	3	14	15	4	9		1	7	2	1		20	18	85	279
8	718	59	58	46	21	4	20	19	2	10	5	1	3	2	2		39	25	87	259
8	723	146	98	67	39	5	7	17	4	3	6	2	13		3		25	14	93	413
8	728	68	47	42	17	4	19	24		3	1	2	14	6	1		37	25	87	252
8	733	93	60	64	27	3	26	10	1	1	7	3	9	12	2		32	32	84	322
8	738	91	63	71	30	3	26	23	2	3	7	2	7	4	1		33	31	104	341
8	743	88	78	67	28	3	23	32		3	6	2	2	5	3		38	28	101	348
32	748	255	124	120	34	1	12	12	1	7		6	3		1		28	19	84	584
8	753	75	44	26	10	5	19	9	1			3	5	2			10	27	55	202
8	758	88	82	52	23	4	31	20					12	4			45	35	92	318
8	763	93	62	68	25	2	37	16	4		4	2	12	1	3		18	41	99	331
8	768	98	87	68	26	1	44	21	2	3	1	3	4	4	3		8	48	109	370
8	773	65	94	70	29	7	33	15	1	1	3	3	6		1		10	43	102	337
8	778	73	73	54	28	3	26	13		3	1		3		1		8	29	78	280
8	783	92	78	47	26		20	14			2	1	2		4		9	21	65	288
8	788	128	120	94	32	3	48	16	2	1		2	5		4		33	53	113	460
16	793	58	105	39	17	1	21	13	2	2	3	1	5	1	1		21	23	63	270
16	798	79	147	58	39	4	30	13	3	1	3		14		5		25	34	105	398
16	803	59	154	61	19	3	34	13	2	4	1	1	11	2	6		34	38	90	373
16	808	71	143	58	35	2	27	7		4	5	1	11		4		30	30	89	370
8	813	79	143	51	38	2	22	15	1				8		3		34	24	87	364
32	818	48	90	47	22	4	18	3	1	1		2	4				6	24	55	240
16	823	68	76	66	34	6	20	5	1	4			2	1	1		18	26	77	289

Fraction (1/)	Depth (cm)	Inf.	pachy (d)	bull.	dut.	sacc.	ruber	trunc.	men.	univ.	pachy (s)	siph	glut.	quin.	scit.	Other	Ben.	Spin	Trops	Total
64	828	46	57	74	17	2	16	8		2	1			1			4	18	47	226
64	833	121	102	120	41		22	9	1	1	1	1	8		4			23	87	435
64	838	152	120	110	28	5	19	6	3	6		3	5	1	1		3	27	79	464
128	843	184	86	111	11	4	27	7	6	4	2	1	5		2		11	32	66	451
256	848	130	67	61	11	2	14	6	1	8		1	4	1	1		1	17	51	311
512	853	122	69	59	17	2	7	6		7	1		6	1			4	9	46	298
256	858	119	102	95	21	2	7	8			2	1	2				6	10	41	359
16	863	62	37	30	9		12	4							1		20	12	25	155
8	868	81	33	35	17	1	18	5	1				6		1		10	19	49	200
8	873	116	96	69	27		20	7	1	2	1		4	3	3		15	20	65	353
8	878	110	97	80	24	4	16	11		1	1	1	9		2		2	21	73	364
8	883	75	93	46	10	3	9	7			2	1	4	5	2		6	13	34	257
16	888	75	102	51	14	4	4	4	1	1	2		3	2	2		5	8	32	266
8	893	100	127	47	31	1	21	13	1	1	1	1	3		3		16	23	76	354
16	898	108	85	59	17	6	13	8		1		2	5		2		12	21	53	307
8	903	88	78	36	17	5	19	7			2	1	3		3		14	25	52	260
8	908	161	145	112	57	6	28	8	3	1	1	1	11		2		13	35	119	541
8	913	181	96	79	32	3	19	10		1	1		3	1	3		7	22	70	431
16	918	77	47	41	13	2	13	3	3			4	3	3			11	19	42	210
16	923	151	86	59	31	11	21	6	3	2		1	2	7	3		6	33	85	392
8	928	164	91	102	67	1	26	9	3	3	1	1	4	1	5		9	28	121	485
16	933	101	54	55	30	5	25	1			1		3	1	2		15	30	69	283
16	938	76	104	68	36	4	19	6			1	3	1	4	1	1	18	26	73	328
16	943	87	220	115	69	4	22	7	1	2	1	1	5	4	5	1	17	27	115	548
16	948	50	112	90	29	2	12	9	1		1	1	4	2			6	15	61	316
16	953	105	238	110	58	2	11	9	2	1	2	3	4	1	2	2	15	16	91	553
16	958	61	129	154	46	8	10	3	2	2	3	3	5	4	6		18	21	79	436
16	963	46	83	122	32	2	12	2	2				12		1		8	14	62	314
16	968	76	128	79	34	2	11	5	3	1	3	2	1	2	3		27	15	62	353
8	973	74	105	83	29	2	9	4	1	1	1	1	5	1	1		13	12	54	319
16	978	75	125	92	40	3	13	1			1	3	1		2		6	19	63	358
16	988	70	153	81	55	2	22	3		5	2	1	6		3		9	25	94	403

Relative abundances of planktonic foraminifera from cores GeoB 3603—3608 (R/V METEOR M34/2)

A.4.

Appendix 4. Relative abundances of planktonic foraminifera from cores GeoB 3603—3608 (R/V Meteor M34/2)

Appendix 4.1. Relative percentages of planktonic foraminifera from GeoB 3603. Abbreviations are as follows: Depth = Depth of core sample (cm); inf. = *Gr. inflata*; bull. = *Gg. bulloides*; dut. = *N. dutertrei*; pachy (d) = *N. pachyderma* (d); pachy (s) = *N. pachyderma* (s); men. = *Gr. menardii*; Tropicals = Tropical planktonic foraminifera (*G. sacculifer* + *G. ruber* + *G. menardii* + *G. siphonifera* + *O. universa*). Sample sizes vary but were generally between 50 and 100 specimens for a preliminary analysis. Data is plotted in *Bleil et al.* (1996).

Depth	inf.	bull.	dut.	pachy (d)	pachy (s)	men.	Tropicals
20	18.31	25.35	4.23	28.17		1.41	19.72
40	16.67	23.33	1.67	36.67	3.33		16.67
60	10.53	14.04	3.51	61.40	1.75		8.77
80	35.38	20.00		40.00		1.54	4.62
100	13.21	39.62	1.89	24.53		1.89	18.87
120	46.15	7.69	5.77	28.85			11.54
140	42.37	30.51	3.39	8.47			11.86
160	12.73	23.64		41.82	1.82		14.55
180	47.37	14.04	3.51	15.79		1.75	14.04
200	30.65	25.81	3.23	12.90	3.23		24.19
220	27.87	24.59		26.23		3.28	21.31
240	29.03	12.90	4.84	30.65	1.61		16.13
260	53.45	10.34	3.45	5.17	3.45	1.72	20.69
280	40.3	14.93		20.9	2.99		14.93
300	38.6	40.35		8.77			8.77
320	31.67	16.67		25.00	1.67	3.33	18.33
340	27.59	29.31	1.72	13.79			15.52
360	29.09	32.73	3.64	12.73			18.18
380	34.92	12.70	1.59	11.11		1.59	39.68
400	51.56	14.06	3.13	9.38	1.56		18.75
420	48.21	12.50	5.36	7.14		1.79	25
440	35.09	17.54	3.51	24.56			17.54
460	30.51	22.03		25.42	1.69		18.64
480	33.33	25.76	1.52	22.73			15.15
500	33.33	28.07	1.75	33.33	1.75		1.75
520	35.19	16.67	3.70	12.96		1.85	27.78
540	31.67	25		26.67	3.33		13.33
560	46.15	13.46		26.92	1.92		9.62
580	63.64	7.27	5.45	10.91			10.91
600	32.76	17.24	3.45	22.41			24.14
620	25.33	26.67		25.33	4.00		18.67
640	38.46	25	1.92	19.23			13.46
660	32.73	9.09	5.45	10.91			40.00
680	52.63	12.28		10.53			21.05
700	29.23	20	7.69	23.08	3.08		16.92
720	39.22	15.69	3.92	5.88			35.29
740	14.81	22.22	3.70	50.00			9.26
760	32	26	2.00	32.00			8.00
780	50	11.54	3.85	26.92			7.69
800	26.92	11.54		51.92			7.69
820	53.7	27.78		16.67	1.85		
840	25	25	5.77	25.00	1.92		17.31
860	35.29	27.45	3.92	13.73			17.65
880	55.17	10.34	10.34	13.79			10.34
900	38.18	7.27	1.82	27.27	1.82		21.82
920	51.92	11.54	3.85	13.46			19.23
940	57.69	11.54		25.00			5.77
960	43.64	16.36		14.55	1.82		20
980	53.57	16.07	1.79	12.50			14.29
1000	55.32	4.26	6.38	4.26			29.79
1020	32.69	13.46	5.77	11.54			32.69
1040	25.93	20.37	16.67	11.11			25.93
1060	31.15	21.31	8.20	27.87	1.64		8.20
1080	32.14	19.64	1.79	28.57			17.86
1100	25.76	34.85	7.58	19.70	1.52		9.09
1120	36.54	25.00	3.85	28.85			5.77

Appendix 4.2. Relative percentages of planktonic foraminifera from GeoB 3604. Abbreviations are as follows: Depth = Depth of core sample (cm); inf. = *Gr. inflata*; bull. = *Gg. bulloides*; pachy (d) = *N. pachyderma* (d); dut. = *N. dutertrei*, pachy (s) = *N. pachyderma* (s); Tropicals = Tropical planktonic foraminifera (*G. sacculifer* + *G. ruber* + *G. menardii* + *G. siphonifera* + *O. universa*). All values are given as percentages of the total planktonic foraminifera. Sample sizes vary but were generally between 50 and 100 specimens for a preliminary analysis. Data is plotted in *Bleil et al.* (1996).

Depth	inf.	bull.	pachy (d)	dut.	pachy (s)	Tropicals
20	67.21	8.20	11.48	3.28		9.84
40	27.27	25.45	25.45	1.82		20.00
60	19.67	14.75	44.26			21.31
80	18.97	12.07	44.83		5.17	15.52
100	7.84	27.45	54.90		1.96	7.84
120	21.88	29.69	28.13		3.13	17.19
140	11.76	30.88	51.47		1.47	4.41
160	18.64	32.20	42.37			6.78
180	9.26	22.22	53.70	1.85	3.70	7.41
200	15.38	23.08	48.08	1.92		11.54
220	15.15	42.42	27.27	1.52		13.64
240	21.57	37.25	29.41			11.76
260	27.27	30.91	30.91	1.82	3.64	5.45
280	17.65	50.98	21.57	3.92		5.88
300	29.63	25.93	27.78	0.00	3.70	12.96
320	13.73	15.69	50.98	1.96	1.96	7.84
340	12.96	22.22	31.48	1.85	1.85	16.67
360	15.94	31.88	17.39	4.35	0.00	24.64
380	37.68	18.84	7.25	2.90	5.80	26.09
400	57.14	21.43				17.86
420	14.52	24.19	38.71		11.29	11.29
440	14.04	35.09	31.58	1.75		17.54
460	13.33	26.67	46.67		1.67	11.67
480	16.98	24.53	47.17		1.89	9.43
500	21.43	19.64	42.86			14.29
520	14.04	17.54	54.39		3.51	10.53
540	12.50	12.50	58.93	1.79		14.29
560	14.29	22.45	46.94	4.08	4.08	6.12
580	20.00	12.73	34.55	3.64	3.64	20.00
600	12.07	29.31	44.83		6.90	3.45
620	18.52	42.59	18.52		5.56	12.96
640	33.33	19.44	33.33	1.39	2.78	8.33
660	36.67	16.67	31.67			11.67
680	14.29	10.20	61.22		6.12	6.12
700	30.36	23.21	41.07	1.79	1.79	1.79
720	17.91	25.37	23.88	5.97		25.37
740	13.46	13.46	65.38		3.85	3.85
760	13.04	11.59	52.17		7.25	7.25
780	16.13	20.97	45.16		11.29	4.84
800	27.42	25.81	45.16			1.61
820	8.33	10.00	73.33		1.67	6.67
840	8.47	13.56	54.24		15.25	1.69
860	37.14	7.14	32.86	4.29	10.00	2.86
880	11.11	9.26	70.37	1.85	1.85	1.85
900	22.03	5.08	64.41		3.39	3.39
920	46.88	6.25	32.81	1.56	4.69	6.25
940	15.52	13.79	60.34	5.17		5.17

Appendix 4.3. Relative percentages of planktonic foraminifera from GeoB 3605. Abbreviations are as follows: Depth = Depth of core sample (cm); inf. = *Gr. inflata*; bull. = *Gg. bulloides*; pachy (d) = *N. pachyderma* (d); dut. = *N. dutertrei*, pachy (s) = *N. pachyderma* (s); Tropicals = Tropical planktonic foraminifera (*G. sacculifer* + *G. ruber* + *G. menardii* + *G. siphonifera* + *O. universa*). All values are given as percentages of the total planktonic foraminifera. Sample sizes vary but were generally between 50 and 100 specimens for a preliminary analysis. Data is plotted in *Bleil et al.* (1996).

Depth	inf.	bull.	pachy (d)	dut.	pachy (s)	Tropicals
5	20.41	12.24	63.27			2.04
20	29.23	21.54	27.69	3.08	1.54	15.38
40	22.95	21.31	39.34		1.64	14.75
60	10.71	21.43	57.14		7.14	1.79
80	13.21	16.98	62.26		3.77	3.77
100	19.40	23.88	43.28		2.99	7.46
120	8.93	25.00	51.79	1.79	3.57	3.57
140	5.08	23.73	55.93		5.08	6.78
160	13.33	18.33	48.33		10.00	1.67
180	31.03	36.21	13.79	1.72		15.52
200	16.39	52.46	22.95		3.28	4.92
220	23.73	38.98	30.51	1.69		1.69
240	20.69	41.38	25.86		5.17	1.72
260	38.71	17.74	17.74	3.23	1.61	20.97
280	16.18	11.76	50.00		10.29	1.47
300	11.48	16.39	34.43		14.75	1.64
320	23.44	21.88	46.88		1.56	3.13
340	20.34	30.51	38.98	1.69	5.08	3.39
360	21.74	26.09	39.13	1.45	1.45	8.70
380	29.82	19.30	38.60		1.75	5.26
400	27.78	23.61	37.50	1.39	2.78	4.17
420	5.88	17.65	50.98	1.96	3.92	15.69
440	13.56	20.34	52.54	1.69	3.39	6.78
460	13.46	11.54	51.92	3.85	9.62	1.92
480	23.53	17.65	50.98		1.96	1.96
500	19.64	0.00	60.71	5.36		12.50
520	24.00	6.00	56.00	2.00	2.00	8.00
540	41.27	6.35	39.68	4.76	1.59	4.76
560	21.31	8.20	29.51	1.64	36.07	1.64
580	7.27	7.27	58.18		18.18	1.82
600	14.29	11.11	49.21		11.11	9.52
620	25.81	35.48	16.13	3.23	8.06	11.29
640	12.50	16.07	51.79	1.79	5.36	12.50
660	43.40	9.43	39.62	1.89	1.89	3.77
680	5.36	16.07	55.36	1.79	14.29	5.36
700	59.26	9.26	25.93		1.85	3.70
720	29.69	9.38	28.13		15.63	12.50
740	20.00	21.54	30.77	1.54	9.23	16.92
760	8.51	12.77	36.17	4.26	21.28	6.38
780	14.55	12.73	45.45	7.27	5.45	14.55
800	25.45	16.36	43.64		3.64	5.45
820	17.24	25.86	53.45	1.72		1.72
840	17.24	8.62	46.55	5.17	10.34	5.17
860	29.09	18.18	36.36	1.82	3.64	7.27
880	38.78	8.16	44.90	4.08	0.00	4.08

Appendix 4.4. Relative percentages of planktonic foraminifera from GeoB 3606. Abbreviations are as follows: Depth = Depth of core sample (cm); inf. = *Gr. inflata*; bull. = *Gg. bulloides*; pachy (d) = *N. pachyderma* (d); pachy (s) = *N. pachyderma* (s); dut. = *N. dutertrei*; Tropicals = Tropical planktonic foraminifera (*G. sacculifer* + *G. ruber* + *G. menardii* + *G. siphonifera* + *O. universa*). All values are given as percentages of the total planktonic foraminifera. Sample sizes vary but were generally between 50 and 100 specimens for a preliminary analysis. Data is plotted in *Bleil et al.* (1996).

Depth	inf.	bull.	pachy (d)	pachy (s)	dut.	Tropicals
20	1.89	28.30	52.83	16.98		
40	1.82	21.82	65.45	9.09	1.82	
60	7.14	23.21	58.93	5.36		
80	3.70	24.07	68.52	1.85		
100	9.43	26.42	60.38	1.89		1.89
120	20.34	33.90	20.34	18.64		1.69
140	22.00	24.00	32.00	16.00		4.00
160	18.87	35.85	33.96	3.77		3.77
180	15.38	23.08	48.08	3.85		9.62
200	1.79	12.50	69.64	10.71	1.79	3.57
220	1.89	15.09	66.04	9.43	5.66	1.89
240		9.80	72.55	9.80	1.96	3.92
260			57.89	38.60		
280	2.17	6.52	82.61	2.17		4.35
300		19.57	56.52	23.91		
320	20.41	12.24	51.02	14.29	2.04	
340	11.11	7.41	64.81	14.81		
400	4.55	6.82	59.09	27.27		
500	1.59	46.03	28.57	17.46		4.76
540	10.71	5.36	73.21	3.57		7.14
560	4.00	6.00	82.00	8.00		
620	16.22	37.84	32.43	8.11		2.70
700	15.56	37.78	37.78			

Appendix 4.5. Relative percentages of planktonic foraminifera from GeoB 3608. Abbreviations are as follows: Depth = Depth of core sample (cm); pachy (d) = *N. pachyderma* (d); pachy (s) = *N. pachyderma* (s); bull. = *Gg. bulloides*; inf. = *Gr. inflata*. All values are given as percentages of the total planktonic foraminifera. Sample sizes vary but were generally between 50 and 100 specimens for a preliminary analysis. Data is plotted in *Bleil et al.* (1996).

Depth	pachy (d)	pachy (s)	bull.	inf.
5	70.49	3.28	3.28	1.64
20	56.00	2.67	10.67	8.00
40	53.62	2.90	10.14	14.49
60	46.03	3.17	26.98	12.70
80	42.19	1.56	42.19	6.25
100	34.29	2.86	38.57	15.71
120	41.94	0.00	50.00	3.23
140	34.67	2.67	41.33	14.67
160	32.20	18.64	33.90	1.69
180	9.52	74.60	9.52	
200	20.00	61.54	12.31	
220	21.13	59.15	5.63	4.23
240	11.32	75.47	9.43	
260	37.70	34.43	18.03	1.64
280	16.67	63.33	6.67	1.67
300	43.55	20.97	17.74	3.23
320	10.17	84.75	1.69	
340	26.15	52.31	15.38	1.54
360	9.09	72.73	7.27	
380	17.24	68.97	5.17	
400	27.14	21.43	25.71	12.86
420	11.29	62.90	9.68	3.23
440	18.03	68.85	8.20	
460	25.49	60.78	1.96	
480	25.00	37.50	17.86	12.50
500	20.37	31.48	29.63	7.41
520	15.25	47.46	28.81	
540	16.07	48.21	19.64	3.57
560	41.82	21.82	21.82	
580	15.49	16.90	57.75	2.82
600	51.56	1.56	37.50	3.13
620	13.33	8.33	63.33	5.00
640	31.48	18.52	44.44	3.70
660	16.98	37.74	24.53	13.21
680	37.50	7.81	37.50	4.69
700	56.36	7.27	27.27	3.64
720	32.88	6.85	39.73	15.07
740	42.86	3.17	33.33	12.70
760	64.91	5.26	12.28	10.53
780	41.67	5.00	35.00	11.67
800	19.72	5.63	25.35	45.07
820	20.31	6.25	12.50	57.81
840	33.33	1.67	13.33	50.00

Published Articles

A.5.

Reprinted from

PALAEO
GEOGRAPHY
CLIMATOLOGY
ECOLOGY

Palaeogeography, Palaeoclimatology, Palaeoecology 130 (1997) 135–161

Rapid palaeoceanographic changes in the Benguela Upwelling System for the last 160,000 years as indicated by abundances of planktonic foraminifera

M.G. Little [a,*], R.R. Schneider [b,1], D. Kroon [a,2], B. Price [a,3], T. Bickert [b,4], G. Wefer [b,5]

[a] *Geology and Geophysics, University of Edinburgh, Kings' Buildings, West Mains Road, Edinburgh EH9 3JW, UK*
[b] *Fachbereich Geowissenschaften, Universität Bremen, Klagenfurter Straße, D-28359 Bremen, Germany*

Received 19 March 1996; revision 28 October 1996; accepted 28 October 1996

ELSEVIER

PALAEO GEOGRAPHY CLIMATOLOGY ECOLOGY

Scope of the journal
Palaeogeography, Palaeoclimatology, Palaeoecology is an international medium for the publication of original studies and comprehensive reviews in the field of palaeo-environmental geology. It is hoped that the journal will contribute to the sound development of this field by bringing together under one cover interesting results in many disciplines involved in palaeo-environment investigations.

US mailing notice — *Palaeogeography, Palaeoclimatology, Palaeoecology* (ISSN 0031-0182) is published monthly by Elsevier Science B.V. (Molenwerf 1, Postbus 211, 1000 AE Amsterdam). Annual subscription price in the USA US$ 2528.00 (US$ price valid in North, Central and South America only), including air speed delivery. Second class postage paid at Jamaica, NY 11431.
USA POSTMASTERS: Send address changes to *Palaeogeography, Palaeoclimatology, Palaeoecology* Publications Expediting, Inc., 200 Meacham Avenue, Elmont, NY 11003.
Airfreight and mailing in the USA by Publication Expediting.

Publication information
Palaeogeography, Palaeoclimatology, Palaeoecology (ISSN 0031–0182). For 1997 volumes 126–134 are scheduled for publication. A combined subscription to *Palaeogeography, Palaeoclimatology, Palaeoecology* and *Global and Planetary Change* (Vols. 15–17) at reduced rate is available. Subscription prices are available upon request from the publisher. Subscriptions are accepted on a prepaid basis only and are entered on a calendar year basis. Issues are sent by surface mail except to the following countries where air delivery via SAL is ensured: Argentina, Australia, Brazil, Canada, Hong Kong, India, Israel, Japan, Malaysia, Mexico, New Zealand, Pakistan, PR China, Singapore, South Africa, South Korea, Taiwan, Thailand, USA. For all other countries airmail rates are available upon request. Claims for missing issues must be made within six months of our publication (mailing) date. For orders, claims, product enquiries (no manuscript enquiries) please contact the Customer Support Department at the Regional Sales Office nearest to you:
New York, Elsevier Science, P.O. Box 945, New York, NY 10159-0945, USA. Tel: (+1) 212 633 3730, [Toll free number for North American customers: 1-888-4ES-INFO (437-4636)], Fax: (+1) 212 633 3680, E-mail: usinfo-f@elsevier.com
Amsterdam, Elsevier Science, P.O. Box 211, 1000 AE Amsterdam, The Netherlands. Tel. (+31) 20-485-3757, Fax: (+31) 20-485-3432, E-mail: nlinfo-f@elsevier.nl
Tokyo, Elsevier Science, 9-15 Higashi-Azabu I-chome, Minato-ku, Tokyo 106, Japan. Tel: (+81) 3-5561-5033, Fax: (+81) 3-5561-5047, E-mail kyf04035@niftyserve.or.jp
Singapore, Elsevier Science, No. 1 Temasek Avenue, #17-01 Millenia Tower, Singapore 039192. Tel.: (+65) 434-3727, Fax: (+65) 337-2230, E-mail: asiainfo@elsevier.com.sg

0031-0182/97/$17.00

♾ The paper used in this publication meets the requirements of ANSI/NISO Z39.48-1992 (Permanence of Paper).

PRINTED IN THE NETHERLANDS

ELSEVIER

Palaeogeography, Palaeoclimatology, Palaeoecology 130 (1997) 135–161

PALAEO

Rapid palaeoceanographic changes in the Benguela Upwelling System for the last 160,000 years as indicated by abundances of planktonic foraminifera

M.G. Little [a,*], R.R. Schneider [b,1], D. Kroon [a,2], B. Price [a,3], T. Bickert [b,4], G. Wefer [b,5]

[a] *Geology and Geophysics, University of Edinburgh, Kings' Buildings, West Mains Road, Edinburgh EH9 3JW, UK*
[b] *Fachbereich Geowissenschaften, Universität Bremen, Klagenfurter Straße, D-28359 Bremen, Germany*

Received 19 March 1996; revision 28 October 1996; accepted 28 October 1996

Abstract

Two sediment cores retrieved from the continental slope in the Benguela Upwelling System, GeoB 1706 (19°33.7′S 11°10.5′E) and GeoB 1711 (23°18.9′S, 12°22.6′E), reveal striking variations in planktonic foraminiferal abundances during the last 160,000 years. These fluctuations are investigated to assess changes in the intensity and position of the upwelling centres off Namibia. Four species make up over 95% of the variation within the core, and enable the record to be divided into episodes characterized by particular planktonic foraminiferal assemblages. The fossil assemblages have meaningful ecological significance when compared to those of the modern day and the relationship to their environment. The cold-water planktonic foraminifer, *Neogloboquadrina pachyderma* sinistral [*N. pachyderma* (s)], dominates the modern-day, coastal upwelling centres, and *Neogloboquadrina pachyderma* dextral and *Globigerina bulloides* characterize the fringes of the upwelling cells. *Globorotalia inflata* is representative of the offshore boundary between newly upwelled waters and the transitional, reduced nutrient levels of the subtropical waters. In the fossil record, episodes of high *N. pachyderma* (s) abundances are interpreted as evidence of increased upwelling intensity, and the associated increase in nutrients. The *N. pachyderma* (s) record suggests temporal shifts in the intensity of upwelling, and corresponding trophic domains, that do not follow the typical glacial–interglacial pattern. Periods of high *N. pachyderma* (s) abundance describe rapid, discrete events dominating isotope stages 3 and 2. The timing of these events correlates to the temporal shifts of the Angola–Benguela Front (Jansen et al., 1997) situated to the north of the Walvis Ridge. Absence of high abundances of *N. pachyderma* (s) from the continental slope of the southern Cape Basin indicates that Southern Ocean surface water advection has not exerted a major influence on the Benguela Current System. The coincidence of increased upwelling intensity with the movement of the Angola–Benguela Front can be interpreted mainly by changes in strength and zonality of the trade wind system.

Keywords: Benguela current; Upwelling; Nutrients; Trade winds; Planktonic foraminifera

* Corresponding author: Tel.: +44-131-6508505. Fax: +44-131-6683184. E-mail: mark.little@glg.ed.ac.uk.
[1] Fax: +49-421-2183116. E-mail: rschneid@zfn.uni-bremen.de.
[2] E-mail: dkroon@glg.ed.ac.uk.
[3] E-mail: brian.price@glg.ed.ac.uk.
[4] E-mail: bickert@zfn.uni-bremen.de.
[5] E-mail: gwefer@zfn.uni-bremen.de.

PII S0031-0182(96)00136-8

1. Introduction

Upwelling systems, and the associated enhanced primary and secondary productivity, make a significant contribution to the total carbon reservoir in the ocean sediments (Shaffer, 1993). It is vital that a proper understanding of upwelling systems, their variability and driving mechanisms is gained to quantify the carbon sinks in the oceans. The southwest African margin is an excellent area to study upwelling dynamics as it is the site of intense upwelling and exceptionally high productivity. Offshore displacement of more oligotrophic subtropical waters by the southeast trade winds allows the intense upwelling of cold, nutrient-rich waters into the surface layer. This stimulates extreme phytoplankton growth (Brown et al., 1991) in a narrow shoreward zone of eutrophy resulting in most of the surface sediments being of biogenic origin. Recent surface Benguela sediment distributions are discussed by Calvert and Price (1983), Rogers and Bremner (1991), Giraudeau et al. (1993), Dingle (1995) and Summerhayes et al. (1995b).

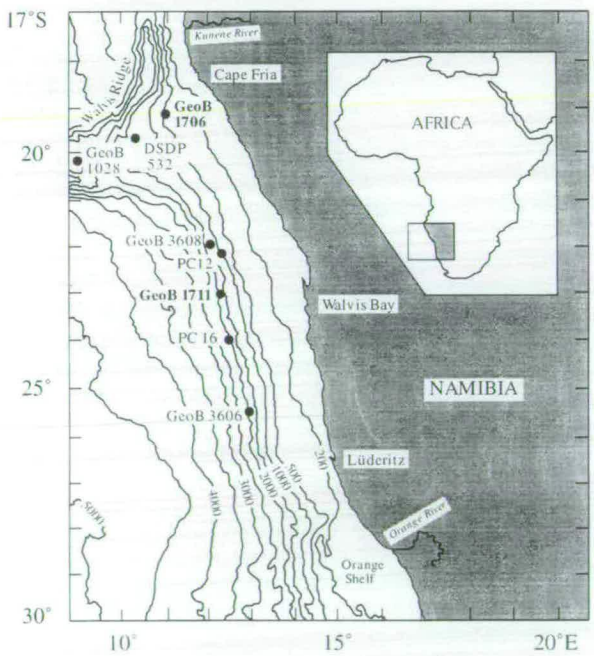

Fig. 1. Study area showing the continental shelf and slope bathymetry, and the locations of the Namibian continental-slope core sites used in text: GeoB 1711, GeoB 1706, GeoB 3608, GeoB 3606, GeoB 1028, DSDP 532, PC 12 and PC 16. Bathymetry of the southwest African coast is given in meters by Dingle and Nelson (1993). Inset shows position with respect to the African continent.

The aim of this study is to assess the variation of planktonic foraminifera to determine changes in the oceanography of the Benguela Upwelling System, in the expectation that this will enable us to assess the extent to which upwelling has changed temporally and spatially, and to determine what controls these changes. The high-resolution planktonic foraminiferal records of cores GeoB 1706, southwest of Cape Fria (19°33.7′S, 11°10.5′E, Fig. 1) and GeoB 1711, off Walvis Bay (23°18.9′S, 12°22.6′E) are used to investigate the variability of palaeoceanography of the Namibian Margin for the last 160 kyr. Two main questions to be investigated are: (1) Can abundance variations of planktonic foraminifera be used to determine past changes of upwelling intensity in the Benguela Upwelling System? (2) To what degree is the Benguela Current System (BCS) influenced by cold-water advection from the Southern Ocean as has previously been suggested (McIntyre et al., 1989; Giraudeau, 1993; Summerhayes et al., 1995b; Giraudeau et al., 1997)?

2. Regional oceanography

The oceanography off South Africa, Namibia and southern Angola is controlled by the coastal branch of the Benguela Current forming the northeastern limb of the anticyclonic gyre of the South Atlantic. The hydrography of the Benguela Current System (BCS) has been described in detail by a number of workers (Shannon, 1985; Lutjeharms and Meeuwis, 1987; Lutjeharms and Stockton, 1987; Summerhayes et al., 1995b; Shannon and Nelson, 1997), and is summarized in Fig. 2. The Benguela Oceanic Current (BOC) is the equatorward drift of cool surface waters flowing from 34°S (Cape Town) past southwestern Africa to 23°S (Walvis Bay), where it diverges from the coast. Inside the shelf break, along the entire coastline, a component of the BOC moves equatorwards forming the Benguela Coastal

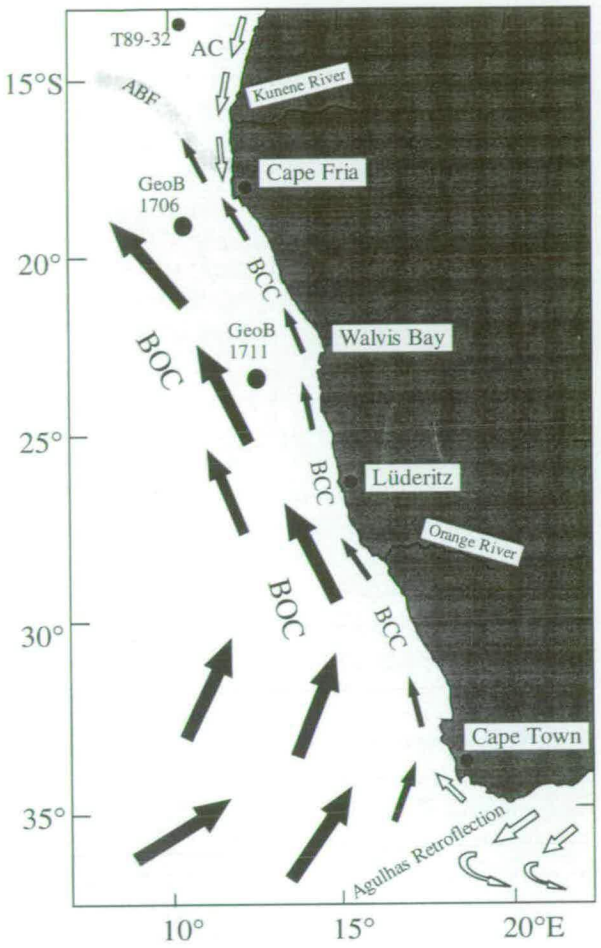

Fig. 2. Map outlining the major oceanographic features of the Benguela Current and neighbouring systems (after Shannon, 1985; Lutjeharms and Stockton, 1987). Black arrows indicate cold-water currents, white arrows warm-water currents. The size of the arrows is relative to the intensity of the respective currents. Core T89-32 (Jansen et al., 1997) is shown for reference. Abbreviations are as used in the text: *BOC*=Benguela Oceanic Current; *BCC*=Benguela Coastal Current; *AC*=Angola Current; *ABF*=Angola–Benguela Front.

Current (BCC). The BCC continues northwards off Angola as far as 14°S (Meeuwis and Lutjeharms, 1990) where the line of upwelling centers terminates. The warm Angola Current (AC), forming the southeasterly limb of the South Equatorial Counter Current (SECC), flows polewards off Angola until it meets the cold BCC between 18 and 14°S at the Angola–Benguela Front (ABF). This is the mixing site of warm, relatively nutrient-poor, waters from the north, and colder, relatively nutrient-rich, waters from the south. The front penetrates, at its greatest extent, 1000 km offshore, with a zone of maximum frontal development within the first 250 km from the shore (Meeuwis and Lutjeharms, 1990). The front has a mean annual shift of 2–3° latitude, with a general frontal NW–SE orientation (Meeuwis and Lutjeharms, 1990). To the south of the Benguela Upwelling System, a component of the warm-water Agulhas Current enters from the Indian Ocean and forms a thermal barrier, the Agulhas Retroflection. This has been observed from satellite imaging (Duncombe-Rae, 1991) as a series of dynamic eddies and rings from the east, effectively limiting the equatorward flow of cool, Subantarctic Surface Water (SASW) filaments into the BOC (Shannon et al., 1989). Movement of the thermal barrier, which is controlled by the relative position and intensity of the Subtropical Convergence (STC) and the Agulhas Current, creates a variable supply of cold Subantarctic waters and warm Agulhas waters into the BCS. This has the effect of controlling the heat flux into the South Atlantic, and will possibly be recorded in the planktonic foraminiferal record by changes in abundance of temperature-dominated species.

Coastal upwelling within the BCS varies with the seasonal extremes of summer and winter (Shannon, 1985). Upwelling intensity and the associated primary productivity is high all year round. However, the seasonal signal has the effect of dividing the system into a Northern Benguela Region (NBR) and a Southern Benguela Region (SBR) (Dingle, 1995). This is seen in the modern-day planktonic foraminiferal distributions (Giraudeau et al., 1993) and has been demonstrated using benthic ostracoda (Dingle, 1995) and satellite imaging (Lutjeharms and Meeuwis, 1987). Seven major upwelling cells can be distinguished: Lüderitz (25°S), Namaqua (29°S), Columbine (32°S), Walvis (22°S), Namibia (19°S), Peninsula (34°S) and Kunene (17°S), in order of decreasing intensity. A strong correlation was found between strength of offshore winds and level of upwelling intensity (Lutjeharms and Meeuwis, 1987). The boundary between the NBR and the SBR (Lüderitz Boundary, LB) is the site of maximum

upwelling intensity at 26–27°S (Lüderitz), which has the coldest and the most persistent upwelling (Fig. 3). Upwelling in the area north of the LB (NBR) is predominantly a winter phenomenon, but the area is typified by year round high productivity and enhanced accumulation of phytoplankton (Brown et al., 1991). Wind speeds are of medium intensity with a wide, oceanic, filamentous, mixing domain (Lutjeharms and Stockton, 1987). Surface sediments are rich in organics with a maximum in the inner-shelf belt of diatomaceous ooze (Bremner, 1983; Rogers and Bremner, 1991). In the Recent setting, the NBR has the lowest dissolved-oxygen, related to a poor oxygen source in the Angola Basin, and the highest marine organic carbon levels and sea surface temperatures (SSTs) (Dingle, 1995). Boyd et al. (1987) found late-summer poleward intrusion of surface and subsurface warm Angolan water south to Walvis Bay to be a common feature.

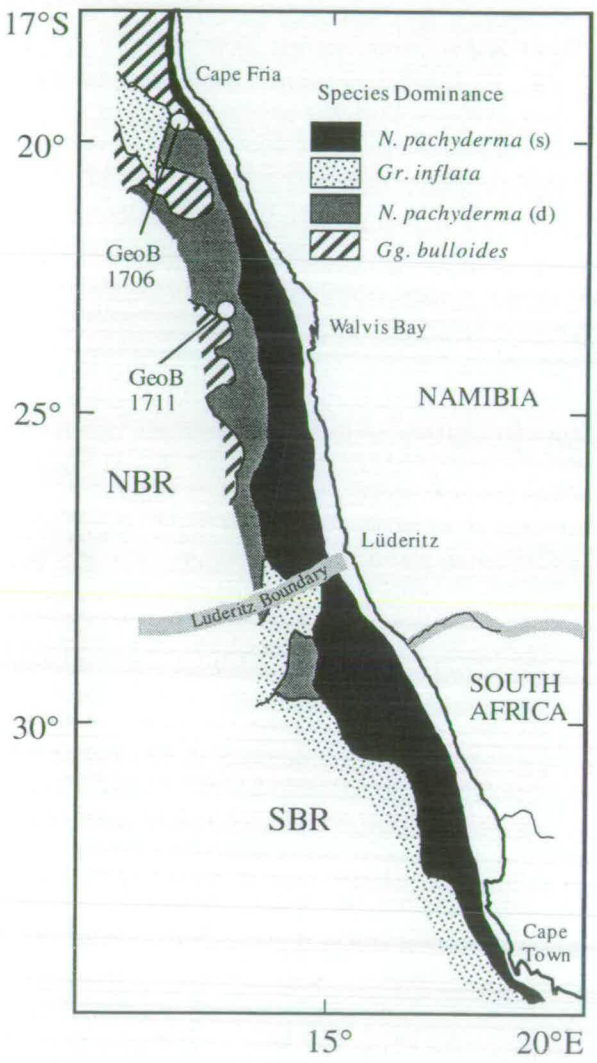

Fig. 3. Recent distribution of planktonic foraminifera in the study area, after Giraudeau (1993): *N. pachyderma* (s) is found in eutrophic, cool upwelled waters; *Gr. inflata* is found in relatively oligotrophic, sub tropical conditions; and, *N. pachyderma* (d) and *Gg. bulloides* are found in the mixed, mesotrophic, subtropical and upwelled waters typical of the offshore Northern Benguela Region (*NBR*). The Lüderitz Boundary represents the boundary between the Northern (*NBR*) and Southern Benguela regions (*SBR*). *N. pachyderma* (s) includes only sinistral forms, whilst *N. pachyderma* (d) includes all dextral forms of *N. pachyderma* and all forms of *N. dutertrei*.

The SBR has a highly seasonal upwelling regime with its maximum in summer, and a restricted mixing domain (Lutjeharms and Meeuwis, 1987; Giraudeau and Rogers, 1994). Offshore there is a strong thermal front between the cold, dense upwelled waters and the displaced subtropical waters. Seasonal variability in nutrient supply and low values of chlorophyll *a* (Giraudeau, 1993) are associated with the variable upwelling intensity. In the Recent sediments, the SBR has the highest dissolved-oxygen levels which support an abundant benthic ostracod population (Dingle, 1995).

The most recent review of the Quaternary upwelling history offshore Namibia was by Summerhayes et al. (1995b). Using geochemical and micropalaeontological analyses of a piston core (PG/PC12, see Fig. 1) from the slope off Walvis Bay, they discussed the dynamics of upwelling in the BCS during the last 70 kyr. They indicated that the most productive time interval, derived from organic carbon data, was during glacial stages 4–2, peaking in isotope stage 3, and coinciding with the coldest SSTs from alkenone data. Upwelling and organic matter flux was found to increase in stages 4 and 3, but decline into stage 2, the Last Glacial Maximum (LGM). This was attributed to an equatorward shift of the trade winds in stage 2, leading to a marked decrease in upwelling at site PG/PC12, northwest of Walvis Bay (Fig. 1). The primary control on the system is believed to be the precessionally controlled posi-

tion of the South Atlantic Anticyclonic Gyre (Summerhayes et al., 1995b) and corresponding variations in the upwelling-inducing trade winds. Aside from this primary control on productivity, Summerhayes et al. (1995a) suggest variations in the supply of nutrients into the system via subsurface waters which sank at the STC, and continued clockwise around the South Atlantic with the Equatorial Undercurrent (EUC) and through the Angola Basin to Namibia.

Jansen et al. (1997) used planktonic foraminifera from three cores on the Angola–Zaire margin to reconstruct palaeo-positions of the ABF for the last 180 kyr. Using a low-resolution record, they suggest that the extreme latitudinal shifts of the BCS can be described by the 100 kyr (eccentricity) period and the meridional shifts by the 23 kyr (precession) component of the Earth's orbital parameters. Jansen et al. (1997) show strong equatorward shifts in stages 4 and substages 3.3–3.1, whilst the southernmost positions (similar to the present situation) were occupied in substages 6.3, 5.5 and stage 1. In agreement with Summerhayes et al. (1995b), they associate the shifting of the ABF, and accompanying upwelling cells, to changes in position and relative intensity of the SAAG and corresponding southeast trade winds, with an additional component from advected Southern Ocean surface or intermediate waters.

3. Modern-day distribution of planktonic foraminifera

The variability of watermasses is important in any discussion of the distribution of planktonic foraminifera. Bé and Tolderlund (1971) grouped planktonic foraminifera into five faunal zones, showing a bipolar and anti-tropical nature of preferred habitats with distinct faunas living in particular latitudinal zones, seemingly governed by the temperature regime. However, other studies brought the dominance of temperature into question, with "typically" cold-water species such as *Globigerina bulloides* d'Orbigny being found in tropical upwelling areas (Thiede, 1975; Prell and Curry, 1981; Kroon, 1991), reinforcing the idea that species distribution is governed by nutrient levels and not by temperature (Reynolds and Thunnel, 1985). Three watermass types adequately describe the BCS as observed by the modern distribution of planktonic foraminifera (Giraudeau, 1993) and satellite imaging (Lutjeharms and Stockton, 1987; Meeuwis and Lutjeharms, 1990).

In the modern setting, Giraudeau (1993) mapped the distribution of planktonic foraminifera and found that the assemblages occur within oceanographically distinct zones or belts, from Cape Town to Cape Fria (Fig. 3). In the SBR, *Globorotalia inflata* d'Orbigny mainly inhabits the offshore waters that are typical of a transitional system with lower nutrient levels and reduced primary productivity compared to the inshore upwelling cells. Inshore, the eutrophic, nutrient-rich, cooler upwelled waters form an area much more agreeable to *Neogloboquadrina pachyderma* sinistral (Ehrenberg) [*N. pachyderma* (s)]. The sharp break between the two zones of foraminiferal domination correlates precisely to the hydrography of the SBR. Bang (1971) studied the water structure between 29 and 32°S (SBR) and distinguished a coast-parallel coastal upwelling front over the continental shelf with a sharply defined thermal anomaly between an offshore divergence zone and the newly upwelled waters of the BCS. Barange and Pillar (1992) extended the observations northwards to 17°S (NBR) and reported that the offshore divergence zone is a permanent feature independent of the wind stress. A "tongue" of warm, oxygen- and nutrient-poor, Angola Basin water filters into the northern BCS intermittently throughout the year (Boyd et al., 1987), further increasing the extent of the filamentous mixing domain in the NBR. As well as the offshore conditions in the SBR, *Gr. inflata* also inhabits the nutrient-poor, subtropical Angola Current filaments injected into the BCS in the NBR. The offshore zone of the NBR is characterized by areas of mixed nutrient levels, suitable for *Neogloboquadrina pachyderma* dextral (Ehrenberg) [*N. pachyderma* (d)] and *Gg. bulloides*. *N. pachyderma* (d) prefers the mesotrophic, but higher nutrient levels of the upwelled filaments, whilst *Gg. bulloides* prefers the relatively lower nutrient levels away from the upwelling filaments

(Giraudeau, 1993). Nearshore waters, which upwell in this area, are of a shallower origin than in the SBR (Shannon and Nelson, 1997), and are less ideal for *N. pachyderma* (s) than the nearshore area to the south.

Oberhänsli (1991) and Schmidt (1992) used the abundances of planktonic foraminifera as indicators of past upwelling processes in the BCS. Both documented cold periods within early stage 6 and stages 4–2 from sites GeoB 1028 and DSDP 532, on the Walvis Ridge (Fig. 1) recorded by the greatest maxima of the cold-water species *N. pachyderma* (s). However, although both showed distinct peaks in the planktonic foraminiferal assemblages, the records were of too low a resolution to ascertain a periodicity for the variations seen and to imply any forcing mechanisms for the system as a whole. Studies of U^k_{37} (Schneider et al., 1995) and organic matter in PG/PC12 (Summerhayes et al., 1995b) reveal similar histories of cooling, suggesting that oceanographic variation may be related to an increased vigour of upwelling, not simply an introduction of cold water from the south.

4. Materials and methods

4.1. Sampling

In this study, we used two gravity cores (GeoB 1706-2 and GeoB 1711-4) both collected on METEOR cruise M20/2 (1991) from 980 m on the upper continental slope of the Walvis Ridge (19°33.7′S, 11°10.5′E) and 1967 m on the Namibian continental slope off Walvis Bay (23°18.9′S, 12°22.6′E), respectively (Fig. 1). The core length of GeoB 1706 was 1113 cm, and of GeoB 1711 1066 cm. Sedimentology and further core characteristics are given in Schulz et al. (1992). Samples were taken at 5 cm intervals throughout the core, allowing geochemical, micropaleontological and isotopic analyses to be carried out at a high resolution. Samples (10 cm^3) for geochemical study were freeze-dried and ground prior to analysis. Micropalaeontological samples (10 cm^3) for foraminiferal work were originally wet-sieved for fractions greater than 63, 125, 250 and 500 μm, but for comparative reasons foraminiferal analysis was made only on the >125 μm size fraction. Archived core material is kept at the Department of Geosciences, University of Bremen, Germany.

4.2. Stable oxygen- and carbon-isotope analysis

Tests of *Gr. inflata* and *Cibicidoides wuellerstorfi* Schwager were hand-picked under a binocular microscope from the 250–500 μm fraction to achieve an analytical weight between 0.05 and 0.10 mg, composed of between 8 and 10 well-preserved and clean specimens. Stable oxygen- and carbon-isotope analysis was conducted on a Finnigan MAT 251 mass spectrometer using a KIEL automated sampling device. The tests of the foraminifera were reacted with concentrated orthophosphoric acid at 75°C. Calibration to the standard Pee Dee Belemnite was via the NBS18, NBS19 and NBS20 standards. Analytical precision for oxygen- and carbon-isotope analyses was ±0.08 and ±0.04‰, respectively.

5. Oxygen-isotope stratigraphy and age model

The planktonic foraminiferal isotope records for GeoB 1706 and GeoB 1711 were produced from the tests of *Gr. inflata*, and the benthic foraminiferal oxygen-isotope record was produced from *C. wuellerstorfi*. The oxygen-isotope records were subsequently correlated with the stacked record of Imbrie et al. (1984) to obtain an age model for the cores. Nine isotopic events within the last 140 kyr were identified in GeoB 1711 by using the benthic foraminiferal oxygen-isotope record, and eight events for GeoB 1706 by using the planktonic foraminiferal oxygen-isotope record (Table 1). For further correlation between the two cores we used seven tie-lines between the two *Gr. inflata* records based on both the oxygen- and carbon-isotope profiles (Fig. 4). Correlation between the planktonic foraminiferal isotope records revealed a period of non-deposition, or a hiatus, at site GeoB 1706 during isotope substages 5.5–5.2.

The GeoB 1706 foraminiferal isotope record illustrates the missing heavy values of $\delta^{13}C$ in

Table 1
Age control-points for the oxygen-isotope curves of GeoB 1706 and GeoB 1711 (Imbrie et al., 1984)

Isotope stage	Depth (cm)		Age (kyr)
	GeoB 1711[a]	GeoB 1706	
1.1		18	6
2.0		78	12
2.2	191	153	19
3.3	461		53
4.2	556		65
5.0		693	71
5.1	686		80
5.2	746	838	87
Hiatus end		843	87.5
5.3	821		99
5.4	901		107
5.5	981		122
Hiatus start		848	126.5
6.0		873	128
6.2	1071	993	135
6.4		1068	151

Time span for the hiatus comes from comparison with $\delta^{18}O$ and $\delta^{13}C$ signatures of GeoB 1711 (Fig. 4) and the benthic foraminiferal isotope record of GeoB 1711 (Fig. 6). Depth measurements for GeoB 1711 are composite depths, and original depth for GeoB 1706.
[a]Denotes benthic foraminiferal isotope record for GeoB 1711.

isotope substage 5.3, and the missing light isotopic values of $\delta^{18}O$ in isotope substage 5.5 compared to the record of GeoB 1711. In all stable oxygen-isotope records from the Angola and Cape Basins, and the continental slope off southwestern Africa and equatorial West Africa (Schneider, 1991; Schneider et al., 1997), substage 5.5 values reach Holocene $\delta^{18}O$ minima. The $\delta^{18}O$ values for GeoB 1706 in isotopic stage 5 are higher than the Holocene values. Detailed examination of carbon- and oxygen-isotope signatures allow the hiatus to be best-fitted between the samples at 848 and 843 cm in GeoB 1706, matching 126.5 and 87.5 kyr, respectively, in GeoB 1711. Fig. 5 shows the carbon-isotope records of GeoB 1711 and GeoB 1706 to directly compare the records adjusted for age. The maximum of $\delta^{13}C$ in substage 5.3 is clearly missing, whilst the excellent correlation in early stage 5 marks the isotope substage 5.5 start of the hiatus. The $\delta^{18}O$ stratigraphy of the complete benthic foraminiferal record (Fig. 6) further clarifies the missing section of sediment within mid-stage 5. Alkenone-derived SST data for both GeoB 1706 and GeoB 1711 reinforce the age model described (Müller, unpubl.), and further suggests the presence of a hiatus between substages 5.5 and 5.2 in GeoB 1706.

6. Results

Twenty eight planktonic foraminiferal species were identified using the taxonomic concepts of Parker (1962) and the Neogene planktonic foraminiferal classification of Kennett and Srinivasan (1983). For the purpose of this paper all dextral neogloboquadrinids are grouped as *N. pachyderma* (d) including all adult forms of *Neogloboquadrina dutertrei* d'Orbigny, thus accounting for the problem of the *N. pachyderma* intergrades of Kipp (1976). Similarly, Mix and Morey (1997) grouped an "upwelling assemblage" of *N. pachyderma* (d), *Gg. bulloides* and *N. dutertrei* as we use here. In both cores, seven species have an average abundance greater than 1%, and of those, four species (*N. pachyderma* (s), *Gg. bulloides*, *N. pachyderma* (d) and *Gr. inflata*) make up, on average, over 95% of the total assemblage (Plate I). The relative abundances of planktonic foraminifera can be divided into a series of discrete episodes described with respect to the dominant species present in that time slice (Figs. 7 and 8).

There are four types of episode characterizing the variation of assemblages seen offshore Namibia. Episode A is dominated by *N. pachyderma* (s) when it is in abundances greater than 40% over all others. Episode B is not dominated by a single species, but consists of $\geq 20\%$ each of *N. pachyderma* (s), *N. pachyderma* (d) and *Gg. bulloides*. Episode C is dominated by two species, *N. pachyderma* (d) and *Gg. bulloides*, both contributing to a total of $\sim 80\%$ of the total assemblage. Finally, *Gr. inflata* dominates episode D when it shows abundances greater than 20%. The graphic representation of the temporal variance in episodes A–D (right hand side of Figs. 7 and 8) shows no obvious correlation with the glacial–interglacial pattern of the isotope stages (left hand side of Figs. 7 and 8).

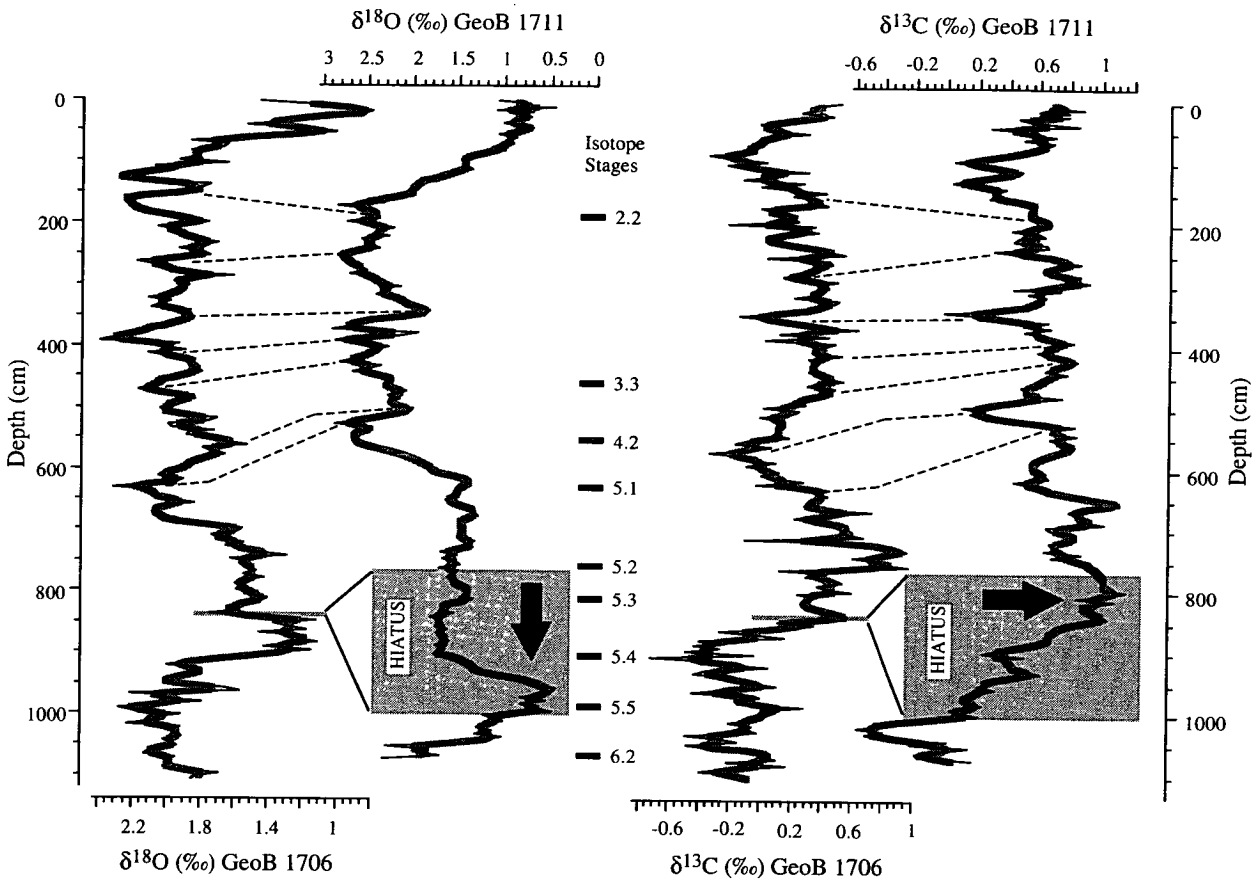

Fig. 4. Oxygen- and carbon-isotope depth profiles for GeoB 1706 and GeoB 1711. Original isotope data (thin dark lines) is superimposed on a three-point average of the same data (broad shaded lines) to help visual correlation. The age control-points for GeoB 1711 are shown to the right of the $\delta^{18}O$ record (these are derived from the benthic foraminiferal stratigraphy of *Cibicidoides wuellerstorfi*, Fig. 6). Tie lines (dashed lines), are derived primarily from the $\delta^{18}O$ signatures, and allow for detailed comparison in isotope stage 3. The tie lines have been applied to the $\delta^{13}C$ records, and agree with the positioning of those in the $\delta^{18}O$ records (see also Fig. 5). The oxygen- and carbon-isotope records highlight the absence of substages 5.5–5.3. The missing excursion to positive $\delta^{13}C$ values (substage 5.3) in GeoB 1711 and the missing excursion to Holocene, or lighter, $\delta^{18}O$ values (substage 5.5) in GeoB 1706, are indicated by arrows. Age control-points are given in Table 1 and Fig. 6.

N. pachyderma (s), which dominates Episode A and forms a substantial part of Episode B, is the second most abundant species. It shows the most notable fluctuations, with maxima over 20%, up to 60% in stages 3–2 and stage 6.4 of GeoB 1706, and similarly in GeoB 1711 with additional maxima in substages 5.5, 5.4 and 5.3. *N. pachyderma* (d), which makes up episodes B and C with *Gg. bulloides*, has an average abundance of 27% and is the most abundant species present. *N. pachyderma* (d) varies substantially with age, showing several maxima throughout the last 160 kyr, and varying between 0 and 80% of the total planktonic foraminifera. With an average abundance of 25%, *Gg. bulloides* records the third highest abundance in the core, commonly recording rapid fluctuations from 10 to 50% throughout the last 160 kyr, relatively independent of glacial–interglacial conditions. Episode D consists largely of *Gr. inflata*, which shows a gradual increase to its peak abundance in stage 5.1 before a drop to previous stage 6 levels.

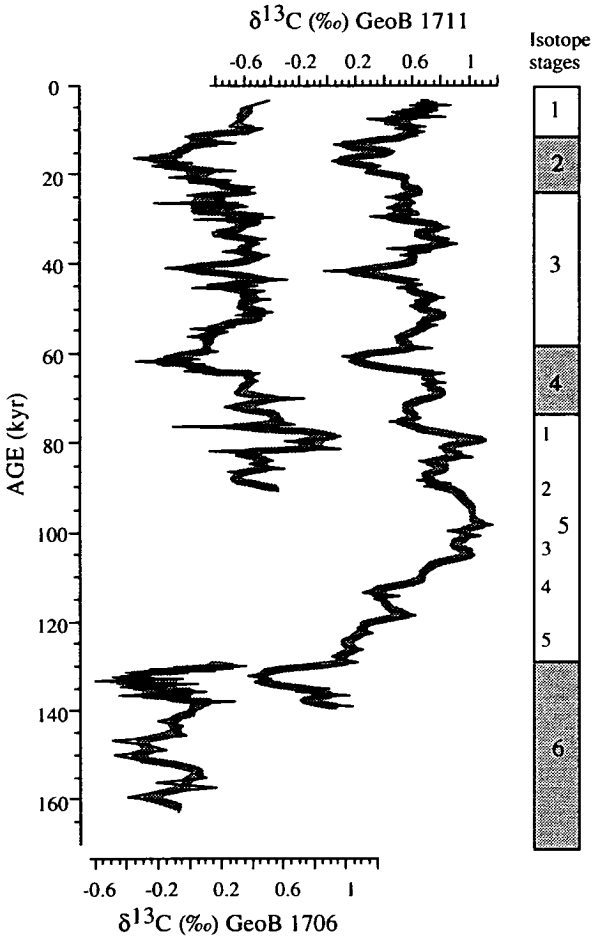

Fig. 5. Carbon-isotope stratigraphy for GeoB 1706 and GeoB 1711 with respect to age. Original data (dark thin line) is superimposed on a three-point average (broad shaded line). The excellent correlation of the two $\delta^{13}C$ records versus age clarifies the positioning of the hiatus boundaries in the interval of substages 5.5–5.2. The record shows an excellent correlation of the two datasets between stages 4–2, where are two records are linked using the $\delta^{18}O$ tie lines (dashed lines, Fig. 4).

7. Discussion

7.1. Planktonic foraminifera and nutrient availability

The planktonic foraminiferal records in the two cores under study are subdivided into episodes characterized by specific foraminiferal assemblages (Figs. 7 and 8). *N. pachyderma* (s), which dominates Episode A, has the greatest influence on the major fluctuations in the system. *N. pachyderma* (s) does not vary with the changes in the global hydrological cycle, described by $\delta^{18}O$ variations (Imbrie et al., 1984), but instead shows a higher frequency of change with abundance maxima throughout isotope stages 6–2, including interglacial stage 5 (Little et al., 1995). Previous investigations within the BCS have distinguished a good agreement with the distribution patterns of the planktonic foraminifera, nutrient levels and surface water hydrography (Giraudeau, 1993; Ufkes and Zachariasse, 1993; Ufkes, 1997). Giraudeau et al. (1997) found a similar pattern when they studied coccolith abundances in the same area. On the basis of factor analysis they correlated the abundances of coccolith species to the modern-day distribution of trophic areas. A comparison of planktonic foraminiferal (Fig. 3) and coccolith distributions in Recent surface sediments (Giraudeau, 1993; Giraudeau et al., 1993; Giraudeau and Rogers, 1994), reveals a striking similarity to the modern-day trophic-level distribution, indicating a relationship between foraminifera type/number and nutrient levels within the Benguela Upwelling System, similar to other oceanic settings (Reynolds and Thunnel, 1985; Kroon and Ganssen, 1989; Kroon, 1991). The fossil assemblages are thus best interpreted with respect to a temporally varying nutrient availability or supply (Figs. 7 and 8). Episodes type A and D infer eutrophic (high) and relatively oligotrophic (low) nutrient levels, respectively, when the observed modern-day nutrient–foraminiferal relationship is applied. Eutrophic Episode A, would be correlated with the trophic situation presently occurring in the nearshore upwelling centres, particularly intense off Lüderitz and further south in the SBR. The offshore, subtropical conditions of the SBR, would be representative of Episode D trophic levels. Episodes B and C would characterize intermediate, mesotrophic conditions, typical of the mixed zone offshore in the NBR, similar to the modern-day situation at the sites of GeoB 1706 and GeoB 1711. At the site of GeoB 1706, eutrophic conditions dominated the oceanographic setting during isotope sub-stage 6.4 and stages 3 and 2. At site GeoB 1711, the planktonic foraminiferal record similarly suggests upwelling conditions throughout stage 3 and into

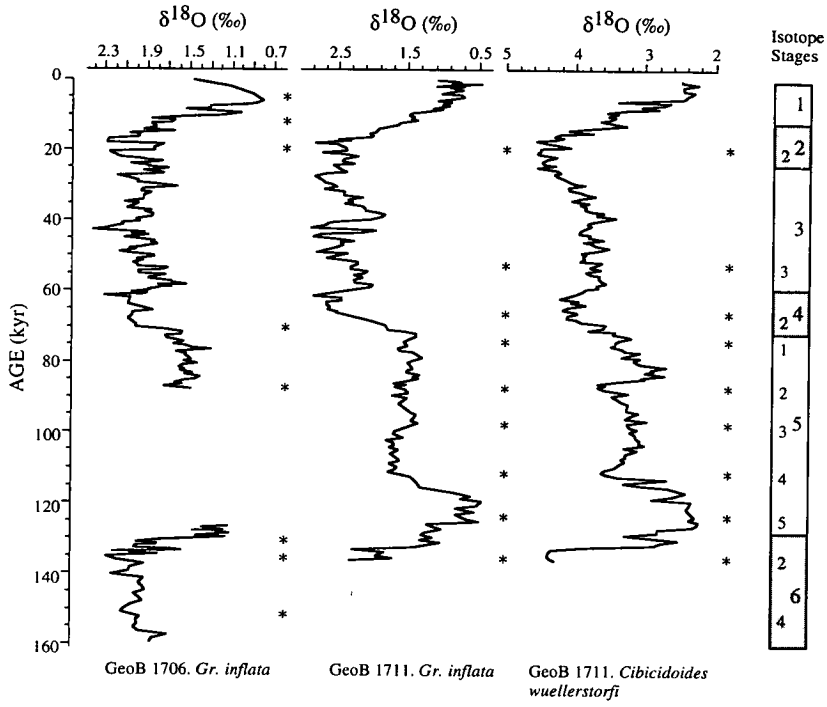

Fig. 6. Oxygen-isotope stratigraphy for GeoB 1706 and GeoB 1711 with respect to age. Planktonic foraminiferal records from *Gr. inflata*, for GeoB 1706 and GeoB 1711, highlight the hiatus in GeoB 1706 in isotope stage 5. Note that isotope values in GeoB 1706 do not reach the light isotopic values of the Holocene, as seen in GeoB 1711. The benthic foraminiferal oxygen-isotope record of GeoB 1711 is shown for comparison. Isotope stages are given on the right hand side, and age control-points are identified (*) to the right of each isotope record.

early stage 2. Both core sites record subtropical, relatively oligotrophic conditions dominating late stage 5.

7.2. Angola–Benguela Front migration, upwelling intensification or cold-water advection?

A fluctuation in nutrient supply could be explained by three different conditions within the BCS. Firstly, upwelling intensity, which would have the effect of widening the zone of *N. pachyderma* (s) displacing further offshore the boundary between eutrophic and mesotrophic watermasses [boundary between *N pachyderma* (s) and other species, Fig. 3]. Secondly, a physical shift of the ABF and corresponding trophic zones equatorwards, bringing increased nutrient levels to the north. Thirdly, a sporadic injection of cold, nutrient-rich water advecting from the Southern Ocean past Cape Town and along the eastern edge of the

Plate I

Photographs of the four main planktonic foraminifera from the Benguela Upwelling System.

1–5. *N. pachyderma* (sinistral), scale bar = 200 μm—note extra bullae in 5, a common feature in the Benguela species.

6–8. *Gg. bulloides*, scale bar = 500 μm—note large offset bullae in 7 and 8, again a common feature of the Benguela species.

9, 10. *N. pachyderma* (dextral), scale bar = 300 μm.

11, 12. *N. pachyderma* (dextral)–*N. dutertrei* intergrades, scale bar = 300 μm.

13. *N. dutertrei* (adult, scale bar = 500 μm). All *N. dutertei* forms are included in *N. pachyderma* (d) counts.

14–17. *Gr. inflata*, scale bar = 400 μm—note bullae in 14, and variance in wall structure similar to *Globorotalia puncticulata*, in 15; however, three chambers in final whorl allows classification as *Gr. inflata*.

PLATE I

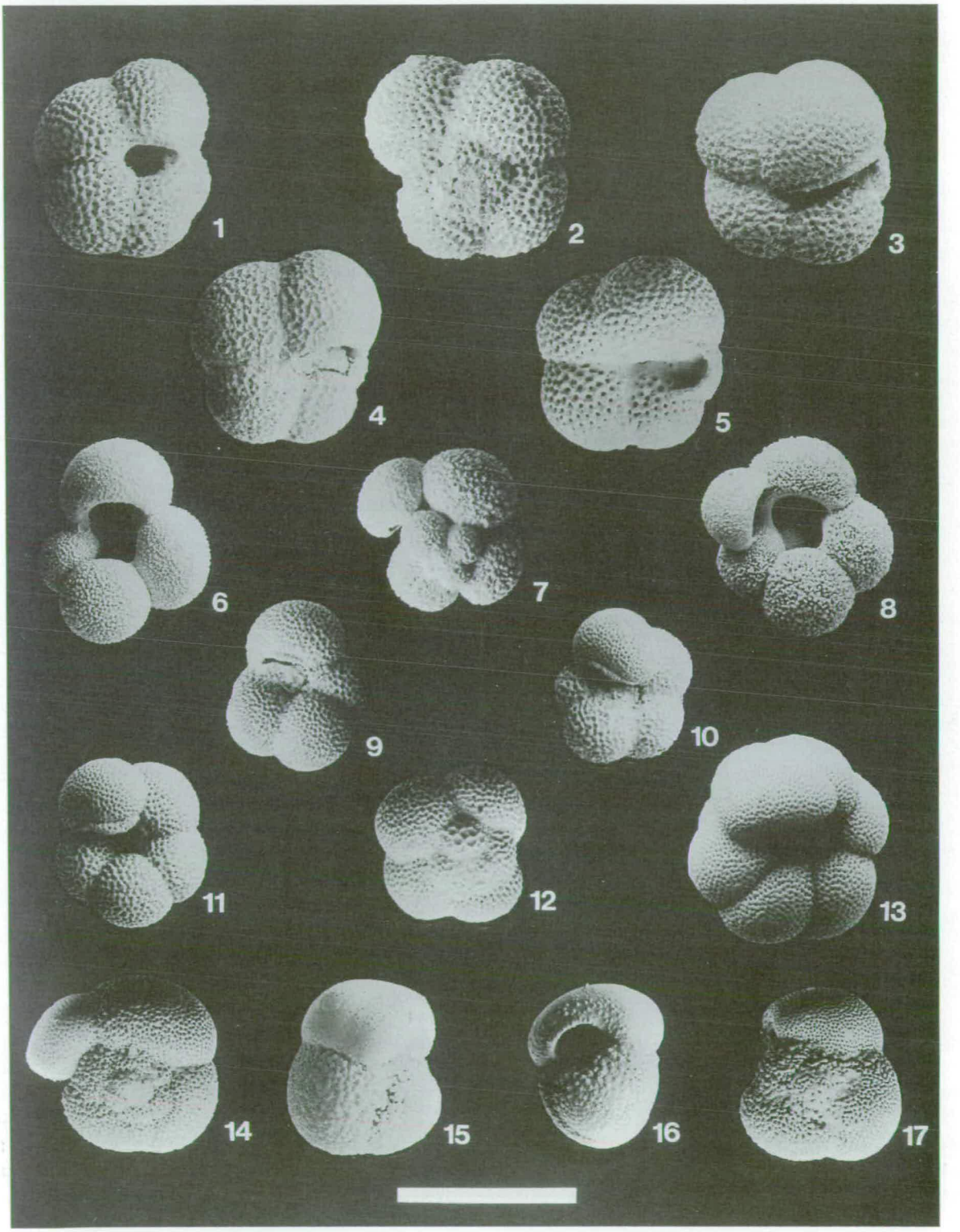

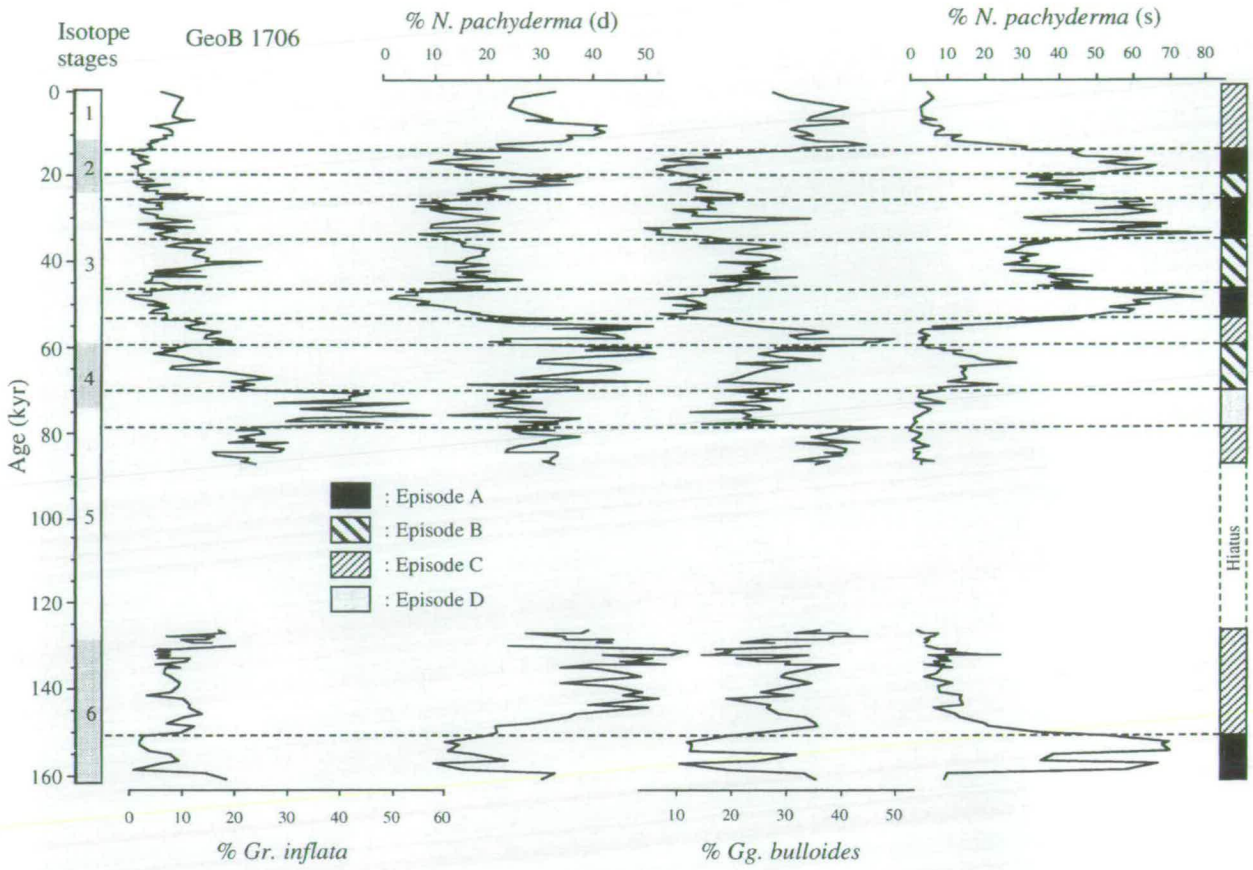

Fig. 7. Fluctuations in the relative abundances of the four major species of planktonic foraminifera with age. Isotope stages are given on the left for reference, whilst a schematic reference for episode dominance is given on the right. Episode *A*: Dominance of *N. pachyderma* (s) > 40% over all others; Episode *B*: 20% each (or >) of *N. pachyderma* (s), *N. pachyderma* (d) and *Gg. bulloides*; Episode *C*: Dominance of *N. pachyderma* (d) + *Gg. bulloides* both contributing to a total of ~80%; Episode *D*: *Gr. inflata* > 20%. See text for discussion.

BCS. All of these conditions would be observed in the fossil record by a relative enhancement of the typical upwelling fauna, in particular *N. pachyderma* (s). An alternative hypothesis, an increase in the nutrient supply by poleward undercurrents from the Angola Basin, was postulated by Summerhayes et al. (1995a) and Struck et al. (1993) using the $\delta^{13}C$ record of the surface dweller *Gg. ruber*, although no firm evidence for nutrient enrichment from the north has been proven.

The distribution of planktonic foraminiferal zones is linked to the oceanographic regimes which are presently occurring off the southwest African coast. The coccoliths and planktonic foraminifera (Giraudeau and Rodgers, 1994) seem to be responding primarily to nutrient availability, and thus upwelling intensification and/or advection of Southern Ocean surface waters. Jansen et al. (1997) recorded high abundances of *N. pachyderma* (s), within the Angola Basin, with maximum abundances throughout the last 160 kyr, and a peak in abundance during early isotope stage 3. The variation in planktonic foraminiferal abundances was correlated to physical shifts of the ABF in response to changes in the intensity and position of the South Atlantic Gyre and the Subtropical Convergence (STC). An equatorwards deflection of the ABF would produce a shift of

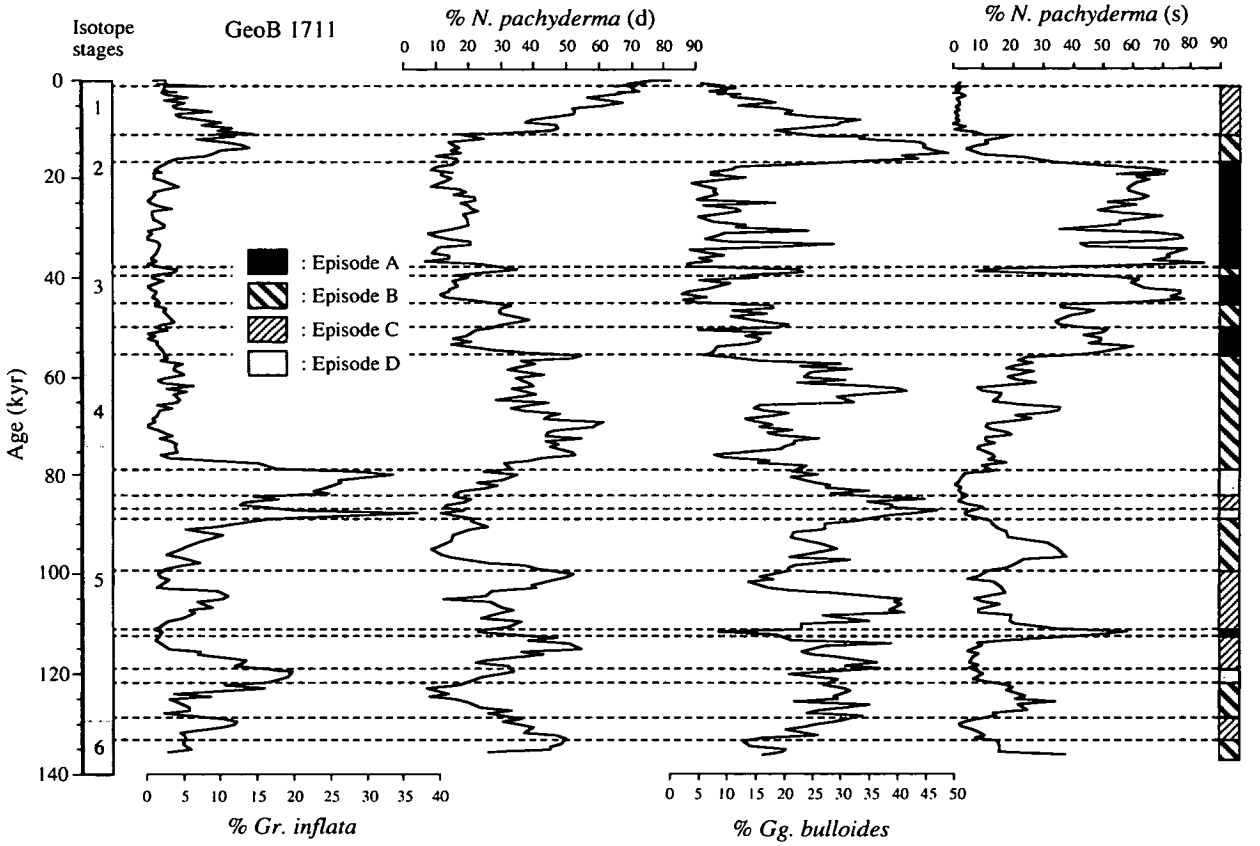

Fig. 8. Fluctuations in the relative abundances of the four major species of planktonic foraminifera with age. Isotope stages are given on the left for reference, whilst a schematic reference for episode dominance is given on the right. Episode *A*: Dominance of *N. pachyderma* (s) > 40% over all others; Episode *B*: 20% each (or >) of *N. pachyderma* (s), *N. pachyderma* (d) and *Gg. bulloides*; Episode *C*: Dominance of *N. pachyderma* (d) + *Gg. bulloides* both contributing to a total of ~80%; Episode *D*: *Gr. inflata* > 20%. See text for discussion.

the more eutrophic areas [dominated by *N. pachyderma* (s)] to the north, whilst a poleward shift would decrease the relative nutrient supply at the Walvis Ridge by moving the upwelling centers south. In the extreme case, a large poleward displacement of the ABF as far as GeoB 1706 could be possible, extending the southerly intrusion of warm Angolan water onto the Walvis Ridge. If the whole Benguela Upwelling System were to move with the ABF, we would predict maxima of *N. pachyderma* (s) at times of equatorward shifts.

The temporal fluctuations in the two planktonic foraminiferal records correlate well with the shifts of the ABF, described by the Benguela Index (Fig. 9). The fluctuations of *N. pachyderma* (s) in GeoB 1706 and GeoB 1711 are directly comparable to similar peaks at 60–70 kyr in stage 4, and 45–50 and 30–35 kyr in stage 3, as seen in T89-32 (14°58.2′S, 10°41.6′E; Fig. 2) and T89-24 (8°54.7′S, 12°03.1′E) from the Angola Basin. Jansen et al. (1997) predict major equatorward shifts in isotope stage 4 and substages 3.3–3.1, and maximum poleward shifts in isotope substages 6.3, 5.5 and stage 1, although not a major equatorward shift at the LGM. In addition, the ABF record shows a similar position in late isotope stage 6–early stage 5 to that of the Holocene. These shifts are mirrored in the Benguela Index records of GeoB 1706 and GeoB 1711, although there are differences, but they are mainly related to discrepancies within the

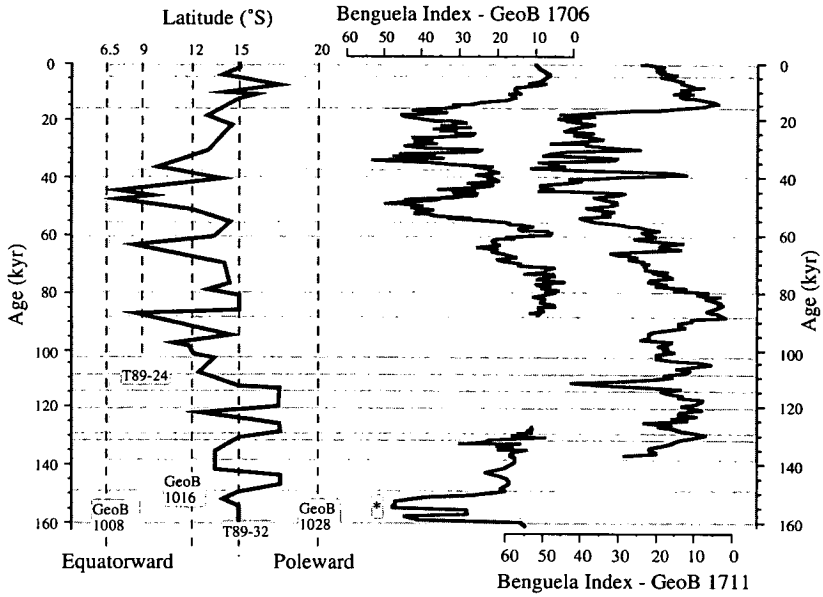

Fig. 9. Comparison of the Benguela Index transfer function of Jansen et al. (1997) (left) with data from GeoB 1706 and GeoB 1711 (right). The Benguela Index function is used to assess relative N–S (equatorward–poleward) movements of the ABF, derived from *N. pachyderma* (s) abundances in five cores from the Angola–Zaire margin. High *N. pachyderma* (s) abundances indicate equatorward shifts of the ABF, and are highlighted for GeoB 1711 and GeoB 1706. The difference in temporal resolution between the Cape and Angola Basin records, probably results in some minor discrepancies, but overall the two records are in agreement. Periods of increased Cape Basin upwelling intensity broadly coincide with equatorward shifts of the ABF. The GeoB 1706 *N. pachyderma* (s) anomaly in isotope stage 6.4 is highlighted (*). The Benguela Index is given as (2/3 × left coiling + 1/3 × right coiling) *N. pachyderma* (Jansen et al., 1997).

age models of the cores. GeoB 1706 records high abundances of *N. pachyderma* (s) in isotope substage 6.4, and much higher abundances of *N. pachyderma* (s) in stage 2, in particular at the LGM, correlating to strong equatorward shifts of the ABF not seen in the Benguela Index of the Angola Basin (Fig. 9).

Alkenone-derived SST estimates (Schneider et al., 1995, 1997; Summerhayes et al., 1995b) indicate that the coolest period in the BCS and the Angola Basin is centred on the lower part of isotope stage 3, exactly when *N. pachyderma* (s) abundances are at their maximum (Figs. 7 and 8). Jansen et al. (1997) proposed the greatest equatorward shift of the ABF at this time based on a maximum of *N. pachyderma* (s) at site T89-32 (Fig. 9). The implied temporal ABF movements are supported by a variety of data, primarily the general agreement of *N. pachyderma* (s) abundances, as seen in GeoB 1706 and GeoB 1711, GeoB 1028 (Schmidt, 1992), DSDP 532 (Oberhänsli, 1991) and T89-32 (Jansen et al., 1997) with alkenone-derived SSTs, which have been recorded by Schneider et al. (1995, 1997) and Summerhayes et al. (1995b). The seemingly anomalous, almost monospecific, assemblage at site GeoB 1706 in stage 6.4, followed by a lack of *N. pachyderma* (s) in late stage 6, is corroborated by SST data from a core on the Angola Margin (GeoB 1016) with a corresponding cool stage 6.4 and a warmer late stage 6 (Schneider et al., 1995).

From cores on the Angola Margin, the Walvis Ridge, the Congo Fan and the equatorial Atlantic Schneider et al. (1995, 1997), using alkenone-derived SSTs, indicated that the ABF has not shifted substantially in the last 200 kyr, and has remained between 12 and 20°S. Jansen et al. (1997), however, recorded high *N. pachyderma* (s) abundances in cores between 6.5 and 20°S implying larger movements of the ABF. The difference

between the two datasets may be related to the habitat of the coccolithophores from which the alkenones and SSTs are derived. The alkenones, and therefore SSTs, are dependent upon the biogeographic limits of coccolithophorids (review by Brassel, 1993). The coccolithophores respond to averaged temperature changes within the water-mass they inhabit, and often co-vary with the global glacial–interglacial regime (Müller et al., 1997, and others therein) and not directly with upwelling (Ten Haven and Kroon, 1991; Emeis et al., 1995). *N. pachyderma* (s) in the BCS, however, is found in the cores of the upwelling cells (Ufkes and Zachariasse, 1993; Ufkes, 1997) and records the immediate, intensification of upwelling seemingly unaffected by the glacial–interglacial pattern. *N. pachyderma* (s) records the maximum fluctuations of the ABF, whilst the coccolith-derived SSTs are measuring the averaged effect of the upwelling cell fringes and global glacial–interglacial regime, not the position of the upwelling cores themselves. Most likely it is the combined effect of the physical movement of the ABF and an increase in upwelling intensity which accounts for the planktonic foraminiferal variations seen in the Angola and Cape basins.

Many of the previous studies in the BCS (McIntyre et al., 1989; Schneider et al., 1995; Summerhayes et al., 1995b; Jansen et al., 1997) have discussed advection of Southern Ocean surface or intermediate waters as a result of equatorward shifts of the Subtropical Convergence (STC). Morley (1989) and Howard and Prell (1992), studied the movements of the STC, situated to the south of Cape Town, marking the boundary between cold, polar-waters from the Southern Ocean and warmer waters of the South Atlantic. Using cores in the southern Indian Ocean, they recorded maximum poleward positions of the STC in isotope stages 11, 9, 5 and 1, from planktonic foraminiferal and radiolarian evidence, whilst maximum equatorward positions were recorded in isotope stages 12, 10, 8, 6 and 4–2. The movements of the STC can be described by a two end-member system: (1) maximum poleward position of the STC, permitting the largest pulses of Indian Ocean water entry into the Atlantic, which is accompanied by maximum equatorward heat advection into the BCS and the maximum poleward position of the ABF; and (2) maximum equatorward position of the STC, limiting the amount of Agulhas Current advecting into the Atlantic by formation of a thermal barrier or gradient off Cape Town. This may, in extreme cases, allow an increase in cold-water advection from either the South Atlantic Surface Water (SASW) or the Antarctic Intermediate Water (AAIW) below, without necessitating an unlikely shift of the polar front (Shannon et al., 1989). However, although the timing of events links well with the shifting of the ABF, as proposed by Jansen et al. (1997) and this paper, it still does not conclusively argue for or against an advectionally controlled system. For further evidence planktonic foraminiferal or SST data from the SBR are needed to record equatorward heat flux around and past the Cape of Good Hope.

New core material and planktonic foraminiferal data (Little, 1997) were collected on the recent leg of the R.V. *Meteor* cruise M32/1 (January 1996). Onboard sampling and foraminiferal analysis has yielded the first conclusive evidence against cold-water advection from the south. Seven cores were recovered from varying water depths along three transects covering the Cape Basin from Cape Point to the Walvis Ridge. The cold-water *N. pachyderma* (s) was found to be almost completely absent in continental-slope cores from 2000 and 3000 m off Cape Town for the last 200,000 years (cores GeoB 3603 and GeoB 3602; Table 2). We are unable to report on the temporal fluctuations of the planktonic foraminiferal abundances in these cores as oxygen-isotope age models have not yet been produced. No obvious sign of selective dissolution was observed and the other planktonic forms, typical of the SBR, were in great abundance with significant numbers of tropical forms, presumably intruding around from the Indian Ocean. A trend to higher maxima and average values is clearly obvious in a traverse from the Southern Cape Basin to the north (Table 2). Full datasets and complete planktonic foraminiferal analyses are given in Little (1997). If northward advection was to play a major role in the planktonic foraminiferal variations seen in the Benguela Upwelling System, then we would almost certainly see the highest

Table 2
Average and maximum relative abundances of sinistral coiling *N. pachyderma* for all cores analysed

Core site (water depth, m) listed north to south	Core position	Average abundance *N. pachyderma* (s)	Maximum abundance *N. pachyderma* (s)
GeoB 1706 (980)	19°33.7'S, 11°10.5'E	29.38	81.76
GeoB 3608 (1972)	22°21.5'S, 12°12.0'E	28.72	75.47
GeoB 1711 (1967)	23°18.9'S, 12°22.6'E	25.90	84.2
GeoB 3606 (1785)	25°28.0'S, 13°05.0'E	11.83	23.91 (38.60)
GeoB 3605 (1375)	31°26.7'S, 15°17.8'E	6.04	21.28 (36.07)
GeoB 3604 (1514)	31°47.1'S, 15°30.0'E	3.00	15.25
GeoB 3603 (2840)	35°07.5'S, 17°32.6'E	0.85	4.00
GeoB 3602 (1885)	34°47.9'S, 17°45.3'E	1.99	8.47 (21.54)

Values for GeoB 3606, GeoB 3605 and GeoB 3602 are marked by single excursions (anomalies) to higher values; first number given is the second highest recorded abundance. Within the three most southerly (poleward) cores (GeoB 3602, GeoB 3603 and GeoB 3604), values of abundance only exceed 10% four times in 30 m of core sampled. Note that average relative abundances are much lower in the southern reaches of the Cape Basin and that there is a positive trend to high values equatorward into the Northern Cape Basin. Core characteristics for GeoB 3602-GeoB 3608 are given in Bleil et al. (1996).

abundances of the cold-water *N. pachyderma* (s) in the south of the region, not the almost zero abundances actually recorded. We would therefore conclude that the ABF and trophic-area shifts described are responding primarily to changes in upwelling intensity via fluctuations in the BCS.

7.3. Trade wind forcing

McIntyre et al. (1989) used planktonic foraminiferal estimates of SST to estimate seasonality in the equatorial Atlantic. Seasonality maxima, largest summer–winter temperature range, are recorded at similar times to greatest upwelling intensity in the BCS, and broadly coincide with the relative shifts of the ABF (Jansen et al., 1997). Trade wind zonality is strongly related to the seasonality at the equator (Mix et al., 1986; Imbrie et al., 1989; McIntyre et al., 1989; Little et al., 1995; Schneider et al., 1995; Mix and Morey, 1997), and also contributes to most of the SST, palaeoproductivity and palaeoceanography variations within the BCS (Schneider et al., 1995; Summerhayes et al., 1995b; Jansen et al., 1997; Mix and Morey, 1997; Schneider et al., 1997, submitted). The records of GeoB 1706 and GeoB 1711 suggest intensification of upwelling in the northern Cape Basin coinciding with increased equatorial and Angola Basin upwelling, at times of increased trade wind zonality. There is no evidence in support of the advection of Southern Ocean water across the STC, and equatorward heat advection, other than that from upwelling via the BCS, plays a minor if not insignificant role in equatorial and Angola Basin palaeoceanography. It is the injection of newly upwelled BCS waters, rather than advection of Southern Ocean water, which McIntyre et al. (1989) observed at the equator. The BCS is driven by atmospheric conditions controlling trade wind intensity and zonality over Southwestern Africa (McIntyre et al., 1989; Schneider et al., 1995, 1997; Mix and Morey, 1997). Times of maximum abundances of *N. pachyderma* (s), indicate maximum offshore divergence and associated upwelling intensity, at times of maximum trade wind intensity and zonality.

Summerhayes et al. (1995b) suggested that upwelling increased in stages 4 and 3, but declined into stage 2. This was attributed to an equatorward shift of the trade winds in stage 2, leading to a marked decrease in upwelling at site PG/PC12. The planktonic foraminiferal record of GeoB 1711, on the continental slope nearby to PG/PC12, indicates that upwelling off Walvis Bay was intense throughout isotope stage 3 into early stage 2, with a decrease of intensity and associated reduction in zonality of the trade winds, from 15 ka to the present.

Trade wind zonality and intensification are intrinsically linked to global-atmosphere-cryo-

sphere changes for at least the last 160,000 yr. Planktonic foraminifera, SST and isotope records from sediment and ice cores in all of the world's major oceans (Yiou et al., 1991; Bond et al., 1992; Grousset et al., 1993; Park et al., 1993; Bender et al., 1994; Hagelberg et al., 1994; Mayewski et al., 1994; Kennett and Ingram, 1995; Little et al., 1995; Behl and Kennett, 1996; Charles et al., 1996), record similar rapid, discrete events to those of the *N. pachyderma* (s) records of the BCS. The Benguela Upwelling system is in an important position that may influence cross-equatorial and inter-ocean heat flux. Further investigation into the timing and correlation of these global events is necessary to understand the complexity of cross-equatorial and inter-ocean teleconnections.

8. Summary

The planktonic foraminiferal records for GeoB 1706 and GeoB 1711 show that the abundance of the cold-water planktonic foraminifer, *N. pachyderma* (s), does not vary with the global glacial–interglacial pattern. Four species make up over 95% of the variation within the core, and enable the record to be divided into episodes characterized by specific planktonic foraminiferal assemblages, with meaningful ecological significance when compared to those of the modern day. *N. pachyderma* (s), dominates the modern-day, coastal upwelling centres; *Gr. inflata* characterizes the oligotrophic, offshore zone of the SBR; and together, *Gg. bulloides* and *N. pachyderma* (d) inhabit the mesotrophic areas of the mixed zone in the NBR. In the fossil record, the planktonic foraminifera are thought to be varying largely with changing nutrient supply, and the subsequent levels of primary productivity, according to local water hydrography and oceanography currently existing offshore Namibia and western South Africa. In cores GeoB 1706 and GeoB 1711, episodes of high *N. pachyderma* (s) abundances are interpreted as evidence of increased upwelling intensity, and the associated increase in nutrients. Periods of high *N. pachyderma* (s) abundances describe rapid, discrete events dominating isotope stages 3 and 2, the timing of which correlate to the temporal shifts of the Angola–Benguela Front situated to the north of the Walvis Ridge. The physical movement of the ABF cannot be disassociated from the increase in upwelling intensity recorded in the fossil record. The absence of high abundances of *N. pachyderma* (s) from the continental slope of the southern Cape Basin conclusively rules out Southern Ocean surface water advection. Upwelling intensification along the entire coast of western and southwestern Africa is generated by changes in the strength and zonality of the trade wind system, responding to similar shifts and intensity of the atmospheric and oceanic gyres. Similar rapid events in all of the world's oceans suggest global variations in cross-equatorial and inter-ocean teleconnections.

Acknowledgements

We thank the crew and scientists aboard R.V. *Meteor* for their help with coring and sampling operations during cruises to the South Atlantic. We are grateful to Colin Summerhayes, Wolfgang Berger, John Rogers and Kate Darling whose comments and critical review significantly improved the manuscript. We would also like to thank Monika Segl and Birgit Meyer-Schack for their assistance with the mass spectrometers and both Alastair Matthewson and Ian Alexander for their helpful advice and discussion. This research was funded by the Natural Environmental Research Council (NERC grant GR3 8344 at Edinburgh University) and the Deutsche Forschungsgemeinschaft (Sonderforschungsbereich 261 at Bremen University, Contribution No. 132).

Appendix A

Oxygen-isotope data from GeoB 1711, using the benthic foraminifer *Cibicidoides wuellerstorfi*. The depth scale is the combined depths of the upper box core and the longer gravity core. The $\delta^{13}C$ and $\delta^{18}O$ values are both parts per thousand (‰)

Depth	$\delta^{18}O$	Depth	$\delta^{18}O$	Depth	$\delta^{18}O$	Depth	$\delta^{18}O$
(cm)	(‰)	(cm)	(‰)	(cm)	(‰)	(cm)	(‰)
1	2.49	271	3.86	541	4.06	811	3.23
6	2.50	276	4.11	546	3.83	816	3.20
11	2.24	281	4.08	551	4.11	821	3.10
16	2.48	286	3.91	556	4.18	826	3.21
21	2.48	291	3.87	561	3.99	831	3.13
26	2.46	296	3.72	566	3.97	836	3.11
31	2.30	301	3.91	571	4.11	841	3.07
36	2.35	306	4.05	576	4.13	846	3.09
41	2.39	311	3.80	581	3.98	851	2.98
46	2.44	316	3.93	586	3.91	856	3.30
51	2.48	321	3.84	591	3.56	861	3.10
56	3.40	326	3.86	596	3.58	866	3.27
61	2.64	331	3.76	601	3.60	871	3.25
66	2.77	336	3.60	606	3.80	876	3.33
71	3.05	341	3.70	611	3.41	881	3.28
76	2.80	346	3.41	616	3.46	886	3.35
81	3.26	351	3.63	621	3.24	891	3.41
86	3.56	356	3.80	626	3.18	896	3.55
91	3.39	361	3.82	631	3.37	901	3.61
96	3.54	366	3.76	636	3.41	906	3.54
101	3.43	371	3.86	641	3.42	911	3.36
106	3.53	376	3.93	646	3.49	916	2.67
111	3.65	381	3.94	651	3.32	921	3.29
116	3.45	386	3.78	656	3.27	926	3.02
121	3.27	391	3.81	661	3.05	931	2.66
126	3.55	396	3.59	666	3.20	936	2.53
131	3.96	401	3.88	671	3.32	941	2.40
136	4.10	406	3.77	676	3.06	946	2.59
141	3.76	411	3.71	681	3.16	951	2.88
146	4.22	416	3.52	686	3.09	956	2.31
151	4.31	421	3.67	691	3.04	961	2.33
156	4.18	426	3.91	696	2.69	966	2.36
161	4.30	431	3.85	701	2.89	971	2.38
166	4.57	436	3.90	706	2.86	976	2.33
171	4.39	441	3.87	711	2.99	981	2.30
176	4.27	446	3.93	716	2.70	986	2.26
181	4.08	451	3.62	721	3.04	991	2.34
186	4.49	456	3.69	726	2.99	996	2.20
191	4.50	461	3.80	731	3.39	1001	2.23
196	4.56	466	3.62	736	3.66	1006	2.30
201	4.51	471	3.83	741	3.55	1011	2.79
206	4.26	476	3.77	746	3.66	1016	2.79
211	4.41	481	3.64	751	3.57	1021	3.27
216	4.48	486	3.67	756	3.22	1026	2.91
221	4.45	491	3.62	761	3.47	1031	2.51
226	4.28	496	3.56	766	3.40	1036	2.76
231	4.55	501	3.70	771	3.33	1041	2.85
236	4.27	506	3.66	776	3.23	1046	3.86
241	4.21	511	3.84	781	3.24	1051	4.32
246	4.31	516	3.89	786	3.25	1056	4.35
251	4.25	521	3.98	791	3.07	1061	4.37
256	4.16	526	4.11	796	3.17	1066	4.34
261	4.08	531	4.21	801	3.26	1071	4.27
266	4.02	536	3.95	806	2.95		

Oxygen- and carbon-isotope data from GeoB 1706, using the planktonic foraminifer *Globorotalia inflata*. The $\delta^{13}C$ and $\delta^{18}O$ values are both parts per thousand (‰)

Depth (cm)	$\delta^{18}O$ (‰)	$\delta^{13}C$ (‰)	Depth (cm)	$\delta^{18}O$ (‰)	$\delta^{13}C$ (‰)	Depth (cm)	$\delta^{18}O$ (‰)	$\delta^{13}C$ (‰)	Depth (cm)	$\delta^{18}O$ (‰)	$\delta^{13}C$ (‰)
3	1.46	0.52	283	1.85	0.15	558	1.67	−0.16	833	1.56	0.48
8	1.12	0.33	288	1.62	0.16	563	1.52	0.06	838	1.74	0.56
13	0.91	0.34	293	1.94	0.49	568	1.80	−0.06	843	1.48	0.56
18	0.81	0.25	298	1.96	0.36	573	1.74	−0.34	848	1.12	0.12
23	0.88	0.46	303	1.87	0.44	578	1.66	−0.04	853	1.37	0.36
28	0.97	0.39	308	1.93	0.34	583	1.78	−0.13	858	1.28	0.20
33	1.31	0.19	313	1.93	0.38	588	1.81	0.10	863	1.17	−0.26
38	1.31	−0.02	318	1.94	0.22	593	1.89	−0.09	868	1.45	−0.05
43	1.53	0.03	323	2.12	0.51	598	1.87	0.02	873	1.18	0.16
48	1.18	0.03	328	1.98	0.47	603	1.91	0.12	878	1.22	−0.41
53	1.01	0.30	333	2.04	0.31	608	2.02	0.00	883	1.11	−0.26
58	1.21	0.01	338	2.10	0.39	613	2.05	0.10	888	1.28	−0.44
63	1.53	−0.01	343	1.86	0.12	618	1.90	0.28	893	1.42	−0.27
68	1.87	0.01	348	1.93	−0.14	623	1.95	−0.03	898	1.15	−0.49
73	1.65	−0.10	353	1.85	0.12	628	2.05	0.23	903	1.40	−0.04
78	1.68	−0.05	358	1.86	0.20	633	2.31	0.45	908	1.42	−0.72
83	1.87	−0.06	363	2.01	0.29	638	2.06	0.36	913	1.74	−0.28
88	1.83	−0.35	368	1.97	0.63	643	2.07	0.44	918	1.88	−0.20
93	1.82	−0.19	373	2.13	0.39	648	2.08	0.34	923	1.99	0.05
98	1.93	0.02	378	2.12	0.12	653	1.99	0.36	928	1.80	−0.35
103	1.65	−0.23	383	2.20	0.44	658	1.84	0.29	933	1.80	−0.43
108	2.07	−0.10	388	2.30	0.03	663	2.03	0.33	938	1.81	−0.16
113	1.98	0.30	393	2.41	0.48	668	2.05	0.73	943	1.99	−0.19
118	1.99	0.04	398	1.93	0.42	673	2.08	0.39	948	2.00	−0.02
123	2.27	0.05	403	2.05	0.33	678	2.04	0.23	953	2.01	0.11
128	2.27	−0.13	408	1.89	0.33	683	2.00	0.37	958	1.66	−0.21
133	2.28	0.27	413	2.11	0.52	688	2.01	0.56	963	1.56	−0.45
138	1.75	−0.00	418	2.00	0.31	693	1.71	0.57	968	2.21	−0.03
148	1.85	0.42	423	1.84	0.36	698	1.56	0.52	973	2.00	0.00
153	1.84	0.20	428	1.85	0.35	703	1.58	0.58	978	2.04	−0.15
158	2.26	0.37	433	1.87	0.33	708	1.73	0.67	983	1.79	−0.13
163	2.25	0.36	438	1.82	0.31	713	1.70	−0.10	988	2.07	0.29
168	2.24	0.42	443	1.80	0.44	718	1.65	0.71	993	2.28	0.02
173	2.20	−0.01	448	1.90	0.40	723	1.55	0.70	998	2.18	0.02
178	2.19		453	1.96	0.54	728	1.64	0.89	1003	1.91	0.01
183	2.14	0.23	458	2.07	0.38	733	1.54	0.97	1008	2.05	−0.02
188	1.97	0.17	463	2.02	0.30	738	1.47	0.85	1013	2.05	−0.21
193	1.92	0.23	468	2.09	0.48	743	1.29	0.60	1018	2.22	−0.05
198	1.76	−0.22	473	2.17	0.43	748	1.62	0.79	1023	1.91	−0.11
203	1.83	0.34	478	2.07	0.44	753	1.52	0.80	1028	1.96	−0.02
208	2.06	0.23	483	1.85	0.25	758	1.53	0.97	1033	1.93	−0.49
213	1.97	0.37	488	1.83	0.22	763	1.50	0.13	1038	1.90	−0.27
218	1.94	0.04	493	2.00	0.29	768	1.47	0.44	1043	2.01	−0.15
223	1.88	0.04	498	1.94	0.02	773	1.55	0.30	1048	1.96	−0.48
228	1.89	0.03	503	2.04	0.24	778	1.42	0.49	1053	1.93	−0.32
233	1.70	0.15	508	2.00	0.19	783	1.55	0.53	1058	2.03	−0.04
238	1.81	0.42	513	1.98	−0.01	788	1.59	0.38	1063	2.09	0.07
243	1.94	0.43	518	1.70	0.15	793	1.54	0.45	1068	2.13	0.04
248	1.80	0.55	523	1.76	0.15	798	1.58	0.60	1073	1.95	0.11
253	1.75	0.03	528	1.99	0.10	803	1.46	0.24	1078	1.99	−0.21
258	1.89	0.44	533	1.97	0.10	808	1.54	0.37	1083	1.97	0.17
263	2.18	0.45	538	1.72	0.12	813	1.40	0.31	1088	2.01	−0.22
268	2.06	0.34	543	1.87	0.08	818	1.44	0.26	1093	1.96	−0.39
273	1.99	0.32	548	1.89	0.18	823	1.55	0.30	1098	1.69	−0.10
278	2.00	0.33	553	1.67	−0.08	828	1.64	0.39	1103	1.83	−0.07
									1108	1.85	−0.07

Oxygen- and carbon-isotope data from GeoB 1711, using the planktonic foraminifer *Globorotalia inflata*. The depth scale is the combined depths of the upper box core and the longer gravity core. The $\delta^{13}C$ and $\delta^{18}O$ values are both parts per thousand (‰)

Depth (cm)	$\delta^{13}C$ (‰)	$\delta^{18}O$ (‰)	Depth (cm)	$\delta^{13}C$ (‰)	$\delta^{18}O$ (‰)	Depth (cm)	$\delta^{13}C$ (‰)	$\delta^{18}O$ (‰)	Depth (cm)	$\delta^{13}C$ (‰)	$\delta^{18}O$ (‰)
1	0.67	1.08	231	0.63	2.52	481	0.74	2.27	796	1.16	1.36
4	0.72	0.82	236	0.64	2.47	486	0.34	2.15	801	1.03	1.39
7	0.65	0.76	241	0.30	2.38	491	0.38	2.27	806	0.85	1.43
10	0.88	0.88	246	0.50	2.66	496	0.10	2.24	811	1.08	1.33
11	0.63	0.46	251	0.74	2.83	501	0.24	2.00	816	0.91	1.49
13	0.58	0.91	256	0.71		506	0.15	2.04	826	0.87	1.66
16	0.78	1.10	261	0.86	2.70	521	0.56	2.63	831	0.97	1.67
19	0.59	0.71	266	0.70	2.67	526	0.83	2.85	836	1.00	1.54
21	0.60	0.90	271	0.62	2.59	531	0.68	2.44	841	1.04	1.78
22	0.77	0.86	276	0.63	2.52	536	0.67	2.45	846	0.93	1.68
25	0.70	0.81	281	0.87	2.69	541	0.84	2.65	851	0.76	1.67
26	0.45	0.72	286	0.77	2.40	546	0.67	2.65	856	0.75	1.73
31	0.55	0.85	291	0.92		551	0.73	2.60	861	0.70	1.61
36	0.84	1.03	296	0.76	2.42	556	0.79	2.65	866	0.66	1.71
41	0.28	0.76	301	0.42	2.14	561	0.83	2.50	876	0.69	1.63
46	0.46	0.70	306	0.73	2.36	566	0.79	2.52	881	0.60	1.59
51	0.50	0.81	311	0.52	2.29	586	0.55	1.98	886	0.48	1.73
56	0.69	1.08	316	0.64	2.40	596	0.56	1.81	891	0.34	1.64
61	0.49	0.87	321	0.60	2.16	606	0.63	1.77	896	0.24	1.67
66	0.68	1.01	326	0.60	2.10	611	0.66	1.54	901	0.51	1.76
71	0.63	0.91	331	0.48	2.10	616	0.43	1.37	906	0.32	1.60
76	0.58	1.15	336	0.44	1.97	621	0.54	1.36	911	0.44	1.44
81	0.47	1.01	341	−0.02	1.83	631	0.70	1.48	921	0.41	1.34
86	0.43	1.25	346	0.29	1.88	636	0.66	1.54	931	0.62	1.29
91	0.20	1.43	351	0.28	2.03	646	0.99	1.48	941	0.25	0.83
96	0.04	1.49	356	0.65	2.56	651	1.11	1.64	946	0.27	0.58
101	0.22	1.42	361	0.49	2.63	656	1.12	1.59	951	0.21	0.72
106	0.31	1.45	366	0.67	2.68	661	0.86	1.42	956	0.32	0.42
111	0.47	1.37	371	0.50	2.88	666	0.79		966	0.11	0.48
116	0.44	1.61	376	0.64	1.95	676	0.91	1.28	971	0.11	0.80
121	0.20	1.65	381	0.59	2.16	681	0.89	1.40	976	0.14	0.53
131	0.03	1.92	386	0.74	2.72	686	1.02	1.49	981	0.24	0.79
141	0.37	1.97	391	0.82	2.86	691	0.65		991	0.04	0.63
146	0.29	2.05	396	0.63	2.50	696	0.68	1.44	996	0.10	0.46
151	0.32	2.00	401	0.71	2.27	701	0.84	1.41	1001	0.21	1.20
156	0.27	2.05	406	0.59	2.47	706	0.83	1.49	1006	−0.05	1.12
161	0.53	2.49	411	0.66	2.42	711	0.84	1.50	1011	−0.45	0.98
166	0.58	2.32	416	0.79	2.51	716	0.67	1.30	1016	−0.38	1.21
171	0.53	2.84	421	0.84	2.65	721	0.69	1.42	1021	−0.57	1.28
176	0.57	2.51	426	0.77	2.80	726	0.75	1.32	1026	−0.40	1.11
181	0.53		431	0.68	2.35	731	0.63	1.48	1031	−0.52	1.29
186	0.52	2.39	436	0.64	2.50	736	0.87	1.68	1036	−0.42	1.01
191	0.66	2.37	441	0.78	2.66	741	0.69	1.51	1041	0.01	1.22
196	0.67	2.74	446	0.62	2.36	746	0.89	1.66	1046	−0.23	1.38
201	0.60	2.44	451	0.60	2.22	751	0.92	1.52	1051	0.15	2.26
206	0.41	2.22	456	0.64	2.22	756	0.93	1.46	1056	−0.05	1.80
211	0.58	2.41	461	0.48	2.32	761	0.98	1.70	1061	−0.20	1.92
216	0.62	2.45	466	0.51	2.31	766	0.99	1.48	1066	−0.17	1.68
221	0.46	2.27	471	0.54	2.07	776	1.03	1.60	1071	0.17	2.30
226	0.43	2.57	476	0.52	2.14	791	1.01	1.44			

Relative abundances of planktonic foraminifera from GeoB 1706. Abbreviations are as follows: N. pachy (s) = *N. pachyderma* (s); Gg. bull. = *Gg. bulloides*; N. pachy (d) = *N. pachyderma* (d); Gr. inf. = *Gr. inflata*

Depth (cm)	N. pachy (s) (%)	Gg. bull. (%)	N. pachy (d) (%)	Gr. inf. (%)	Depth (cm)	N. pachy (s) (%)	Gg. bull. (%)	N. pachy (d) (%)	Gr. inf. (%)
3	4.38	27.49	33.07	5.98	288	36.56	21.51	15.05	11.83
8	6.30	30.71	25.20	10.24	293	69.59	9.36	9.36	1.75
13	2.93	41.37	24.10	9.12	298	56.52	12.56	9.18	12.56
18	3.37	34.46	30.34	8.24	303	68.07	4.20	17.65	4.20
23	6.90	33.85	32.52	10.24	308	45.86	6.77	22.56	9.02
28	2.92	40.00	27.42	12.58	313	81.76	6.29	6.92	5.03
33	3.31	41.37	32.39	8.75	318	57.32	15.85	11.59	6.71
38	6.11	32.58	42.99	5.20	323	46.27	19.40	13.43	9.95
43	7.76	32.54	41.49	4.18	328	29.95	14.01	15.94	15.46
48	8.88	30.89	40.54	7.34	333	37.50	21.88	15.10	9.90
53	6.94	33.80	42.59	8.33	338	30.95	29.05	15.24	7.14
58	6.50	34.98	40.25	8.36	343	29.22	22.84	20.16	14.40
63	13.45	31.84	35.43	6.73	348	26.00	20.80	19.20	12.80
68	11.34	33.33	36.43	7.22	353	34.60	27.00	19.39	12.17
73	11.44	36.36	34.90	4.11	358	29.80	28.81	16.23	15.23
78	12.18	40.96	35.06	5.54	363	31.96	25.95	15.19	14.56
83	21.03	44.84	21.83	3.57	368	31.93	17.65	10.08	25.21
88	31.33	33.08	22.31	4.26	373	25.29	26.05	20.31	14.94
93	31.12	30.51	30.51	2.72	378	40.35	22.81	14.04	11.40
98	46.15	28.21	14.42	0.64	383	35.35	25.25	14.14	5.05
103	44.00	14.91	13.45	0.36	388	27.06	22.35	20.59	13.53
108	46.62	18.15	20.28	3.56	393	35.90	26.92	15.38	3.85
113	50.00	11.80	22.47	1.69	398	49.33	16.00	20.00	14.67
118	63.21	7.14	12.50	2.14	403	37.68	31.88	14.49	4.35
123	51.46	15.48	8.79	3.77	408	39.91	17.37	26.76	4.23
128	58.56	7.73	20.99	1.66	413	48.00	25.00	8.00	3.00
133	66.95	9.75	13.98	0.42	418	38.22	22.29	11.46	6.37
138	64.04	6.40	16.26	1.48	423	43.59	20.51	16.67	7.69
148	46.24	12.90	28.23	1.61	428	34.54	19.59	19.07	13.92
153	33.45	11.85	37.98	2.09	433	53.90	15.60	7.80	7.80
158	31.46	15.56	34.11	2.32	438	39.71	23.44	23.44	7.18
163	38.36	16.14	29.89	3.17	443	69.91	15.04	4.42	2.65
168	35.02	12.44	35.02	4.61	448	55.56	15.87	6.35	3.97
173	45.69	12.50	24.57	0.86	453	64.46	14.88	6.61	4.13
178	38.61	8.91	31.68	1.49	458	70.35	11.50	5.31	1.33
183	28.70	13.90	36.32	7.62	463	69.74	13.16	2.63	0.00
188	49.59	15.29	23.14	2.48	468	79.52	7.23	1.20	1.20
193	47.21	13.44	21.97	3.61	473	73.03	11.18	2.63	0.66
198	49.38	13.58	17.90	3.09	478	61.14	13.47	8.81	4.66
203	47.44	13.95	17.21	5.12	483	62.98	15.22	6.57	6.92
208	41.80	14.21	21.58	5.46	488	65.03	9.48	9.15	3.59
213	45.08	21.97	14.39	5.30	493	54.42	15.31	13.95	7.48
218	34.97	20.51	19.81	10.96	498	60.99	11.81	13.74	4.67
223	38.21	22.33	24.07	5.96	503	59.33	11.94	18.66	3.73
228	38.43	13.22	14.88	14.05	508	54.85	6.80	16.99	6.80
233	53.37	19.95	16.32	4.15	513	48.98	10.20	21.94	7.14
238	62.36	14.04	14.04	2.25	518	28.74	20.24	35.22	6.07
243	63.64	16.72	7.04	3.81	523	45.75	17.65	18.30	11.11
248	56.73	15.87	10.10	6.25	528	29.01	20.61	25.19	14.50
253	59.24	15.84	12.32	5.28	533	6.02	25.00	51.85	10.65
258	65.45	15.61	6.31	5.98	538	14.08	32.39	32.75	11.97
263	50.67	17.33	19.11	6.22	543	3.55	33.10	47.52	11.58
268	58.70	9.42	9.06	2.17	548	2.33	37.74	38.13	17.51
273	66.99	13.69	11.49	2.69	553	5.18	30.79	44.96	14.71
278	57.46	12.71	16.57	5.52	558	2.53	32.58	46.35	14.33
283	30.99	34.50	22.22	5.26	563	4.59	50.18	23.32	16.61

Depth (cm)	N. pachy (s) (%)	Gg. bull. (%)	N. pachy (d) (%)	Gr. inf. (%)	Depth (cm)	N. pachy (s) (%)	Gg. bull. (%)	N. pachy (d) (%)	Gr. inf. (%)
568	3.25	47.15	24.39	19.51	843	3.17	35.73	33.14	24.21
573	3.56	46.31	20.61	15.78	848	2.14	36.36	39.57	17.11
578	3.55	45.08	21.86	16.12	853	3.42	31.62	38.03	18.38
583	3.28	44.26	23.28	20.33	858	7.92	41.25	27.50	17.92
588	2.64	43.17	30.84	17.18	863	6.43	42.17	34.14	8.43
593	5.88	36.86	34.12	15.29	868	5.86	45.05	35.14	7.21
598	3.55	43.20	27.22	11.83	873	6.15	38.97	34.87	16.41
603	5.09	28.00	51.64	9.09	878	4.13	37.73	35.40	14.73
608	9.47	34.74	44.91	5.96	883	5.22	26.91	44.18	10.04
613	7.66	35.59	42.79	8.56	888	4.37	21.84	41.26	12.14
618	9.64	37.35	38.96	8.03	893	4.08	24.85	43.88	15.73
623	14.18	32.57	41.76	6.51	898	4.44	27.99	43.34	13.65
628	11.48	28.96	48.63	8.74	903				
633	11.79	25.13	52.31	4.62	908	4.31	34.51	24.31	20.39
638	17.37	28.96	39.77	10.04	913	7.72	20.58	54.98	9.32
643	19.66	36.52	30.34	11.80	918	12.37	17.20	52.69	5.38
648	28.85	21.15	29.81	17.31	923	12.23	20.50	52.52	7.91
653	13.79	30.34	44.14	8.28	928	10.84	18.88	58.63	4.82
658	15.19	26.58	45.57	7.59	933	9.75	19.86	57.40	7.58
663	14.29	24.49	38.78	18.37	938	18.97	16.38	55.46	5.46
668	15.50	20.93	25.58	27.13	943	24.40	14.78	52.23	5.15
673	10.46	17.65	50.98	19.61	948	5.30	34.09	42.42	7.58
678	23.91	31.52	16.30	23.91	953	10.27	27.40	51.03	5.48
683	7.87	29.21	37.64	19.66	958	7.88	21.16	51.87	11.62
688	8.55	18.80	37.61	23.93	963	11.24	25.28	48.31	10.67
693	2.59	26.72	21.55	45.69	968	6.67	30.74	45.56	11.11
698	2.15	23.12	28.49	41.94	973	8.33	29.90	54.41	4.90
703	6.25	29.69	20.31	42.19	978	9.59	30.31	45.08	6.99
708	9.52	17.69	30.61	27.89	983	4.11	39.85	40.36	6.94
713	1.72	17.24	24.14	53.45	988	11.69	34.77	34.15	9.54
718	2.38	25.40	21.43	44.44	993	9.22	35.46	40.07	6.74
723	5.71	27.14	26.19	32.86	998	7.19	30.00	47.19	6.56
728	4.35	12.50	31.52	44.02	1003	3.99	29.24	49.50	7.97
733	3.94	22.05	28.74	41.34	1008	11.69	34.77	34.15	9.54
738	2.78	23.61	12.50	57.64	1013	7.85	31.42	44.11	9.37
743	1.26	22.27	37.82	33.19	1018	8.03	25.70	49.80	8.03
748	1.67	26.67	33.00	30.00	1023	13.89	31.48	46.30	3.24
753	1.96	27.84	26.27	39.61	1028	13.86	19.28	53.01	10.24
758	1.23	14.72	33.74	48.47	1033	14.66	27.16	39.66	11.64
763	0.31	47.68	22.60	25.08	1038	6.51	26.63	50.89	11.24
768	0.00	39.79	33.07	20.41	1043	12.29	29.05	37.43	13.97
773	0.45	41.31	25.06	25.06	1048	13.68	33.68	35.79	10.53
778	3.34	39.20	26.73	25.84	1053	20.29	35.51	28.26	7.25
783	2.48	34.78	37.89	21.12	1058	21.74	36.02	21.74	12.42
788	0.87	38.26	32.17	23.91	1063	35.27	25.31	21.99	9.96
793	2.88	43.75	30.29	19.23	1068	53.26	19.57	20.11	2.72
798	2.13	31.91	31.38	30.32	1073	70.59	11.76	11.76	1.76
803	5.47	39.05	26.28	24.45	1078	68.78	12.68	14.63	1.95
808	1.13	41.24	24.29	29.38	1083	70.99	12.35	12.35	3.70
813	1.18	40.78	23.53	28.63	1088	39.19	31.98	17.57	7.66
818	2.70	37.16	33.78	16.22	1093	35.71	25.00	23.81	9.52
823	2.07	40.69	33.79	16.55	1098	67.67	10.53	9.77	6.02
828	1.14	34.86	32.57	22.86	1103	58.99	19.42	15.83	0.72
833	6.56	31.69	32.24	22.40	1108	10.27	33.51	32.97	14.59
838	3.40	38.11	30.94	21.51	1113	9.29	35.71	30.71	18.57

Relative abundances of planktonic foraminifera from GeoB 1711. Abbreviations are as follows: N. pachy. (s) = *N. pachyderma* (s); Gg. bull. = *Gg. bulloides*; N. pachy (d) = *N. pachyderma* (d); Gr. inf. = *Gr. inflata*. The composite depth scale incorporates the upper box core (BC) and the longer gravity core

Depth (cm)	N. pachy. (s) (%)	Gg. bull. (%)	N. pachy. (d) (%)	Gr. inf. (%)	Depth (cm)	N. pachy. (s) (%)	Gg. bull. (%)	N. pachy. (d) (%)	Gr. inf. (%)
BC 1	2.2	6.8	82.1	0.7	251	70.4	6.0	18.1	0.5
BC 4	2.3	6.5	77.0	2.3	256	55.6	8.6	19.4	0.6
BC 7	1.4	10.0	68.9	2.3	261	55.9	14.2	19.5	1.5
BC 10	1.0	7.8	74.1	1.3	266	46.8	12.4	19.9	2.1
11	2.3	12.2	64.6	8.0	271	35.3	24.7	16.9	2.0
BC 13	0.8	11.5	69.6	2.3	276	66.9	10.4	12.5	0.0
16	1.9	7.8	70.6	2.2	281	75.8	9.3	7.2	0.5
BC 19	0.9	10.5	70.3	2.0	286	77.4	7.0	9.7	0.0
21	1.3	9.2	72.4	2.6	291	68.8	10.5	13.9	0.0
BC 22	1.1	10.9	66.2	2.0	296	42.7	29.2	20.5	1.2
BC 25	0.0	13.2	68.5	3.8	301	44.6	17.9	20.4	1.7
26	2.2	12.4	69.0	1.8	306	78.5	4.7	10.7	1.4
31	3.8	11.5	65.1	2.4	311	71.9	10.4	8.7	1.0
36	1.1	17.0	56.3	5.4	316	72.5	6.2	14.2	0.6
41	2.1	19.1	62.2	2.1	321	67.1	8.2	13.7	0.4
46	2.3	12.8	67.1	4.9	326	84.2	4.2	6.5	1.0
51	0.8	19.2	61.0	3.3	331	55.6	4.5	23.3	0.0
56	2.1	22.1	51.8	3.9	336	16.1	22.8	29.5	1.6
61	0.3	20.6	52.4	8.7	341	7.7	23.9	34.9	3.9
66	1.5	25.2	52.3	3.6	346	38.4	14.4	25.9	3.4
71	0.7	33.7	46.9	4.2	351	54.9	16.3	16.3	0.5
76	2.1	30.4	39.6	7.4	356	62.2	6.3	19.4	0.5
81	0.0	29.8	37.3	9.9	361	59.8	11.2	14.9	2.0
86	4.0	24.2	46.9	7.3	366	64.6	7.9	16.4	0.0
91	0.3	19.1	47.6	11.4	371	76.5	4.3	14.2	0.3
96	7.5	22.2	45.6	9.7	376	76.3	3.2	13.7	1.1
101	9.8	26.6	26.2	14.5	381	73.0	7.4	11.1	0.8
106	19.8	34.3	16.4	9.3	386	77.6	3.3	12.9	0.4
111	15.8	33.7	20.8	11.9	391	64.1	5.9	20.3	1.2
116	10.7	43.8	24.5	6.6	396	35.8	18.6	28.3	1.3
121	11.4	44.7	13.5	10.5	401	36.3	18.8	33.1	0.8
126	7.5	44.6	15.0	12.7	406	47.0	11.9	30.0	2.4
131	4.3	46.2	16.8	13.9	411	44.2	17.5	29.2	1.9
136	7.2	48.7	14.4	9.7	416	39.2	11.4	30.1	2.4
141	10.0	40.9	17.3	9.1	421	34.1	17.3	38.7	3.1
146	23.8	43.6	10.0	7.8	426	35.6	21.2	34.9	3.4
151	29.5	33.7	16.1	3.9	431	40.9	18.9	29.1	1.6
156	35.8	23.8	16.6	2.6	436	51.6	5.9	26.9	1.1
161	53.2	12.4	14.9	2.2	441	50.0	18.2	22.1	2.6
166	65.9	11.8	10.0	1.4	446	43.9	14.1	20.5	0.0
171	71.7	8.1	8.1	0.8	451	49.5	16.7	19.0	1.0
176	54.7	9.8	15.0	1.9	456	49.8	16.3	14.9	0.0
181	70.8	8.0	11.5	0.7	461	45.4	14.2	20.8	1.3
186	61.6	14.1	11.8	0.8	466	60.4	9.1	14.4	1.1
191	66.1	8.7	14.4	0.7	471	50.6	8.4	27.1	1.8
196	61.6	4.9	13.1	1.9	476	42.5	7.0	37.5	2.0
201	58.3	8.9	8.0	4.0	481	24.7	12.6	54.5	2.0
206	58.7	8.4	16.8	2.4	486	21.8	16.0	51.9	2.5
211	61.9	9.3	18.9	0.7	491	26.5	30.4	36.5	1.7
216	65.4	7.4	15.3	0.9	496	21.3	23.4	40.4	4.5
221	63.1	5.8	21.5	0.5	501	18.0	32.3	36.4	3.5
226	51.8	19.0	21.9	0.0	506	27.0	25.3	32.0	3.4

Depth (cm)	N. pachy. (s) (%)	Gg. bull. (%)	N. pachy. (d) (%)	Gr. inf. (%)	Depth (cm)	N. pachy. (s) (%)	Gg. bull. (%)	N. pachy. (d) (%)	Gr. inf. (%)
231	61.5	6.8	17.4	0.3	511	18.4	24.1	43.4	4.8
236	53.7	12.4	19.8	1.2	516	20.8	31.2	34.6	2.3
241	48.4	13.3	20.7	3.1	521	27.8	22.9	36.4	1.2
246	56.3	10.4	23.0	0.5	526	18.8	34.7	38.8	1.8
531	8.2	40.1	40.1	6.0	811	20.2	22.6	25.7	7.0
536	10.1	41.9	33.3	2.3	816	17.8	21.3	37.8	4.4
541	16.1	34.7	38.1	5.1	821	12.1	21.1	41.0	2.3
546	16.0	29.8	41.0	3.2	826	8.6	16.5	52.3	1.2
551	13.5	32.6	28.4	4.3	831	4.7	18.7	50.2	1.7
556	22.9	16.6	44.8	3.6	836	13.8	14.6	46.9	2.7
561	36.0	15.6	38.7	1.1	841	16.2	17.7	39.4	1.5
566	35.6	17.1	32.9	3.2	846	16.9	21.3	41.0	1.1
571	30.8	21.3	37.1	1.4	851	17.4	29.8	27.2	9.4
576	21.0	18.1	47.9	1.3	856	7.4	40.9	25.1	10.8
581	26.3	14.1	44.5	1.1	861	9.4	39.6	11.9	10.1
586	20.5	15.7	43.2	0.5	866	15.7	40.9	26.8	6.6
591	12.0	18.5	61.6	0.9	871	8.7	38.8	30.2	8.7
596	11.0	16.4	59.4	0.0	876	8.6	41.4	33.8	5.6
601	12.9	21.9	58.2	0.0	881	19.5	27.4	29.0	6.2
606	17.8	17.8	46.6	1.3	886	19.0	35.3	23.5	4.6
611	19.7	19.4	44.4	2.0	891	20.3	23.7	36.1	2.5
616	11.2	26.7	43.6	3.0	896	35.3	23.7	32.1	1.3
621	11.3	22.3	54.6	1.4	901	58.6	9.5	24.9	0.6
626	14.2	22.5	43.8	3.0	906	48.8	19.1	22.7	1.8
631	8.9	20.6	47.7	3.7	911	18.3	21.8	47.0	1.1
636	8.1	20.0	45.1	3.4	916	8.3	39.0	38.2	0.9
646	13.8	8.8	51.9	3.8	921	9.7	27.6	51.1	1.6
651	14.1	10.4	52.6	1.5	926	5.0	23.7	54.8	2.7
656	11.9	18.1	42.5	2.7	931	8.6	25.3	36.4	7.1
661	18.0	16.3	39.0	8.7	936	7.0	29.7	42.8	6.6
666	9.9	24.6	31.0	15.1	941	5.8	36.7	25.4	13.3
676	13.6	22.0	32.8	17.7	946	8.5	31.1	21.9	13.0
681	4.2	26.5	24.7	28.3	951	5.5	37.2	32.1	11.9
686	3.2	21.7	34.9	33.3	956	10.1	21.3	33.7	19.7
691	2.1	25.9	30.0	25.9	966	7.1	29.9	24.1	19.1
696	0.7	28.5	22.4	26.4	971	17.9	27.4	19.2	16.2
701	2.8	27.7	28.9	25.3	976	19.9	30.9	17.1	10.4
706	2.1	35.3	24.4	23.9	981	17.7	32.0	6.9	16.0
711	2.8	28.8	17.6	22.6	986	24.0	29.3	13.5	3.4
716	5.0	35.4	15.8	24.6	991	20.9	29.9	7.7	8.5
721	2.9	44.8	15.4	14.5	996	34.3	22.2	15.7	2.8
726	2.0	35.0	20.7	17.7	1001	21.4	35.2	19.6	3.8
731	5.2	39.3	18.4	13.1	1006	25.2	26.4	23.3	5.5
736	10.4	38.9	13.2	12.5	1011	13.5	24.5	33.0	5.5
741	8.4	46.9	12.4	16.4	1016	14.6	34.2	25.9	1.9
746	4.0	43.6	18.1	20.1	1021	4.3	29.8	36.2	10.1
751	4.3	38.5	11.1	36.8	1026	2.1	26.4	30.5	12.0
756	12.8	33.0	21.3	17.0	1031	3.0	23.9	36.0	11.7
761	13.1	27.7	20.8	14.2	1036	6.8	20.9	40.0	10.0
766	15.3	27.6	25.8	9.2	1041	10.9	26.4	37.3	4.1
771	18.0	22.3	20.5	4.9	1046	7.7	17.2	47.3	4.7
776	18.3	21.8	14.7	10.2	1051	14.8	13.7	49.7	4.9
786	31.6	26.6	14.3	7.4	1056	15.8	14.8	48.5	4.6
791	34.9	29.8	10.7	5.2	1061	15.7	20.9	45.2	5.2
796	35.7	27.4	8.3	4.5	1066	15.2	20.1	45.1	5.7
801	37.8	21.5	11.4	2.4	1071	37.3	16.9	25.9	2.5
806	23.8	32.1	14.5	4.1					

References

Bang, N.D., 1971. The southern Benguela Current region in February 1966. Part 2. Bathymetry and air/sea interactions. Deep-Sea Res., 18: 209–265.

Barange and Pillar, 1992. Cross-shelf circulation, zonation and maintenance mechanisms of *Nyctiphanes capensis* and *Euphasia hanseni* (Euphausiacea) in the northern Benguela upwelling system. Cont. Shelf Res., 12: 1027–1042.

Bé, A.W.H. and Tolderlund, D.S., 1971. Distribution and ecology of living planktonic foraminifera in surface waters of the Atlantic and Indian Oceans. In: B.M. Funnel and W.R. Riedel (Editors), The Micropalaeontology of the Oceans. Cambridge Univ. Press, pp. 105–149.

Behl, R.J. and Kennett, J.P., 1996. Brief interstadial events in the Santa Barbara Basin, NE Pacific, during the past 60 kyr. Nature, 379: 243–246.

Bender, M., Sowers, T., Dickson, M.-L., Orchado, J., Grootes, P., Mayeweski, P.A. and Meese, D.A., 1994. Climate correlations between Greenland and Antarctica during the past 100,000 years. Nature, 372: 663–666.

Bleil, U. and participants, 1996. Bericht und erst Ergenbnisse über die METEOR-Fahrt M32/1, Cape Town–Walvis Bay, 2.1.1996–28.1.1996. Ber Fachbereich Geowiss., Univ. Bremen.

Bond, G., Heinrich, H., Broecker, W., Labeyrie, L., McManus, J., Andrews, J., Huon, S., Jantschik, R., Clasen, S., Simet, C., Tedesco, K., Klas, M., Bonani, G. and Ivy, S., 1992. Evidence for massive discharges of icebergs into the North Atlantic ocean during the last glacial period. Nature, 360: 245–249.

Boyd, A.J., Salat, J. and Maso, M., 1987. The seasonal intrusion of relatively saline water on the shelf off northern and central Namibia. S. Afr. J. Mar. Sci., 5: 107–120.

Brassel, S.C., 1993. Applications of biomarkers for delineating marine palaeoclimatic fluctations during the Pleistocene. In: M.H. Engel and S.A. Macko (Editors), Organic Geochemistry: Principles and Applications. Plenum Press, pp. 699–738.

Bremner, J.M., 1983. Biogenic sediments on the South West African (Namibian) continental margin. In: J. Thiede and E. Suess (Editors), Coastal Upwelling: Its Sediment Record. Part B: Sedimentary Records of Ancient Coastal Upwelling. Plenum Press, pp. 73–104.

Brown, P.C., Painting, S.J. and Cochrane, K.L., 1991. Estimates of phytoplankton and bacterial biomass and production in the northern and southern Benguela ecosystems. S. Afr. J. Mar. Sci., 11: 537–564.

Calvert, S.E. and Price, N.B., 1983. Geochemistry of Namibian shelf sediments. In: E. Suess and J. Thiede (Editors), Coastal Upwelling, its Sediment Record: Part A: Responses of the Sediment Regime to Present and Coastal Upwelling. Plenum Press, pp. 337–375.

Charles, C.D., Lynch-Stieglitz, J., Ninnemann, U.S. and Fairbanks, R.G., 1996. Climate connections between the hemisphere revealed by deep sea sediment core/ice core correlations. Earth Planet. Sci. Lett., 142: 19–27.

Dingle, R.V., 1995. Continental shelf upwelling and benthic ostracoda in the Benguela System (southeastern Atlantic Ocean). Mar. Geol., 122: 207–225.

Dingle, R.V. and Nelson, G., 1993. Sea bottom temperature, salinity and dissolved oxygen on the continental margin off south-western Africa. S. Afr. J. Mar. Sci., 13: 33–49.

Duncombe-Rae, C.M., 1991. Agulhas retroflexion rings in the South Atlantic Ocean: an overview. S. Afr. J. Mar. Sci., 11: 327–344.

Emeis, K.-C., Anderson, D.M., Doose, H., Kroon, D. and Schultz-Bull, D., 1995. Sea surface temperatures and the history of monsoon upwelling in the NW Arabian Sea during the last 500 kyr. Quat. Res., 43: 355–361.

Giraudeau, J., 1993. Planktonic foraminiferal assemblages in surface sediments from the southwest African continental margin. Mar. Geol., 110: 1–16.

Giraudeau, J. and Rogers, J., 1994. Phytoplankton biomass and sea-surface temperature estimates from sea-bed distribution of nannofossils and planktonic foraminifera in the Benguela Upwelling System. Micropalaeontology, 40(3): 275–285.

Giraudeau, J., Monteiro, P.M.S. and Nikodemus, K., 1993. Distribution and malformation of living coccolithophores in the northern Benguela upwelling system off Namibia. Mar. Micropalaeontol., 22: 93–110.

Giraudeau, J., Summerhayes, C.P. and Kroon, D., 1997. Upwelling variability off Namibia from phytoplankton biomass estimates over the last 70,000 years (in prep.).

Grousset, F.E., Labeyrie, L., Sinko, J.A., Cremer, M., Bond, G., Duprat, J., Cortijo, E. and Huon, S., 1993. Patterns of ice rafted detritus in the glacial North Atlantic (40–55°N). Paleoceanography, 8: 175–192.

Hagelberg, T.K., Bond, G. and de Menocal, P., 1994. Milankovitch band forcing of sub-Milankovitch climate variability during the Pleistocene. Paleoceanography, 9: 545–558.

Imbrie, J., Hays, J.D., Martinson, D.G., McIntyre, A., Mix, A.C., Morley, J.J., Pisias, N.G., Prell, W.L. and Shackleton, N.J., 1984. The orbital theory of pleistocene climate: support from a revised chronology of the marine $\delta^{18}O$ record. In: A. Berger, J. Imbrie, J. Hays, G. Kukla and B. Saltzman (Editors), Milankovitch and Climate, Part I. Reidel, pp. 269–305.

Imbrie, J., McIntyre, A. and Mix, A., 1989. Oceanic response to orbital forcing in the Late Quaternary: Observational and experimental strategies. In: A. Berger (Editors), Climate and Geo-Sciences. Kluwer Academic Publishers, pp. 121–164.

Jansen, F., Ufkes, E. and Schneider, R., 1997. Late Quaternary movements of the Angola–Benguela Front, SE Atlantic, and their response to orbital forcing. In: G. Wefer, W.H. Berger, G. Siedler and D. Webb (Editors), The South Atlantic: Present and Past circulation. Springer, Berlin, pp. 553–575.

Kennett, J.P. and Ingram, B.L., 1995. A 20,000 year record of ocean circulation and climate change from the Santa Barbara Basin. Nature, 377: 510–513.

Kennett, J.P. and Srinivasan, M.S., 1983. Neogene planktonic foraminifera: A Phylogenetic Atlas. Hutchison Ross, Stroudsburg, PA, 265 pp.

Kipp, N.G., 1976. New transfer function for estimating past sea-surface conditions from sea-bed distribution of planktonic foraminiferal assemblages in the North Atlantic. In:

R.M. Cline and J.D. Hays (Editors), Investigation of Southern Ocean Palaeoceanography and Palaeoclimatology. Geol. Soc. Am. Mem. 145.

Kroon, D., 1991. Distribution of extant planktic foraminiferal assemblages in Red Sea and nothern Indian Ocean surface waters. Rev. Esp. Micropaleontol., 23(1): 37–74.

Kroon, D. and Ganssen, G., 1989. Northern Indian Ocean upwelling cells and the stable isotope composition of living planktonic foraminifera. Deep Sea Res., 36: 1219–1236.

Little, M.G., 1997. Late Quaternary Palaeoceanography of the Benguela Upwelling System, Eastern South Atlantic Ocean. Ph.D. Thesis, Edinburgh Univ.

Little, M.G., Kroon, D., Schneider R.R., Price, B., Müller, P. and Wefer, G., 1995. Late Quaternary palaeoceanography and palaeoproductivity of the Benguela upwelling system for the last 180,000 years. ICP V Halifax, Nova Scotia. Abstract volume, pp. 133–134.

Little, M. G., Kroon, D., Schneider, R.R., Price, N.B. and Summerhayes, C., in press. Trade Wind forcing of upwelling, seasonality, and Heinrich events as a response to sub-Milankovitch climate variability. Paleoceanography.

Lutjeharms, J.R.E. and Meeuwis, J.M., 1987. The extent and variability of SE Atlantic upwelling. S. Afr. J. Mar. Sci., 5: 51–62.

Lutjeharms, J.R.E. and Stockton, P.L., 1987. Kinematics of the upwelling front off southern Africa. S. Afr. J. Mar. Sci., 5: 35–49.

Mayewski, P.A., Meeker, L.D., Whitlow, S., Twickler, M.S., Morrison, M.C., Bloomfield, P., Bond, G.C., Alley, R.B., Gow, A.J., Grootes, P.M., Meese, D.A., Ram, A., Taylor, K.C. and Wumkes, W., 1994. Changes in atmospheric circulation and ocean ice cover over the North Atlantic during the last 41,000 years. Science, 263: 1747–1751.

McIntyre, A., Ruddiman, W.F., Karlin, K. and Mix, A.C., 1989. Surface water response of the equatorial Atlantic Ocean to orbital forcing. Paleoceanography, 4: 19–55.

Meeuwis, J.M. and Lutjeharms, J.R.E., 1990. Surface thermal characteristics of the Angola–Benguela front. S. Afr. J. Mar. Sci., 9: 261–279.

Mix, A.C. and Morey, A.E., 1997. Climate feedback and Pleistocene variations in the Atlantic South Equatorial Current. In: G. Wefer, W.H. Berger, G. Siedler and D. Webb (Editors), The South Atlantic: Present and Past Circulation. Springer, Berlin, pp. 503–525.

Mix, A.C., Ruddiman, W.F. and McIntyre, A., 1986. Late Quaternary paleoceanography of the tropical Atlantic, 2: The seasonal cycle of sea surface temperatures, 0–20,000 years B.P. Paleoceanography, 1: 339–353.

Morey, J.J., 1989. Variations in high-latitude oceanographic fronts in the southern Indian Ocean: An estimation based on faunal changes. Paleoceanography, 4: 547–554.

Müller, P.J., Cepek, M., Ruhland, G. and Schneider, R.R., 1997. Alkenone and coccolithophorid species changes in late Quaternary sediments from the Walvis Ridge: Implications for the alkenone palaeotemperature method. Palaeogeogr., Palaeoclimatol., Palaeoecol. (submitted).

Oberhänsli, H., 1991. Upwelling signals at the northeastern Walvis Ridge during the past 500,000 years. Paleoceanography, 6: 53–71.

Parker, F.L., 1962. Planktonic foraminiferal species in Pacific sediments. Micropalaeontology, 8: 219–254.

Park, J., D'Hondt, L.D., King, J.W. and Gibson, C., 1993. Late Cretaceous precessional cycles in double time: A warm-Earth Milankovitch response. Science, 261: 1431–1434.

Prell, W.L. and Curry, W.B., 1981. Faunal and isotopic indices of monsoonal upwelling: Western Arabian Sea. Oceanol. Acta 4.

Reynolds, L.A. and Thunnel, R.C., 1985. Seasonal succession of planktonic foraminifera in the subpolar North Pacific. J. Foraminiferal Res., 15: 282–301.

Rogers, J. and Bremner, J.M., 1991. The Benguela Ecosystem. Part VII. Marine geological aspects. Oceanogr. Mar. Biol. Annu. Rev., 29: 1–85.

Schmidt, H., 1992. Der Benguela Strom im Bereich des Walfisch Rückens im Spätquartär. Ph.D. Thesis, Univ. Bremen, 28, 172 pp.

Schneider, R.R., 1991. Spätquartäre Produktivitätsänderungen im östlichen Angola-Becken: Reaktion auf Variationen im Passat–Monsun-Windsystem und in der Advektion des Benguela-Küstenstroms. Ph.D. Thesis, Univ. Bremen, 21, 198 pp.

Schneider, R.R., Müller, P.J. and Ruhland, G., 1995. Late Quaternary surface circuation in the east-equatorial south Atlantic: Evidence from Alkenone sea-surface temperatures. Paleoceanography, 10: 197–219.

Schneider, R.R., Müller, P.J., Ruhland, G., Meinecke, G., Schmidt, H. and Wefer, G., 1997. Late Quaternary surface temperatures and productivity in the east-equatorial South Atlantic: Response to changes in Trade/Monsoon Wind forcing and surface water advection. In: G. Wefer, W.H. Berger, G. Siedler and D. Webb (Editors), The South Atlantic: Present and Past Circulation. Springer, Berlin, pp. 527–551.

Schneider, R.R., Müller, P.J., Kroon, D., Price, B. and Alexander, I., in press. Monsoon related Zaire (Congo) discharge fluctuations and influence of fluvial silicate supply on marine productivity in the east equatorial Atlantic over the last 200,000 years. Paleoceanography.

Schulz, H.D. and cruise participants, 1992. Bericht und erst Ergenbnisse über die METEOR-Fahrt M20/2, Abidjan–Dakar, 27.12.1991–3.2.1992. Ber. Fachbereich Geowiss. Univ. Bremen 25, 173 pp.

Shaffer, G., 1993. Effects of the marine biota on global carbon cycling. In: M. Heinmann (Editor), The Global Carbon Cycle. Springer Verlag.

Shannon, L.V., 1985. The Benguela Ecosystem Part 1: Evolution of the Benguela, physical features and processes. Oceanogr. Mar. Biol. Annu. Rev., 23: 105–182.

Shannon, L.V. and Nelson, G., 1997. The Benguela physical features, shelf dynamics and system variability. In: G. Wefer, W.H. Berger, G. Siedler and D. Webb (Editors), The South Atlantic: Present and Past Circulation. Proc. S. Atlantic Conf., Bremen, 15–19 August, Springer, Berlin, pp. 163–210.

Shannon, L.V., Lutjeharms, J.R.E. and Agenbag, J.J., 1989.

Episodic input of Subantarctic water into the Benguela region. S. Afr. Tydskr. Wet. 85.

Struck, U., Sarnthein, M., Westerhausen, L., Barnola, J.M. and Raynauld, D., 1993. Ocean–atmosphere carbon exchange: impact of the "biological pump" in the Atlantic equatorial upwelling belt over the last 330,000 years. Palaeogeogr., Palaeoclimatol., Palaeoecol., 103: 41–56.

Summerhayes, C.P., Emeis, K.C., Angel, M.V., Smith, R.L. and Zeitzschel, B., 1995a. Upwelling in the ocean: Modern processes and ancient records. In: C.P. Summerhayes, K.C. Emeis, M.V. Angel, R.L. Smith and B. Zeitzschel (Editors), Upwelling in the Ocean. Dahlem Workshop Report. Wiley, pp. 1–38.

Summerhayes, C.P., Kroon, D., Rosel-Melé, A., Jordan, R.W., Schrader, H.J., Hearn, R., Villanueva, J., Grimalt, J.O. and Eglinton, G., 1995b. Variability in the Benguela Current System over the last 70,000 years. Prog. Oceanogr., 35: 207–251.

Ten Haven, H.L. and Kroon, D., 1991. Late Pleistocene sea surface temperature variations off Oman as revealed by the distribution of long-chain alkenones. Proc. ODP, Sci. Results, 117: 445–452.

Thiede, J., 1975. Distribution of foraminifera in surface waters of a coastal upwelling area. Nature, 253: 712–714.

Ufkes, E., 1997. Planktonic foraminifera in the surface waters of the eastern South Atlantic during springtime. Oceanol. Acta (submitted).

Ufkes, E. and Zachariasse, W.-J., 1993. Origin of coiling differences in living negloboquadrinids in the Walvis Bay region, off Namibia, Southwest Africa. Micropalaeontology, 39: 283–287.

Yiou, P., Genthon, C., Ghil, M., Jouzel, J., Le Treut, H., Barnola, J.M., Lorius, C. and Korotkevitch, Y.N., 1991. High-frequency palaeovariability in climate and CO_2 levels from Vostock ice core records. J. Geophys. Res., 96: 20,365–20,378.

Quaternary Geology and Geomorphology of South America

by C.M. Clapperton

This monograph reviews the nature of Quaternary environmental changes over the largest continent in the Southern Hemisphere. Moreover, since South America makes a transect across most climatic belts of an entire hemisphere, it provides a unique opportunity to examine the impact of changing Quaternary climates on a variety of environments. It also forms the basis for judging the synchrony or non-synchrony of Quaternary climatic changes between hemispheres and this has important implications for climatic modelling.

The book is lavishly illustrated with photographs and line diagrams. As it provides a compendium of data and analyses about Quaternary changes for a whole continent, this book should appeal to a wide range of environmental disciplines.

Contents: 1. The Physical Geography of South America. 2. Quaternary Tectonics of South America. 3. Quaternary Volcanism in South America. 4. Characteristics of the Quaternary Volcanic Zones. 5. Quaternary of the Alluvial Basins. Part I: Structure and Quaternary Stratigraphy. 6. Quaternary of the Alluvial Basins. Part II: Fluvial Landforms and Sediments. 7. Quaternary of the Alluvial Basins. Part III: Aeolian Features: Palaeoclimate. 8. Quaternary of the South American Highlands. Part I: Highlands of the Brazilian Shield. 9. Quaternary of the South American Highlands. Part II: Case Studies in Southeast Brazil: Campos do Jordão and Serra da Itatiaia. 10. Quaternary of the South American Highlands. Part III: The Northern and Southern Highlands. 11. The Glaciers and Glacial Landforms of South America.12. Late Cenozoic Glacial History of the Andes. Part I: Late Miocene-Middle Pleistocene. 13. Late Cenozoic Glacial History of the Andes. Part II: The Late Quaternary (Isotope Stages 7-3). 14. Late Cenozoic Glacial History of the Andes. Part III: The Last Glaciation Maximum (Isotope Stage 2). 15. Late Cenozoic Glacial History of the Andes. Part IV: The Late-Glacial and Holocene. 16. Quaternary Gravel Formations of Southern South America. 17. Quaternary Palaeolakes of the Arid Regions of South America. 18. Quaternary Geocryogenic Features of South America and the Falkland Islands (Islas Malvinas). 19. Quaternary of the South American Coasts. 20. Quaternary Palynological Studies in South America. Part I: Pre-Quaternary-Late Quaternary. Introduction. 21. Quaternary Palynological Studies in South America. Part II: The Last Glaciation. 22. Palaeoecology of the Late-Glacial and Holocene Intervals. 23. The Quaternary of South America: Overview and Implications. References. Subject Index.

©1993 800 pages
Dfl. 350.00 (US $ 200.00)
ISBN 0-444-882472

ELSEVIER SCIENCE B.V.
P.O. Box 1930
1000 BX Amsterdam
The Netherlands

P.O. Box 945
Madison Square Station
New York, NY 10160-0757

The Dutch Guilder (Dfl.) prices quoted apply worldwide. US $ prices quoted may be subject to exchange rate fluctuations. Customers in the European Community should add the appropriate VAT rate applicable in their country to the price.

ELSEVIER SCIENCE B.V.

(continued from inside front cover)

Advertising information
Advertising orders and enquiries may be sent to: Elsevier Science, Advertising Department, The Boulevard, Langford Lane, Kidlington, Oxford OX5 1GB, UK, tel.: (+44) (0) 1865 843565, fax: (+44) (0) 1865 843976. *In the USA and Canada*: Weston Media Associates, attn. Dan Lipner, P.O. Box 1110, Greens Farms, CT 06436-1110, USA, tel.: (203) 261 2500, fax: (203) 261 0101. *In Japan*: Elsevier Science Japan, Marketing Services, 1-9-15 Higashi Azabu, Minato-ku, Tokyo 106; Tel. +81 5 5561 5033; Fax +81 5 5561 5047.

NOTE TO CONTRIBUTORS
A detailed Guide for Authors is available upon request. Please pay special attention to the following notes:

Preparation of the text
a) The manuscript should preferably be prepared on a word processor and printed with double spacing and wide margins and include an abstract of not more than 500 words. **Also provide 4 to 6 keywords. These must be taken from the most recent edition of the AGI GeoRef Thesaurus and should be placed beneath the abstract.**
b) Authors should use IUGS terminology. The use of S.I. units is also recommended.
c) The title page should include the name(s) of the author(s), their affiliations, fax and e-mail numbers. In case of more than one author, please indicate to whom the correspondence should be addressed.

References
a) References in the text consist of the surname of the author(s), followed by the year of publication in parentheses. All references cited in the text should be given in the reference list and vice versa.
b) The reference list should be in alphabetical order.

Tables
Tables should be compiled on separate sheets and should be numbered according to their sequence in the text. Tables can also be sent as glossy prints to avoid errors in typesetting.

Illustrations
a) All illustrations should be numbered consecutively and referred to in the text.
b) Drawings should be lettered throughout, the size of the lettering being appropriate to that of the drawings, but taking into account the possible need for reduction in size. The page format of the journal should be considered in designing the drawings.
c) Photographs must be of good quality, printed on glossy paper.
d) Figure captions should be supplied on a separate sheet.
e) Colour figures can be accepted providing the reproduction costs are met by the author. Please consult the publisher for further information.

Page proofs
One set of page proofs will be sent to the corresponding author, to be checked for typesetting/editing. The author is not expected to make changes or corrections that constitute departures from the article in its accepted form. Proofs should be returned within 3 days.

Reprints
Fifty reprints of each article are supplied free of charge. Additional reprints can be ordered on a reprint order form which will be sent to the corresponding author upon receipt of the accepted article by the publisher.

Submission of manuscripts
Authors are requested to submit, with their manuscripts, the names and addresses of *four* potential referees.
All manuscripts should be sent in triplicate to: Editorial Office *Palaeogeography, Palaeoclimatology, Palaeoecology*, P.O. Box 1930, 1000 BX Amsterdam, The Netherlands. Illustrations should also be submitted in triplicate. One set should be in a form ready for reproduction: the other two may be of lower quality.
The indication of a fax and e-mail number on submission of the manuscript could assist in speeding communications. The fax number for the Amsterdam office is +31-20-4852696.
Submission of an article is understood to imply that the article is original and unpublished and is not being considered for publication elsewhere.
Upon acceptance of an article by the journal, the author(s) resident in the U.S.A. will be asked to transfer the copyright of the article to the publisher. This transfer will ensure the widest possible dissemination of information under the U.S. Copyright Law.

Submission of electronic text
Authors are encouraged to submit the final text on a 3.5" or 5.25" diskette. Both double density (DD) and high density (HD) diskettes are acceptable. Make sure, however, that the diskettes are formatted according to their capacity (HD or DD) before copying the files onto them. As with the requirements for manuscript submission, the main text, list of references, tables and figure captions should be stored in separate text files with clearly identifiable file names. The format of these files depends on the word processor used. Texts made with Display Write, MultiMate, Microsoft Word, Samna Word, Sprint, TEX, Volkswriter, Wang PC, WordMARC, WordPerfect and Wordstar or supplied in DCA/RFT or DEC/DX format can be readily processed. In all other cases the preferred format is DOS text or ASCII. It is essential that the name and version of the word processing program, the type of computer on which the text was prepared, and the format of the text files are clearly indicated.
Authors are requested to ensure that the contents of the diskette **correspond exactly** to the contents of the hard copy manuscript. Discrepancies can lead to proofs of the wrong version being made. The word processed text should be single column format. Keep the layout of the text as simple as possible; in particular, do not use the word processor's options to justify or to hyphenate the words.

If available, electronic files of the figures should also be included on a separate floppy disk.

Authors in Japan please note: Upon request, Elsevier Science Japan will provide authors with a list of people who can check and improve the English of their paper (*before submission*). Please contact our Tokyo office: Elsevier Science Japan, 1-9-15 Higashi Azabu, Minato-ku, Tokyo 106; Tel. +81 3 5561 5032; Fax +81 3 5561 5045.

Teller, 1990; *Andrews et al.,* 1993; *Bond et al.,* 1993; *Paillard and Labeyrie,* 1994], decreasing the salinity, and therefore the density, of the Gulf Stream and lowering its potential to sink in the polar regions of the North Atlantic, thus reducing the rate of convective overturn and deep water mixing. The subsequent decrease in warm-water advection from the tropics is suggested to stimulate a rapid cooling and sudden ice sheet build up, with ice sheets expanding to their maximum seaward position before final collapse and release of icebergs into the North Atlantic, further cooling the surface polar waters [*Johnson and Andrews,* 1979; *Paillard and Labeyrie,* 1994]. If this model is coupled with the Gulf Stream and the cross-equatorial transfer of heat and moisture from the South Atlantic to the North Atlantic, as previous models of oceanic convection suggest [*Stommel,* 1980; *Gordon,* 1986; *Imbrie et al.,* 1989; *Berger,* 1990; *Gordon et al.,* 1992; *Berger and Kroon,* 1995; *Macdonald and Wunsch,* 1996], then the impact of thermohaline changes on the conveyor could also be affected by changes in the rate of moisture and heat input from the tropics at times of increased trade wind intensity [*Ruddiman and McIntyre,* 1981; *Imbrie et al.,* 1989; *Little et al.,* 1997]. An increase in moisture supply to the North Atlantic ice sheets, contemporaneous with a northern hemisphere cooling, would enhance rapid ice buildup and subsequent calving as ice sheets reach their maximum

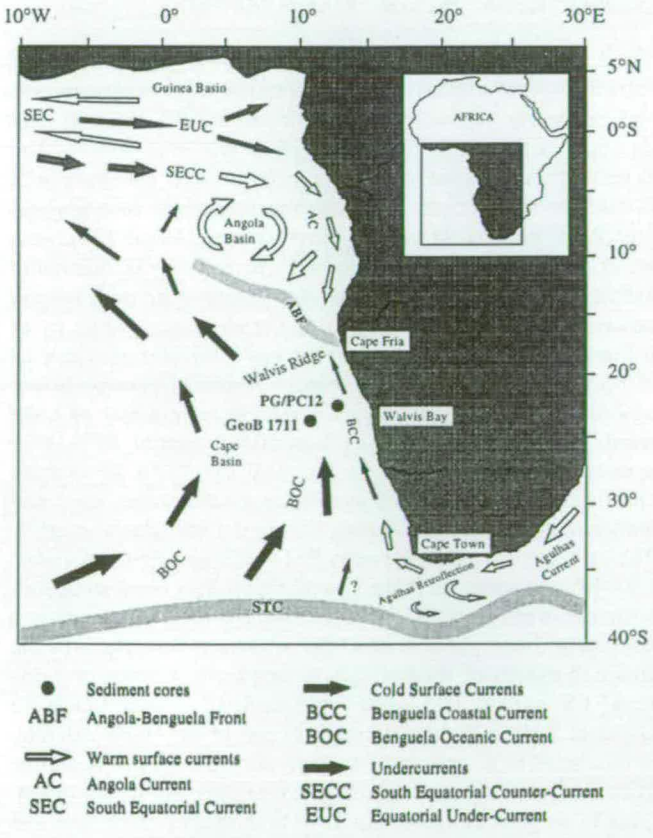

Figure 1. Map outlining the major oceanographic features of the southeastern and equatorial South Atlantic [after *Shannon,* 1985; *Lutjeharms and Stockton,* 1897; *Schneider,* 1991], with sediment core positions (solid circles) on the continental slope. Hydrography is summarized from *Jansen et al.* [1984], *Shannon et al.* [1987], *Stramma and Peterson* [1989], *Gordon and Bosley* [1991].

latitudinal extent [*Boulton and Payne,* 1994], and would account for the anomalous warm water sea surface temperatures (SSTs) which prevail into the phase of maximum ice building in the northwestern subtropical gyre and subpolar ocean [*Ruddiman and McIntyre,* 1981].

The hydrography of the Benguela Current system ((BCS) Figure 1) has been described in detail by a number of workers [*Shannon,* 1985; *Lutjeharms and Meeuwis,* 1987; *Lutjeharms and Stockton,* 1987; *Meeuwis and Lutjeharms,* 1990; *Summerhayes et al.,* 1995], with additional reviews of the regional oceanography given by *Little et al.* [1997] (Cape Basin), *Schneider* [1991] (Angola Basin), and *Peterson and Stramma* [1991] (South Atlantic). The oceanography off southwestern Africa is governed in the south by the warm-water Agulhas Current entering from the Indian Ocean [*Gordon,* 1986; *Gordon et al.,* 1992; *Macdonald and Wunsch,* 1996; *Schmitz,* 1996], in the north by the warm-water Angola Current and South Atlantic cyclonic gyre [*Moroshkin et al.,* 1970; *Gordon and Bosley,* 1991], and offshore Namibia and South Africa by the coastal branch of the Benguela Current, forming the northeastern limb of the anticyclonic gyre of the South Atlantic. Along the entire eastern and equatorial margin of the South Atlantic the coastal regions are characterized by seasonally variable upwelling generated by changes in the strength and zonality of the trade wind system. Meridional to zonal changes in trade wind direction generate greater offshore displacement of tropical and subtropical waters and the upwelling and intermixing of cooler, nutrient-rich waters, supporting a diverse plankton community.

Materials and Methods

Gravity core GeoB 1711-4 was collected on R/V *METEOR* cruise M20/2 (1991) from a water depth of 1967 m on the continental slope of the Cape Basin (23°18.9'S 12°22.6'E). Core length of GeoB 1711 was 1066 cm. Sedimentology and further core characteristics are given by *Schulz et al.* [1992]. Piston core PC12, with its accompanying gravity core PG12 collected on R/V *CHAIN* cruise 115 (1973), was recovered from 1017 m on the continental slope just north of Walvis Bay (22°16.0'S, 12°32.3'E). Core length of PC12 was 620 cm with the bottom 82 cm discarded due to "flow in" and PG12 was 82 cm long. Combined (PG/PC12) they represent at least 620 cm of sediment record, with a small hiatus between the two sediment cores, confirmed using carbonate content profiles from four other cores near the slope of PG/PC12 (PC16, 4778, 4804 and 4805) [*Summerhayes et al.,* 1995].

For a high-resolution study, samples were taken at 5-cm intervals along GeoB 1711 and at 10-cm intervals along PG/PC12, allowing geochemical, micropaleontological, and stable isotopic analysis to be carried out at an average sample interval of about 650 years. GeoB 1711 samples (10 cm^3) for foraminiferal counts and stable isotope measurements were wet sieved, before foraminiferal analysis was made on the >125-μm size fraction. GeoB 1711 archived core material is kept at the Department of Geosciences, University of Bremen, Germany. PC12 and PG12 were sampled and prepared separately. In October 1995 the cores were re-sampled at 10-cm intervals for planktonic foraminifera, and the samples wet sieved for fractions >125-μm. Archived core material is kept at the Woods Hole Oceanographic Institution, Woods Hole,

Massachusetts, and archived foraminiferal samples are kept at the Department of Geology and Geophysics, Edinburgh University, Edinburgh, Scotland.

A stratigraphic framework for the cores was gained by correlation of the planktonic oxygen isotope profiles (and benthic oxygen isotope profile for GeoB 1711) with the normalized SPECMAP standard record [*Imbrie et al.*, 1984]. For GeoB 1711 the tests of *Globorotalia inflata* d'Orbigny and *Cibicidoides wuellerstorfi* Schwager were hand-picked under a binocular microscope from the 250—500 μm fraction to achieve an analytical weight between 0.05 and 0.10 mg, composed of between eight and ten well-preserved and clean *Gr. inflata* specimens and between two and four *C. wuellerstorfi* specimens. Stable oxygen and carbon isotope analysis was conducted on a Finnigan MAT 251 mass spectrometer at the Fachbereich Geowissenschaften, Bremen, Germany. The tests of the foraminifera were reacted with concentrated ortho-phosphoric acid at 75°C. Calibration to the standard Pee Dee belemnite was via the NBS18, NBS19, and NBS20 standards. Analytical precision for oxygen and carbon isotope analyses was ±0.08‰ and ±0.04‰, respectively. The oxygen isotope records were subsequently correlated with the stacked record of *Imbrie et al.* [1984] to obtain an age model for the cores. Eight stable isotope events between 45 and 140 kyr were identified from the benthic record for GeoB 1711 (Figure 2). Oxygen isotope analysis for PG/PC12 was carried out using *N. pachyderma* specimens; detailed sampling and isotope analysis methodology and stratigraphy of PG/PC12 is documented by *Summerhayes et al.* [1995].

For further chronostratigraphic control in both records, radiocarbon ages were measured on planktonic foraminifera extracted from selected sample intervals. Carbon dioxide generated from the samples by acid hydrolysis was reacted to form graphite using Fe/H_2 catalytic reduction at the Fachbereich Geowissenschaften, Bremen, Germany. Graphite was pressed into targets which were analyzed along with standards and process blanks on an accelerator mass spectrometer (AMS) at the Leibniz-Labor AMS facility, Christian-Albrechts-University, Kiel, Germany, following the procedures described in *Nadeau et al.* (1997). Analytical radiocarbon ages were calculated using 5568 (years) as the half-life of radiocarbon. The analytical ^{14}C ages obtained must be corrected for the age difference between atmosphere and the surface ocean. For the low-latitude range the reservoir age is generally 400 years and is not likely to have changed by more than 100-200 years during the late Pleistocene [*Bard*, 1988; *Bard et al.*, 1990b]. We have corrected the analytical data ages for reservoir effect by + 400 years, and further calculated radiocarbon ages to calendar years according to *Bard et al.* [1990a, b] and *Bard et al.* [1993] (Table 1).

Results

The changing downcore abundance of the cold-water planktonic foraminifera *N. pachyderma* (s) records rapid oscillations in relative abundances between 0 and 90% of the total planktonic foraminiferal assemblage (Figure 2). The *N. pachyderma* (s) records do not follow the glacial-interglacial regime described by the oxygen isotope profile, but instead show a higher frequency of change on a sub-Milankovitch cyclicity, with *N. pachyderma* (s) maxima describing discrete PS events (pachyderma sinistral) (Table 2).

Table 1. Calendar Age Calculation

Core	Depth[a]	Age,[b] kyr	Error (+/-)	Calendar Age,[c] kyr	Error (+/-)
PG/PC12[d]	10	5.99	75	6.09	93
PG/PC12[d]	45	7.88	40	8.44	49
PG/PC12[d]	75	10.50	55	11.69	68
PG/PC12[d]	113	14.10	55	16.15	67
PG/PC12[e]	142	16.85	80	19.49	95
PG/PC12[e]	167	19.25	85	22.33	101
PG/PC12[e]	217	23.80	120	27.54	134
PG/PC12[e]	267	28.50	190	32.68	202
GeoB 1711[f1]	116	12.68	70	14.39	87
GeoB 1711[f2]	191	17.14	120	19.84	144
GeoB 1711[f3]	251	18.74	130	21.73	154
GeoB 1711[f4]	341	35.37	980	39.71	959

[a]Composite depth (cm).
[b]No reservoir corrections or calibration to calendar years.
[c]Ages converted to calendar years following the methods of *Bard et al.* [1990a, b], and *Bard et al.* [1993] after a 400-years correction for marine reservoir effect.
[d]Age from *N. pachyderma* right coiling specimens.
[e]Age from *N. pachyderma* left coiling specimens.
[f]Age from *Globorotalia inflata* specimens. Sample identification numbers: [1]KIA557; [2]KIA556; [3]KIA555; [4]KIA554.

The *N. pachyderma* (s) records off southwest Africa have been shown to vary primarily according to the local oceanographic and upwelling regime, which is driven by the intensity and direction of the southeast trade winds [*Little et al.*, 1997]. The extent of the coastal upwelling cells at any one time will dictate the hydrography and therefore planktonic foraminiferal record. Owing to its geographical position, GeoB 1711, at a water depth of 1967 m, is thought to reflect the maximum extent of the upwelling offshore and therefore the most intense upwelling and corresponding strong trade winds, while cores inshore of GeoB 1711 generally have broader maxima of *N. pachyderma* (s) reflecting a more sustained position below upwelling cells not reflecting the maximum intensity of trade winds [*Little et al.*, 1997]. Upwelling events PS1—PS9 punctuate the record for the last 140 kyr, with an average spacing of the order of 10 kyr in the glacial stages 4—2 and with a longer (~20 kyr) spacing during the interglacial stage 5. The calendar ages for PS events PS1—PS9 and Heinrich events H1—H6 are given in Table 2, with PS1—PS6 correlating well with the timing of H1—H6 in the North Atlantic with a consistent 3-kyr phase lead of the southern hemisphere to the Heinrich events of the northern hemisphere. Considering this lead, PS events PS1—PS6 in GeoB 1711 and PG/PC12 correlate well to the six Heinrich events in the North Atlantic, within analytical and calendar age correction error margins. With regard to PS and Heinrich events preceding H6 (PS6), there is no general agreement as to how many events exist and their exact timing. *Heinrich* [1988] observed an "extra" five IRD events during interglacial stage 5 and more recently *McManus et al.*, [1994] reported the occurence of IRD deposits together with increased abundance of *N. pachyderma* (s) during interglacial stage 5. Heinrich events H1—H6 from sediment

PALEOCEANOGRAPHY, VOL. 12, NO. 4, PAGES 568-576, AUGUST 1997

Trade wind forcing of upwelling, seasonality, and Heinrich events as a response to sub-Milankovitch climate variability

Mark G. Little,[1] Ralph R. Schneider,[2] Dick Kroon,[1] Brian Price,[1]
Colin P. Summerhayes,[3] and Monika Segl[2]

Abstract. Planktonic foraminifera recovered from two cores in the northern Benguela upwelling system reveal a history of rapid events with a variability at sub-Milankovitch frequencies during the last 140 kyr. The "cold-water" planktonic foraminifer, left coiling *Neogloboquadrina pachyderma* (Ehrenberg), shows rapid fluctuations in relative abundance, indicating changes in upwelling intensity. The periods of high abundance in left coiling *N. pachyderma* are referred to as "PS events" (pachyderma sinistral) and indicate increased intensity and zonality of the South Atlantic trade winds controlling the Benguela upwelling system. The good correlation between PS events, the North Atlantic Heinrich events, and the Dansgaard-Oeschger cycles from the Greenland Ice Sheet Program (GISP2) ice core suggests large-scale global oceanographic or climatic teleconnections between the South and North Atlantic via the trade wind system. The radiocarbon constrained timing of PS events younger than 45 kyr indicates that the South Atlantic leads the North Atlantic's response to trade wind changes, particularly during isotope stages 4—2 when the Earth was dominated by large ice sheets. At times of increased trade wind strength, tropical and subtropical waters are forced across the equator enhancing the pool of warm water to be transferred to the high latitudes of the North Atlantic via the Gulf Stream and North Atlantic Drift, increasing the pull of the thermohaline convective conveyor. The increased supply of warm water to the polar regions of the northern hemisphere increases the ice-ocean moisture gradient and accelerates ice sheet growth, leading to eventual instability and collapse.

Introduction

Planktonic foraminifera collected from two cores in the Benguela upwelling system in the southeastern Atlantic Ocean are used to assess the South Atlantic influence on North Atlantic and global climate change for the past 140 kyr. The high abundances of the left coiling planktonic foraminifer, *Neogloboquadrina pachyderma* (Ehrenberg) (*N. pachyderma* (s)), fluctuate with a higher frequency of change than would be expected if the system was dominated by the global glacial/interglacial cycle [*Little et al.*, 1997]. These rapid events are investigated to ascertain the extent, cause, and timing of South Atlantic-North Atlantic teleconnections in global thermohaline/geostrophic circulation. Here we examine the relative abundances of planktonic foraminifera from cores GeoB 1711 and PG/PC12 from the northern Cape Basin in the South Atlantic Ocean for evidence of short-lived climate events related to the southern hemisphere trade wind system and their link to equatorial seasonality and Heinrich events.

Many authors have studied the well-defined rapid pulses of ice-rafted debris (IRD) in marine sediments during the last glacial cycle [*Pastouret et al.*, 1975; *Ruddiman*, 1977; *Aksu and Piper*, 1979; *Fillon and Duplessy*, 1980; *Ruddiman et al.*, 1980; *Molnia*, 1983; *Broecker*, 1988; *Jansen and Veum*, 1990; *Bond et al.*, 1992; *Duplessy et al.*, 1992; *Bond et al.*, 1993; *Grousset et al.*, 1993; *Keigwin and Lehman*, 1994; *Maslin et al.*, 1995; *Porter and Zhisheng*, 1995; *van Kreveld et al.*, 1996]. These short-lived "Heinrich events" occur on sub-Milankovitch timescales at intervals of between 8 and 11 kyr, and are commonly associated with peak abundances of Arctic/sub-Arctic faunas, as represented by *N. pachyderma* (s) [*Bond et al.*, 1992; *Broecker and Maier-Reimer*, 1992; *Bond et al.*, 1993; *Grousset et al.*, 1993; *van Kreveld et al.*, 1996]. Periods of cooling terminated by an abrupt warming represent similar climate changes in the Greenland ice cores and suggest fluctuations at a higher frequency than Milankovitch orbital forcing with more oscillations in the last 60 ka than are recorded in either the *N. pachyderma* (s) or IRD records from the North Atlantic sediments [*Broecker et al.*, 1990a; *Johnsen*, 1992; *Bond et al.*, 1993; *Dansgaard et al.*, 1993; *Grootes et al.*, 1993; *Bender et al.*, 1994]. *Dansgaard et al.* [1993], showed that the $\delta^{18}O$ record from the GRIP ice core contains 23 interstadials within the last 120 kyr, with 17 interstadials recognized between the LGM (last glacial maximum) and oxygen isotope stage 4, compared with only five Heinrich events recognized in marine sediments within this period [*Heinrich*, 1988; *Bond et al.*, 1992; *Bond et al.*, 1993; *Grousset et al.*, 1993].

The Heinrich events are thought to be the result of fluctuations in the thermohaline convective conveyor which draws warm, tropical, saline-rich waters from the equatorial regions into the high latitudes of the North Atlantic via the Gulf Stream and North Atlantic Drift [*Broecker and Denton*, 1989; *Berger*, 1990; *Broecker et al.*, 1990a; *Bond et al.*, 1993; *Paillard and Labeyrie*, 1994]. Previously, meltwater input from the large Laurentide ice sheets was thought to be the principal cause of disturbance to the thermohaline convection [*Broecker et al.*, 1985; *Watts*, 1985; *Broecker*, 1988; *Broecker and Denton*, 1989; *Berger*, 1990; *Broecker et al.*, 1990a, b;

[1]Department of Geology and Geophysics, University of Edinburgh, Edinburgh, Scotland.
[2]Fachbereich Geowissenschaften, Universitat Bremen, Bremen, Germany.
[3]Southampton Oceanography Centre, Southampton, England.

Paper number 97PA00823.
0883-8305/97/97PA-00823$12.00

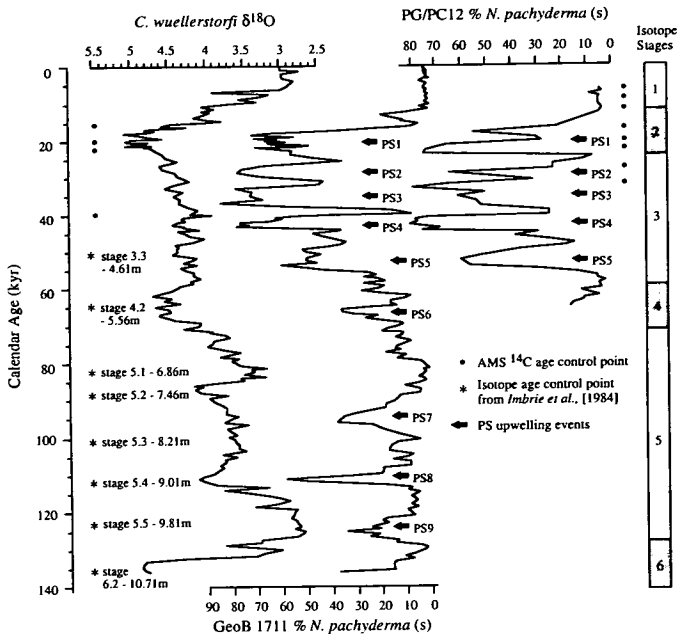

Figure 2. Planktonic foraminifera derived oxygen isotope stratigraphy for GeoB 1711 versus calendar age (kiloyears before present). The $\delta^{18}O$ age control points (asterisks) and ^{14}C AMS age control points (solid circles) for GeoB 1711 are shown to the left of the $\delta^{18}O$ *C. wuellerstorfi* record, and to the right of the *% N. pachyderma* (s) data for PG/PC12. PS (pachyderma sinistral) upwelling events are highlighted on the GeoB 1711 and PG/PC12 *N. pachyderma* (s) abundance data. Graphic representation of the isotope stages is given to the right of the figure.

records in the North Atlantic are associated with peak abundances of *N. pachyderma* (s) and large fluxes of IRD principally at times of large ice sheets during global cooling, specifically glacial isotope stages 4—2. During warmer interglacial periods, when ice sheets are near their minimum size and insolation is near a maximum, it is unlikely that fluctuations in ice sheet growth will be recorded in IRD and *N. pachyderma* (s) abundances, as ice sheets will never grow to a sufficient size to enable ice sheet calving or to produce Heinrich events. The presence of PS events during interglacial stage 5 further supports the studies of *Heinrich* [1988] and *McManus et al.*, [1994] for climate instability during non-glacial periods when high latitude climate amplification is not as pronounced.

Using a graphic correlation similar to that used in previous studies of Heinrich events [*Bond et al.*, 1993; *Dansgaard et al.*, 1993; *Grousset et al.*, 1993; *Bender et al.*, 1994], tie-lines have been drawn between the distinct cool periods in GeoB 1711 and their temporal equivalents in the GISP2 ice core [Figure 3]. Additionally, the equatorial seasonality record derived from planktonic foraminiferal abundances at core RC24-16 (5°2.3'S 10°11.5'W [*McIntyre et al.* , 1989]) is also correlated with the GeoB 1711 *N. pachyderma* (s) record. *Bender et al.* [1994] following the stratigraphy of *Dansgaard et al.* [1993], correlated the 23 interstadials found in the GRIP ice core record to those in the nearby Greenland ice core, GISP2. The graphic correlation in Figure 3 suggests that almost all of the 23 interstadials, particularly in the glacial stages 4—2 (IS1—IS20 [*Bender et al.*, 1994]), can be found in the GeoB 1711 *N. pachyderma* (s) record as maxima in *N. pachyderma* (s) abundances and therefore cold upwelling events at site GeoB 1711. All of the short-term features of upwelling events PS1—PS8 can also be found in the RC24-16 seasonality record with cooler upwelling maxima occuring simultaneous with maximum eastern equatorial seasonality and therefore maximum seasonal SST variability between summer and winter extremes. Notably, it is the minima in the *% N. pachyderma* (s) record, and hence warm intervals of reduced upwelling intensity, that match $\delta^{18}O$ minima in the GISP2 ice core and minima in the equatorial seasonality record (Figure 3). The *N. pachyderma* (s) abundances suggest that the pronounced upwelling events PS6, PS7 and PS8 record cold stages in a predominantly warm interglacial period, while PS1—PS5 record the base values in a cold glacial period punctuated by anonamously low *% N. pachyderma* (s) values. The correlation suggests that the cold periods within the GeoB 1711 and RC24-16 records consistently lead the corresponding cold periods within the GISP2 record , in the ^{14}C constrained 0—45 kyr period, consistent with the findings of *Bender et al.* [1994] and *Charles et al.* [1996], or alternatively, warming in the southern hemisphere is in phase with cooling in the Greenland ice core record and vice versa.

The South and equatorial Atlantic lead the North Atlantic response documented by Heinrich layers and are opposing at the higher frequency scale of atmospheric response indicated by the interstadials IS1—IS23. Supporting planktonic foraminiferal abundances from cores GeoB 1706 on the Walvis Ridge and PG/PC12 (Figure 2) on the continental slope demonstrate that with further AMS ^{14}C control on the younger part of these records, the apparent lead visible in Figure 3 and calculated in Table 2 is a true feature of the South Atlantic

Table 2. Pachyderma Sinistral and Heinrich Event Correlations

Pachyderma Sinistral		Heinrich			
Event	Calendar Age, kyr	Event	Age,[a] kyr	Error (+/-)	Calendar Age,[b] kyr
PS1	19.2-21.7	H1	13.65-14.99	90-230	15.59-17.25
PS2	26.1-29.0	H2	20.37-21.77	330-220	23.64-25.25
PS3	32.7-36.7	H3	26.57-29.57	310-660	30.60-33.80
PS4	42.4	H4[c]			38-42
PS5	53	H5[c]			50-52
PS6	65-71	H6[c]			67[d]
PS7	95				
PS8	111				
PS9	125				

PS event calendar age ranges are taken as an average from cores PG/PC12 and GeoB 1711.

[a]Analytical age from *Bond et al.* [1992].

[b]Ages converted to calendar years following the methods of *Bard et al.* [1990a, b], and *Bard et al.* [1993] after a +400-years correction for reservoir effect.

[c]From *Grousset et al.* [1993].

[d]H6 covers the whole of stage 4 [*Bond et al.*, 1992] but peaks at 67 kyr.

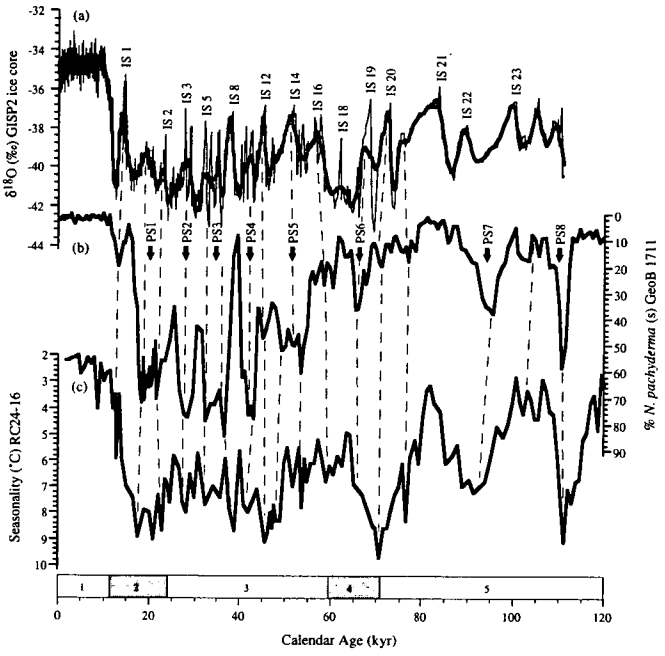

Figure 3. Correlation between (a) Greenland, GISP2 ($\delta^{18}O$) ice core, (b) *N. pachyderma* (s) from GeoB 1711 (% of total planktonic foraminifera), (c) Equatorial seasonality (°C) [*McIntyre et al.*,1989]. The GISP2 $\delta^{18}O$ data [*Grootes et al.*, 1993] have been smoothed for graphic correlation [thick line; 21pt smooth < 70 kyr, 9 pt smooth > 70 kyr], with the original data (thin line) superimposed. *N. pachyderma* (s) maxima (PS events) are labeled PS1—PS8. Interstadials in the GISP2 ice core record are labeled IS1—IS23 (after *Bender et al.*, 1994).

records [*Little*, 1997; *Little et al.*, 1997]. Indeed, *Imbrie et al.* [1989] showed that South Atlantic SST records consistently lead the North Atlantic SST response by 3-kyr in the precessional cycle. The interhemispheric correlation suggests that the cross-equatorial geostrophic/thermohaline flux plays an important role in northern hemisphere climate change. Moreover, all sediment and ice records, in particular equatorial seasonality, show an interesting feature whereby the data show a clear change of dominant frequency at about 65 ka. Visual inspection of the seasonality record in particular shows greatest amplitudinal variations in the earlier part of the record with an enhanced 23-kyr frequency, while the period between 15 and 65 ka has a much higher frequency of change. The variable frequency of change suggest that precession seems to be more dominant before 65 ka in the warmer global interglacial regime, but younger than this, the northern Cape Basin is affected by a higher frequency of change, at a time when the normal precessional variation, and insolation, are at their weakest [*Berger et al.*, 1984] and the average global temperature is reduced. The change at 65 ka is also reflected in the GISP2 ice core, with an overall trend from longer-term cycles before isotope stage 4, to shorter higher-frequency change in the glacial stages 4—2.

Discussion

Correlation of Paleoceanographic Proxies in the South Atlantic

The *N. pachyderma* (s) abundances from the South Atlantic Ocean show a history of rapid events punctuating the last 140 kyr, temporally consistent with equatorial seasonality, and with most of the events recognizable in Greenland ice records. Before discussing the implications for the North Atlantic, it is necessary to understand the forcing mechanisms behind the observed rapid changes in the Cape Basin and at the equator .

Using planktonic foraminifera derived SST from sediment cores in the eastern equatorial Atlantic Ocean, *McIntyre et al.* [1989] concluded that the variations seen in the seasonality records were controlled by two separate factors. First is equatorial trade wind and monsoon-controlled divergence, which controls trade wind meridionality/zonality and, in turn, upwelling intensity. Second is the increased abundance of transitional and subpolar fauna in the equatorial Atlantic, which led them to believe that heat advection from high southern latitudes also plays a significant role. These mechanisms were linked into a two end-member system: (1) furthest southerly position of the subtropical convergence (STC), permitting the greatest pulses of Indian Ocean water to enter into the Atlantic, accompanied by maximum northward heat advection into the Benguela Current; and (2) farthest northerly position of the STC preventing Indian Ocean water entry into the Atlantic by formation of a thermal barrier south of Cape Town and accompanied by equatorward advection of cold water from south of the STC. *Schneider et al.* [1995] have also suggested that advection of cold surface waters from the Southern Ocean was directed to the equatorial Atlantic with a more offshore Benguela Oceanic Current at times of increased trade wind zonality and reduced monsoon intensity.

Equatorward advection of cold waters from the STC should be reflected in very high abundances of cold-water planktonic foraminifera as are used to describe cool SSTs at the equator. Cores taken from the southern Cape Basin [*Little*, 1997] show that the cold-water *N. pachyderma* (s) was almost completely absent offshore Cape Town for at least the last 200,000 years and in abundances less than 50% in the north of the southern Cape Basin even though it is in abundances of up to 90% in the northern Cape Basin [*Oberhänsli*, 1991; *Schmidt*, 1992; *Jansen et al.*, 1997; *Little et al.*, 1997]. If northward advection of cool Southern Ocean surface and intermediate waters was to be playing a major role in the planktonic foraminiferal variations seen in the Benguela upwelling system, then we would almost certainly see the highest abundances of the cold-water *N. pachyderma* (s) in the south of the region. Their absence strongly suggests against cold-water advection of sub-Antarctic waters from the STC.

A third possibility we must consider is the extension of the Benguela Current into the more northerly Angola Basin and equatorial Guinea Basin by the intensification of the along shore component of the Benguela Current in glacial periods [*Gardner and Hays*, 1976; *Morley and Hays*, 1979; *Diester-Haass*, 1985; *Pokras*, 1987; *Diester-Haass et al.*, 1988; *Mix and Morey*, 1997]. This necessitates a westward deflection of the Benguela Coastal Current in the region of 0°—5°S and a shift from the present cyclonic gyre where the Benguela Current is deflected at 23°S. Recent studies do not indicate an intensification of the along-shore component of the Benguela Current into the Angola or Guinea Basins [*Jansen and Van Iperen*, 1991; *Schneider et al.*, 1995; *Jansen et al.*, 1997; *Mix and Morey*, 1997]. *Schneider et al.* [1995], with SST records from the Angola Basin and on the Walvis Ridge, show that the

Angola-Benguela Front has remained between 12° and 20°S during the last 200 kyr and that the current cyclonic gyre centred on the Angola Basin has existed during this time. *Little et al.* [1997] strongly argue that upwelling in the Benguela system is dominated by the trade winds and that its fluctuation corresponds to the movements of the Angola-Benguela Front, marking the boundary of the Angola and Benguela Current systems.

Direct along-shore intensification of the Benguela Current into the Angola Basin is not significant, and instead, an intensification of equatorial upwelling coinciding with intensification of upwelling farther south in the northern Cape Basin should be considered, the result correlating to cold SSTs in the equatorial region and an increased annual SST range promoting increased equatorial seasonality [*Mix et al.*, 1986a, b; *Imbrie et al.*, 1989; *McIntyre et al.*, 1989; *Mix and Morey*, 1997]. Our data set clearly shows intensification of upwelling in the northern Cape Basin at regular intervals over the past 140 kyr, in particular, the LGM and isotope stages 2 and 3; similar planktonic foraminiferal analysis, although at a lower resolution, agrees in most part with this assessment [*Oberhänsli*, 1991; *Diester-Haass et al.*, 1992; *Schmidt*, 1992; *Jansen et al.*, 1997; *Little et al.*, 1997; J. Giraudeau et al., manuscript in preparation, 1997]. There is no evidence in support of the advection of sub-Antarctic waters across the STC, but instead there is ample evidence of extensive cooling associated with trade wind driven upwelling. It is the input of this latter type of cold upwelled water, simultaneous with Namibian coastal upwelling, which *McIntyre et al.* [1989] observed at the equator rather than advection of cold Southern Ocean surface waters.

It seems that trade wind zonality is strongly related to the seasonality at the equator, as *McIntyre et al.* [1989], *Imbrie et al.* [1989], *Schneider et al.* [1995] and *Mix and Morey* [1997] have suggested; equatorward cold-water advection, other than that from upwelling, plays a minor if not insignificant role. At times of maximum trade wind zonality, the eastern boundary of the South Atlantic Ocean and equatorial seasonality records, respond to increased upwelling intensity and relatively cooler SSTs. Equatorial seasonality could be further enhanced if offshore divergence of the Benguela Oceanic Current intensified the direct input into the equatorial regions via the South Equatorial Countercurrent. Increased trade wind zonality along the entire eastern margin of the South Atlantic should increase the divergence of warm surface waters away from the coastal upwelling cells and force tropical and subtropical waters across the equator via the South Equatorial Current. This will increase the equatorial pool of heat which can be transported to the high northern latitudes by the Gulf Stream and North Atlantic Drift.

Teleconnections in the Atlantic Oceanic and Atmospheric Circulation System

During the period of increased trade wind and upwelling intensity in glacial stages 4—2, the *N. pachyderma* (s) record is punctuated by anomalous abundance minima. These periods of low % *N. pachyderma* (s) represent rapid short-lived warmer intervals at a time of glacial cooling, reflecting decreased trade wind strength as monsoonal winds increased over eastern and central Africa. Contrary to this, the cool PS events, which are thought to be typical for the eastern South Atlantic continental margin, correlate to warmer climate intervals in the Greenland ice records and subpolar ocean SSTs [*Ruddiman and McIntyre*, 1981]. The Benguela Current system could be regarded as the major component influencing cross-equatorial teleconnections between the South Atlantic and North Atlantic via the South Equatorial and the North Brasil Currents into the Gulf Stream, driven by variations in atmospheric conditions controlling trade wind intensity and zonality. Cold water resulting directly from intense upwelling will produce cold SSTs and lowered salinities along the entire eastern South Atlantic margin, enhancing seasonality at the equator. Direct cross-equatorial transfer of this cooler water into the Gulf Stream, similar to that from hypothesized meltwater models, would have had an almost instantaneous cooling effect on North Atlantic records rather than a lead of 3-kyr as is implied from correlation with the timing of Heinrich events. With respect to northern hemisphere climate change indicated in the GISP2 record it appears that southern hemisphere trade winds have been reduced at times of maximum cooling and vice versa. *Ruddiman and McIntyre* [1981] discussed similar results using SST data from the northwestern subtropical gyre and the subArctic ocean which remain near their maximum SST into the phase of maximum ice building, creating optimal conditions for rapid ice growth by providing moisture due to the large temperature gradient between the atmosphere and ocean. The GeoB 1711 data set reinforces this relationship but suggests that enhanced cross-equatorial transfer of warm waters into the Gulf Stream, at times of trade wind zonality, increases warm-water advection to the higher latitudes of the North Atlantic and maintains the elevated SSTs into the phase of maximum ice building. Without very high resolution records the precise timing of events in the northern and southern hemisphere cannot be quantified conclusively, but the phase difference suggested by this and previous work ([*Imbrie et al.*, 1989; *Charles et al.*, 1996] suggests a real lead of the South Atlantic Ocean.

Boulton and Payne [1994] modeled midlatitude northern hemisphere ice sheet growth and have suggested that Heinrich scale instabilities and ice calving could result from internal thermal instabilities as a result of changes in the basal boundary conditions of the ice sheets. A reduction in basal friction initiating iceberg calving could result from an increase in the accumulation rate of snow. Modelled results suggest that ice sheet calving could occur approximately every 4-kyr, following a 2—3 kyr increase in the accumulation of snow, as is predicted by the 3-kyr lead of the Southern Atlantic Ocean. A relative increase in moisture supply to the atmosphere in the higher latitudes of the North Atlantic would be enough to create basal instability leading to a rapid calving event and IRD deposit [*Boulton and Payne*, 1994]. We hypothesize that the intensification of the trade winds, increases cross equatorial flow and delivers more warm water into the tropical pool for delivery northwards. The increase in heat flux from the equator to the high latitudes of the North Atlantic via the Gulf Stream, leads to an increased accumulation of ice and increased thermal instabilities in the northern hemisphere ice sheets, as the ice-ocean moisture gradient is increased. This will result in rapid ice sheet calving and stimulate further moisture feedback mechanisms and further ice sheet collapse [*Ruddiman and McIntyre*, 1981].

Our observations suggest millenial scale "conveyor belt" changes occur in all of the Earth's major ocean basins in both northern and southern hemispheres. The entire data set is strongly suggestive of a globally linked atmosphere-ocean-cryosphere system varying via changes in trade wind intensity and zonality, linked to sub-Milankovitch climate variability derived from the insolation-linked precessional band.

Conclusions

Relative abundances of the cold-water planktonic foraminifera *N. pachyderma* (s) record rapid upwelling intervals (PS events) punctuating the last 140 kyr on a sub-Milankovitch cyclicity. Records in the equatorial Guinea Basin and the more southerly Angola and Cape Basins have shown upwelling intensification to be the primary control on faunal and SST patterns. Correlation between *N. pachyderma* (s) abundances from the northern Cape Basin and eastern equatorial seasonality record [*McIntyre et al.*, 1989] suggests that the entire eastern margin of the South Atlantic is dominated by fluctuations in trade wind zonality and intensity. Radiocarbon dating for the last 45 kyr permits a further correlation between PS events in the northern Cape Basin with Heinrich events of the North Atlantic and suggests teleconnections in South Atlantic—North Atlantic and global heat transfer. Maximum abundances of *N. pachyderma* (s) coincide with interstadials in the GISP2 ice core and further suggest that warm-water advection to the North Atlantic stimulates rapid ice sheet growth.

We hypothesize that intense upwelling events on a sub-Milankovitch cyclicity occurred throughout the last 140 kyr, in particular during the last glacial cycle (isotope stages 4—2), controlled by changes in intensity and zonality of the trade winds at times of maximum ice buildup and mimimum solar insolation and indicate a 3-kyr phase lead of the South Atlantic to corresponding changes in northern hemisphere sediment records. The increase in trade wind controlled offshore displacement of tropical and subtropical waters, may have implications for the strength of equatorial transfer into the North Atlantic, via the South Equatorial Current and Gulf Stream, and for the global thermohaline conveyor and Atlantic convection. The tropical warm water which is forced across the equator, is transported to the high latitudes of the North Atlantic into the phase of maximum ice building. This intensifies the moisture gradient between the subArctic ocean and the northern hemisphere ice sheets, increasing the rate of snow accumulation until eventual ice sheet collapse and iceberg calving.

Furthermore, the sub-Milankovitch frequencies at which these rapid upwelling events occur have also been described for sediment cores within the Pacific [*Kennett and Ingram*, 1995; *Behl and Kennett*, 1996], northern [*Hagelberg et al.*, 1994], and southern Atlantic Oceans [*Park et al.*, 1993; *Charles et al.*, 1996] and within the Greenland [*Bender et al.*, 1994; *Mayewski et al.*, 1994] and Vostok [*Yiou et al.*, 1991] ice cores. The paleoceanographic records analyzed in this study demonstrate further that high-frequency sub-Milankovitch cyclicity is a global phenomenon and that cross-equatorial heat transfer via trade wind intensification may have serious repercussions for global climate.

Acknowledgments. We thank the crew and scientists aboard R/V METEOR for their help with coring and sampling operations during cruises to the South Atlantic. We are grateful to Andrew McIntyre, Katharina Billups, and an anonymous reviewer, whose comments and critical review significantly improved the manuscript. We also thank the Leibniz-Labor AMS facility, Christian-Albrechts-University, Kiel, Germany for measuring the AMS ^{14}C dates, Birgit Meyer-Schack for her assistance with the mass spectrometers, and Sandy Tudhope for his helpful advice which greatly improved the data presentation. This research was funded by the Natural Environmental Research Council (NERC grant GR3 8344 at Edinburgh University) and the Deutsche Forschungsgemeinschaft (Sonderforschungsbereich 261 at Bremen University, contribution N° 146).

References

Aksu, A.E., and D.J.W. Piper, Baffin Bay in the past 100,000 yr, Geology, 7, 245-248, 1979.

Andrews, J.T., A.S. Dyke, K. Tedesco, and J.W. White, Meltwater along the Arctic margin of the Laurentide Ice Sheet (8-12 ka): Stable isotopic evidence and implications for past salinity anomalies, *Geology, 21*, 881-884, 1993.

Bard, E., Correction of accelerator mass spectrometer ^{14}C ages measured in planktonic foraminifera, *Paleoceanography, 3*, 635-645, 1988.

Bard, E., B. Hamelin, and R.G. Fairbanks, U-Th ages obtained by mass spectrometry in corals from Barbados: Sea level during the past 130,000 years, *Nature, 346*, 456-458, 1990a.

Bard, E., B. Hamelin, R.G. Fairbanks, and A. Zindler, Calibration of the ^{14}C timescale over the past 30,000 years using mass spectrometric U-Th ages from Barbados corals, *Nature, 345*, 405-410, 1990b.

Bard, E., M. Arnold, R.G. Fairbanks and B. Hamelin, ^{230}U, ^{234}U and ^{14}C ages obtained by mass spectrometry on corals, *Radiocarbon, 35*, 191-199, 1993.

Behl, R.J., and J.P. Kennett, Brief interstadial events in the Santa Barbara Basin, NE Pacific, during the past 60 kyr, *Nature, 379*, 243-246, 1996.

Bender, M., T. Sowers, M.-L. Dickson, J. Orchado, P. Grootes, P.A. Mayeweski, and D.A. Meese, Climate correlations between Greenland and Antarctica during the past 100,000 years, *Nature, 372*, 663-666, 1994.

Berger, W.H., The Younger Dryas cold spell - a quest for causes., *Paleogeog. Paleoclim. Paleoecol., 89*, 219-237, 1990.

Berger, A., J. Imbrie, J. Hays, G. Kukla, and B. Saltzman, *Milankovitch and Climate*, 510 pp., D. Reidel, Norwella, Mass., 1984.

Berger, W.H., and D. Kroon, Possible causes for the Younger Dryas: A brief survey, in *The Younger Dryas*, edited by S.R. Troelstra, J.E. van Hinte, and G.M. Ganssen, G. M., pp. 221-224, North-Holland, New York, 1995.

Bond, G., et al., Evidence for massive discharges of icebergs into the North Atlantic ocean during the last glacial period, *Nature, 360*, 245-249, 1992.

Bond, G., W. Broecker, S. Johnsen, J. McManus, L. Labeyrie, J. Jouzel, and G. Bonani, Correlations between climate records from North Atlantic sediments and Greenland ice, *Nature, 365*, 143-147, 1993.

Boulton, G.S., and T. Payne, Mid-latitude ice sheets through the last glacial cycle: Glaciological and geological reconstructions, In *Long Term Climatic Variations*, edited by J.-C. Duplessy, and M.-T. Spyriadakis, M.-T., *NATO ASI Series, I22*, pp. 177-212, 1994.

Broecker, W.S., The chronology of the last glaciation: Implications to the causes of the Younger Dryas event, *Paleoceanography, 3*, 1-19, 1988.

Broecker, W.S., and G.H. Denton, The role of ocean-atmosphere reorganizations in glacial cycles, *Geochim. Cosmochim. Acta, 53*, 2465-2501, 1989.

Broecker, W.S., and E. Maier-Reimer, The influence of air and sea exchange on the carbon isotope distribution in the sea, *Global Biogeochem. Cycles, 6*, 315-320, 1992.

Broecker, W.S., D.M. Peteet, and D. Rind, Does the ocean-atmosphere system have more than one stable mode of operation?, *Nature, 315*, 21-26, 1985.

Broecker, W.S., G. Bond, M. Klas, G. Bonani, and W. Wolfli, A salt oscillator in the glacial Atlantic?, 1, The concept, *Paleoceanography, 5*, 469-477, 1990a.

Broecker, W.S., T.H. Peng, J. Jouzel, and G. Russell, The magnitude of global fresh-water transports of importance to ocean circulation, *Clim, Dyn., 4*, 73-79, 1990b.

Charles, C.D., J. Lynch-Stieglitz, U.S. Ninnemann, and R.G. Fairbanks, Climate connections between the hemisphere revealed by deep sea sediment core/ice core correlations, *Earth Planet. Sci. Lett., 142*, 19-27, 1996.

Dansgaard, W., et al., Evidence for general instability of past climate from a 250-kyr ice-core-record, *Nature, 364*, 218-220, 1993.

Diester-Haass, L., Late Quaternary sedimentation on the eastern Walvis Ridge, SE Atlantic (HPC 532, Leg 75, and four piston cores), *Mar. Geol., 65*, 145-189, 1985.

Diester-Haass, L., K. Heine, P. Rothe, and H. Schrader, Quaternary history of continental climate and the Benguela Current off southwest Africa, *Palaeogeog. Palaeoclim. Palaeoecol. 65*, 81-91, 1988.

Diester-Haass, L., P.A. Meyers, and P. Rothe, The Benguela Current and associated upwelling on the southwest African Margin: A synthesis of the Neogene-Quaternary sedimentary record at DSDP sites 362 and 532. In *Upwelling Systems: Evolution Since the Early Miocene*, edited by C.P. Summerhayes, W.L. Prell, and K.C. Emeis, *Geol. Soc. Spec. Publ.*, 64, 331-342, 1992.

Duplessy, J.C., L. Labeyrie, M. Arnold, M. Paterne, J. Duprat, and T.C.E. van Weering, Changes in surface salinity of the North Atlantic Ocean during the last deglaciation, *Nature, 358*, 485-487, 1992.

Fillon, R.H., and J.C. Duplessy, Labrador Sea bio-, tephro-, oxygen isotopic stratigraphy and Late Quaternary palaeoceanographic trends, *Canad. J. Earth Sci. 17*, 831-854, 1980.

Gardner, J.V., and J.D. Hays, Responses of sea-surface temperature and circulation to global climate changes during the past 200,000 years in the eastern equatorial Atlantic Ocean, *Mem. Geol. Soc. Am., 145*, 221-246, 1976.

Gordon, A.L., Interocean exchange of thermocline water, *J. Geophys. Res., 91*, 5037-5046, 1986.

Gordon, A.L., and K.T. Bosley, Cyclonic gyre in the tropical South Atlantic, *Deep Sea Res., 38*, S323-S343, 1991.

Gordon, A.L., R.F. Weiss, W.M. Smethie, and M.J. Warner, Thermocline and intermediate water communication between the South Atlantic and Indian Oceans, *J. Geophys. Res., 97*, 7223-7240, 1992.

Grootes, P.M., M. Stuiver, J.W.C. White, S. Johnsen, and J. Jouzel, Comparison of oxygen isotope records from the GISP2 and GRIP Greenland ice cores, *Nature, 366*, 552-554, 1993.

Grousset, F.E., L. Labeyrie, J.A. Sinko, M. Cremer, G. Bond, J. Duprat, E. Cortijo, and S. Huon, Patterns of ice rafted detritus in the glacial North Atlantic (40°-55°N), *Paleoceanography, 8*, 175-192, 1993.

Hagelberg, T.K., G. Bond, and P. deMenocal, Milankovitch band forcing of sub-Milankovitch climate variability during the Pleistocene, *Paleoceanography, 9*, 545-558, 1994.

Heinrich, H., Origin and consequences of cyclic ice rafting in the northeast Atlantic Ocean during the past 130,000 years, *Quat. Res., 29*, 142-152, 1988.

Imbrie, J., J.D. Hays, D.G. Martinson, A. McIntyre, A.C. Mix, J.J. Morley, N.G. Pisias, W.L. Prell, and N.J. Shackleton, The orbital theory of pleistocene climate: Support from a revised chronology of the marine $\delta^{18}O$ record, in *Milankovitch and Climate, Part I*, edited by A. Berger, et al., pp. 269-305, D. Reidel, Norwell, Mass., 1984.

Imbrie, J., A. McIntyre, and A. Mix, Oceanic response to orbital forcing in the late Quaternary: Observational and experimental strategies, in *Climate and Geo-Sciences*, edited by A. Berger, pp. 121-164, Kluwer Acad., Norwell, Mass., 1989.

Jansen, E., and T. Veum, Evidence for two-step deglaciation and its impact on North Atlantic deep-water circulation, *Nature, 343*, 612-616, 1990.

Jansen, F., E. Ufkes, and R.R. Schneider, Late Quaternary movements of the Angola-Benguela Front, SE Atlantic, and implications for advection in the equatorial Ocean, in *The South Atlantic: Present and Past Circulation*, G. Wefer, W.H. Berger, G. Siedler, and D. Webb, pp. 553-575, Springer-Verlag, New York, 1997.

Jansen, J.H.F., and J.M. van Iperen, A 220,000-year climatic record for the east-equatorial Atlantic Ocean and equatorial Africa: Evidence from diatoms and opal phytoliths in the Zaire (Congo) deep-sea fan, *Paleoceanography, 6*, 573-591, 1991.

Jansen, J.H.F., T.C.E. van Weering, R. Gieles, and J. van Iperen, Late Quaternary oceanography and climatology of the Zaire-Congo fan and the adjacent eastern Angola Basin, *Neth. J. Sea Res., 17*, 201-249, 1984.

Johnsen, S.J., Irregular glacial interstadials recorded in a new Greenland ice core, *Nature, 359*, 311-312, 1992.

Johnson, R.G., and J.T. Andrews, Rapid ice sheet growth and initiation of the last glaciation, *Quat. Res., 12*, 119-134, 1979.

Keigwin, L.D., and S.J. Lehman, Deep circulation linked to Heinrich event 1 and Younger Dryas in a middepth North Atlantic core, *Paleoceanography, 9*, 185-194, 1994.

Kennett, J.P., and B.L. Ingram, A 20,000 year record of ocean circulation and climate change from the Santa Barbara Basin, *Nature, 377*, 510-513, 1995.

Kreveld, S.A. van, M. Knappertsbusch, J. Ottens, G.M. Ganseen, and J.E. van Hinte, Biogenic carbonate and IRD (Heinrich Layer) accumulation in deep sea sediments from a northeast Atlantic piston core, *Mar. Geol., 131*, 21-46, 1996.

Little, M.G., Late Quaternary palaeoceanography of the Benguela upwelling system. Ph.D. thesis, Edinburgh Uni., Edinburgh, Scotland, 1997.

Little, M.G., R.R. Schneider, D. Kroon, N.B. Price, T. Bickert, and G. Wefer, Rapid palaeoceanographic changes in the Benguela upwelling system for the last 160,000 years, as indicated by abundances of planktonic foraminifera, *Palaeogeogr. Palaeoclim. Palaeoecol.*, in press, 1997.

Lutjeharms, J.R.E., and J.M. Meeuwis, The extent and variability of SE Atlantic upwelling, *S. Afr. J. Mar. Sci., 5*, 51-62, 1987.

Lutjeharms, J.R.E., and P.L. Stockton, Kinematics of the upwelling front off southern Africa, *S. Afr. J. Mar. Sci., 5*, 35-49, 1987.

Macdonald, A.M., and C. Wunsch, An estimate of global circulation and heat fluxes, *Nature, 382*, 436-439, 1996.

Maslin, M.A., N.J. Shackleton, and U. Pflaumann, Surface water temperature, salinity, and density changes in the northeast Atlantic during the last 45,000 years: Heinrich events, deep water formation, and climatic rebounds, *Paleoceanography, 10*, 527-544, 1995.

Mayewski, P.A., et al., Changes in atmospheric circulation and ocean ice cover over the North Atlantic during the last 41,000 years, *Science, 263*, 1747-1751, 1994.

McIntyre, A., W.F. Ruddiman, K. Karlin, and A.C. Mix, Surface water response of the equatorial Atlantic Ocean to orbital forcing, *Paleoceanography, 4*, 19-55, 1989.

McManus, J.F., G.C. Bond, W.S. Broecker, S. Johnsen, L. Labeyrie and S. Higgins, High-resolution climate records from the North Atlantic during the last interglacial, *Natrue, 371*, 326-329, 1994.

Meeuwis, J.M., and J.R.E. Lutjeharms, Surface thermal characteristics of the Angola-Benguela front, *S. Afr. J. Mar. Sci., 9*, 261-279, 1990.

Mix, A.C., and A.E. Morey, Climate feedback and Pleistocene variations in the Atlantic South Equatorial Current, in *The South Atlantic: Present and Past Circulation*, G. Wefer, W.H. Berger, G. Siedler, and D. Webb, pp. 503-525, Springer-Verlag, New York, 1997.

Mix, A.C., W.F. Ruddiman, and A. McIntyre, Late Quaternary paleoceanography of the tropical Atlantic, 1: Spatial variability of annual mean sea surface temperatures, 0—20,000 years B.P., *Paleoceanography, 1*, 43-66, 1986a.

Mix, A.C., W.F. Ruddiman, and A. McIntyre, Late Quaternary paleoceanography of the tropical Atlantic, 2, The seasonal cycle of sea surface temperatures, 0-20,000 years B.P., *Paleoceanography, 1*, 339-353, 1986b.

Molnia, B.F. Distal glacial-marine sedimentation: Abundance, composition and distribution of North Atlantic ocean Pleistocene ice-rafted sediment. in *Glacial-Marine Sedimentation* edited by B.F. Molnia, pp. 593-629, Plenum, New York, 1983.

Morley, J.J., and J.D. Hays, Comparison of glacial and interglacial oceanographic conditions in the South Atlantic from variations in calcium carbonate and radiolarian distribution, *Quat. Res., 12*, 396-408, 1979.

Moroshkin, K.V., V.A. Bubnov, and R.P. Bulatov, Water circulation in the eastern South Atlantic, *Oceanology, Engl. Transl, 10*, 27-34, 1970.

Nadeau, M.-J., M. Schleicher, P.M. Grootes, H. Erlenkeuser, A. Gottdang, D.J.W. Mous, J.M. Sarnthein, and H. Willkomm, Nuclear Instruments and Methods, B., in press, 1997.

Oberhänsli, H., Upwelling signals at the northeastern Walvis Ridge during the past 500,000 years, *Paleoceanography, 6*, 53-71, 1991.

Paillard, D., and L. Labeyrie, Role of the thermohaline circulation in the abrupt warming of the Heinrich events, *Nature, 372*, 162-164, 1994.

Park, J., L.D. D'Hondt, J.W. King, and C. Gibson, Late Cretaceous precessional cycles in double time: A warm-Earth Milankovitch response, *Science, 261*, 1431-1434, 1993.

Pastouret, L., G.A. Auffret, M. Hoffert, H.D. Needham, and C. Latouche, Sedimentation sur la ride de Terre-Neuve, *Can. J. Earth Sci., 12*, 1019-1035, 1975.

Peterson, R.G., and L. Stramma, Upper-level circulation in the South Atlantic Ocean, *Prog. Oceanogr., 26*, 1-73, 1991.

Pokras, E.M., Diatom record of Late Quaternary climatic change in the eastern equatorial Atlantic and tropical Africa, *Paleoceanography, 2*, 273-286, 1987.

Porter, S.C., and A. Zhisheng, Correlation between climate events in the North Atlantic and China during the last glaciation, *Nature, 375*, 305-308, 1995.

Ruddiman, W.F., Late Quaternary deposition of ice rafted sand in the subpolar North Atlantic (lat 40-65N), *Geol. Soc. Am. Bull., 88*, 1813-1827, 1977.

Ruddiman, W.F., and A. McIntyre, Oceanic mechanisms for amplification of the 23,000-year ice-volume cycle, *Science, 212*, 617-627, 1981.

Ruddiman, W.F., A. McIntyre, V. Niebler-Hunt, and J.T. Durazzi, Oceanic evidence for the mechanism of rapid northern hemisphere glaciation, *Quat. Res., 13*, 33-64, 1980.

Schmidt, H., Der Benguela Strom im Bereich des Walfisch Rückens im Spätquartär. Ph.D. thesis, Univ. Bremen,172 pp., Bremen, Germany, 1992.

Schmitz, W.J., On the eddy field in the Agulhas Retroflection, with some global considerations, *J. Geophys. Res., 101*, 16,259-16,271, 1996.

Schneider, R.R., Spätquartäre Produktivitätsänderungen im östlichen Angola-Becken: Reaktion auf Variationen im Passat-Monsun-Windsystem und in der Advektion des Benguela-Küstenstroms. Ph.D. thesis, 198 pp., Univ. Bremen, Bremen, Germany, 1991.

Schneider, R.R., P.J. Müller, and G. Ruhland, Late Quaternary surface circuation in the east-equatorial south Atlantic: Evidence from Alkenone sea surface temperatures, *Paleoceanography, 10*, 197-219, 1995.

Schulz, H.D., et al., Bericht und erst Ergenbnisse über die METEOR-Fahrt M20/2, Abidjan-Dakar, 27.12.1991 - 3.2.1992, *25*, 173pp, Ber. Fachber. Geowissenschaften, Univ. Bremen, Bremen, Germany, 1992.

Shannon, L.V., The Benguela ecosystem, Part 1, Evolution of the Benguela, physical features and processes, *Oceanogr Mar. Bio. Ann. Rev., 23*, 105-182, 1985.

Shannon, L.V., J.J. Agenbag, and M.E.L. Buys Large and mesoscale features of the Angola-Benguela Front, in *The Benguela and Comparable Ecosystems*, A.L.L. Payne, J.A. Gulland, and K.H. Brink, *S. Afr. J. Mar. Sci., 5*, 11-34, 1987.

Stommel, H., Asymmetry of interoceanic fresh-water and heat fluxes, *Proc. Nat. Acad. Sci., U.S.A., 77*, 2377-2381, 1980.

Stramma, L., and R.G. Peterson, Geostrophic transport in the Benguela Current region, *J. Phys. Oceanogr., 19*, 1440-1448, 1989.

Summerhayes, C.P., D. Kroon, A. Rosel-Melé, R.W. Jordan, H.J. Schrader, R. Hearn, J. Villanueva, J.O. Grimalt, and G. Eglinton, Variability in the Benguela Current System over the last 70,000 years., *Prog. Oceanogr., 35*, 207-251, 1995.

Teller, J.T., Meltwater and precipitation runoff to the North Altantic, Arctic, and Gulf of Mexico from the Laurentide ice sheet and adjacent regions during the Younger Dryas, *Paleoceanography, 5*, 897-905, 1990.

Watts, R.G., Global climate variations due to fluctuations in the rate of deep water formation, *J. Geophys. Res., 90*, 8067-8070, 1985.

Yiou, P., C. Genthon, M. Ghil, J. Jouzel, H. Le Treut, J.M. Barnola, C. Lorius, and Y.N. Korotkevitch, High-frequency palaeovariability in climate and carbon dioxide levels from Vostok ice core records, *J. Geophys. Res., 96*, 20,365-20,378, 1991.

D. Kroon, M.G. Little (corresponding author), and B. Price, Department of Geology and Geophysics, University of Edinburgh, West Mains Road, Edinburgh EH9 3JW, Scotland.
(e-mail: dick.kroon@glg.ed.ac.uk; mark.little@glg.ed.ac.uk; brian.price@glg.ed.ac.uk)

R.R. Schneider and M. Segl, Fachbereich Geowissenschaften, Universitat Bremen, Klagenfurter Strasse, D-28359 Bremen, Germany.
(e-mail: rschneid@zfn.uni-bremen.de; segl@allgeo.uni-bremen.de)

C.P. Summerhayes, Southampton Oceanography Centre, Empress Dock, Southampton, SO14 3ZH, England.
(e-mail: colin.p.summerhayes@soc.soton.ad.uk)

(Received August 15, 1996; revised February 25, 1997;
accepted March 17, 1997.)

5 April 1997 No2076 Weekly £1·85 US$3·75

ISSN 0262 4079

New Scientist

Build the smallest they said

Four weird m

Dirty politics

Hunting the s

Southern oceans hold key to climate

Fred Pearce

THE waxing and waning of ocean currents almost as far south as Antarctica may have triggered regular growth spurts in Arctic ice sheets over the past 140 000 years. Researchers in Britain and Germany studying fossilised protozoans in the southern Atlantic say that their finding may lead to better predictions of the rate of global warming.

Many scientists believe that major climate changes are triggered by events in the northern hemisphere alone. But in a study to be published in *Paleoceanography*, Mark Little and Dick Kroon of the University of Edinburgh and their colleagues claim that that there may have been dramatic swings in the southern climate every 8000 to 10 000 years.

Not only are these sudden changes in step with events in the far north, they appear to precede them by about 3000 years. Kroon admits that he cannot be sure about this. "They could be 7000 years behind," he says. "But at any rate there is a clear link."

How might they be linked? The researchers argue that the southern climate swings may coincide with changes in the strength of the Benguela current that brings cold, deep Antarctic water north along the eastern shore of the southern Atlantic Ocean. This current grows stronger or weaker depending on the strength of the trade winds close to the equator. When strong trade winds blow aside surface waters, the current strengthens as it wells up to the surface.

Images

Cold storage: strong currents in the South Atlantic may build up ice sheets in the far north

"climate is not made in the North Atlantic as so many authors suggest".

At issue is the genesis of Heinrich events, regular surges and collapses of ice sheets that occur in the northern hemisphere every 8000 to 10 000 years. During an event, the ice sheets over North America, Greenland and Eurasia grow when the climate is cold and when the sheets are supplied with large amounts of moisture in the form of snow. But eventually the ice sheets become unstable and collapse into the oceans, releasing vast flows of icebergs. These icebergs carry boulders that end up on the ocean bed.

Now Little, Kroon and their colleagues report that similar cycles of rapid climate change have occurred in the southern Atlantic Ocean. The researchers found their evidence in rock cores taken from the seabed off the coast of Namibia. These cores showed that at regular intervals, several polar species of protozoan known as planktonic Foraminifera suddenly appeared or disappeared. The researchers conclude, after radiocarbon dating the protozoans,

Little and Kroon believe that the periodic strengthening of the cold southern current, revealed by the protozoans, pushes so much water into the tropical Atlantic that it strengthens the Gulf Stream in the northern Atlantic. This current then transports large amounts of warm water from the tropics northwards. There, the meeting of warm water and cold air generates large amounts of extra precipitation—enough to cause the rapid growth of the ice sheets.

"We can see here part of a global phenomenon," says Little. The researchers say that if the oceans play as great a role in climate change as the results suggest, predictions about the impact of greenhouse gas emissions may have to be revised. "This seems to show that the oceans control the world's climate as much as carbon dioxide does," says Kroon. "That could have important implications for our understanding of global warming." □

14

9 770262 407084

Extract from: EUG 9 (1997) Abstracts volume; Proxies 67/4B38 pp 613.

European Union of Geosciences 9

"Proxies in palaeoceanography and palaeoclimatology"

STRASBOURG, FRANCE

67/4B38

'HEINRICH-EVENTS' IN THE SOUTH ATLANTIC OCEAN: IMPLICATIONS FOR CROSS-EQUATORIAL AND GLOBAL HEAT TRANSFER AND SUB-MILANKOVITCH CLIMATE VARIABILITY

Mark G. Little[1] (Mark.Little@glg.ed.ac.uk),
Dick Kroon[1] (Dirk.Kroon@glg.ed.ac.uk) &
Ralph R. Schneider[2]
(Rschneid@zfn.uni-bremen.de)

[1] Geology and Geophysics, University of Edinburgh, West Mains Road, Edinburgh, EH9 3JW, Scotland, U.K.
[2] Fachbereich Geowissenschaften, Universitat Bremen, Klagenfurter Strasse, D-28359 Bremen, Germany.

Changes in the abundances of planktonic foraminifera, recovered from sediment cores in the Benguela upwelling system, reveal a history of rapid upwelling events during the last 140,000 years. The cold-water planktonic foraminifer, left-coiling *Neogloboquadrina pachyderma* (Ehrenberg), records changes in abundance of over 50% in less than 5 kyr. These discrete episodes regularly punctuate the fossil record, and are referred to as PS-events, which can be correlated between cores in the Cape Basin. The timing of the PS-events suggests a sub-Milankovitch forcing in the order of 10 kyr, and with AMS ^{14}C chronological control, suggests that the history of upwelling in the Benguela system reflects the equatorial seasonality record from core RC24-16. During the last 65 kyr when precessional forcing is weakest, in the glacial stages 2-4, the 10 kyr cyclicity is very pronounced in both equatorial and Cape Basin records. ^{14}C dates for the last 45 kyr in GeoB 1711, enable a good correlation with Heinrich-events H1-H4 in the North Atlantic marine and ice-core records. The further dating of three cores in the northern Cape Basin (GeoB 1711, GeoB 1706 and PG/PC12) reveals a constant 2-3 kyr lead of the South Atlantic upwelling record relative to the North Atlantic Heinrich-events and the GISP2 $\delta^{18}O$ ice core record for at least the last 80 kyr. The similarity in timing of the PS-events with foraminifera-derived equatorial seasonality and northern hemisphere Heinrich records, further suggests global teleconnections in the atmosphere-ocean-cryosphere system. We suggest that we are recording evidence for high frequency cycling driven by non-linear harmonics in the precessional band, as a result of changes in net global insolation and the resultant intensity of the Trade Wind system, affecting cross-equatorial and global heat transfer.

Extract from: ICP V (1995) Abstracts volume; Session 5: Ocean Fluxes pp133-134.

Fifth Internation Conference On Paleoceanography
"The role of paleoceanographic linkages in the global system"
HALIFAX, NOVA SCOTIA, CANADA

LATE QUATERNARY PLANKTONIC FORAMINIFERAL RECORD OF PALAEOCEANOGRAPHIC CHANGE IN THE BENGUELA UPWELLING SYSTEM FOR THE LAST 180,000 YEARS.

Little, M.G., Department of Geology and Geophysics, Grant Institute, University of Edinburgh, West Mains Road, Edinburgh, EH9 3JW, Scotland, UK; Kroon, D.; Schneider, R.R.; Wefer, G. & Price, N.B.

A new core from the Walvis Ridge (20°S, 11°E), Namibia reveals striking downcore variations in foraminiferal abundances. Fluctuations are investigated to assess changes in the intensity and position of the upwelling centres offshore Namibia during the last 180 kyr.

Four taxa make up over 95% of the variation within the assemblage, and together with correlation and factor analysis allow the Late Quaternary to be divided into episodes of taxa dominance as seen in the modern-day distribution patterns. The episodes are interpreted as fluctuations in nutrient supply indicating changes in upwelling intensity. In the region south of 27°S the area consists of near shore intense upwelling centres dominated by Neogloboquadrina pachyderma, and a sharp thermal barrier separating oligotrophic, tropical waters dominated by Globorotalia inflata. The region north of 27°S has a narrow, near shore, low intensity, upwelling centre and an offshore, mesotrophic mixing domain dominated by Neogloboquadrina dutertrei and Globigerina bulloides.

The foraminiferal record suggests shifts in the type and intensity of upwelling processes, and corresponding trophic domains, which do not follow the typical Glacial-Interglacial pattern. Fluctuations in the major components show a precessional cyclicity, and match well with the seasonality record of the N. Atlantic; whilst the shifts of the trophic domains correspond to movement of the equatorward Angola-Benguela Front. An anomalous cool event between 53 and 41 kyr, at a time of reduced upwelling intensity, can be explained by the advection of Subantarctic Surface Water into the Benguela system. Variations in position of the South Atlantic gyre and corresponding trade wind intensities are interpreted to be the main forcing mechanisms for the fluctuations seen.

DER SPIEGEL

Nr. 22/26.5.97 · 5,00 DM

4 390700 705005 22

HONGKONG

Chinas reiche Beute

Prisma

Wissenschaft

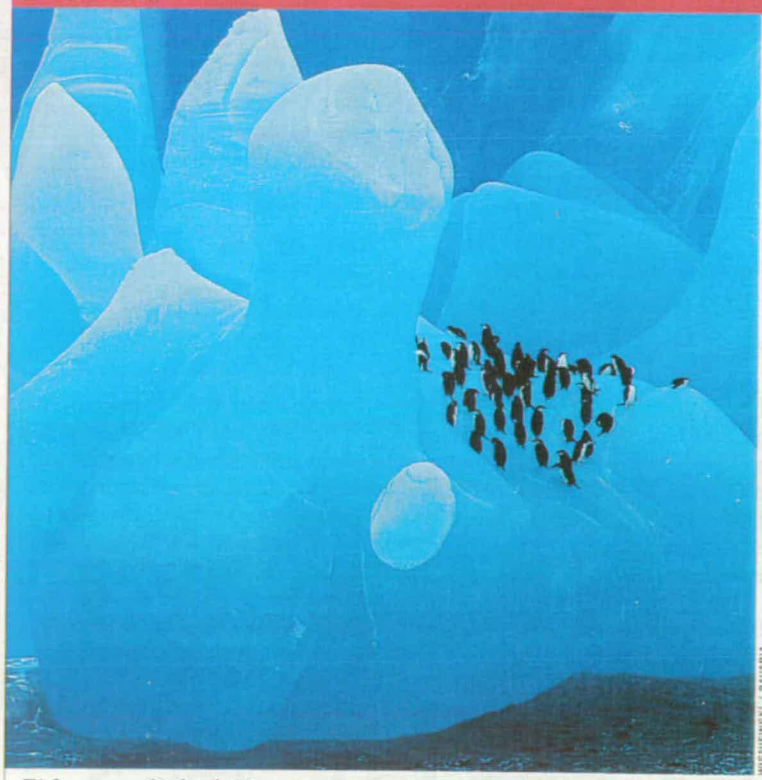

WISNIEWSKI / BAVARIA

Eisberg am Südpol, Pinguine

KLIMA

Kalter Süden

Globale Klimaveränderungen, die mit regelmäßigem An- und Abschwellen von Schnee- und Eismassen auf der nördlichen Halbkugel einhergehen, haben ihren Ursprung in einer kühlen Meeresströmung aus dem Südatlantik. Zu diesem Ergebnis gelangte eine deutsch-britische Forschergruppe, die in Sedimentproben vom Meeresgrund vor der Küste des südafrikanischen Staates Namibia Anzahl und Alter fossilisierter Einzeller untersuchten. Die Urtierchen erlauben Rückschlüsse auf die Stärke der Passatwinde, die offenbar ein Motor des Weltklimas sind. Geowissenschaftler der Universitäten Bremen und Edinburgh deuten die Befunde als Nachweis dafür, daß auch die Eismassen am Südpol entgegen vorherrschender Meinung in Abständen von wenigen tausend Jahren plötzlich anwuchsen oder abschmolzen und verantwortlich waren für die Intensivierung der Passatwinde auf der Südhalbkugel. Die unterschiedliche Stärke der Passatwinde bewirkt, so die Forscher, eine Veränderung der Benguela-Meeresströmung, die südpolare Wassermassen in äquatoriale Breitengrade bringt. Dabei wird auch der Wärmetransport über den Äquator und in den Golfstrom verstärkt. Seine wärmeren Wassermassen treffen in nördlichen Breiten auf Kaltluft und sorgen so für erhöhten Schneefall und Vereisung. Die Bremer Forscher Ralph Schneider und Gerold Wefer sind deshalb überzeugt, daß die starke Vereisung auf der Nordhalbkugel auch im Südozean verursacht wird.

Bernste
Die Stasi-Co